



Doctoral Dissertation

Submitted to obtain the title of

JUSTUS-LIEBIG-
UNIVERSITÄT
GIESSEN



Doctor in Chemistry from the Université de Bourgogne and the Justus-Liebig-Universität Giessen

By

Maria Agatha E. GUNAWAN

Ingénieur de l'Ecole Nationale Supérieure de Chimie de Clermont-Ferrand

Functionalization and Metallization of Diamondoids

Defended on 21 May 2015 in Dijon, France, in front of board of reviewers:

Prof. Bruno DOMENICHINI Professor in Université de Bourgogne, Dijon	Chairman
Prof. Philippe SERP Professor in Ecole Nationale Supérieure des Ingénieurs en Art Chimique et Technologique, Toulouse	Reviewer
Prof. Doris KUNZ Professor in Tübingen University, Tübingen	Reviewer
Prof. Armin DE MEIJERE Professor in Georg-August-Universität, Göttingen	Examiner
Prof. Peter R. SCHREINER Professor in Justus-Liebig-Universität, Giessen	Thesis co-supervisor
Prof. Jean-Cyrille HIERSO Professor in Université de Bourgogne, Dijon	Thesis co-supervisor



Acknowledgements

This research work was carried out for 18 months in France and 18 months in Germany: in the laboratory of *Institut de Chimie Moléculaire de l'Université de Bourgogne* (ICMUB) in the team of *OrganoMétallique et Catalyse pour une Chimie Bio- et éco-Compatible* (OMBC³) and *Institut für Organische Chemie, Justus-Liebig-Universität* in the team of Prof. Dr. Peter R. Schreiner's group. The financial support for 3 years was assured equally by *Conseil Régional de Bourgogne* and Prof. Schreiner's group. The mobility and the defense were supported by *Université Franco-Allemande*.

I would like to express my deepest appreciation to my co-supervisors, Prof. Jean-Cyrille Hierso and Prof. Peter R. Schreiner, who gave me the opportunity to work in this multidisciplinary subject. Thank you for the understanding, wisdom, patience, enthusiasm, and for pushing me farther than I thought I could go.

I would like to thank Prof. Bruno Domenichini that also supervised me from the very beginning of this project until the end and become the chairman during my defense. I am really enjoyed the discussion and the explanation about physical phenomena.

I take this opportunity to express my gratitude to Prof. Philippe Serp, Prof. Doris Kunz, and Prof. Armin de Meijere for reviewing the manuscript in spite of their very busy schedule.

To Didier Poinot, I am extremely grateful for your assistance, suggestions throughout my project, and continuous encouragement during the hardest time. Also with his humor that always brightened my days.

I would like to express my sincere gratitude to Patrice Renaut that helped me with the discussion and advise that always work for my synthesis.

I would never forget the help I got from Prof. Philip Richard, H  l  ne Cattey, Jonathan Becker, Sylviane Royer, Claire-H  l  ne Branchais, Paul Maurice Peterle, Nicolas Zanfoni, Jacques Andrieu, Regine Amardeil, Dominique Vervandier-Fasseur, Julien Roger, Prof. Nadine Pirio, Fr  d  ric Herbst, Remi Chassagnon,

Acknowledgements

Celine Dirand, Prof. Sebastien Chevalier, Boryslav Tkachenko, Natalie Fokina, Prof. Andrey Fokin, and Radim Hrdina.

I owe a lot to my colleagues, Sophal Mom, Fatima Allouch, Nejib Dwadnia, Emmanuel Lerayer, Philipp Wagner, Michael Linden, Sascha Combe, Paul Kahl, Christine Hofmann, Honman Yau, and all my friends in French and German groups who supported me in during my stay in Dijon and Giessen.

"This thesis work is dedicated to Jesus Christ who is my rock, my fortress, and my deliverer.

This work is also dedicated to my husband, Michael."

Abstract

The thesis deals with development of synthetic methods for preparation of novel carbon-metal organohybrid based on diamondoid and palladium.

The vapor pressure of various diamondoids was measured from a new measurement protocol at solid-vapor thermodynamic equilibrium state. Their volatile tendency opened a possibility to do deposition from gas phase and at various pressure (ambient, primary vacuum, and high vacuum) of diamondoids on silicon or mica substrates. SEM observations have shown that depending on the type of functional groups on the diamondoid, different crystal shapes can be produced (rods, needles, triangles, truncated octahedral form).

OMCVD of palladium on functionalized diamantanes showed that Pd deposition occurs preferentially on the oxide native layer on silicon substrates than on diamondoid crystals bearing hydroxyl or fluorine groups. This urged the synthesis new diamondoids with phosphino groups in order to make strong covalent bonding between the modified diamondoid and palladium.

A full set of functionalized diamondoid phosphines were synthesized with unexpected air-stability of some primary diamondoid phosphines were observed.

It has been shown that the use of P(III) phosphine as anchoring sites allowed the formation of hybrid material **Pd@PH₂-Diam-OH**. Different characterizations (XPS, SEM, TEM, and EDX) indicated that an insulator material **Pd@PH₂-Diam-OH** formed during the CVD deposition with P-Pd interaction.

Résumé

Ces travaux de thèse développent des méthodes pour la synthèse de nouveaux organohybrides carbone-métal basés sur les diamantoïdes et le palladium.

Les pressions de vapeur de divers diamantoïdes ont été mesurées grâce à un protocole original de mesures de l'état d'équilibre thermodynamique solide-vapeur. Leur relative volatilité a permis de réaliser des dépôts de diamantoïdes en phase vapeur, à diverses pressions (ambiante, vide primaire, et vide poussé) sur des substrats comme le silicium ou le mica. Les observations au MEB ont montré que, selon le type de groupes fonctionnels présents sur le diamantoïde, différentes formes cristallines peuvent être produites (tiges, aiguilles, triangles, formes octaédriques tronquées).

L'OMCVD de palladium sur les diamantanes fonctionnalisés montre que le palladium se dépose préférentiellement sur le substrat du silicium plutôt que sur les cristaux de diamantoïdes portant des groupes hydroxy ou fluor. Nous avons alors envisagé la synthèse de nouveaux diamantoïdes portant des groupes phosphino, qui pourraient former une liaison covalente entre le diamantoïde modifié et le palladium.

Un ensemble complet de diamantoïdes fonctionnalisés par des phosphines a été synthétisé. Certaines nouvelles phosphines primaires ont révélées une stabilité à l'air inattendue.

Il a été montré que l'utilisation de phosphine P(III) comme sites d'ancrage a permis la formation du matériau hybride **Pd@PH₂-Diam-OH**. Différentes caractérisations (XPS, MEB, MET, et EDX) ont montré que le matériau **Pd@PH₂-Diam-OH** formé est isolant, et présente des interactions Pd-P.

Table of content

Abbreviations

General introduction	1
Chapter 1: Diamondoids and their functionalization	5
1.1. Introduction	5
1.2. Historical background: from the synthesis of detonation nanodiamond to the isolation and characterization of higher diamondoids	6
1. Nanodiamond vs. diamondoids: the case of polymantanes	6
2. Synthesis of polymantanes vs. extraction from the geosphere	7
3. Diamondoid nomenclature and characterization	10
1.3. Functionalization of adamantane, diamantane, and higher diamondoids	13
1. Diamondoid halides	13
2. Hydroxylated diamondoids	17
3. Metallated nucleophilic diamondoids	20
4. Amino- and nitrodiamondoids and their derivatives	21
5. Polyfunctionalized diamondoids with different reactive functionalities	24
6. Alkyl-, aryl-, alkenyl-, phosphinyl-, cyano- and thiol- substituted diamondoids	27
1.4. Organohybrids built on nanodiamond and diamondoids and their applications	32
1. Biological applications of nanodiamond and diamondoid-based hybrids	32
2. Polymeric diamondoid materials	37
3. Molecular mechanics and electronics innovations from diamond nanoassembly	38
4. Synthetic and catalytic applications associated with modified diamondoids	41
1.5. Conclusion	43
Chapter 2: Vapor pressure measurements for vapor deposition of diamondoids as crystalline self-assemblies	45
2.1. Introduction	45
2.2. Diamondoid volatility	46
2.3. Vapor pressure measurement of diamondoids	48

1. Mass-loss method	48
2. Measurement of vapor pressure at equilibrium state	50
3. Comparison with volatile organometallics	52
2.4. Deposition of diamondoids as crystalline self-assemblies	53
1. Vapor deposition under atmospheric pressure	54
2. Scanning electron microscopy (SEM) of deposits	61
3. Vapor deposition under primary vacuum (P = 5 mbar)	64
2.5. Physical vapor deposition (PVD) under high-vacuum	68
2.6. Conclusion	72
Chapter 3: CVD of Pd on functionalized diamantanes	73
3.1. Introduction to vapor phase deposition techniques	73
1. Physical vapor deposition (PVD)	73
2. Chemical vapor deposition (CVD)	74
3. Organometallic precursors and essential features	76
3.2. Metal deposition on diamondoids by CVD at very low temperature	77
1. Palladium CVD on 1-hydroxydiamantane (30) and 4-fluorodiamantane (25) at 65 °C	77
2. Palladium CVD on 1-hydroxydiamantane (30) at 30 °C	79
3.3. Conclusion	80
Chapter 4: Functionalization of diamondoid phosphines	83
4.1. Short review of the synthesis and applications of diamondoid phosphines	83
4.2. Synthesis of functionalized diamondoid phosphines and derivatives	89
1. Phosphorylation and hydroxylation of diamondoids	91
2. Reduction of phosphorylated diamondoids	94
3. Arylation and benzylation of phosphorylated diamondoids	97
4. Reduction of diamondoid phosphine oxide/selenide/sulfide	99
4.3. Conclusion	101
Chapter 5: Palladium CVD under mild conditions on functionalized diamondoid phosphines	103
5.1. Introduction	103
5.2. Palladium-diamantane phosphine hybrids construction by vapor deposition	104

1. Self-assembly of (9-hydroxydiamant-4-yl)phosphonic dichloride (182)	104
2. Palladium CVD on (9-hydroxydiamant-4-yl)phosphonic dichloride (182)	105
3. Self-assembly of 9-phosphinodiamantan-4-ol (190)	109
4. Palladium CVD on 9-phosphinodiamantan-4-ol (190)	113
5. XPS analysis of the organohybrid Pd@PH ₂ -Diam-OH	124
6. TEM analysis of the organohybrid Pd@PH ₂ -Diam-OH	144
5.3. Conclusion	151
Chapter 6: Experimental part	153
6.1. Clausius-Clayperon calculation for vapor pressure of diamondoids	153
1. General conditions	153
2. Vapor pressure measurements of diamondoids and thermodynamics data	153
6.2. Vapor deposition conditions and apparatus	162
1. Deposition at atmospheric pressure or low vacuum	162
2. Vapor deposition apparatus for experiments under high vacuum (PVD)	162
6.3. CVD conditions and apparatus	165
6.4. Synthesis of diamondoid phosphines and precursors	167
1. General information	167
2. Procedures	167
3. NMR spectra	192
6.5. X-Ray structure analyses of diamondoids	271
Conclusions and perspectives	283
Structures numbering	

Abbreviations

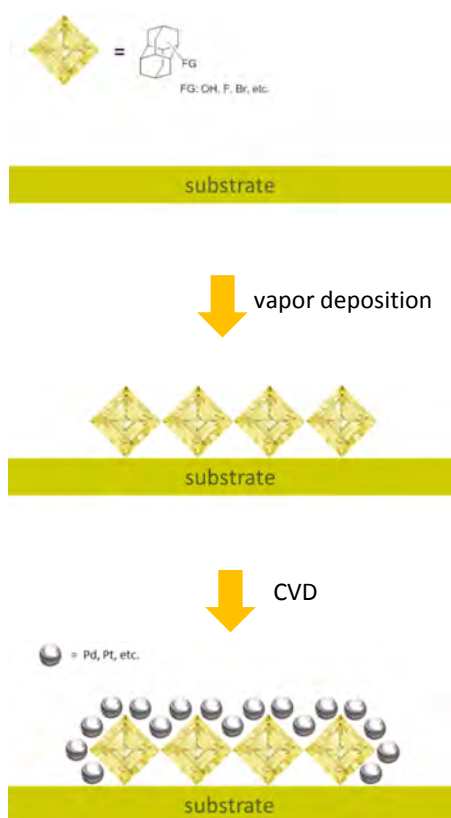
AFM	=	atomic force microscopy
ATRP	=	atom-transfer radical-polymerization
BE	=	binding energy
BODIPY	=	4,4-difluoro-4-bora-3a,4a-diaza-s-indacene
CD	=	cyclodextrin
<i>m</i> -CPBA	=	<i>m</i> -chloroperbenzoic acid
CP-MAS	=	cross-polarization magic angle spinning
CVD	=	chemical vapor deposition
CyH	=	cyclohexane
DAST	=	diethylaminosulfur trifluoride
DBU	=	1,8-diazabicyclo[5.4.0]undec-7-ene
DCE	=	1,2-dichloroethane
DCM	=	dichloromethane
DEG	=	diethylene glycol
DMDO	=	dimethyldioxirane
Di-Ac	=	diacetyl (butane-2,3-dione)
DOX-ND	=	doxorubicin hydrochloride-nanodiamond
DSC	=	differential scanning calorimetry
EDX	=	Energy-dispersive X-ray spectroscopy
EXAFS	=	extended X-ray absorption fine structure
FDD	=	functionalized diamondoid
FTIR	=	Fourier transform infrared spectroscopy
h	=	hour
LED	=	light-emitting diode
LiHMDS	=	lithium bis(trimethylsilyl)amide
min	=	minute
NEA	=	negative electron affinity
nry.	=	no reported yield
OMCVD	=	organometallic chemical vapor deposition
PCC	=	pyridinium chlorochromate

Abbreviations

PL	= poly-L-lysine
PPST	= 1,3-propane sultone
PTC	= phase-transfer condition
PVD	= physical vapor deposition
Pyr	= pyridine
r.t.	= room temperature
SAED	= selected area electron diffraction
SAMs	= self-assembled monolayers
SEM	= scanning electron microscopy
SMFM	= single-molecule fluorescence microscopy
STS	= scanning tunneling spectroscopy
SXE	= soft-X-ray emission
T_d	= thermal decomposition temperature
TEM	= transmission electron microscopy
TG	= thermogravimetry
T_g	= glass transition temperature
TMSOI	= trimethylsulfoxonium iodide
<i>p</i> -TSA	= <i>p</i> -toluenesulfonic acid
TU	= thiourea
XAS	= X-ray absorption
XPS	= X-ray photoelectron spectroscopy
yd.	= yield

General introduction

The main goal in this fundamental research is to make novel hybrid materials that combine pure sp^3 carbon (diamondoids) and transition metals into unique ordered structures. With combined metal-carbon electronic structures of these hybrid edifices, we would –in midterms– like to examine their physical properties and apply the new hybrids in transition metal-promoted catalysis. We envision thus a “bottom-up” synthesis of diamond-like structures with the intention to capture some key properties of bulk diamond at nanoscale. Ideally, long-term applications may concern the growth of diamond-like films with controlled purity by vapor phase deposition techniques and chemical methods (PVD, CVD) inspired by transition metal reactivity (C–H bond activation and transition metal promoted C–C bond formation).



The name “diamondoid” has been used to term cage hydrocarbon molecules of a size larger than adamantane ($C_{10}H_{16}$) that are totally or mostly superimposable on the cubic diamond lattice. Thus, most diamondoids are unique hydrocarbon nanostructures that can be described as fully hydrogen-terminated nanometer-sized diamonds.¹ Judging from the revolutionary progress during the last decade in novel carbon nanomaterials, such as sp^2 -C-based fullerenes, nanotubes, and graphenes, the sp^3 -C-based diamondoids are exciting new materials. They are complementary to the sp^2 -C-based materials and combine the unique features of both diamond and carbon nanostructures. They provide new opportunities for scientific discoveries and technological applications over a wide range of disciplines and at the same time affect multiple industrial applications concerning energy, electronics, biopharmaceuticals, and even consumer goods.

¹ H. Schwertfeger, A. A. Fokin, P. R. Schreiner. *Angew. Chem. Int. Ed.*, **2008**, 47, 1022-1036. Diamonds are a chemist’s best friend: diamondoid chemistry beyond adamantane.

Diamond is an attractive material for research and technical applications because of its unique properties, such as hardness, chemical inertness, high thermal conductivity, and low thermal expansion coefficient. It is optically transparent over a very large range of the electromagnetic spectrum, has a high refractive index and technically highly desirable luminescent properties. Despite these features, diamond is mainly utilized (beside jewelry) as an abrasive and as a cutting tool. This is partly due to the complications in processing diamond “top-down”. The most common nanoscale diamond material is called “nanodiamond” (without “s” due to its mixed nature) and is obtained from detonation chemistry.² Reducing the size of bulk diamond into nanosize material still keeps most of its properties, including mechanic, optic, electronic, chemistry, fluorescence, biocompatibility, etc. However, nanodiamond has several issues, such as surface stability, purity, varied size, prone to aggregation, and functionalization of its surface (only qualitatively identified).³ With such limitation, nanodiamond has already shown their huge potential applications. In our case, we focused on the “bottom-up” construction of hybrid diamond-like micro- and nanostructures from well-defined diamondoid building blocks modified with transition metals active for C–C bond forming reactions. To form these carbon-metal hybrids we choose to investigate the Chemical Vapor Deposition (CVD) process.

CVD is a powerful method that allows growing particles and films, including diamond films⁴ and higher diamondoids.⁵ Classical organometallic CVD (OMCVD) uses metal complexes stabilized by organic ligands (organometallics) and operates at moderate to high temperature and pressure. In the present case, we used very mild conditions for metal deposition due to the sensitive nature of the organic substrate for deposition (diamondoid).⁶ We expected that mild temperature OMCVD preserved the original carbon architecture, while the functions on the diamondoids may be thermodynamically high potential sites for germination and growth of metallic nanoparticles.

The content of this thesis is the following:

² N. R. Greiner, D. S. Phillips, J. D. Johnson, F. Volk. *Nature*, **1988**, 333, 440–442. Diamonds in detonation soot.

³ V. N. Mochalin, O. Shenderova, D. Ho, Y. Gogotsi. *Nature*, **2012**, 11–23. The properties and applications of nanodiamonds.

⁴ Y.-C. Chen, L. Chang. *RSC Adv.*, **2014**, 4, 18945–18950. Chemical vapor deposition of diamond on an adamantane-coated sapphire substrate.

⁵ J. E. P. Dahl, J. M. Moldowan, Z. Wei, P. A. Lipton, P. Denisevich, R. Gat, S. Liu, P. R. Schreiner, R. M. K. Carlson. *Angew. Chem. Int. Ed.*, **2010**, 49, 9881–9885. Synthesis of higher diamondoids and implications for their formation in petroleum.

⁶ J.-C. Hierso, C. Satto, R. Feurer, P. Kalck. *Chem. Mater.*, **1996**, 8, 2481–2485. Organometallic chemical vapor deposition of palladium under very mild conditions of temperature in the presence of a low reactive gas partial pressure.

- *Chapter 1* is devoted to a comprehensive review of diamondoid functionalizations (mainly adamantane and diamantane with some higher diamondoids), including a historical background and pertinent applications in biology, polymer, electronic, and catalysis sciences. The content of this chapter was mainly published in a book and a literature review:

Nanodiamonds: emergence of functionalized diamondoids and their unique applications. M. A. Gunawan, D. Poinso, B. Domenichini, P. R. Schreiner, A. A. Fokin, J.-C. Hierso. in *Chemistry of Organo-Hybrids: Synthesis and Characterization of Functional Nano-Objects*, first edition, Editors B. Charleux, C. Copéret, E. Lacôte, John Wiley & Sons, Inc. USA, **2015**, 69-113.

Diamondoids: Functionalization and subsequent applications of perfectly defined molecular cage hydrocarbons. M. A. Gunawan, J.-C. Hierso, D. Poinso, A. A. Fokin, N. A. Fokina, B. A. Tkachenko, P. R. Schreiner. *New J. Chem.*, **2014**, 38, 28-41. (Inside Cover of New Journal of Chemistry for edition 2014, volume 38).

- *Chapter 2* is focused on the determination of the vapor pressure of diamondoids to conduct their self-assembly by simple vapor deposition methods to get well-ordered crystalline deposits of micrometer size. A selected diamondoid was then deposited by PVD under ultra-high vacuum to get nanosized crystalline self-assemblies. These kinds of functionalized deposits are the substrates for hybrid formation. The content of this chapter was published in an original article:

The functionalization of molecular nanodiamonds (diamondoids) as key parameter of their easily controlled self-assembly in micro- and nanocrystals from vapor phase. M. A. Gunawan, D. Poinso, B. Domenichini, C. Dirand, S. Chevalier, A. A. Fokin, P. R. Schreiner, J.-C. Hierso. *Nanoscale*, **2015**, 7, 1956-1962.

- *Chapter 3* treats metal deposition on selected functionalized diamondoids (F, OH) by OMCVD. It was characterized by Scanning Electron Microscopy (SEM) and Energy-dispersive X-ray spectroscopy (EDX analysis). It will be published in combination with Chapter 5.
- *Chapter 4* focuses on the synthesis of new phosphorylated diamondoids. It covers the phosphorylation, hydroxylation, arylation, and alkylation of diamondoids. The objective was to develop specifically difunctionalized diamondoids bearing a phosphino group in order to generate efficient covalent bonding to late transition metals; the other function (hydroxy, chloro) would allow

efficient anchoring or/and self-assembly of diamondoids on virtually any kind of substrate. The content has been disclosed in two articles:

Selective Preparation of Diamondoid Phosphonates. A. A. Fokin, R. I. Yurchenko, B. A. Tkachenko, N. A. Fokina, M. A. Gunawan, D. Poinot, J. E. P. Dahl, R. M. K. Carlson, M. Serafin, H. Cattey, J.-C. Hierso, P. R. Schreiner. *J. Org. Chem.*, **2014**, 79, 5369-5373.

Functionalized Adamantyl and Diamantyl Phosphines. M. A. Gunawan, D. Poinot, H. Cattey, J. Becker, R. I. Yurchenko, E. D. Butova, H. Hausmann, A. A. Fokin, P. R. Schreiner, J.-C. Hierso. In preparation for *J. Org. Chem.* **2015**.

- *Chapter 5* finally describes the use of the novel functionalized diamondoid phosphines as substrates for palladium deposition by CVD under very mild conditions. From the organometallic precursor [Pd(allyl)Cp] and H₂ as a reactive gas, a fully new hybrid material was obtained and characterized. This hybrid opens pathways for catalytic applications and physical studies, which are the subject of current studies in the laboratory.

Chapter 1: Diamondoids and their functionalization

1.1. Introduction

After the blooming of fullerene and carbon nanotube chemistry, various forms of nanodiamonds (NDs) represent the most recently explored exciting class of carbon allotropes.[#] These species are generally defined as nanometer-sized particles having a perfect diamond cubic lattice. Their well-defined dimensions, unique surface properties, ready availability, and biocompatibility paved the way for applications that span the disciplines of organic and inorganic chemistry, physics, materials science, bioengineering, medicine, and beyond.^{1,2a,3} Detonation or CVD nanodiamond (*in singular form to differentiate these product mixtures from pure diamondoids, which we also call nanodiamonds*) are hydrogen-terminated graphitization, leading to sp^2 bonding carbon regimes (i.e., onion-like surfaces).^{4,5} In contrast, diamondoids (or molecular NDs), which are the main object of this chapter, are unique hydrogen-terminated carbon nanostructures that can be described as nanometer size, perfectly defined diamonds (**Fig. 1.1**). These very stable polycyclic hydrocarbons possess carbon atoms of different but precisely defined “environments” (as exemplified in **Fig. 1.1** with diamantane). As a consequence, their functionalization leads to well-defined products in the chemical sense that can be characterized precisely by chemical and physical methods. Functionalized diamondoids thus represent molecularly-defined cage hydrocarbons whose carbon skeletons are superimposable on the diamond lattice.

This chapter focuses on the origin and descriptions of molecularly defined NDs and their functionalization. Properties of organohybrids built from such species will be emphasized, in particular, by an examination of their applications spanning important scientific fields from synthetic chemistry to

[#] Formally, small diamondoids are not carbon allotropes as they are hydrogen terminated. However, as they end up being diamonds upon growth we subsume them under the header of carbon allotropes.

¹ O. A. Shenderova, V. V. Zhirnov, D. W. Brenner. *Crit. Review. Sol. State Mater. Sci.*, **2002**, 27, 227-356. Carbon Nanostructures.

² (a) H. Schwertfeger, A. Fokin, P. R. Schreiner. *Angew. Chem. Int. Ed.*, **2008**, 47, 1022-1036. Diamonds are a chemist's best friend. Diamondoid chemistry beyond adamantane. (b) H. Decker. *Z. Angew. Chem.*, **1924**, 37, 795. (c) R. A. Alexander, C. E. Knight. US 4952748, **1990**. Purification of hydrocarbonaceous fractions.

³ A. M. Schrand, S. A. Ciftan Hens, O. A. Shenderova. *Crit. Review. Sol. State Mater. Sci.*, **2009**, 34, 18-74. Nanodiamond Particles: Properties and Perspectives for Bioapplications.

⁴ S. P. Adiga, L. A. Curtiss, D. M. Gruen. Molecular Dynamics Simulations of Nanodiamond Graphitization. In: *Nanodiamonds Applications in Biology and Nanoscale Medicine*; Dean Ho, Ed. Springer, **2010**, p. 35-54.

⁵ D. Ugarte. *Nature*, **1992**, 359, 707-709. Curling and closure of graphitic networks under electron-beam irradiation.

materials science. Chemistry of nanodiamond derived from detonation processes is not detailed herein, and has been the subject of other recent reviews and book chapters.^{6,7,8,9}

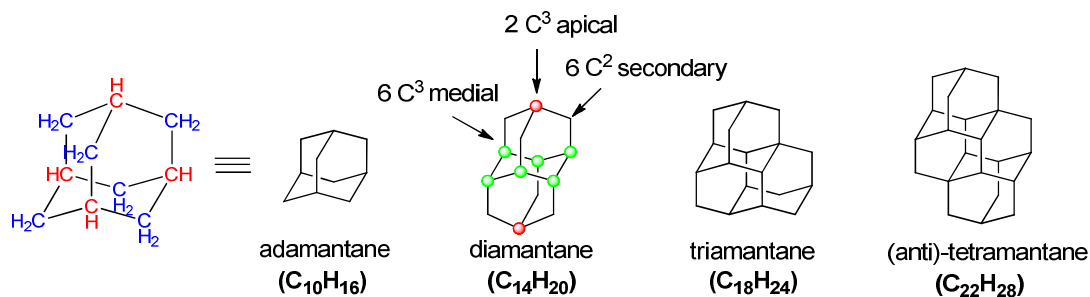


Figure 1.1. Primary diamondoid structures superimposable on the diamond lattice and built on n -fused adamantane units (general formula $[C_{4n+6}H_{4n+12}]$, $n = 1-4$). Several isomeric forms exist for $n > 3$, and some higher diamondoids of high symmetry do not follow this brutto formula.

1.2. Historical background: from the synthesis of detonation nanodiamond to the isolation and characterization of higher diamondoids

1. Nanodiamond vs. diamondoids: the case of polymantanes

Diamond-like carbon particles with characteristic sizes of 4–10 nm in diameter are frequently called “ultradispersed diamond”, and they are obtained mostly as “detonation nanodiamond”, and alternatively from shock wave high-pressure experiments on graphitic materials in the presence of metal powders (Al, Fe, Co, Ni, Cu).^{1,10,11} Detonation nanodiamond has been produced mainly in Russia by detonation of carbon-containing explosives early on in the 1960s for military research purposes. Therefore, by mixing 2,4,6-trinitrotoluene (TNT) with carbon-rich solid materials, for instance triaminonitrobenzene, and by detonating the mixture in an inert gas confined atmosphere, spheroidal diamond particles can be produced that are approximately 4 nm in diameter.^{10,12} However, the denomination “ultradispersed diamond” could be somewhat misleading because stubborn aggregation

⁶ O. Shenderova and D. Gruen, Eds. *Ultrananocrystalline Diamond: Synthesis, Properties and Applications*, William-Andrew Publishing, Norwich, NY, **2006**.

⁷ A. Krueger. *Chem. Eur. J.*, **2008**, *14*, 1382-1390. New carbon materials: Biological applications of functionalized nanodiamond materials.

⁸ A. Aleksenskiy, M. Baidakova, V. Osipov, A. Vul'. The fundamental Properties and Characteristics of Nanodiamonds. In: *Nanodiamonds Applications in Biology and Nanoscale Medicine*; Dean Ho, Ed. Springer, **2010**, p. 55-77.

⁹ A. Krueger, D. Lang. *Adv. Funct. Mater.*, **2012**, *22*, 890-906. Functionality is Key: Recent Progress in the Surface Modification of Nanodiamond.

¹⁰ N. R. Greiner, D. S. Phillips, J. D. Johnson, F. Volk. *Nature*, **1988**, *333*, 440-442. Diamonds in detonation soot.

¹¹ A. Krueger. *Adv. Mater.*, **2008**, *20*, 2445-2449. Diamond Nanoparticles: Jewels for Chemistry and Physics.

¹² G. Galli. Structure, Stability and Electronic Properties of Nanodiamonds. In: *Computer-Based Modeling of Novel Carbon Systems and their Properties beyond Nanotubes*; L. Colombo, A. Fasolino, Eds. Springer, **2010**, p 37-56.

in such raw products is observed, which stems from the interaction of primary particles of 60 to 200 nm in size.¹³ A critical issue for the satisfactory application of detonation nanodiamond is therefore the separation of their agglomerates and its efficient purification from soot and other forms of graphitic carbon.^{11,13}

The term “diamondoid”, first coined by Decker as early as 1924,^{2b} is used to describe cage hydrocarbon molecules of a size larger than adamantane (C₁₀H₁₆) that are totally or mostly superimposable on the diamond lattice.¹⁴ Among diamondoids the family of polymantanes includes the molecules that can *only be formed by the face-fusing of adamantane units*, sharing thus six carbon atoms per pair of adamantane units. The polymantanes form a series starting with the smallest molecules for which the general formula [C_{4n+6}H_{4n+12}] does not comprise any further isomer, namely adamantane, diamantane, and triamantane (**Fig. 1.1**); these are called lower diamondoids. Depending on the spatial arrangement of adamantane units, higher polymantanes (n>3) theoretically present several (numerous) isomers. For instance, the three possible tetramantanes that share the general formula C₂₂H₂₈ are called *iso*-tetramantane (C_{3v} point group), *anti*-tetramantane (C_{2h} point group), and chiral *skew*-tetramantane (C₂ point group). Then, there are four possible pentamantanes (not including enantiomers); thirty-nine isomeric arrangements are theoretically possible for hexamantane, and so forth.¹⁵

2. Synthesis of polymantanes vs. extraction from the geosphere

From a historical perspective adamantane was first isolated in 1933 from a sample of petroleum collected in Czechoslovakia.¹⁶ Efficient synthetic preparations of lower diamondoids have been reported in 1957 by Schleyer for adamantane,¹⁷ and in 1965 by Cupas, Schleyer and Trecker for diamantane.¹⁸ In the same period diamantane was also isolated from petroleum.¹⁹ In 1966 the synthesis of triamantane was reported by Williams *et al.*²⁰ The first higher diamondoid was synthesized in 1976 by Burns *et al.* which successfully synthesized *anti*-tetramantane that holds this name from its structural similarity with

¹³ E. Ōsawa. Single-Nano Buckydiamond Particles. In: *Nanodiamonds Applications in Biology and Nanoscale Medicine*; Dean Ho, Ed. Springer, **2010**, p. 1-33.

¹⁴ This definition prevents thus the inclusion of cyclohexane and other simple alkanes. See also reference 32 for various examples of non-polymantane diamondoids.

¹⁵ H. Hopf. *Angew. Chem. Int. Ed.*, **2003**, 42, 2000-2002. Diamonds from Crude Oil?

¹⁶ S. Landa, V. Machacek. *Collect. Czech. Chem. Commun.*, **1933**, 5, 1-5. Adamantane, a new hydrocarbon extracted from petroleum.

¹⁷ P. von R. Schleyer. *J. Am. Chem. Soc.*, **1957**, 79, 3292-3292. A simple preparation of Adamantane.

¹⁸ C. A. Cupas, P. von R. Schleyer, D. J. Trecker. *J. Am. Chem. Soc.*, **1965**, 87, 917-918. Diamantane

¹⁹ S. Hala, S. Landa, V. Hanus. *Angew. Chem. Int. Ed.*, **1966**, 5, 1045-1046. Isolation of diamantane from petroleum.

²⁰ V. Z. Williams, P. von R. Schleyer, G. J. Gleicher, L. B. Rodewald. *J. Am. Chem. Soc.*, **1966**, 88, 3862-3863. Triamantane.

butane in its *anti*-conformation.²¹ Schleyer reported an elaborate perspective of this exciting period of synthetic success, which ended with the synthetic attempts toward higher diamondoids.²² Synthetic efforts to access higher diamondoids *via* carbocation rearrangements similar to those successfully devised to prepare the lower diamondoids irremediably failed.²³ Those have been apparently blocked by the large number of possible intermediates, and the complex reaction pathways and kinetics involved in the processes.



Figure 1.2. Carbon framework of cyclohexamantane $C_{26}H_{30}$ based on single-crystal X-ray diffraction with a view along a diamond (111) crystal-lattice plane (left), and “wheel-like” side view of the same molecule (right).

In the 1990's the isolation of diamondoids from the geosphere clearly leaped ahead their chemical synthesis, starting with the patents filed by the Mobil Oil Corporation.^{2c} In 1995 higher diamondoids up to hexamantane ($C_{30}H_{36}$) had been shown to exist in petroleum by Lin and Wilk on the basis of gas chromatography/mass spectrometry analysis.²⁴ It was suggested later in 1999 by Dahl *et al.* that diamondoids may occur largely in all petroleum sources and thus may be used as decisive indicators of natural oil cracking.²⁵ The breakthrough evidence of diamondoid's ubiquity in oils and fuels was provided by Dahl *et al.* in 2003 through the isolation and identification of twenty-one different higher polymantanes by HPLC techniques.²⁶ Dahl *et al.* also provided structural proofs for cyclohexamantane (X-ray characterization), which displays a highly symmetrical (D_{3d}) beautiful hexagonal arrangement of six

²¹ W. Burns, T. Mitchell, M. McKervey, J. Rooney, G. Ferguson, P. Roberts. *J. Chem. Soc. Chem. Commun.*, **1976**, 21, 893-895. Gas-phase reactions on platinum. Synthesis and crystal structure of anti-tetramantane, a large diamondoid fragment.

²² P. von R. Schleyer. My Thirty Years in Hydrocarbon Cages: From Adamantane to Dodecahedrane. In: *Cage Hydrocarbons*; G. A. Olah Ed., John Wiley, New York, **1990**, p. 1-38.

²³ R. C. Fort Jr, P. von R. Schleyer. *Chem. Rev.*, **1964**, 64, 277-300. Adamantane: Consequences of the Diamondoid Structure.

²⁴ R. Lin, Z. A. Wilk. *Fuel*, **1995**, 74, 1512-1521. Natural occurrence of tetramantane ($C_{22}H_{28}$), pentamantane ($C_{26}H_{32}$) and hexamantane ($C_{30}H_{36}$) in a deep petroleum reservoir.

²⁵ J. E. Dahl, J. M. Moldowan, K. E. Peters, G. E. Claypool, M. A. Rooney, G. E. Michael, M. R. Mello, M. L. Kohnen. *Nature*, **1999**, 399, 54-57. Diamondoid hydrocarbons as indicators of natural oil cracking.

²⁶ J. E. Dahl, S. Liu, R. M. K. Carlson. *Science*, **2003**, 299, 96-99. Isolation and Structure of Higher Diamondoids, Nanometer-Sized Diamond Molecules.

fused-face adamantane units; this pericondensed hexamantane is the only diamondoid of formula $C_{26}H_{30}$ (**Fig. 1.2**).²⁷

Early hypotheses on diamondoid formation in the geosphere postulated the involvement of carbocation-mediated rearrangements when petroleum hydrocarbons containing reactive functions such as double bonds could react with superacid sites on naturally occurring clay minerals. The formation of the lower diamondoids, adamantane and diamantane, from aliphatic alkanes under conditions of cracking was shown afterwards,²⁸ gathering evidence that thermal pathways involving free radicals in the absence of acid catalyzed carbocation rearrangements may also occur. Dahl and Schreiner indicated that “*Such mechanistic proposals underline the notion that diamondoids are thermodynamically the most stable hydrocarbons,... more stable than nanographenes...of comparable molecular weight*”.²⁹ In addition, the relative stabilities of carbocations and alkyl radicals are different for polycyclic structures. Indeed, while the secondary and tertiary diamondoid C–H bonds have practically the same homolytic bond dissociation energies, the heterolytic cleavages of these bonds differ significantly in energy. Since the isomer distribution in raw oil extraction is inconsistent with the thermodynamic stability of the diamondoids or of their cations, a different formation mechanism may be involved. This was further evidenced by the direct synthesis of higher diamondoids from lower diamondoids under CVD growth conditions.²⁹ Up to 1.5 mol% of tetramantanes could be formed by pyrolyzing triamantane in a sealed gold tube for 96 h. Under similar cracking conditions that generate free alkyl radicals, up to 0.75 mol% of various pentamantanes were obtained, coming from either *iso*-tetramantane, or *anti*-tetramantane or *skew*-tetramantane. Pentamantanes formed by the replacement of three hydrogen “face-related” atoms on tetramantanes with four carbon atoms, to produce an additional cage *without breaking any of the original tetramantane bonds*. Each cage closure formally necessitates an isobutyl moiety, and consistently the addition of isobutane or isobutene in the cracking atmosphere lead to larger amounts of products. Formation of pentamantanes *n* that would have needed the breaking of the original *n*-1 tetramantane to be formed just did not occur. This observation led to the conclusion of a mechanism analogous to CVD growth of diamond. This work shows that it is highly likely that atomic layer

²⁷ J. E. P. Dahl, J. M. Moldowan, T. M. Peakman, J. C. Clardy, E. Lobkovsky, M. M. Olmstead, P. W. May, T. J. Davis, J. W. Steeds, K. E. Peters, A. Pepper, A. Ekuan, R. M. K. Carlson. *Angew. Chem. Int. Ed.*, **2003**, 42, 2040-2044. Isolation and Structural Proof of the Large Diamond Molecule, Cyclo-hexamantane ($C_{26}H_{30}$).

²⁸ G. N. Gordadze, M. V. Giruts. *Pet. Chem.*, **2008**, 48, 414-419. Synthesis of adamantane and diamantane hydrocarbons by high-temperature cracking of higher n-alkanes.

²⁹ J. E. P. Dahl, J. M. Moldowan, Z. Wei, P. A. Lipton, P. Denisevich, R. Gat, S. Liu, P. R. Schreiner, R. M. K. Carlson. *Angew. Chem. Int. Ed.*, **2010**, 49, 9881-9885. Synthesis of Higher Diamondoids and Implications for Their Formation in Petroleum.

deposition, a parent method of classical CVD, may in the future be used as a controlled synthetic way towards higher diamondoids from polymantane seeds.

3. Diamondoid nomenclature and characterization

3.1. Nomenclature

The von Baeyer system is used for IUPAC naming of polycyclic hydrocarbons, including diamondoids and polymantanes.³⁰ The name is determined by the identification of the largest ring, the largest bridge across this main ring and the lengths and positions of the other bridges in the structure.³¹ The complete name indicates the *number of rings* (prefix), the *lengths* and *positions* of the bridges (numbers in brackets) and the *total number of skeletal atoms* in the ring system suffix. Thus, adamantane following the von Baeyer system is named: tricyclo[3.3.1.1^{3,7}]decane. Indeed, the largest ring in adamantane is eight carbon atoms long (C1 to C8, **Fig. 3**) with two bridges of one atom across it. Two tertiary carbons C1 and C5 are selected as bridgeheads to determine the lengths and positions of the bridges. Between these C1 and C5 bridgehead atoms, two bridges of three atoms (C2, C3, C4 and C6, C7, C8) and one bridge of one atom (C10) exist: giving the [3.3.1] combination. In addition, a last bridge of one atom (C9) exists between C3 and C7, giving the last number [1^{3,7}]. Since the global number of fused rings is three (tricyclo) and the total number of atoms is ten (decane) the final nomenclature of adamantane is effectively tricyclo[3.3.1.1^{3,7}]decane.

For specifically naming polymantanes, which are very regularly repeating fused adamantane units, the von Baeyer system can be advantageously substituted by a representation introduced by Balaban and Schleyer³² (diamantane in the von Baeyer system is named pentacyclo[7.3.1.1.^{4,12}.0^{2,7}.0^{6,11}]tetradecane).³³ This system is based on graph theory and thus considers step by step growth of cages.³¹ Starting with a single adamantane a maximum of four directions exists in which a polymantane molecule could grow (see **Fig. 1.3**). These directions are labeled with the numbers 1, 2, 3, and 4. The graphical construction of [1]diamantane, [12]triamantane and [121]tetramantane is the simplest application of this useful nomenclature mode (**Fig. 1.3**).

³⁰ G. P. Moss. *Pure Appl. Chem.*, **1999**, 71, 513-529. Extension and revision of the von Baeyer system for naming polycyclic compounds (including bicyclic compounds).

³¹ A didactic and useful short summary of the basic applications of nomenclature for diamondoids was given by J. Filik, see reference 36.

³² A. T. Balaban, P. von R. Schleyer. *Tetrahedron*, **1978**, 34, 3599-3609. Systematic classification and nomenclature of diamond hydrocarbons. I. Graph-theoretical enumeration of polymantanes.

³³ A. T. Balaban, D. J. Klein, J. E. Dahl, R. M. K. Carlson. *Open Org. Chem. J.*, **2007**, 1, 13-31. Molecular Descriptors for Natural Diamondoid Hydrocarbons and Quantitative Structure-Property Relationships for Their Chromatographic Data.

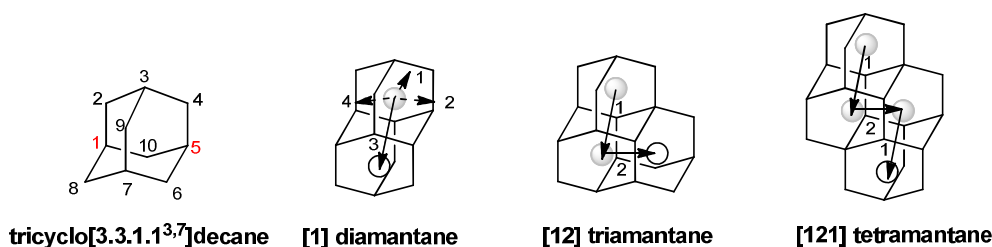


Figure 1.3. Adamantane nomenclature following von Baeyer system (left), and diamantane, triamantane and *anti*-tetramantane names following the Schleyer and Balaban representation.

3.2. Physical properties and modes of characterization

Lower diamondoids are nearly strain-free and chemically, as well as thermally, very stable. These characteristics are typically accompanied with high melting points in comparison to other hydrocarbons of comparable molecular weight. The melting points of adamantane, diamantane and triamantane are estimated between 200 °C and 270 °C, but they readily sublime at room temperature under normal or slightly reduced pressure. Only few reports of physical data concerning functionalized diamondoids are available. Solid and liquid vapor pressures for adamantane and diamantane as well as alkylated congeners have been gathered and reviewed: data such as molar enthalpies, molar entropies, molar heat capacities, enthalpies of formation, sublimation, combustion, etc. are available.³⁴ Solubility limits of adamantane and diamantane in liquid organic solvents at 25 °C (alkanes, benzene, toluene, THF) have been also reported.³⁵

The most commonly used spectroscopic methods to analyze diamondoids are nuclear magnetic resonance,²² and Raman spectroscopy.³⁶ The Raman spectra of lower diamondoids were reported early,³⁷ then both Raman and infrared spectra of higher diamondoids up to hepta- and hexamantane have been studied, and the spectra show in general good agreement with density functional theory

³⁴ (a) J. S. Chickos, W. E. Acree Jr. *J. Phys. Chem. Ref. Data*, **2002**, 31, 537-698 and references cited therein. (b) T. Clark, T. Knox, H. Mackle, M. A. McKervey, H. Mackle, J. J. Rooney. *J. Am. Chem. Soc.*, **1979**, 101, 2404-2410. Thermochemistry of bridged-ring substances. Enthalpies of formation of some diamondoid hydrocarbons and of perhydroquinacene. Comparisons with data from empirical force field calculations. (c) T. Clark, T. Knox, M. A. McKervey, H. Mackle. *J. Chem. Soc. Perkin Trans. 2*, **1980**, 1686-1689. Thermochemistry of bridged-ring substances. Enthalpies of formation of diamantan-1-, -3-, and -4-ol and of diamantanone.

³⁵ J. Filik. Diamondoid Hydrocarbons. In: *Carbon-Based Nanomaterials, Materials Science Foundations* (monograph series), N. Ali, A. Öchsner, W. Ahmed, Eds. Trans Tech, Switzerland, **2010**, p. 1-26.

³⁶ J. Filik. Diamondoid Hydrocarbons. In: *Carbon-Based Nanomaterials, Materials Science Foundations* (monograph series), N. Ali, A. Öchsner, W. Ahmed, Eds. Trans Tech, Switzerland, **2010**, p. 1-26.

³⁷ T. E. Jenkins, J. Lewis. *Spectrochim. Acta A*, **1980**, 36, 259-264. A Raman study of adamantane, diamantane and triamantane between 10 K and room temperature.

computations.³⁸ Raman spectroscopy of diamondoids has been compared with nanophase and bulk diamonds.²⁷ One of the significant differences is in the CCC deformation corresponding to “cage-breathing” modes which produces the highest intensity Raman signals in the region of the spectra below 800 cm⁻¹.

The relationship possibly existing between the electronic structures of the diamondoids, nanocrystalline diamonds, and bulk diamonds is essential to correlate band gaps with the sizes and structures of the considered species. X-ray absorption (XAS) measurements in the gas phase on polymantanes ranging from adamantane to cyclohexamantane have been reported.³⁹ The data show that the unoccupied states that are bulk-related do not exhibit quantum confinement behavior, *i. e.*, no increasing band edge blue shifts with decreasing particle size, a behavior that is generally expected from semiconductors. These findings indicated that in the ultimate size limit for nanocrystals possibly a molecular description is better suited since the hydrogen atoms on the surface have a large influence on the diamondoids’ electronic structures by dominating the lowest unoccupied states. However, these results were further refined with measurements performed on technologically pertinent condensed-phase diamondoids as opposed to previous gas-phase work.⁴⁰ Thus, XAS from the carbon 1s level probes the unoccupied states and indicates the relative energy position of the lowest unoccupied orbitals, while soft-X-ray emission (SXE) spectroscopy aptly probed the highest occupied *sp*³ hybridized states in diamondoids. XAS and SXE provided independent measures of the unoccupied and occupied states, and gave an indication of the LUMO and HOMO relative energies. From these data, the gaps of the diamondoids have been estimated and compared to the various computations. Solid-state diamondoid X-ray absorption data indicated, as previously observed in the gas phase, that the lowest unoccupied states are relatively fixed in energy and dominated by states associated with the hydrogen-terminated surfaces. However the HOMO-LUMO gaps increase with decreasing size, where energy shifting and consequently quantum confinement occurs only in the occupied states. Finally, the changes in electronic structures induced by chemical functionalization of the diamondoids have been explored using valence

³⁸ (a) J. Filik, J. N. Harvey, N. L. Allan, P. W. May, J. E. P. Dahl, S. Liu, R. M. K. Carlson. *Spectrochim. Acta A*, **2006**, 64, 681-692. Raman spectroscopy of diamondoids. (b) J. Oomens, N. Polfer, O. Piral, Y. Ueno, R. Maboudian, P. W. May, J. Filik, J. E. Dahl, S. Liu, R. M. K. Carlson. *J. Mol. Spectrosc.*, **2006**, 238, 158-167. Infrared spectroscopic investigation of higher diamondoids.

³⁹ T. M. Willey, C. Bostedt, T. van Buuren, J. E. Dahl, S. G. Liu, R. M. Carlson, L. J. Terminello, T. Möller. *Phys. Rev. Lett.*, **2005**, 95, 113401/1-113401/4. Molecular Limits to the Quantum Confinement Model in Diamond Clusters.

⁴⁰ T. M. Willey, C. Bostedt, T. van Buuren, J. E. Dahl, S. G. Liu, R. M. K. Carlson, R. W. Meulenberg, E. J. Nelson, L. J. Terminello. *Phys. Rev. B*, **2006**, 74, 205432. Observation of quantum confinement in the occupied states of diamond clusters.

photoelectron spectroscopy.⁴¹ Through the variation of functional group (thiol, hydroxy, or amino groups), cage size (adamantane, diamantane, triamantane, [121]tetramantane, and [1(2,3)4]pentamantane), and functionalization site (apical or medial) was examined to what degree such alterations affect the electronic structures of the molecule. The ionization potentials did not show a linear dependence on the electronegativity of the functional group, but instead a linear correlation between the HOMO-1 ionization potential and the functional group electronegativity. This was attributed to localization of the HOMO on the functional group, and of the HOMO-1 on the diamondoids cage.

1.3. Functionalization of adamantane, diamantane, and higher diamondoids

1. Diamondoid halides

The functionalization of the smallest diamondoid, adamantane, was developed during its first synthetic preparation in 1941.⁴² Compared to the polymantanes such as diamantane and triamantane the selective functionalization of adamantane is the easiest because of the existence of only one type of secondary (six C^2) and one type of tertiary (4 C^3) carbon atoms (**Fig. 1.1**). Adamantane mono-functionalized with all possible halogens have been reported, these species are functionalized on the bridgehead tertiary carbon (**Scheme 1.1**). Monobromination and dibromination using Br_2 in the absence or presence of aluminum Lewis catalyst lead from adamantane **1** respectively to bromoadamantane **2** and 1,3-dibromoadamantane **3** with satisfactory yields.⁴³ Under these conditions the formation of tri- and tetrabromoadamantanes **4** and **5** is also possible. Modifications aiming at the optimization of the synthesis of the dibromo analogue **3** have been explored (**Scheme 1.1, (b), (c)**).^{44,45} Iodoadamantane **7**^{46,47} can be obtained from iodination of 1-adamantanol **6**, which is itself obtained by direct ozonation of adamantane **1**;⁴⁸ direct access is also possible through phase-transfer catalyzed iodination.⁴⁹ 1-

⁴¹ T. Rander, M. Staiger, R. Richter, T. Zimmermann, L. Landt, D. Wolter, J. E. Dahl, R. M. K. Carlson, B. A. Tkachenko, N. A. Fokina, P. R. Schreiner, T. Möller, C. Bostedt. *J. Chem. Phys.*, **2013**, 138, 024310/1-024310/7. Electronic structure tuning of diamondoids through functionalization.

⁴² V. Prelog, R. Seiwert. *Ber. Dtsch. Chem. Ges.*, **1941**, 74, 1644-1648. Über die Synthese des Adamantans ("On the Synthesis of Adamantanes").

⁴³ G. L. Baughman. *J. Org. Chem.*, **1964**, 29, 238-240. Dibromination of Adamantane.

⁴⁴ T. M. Gorrie, P. von R. Schleyer. *Org. Prep. Proc. Int.*, **1971**, 3, 159-162. The Preparation of 1,3-dibromoadamantane.

⁴⁵ E. R. Talaty, A. E. Cancienne Jr., A. E. Dupuy Jr. *J. Chem. Soc. C*, **1968**, 1902-1903. Selective Dibromination of Adamantane.

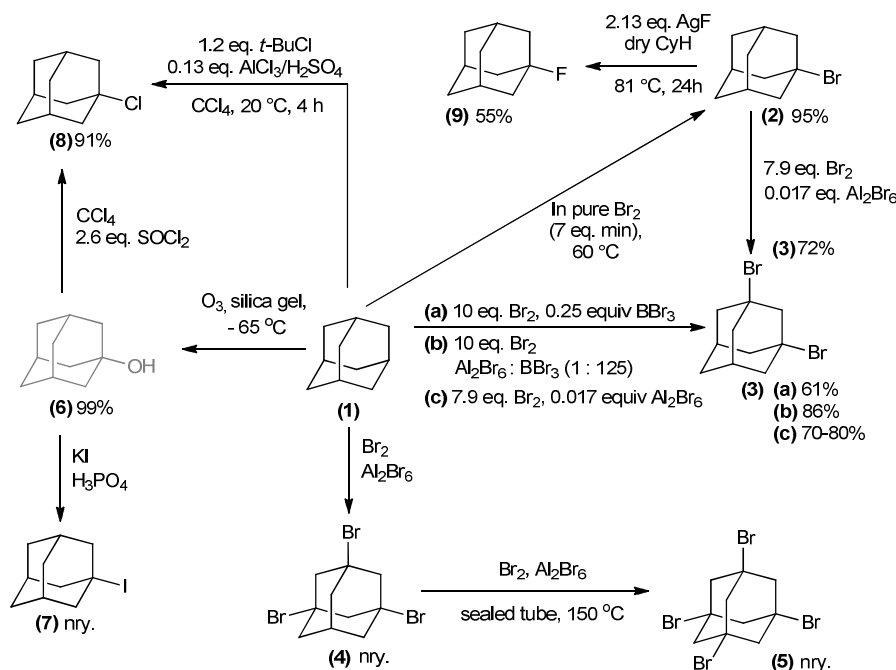
⁴⁶ H. Stone, H. Shechter. *J. Org. Chem.*, **1950**, 15, 491-495. A New Method for the Preparation of Organic Iodides.

⁴⁷ J. H. Wieringa, J. Strating, H. Wynberg. *Synthetic Commun.*, **1972**, 2, 191-195. 1-Lithioadamantane.

⁴⁸ Z. Cohen, E. Keinan, Y. Mazur, T. H. Varkony. *J. Org. Chem.*, **1975**, 40, 2141-2142. Dry Ozonation. A Method for Stereoselective Hydroxylation of Saturated Compounds on Silica Gel.

⁴⁹ P. R. Schreiner, O. Lauenstein, E. D. Butova, A. A. Fokin. *Angew. Chem. Int. Ed.*, **1999**, 38, 2786-2788. The first efficient iodination of unactivated aliphatic hydrocarbons.

Adamantanol **6** can be also treated with a mixture of thionyl chloride and CCl_4 to provide chloroadamantane **8** in excellent yield.⁵⁰ A direct route to **8** from adamantane **1** with also excellent yield is possible by treating it with *tert*-butyl chloride and AlCl_3 .⁵¹ An alternative way to **8** and 2-chloroadamantane is the photochemical chlorination of adamantane with Cl_2 .⁵² Fluoroadamantane **9** has been obtained from bromoadamantane **2**,^{53,54} and other methods of fluorination and polyfluorination exist, using for instance iodine pentafluoride on **1**,⁵⁵ or starting from **6**.^{56,57} An electrochemical method using adamantane with $\text{Et}_3\text{N}\cdot 5\text{HF}$ as both electrolyte and fluorine source has been also disclosed.⁵⁸



Scheme 1.1. Synthetic pathways to adamantyl halides **2-5**, and **7-9**.

(*nry.* stands for no reported yield).

⁵⁰ G. Molle, P. Bauer. *J. Am. Chem. Soc.*, **1982**, 104, 3481-3487. The Barbier Synthesis: A One-Step Grignard Reaction?

⁵¹ R. Jalal, R. Gallo. *Synthetic Commun.*, **1989**, 19, 1697-1704. Improved Synthesis of 1-Chloroadamantane by Hydride Transfer Induced by Tertiarybutylchloride.

⁵² G. W. Smith, H. D. Williams. *J. Org. Chem.*, **1961**, 26, 2207-2212. Some Reactions of Adamantane and Adamantane Derivatives.

⁵³ R. C. Fort Jr., P. von R. Schleyer. *J. Org. Chem.*, **1965**, 30(3), 789-796. The Proton Magnetic Resonance Spectra of Adamantane and Its Derivatives.

⁵⁴ F. Leroux, L.Garamszegi, M. Schlosser. *J. Fluor. Chem.*, **2002**, 117, 177-180. A simple method for the displacement of bromine by fluorine at tertiary, benzylic or non-classical secondary sites.

⁵⁵ S. Hara, M. Aoyama. *Synthesis*, **2008**, 2510-2512. Direct fluorination of adamantanes with iodine pentafluoride.

⁵⁶ I. Bucsi, B. Török, A. I Marco, G. Rasul, G. K. S. Prakash, G. A. Olah. *J. Am. Chem. Soc.*, **2002**, 124, 7728-7736. Stable Dialkyl Ether/Poly(Hydrogen Fluoride) Complexes: Dimethyl Ether/Poly(Hydrogen Fluoride). A New, Convenient, and Effective Fluorinating Agent.

⁵⁷ V. A. Petrov, S. Swearingen, W. Hong, W. Chris Petersen. *J. Fluor. Chem.*, **2001**, 109, 25-31. 1,1,2,2-Tetrafluoroethyl-N,N-dimethylamine: a new selective fluorinating agent.

⁵⁸ M. Aoyama, T. Fukuhara, S. Hara. *J. Org. Chem.*, **2008**, 73, 4186-4189. Selective Fluorination of Adamantanes by an Electrochemical Method.

Bromination of diamantane **10** is a more intricate process (**Scheme 1.2**), since by the use of Lewis acid catalysts the conditions have to be tuned to improve the selectivity in the three isomers obtained in majority: **11**, **12** and **13**. In pure Br₂ 1-bromodiamantane **11** is selectively obtained in good yield (**Scheme 1.2, (a)**).^{59,60} The apical isomer 4-bromodiamantane **12** can be obtained in a satisfactory yield in the presence of traces of AlBr₃ with *tert*-butyl bromide (**b**), albeit in a mixture with **11** that can be separated by column chromatography on alumina directly or after conversion to the corresponding alcohols.⁶¹ Bromination of **10** under phase transfer conditions (PTC) with CBr₄ and NaOH/*n*-Bu₄NBr (**c**) allowed the isolation of secondary-C functionalized 3-bromodiamantane **13** in low yield.⁶¹ Access to **13** in overall better yield is possible in three steps via 3-diamantanone **31**, which can be obtained in satisfactory yield from sulfuric acid oxidation of diamantane **10**.^{62,63} Reduction of **31** to the corresponding alcohol **32** can be easily followed by tosylation, bromination (PBr₅) or chlorination (SOCl₂) to give 3-bromodiamantane **13** and 3-chlorodiamantane **33**,⁶⁴ respectively.

By forcing the conditions used for monobromination, di, tri and even tetrabromination of diamantane **10** was possible delivering the dibromide diamondoids **14** and **15**,⁵⁹ as well as **16**, and tribromide **17** and tetrabromide **18** all substituted at a tertiary carbon.⁶⁰ 1-Iododiamantane **19**, 4-iododiamantane **20**, and 3-iododiamantane **21** formed from iodination of **10** under phase transfer conditions with CHI₃ and NaOH in CH₂Cl₂,⁶¹ but **20** and **21** are difficult to isolate. Direct access to 1-chlorodiamantane **22** and 4-chlorodiamantane **23** from **10** has been reported in moderate yield (due to unreacted diamantane), the compounds were obtained as a mixture isolated from co-formed 1-hydroxydiamantane **30**.⁶¹ The tertiary-C brominated diamantanes are excellent precursors to form the corresponding fluorodiamantanes employing the fluorinating agent silver fluoride (the corresponding hydroxylated precursors can also be used with diethylaminosulfur trifluoride, DAST).⁶⁵ The mono-**24,25**, di-**26,27**, tri-

⁵⁹ T. M. Gund, P. von R. Schleyer. *Tetrahedron Lett.*, **1971**, 19, 1586-1586. The Ionic Bromination of Diamantane.

⁶⁰ T. M. Gund, P. von R. Schleyer, G. D. Unruh, G. J. Gleicher. *J. Org. Chem.*, **1974**, 39, 2995-3003. Diamantane. III Preparation and Solvolysis of Diamantyl Bromides.

⁶¹ A. A. Fokin, B. A. Tkachenko, P. A. Gunchenko, D. V. Gusev, P. R. Schreiner. *Chem. Eur. J.*, **2005**, 11, 7091-7101. Functionalized Nanodiamonds Part I. An Experimental Assessment of Diamantane and Predictions for Higher Diamondoids.

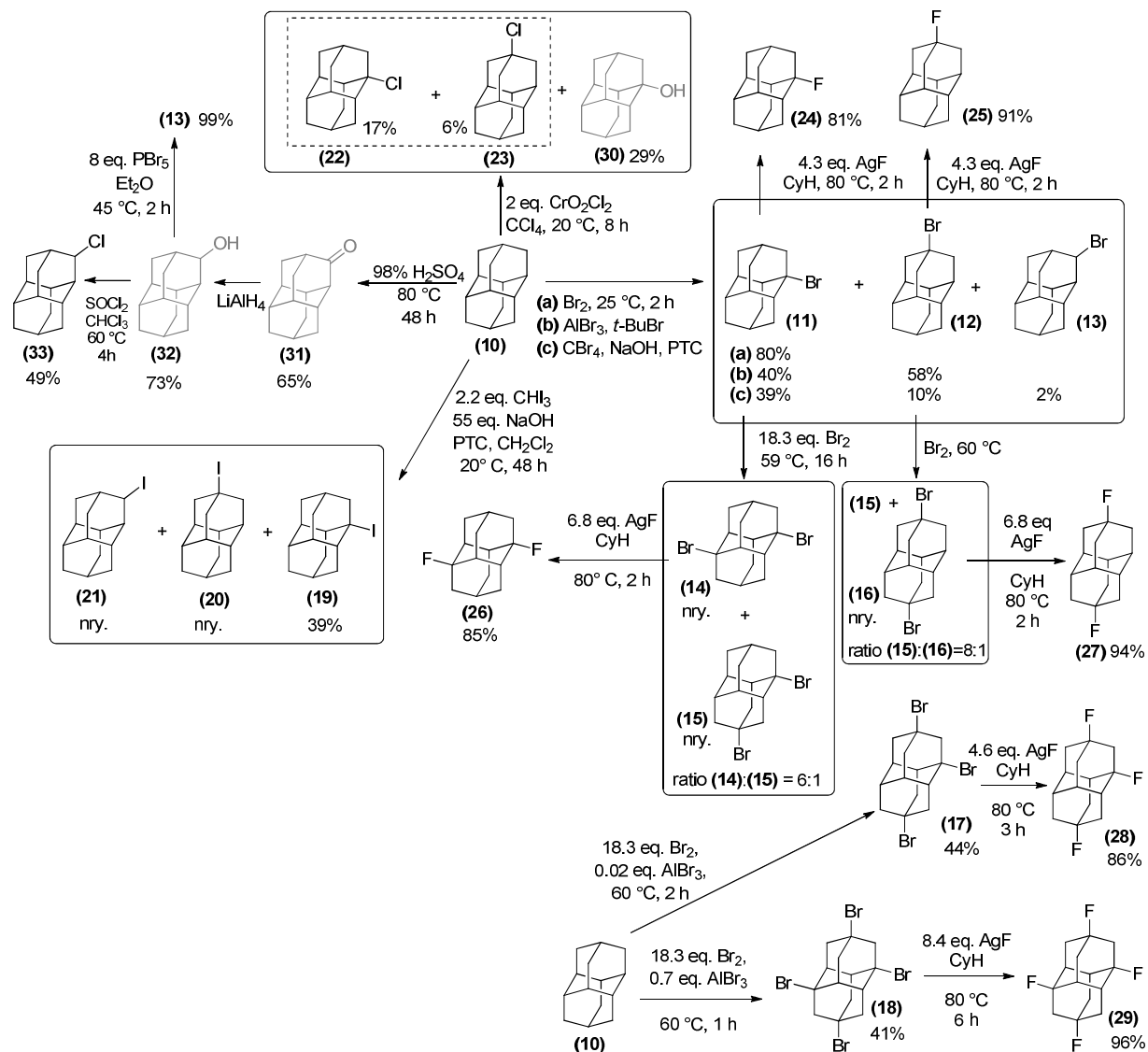
⁶² T. M. Gund, M. Nomura, V. Z. Williams Jr., P. von R. Schleyer. *Tetrahedron Lett.*, **1970**, 56, 4875-4878. The Functionalization of Diamantane (Congressane).

⁶³ A. A. Fokin, T. S. Zhuk, A. E. Pashenko, P. O. Dral, P. A. Gunchenko, J. E. P. Dahl, R. M. K. Carlson, T. V. Koso, M. Serafin, P. R. Schreiner. *Org. Lett.*, **2009**, 11, 3068-3071. Oxygen-Doped Nanodiamonds: Synthesis and Functionalizations.

⁶⁴ T. M. Gund, M. Nomura, P. von R. Schleyer. *J. Org. Chem.*, **1974**, 39, 2987-2994. Diamantane. II. Preparation of Derivatives of Diamantane.

⁶⁵ H. Schwertfeger, C. Würtele, H. Hausmann, J. E. P. Dahl, R. M. K. Carlson, A. A. Fokin, P. R. Schreiner. *Adv. Synth. Catal.*, **2009**, 351, 1041-1054. Selective Preparation of Diamondoid Fluorides.

28 and tetrafluorinated diamantanes **29**, are all obtained in excellent yields above 80% after a few hours of heating under reflux in cyclohexane (CyH).



Triamantane, tetramantane and even pentamantane bromides and fluorides have been synthesized (**Fig. 1.4**) as well. Triamantane treated with neat Br₂ for 5 min at 0 °C, gives 2-bromotriamantane **34**, which was isolated in 43% yield as the major isomer in a mixture of four monobrominated

triamantanes.⁶⁶ Fluorotriamantanes **35a-d** are mostly obtained by treatment of hydroxylated analogues⁶⁷ with DAST.⁶⁵ Treatment of [121]tetramantane with Br₂ for 16 h at 20 °C gives 2,17-dibrominated **36** in modest 17% yield.⁶⁷ The syntheses of 6-fluoro[121]tetramantane **37a** and 6,13-difluoro[121]tetramantane **37b** have been also reported with good yields from their alcohol precursors.⁶⁵ [1(2,3)4]-Pentamantane is the highest diamondoid that has been efficiently functionalized with halogen (and hydroxy, thiol and nitroso substituents) since it reacts with electrophiles more selectively than triamantane and [121]tetramantane. It gave in multistep reactions overall yields of 25–75% the mono and dibrominated analogues **38a-d**.⁶⁸ 7-Fluoro[1(2,3)4]pentamantane **39** was isolated from fluorination of the corresponding alcohol after HPLC purification (65%).⁶⁵

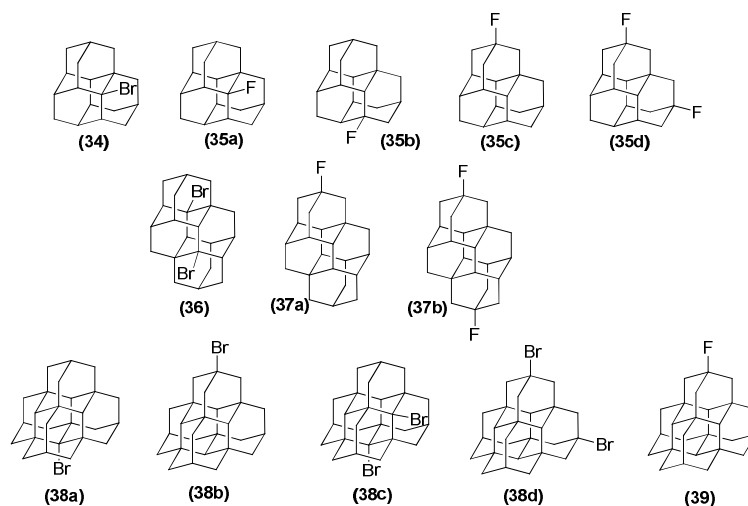


Figure 1.4. Triamantane (**34** and **35**), tetramantane (**36** and **37**) and pentamantane (**38** and **39**) bromides and fluorides.

2. Hydroxylated diamondoids

The alcohol derivatives of **1** can be obtained either by hydrolysis of the corresponding halides or by direct functionalization, as illustrated in **Scheme 1.3** with a selection of mono-, di- and tetrahydroxylated adamantanes: **6** and **42**,⁴⁸ **40**,⁴³ and **43**.⁶⁹ 2-Hydroxyadamantane functionalized at the secondary-C can be

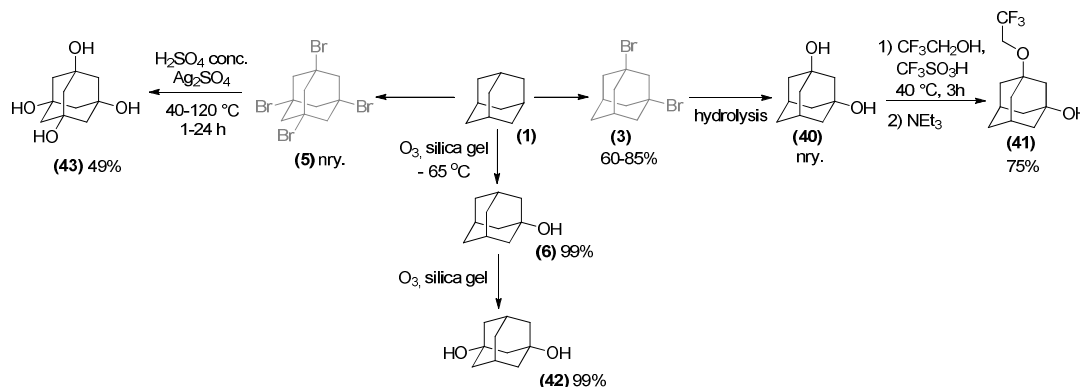
⁶⁶ P. R. Schreiner, N. A. Fokina, B. A. Tkachenko, H. Hausmann, M. Serafin, J. E. P. Dahl, S. Liu, R. M. K. Carlson, A. A. Fokin. *J. Org. Chem.*, **2006**, 71, 6709–6720. Functionalized Nanodiamonds: Triamantane and [121]Tetramantane.

⁶⁷ N. A. Fokina, B. A. Tkachenko, A. Merz, M. Serafin, J. E. P. Dahl, R. M. K. Carlson, A. A. Fokin, P. R. Schreiner. *Eur. J. Org. Chem.*, **2007**, 4738–4745. Hydroxy Derivatives of Diamantane, Triamantane, and [121]Tetramantane: Selective Preparation of Bis-Apical Derivatives.

⁶⁸ A. A. Fokin, P. R. Schreiner, N. A. Fokina, B. A. Tkachenko, H. Hausmann, M. Serafin, J. E. P. Dahl, S. Liu, R. M. K. Carlson. *J. Org. Chem.*, **2006**, 71, 8532–8540. Reactivity of [1(2,3)4]Pentamantane (T_σ-Pentamantane): A Nanoscale Model of Diamond.

⁶⁹ S. Liu, J. Guo, D. Jia. *Pat. CN*, **2007**, 1974515 A. Synthesis of 1,3,5,7-tetrahydroxyadamantane.

obtained by reduction or hydrogenation of 2-adamantanone⁷⁰ with various reagents.^{71,72} The monoprotected diol **41** provides access to unequally functionalized adamantanes (**Scheme 1.3**).⁷³



Scheme 1.3. Hydroxylated adamantanes **6** and **40-43** (*nry.* stands for no reported yield).

The methods for the preparation of hydroxylated diamondanes have been reviewed by Schreiner and co-workers.² **Scheme 1.4** summarizes various conditions for the oxidation of diamondane **10** (a-f) to prepare the hydroxylated diamondanes **30**, **48** and **49** as mixtures, further isolated by silica gel chromatography workup.^{61,67}

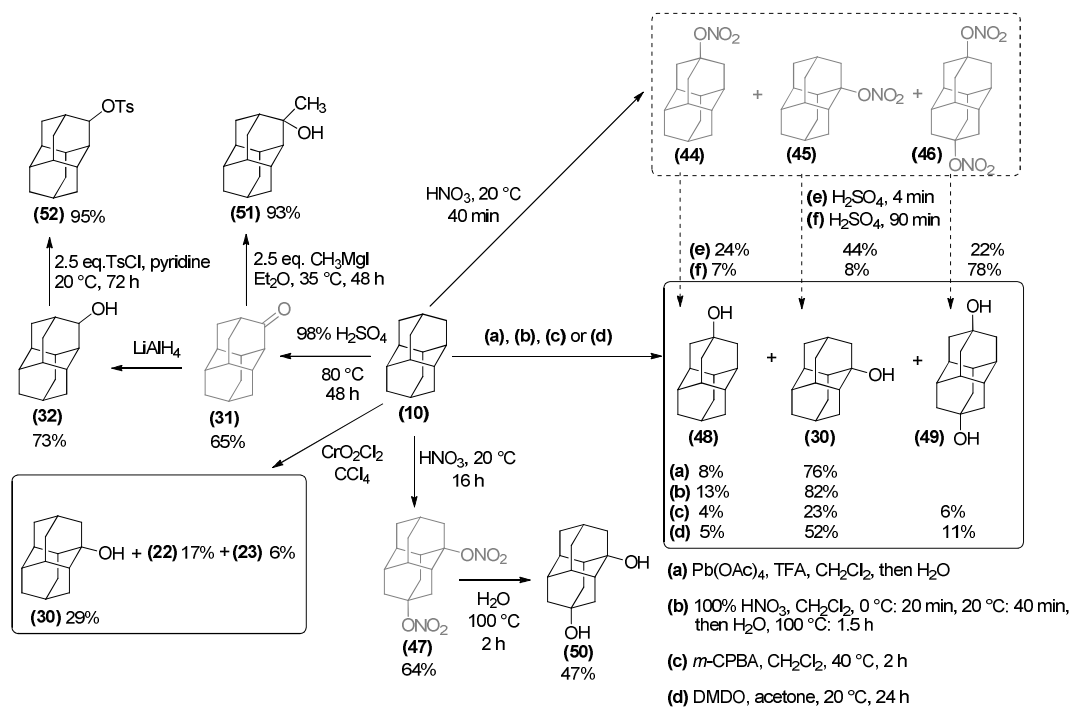
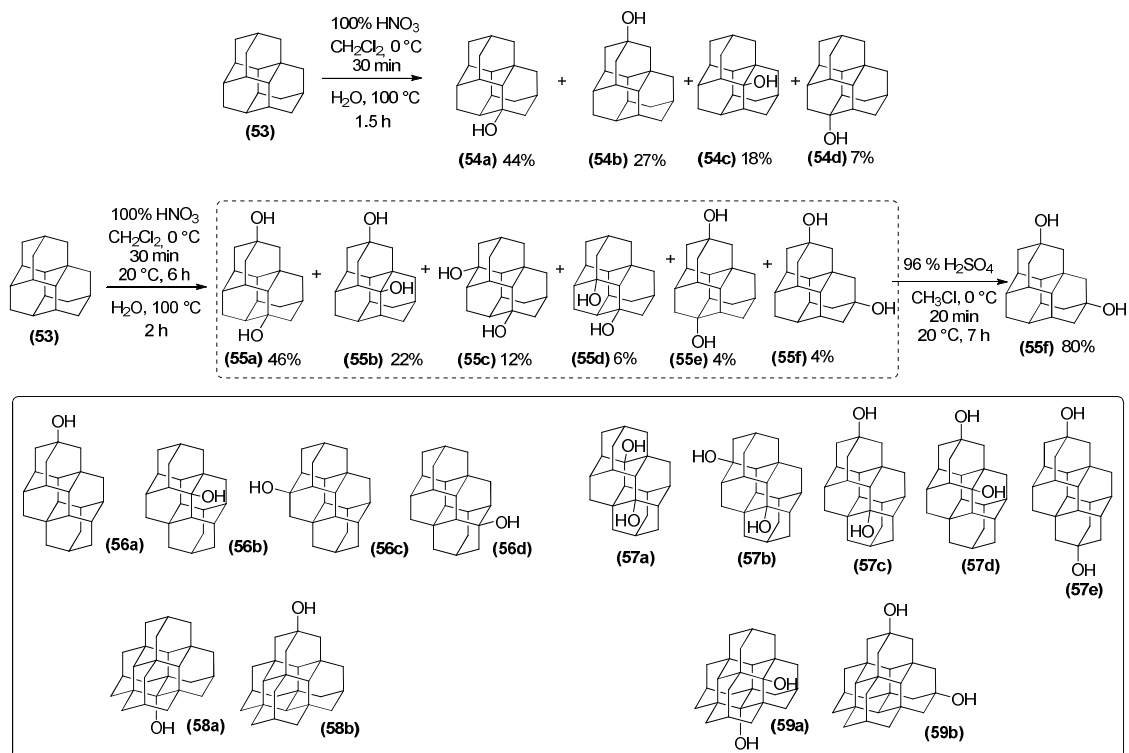
1,4-Dihydroxydiamondane **50** can be prepared from 1,4-dinitroxydiamondane **47** formed by treatment of **10** with HNO_3 .⁶⁷ Other alcohols functionalized on a secondary carbon were also obtained.⁶²⁻⁶⁴ For instance **51** bearing both a hydroxyl and a methyl group in position-2 can be prepared through a classical Grignard reaction with the ketone **31**; this ketone can be used as well to form 2-tosyloxydiamondane **52**, obtained in excellent yield, albeit in a rather long reaction time. The oxidation of triamantane **53** with HNO_3 is also suited to prepare the alcohols **54a-d** as a separable mixture (**Scheme 1.5**).⁶⁷ Except for **54d** the alcohols **54** have also been prepared by other routes.⁶⁶

⁷⁰ K. Tanaka, M. Yamaguchi, T. Shiiki. *Jpn. Kokai Tokkyo Koho*, **2003**, JP 2003267906 A 20030925. Preparation of 2-adamantanone from adamantane.

⁷¹ S. Enthaler, B. Eckhardt, S. Inoue, E. Irran, M. Driess. *Chem. Asian J.*, **2010**, 5, 2027-2035. Facile and Efficient Reduction of Ketones in the Presence of Zinc Catalysts Modified by Phenol Ligands.

⁷² Y. Fujiwara, Y. Iwasaki, T. Maegawa, Y. Monguchi, H. Sajiki. *ChemCatChem*, **2011**, 3, 1624-1628. Facile Hydrogenation of Ketones Catalyzed by Platinum on Carbon under Ordinary Pressures and Temperatures.

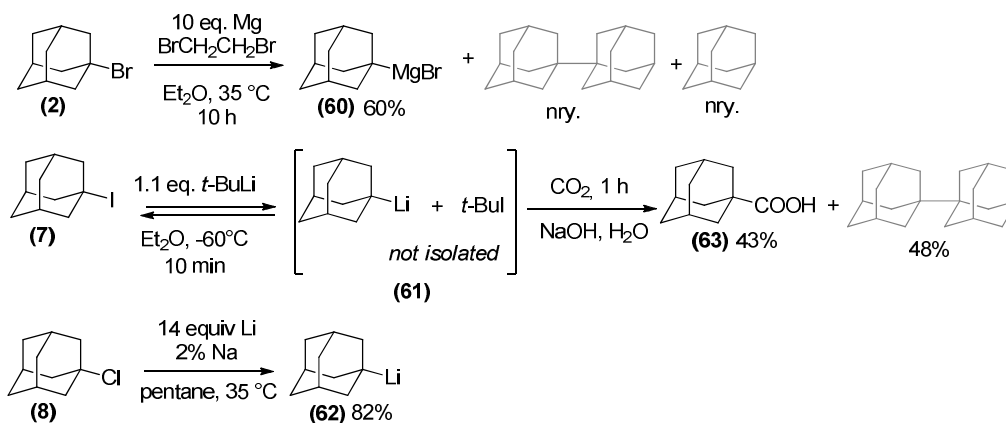
⁷³ H. Schwertfeger, C. Würtele, M. Serafin, H. Hausmann, R. M. K. Carlson, J. E. P. Dahl, P. R. Schreiner. *J. Org. Chem.*, **2008**, 73, 7789-7792. Monoprotection of Diols as a Key Step for the Selective Synthesis of Unequally Disubstituted Diamondoids (Nanodiamonds).


 Scheme 1.4. Hydroxylated diamantanes **30**, **32**, **48-51**, and tosyloxy derivative **52**.

 Scheme 1.5. Polymantane alcohols **54-59**.

By forcing the nitroxilation conditions on **53**, the diols **55a-f** have been obtained under kinetic control but their separation was difficult.⁶⁷ A selective preparation of 9,15-dihydroxytriamantane **55f**, obtained from isomerization of the previous mixture **55a-f**, is possible under thermodynamic conditions.⁶⁷ Hydrolysis of bromide or nitroso precursors yield the monohydroxylated **56a-d**^{66,73} and dihydroxylated [121]tetramantanes **57a-e**.^{67,74} Similarly, the mono- and dihydroxylated [1(2,3)4]pentamantanes (**58a,b** and **59a,b** respectively) can be obtained.⁶⁸

3. Metallated nucleophilic diamondoids

Only a limited number of metallated diamondoids have been prepared, mainly derived from adamantane. The synthesis of the Grignard reagents R-MgX where R is a cage structure apparently is very difficult due to the tendency for radical recombination to give R-R cage dimers (**Scheme 1.6**). Experimental conditions coined with the term “static process” have been reported, which, from kinetic studies, aim at maintaining a magnesium surface state that limits the diffusion of cage radicals R[•] into the reaction mixture.⁷⁵ Thus, under optimized conditions, the Grignard reagent 1-adamantylmagnesium bromide **60** has been obtained in 60% yield in Et₂O and *n*-Bu₂O, while THF was found not to be a suitable solvent.⁷⁵



Scheme 1.6. Adamantyl Grignard reagent and lithiated adamantane **60-62**, and quenching derivative **63**.

⁷⁴ B. A. Tkachenko, N. A. Fokina, L. V. Chernish, J. E. P. Dahl, S. Liu, R. M. K. Carlson, A. A. Fokin, P. R. Schreiner. *Org. Lett.*, **2006**, 8, 1767-1770. Functionalized Nanodiamonds Part 3: Thiolation of Tertiary/Bridgehead Alcohols.

⁷⁵ (a) J. E. Dubois, P. Bauer, G. Molle, J. Daza. *C. R. Acad. Sc. Paris, Serie C : Sci. Chim.*, **1977**, 284, 145-148. Congested Cage-structure Organomagnesium Compounds: Synthesis of 1-Adamantylmagnesium bromide. (b) G. Molle, P. Bauer, J. E. Dubois. *J. Org. Chem.*, **1982**, 47, 4120-4128. Formation of cage-structure organomagnesium compounds. Influence of the degree of adsorption of the transient species at the metal surface.

1-Adamantyllithium **62** and its congeners 2-adamantyllithium and 1-diamantyllithium have been directly synthesized from the reaction of bromide and chloride precursors with lithium metal.⁷⁶ Here also the control of metal-solution interface is crucial to achieve the highest yields, and to avoid diamondoid homologation. Previous attempts at the direct metallation of secondary or tertiary adamantyl iodides had used an excess of *tert*-butyllithium **61**, which allowed the preparation of 1-adamantanecarboxylic acid **63**.^{47,77}

4. Amino and nitro diamondoids and their derivatives

The development of acetamide and amine derivatives of lower diamondoids has been motivated by their associated pharmacological applications that are well illustrated by the emblematic antiviral and anti-Parkinsonian 1-aminoadamantane **64** (or amantadine, **Scheme 1.7**).⁷⁸ In addition, amino derivatives are important for further functionalization towards, e.g., artificial amino acids and peptides (see section IV.4.). Various methods for the synthesis of adamantylamines and hydrochloride derivatives have been patented,^{79,80,81} such as the lithiation of adamantyl halides in the presence of an aminating agent under ultrasound that produces 1-aminoadamantane **64** in 54% yield (**Scheme 1.7**). The synthesis of **64** in high yield has been also reported directly from **1** on a 20 g scale by treatment with trichloroamine (*caution: explosive, sensitive to light, heat, and shock*) under Friedel-Crafts conditions, followed by solvolysis with HCl.⁸² The nitrite ester of adamantane **66** can be obtained by the reaction of adamantane with concentrated nitric acid; further treatment with sulfuric acid in the presence of acetonitrile gives 1-acetamidoadamantane **67** in good yield.⁸³ Compound **67** has also been obtained in moderate 38% yield from direct nucleophilic amidation of **1** with CH₃CONH₂.⁸⁴ Notably, **67** can be reacted with NaOH to give the hydrochloride salt of amantadine **68** in excellent yield. The relevant nitro derivative **65** is not easily

⁷⁶ G. Molle, P. Bauer, J. E. Dubois. *J. Org. Chem.*, **1983**, 48, 2975-2981. High-Yield Direct Synthesis of a New Class of Tertiary Organolithium Derivatives of Polycyclic Hydrocarbons.

⁷⁷ P. T. Lansbury, J. D. Sidler. *J. Chem. Soc. Chem. Commun.*, **1965**, 16, 373. 1-Adamantyl-lithium.

⁷⁸ L. Wanka, K. Iqbal, P. R. Schreiner. *Chem. Rev.*, **2013**, 113, 3516-3604. The Lipophilic Bullet Hits the Targets: Medicinal Chemistry of Adamantane Derivatives

⁷⁹ G. A. Kraus. *Pat. U.S.*, **1997**, US 5599998 A. Method for the Synthesis of Adamantane Amines.

⁸⁰ C. Schickaneder. *Eur. Pat. Appl.*, **2007**, EP 1820792 A1 20070822. Process for the Preparation of Adamantanamines.

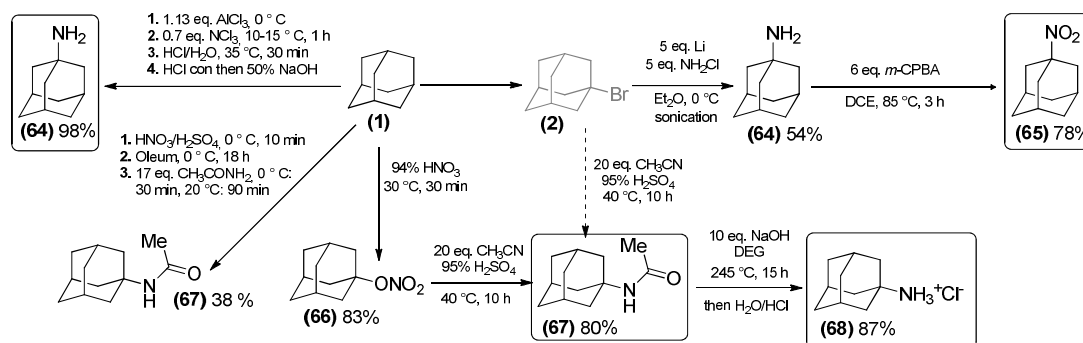
⁸¹ G. M. Butov, V. V. Pershin, V. V. Burmistrov. *Pat. Russ.*, **2012**, RU 2440971 C1 20120127. Method of producing hydrochlorides of amine-derivatives of adamantane.

⁸² (a) P. Kovacic, P. D. Roskos. *J. Am. Chem. Soc.*, **1969**, 91, 6457-6460. Chemistry of N-Halamines. XIII. Amination of Adamantanes and Their Precursors with Trichloroamine-Aluminum Chloride. (b) P. Kovacic, P. D. Roskos. *Tetrahedron Lett.*, **1968**, 56, 5833-5835. A Novel, Simple Synthesis of Aminoadamantanes.

⁸³ I. K. Moiseev, R. I. Doroshenko, V. I. Ivanova. *Pharm. Chem. J.*, **1976**, 10, 450-451. Synthesis of Amantadine via the Nitrate of 1-Adamantanol.

⁸⁴ L. Wanka, C. Cabrele, M. Vanejews, P. R. Schreiner. *Eur. J. Org. Chem.*, **2007**, 1474-1490. γ -Aminoadamantanecarboxylic Acids Through Direct C-H Bond Amidations.

obtained by direct nitration of adamantane with concentrated nitric acid, but its expedient synthesis by reaction of 1-aminoadamantane with *m*-chloroperbenzoic acid has been reported.⁸⁵



Scheme 1.7. Synthetic roads to amine, amide and nitro-functionalized adamantanes **64-68**.

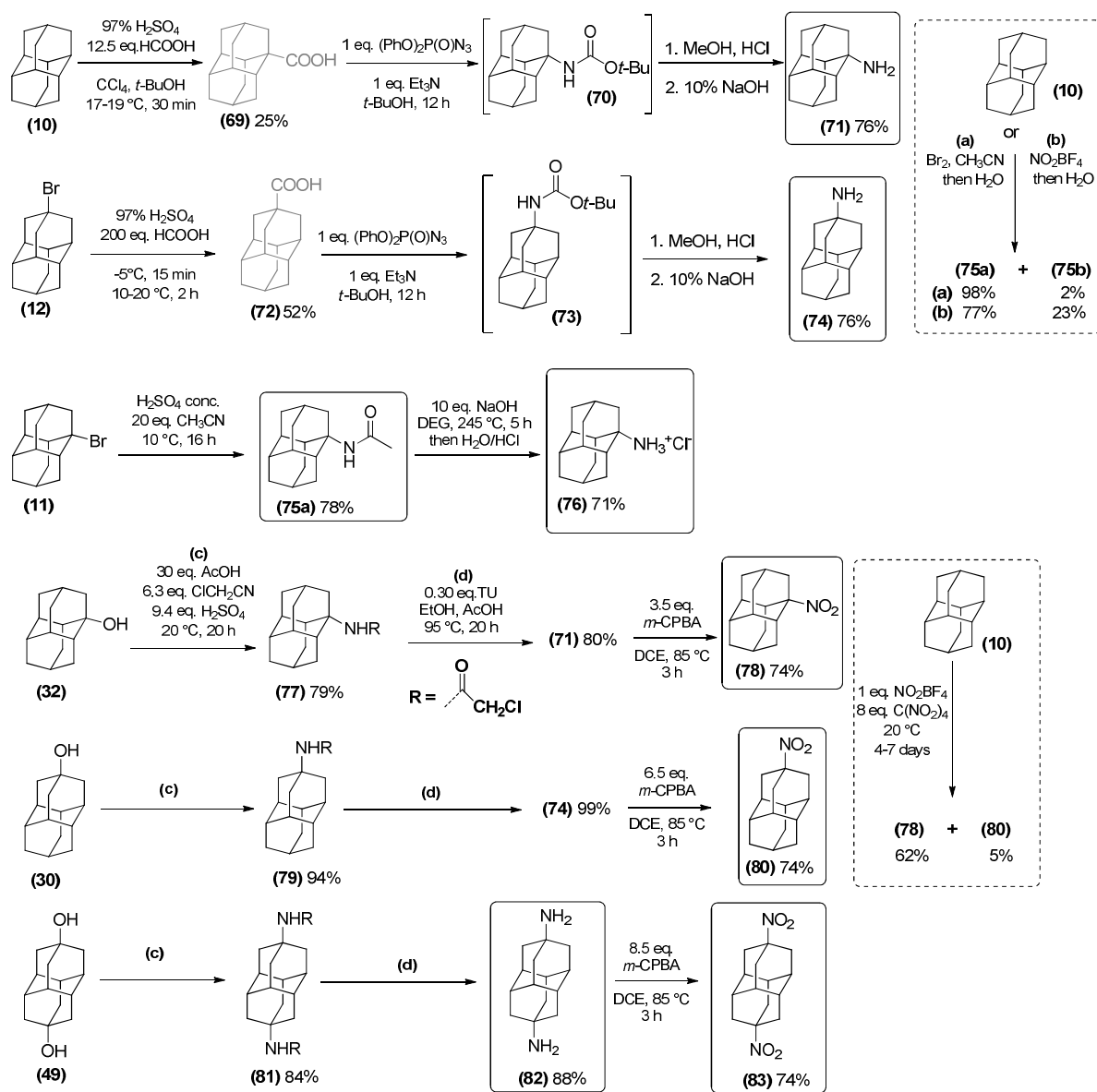
Aminodiamantanes and their derivatives can be prepared from diamantane **10**, 1-bromodiamantane **11**, 4-bromodiamantane **12**, 1-hydroxydiamantane **32**, 4-hydroxydiamantane **30** and 4,9-dihydroxydiamantane **49** (**Scheme 1.8**). Diamantanecarboxylic acids **69** and **72**^{62,64} have been treated with diphenylphosphoryl azide and *tert*-butyl alcohol to give the intermediary carbamates **70** and **73**, respectively, that can be hydrolyzed to 1-amino- and 4-aminodiamantane **71** and **74**.⁸⁶ From 1-bromodiamantane **11** the synthesis of 1-acetamidodiamantane **75a** by a Ritter reaction ($\text{CH}_3\text{C}\equiv\text{N}/\text{H}_2\text{SO}_4$) gives **76** after hydrolysis as the hydrochloride salt of **71**. 1-Acetamidodiamantane **75a** can be directly obtained in a mixture with its isomer 4-acetamidodiamantane **75b**; it is also available by oxidation of diamantane **10** with neat bromine or nitronium tetrafluoroborate, NO_2BF_4 , in acetonitrile (conditions (a) and (b) in **Scheme 1.8**).⁶¹

The aminodiamantanes **71**, **74**, and **82** can be prepared by acidic exchange of the hydroxyl groups of diamantanols **32**, **30**, and **49**, respectively; treatment with chloroacetonitrile and cleavage gave **77**, **79**, and **81**.⁸⁶ Treatment of aminodiamantanes **71**, **74**, and **82** with *m*-CPBA in dichloroethane leads to the corresponding nitro-functionalized compounds **78**, **80** and **83** in yields around 75%.⁸⁵ The synthesis of **78** and **80** as a 12:1 mixture has been reported directly from diamantane **10** upon treatment with NO_2BF_4 in

⁸⁵ H. Schwertfeger, C. Würtele, P. R. Schreiner. *Synlett.*, **2010**, 3, 493-495. Synthesis of Diamondoids Nitro Compounds from Amines with *m*-Chloroperbenzoic Acid.

⁸⁶ A. A. Fokin, A. Merz, N. A. Fokina, H. Schwertfeger, S. L. Liu, J. E. P. Dahl, R. K. M. Carlson, P. R. Schreiner. *Synthesis*, **2009**, 6, 909-912. Synthetic Routes to Aminotriamantanes, Topological Analogues of the Neuroprotector Memantine®.

nitromethane.⁸⁷ Similar synthetic routes can be applied to give various biologically pertinent aminotriamantanes.⁸⁶

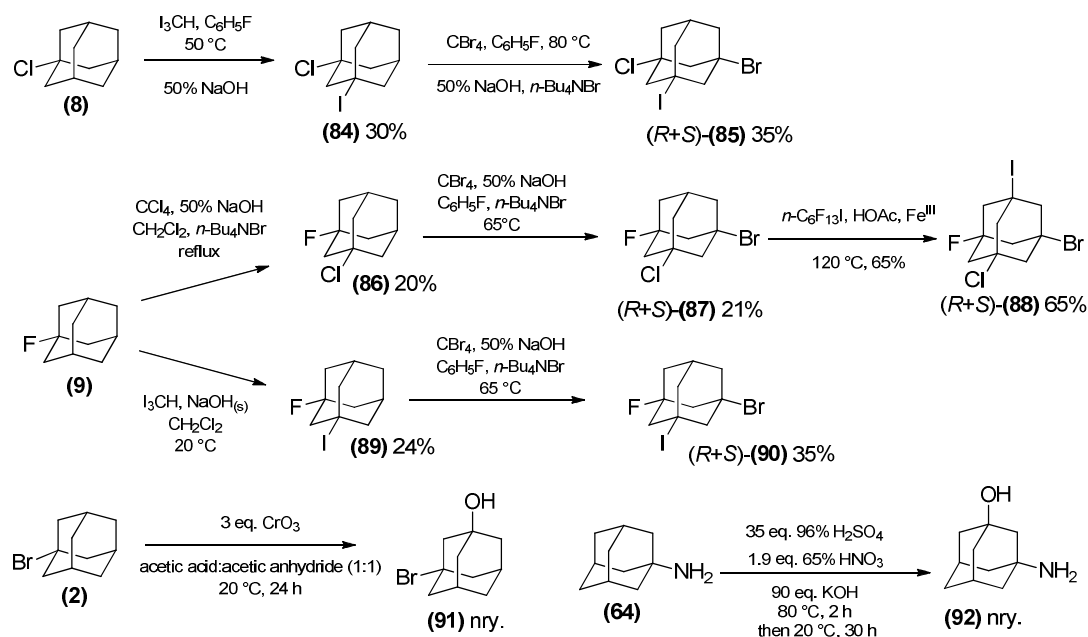


Scheme 1.8. Main synthetic pathways to amino-, acylamino-, and nitro-functionalized diamantanes **71**, and **74-83**.

⁸⁷ G. A. Olah, P. Ramaiah, C. B. Rao, G. Sandford, R. Golam, N. J. Trivedi, J. A. Olah. *J. Am. Chem. Soc.*, **1993**, 115, 7246-7249. Nitration of adamantane and Diamantane with Nitronium Tetrafluoroborate.

5. Polyfunctionalized diamondoids with different reactive functionalities

The synthesis of polyfunctionalized diamondoids with mixed reactive functions is of particular interest to build unequally substituted organohybrids based on the reactivity differences of the functions introduced. **Scheme 1.9** summarizes some interesting mixed polyfunctionalized halo-, hydroxy-, and amino-adamantanes formed from tertiary-C functionalized bromo-, chloro- and fluoroadamantane.



Scheme 1.9. Syntheses of polyfunctionalized adamantanes **84-92** bearing different halo-, hydroxy-, and amino-functions.

Several interesting polyhaloadamantanes have been synthesized in moderate yields by successive multistep reactions under phase-transfer condition (PTC).⁸⁸ Stepwise iodination with iodoform and bromination with CBr_4 of 1-chloroadamantane **8** led successively to the formation of 1-chloro-3-iodoadamantane **84**, and 1-chloro-3-bromo-5-iodoadamantane **85** as a racemic mixture.⁸⁹ Chlorination of fluoroadamantane **9** with CCl_4 gave **86**, which was brominated to give **87**, which was iodinated⁹⁰ with $n\text{-C}_6\text{F}_{13}\text{I}$ to give the remarkable tetrahalide 1-bromo-3-chloro-5-fluoro-7-iodoadamantane **88**. Successive iodination and bromination of 1-fluoroadamantane **9** provided first 1-fluoro-3-iodoadamantane **89** then

⁸⁸ P. R. Schreiner, A. A. Fokin, O. Lauenstein, Y. Okamoto, T. Wakita, C. Rinderspacher, G. H. Robinson, J. K. VoHS, C. F. Campana. *J. Am. Chem. Soc.*, **2002**, 124, 13348-13349. Pseudotetrahedral Polyhaloadamantanes as Chirality Probes: Synthesis, Separation, and Absolute Configuration.

⁸⁹ A. A. Fokin, O. Lauenstein, P. A. Gunchenko, P. R. Schreiner. *J. Am. Chem. Soc.*, **2001**, 123, 1842-1847. Halogenation of Cubane under Phase-Transfer Conditions: Single and Double C-H-Bond Substitution with Conservation of the Cage Structure.

⁹⁰ L. Liguori, H.-R. Bjørsvik, A. Bravo, F. Fontana, F. Minisci. *Chem. Commun.*, **1997**, 1501-1502. A New Direct Homolytic Iodination Reaction of Alkanes by Perfluoroalkyl Iodides.

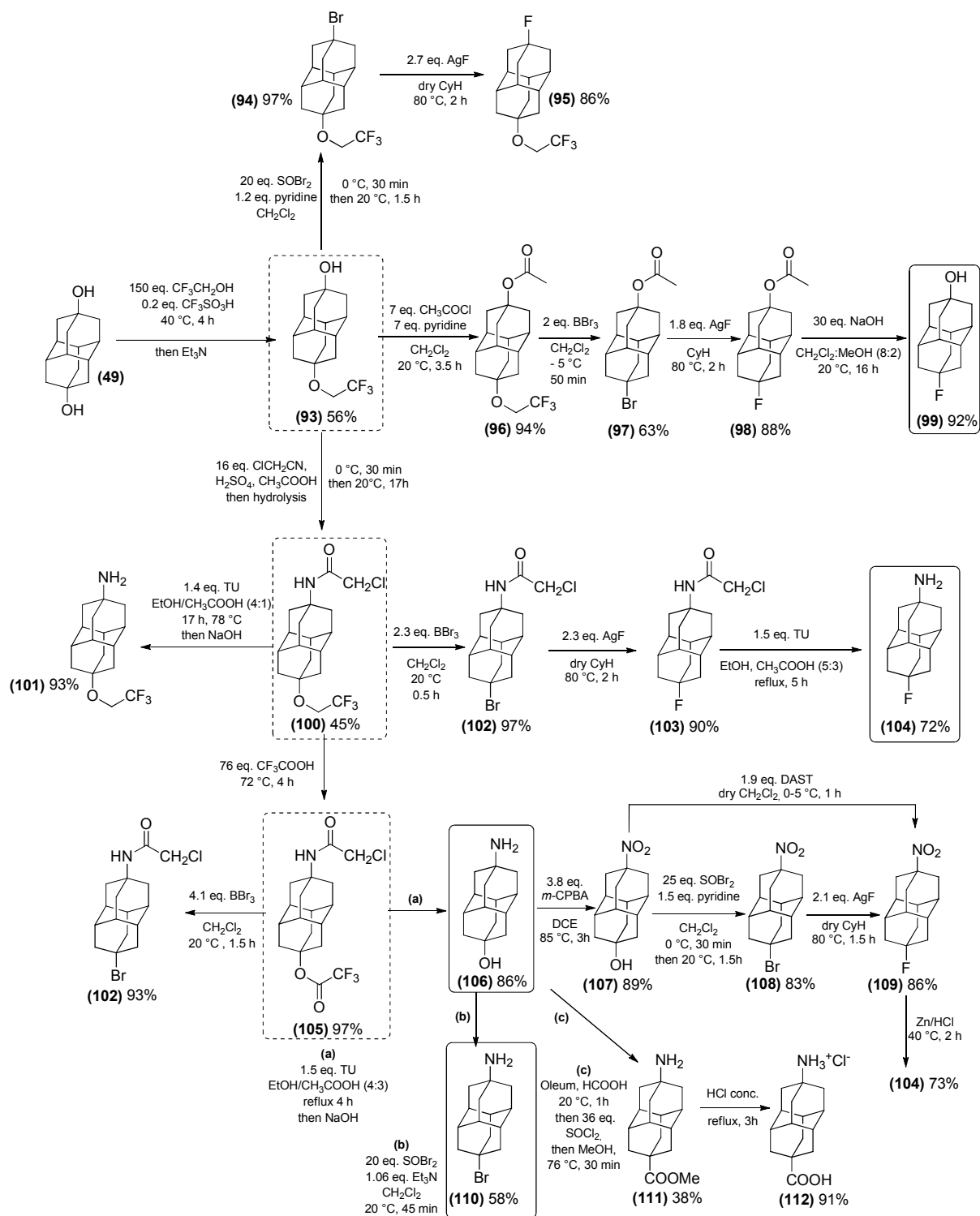
1-fluoro-3-bromo-5-iodoadamantane **90** as a racemic mixture. 3-Bromoadamantan-1-ol **91**, and its chloro-congener, have been synthesized and isolated en route to 1,3-diiodoadamantane, which was obtained by addition of hydroiodic acid to any of those compounds.⁹¹ From **91** the formation of 1-bromo-3-chloroadamantane (using thionyl chloride) and 1,3-dibromoadamantane **3** (using hydrobromic acid) were also reported.⁹¹ The formation of 1-aminoadamantane-3-ol **92** has been described from reaction of the hydrochloric salt of 1-aminoadamantane in a mixture H₂SO₄/HNO₃ followed by quenching with KOH.⁹²

As summarized in **Scheme 10**, the monoprotection of diamantane-4,9-diol **49** by a fluoroalkyl ether function is an important achievement at the origin of the synthesis for a great number of unequally difunctionalized diamantanes **93-112**.^{65,73} By employing 2,2,2-trifluoroethanol under acidic conditions on **49**, the precursor **93** forms in 56% yield; it can be separated from the diether (9%) and unreacted diol (30%) by silica gel column chromatography. Compound **93** has allowed the synthesis of the pivotal protected amido **100** and ester **105** diamantane derivatives.⁷³

These precursors provided access to 9-fluorodiamantan-4-ol **99**, 4-amino-9-fluorodiamantane **104**, 4-amino-9-bromodiamantane **110**,⁶⁵ as well as 9-aminodiamantan-4-ol **106**,⁷³ with yields generally above 70% (mainly from selective deprotection). The syntheses of mixed difunctionalized derivatives **101**, **107**, **111**, and **112** have also been detailed,⁷³ as well as for **94-98**, **102**, **103**, **108**, and **109**.⁶⁵

⁹¹ A. E. Lukach, A. N. Santiago, R. A. Rossi. *J. Org. Chem.*, **1997**, 62, 4260-4265. Reactions of 1,3-Dihaloadamantanes with Carbanions in DMSO: Ring-Opening Reactions to Bicyclo[3.3.1]nonane Derivatives by the S_{RN}1 Mechanism.

⁹² U. Hassiepen, M. Kittelmann. *PCT Int. Appl.*, **2009**, WO 2009068531 A2. Preparation of Adamantly glucuronic acids as Enzyme Inhibitors and Antidiabetic Agents.



Scheme 1.10. Synthetic roads to difunctionalized mixed hydroxy-, halo- and amino-diamantanes from their protected parent compounds, **93-112**.

6. Alkyl-, aryl-, alkenyl-, phosphinyl-, cyano- and thiol-substituted diamondoids

Adamantane substituted with phosphine, alkenyl, or simple alkyl fragments have been studied because these species have biological interest (*alkyls*),⁹³ can be used as monomers in polymerizations (*alkenes*), or are ligands for transition metals with outstanding properties (*phosphines*). The preparation of 2-adamantyl-1,3-butadiene **115** (**Scheme 1.11**)⁹⁴ was conducted from adamantane via the selective photochemical preparation of 1-acetyladamantane **113**,⁹⁵ followed by oxetane **114** formation and ring opening. Adamantane is also the precursor for the formation of di-1-adamantyl phosphinic acid chloride **116**,⁹⁶ which gives access to the organophosphorus compounds di-1-adamantylphosphine **117**, di-1-adamantylchlorophosphine **118**, and di-1-adamantylphosphine oxide **119**. They are obtained in excellent yields above 85% at a scale of several grams, and notably without the need for metallated adamantyl nucleophilic reagents. Chlorophosphine **118** can be treated with phenyl magnesium bromide/CuBr to give the dialkylaryl phosphine **120** in 65% yield.⁹⁷ The preparation of the parent trialkylphosphines **123** by reacting **118** with organometallic reagents such as alkyllithium, alkylmagnesium or alkylzinc (alkyl = *n*-butyl, *tert*-butyl, benzyl, etc.) has been patented,⁹⁸ and has led to the commercialization of the ligands CataCXium® useful for group 10 metal-catalyzed cross-coupling reactions.⁹⁹ The secondary phosphine **117** has been used to prepare the zwitterionic phosphonium salts **121**¹⁰⁰ and **122**,¹⁰¹ applicable as ligands for transition metals under conditions of biphasic and aqueous-phase catalysis.

⁹³ (a) S. Samnick, S. Ametamey, K. L. Leenders, P. Vontobel, G. Quack, C. G. Parsons, Henrik Neu, Pius A. Schubiger. *Nucl. Med. Biol.*, **1998**, 25, 323-330. Electrophysiological Study, Biodistribution in Mice, and Preliminary PET Evaluation in a Rhesus Monkey of 1-Amino-3-[¹⁸F]fluoromethyl-5-methyl-adamantane (¹⁸F-MEM): A Potential Radioligand for Mapping the NMDA-Receptor Complex. (b) B. Reisberg, R. Doody, A. Stöffler, F. Schmitt, S. Ferris, H. J. Möbius. *N. Engl. J. Med.*, **2003**, 348, 1333-1341. Memantine in Moderate-to-Severe Alzheimer's Disease.

⁹⁴ A. A. Fokin, E. D. Butova, L. V. Chernish, N. A. Fokina, J. E. P. Dahl, R. M. K. Carlson, P. R. Schreiner. *Org. Lett.*, **2007**, 9, 2541-2544. Simple Preparation of Diamondoid 1,3-Dienes via Oxetane Ring Opening.

⁹⁵ (a) I. Tabushi, S. Kojo. *Tetrahedron Lett.*, **1973**, 26, 2329-2332. Photoacetylation of Substituted Adamantanes. Exclusive Bridgehead Substitution and Large ρ^* value. (b) I. Tabushi, S. Kojo, K. Fukunishi. *J. Org. Chem.*, **1978**, 43, 2370-2374. Mechanism of Photoacetylation of Substituted Adamantanes.

⁹⁶ J. R. Goerlich, R. Schmutzler. *Phosphorus, Sulfur, and Silicon*, **1995**, 102, 211-215. Organophosphorus Compounds with Tertiary alkyl substituents. VI: A convenient Method for the Preparation of di-1-adamantylphosphine and di-1-adamantylchlorophosphine.

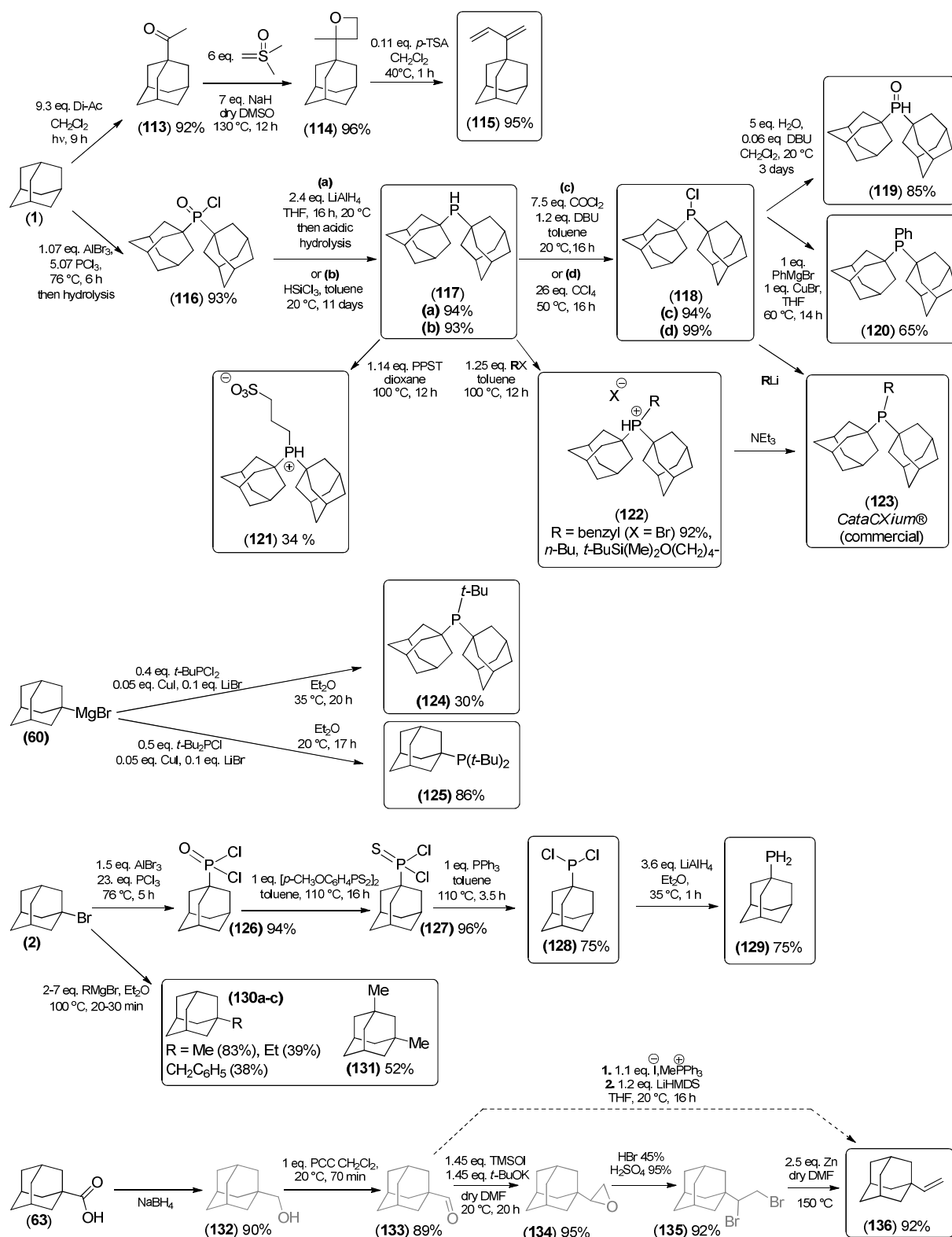
⁹⁷ A. Köllhofer, H. Plenio. *Chem. Eur. J.*, **2003**, 9, 1416-1425. Homogeneous Catalysts Supported on Soluble Polymers: Biphasic Sonogashira Coupling of Aryl Halides and Acetylenes Using MeOPEG-Bound Phosphine-Palladium Catalysts for Efficient Catalyst Recycling.

⁹⁸ M. Beller, A. Ehrentraut, C. Fuhrmann, A. Zapf. *PCT Int. Appl.*, **2002**, WO 2002010178 A1 20020207. Preparation of novel phosphine ligands and use in catalytic reactions.

⁹⁹ A. Zapf, M. Beller. *Chem. Commun.*, **2005**, 431-440. The development of efficient catalysts for palladium-catalyzed coupling reactions of aryl halides.

¹⁰⁰ W. S. Brown, D. D. Boykin, M. Q. Sonnier Jr, W. D. Clark, F. V. Brown, K. H. Shaughnessy. *Synthesis*, **2008**, 12, 1965-1970. Sterically Demanding, Zwitterionic Trialkylphosphonium Sulfonates as Air-Stable Ligand Precursors for Efficient Palladium-Catalyzed Cross-Couplings of Aryl Bromides and Chlorides.

¹⁰¹ C. A. Fleckenstein, H. Plenio. *Chem. Soc. Rev.*, **2010**, 39, 694-711. Sterically Demanding Trialkylphosphines for Palladium-catalyzed Cross Coupling Reactions – Alternatives to P(*t*-Bu₃).


 Scheme 1.11. Olefin-, phosphorus- and alkyl-substituted adamantanes **115-130**, and **136**.

Another synthetic pathway to adamantylalkylphosphines is the reaction of halophosphines with adamantylmagnesium bromide **60**,⁷⁵ which gives the monoadamantylphosphine **125** in excellent yield, but the diadamantyl analogue **124** only in moderate yield.¹⁰²

1-Bromoadamantane **2** treated with a large excess of PCl_3 in the presence of AlBr_3 leads to 1-adamantylphosphonic acid dichloride **126**, the parent of **116** in excellent yield on a multigram scale,¹⁰³ the dibromide analogue of **126** is accessible by using PBr_3 , albeit in lower yield (24%).¹⁰⁴ 1-Adamantyl-dichlorophosphine **128** can be prepared from compound **126** through reaction with Lawesson's reagent (*via* 1-adamantyl-dichlorophosphine sulfide **127**) in 68% overall yield. The direct phosphorylation of **1** is possible with AlCl_3 and PCl_3 to produce **126** in 64% yield.¹⁰⁵ The primary phosphine **129** is an oily product obtained in 75% yield by reduction of **128** with LiAlH_4 .¹⁰⁴ 1-Bromoadamantane **2** is also an interesting precursor for the alkylation of adamantane by reacting it with Grignard reagents to yield products **130a-c**;^{106a} Optimization of the reaction has been reported^{106b} together with multistep polyalkylation conditions which give for instance **131** and 1,3-dimethyladamantane analogue.

The adamantanecarboxylic acid **63**¹⁰⁷ is a useful reagent that has been used to prepare 1-vinyladamantane **136** by two different routes,^{108,109} *via* the reduction of **63** to adamantan-1-ylmethanol **132**,¹¹⁰ followed by oxidation to adamantane-1-carbaldehyde **133**.¹⁰⁹ The oxirane **134** forms in excellent yield from **133** and its ring opening led to 1-adamantyl-1,2-dibromoethane **135**, which is debrominated

¹⁰² J. P. Stambuli, S. R. Stauffer, K. H. Shaughnessy, J. F. Hartwig. *J. Am. Chem. Soc.*, **2001**, 123, 2677-2678. Screening of Homogeneous Catalysts by Fluorescence Resonance Energy Transfer. Identification of Catalysts for Room-Temperature Heck Reactions.

¹⁰³ M. Gouygou, G. Etemad-Moghadam, M. Koenig. *Synthesis*, **1987**, 5, 508-509. A Convenient Method for the Synthesis of 1-Adamantyl-dichlorophosphine.

¹⁰⁴ H. Duddeck, M. Hani, A. Elgamal, A. G. Hanna. *Phosphorus and Sulfur*, **1986**, 28, 307-314. Synthesis and Mass Spectra of Adamantylphosphoryl Derivatives.

¹⁰⁵ G. A. Olah, O. Farooq, Q. Wang, A. Wu. *J. Org. Chem.*, **1990**, 55, 1224-1227. AlCl_3 -Catalyzed Dichlorophosphorylation of Saturated Hydrocarbons with PCl_3 in Methylene Chloride Solution.

¹⁰⁶ (a) E. Ōsawa, Z. Majerski, P. von R. Schleyer. *J. Org. Chem.*, **1971**, 36, 205-207. Preparation of Bridgehead Alkyl Derivatives by Grignard Coupling. (b) G. Molle, J. E. Dubois, P. Bauer. *Can. J. Chem.*, **1987**, 65, 2428-2433. Contribution à l'étude des réactions d'alkylation et de polyalkylation de l'adamantane et de ses homologues.

¹⁰⁷ H. Koch, W. Haaf. *Org. Synth.*, **1964**, 44, 1-3 (or collective volume n° V; H. E. Baumgarten, Ed.; **1973**, 20-22). 1-Adamantanecarboxylic acid.

¹⁰⁸ A. A. Fokin, E. D. Butova, A. V. Barabash, N. N. Huu, B. A. Tkachenko, N. A. Fokina, P. R. Schreiner. *Synth. Commun.*, **2013**, 43, 1772-1777. Preparative Synthesis of Vinyl Diamondoids.

¹⁰⁹ J. A. Wright, M. J. Gaunt, J. B. Spencer. *Chem. Eur. J.*, **2006**, 12, 949-955. Novel Anti-Markovnicov Regioselectivity in the Wacker Reaction of Styrenes.

¹¹⁰ (a) R. P. McGearry. *Tetrahedron Lett.*, **1998**, 39, 3319-3322. Facile and chemoselective reduction of carboxylic acids to alcohols using BOP reagent and sodium borohydride. (b) G. Nagendra, C. Madhu, T. M. Vishwanatha, V.V Sureshbabu. *Tetrahedron Lett.*, **2012**, 53, 5059-5063. An expedient route for the reduction of carboxylic acids to alcohols employing 1-propanephosphonic acid cyclic anhydride as acid activator.

to **136** with an overall yield of 80%.¹⁰⁸ Compound **133** can alternatively undergo a Wittig reaction to give **136** in 65% yield.¹⁰⁹

Diamantane **10** and a variety of its derivatives (bromides, alcohols, ketones, esters and carboxylic acids): **11**, **30**, **31**, **48**, **49**, **140**, **144**, **151** and **155** are precursors of compounds that incorporate aryl, alkyl, alkenyl, phosphino, and thiol groups as depicted in **Scheme 1.12**.

Cyanoaryldiamantane **137** has been obtained photochemically directly from **10**.⁶¹ Diamantanylphosphonic acid dichloride **138** and diamantylphosphinic acid chloride **139** can also be prepared from **10**, and then reduced to the corresponding phosphines.¹¹¹ Photochemistry has also been successfully used to form acetyldiamantanes **140** and **141**.^{112,113} Photoacetylation can be applied to [123]tetramantane and to some pentamantanes to selectively form apical acetyl derivatives.¹¹³ Compound **140** allowed the preparation of diamantylbutadiene **143** in 94% overall yield *via* the formation and ring-opening of oxetane derivative **142**.⁹⁴

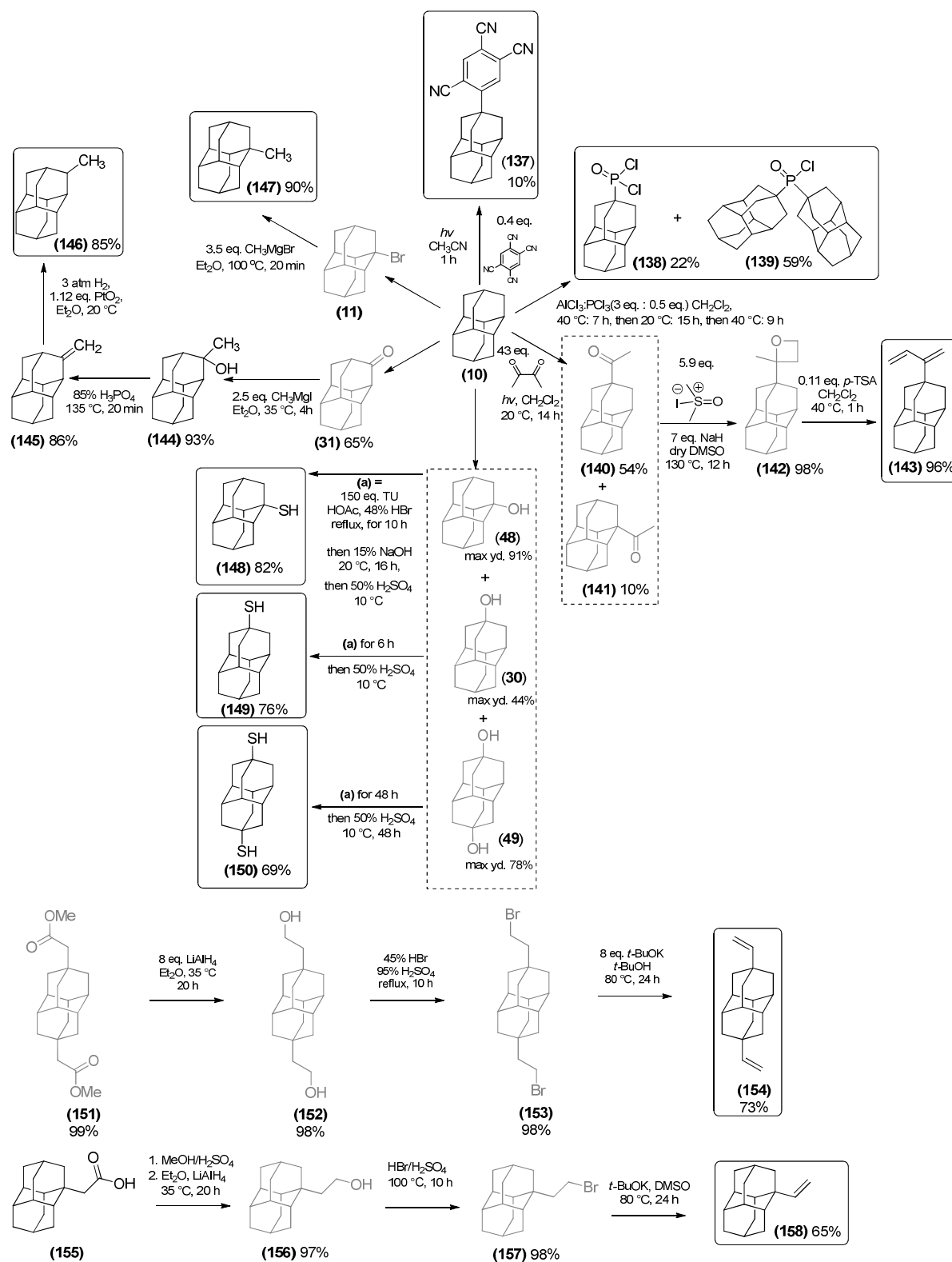
Diamantan-3-one **31** undergoes an efficient reaction with CH_3MgI to form **144**,⁶³ which after dehydration to **145** and further platinum-catalyzed hydrogenation gave 3-methyldiamantane **146** in 68% overall yield.^{62,64} Isomeric 1-methyldiamantane **147** forms from its bromide analogue **11** in very good yield by Grignard reaction.¹⁰⁶

Diamantanols are ideal precursors for the corresponding thiols **148-150** by treatment with thiourea (TU) in the presence of hydrobromic and acetic acid.⁷⁴ The conditions of thiolation can be extended to higher diamondoids such as triamantane and the tetramantanes; the resulting molecules are of particular interest for nanoelectronic devices (see section **1.4** part **3**). Noteworthy, the 1-vinyl- and 4,9-divinyl-substituted diamantanes **158** and **154** have been obtained from carboxylic acid, ester, alcohol, and bromide derivatives **151-153** and **155-157**.¹⁰⁸ Unsaturated compounds such as vinyldiamondoids are expected to play a role for the immobilization of organic molecules on semiconductors for nanoelectronics.

¹¹¹ H. Schwertfeger, M. M. Machuy, C. Würtele, J. E. P. Dahl, R. M. K. Carlson, P. R. Schreiner. *Adv. Synth. Catal.*, **2010**, 352, 609-615. Diamondoid Phosphines – Selective Phosphorylation of Nanodiamonds.

¹¹² I. Tabushi, S. Kojo. P. von R. Schleyer, T. M. Gund. *J. Chem. Soc., Chem. Comm.*, **1974**, 591. Selective Functionalization of Unactivated Methine Positions. 4-Acetyldiamantane.

¹¹³ A. A. Fokin, P. A. Gunchenko, A. A. Novikovskiy, T. E. Shubina, B. V. Chernyaev, J. E. P. Dahl, R. M. K. Carlson, A. G. Yurchenko, P. R. Schreiner. *Eur. J. Org. Chem.*, **2009**, 5153-5161. Photoacetylation of Diamondoids: Selectivities and Mechanism.



Scheme 1.12. Synthetic routes to aryl-, alkyl-, alkenyl-, phosphinyl-, and thiol-substituted diamondanes **137-139**, **143-150**, **154** and **158**.

1.4. Organohybrids built on nanodiamond and diamondoids and their applications

The functionalization of diamondoids (see section 1.3), and ultradispersed detonation nanodiamond^{7,114} has opened the way for the construction of a very large diversity of nanohybrids. The resulting compounds have been used in applications that span fields extending from basic synthetic methods (section 1.4 part 4) up to highly technological applications towards advanced nanoelectronic devices (section 1.4 part 3). The use of detonation nanodiamond in materials and biomaterials is certainly the most developed area of research up to now (section 1.4 part 2 and 1.4 part 1). In the following we introduce some representative examples of organohybrids purposely developed for novel applications. This selection mainly concerning lower diamondoids, includes some pertinent examples that also illustrate the great potential of higher diamondoids and ultradispersed detonation nanodiamond.

1. Biological applications of nanodiamond and diamondoid-based hybrids

Nanoparticles of various origins are now intensively examined for biological applications such as imaging, diagnostic, or drug delivery. The inevitable requirements when employing nanoparticles in bio-applications are: (i) control of surface properties, (ii) proper dispersion in physiological solutions, (iii) biocompatibility criteria, (iv) efficient and selective targeting of intracellular locations. The interest of nanoparticles for biological applications is highly dependent on their sizes, shapes, purities and their mode of administration and elimination. Ultradispersed detonation nanodiamond has been studied for biomedical use due to its small primary particle sizes (4 to 5 nm at best) and retention of high cellular viability. This work has been comprehensively surveyed.^{3,7,115} In general, the features of detonation nanodiamond that are accurately controlled are their aggregation state, surface chemistry as well as localization and accumulation within the body. Comparisons between *in vitro* and *in vivo* testing for biocompatibility is also required before the full biomedical potential of detonation nanodiamond can be realized.

¹¹⁴ W. S. Yeap, K. P. Loh. Functionalization of Nanodiamond for specific biorecognition. In: *Nanodiamonds Applications in Biology and Nanoscale Medicine*; Dean Ho, Ed. Springer, **2010**, p. 117-125.

¹¹⁵ V. N. Mochalin, O. Shenderova, D. Ho, Y. Gogotsi. *Nat. Nanotechnol.*, **2012**, 7, 11-23. The properties and applications of nanodiamonds.

Detonation nanodiamond, when accurately pretreated can be a versatile platform for the controlled functionalization and delivery of therapeutics in the form of hydrogels.¹¹⁶ Specifically prepared detonation nanodiamond has been employed and before coating the drug onto the nanodiamond, the chemical nature and purity of the material had been investigated with FTIR, Raman spectroscopy, thermogravimetric analysis and TEM, to establish that the size of the NDs was in the range of 2-8 nm and its purity was over 90 wt %. Such nanodiamond mixture was functionalized at the surface with hydroxyl and carboxyl hydrophilic functions. As such, this material can serve as a chemotherapeutic drug carrier. Doxorubicin hydrochloride (DOX), an apoptosis-inducing drug was coated on nanodiamond or embedded into nanodiamond aggregates and introduced into living cells. A stable dispersion of the nanodiamond in water (<100 µg/mL) has been achieved *via* mild ultrasonication. Because the nanodiamond material is negatively charged (NDCOO⁻) and doxorubicin ions (D-NH₃⁺) are cationic, the interaction between nanodiamond material and DOX might have appeared to be straightforward. However, DOX ions were not easily adsorbed by the nanodiamond mixture due to the high aqueous dispersibility of both cations and anions. To yield DOX-ND (doxorubicin hydrochloride-nanodiamond) composites precipitating from their aqueous suspension upon centrifuging, the addition of salts such as NaCl was necessary. Without the addition of NaCl, less than 0.5 wt % of DOX could be adsorbed onto the nanodiamond. Conversely, 10 wt % adsorption of DOX on nanodiamond was achieved with the addition of NaCl (10 mg/mL). Reversible release of DOX from nanodiamond could be achieved by desalination. To check nanodiamond movement as drug carriers into living cells, fluorescent FITC-linked poly-L-lysine was also coated onto the material (10 wt %) *via* a physical adsorption mechanism analogous to the adsorptive mechanism employed for DOX-ND interfacing. The cells were grown with the fluorescent agent modified nanodiamond and many of the fluorescent ND aggregates were detected inside the cells by confocal imaging within 10 h of incubation. The biocompatibility of such modified nanodiamond for use as drug delivery material was investigated *in vitro* by examining the cellular response towards incubation with unmodified precursor nanodiamond. Cell viability during growth in culture media was monitored at 24-72 h, and the response of genes involved in inflammation was also assessed. Specifically, interleukin-6 (IL-6), tumor necrosis factor α (TNF α), and inducible nitric oxide synthase (iNOS) expression were evaluated, which all confirmed sufficient nanodiamond biocompatibility. DOX-ND composites have been applied toward the HT-29 human colorectal cancer cell line. Cell viability assays were done using seeded HT-29 human colorectal adenocarcinoma cells in which nanodiamond was added at a final concentration

¹¹⁶ H. Huang, E. Pierstorff, E. Ōsawa, D. Ho. *Nano Lett.*, **2007**, 7, 3305-3314. Active Nanodiamond Hydrogels for Chemotherapeutic Delivery.

of 25 $\mu\text{g}/\text{mL}$. No difference was seen in cell viability when cells were grown in the presence of unmodified nanodiamond, which supported the biocompatibility of the material.^{117,118} Conversely, in the presence of doxorubicin alone at a concentration of 2.5 $\mu\text{g}/\text{mL}$, or of DOX-ND at concentrations of 2.5 and 25 $\mu\text{g}/\text{mL}$, respectively, a significant decrease of cell viability was observed. The effect of the doxorubicin was attenuated through ND mediated DOX sequestering. Therefore, nanodiamond “*can serve as concentration-tuning substrates that can be interfaced with a chemotherapeutic drug while further serving as stabilization matrices to preserve drug functionality*”,^{116,119} *in vivo* studies confirmed their interest.¹²⁰

A frustrating limitation of detonation nanodiamond modified by adsorption or conjugation of bioactive species is the absence of precise molecular characterization of the hybrid construction. Conversely, functionalized lower diamondoids have been used to build molecularly well-defined composite edifices. Simple adamantane derivatives have long been known for their antiviral activity against Influenza A, and HIV viruses (**Fig. 1.5**).^{121,122} Bio-properties of adamantane derivatives are also associated with central nervous system (against Parkinson’s and Alzheimer’s diseases), and some antimicrobial, anti-inflammatory and antifungal activities have been recognized.^{78,123}

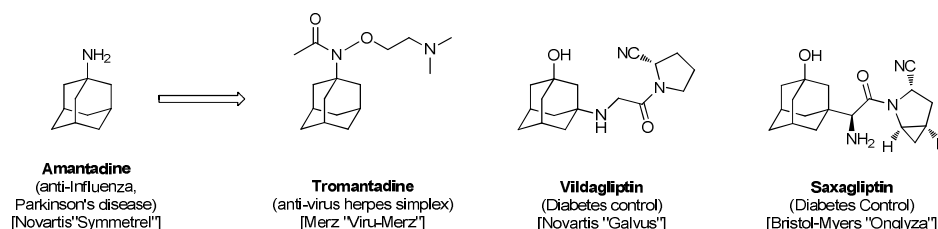


Figure 1.5. Adamantane derivatives with biological activity: from simple Amantadine to polyfunctionalized Saxagliptin.

¹¹⁷ A. M. Schrand, H. Huang, C. Carlson, J. J. Schlager, E. Ōsawa, S. M. Hussain, L. Dai. *J. Phys. Chem. B*, **2007**, 111, 2-7. Are Diamond Nanoparticles Cytotoxic?

¹¹⁸ A. M. Schrand, L. Dai, J. J. Schlager, S. M. Hussain, E. Ōsawa. *Diam. Relat. Mater.*, **2007**, 16, 2118-2123. Differential biocompatibility of carbon nanotubes and nanodiamonds.

¹¹⁹ X. Li, J. Shao, Y. Qin, C. Shao, T. Zheng, L. Ye. *J. Mater. Chem.*, **2011**, 21, 7966–7973. TAT-conjugated nanodiamond for the enhanced delivery of doxorubicin.

¹²⁰ E. K. Chow, X.-Q. Zhang, M. Chen, R. Lam, E. Robinson, H. Huang, D. Schaffer, E. Ōsawa, A. Goga, D. Ho. *Sci. Transl. Med.*, **2011**, 3, 73ra21. Nanodiamond therapeutic delivery agents mediate enhanced chemoresistant tumor treatment.

¹²¹ I. Stylianakis, A. Kolocouris, N. Kolocouris, G. Fytas, G. B. Foscolos, E. Padalko, J. Neyts, E. De Clercq. *Bioorg. Med. Chem. Lett.*, **2003**, 13, 1699-1703. Spiro[pyrrolidine-2,2'-adamantanes]: Synthesis, Anti-Influenza Virus Activity and Conformational Properties.

¹²² See for instance reference 84 and references cited therein.

¹²³ K. Omar, A. Geronikaki, P. Zoumpoulakis, C. Camoutsis, M. Soković, Ana Ćirić, J. Glamočlija. *Bioorg. Med. Chem. Lett.*, **2010**, 18, 426-432. Novel 4-thiazolidinone derivatives as potential antifungal and antibacterial drugs.

Due to the ability of adamantane and its derivatives to attach to DNA, it has been possible to construct well-defined nanostructures consisting of DNA fragments as linkers between adamantane cores. Conversely, only a few derivatives of higher diamondoids have been investigated for biological and pharmaceutical potential use.¹²⁴ Adamantane, diamantane, and triamantane motifs can be introduced into DNA by chemical and enzymatic methods.¹²⁵ This was achieved by the synthesis of diamond-modified triphosphates and phosphoramidites from the lower brominated diamondoids **2**, **12**, and **34** via 1-*O*-diamondoid-yl-4-*O*-propargyltriethylene glycol. These artificial nucleotides were then incorporated into DNA in two ways, either DNA polymerase or automated solid phase synthesis. Remarkably, the β -conformation of DNA double helix is tolerated by the diamond-modified nucleotides.¹²⁵

Organohybrid structures have been studied that combine diamondoids and sugar supramolecular rings cyclodextrins (CDs). Inclusion complexes of CDs can form host-guest pairs for which stability is mainly determined by the shape and hydrophobicity of the guest molecules. Several inclusion complexes of both hydrophilic lower diamondoid-carboxylic acids¹²⁶ and their 5-aminoisophthalic acid derivatives (**Fig. 1.6(a)**, top) with β -CD and γ -CD (7-membered and 8-membered sugar ring molecules, respectively) have been studied and characterized.¹²⁷

Due to their hydrophobicity and symmetry, it was expected that the cages of these diamondoids would be excellent guests for CDs. In addition, no inclusion of the pendant hydrophilic aromatic moiety (R) in the CDs cavity is expected. All modified diamondoids studied have been shown to interact with β -CD, but only the bulkiest ones (mainly triamantanes) interacted with γ -CD. γ -CD is more flexible than β -CD, and in solution the cavity of γ -CD partially collapses. Therefore, its tendency to replace internal hydration water with a suitable hydrophobic guest is significantly reduced. The stoichiometry of host-guest complexes was found to be 1:1 and their interaction is endothermic in each case, with increasingly negative ΔH for the larger diamondoid acids.

¹²⁴ See reference 2 for an overview of the main studies and patented works.

¹²⁵ Y. Wang, B. A. Tkachenko, P. R. Schreiner, A. Marx. *Org. Biomol. Chem.*, **2011**, 9, 7482-7490. Diamondoid-modified DNA.

¹²⁶ N. A. Fokina, B. A. Tkachenko, J. E. P. Dahl, R. M. K. Carlson, A. A. Fokin, P. R. Schreiner. *Synthesis*, **2012**, 259-264. Synthesis of Diamondoid Carboxylic Acids.

¹²⁷ J. Voskuhl, M. Waller, S. Bandaru, B. A. Tkachenko, C. Fregonese, B. Wibbeling, P. R. Schreiner, B. J. Ravoo. *Org. Biomol. Chem.*, **2012**, 10, 4524-4530.

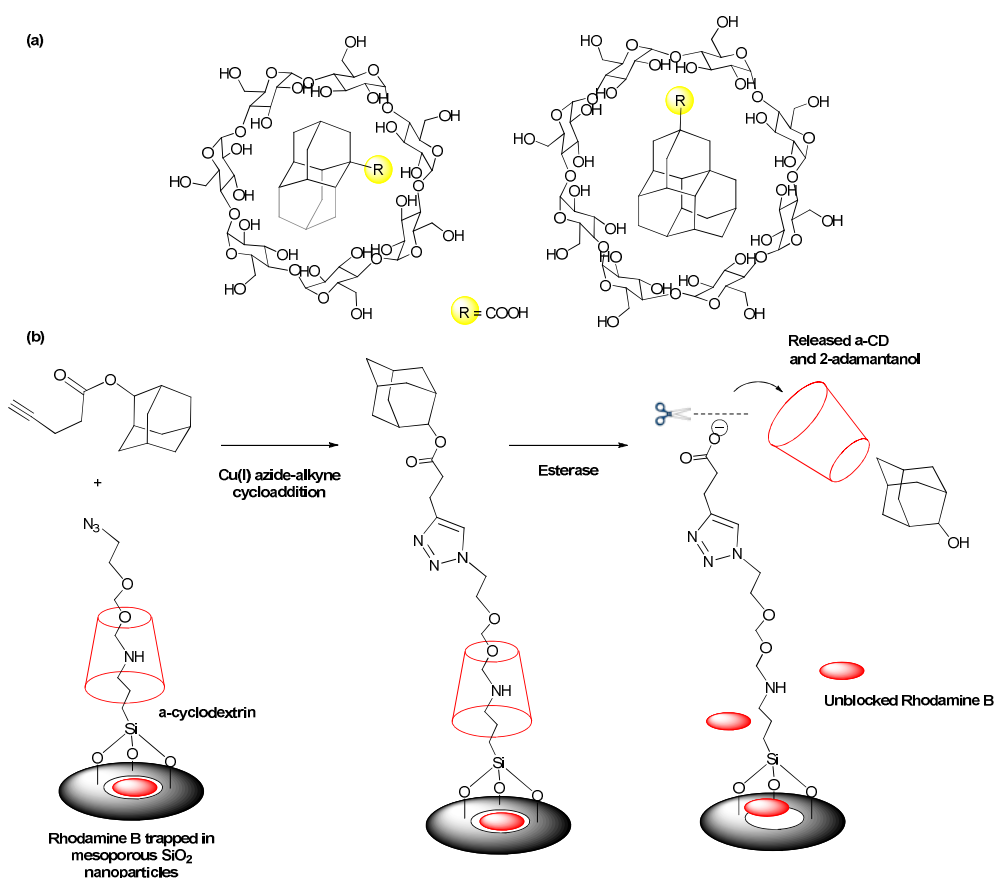


Figure 1.6. (a) Host-guest inclusion complexes with carboxylic acid and peptide derivatives of adamantane, diamantane, and triamantane in β -CD and γ -CD. (b) Enzyme-responsive snap-top covered silica nanocontainers.

From a different “non-inclusive” approach, a nanocontainer was constructed to encapsulate luminescent Rhodamine B and control its release by removal of a snap-top adamantyl ester motif blocking an α -CD (**Fig. 1.6(b)**, bottom).¹²⁸ Azide-modified silica particles can be loaded with Rhodamine B molecules and incubated with α -CD. The α -CD tori thread onto the tri(ethylene)glycol effectively blocked the nanopores, while the azide function serves as a handle to covalently attach an adamantyl stopper group to the snap-top precursors by using a Cu(I)-catalyzed “click” cycloaddition reaction. The hydrolysis of the adamantyl ester stopper resulted in dethreading of the α -CD, and release of the Rhodamine B from the pores. The result of this work is a biocompatible controlled release system that can exploit enzymatic specificity for controlled delivery of small molecules.

¹²⁸ K. Patel, S. Angelos, W. R. Dichtel, A. Coskun, Y.-W. Yang, J. I. Zink, J. F. Stoddart. *J. Am. Chem. Soc.*, **2008**, 130, 2382-2383. Enzyme-Responsive Snap-Top Covered Silica Nanocontainers.

2. Polymeric diamondoid materials

Unsaturated lower diamondoids derivatives have been used for polymerization and copolymerization with the objective of transferring some diamond properties to the polymeric materials obtained.³⁴ 1-Ethynyladamantane, 1,3-diethynyladamantane,¹²⁹ and 1,4-, 4,9- and 1,6-diethynyldiamantane¹³⁰ have been synthesized and oligomerized, polymerized or co-polymerized, to eventually give thermoset resins thermally stable above 450 °C from an adamantane framework, and 500 °C from a diamantane. Diamondoids have been also incorporated as co-monomers which increase the rigidity and thermal stability of light emitting polyolefins.¹³¹ Thus, these polymers show good solubility, and the incorporation of an adamantane unit in the repeating motif significantly increases the T_g and T_d of the polymers. The adamantane unit is an efficient π -conjugation interrupter and prevents interchain interactions. Blue or green light emission and low turn-on voltages were obtained from a single-layer LED fabricated from the polymers.¹³¹

Besides modified polyolefins, several polycondensation polymers such as polyamides and polyimides have also been produced with diamondoids in the main chain.^{132,133} These polymers were respectively obtained from direct polycondensation of 1,3-bis[4-(4-carboxyphenoxy)phenyl]adamantane with various diamines, and from 1,6-bis[4-(4-aminophenoxy)phenyl]diamantane and various aromatic tetracarboxylic dianhydrides. Dynamic mechanical analysis revealed that further incorporation of rigid and bulky diamantane into adamantane-polyamides led to T_g around 300 °C and T_d above 400 °C.¹³² These diamantane-based polyimides exhibit low dielectric constants (2.56-2.78), low moisture absorption (<0.3%), good solubility, and high number-average molecular weights; they can form a tough and transparent film after cyclodehydration.¹³³

In most recent studies, various uses of diamondoid derivatives have been envisioned. 1,3,5,7-Tetrabromoadamantane **5** was employed to synthesize 1,3,5,7-tetrakis(4-aminophenyl)adamantane that was then used as cross-linker for the incorporation of adamantane into a commercial epoxy resin

¹²⁹ T. G. Archibald, A. A. Malik, K. Baum. *Macromolecules*, **1991**, 24, 5261-5265. Thermally Stable Acetylenic Adamantane Polymers.

¹³⁰ A. A. Malik, T. G. Archibald, K. Baum. *Macromolecules*, **1991**, 24, 5266-5268. New High-Temperature Polymers Based on Diamantane.

¹³¹ S. Zheng, J. Shi, R. Mateu. *Chem. Mater.*, **2000**, 12, 1814-1817. Novel Blue Light Emitting Polymer Containing an Adamantane Moiety.

¹³² Y.-T. Chern, H.-C. Shiue, S. C. Kao. *J. Polym. Sci. Polym. Chem.*, **1998**, 36, 785-792. Synthesis and Characterization of New Polyamides Containing Adamantyl and Diamantyl Moieties in the Main Chain.

¹³³ Y.-T. Chern. *Macromolecules*, **1998**, 31, 5837-5844. Low Dielectric Constant Polyimides Derived from Novel 1,6-Bis[4-(4-aminophenoxy)phenyl]diamantane.

network.¹³⁴ A new epoxy material obtained exhibited, as expected, superior thermal properties (high glass transition temperatures) with low dielectric constants in the GHz frequency range. Not only polymers with diamondoids within the main chain backbone can be prepared, but also polymers containing side-chain adamantane.¹³⁵ 1-Adamantylacrylate, 1-vinyladamantane, and 1-diamantylacrylate were employed respectively in atom-transfer radical-polymerization (ATRP), cationic, and free radical polymerization. Soluble colorless polymers of rather low molar masses, containing pendant diamondoid moieties, were synthesized and characterized. The materials exhibited an unusual combination of moderately high refractive index with low optical dispersion, making the polymers potentially applicable as thin film specialty optical plastics.¹³⁵ An even simpler way of using diamondoids in making new polymer materials is to use them as additives; this has been done, for instance, for polypropylene and polycarbonate polymers, for which they can behave as plasticizers or antiplasticizers.¹³⁶

3. Molecular mechanics and electronics innovations from diamond nanoassembly

Higher diamondoids and detonation nanodiamond inherit a lot of the attractive properties of bulk diamond such as superior hardness and Young's modulus, optical properties and fluorescence, high thermal conductivity and electrical resistivity.¹¹⁵ However, degradation in properties can occur when impure or aggregated nanodiamond is used, emphasizing the necessity to control the dispersion of properly functionalized materials. In this respect, the use of diamondoids has been demonstrated to give very innovative applications in molecular mechanics and electronics.

[121]Tetramantane-6-thiol (of the family of diamondoids **148-150**) has been used to form large areas of self-assembled monolayers (SAMs) on silver and gold surfaces (**Fig. 1.7**).¹³⁷ SAMs were prepared in solution at room temperature via self-assembly from ethanol/toluene solution, by immersing the metal surfaces into the solutions for 24-48 h. For SAMs deposited on Au, a layer of 3 nm Ti followed by 100 nm Au was deposited by electron beam evaporation at low pressure onto either Au or Ag substrates with an

¹³⁴ Q. Wei, A. Lazzeri, F. Di Cui, M. Scalari, E. Galoppini. *Macromol. Chem. Phys.*, **2004**, 205, 2089-2096. New epoxy resins cured with tetraaminophenyladamantane (TAPA).

¹³⁵ D. R. Robello. *J. Appl. Polym. Sci.*, **2013**, 127, 96-103. Moderately high refractive index, low optical dispersion polymers with pendant diamondoids.

¹³⁶ A. Ghosh, S. F. Sciamanna, J. E. Dahl, S. Liu, R. M. K. Carlson, D. A. Schiraldi. *J. Polym. Sci. Polym. Phys.*, **2007**, 45, 1077-1089. Effect of Nanoscale Diamondoids on the Thermomechanical and Morphological Behaviors of Polypropylene and Polycarbonate.

¹³⁷ W. L. Yang, J. D. Fabbri, T. M. Willey, J. R. I. Lee, J. E. Dahl, R. M. K. Carlson, P. R. Schreiner, A. A. Fokin, B. A. Tkachenko, N. A. Fokina, W. Meevasana, N. Mannella, K. Tanaka, X. J. Zhou, T. van Buuren, M. A. Kelly, Z. Hussain, N. A. Melosh, Z.-X. Shen. *Science*, **2007**, 316, 1460-1462. Monochromatic Electron Photoemission from Diamondoid Monolayers.

area of approximately 1 cm^2 . Photoelectron spectra of the diamondoid monolayers exhibited a peak at the low-kinetic energy threshold and up to 68% of all emitted electrons were emitted within this single energy peak. With an energy distribution width of about 0.3 electron volts, this source of monochromatic electrons may find application in technologies such as electron microscopy, electron beam lithography, and field-emission flat-panel displays.¹³⁸

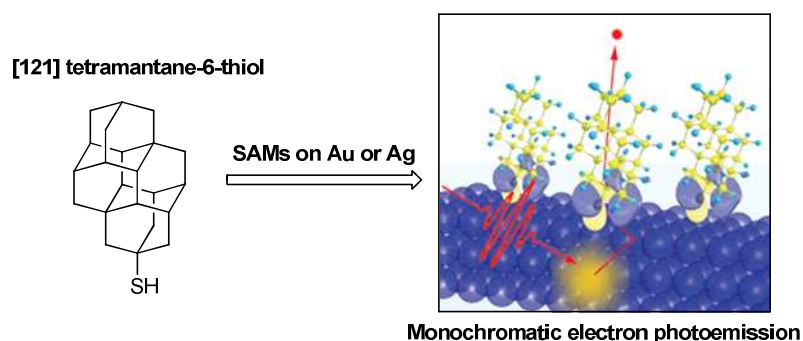


Figure 1.7. Monochromatic electron photoemission from self-assembled monolayers of [121]tetramantane-6-thiol on Au or Ag (*right picture is reproduced with permission from ref. 140, copyright Elsevier publisher*).

This unusual property was explained by negative electron affinity (NEA),^{139,140} in conjunction with strong electron-phonon scattering within the monolayer.¹⁴¹ To demonstrate the peculiar role of a monolayer of functionalized diamondoids as opposed to a thin film of pristine diamondoids, a comparison of [121]tetramantane-6-thiol SAMs with [121]tetramantane films had been also explored.¹³⁷ The spectrum of a [121]tetramantane film shows a small peak at low kinetic energy, in marked contrast with the data for [121]tetramantane-6-thiol. The poor electron conductivity within the thicker films versus that through the monolayers, and the role that the thiol groups play in the SAM samples could be the origin of this difference. In particular, the strong electron emission does not occur solely from the diamondoid surface, but the metal substrate is also intimately involved in the process. By analyzing photoemission

¹³⁸ Electron emitters materials are of interest because electrons emitted into vacuum can be precisely controlled and integrated into devices. One of the challenges in the field is to develop large, uniform surfaces that emit electrons with a sharp energy distribution.

¹³⁹ For electrons the energy level in vacuum is lower than those of diamond conduction bands, meaning that at surfaces with NEA, electrons excited into the conduction band will spontaneously be emitted into vacuum even at low temperature.

¹⁴⁰ S. Roth, D. Leuenberger, J. Osterwalder, J. E. Dahl, R. M. K. Carlson, B. A. Tkachenko, A. A. Fokin, P. R. Schreiner, M. Hengsberger. *Chem. Phys. Lett.*, **2010**, 495, 102-108. Negative-electron-affinity diamond monolayers as high-brilliance source for ultrashort electron pulses.

¹⁴¹ W. A. Clay, Z. Liu, W. Yang, J. D. Fabbri, J. E. Dahl, R. M. K. Carlson, Y. Sun, P. R. Schreiner, A. A. Fokin, B. A. Tkachenko, N. A. Fokina, P. A. Pianetta, N. Melosh, Z.-X. Shen. *Nanoletters*, **2009**, 9, 57-61. Origin of the Monochromatic Photoemission Peak in Diamondoid Monolayers.

spectroscopy data the mean free path for scattering was estimated.¹³⁷ The mean free path measurement demonstrates that diamondoids SAMs do have a much shorter interaction length than most of the known related materials.

In the exciting field of molecular machines, diamondoid structures can have various functions owing to their specific rigidity and sphericity. This is well-illustrated in the pertinent following examples. A modified diamantane, 4,9-bis(4-iodophenyl)diamantane has been used to build one of several nanostructures that emulate macroscopic gyroscopes within a rigid crystalline environment (**Fig. 1.8a**).¹⁴²

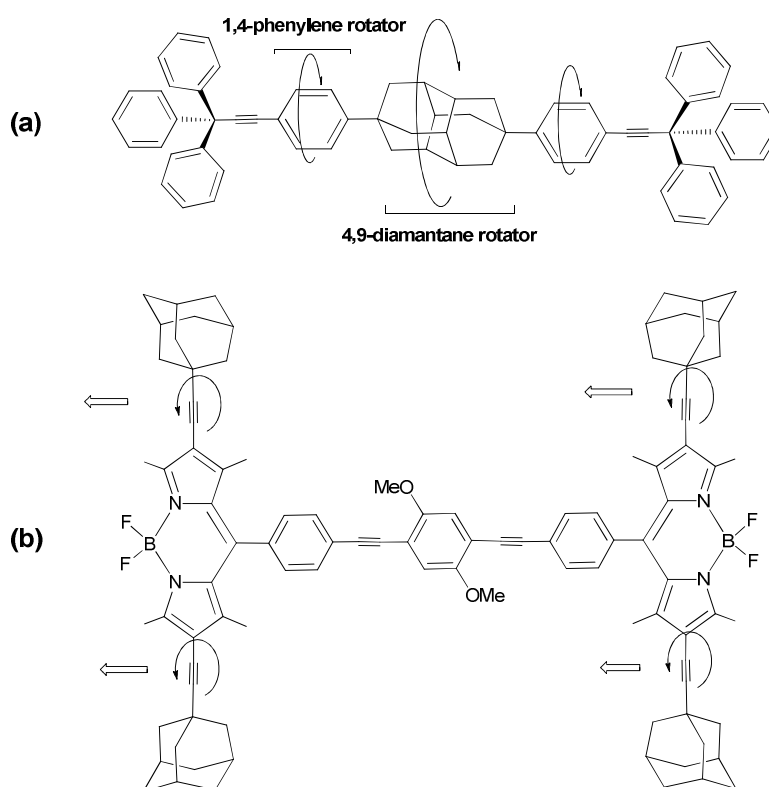


Figure 1.8. Diamondoids in molecular machines: (a) *nanogyroscope* with fast diamantane rotator and (b) highly mobile adamantane-wheeled *nanocars*.

The key elements for the construction of a molecular gyroscope are a rotator, a stator, and an axle that joins them.¹⁴³ Solid state ^2H NMR has shown that the rotary dynamics of nanogyroscopes depend primarily on steric shielding. While structures ending with triptycyls are static, molecular gyroscopes with

¹⁴² S. D. Karlen, R. Ortiz, O. L. Chapman, M. A. Garcia-Garibay. *J. Am. Chem. Soc.*, **2005**, *127*, 6554-6555. Effects of Rotational Symmetry Order on the Solid State Dynamics of Phenylene and Diamantane Rotators.

¹⁴³ S. D. Karlen, M. A. Garcia-Garibay *Top. Curr. Chem.*, **2005**, *262*, 179-228. Amphidynamic Crystals: Structural Blueprints for Molecular Machines.

trityl groups display 180 ° rotation with rates of ca. 500 Hz at 300 K, and compounds with *tert*-butyl-substituted trityl frames reach rates about 100 MHz at the same temperature.¹⁴² The motifs used as rotators can show very different dynamics. Thus, two-fold phenylene and three-fold adamantane rotators were first deduced by comparison of a normal ¹³C CP-MAS spectrum and one acquired with dipolar dephasing at 25 °C. It was shown that despite their proximity and sharing a close environment, the adamantane group rotates ca. 20,000 times faster than the phenylenes at 300 K. These observations support the notion that the more cylindrical high order rotators should have much faster rates in solids.

In the search for miniaturizing devices and machines, a family of “nanovehicles” termed “nanocars” has been developed which can translate on surfaces with controlled directionality. These “nanocars” in comparison with their macroscopic analogues also consist of a chassis, axles, and wheels. The synthesis of fluorescent nanocars equipped with adamantane wheels was reported (**Fig. 1.8b**),¹⁴⁴ and their behaviors were analyzed by single-molecule imaging SMFM, single-molecule fluorescence microscopy). The nanocars were imaged using 4,4-difluoro-4-bora-3a,4a-diaza-s-indacene (BODIPY) as the chromophore. The BODIPY was rigidly incorporated into the molecule chassis via acetylenic cross-coupling. For the adamantane four-wheeled nanocar, the percentage of moving nanocars and the diffusion constant show a significant improvement over *p*-carborane-wheeled nanocars with the same chassis.¹⁴⁴ The mobility of the nanocars was determined from fluorescence images taken as a function of time. Each series of time-lapse images contained twenty frames and was analyzed taking into account phenomenon of photo blinking and photo bleaching of fluorescent molecules. The interaction energy between the chosen wheels (diamondoid or carborane) and the glass substrate determines the mobility of the nanocars (weak van der Waals forces or hydrogen bonding, respectively). The final results are consistent with a wheel-like rolling motion associated to the sphericity of adamantane.

4. Synthetic and catalytic applications associated to modified diamondoids

The synthetic applications of diamondoids in catalysis are promising since the existing examples of decorating phosphines with adamantyl^{145,146} or diamantyl¹⁴⁷ fragments have given spectacular results in

¹⁴⁴ P.-L. E. Chu, L. Y. Wang, S. Khatua, A. B. Kolomeisky, S. Link, J. M. Tour. *ACS Nano*, **2013**, 7, 35-41. Synthesis and Single-Molecule Imaging of Highly Mobile Adamantane-Wheeled Nanocars.

¹⁴⁵ A. Tewari, M. Hein, A. Zapf, M. Beller. *Tetrahedron*, **2005**, 61, 9705-9709. Efficient palladium catalysts for the amination of aryl chlorides: a comparative study on the use of phosphonium salts as precursors to bulky, electron-rich phosphines.

¹⁴⁶ L. Ackermann. *Org. Lett.*, **2005**, 7, 3123-3125. Phosphine oxides as pre-ligands in ruthenium-catalyzed arylations via C–H bond functionalization using aryl chlorides.

terms of catalytic efficiency and scope. The bulky electron-rich framework provided by these sp^3 -C polyalkyl fragments is highly useful for activating valuable chloride substrates, in cross-coupling reactions. The stability conferred by the carbon cages provides also metal catalytic systems with an enhanced life-time even at high temperature in solution, or under gas high pressure. In line with these results, decorating carbenes with diamondoid fragments for catalysis has been also briefly investigated.¹⁴⁸

Organocatalysts incorporating adamantane have also been proven highly promising. In particular, the chiral tetrapeptide platform (**A**) incorporating an artificial aminoacid, γ -aminoadamantanecarboxylic acid, is an efficient organocatalyst for enantioselective kinetic resolution of *trans*-cycloalkane-1,2-diols (**Fig. 1.9**, left).¹⁴⁹ The kinetic resolution of chiral *trans*-cycloalkane-1,2-diols is challenging and limitations exist even with enzymatic approaches. The tetrapeptide **A**, synthesized by automated solid-phase peptide-coupling methods, stereoselectively transfers acyl groups onto *trans*-cycloalkane-1,2-diols with enantiomeric excess above 99%.

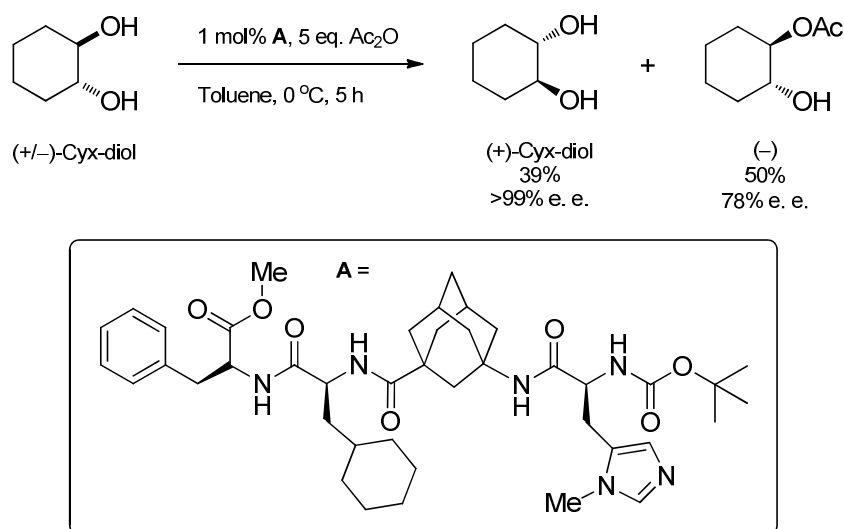


Figure 1.9. Chiral tetrapeptide platform (**A**) incorporating γ -aminoadamantane carboxylic acid as organocatalyst for enantioselective kinetic resolution of *trans*-cycloalkane-1,2-diols.

¹⁴⁷ G. Eastham, N. Tindale. *PCT Int. Appl.*, **2005**, WO 2005079981 A1 20050901. Catalyst system for carbonylating ethylenically unsaturated compounds.

¹⁴⁸ H. Richter, H. Schwertfeger, P. R. Schreiner, R. Fröhlich, F. Glorius. *Synlett.*, **2009**, 2, 193-197. Synthesis of Diamantane-Derived N-Heterocyclic Carbenes and Applications in Catalysis.

¹⁴⁹ C. E. Müller, L. Wanka, K. Jewell, P. R. Schreiner. *Angew. Chem. Int. Ed.*, **2008**, 47, 6180-6183. Enantioselective Kinetic Resolution of *trans*-Cycloalkane-1,2-diols.

This chemical kinetic resolution currently provided some remarkably high selectivity for such a reaction, and this derives from the rigid and lipophilic adamantyl γ -amino acid. A structural selectivity model was determined from a molecular dynamics search for low-lying conformations of the organocatalyst/acylium ion adduct. The *N*- π -methylhistidine moiety is responsible for the acyl transfer while the hydrophobic proximal groups provide some key interactions with the substrate.

The absence of secondary structure in the free catalyst strongly suggests that the determining factors for stereoselection are established within the complex formed from the charged acylium ion and the peptide catalyst: the two homochiral C* stereogenic centers determine the final stereochemistry.

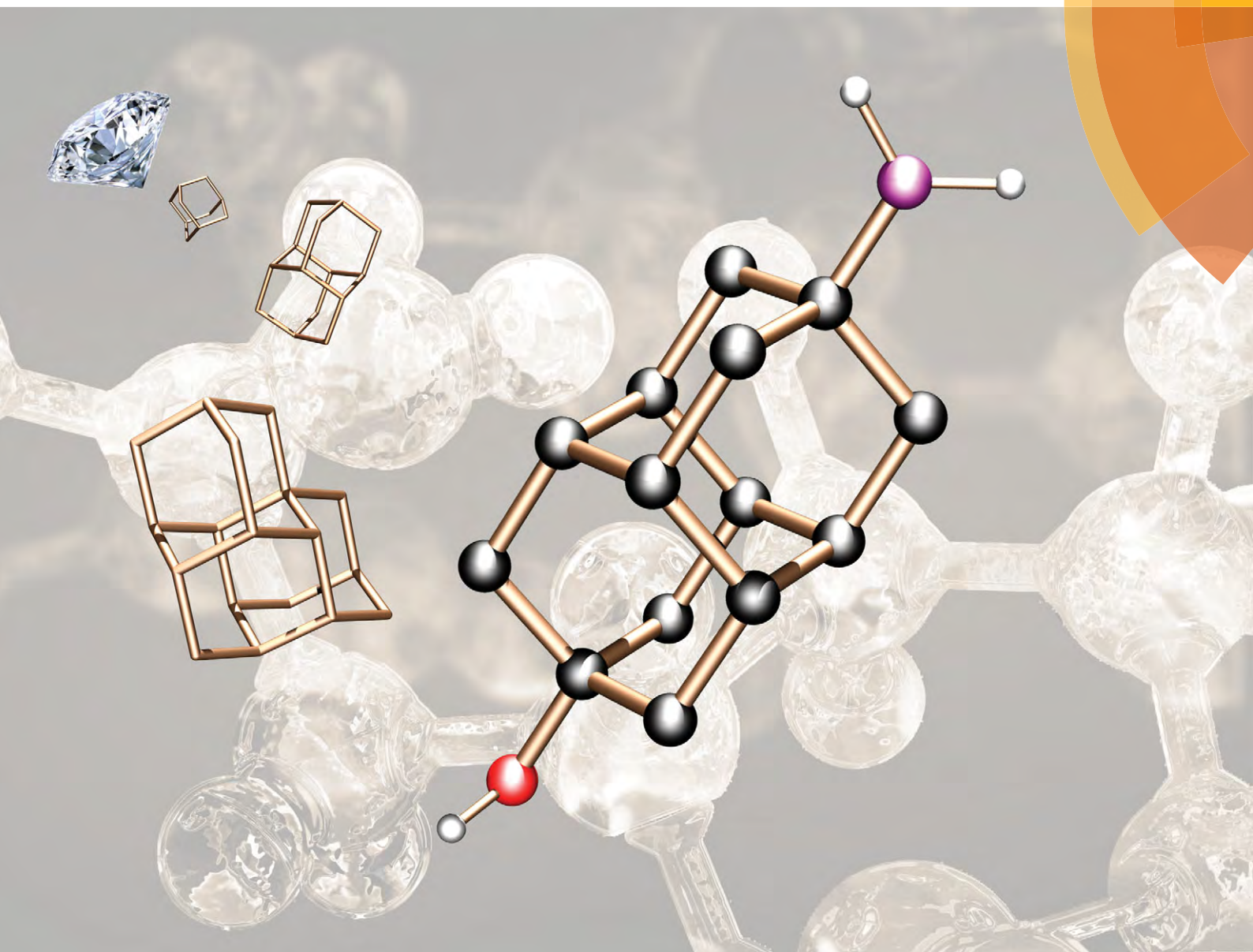
1.5. Conclusion

Synthetic modifications of adamantane and diamantane are well developed. Their applications have covered multidisciplinary studies, including fields such as biology, materials, electronics, and catalysis. Therefore the versatility of diamondoids has been already largely proven, and further exciting development are achievable. The present bibliographical chapter constitutes a valuable foundation for the carbon-metal organohybrid construction we aim based on functionalized diamondoids.

NJC

New Journal of Chemistry
www.rsc.org/njc

A journal for new directions in chemistry



ISSN 1144-0546



ROYAL SOCIETY
OF CHEMISTRY

PERSPECTIVE

Jean-Cyrille Hierso, Peter R. Schreiner *et al.*
Diamondoids: functionalization and subsequent applications of perfectly defined molecular cage hydrocarbons



Diamondoids: functionalization and subsequent applications of perfectly defined molecular cage hydrocarbons

Cite this: *New J. Chem.*, 2014, 38, 28

Maria A. Gunawan,^{ab} Jean-Cyrille Hierso,^{*ac} Didier Poinso,^a Andrey A. Fokin,^{bd} Natalie A. Fokina,^b Boryslav A. Tkachenko^b and Peter R. Schreiner^{*b}

Received (in Montpellier, France)
18th May 2013,
Accepted 17th September 2013

DOI: 10.1039/c3nj00535f

www.rsc.org/njc

The term “diamondoid” describes cage hydrocarbon molecules that are superimposable on the diamond lattice. Diamondoids that are formally built by face-fusing of adamantane units, namely diamantane, triamantane, tetramantane, etc., have fascinated chemists since the beginning of the last century. The functionalization of these perfectly defined (C,H)-molecules is described here. Thus, diamondoid halides and diamondoid alcohols are first rank precursors for amino and phosphine-substituted diamondoids that have proved to be highly useful in therapeutic applications and metal catalysis, respectively. The extent of functionalization and polyfunctionalization achieved for adamantane and diamantane, and the synthesis and applications of the resulting organohybrids are illustrated, revealing their high potential in fields such as organocatalysis, polymers, molecular electronics and mechanics.

^a *Université de Bourgogne, Institut de Chimie Moléculaire de l'Université de Bourgogne (ICMUB), UMR CNRS 6302, 9 avenue Alain Savary, 21078 cedex, Dijon, France. E-mail: hiersojc@u-bourgogne.fr; Fax: +33 (0)38039 3682; Tel: +33 (0)38039 6107*

^b *Institut für Organische Chemie, Justus-Liebig-Universität, Heinrich-Buff-Ring 58, 35392 Giessen, Germany. E-mail: prs@uni-giessen.de; Fax: +49 641 99 34309; Tel: +49 641 99 34300*

^c *Institut Universitaire de France (IUF), France*

^d *Department of Organic Chemistry, Kiev Polytechnic Institute, pr. Pobedy 37, 03056, Kiev, Ukraine*

1. Introduction

Nanometre-sized particles possessing a perfect diamond cubic lattice are fascinating molecules that have recently been employed for applications that span the fields of organic and inorganic chemistry, physics, materials science, bioengineering, medicine and beyond.^{1–3} The term “diamondoid” has been used to name cage hydrocarbon molecules of a size larger than adamantane (C₁₀H₁₆) that are totally or mostly superimposable



Maria A. Gunawan

Maria A. Gunawan was born in Malang (Indonesia). She studied chemistry at Clermont-Ferrand's Superior National School of Chemistry and achieved in 2010 both an engineering degree and a master's degree from Blaise Pascal University in Clermont-Ferrand. She is now an international PhD student under the joint supervision of Prof. Jean-Cyrille Hierso (Dijon, France) and Prof. Peter R. Schreiner (Giessen, Germany) on the topic of diamondoids functionalization and metallization.



Jean-Cyrille Hierso

Jean-Cyrille Hierso was born in Toulouse (France) in 1971. He is Full Professor of Chemistry, heading the group of “Organometallic Chemistry and Catalysis” in the Institute of Molecular Chemistry at the University of Burgundy (Dijon, France). He is interested in metals and ligands chemistry, catalysis, and nanomaterials. In 2011 he was awarded the Prize for Coordination Chemistry from the French Chemical Society (SCF). In 2012 he received the EurJIC Young Researcher Award and he was appointed Member of the Institut Universitaire de France (IUF). He shares with his friend Peter R. Schreiner a passion for nanodiamonds (less expensive for girls. . .).

on the cubic diamond lattice.⁴ In this context most diamondoids are unique hydrocarbon nanostructures that can be described as fully hydrogen-terminated nanometre-sized diamonds (Scheme 1), and they have rightly been termed *nanodiamonds* (or *molecular nanodiamonds*), as opposed to *detonation nanodiamond*^{2,3} for which a clearly defined surface functionalization is particularly challenging. Thus, among diamondoids the family of polymantanes includes molecules that can only be formed by the face-fusing of adamantane units, sharing six carbon atoms per pair of adamantane units. The polymantanes form a series of which the smallest molecules are called *lower diamondoids*. For adamantane through triamantane the general formula ($C_{4n+6}H_{4n+12}$) does not comprise isomers whereas the next higher member of this series ($C_{22}H_{28}$) corresponds to four tetramantane stereoisomers (Scheme 1), including one pair of enantiomers. Diamondoids are very stable and possess carbon atoms of different but precisely defined “environments” (as exemplified in Scheme 1 with diamantane). As a consequence, their surface functionalization is expected to be conducted accurately by chemical means.

The Baeyer system is used for IUPAC naming of polycyclic hydrocarbons, including diamondoids and polymantanes.⁵ For naming polymantanes, which are regularly repeating fused adamantane units, the Baeyer system can be advantageously substituted by a nomenclature introduced by Balaban and Schleyer.⁴

Indeed, for instance, diamantane is named pentacyclo-[7.3.1.1.^{4,12}.0.^{2,7}0^{6,11}]tetradecane in the Baeyer system. In contrast, Balaban and Schleyer nomenclature system is based on graph theory and thus considers a step by step growth of adamantane cages. With this convenient convention the first lower diamondoids, after adamantane, are named [1]diamantane, [12]triamantane and [121]tetramantane (*anti*-tetramantane), and the higher diamondoids are easily pictured following the vectors indicated in brackets for adding further cages; this was nicely illustrated recently by Filik.⁶

From a historical perspective, adamantane was identified in 1933 from a sample of petroleum collected in Czechoslovakia.⁷ It was a real breakthrough for alkane chemistry when Landa showed that adamantane reacts with neat bromine at room temperature to give the tertiary monobromo derivative almost quantitatively.⁸ Efficient synthetic preparation of lower diamondoids has been reported for adamantane⁹ and for diamantane;^{10,11} the latter hydrocarbon was also isolated from petroleum.¹² In 1966 the challenging synthesis of triamantane was also reported.¹³ The first higher diamondoid was synthesized in 1976: *anti*-tetramantane (= [121]tetramantane) received this name from its structural similarity to butane in its *anti*-conformation.¹⁴ Schleyer reported a perspective on this period of synthetic success, which has ended with the synthetic attempts of higher diamondoids.¹⁵ Synthetic efforts for higher



Natalie A. Fokina

Natalie A. Fokina was born in Kiev (Ukraine). She studied chemistry at the National Technical University of Ukraine “Kiev Polytechnic Institute”, and after obtaining her MS (1983) she worked as a production designer at Scientific Technological Institute of Domestic Chemistry (Kiev). She obtained a PhD (2002) in Bioorganic Chemistry at the Institute of Bioorganic Chemistry and Petrochemistry NAS of Ukraine and there served

as Deputy Head of the Department of Fine Organic Synthesis. Since 2004 she has been working in the group of P. R. Schreiner as a research associate. She is the author of 25 publications on the chemistry of cage compounds and chemo-enzymatic approaches to the synthesis of fluorinated amino acids.



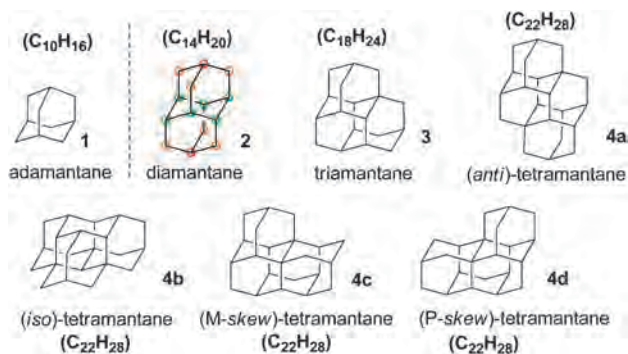
Andrey A. Fokin

Andrey A. Fokin is a Head of the Department of organic chemistry at the National Technical University of Ukraine “Kiev Polytechnic Institute”. He obtained his Candidate (1985) and Doctor of Chemical Sciences (1995) degrees from this institution. He was a DAAD (1996) and Alexander von Humboldt (1997–1998) research fellow in the group of Professor P. v. R. Schleyer at the University of Erlangen-Nürnberg (Germany).

He is the author of over 150 publications on the chemistry of cage compounds, pesticide chemistry, alkane activation mechanisms, computational chemistry of radicals and radical ions, and the generation and transformations of hydrocarbon radical cations.

Didier Poinsot was born in Strasbourg (France) in 1972. He studied physical chemistry at the University Louis Pasteur of Strasbourg (master's degree in thin film materials, 1998). He became assistant engineer in CNRS, at the University of Burgundy (1999), and is in charge of the “Catalytic tests under pressure laboratory” in the Institute of Molecular Chemistry. He joined with enthusiasm the French-German cooperation team built in 2011 around “nanodiamonds for chemical vapour deposition”.

Boryslav A. Tkachenko was born in Kyiv (Ukraine) in 1976. He studied chemistry at the National Technical University of Ukraine “Kyiv Polytechnic Institute” (Ukraine) where he received his MS (1999) and Candidate of Chemical Sciences (2003, PhD) degrees in Organic Chemistry. Currently he is a research associate in the group of P. R. Schreiner and a member of the diamondoid research team.



Scheme 1 Lower diamondoids: polymantanes (2–4d) are built by face-fusing of adamantane (1) units.

diamondoids preparation *via* carbocation rearrangements similar to those successfully devised to prepare the lower diamondoids failed,¹⁶ apparently blocked by the large number of possible intermediates and the complex reaction pathways involved in the processes. Nevertheless, higher diamondoids up to hexamantane ($C_{30}H_{36}$) have been shown to exist in petroleum on the basis of gas chromatography/mass spectrometry analysis.¹⁷ It was suggested later that diamondoids may occur largely in all petroleum sources and thus may be used as decisive indicators of natural oil cracking.¹⁸ The breakthrough evidence of diamondoids' ubiquity in oils and fuels was provided in 2003 through the isolation and identification of twenty-one different higher polymantanes by HPLC techniques.¹⁹ Additionally, there is a method akin to chemical vapour deposition that yields higher diamondoids, albeit in low yields.²⁰ Lower diamondoids are low-strained, and kinetically as well as thermodynamically very stable. These characteristics are accompanied by high melting points in comparison to other hydrocarbons; for adamantane, diamantane and tetramantane, melting points are estimated between 220 and 270 °C (they fairly easily sublime at



Peter R. Schreiner

serves also as Vice President for Research. P. R. Schreiner received the Dirac Medal (2003) and the ADUC-Prize (1999). He was bestowed with honorary lifetime memberships of the Israel (2009) and the Polish (2013) Chemical Society. In 2013 he became a member of the German National Academy of Science (Leopoldina). In the little spare time he has, he enjoys playing fierce tennis matches and loud rock music.

Peter R. Schreiner (b. 1965) studied and received his Dr. rer. nat. (1994) in organic chemistry at the University of Erlangen-Nürnberg (Germany) and a PhD (1995) in Computational Chemistry from the University of Georgia (UGA), USA. He was assistant professor in Göttingen and associate professor at UGA before accepting the chair of organic chemistry at the Justus-Liebig University Giessen (Germany) in 2002, where he

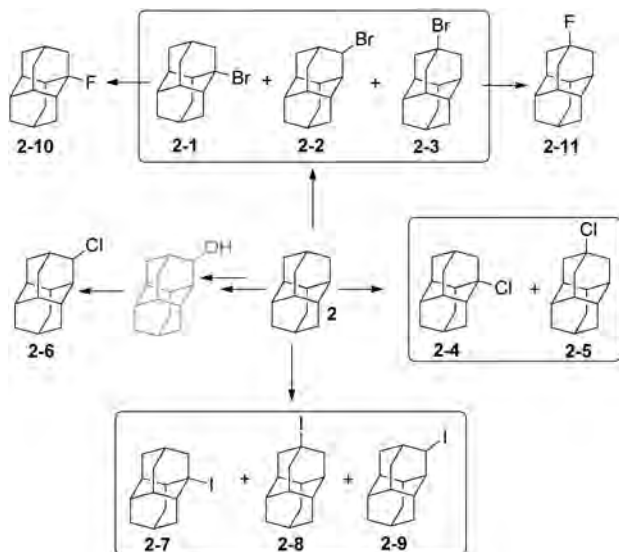
room temperature under normal or low pressure). Solubility limits of adamantane and diamantane in liquid organic solvents at 25 °C (alkanes, benzene, *etc.*) have been reported.²¹ Commonly used spectroscopic methods to analyse diamondoids are NMR, FT-IR and Raman spectroscopy;⁶ Raman spectra of lower diamondoids have been reported.²² The vibrational spectra of diamondoids have been compared with macroscopic diamond entities such as nanocrystalline and bulk diamond.²³ A significant difference is found in the CCC deformation vibration corresponding to “cage-breathing” modes, which produce the highest intensity Raman signals in the spectral region below 800 cm^{-1} .

Stimulated by the perspective of a transposition of the properties of diamond in the nanoscale range, a large body of work has been devoted to the development of methods to selectively and efficiently functionalize diamondoids. These efforts have generated a great number of molecules having high potential for applications in biology, polymer chemistry, molecular electronics, molecular mechanics, synthesis and catalysis. We review herein the most practical functionalizations of lower diamondoids together with the related applications of the resulting compounds in the transdisciplinary fields mentioned above.

2. Direct functionalization of diamondoids

2.1 Halogenation

The functionalization of adamantane (1) is more selective than for polymantanes because there are only two different types of C–H bonds (Scheme 1). Monofunctionalized adamantane derivatives at a bridgehead tertiary carbon with all possible halides have been reported.^{24–26} Bromination and dibromination of 1 with Br_2 in the absence or presence of aluminum Lewis catalyst leads directly to 1-bromoadamantane (1-1) and 1,3-dibromoadamantane, respectively.²⁷ The bromination of diamantane (2) is a more intricate process (Scheme 2). When using Lewis acid catalysts the conditions have to be tuned to improve the selectivity for one of the three isomers obtained: 2-1, 2-2 and 2-3. Neat Br_2 selectively gives 1-bromodiamantane (2-1) in 80% yield,^{28,29} while the apical isomer 4-bromodiamantane (2-3) forms in the presence of traces of $AlBr_3$ with *tert*-butyl bromide in 58% yield albeit in a mixture with 2-1.²⁹ Radical bromination of diamantane under phase transfer catalytic (PTC) conditions with CBr_4 and $NaOH/n-Bu_4NBr$ predominantly gives 2-1 (56%), some 2-3 (23%) and traces of the secondary-C functionalized 3-bromodiamantane (2-2) (11%).³⁰ The latter can be prepared in 47% overall yield in two steps from 3-diamantanone.³¹ A mixture of 1-chlorodiamantane (2-4) and 4-chlorodiamantane (2-5) ensues in moderate yield (25%) from the reaction of 2 with CrO_2Cl_2 in CCl_4 , with 1-hydroxydiamantane as the side product.³² The synthesis of secondary-C functionalized 3-chlorodiamantane (2-6) is possible in three steps from 2 *via* 3-diamantanol formation followed by chlorination with $SOCl_2$ (yield 49%).³³ 1-Iododiamantane (2-7), 4-iododiamantane (2-8) and 3-iododiamantane (2-9) form in the direct iodination of 2 under PTC conditions with CHI_3 and $NaOH$ in CH_2Cl_2 .³⁰ Compound 2-7 is the major halide formed in 39% yield. Fluorodiamantanes 2-10



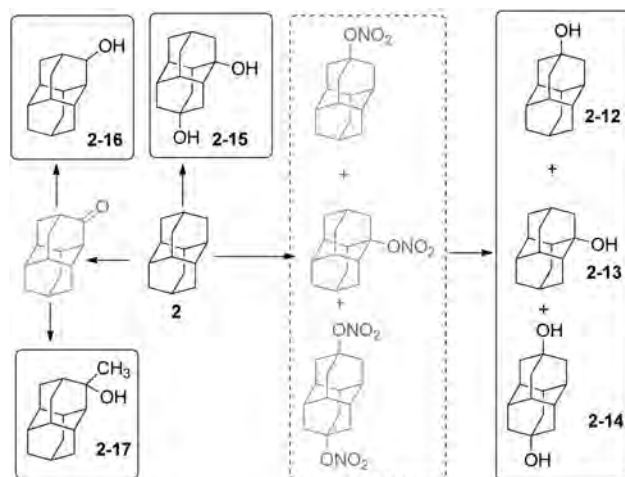
Scheme 2 Diamantylhalides 2-1–2-11.

and 2-11 are obtained in excellent yields from the corresponding bromides 2-1 and 2-3, respectively; AgF is used as the fluorinating agent in cyclohexane, and alternatively the corresponding hydroxylated diamantanes can also be used as precursors for reactions with diethylaminosulfur trifluoride (DAST).³⁴

Triamantane, tetramantane, and pentamantane bromides and fluorides have been also synthesized.³⁵ Fluorotriamantanes are obtained by treatment of hydroxylated analogues³⁶ with DAST.³⁴ From *anti*-tetramantane treated with Br₂ the access to dibrominated analogue is possible in a modest 17% yield.³⁶ [1(2,3)4]-Pentamantane is the higher diamondoid which has been efficiently functionalized with halides and surprisingly reacts more selectively with electrophiles than triamantane and *anti*-tetramantane. This pentamantane gives in multistep reactions overall yields of 25 to 75% of mono- or dibrominated products.³⁷

2.2 Hydroxylation

The hydroxy derivatives of 1 can be obtained either by hydrolysis of the corresponding halides or by direct functionalization of 1; mono-, di- and tetrahydroxylated adamantanes have been made.^{38–40} Scheme 3 summarizes the main methods for the preparation of hydroxylated diamantanes. 1-Hydroxydiamantane (2-13) forms in 23% to 82% yield upon treatment of 2 with various oxidants (*m*-chloroperbenzoic acid, Pb(OAc)₄, dimethyldioxirane, nitric acid), among which HNO₃ is the most efficient.^{32,36} Concomitant formation of 4-hydroxydiamantane (2-12) and 4,9-dihydroxydiamantane (2-14) in low yields (5–13% and 6–11%, respectively) generally occurs; these can be separated by silica gel chromatography. 1,4-Dihydroxydiamantane (2-15) can be synthesized *via* treatment of 2 with HNO₃ *via* 1,4-dinitroxydiamantane as an isolatable intermediate (overall yield of 2-15: 30%).³⁶ Other hydroxy derivatives can be obtained such as the species functionalized on a secondary-C 2-16 and 2-17.^{31,33} 2-Methyldiamantan-2-ol (2-17) is accessible in 93% yield from a Grignard reaction of 2-diamantanone; the latter

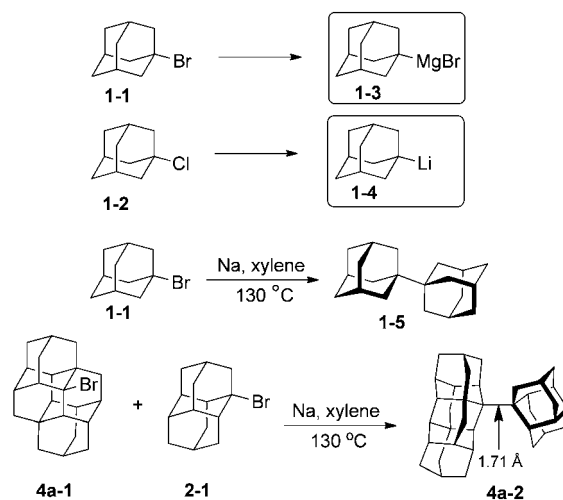


Scheme 3 Diamantans 2-12–2-17.

can alternatively be reduced by LiAlH₄ for the formation of 2-16 (73%). The oxidation of triamantane (3) with HNO₃ is also appropriate to produce the mono- or dihydroxylated analogues.³⁶ Conditions to yield the monohydroxylated^{35,41} and dihydroxylated [121]tetramantanes have been reported *via* the hydrolysis of bromide or nitroxy precursors.^{37,42} Similarly, the mono- and dihydroxylated [1(2,3)4]pentamantanes can be obtained.³⁷

2.3 Metallation and coupling

A limited number of metallated diamondoids have been prepared, mainly from adamantane (1) (Scheme 4). Grignard reagent 1-adamantylmagnesiumbromide (1-3) has been obtained in 60% yield from the reaction of 1-bromoadamantane 1-1 with an excess of magnesium in the presence of BrCH₂CH₂Br in Et₂O and *n*-Bu₂O; THF was found to be unsuitable.⁴³ 1-Adamantyl lithium (1-4) and its congeners 2-adamantyl lithium as well as 1-diamantyl lithium have been directly synthesized from the reactions of their chloride precursors with lithium metal in pentane (82, 85 and 76% respectively).⁴⁴ In these reactions the



Scheme 4 Metallated diamondoids and (homo)coupling reactions.

control of the metal–solution interface is crucial to avoid diamondoid homologation.

Metallated derivatives are intermediates in the diamondoid couplings with sodium (Wurtz reaction). Simplest coupled 1,1-diadamantyl (1-5) resembles part of the diamond lattice and may be viewed as a diamondoid of larger size. Recently prepared coupled higher diamondoids represent even larger nanodiamond particles and contain extremely long C–C bonds.⁴⁵ For instance coupling of the respective bromo derivatives of adamantane 2-1 and tetramantane 4a-1 gives diamondoid 4a-2, which contains the C–C bond of 1.71 Å lengths, the longest so far observed in alkanes.⁴⁶ Despite pronounced geometrical distortions coupled diamondoids display high thermal stabilities.

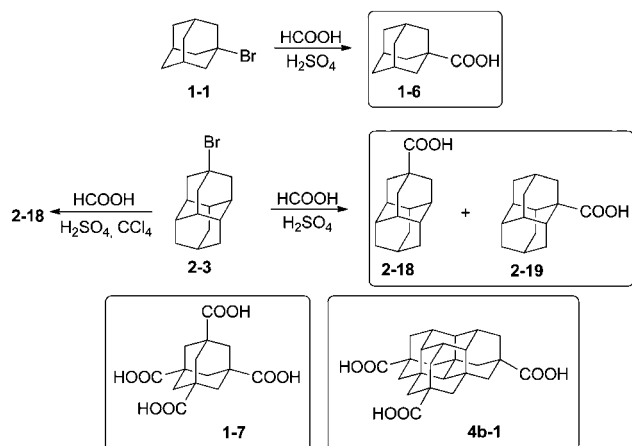
2.4 Carboxylation

The preparation of 1-adamantane carboxylic acid (1-6) utilizes the Koch–Haaf reaction of adamantane derivatives with formic acid in sulfuric acid.⁴⁷ The carboxylation of adamantane derivatives is accompanied by an intermolecular hydride transfer reaction, which results in the formation of a mixture of apical and medial adamantane carboxylic acids. The selective conversion of the 4-bromodiamantane (2-3) to the adamantane-4-carboxylic acid (2-18) is possible under high dilution conditions that prevent the intermolecular hydrogen exchange (Scheme 5).⁴⁸

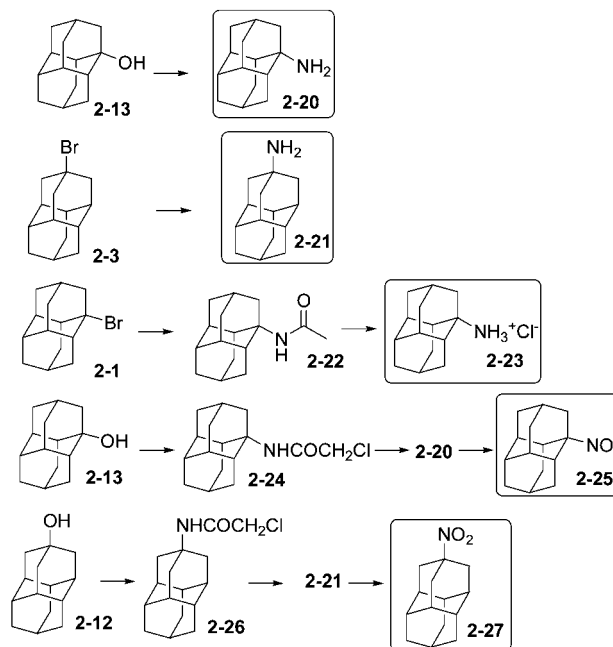
The Koch–Haaf carboxylation was recently applied for the preparation of triamantane, tetramantane, and pentamantane carboxylic acids in good yields.⁴⁹ The diamondoid polycarboxylic acids are useful as 3D-building blocks, and can be prepared through C–H-photocarbonylation or, better, through hydrolysis of the corresponding nitriles, as was demonstrated in the preparation of adamantane-1,3,5,7-tetracarboxylate (1-7).⁵⁰ For higher diamondoids direct Koch–Haaf carboxylation allows preparation of [1(2)3]tetramantane-7,11,17-tricarboxylate (4b-1), which can be used as a building block for various tripodal rigid surface anchors.⁵¹

2.5 Amination, amidation, and nitration

The development of acetamide and amine derivatives of adamantane has been motivated by their pharmacological applications that have been recently reviewed.⁵² Monoaminodiamantanes



Scheme 5 Diamondoid carboxylic acids 1-6–4b-1.

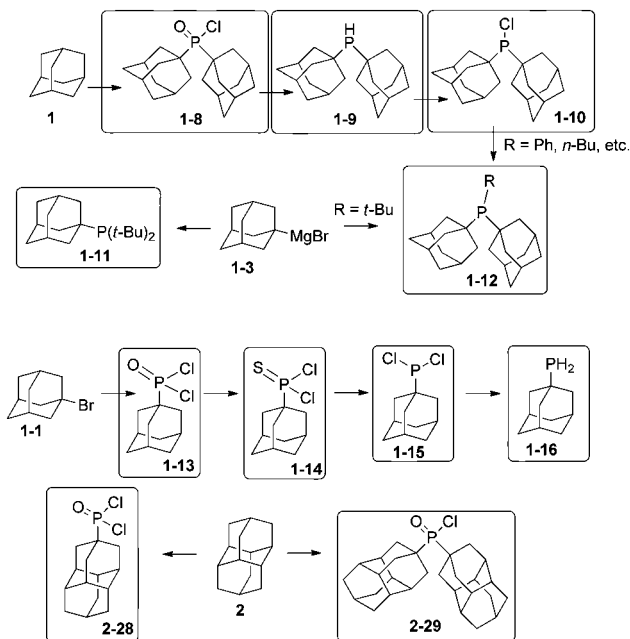


Scheme 6 Amino-, amido-, and nitrodiamantanes 2-20–2-27.

(Scheme 6) and their derivatives have been prepared from adamantane (2), *via* 1-bromodiamantane (2-1), 4-bromodiamantane (2-3), 1-hydroxydiamantane (2-13), and 4-hydroxydiamantane (2-12). Compounds 2-13 and 2-3 can be converted in one step to the corresponding carboxylic acids, which further form intermediary carbamates that can then be hydrolysed to 1-amino- and 4-aminodiamantane (2-20) and (2-21) with overall yields of about 20% and 40%, respectively.⁵³ 1-Bromodiamantane (2-1) gives 1-acetamidodiamantane (2-22) by a Ritter reaction (using $\text{CH}_3\text{CN}/\text{H}_2\text{SO}_4$), 2-22 after hydrolysis forms 2-23 as the hydrochloride salt of 2-20 (overall yield 55%).⁵³ Aminodiamantanes 2-20 and 2-21 form in good yields (63 and 93%, respectively) by acidic exchange of the hydroxyl groups of adamantanol 2-13 and 2-12, respectively: treatment with chloroacetonitrile– H_2SO_4 in acetic acid gives 2-24 and 2-26, which can be cleaved in the presence of thiourea.⁵³ Aminodiamantanes 2-20 and 2-21 react with *m*-chloroperbenzoic acid in dichloroethane to give the nitro-functionalized compounds 2-25 and 2-27 in 74% yield.⁵⁴ 4,9-Diamino- and dinitrodiamantane have been also described.^{53,54}

2.6 Phosphorylation and phosphination

Diamondoids substituted with alkyl phosphines are ligands for transition metals with exceptional properties. Adamantane (1) can be used for the formation of di(1-adamantyl)phosphinic acid chloride (1-8), which provides access to the organophosphorus compounds di(1-adamantyl)phosphine (1-9) and di(1-adamantyl)chlorophosphine (1-10) (Scheme 7).⁵⁵ They are obtained in excellent yields of above 85% on a scale of several grams. Compound 1-10 is ideal for generating trialkyl phosphine 1-12.^{56–58} Another synthetic pathway to adamantylalkylphosphines is the reaction of halophosphines with the precursor adamantyl magnesium bromide 1-3,⁴³ which gives the monoadamantylphosphine 1-11 in excellent 86% yield, but the diadamantyl analogue 1-12 only in

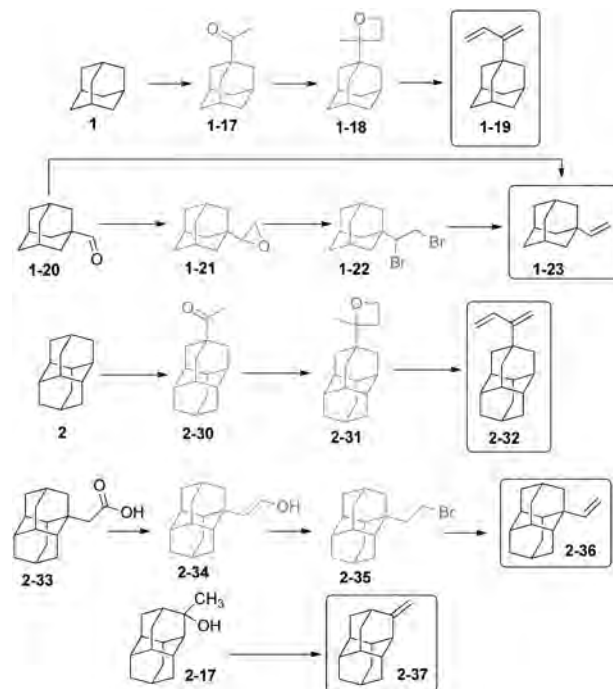


Scheme 7 Phosphorus-substituted adamantanes and diamantanes **1-8-1-16** and **2-28, 2-29**.

moderate 30% yield.⁵⁹ 1-Bromoadamantane (**1-1**) treated with a large excess of PCl_3 in the presence of AlBr_3 leads to 1-adamantyl phosphonic acid dichloride (**1-13**) in 94% yield on a several grams scale.⁶⁰ 1-Adamantyl dichlorophosphine (**1-15**) can be prepared in 68% overall yield from **1-13** through reaction with Lawesson's reagent *via* 1-adamantyl dichlorophosphine sulphide (**1-14**).⁶¹ The primary phosphine **1-16** is an oily product obtained in 75% yield from the reaction of dichlorophosphine **1-15** with LiAlH_4 .⁶² 4-Diamantyl phosphonic acid dichloride (**2-28**) and di-4-diamantyl phosphonic acid chloride (**2-29**) are prepared from **2** in 22% and 59% yield respectively,⁶³ and **2-29** can be further reduced with HSiCl_3 to its corresponding secondary phosphine (84%), which is highly oxygen-sensitive. The triamantyl phosphine analogues of the latter have been also synthesized.⁶²

2.7 Olefination and alkylation

Diamondoids substituted with olefinic moieties can be used as monomers in polymerization reactions. Unsaturated compounds such as vinyl diamondoids are also expected to play a role in the immobilization of organic molecules on semiconductors for nanoelectronics. The preparation of 2-adamantylbutadiene-1,3 (**1-19**) (Scheme 8)⁶⁴ was conducted from **1** *via* the selective photochemical preparation of 1-acetyladamantane (**1-17**),⁶⁵ followed by oxetane **1-18** formation and a dehydrating ring opening catalysed by *p*-toluenesulfonic acid. Adamantyl-1-carbaldehyde (**1-20**) undergoes a Wittig reaction to give 1-vinyl adamantane (**1-23**) in 65% yield.⁶⁶ Alternatively, the adamantyloxirane **1-21** forms in excellent yield from adamantane-1-carbaldehyde, and its acidic ring opening ($\text{HBr-H}_2\text{SO}_4$) leads to 1-adamantyl-1,2-dibromoethane (**1-22**), which is debrominated to **1-23** (using Zn in DMF at 150 °C) with an overall yield of 72%.⁶⁷



Scheme 8 Diene and olefinic adamantane and diamantane **1-19, 1-23, 2-32, 2-36** and **2-37**.

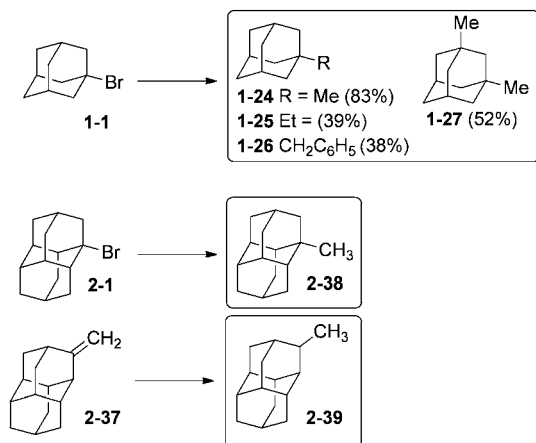
Photoacetylation has been also successfully used on the diamondoids, *e.g.*, for **2** to prepare acetyldiamantane **2-30**, which allowed the preparation of diamantylbutadiene **2-32** in 94% overall yield *via* the formation and ring-opening of the corresponding oxetane **2-31**.^{68,69} 1-Vinyldiamantane (**2-36**) has been obtained from diamantane acetic acid **2-33**, after reduction to the alcohol **2-34**, subsequent bromination to **2-35**, and then its dehydrobromination – the overall yield of **2-36** was 62%;⁶⁷ Its 4,9-divinyl substituted cousin was obtained similarly. Dehydration of **2-17** can be achieved at 135 °C in the presence of H_3PO_4 to give **2-37** in 86% yield.

Diamondoids substituted with simple alkyl fragments are of practical value for biomedical applications.^{52,70} For instance, 3,5-dimethyladamantyl-1-amine, also called Memantine[®], has been found to give some symptomatic improvement in moderate to severe Alzheimer's disease.^{70b}

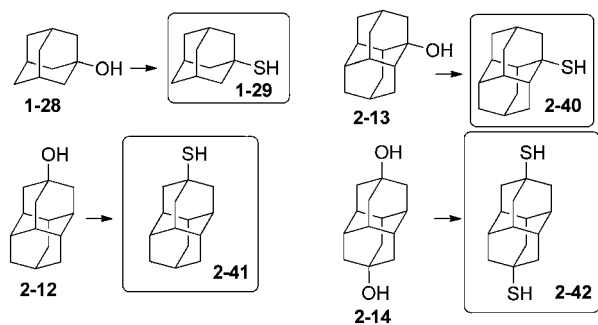
Diamondoid halides are useful alkylation reagents. 1-Bromoadamantane (**1-1**) undergoes reaction with alkyl Grignard reagents R-MgBr ($\text{R} = \text{Me, Et, CH}_2\text{Ph}$) to yield in moderate to good yields compounds **1-24-1-26** (Scheme 9).⁷¹ Multistep polyalkylation conditions can also give, for instance, **1-27** and 4,9-dimethyldiamantane. Compound **1-24** can also be obtained in 94% yield by reaction of 1-fluoroadamantane with AlMe_3 .⁷² 1-Methyldiamantane (**2-38**) forms in 90% yield from bromide **2-1** by reaction with CH_3MgBr .⁷¹ Isomeric 2-methyldiamantane (**2-39**) can be obtained in 85% yield from hydrogenation of olefin **2-37** catalysed by PtO_2 under H_2 pressure.^{33b}

2.8 Thiolation

Incorporation of thiol groups into diamondoids allows their attachment to noble metal surfaces to form self-assembled



Scheme 9 Alkylated adamantanes and diamantanes **1-24–1-27** and **2-38, 2-39**.



Scheme 10 Adamantane- and diamantanethiols **1-29, 2-40–2-42**.

monolayers (SAMs) that have applications in molecular electronics. Fokin and Schreiner *et al.* have shown that treatment of tertiary mono- and dihydroxy hydrocarbon derivatives (diamondoid alcohols) with thiourea in the presence of hydrobromic and acetic acid is a one-step route to prepare the respective tertiary thiols and dithiols.⁴² This procedure was used for the preparation of diamondoid thiols of adamantane and diamantane in satisfactory yields (Scheme 10): **1-29** (57%), **2-40** (82%), **2-41** (76%) and **2-42** (69%). The thiolation conditions can be extended to higher diamondoids such as triamantane, tetramantanes and pentamantanes. Interestingly, reactions with 1-bromoadamantane (**1-1**) involving hydrogen sulfide, organolithium reagents with elemental sulfur, potassium thioacetate and ethyl xanthogenate, sodium dimethyldithiocarbamate, hydrosulfide, or thiosulfate resulted at best in unsatisfactory yields of the expected adamantane-1-thiol (**1-29**);⁴² conversely, the reaction with thiourea gave satisfactory yield.⁷³

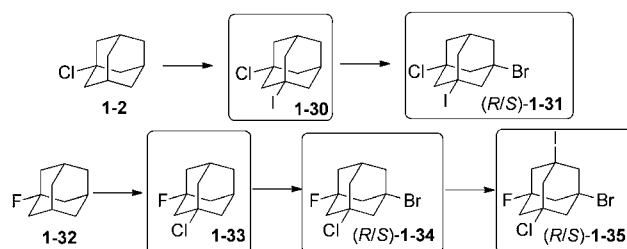
3. Unequal difunctionalization of diamondoids

The synthesis of diamondoids having two different reactive functions is a requirement for their use as platforms or linkers.

Step by step building of composites can be envisaged based on the differences in reactivity of the functions.

3.1 Di- and polyfunctionalized diamondoid halides

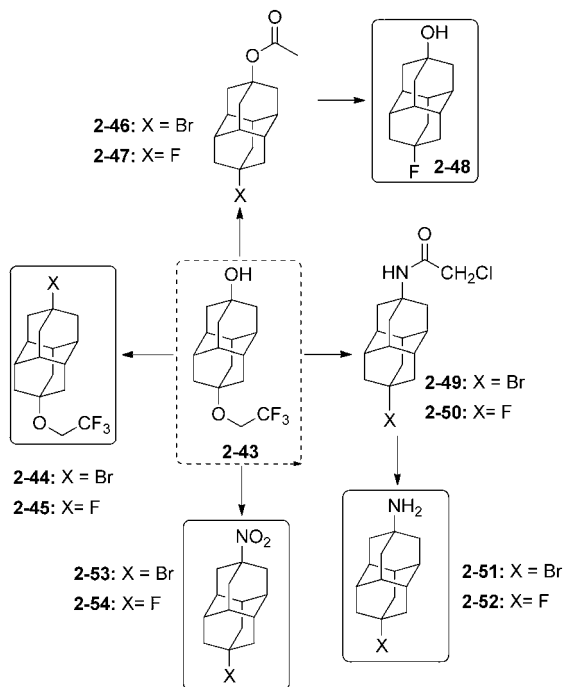
Unequally substituted di- and polyhaloadamantanes have been synthesized by successive multistep reactions under PTC conditions.⁷⁴ Stepwise iodination with iodoform and bromination with CBr_4 of 1-chloroadamantane (**1-2**) (Scheme 11)⁷⁵ led successively to the formation of 1-chloro-3-iodoadamantane **1-30** (30%) and 1-chloro-3-bromo-5-iodoadamantane **1-31** (35%) as a racemic mixture.⁷⁴ Chlorination of 1-fluoroadamantane (**1-32**) with CCl_4 gave **1-33** (20%), which was brominated to give **1-34** (21%), which was iodinated with $n\text{-C}_6\text{F}_{13}\text{I}$ to give the remarkable tetrahalide 1-bromo-3-chloro-5-fluoro-7-iodoadamantane (**1-35**) (65%).⁷⁴ Following this strategy, successive iodination and bromination of 1-fluoroadamantane (**1-32**) provided first 1-fluoro-3-iodoadamantane (24%) and then 1-fluoro-3-bromo-5-iodoadamantane as a racemic mixture (35%).⁷⁴ 3-Bromo-adamantan-1-ol and 3-chloroadamantan-1-ol have also been synthesized and isolated *en route* to 1,3-diiodoadamantane, which is obtained by addition of hydroiodic acid to any of those compounds.⁷⁶



Scheme 11 Selection of polyhalogenated adamantanes **1-30–1-35**.

The selective protection of one of the hydroxyl functions of 4,9-dihydroxydiamantane (**2-14**) by a fluoroalkyl ether function is performed with $\text{CF}_3\text{CH}_2\text{OH}$ in the presence of 20 mol% $\text{CF}_3\text{SO}_3\text{H}$ to give compound **2-43** (Scheme 12). This selective protection is very important as **2-43** is the precursor for the synthesis of a great number of unequally difunctionalized diamantanes and especially diamantane bromides and fluorides.⁴¹

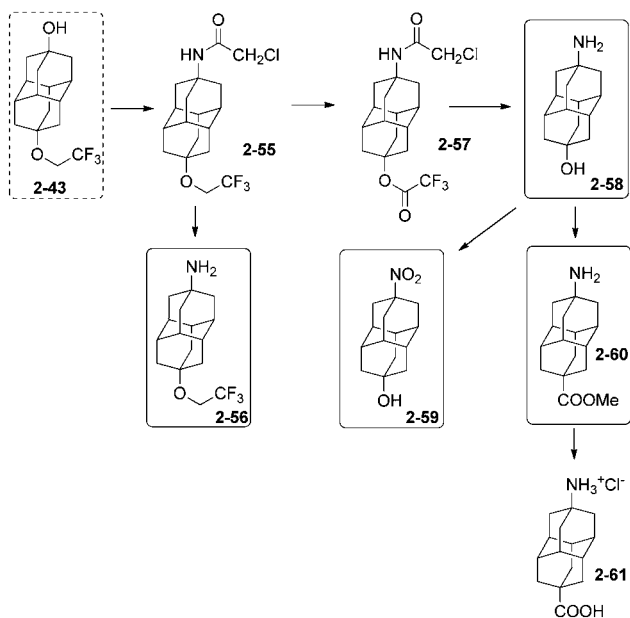
Selective bromination of **2-43** at the hydroxyl position with SOBr_2 gives **2-44** (97%), which is further converted with AgF in cyclohexane to **2-45** (86%).³⁴ The hydroxyl group of **2-43** can also be protected by an acetoxy group with CH_3COCl in pyridine to consecutively give halides **2-46** (63%) in reaction with BBr_3 and **2-47** (88%) in reaction with AgF . Fluorodiamantanol **2-48** is obtained in high 92% yield from **2-47** deprotected in excess of NaOH . The amido-protected analogue of **2-43** gives access to the amido-halides **2-49** (97%) and **2-50** (90%) by using consecutively BBr_3 and AgF .³⁴ Amino and nitro groups can also be introduced to form the difunctionalized amino-halides **2-51** (58% from its hydroxy analogue reacted with SOBr_2), and **2-52** (72% from **2-50** and thiourea), and the nitro-halides **2-53** (83% from hydroxy analogue with SOBr_2) and **2-54** (86% from **2-53** and AgF).³⁴



Scheme 12 Unequally difunctionalized adamantane halides 2-43–2-54.

3.2 Unequally substituted adamantoid alcohols and amines

9-Trifluoroethoxyadamantan-4-ol (2-43) (Scheme 13) is very useful to generate the adamantane amino alcohol 2-58 in three synthetic steps (37% overall yield), *via* acetamide 2-55 (obtained in 45% yield from the action of chloroacetonitrile–H₂SO₄ in acetic acid on 2-43), followed by conversion of the fluoroalkyl ether function into trifluoroacetoxy ester function (2-57, 97% from reflux in trifluoroacetic acid). 2-58 (86%) is obtained



Scheme 13 Disubstituted adamantane alcohols and amines and derivatives 2-55–2-61.

from 2-57 after treatment with thiourea in EtOH–acetic acid, then NaOH.

Attempts to synthesize the amino alcohol 2-58 in one step from 2-55 by directly using thiourea mixed with acetic or trifluoroacetic acid (trying to convert the ether into a base labile ester) resulted in the predominant formation of amino ether 2-56 (93%). The adamantane amino alcohol 2-58 can be efficiently oxidized to the nitro alcohol 2-59 (89%) by using *m*-chloroperbenzoic acid in 1,2-dichloroethane. Clean conversion of 2-58 to the corresponding amino acid 2-61 is more difficult (overall yield 34%) but possible *via* the formation of the methyl ester 2-60 (38%), subsequently hydrolysed in concentrated hydrochloric acid.

4. Applications of functionalized adamantoids

We illustrate herein a selection of salient recent examples of the various fields of applications in which lower adamantoids (adamantane to triamantane derivatives) have been successfully employed.

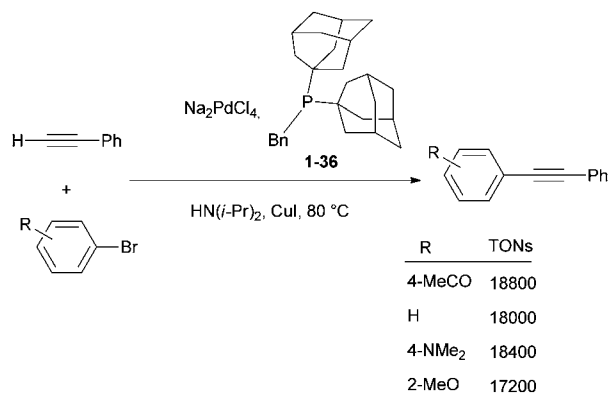
4.1 Homogeneous and heterogeneous catalysis

The applications of adamantoids in homogeneous and heterogeneous catalysis for organic synthesis by transition metals are attractive. Phosphine ligands bearing adamantyl⁷⁷ or diamantyl⁷⁸ fragments (Scheme 7) have given spectacular results in terms of catalytic efficiency and scope in various reactions. The bulky electron-rich framework provided by the hydrocarbon cage to phosphine ligands allows for the activation of valuable organic bromide and chloride substrates in metal-catalysed cross-coupling reactions. The following selected examples illustrate this potential well. By using bis(1-adamantyl)(benzyl)phosphine (1-36) as a ligand (Scheme 14) Köllhofer and Plenio have achieved high turnover numbers (TONs) for the palladium-catalysed arylation of terminal alkynes with a variety of aryl bromides (Scheme 14).⁷⁹ Coupling of various aryl bromides with phenylacetylene was performed at catalyst loadings as low as 0.005 mol%, in excellent yields with Na₂PdCl₄ as a catalyst and HN(*i*-Pr)₂ as a base and solvent. A TON of 17 200 was obtained for the reaction of the electronically deactivated aryl bromide 2-methoxybromobenzene with phenylacetylene.⁷⁹

The same authors have studied heterogenization of bulky electron-rich phosphanes by attaching a bis(1-adamantyl)-phosphanyl group to a monomethyl polyethylene glycol ether support. They formed a polymeric phosphane (Ad₂P-MeOPEG) soluble in water and polar solvents and insoluble in alkanes. The recoverable catalytic system, combining 1 mol% Na₂[PdCl₄], 2 mol% Ad₂P-MeOPEG, 0.7 mol% CuI, and HN(*i*-Pr)₂ as a base in DMSO at 75 °C, allowed the arylation of phenylacetylene, 1-octyne, and trimethylsilylacetylene with various activated and deactivated aryl bromides in excellent yields.⁸⁰

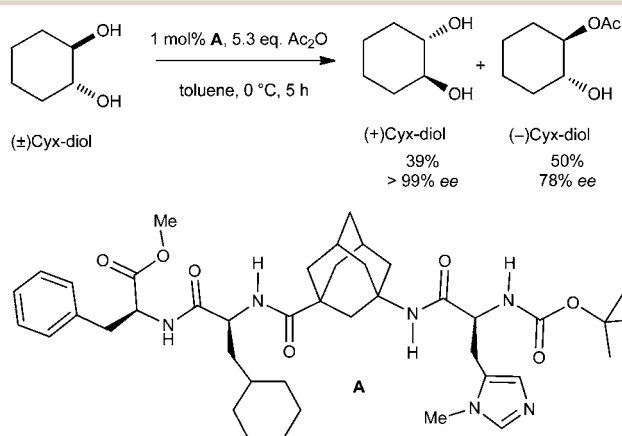
4.2 Asymmetric organocatalysis

Organocatalysts incorporating adamantane (1) have also proven to be highly promising. A chiral tetrapeptide platform incorporating



Scheme 14 Palladium-catalysed arylation of phenylacetylene using as a catalyst [Pd/(1-Ad)₂PBn].

an artificial amino acid, γ -aminoadamantane carboxylic acid, is an efficient organocatalyst for enantioselective kinetic resolution of *trans*-cycloalkane-1,2-diols (Scheme 15).⁸¹ The kinetic resolution of chiral *trans*-cycloalkane-1,2-diols is challenging, and severe limitations exist even with enzymatic approaches (selectivity factors $S < 5$). The tetramer synthesized by automated solid-phase peptide-coupling methods enantioselectively transfers acyl groups onto *trans*-cycloalkane-1,2-diols with enantiomeric excess above 99% ($S \gg 50$). This kinetic resolution currently provides the highest selectivity for these types of reactions, and this is to a large part due to the rigid and lipophilic adamantyl γ -amino acid.⁸² The absence of secondary structure in the organocatalyst suggests that the determining factors for stereoselection are established within the complex formed from the charged acylium ion and the peptide catalyst. The stereogenic centers of the artificial peptide determine the final stereochemistry of the diol.



Scheme 15 Tetrapeptide chiral platform incorporating γ -aminoadamantane carboxylic acid applied as organocatalyst in kinetic resolution of *trans*-cycloalkane-1,2-diols (racemic cyclohexane-1,2-diol is shown as an example).

4.3 Biological and medical applications

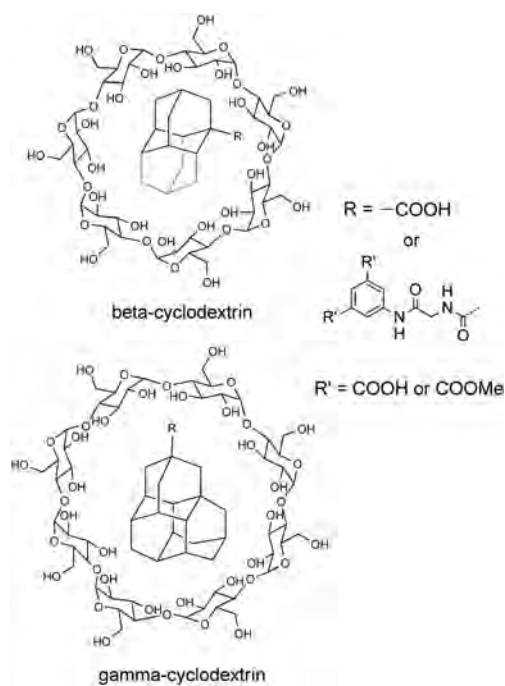
Simple adamantane derivatives have long been known for their antiviral activity against Influenza A and HIV viruses. Biological properties observed for adamantane derivatives are

also associated with the central nervous system (against Parkinson's and Alzheimer's diseases), and some antimicrobial, anti-inflammatory and antifungal activities have been recognized.^{52,83} Conversely, diamondoid derivatives of higher rank have been less investigated so far for biological and pharmaceutical potential use. This is clearly an oversight by the pharmaceutical industry that is likely due to the unforeseen isolation and chemical functionalization of diamondoids higher than adamantane. The large majority of derivatives where adamantane is replaced by a larger diamondoid moiety still await their preparation and utilization.

Adamantane, diamantane, and triamantane motifs can be introduced into DNA by chemical and enzymatic methods.⁸⁴ This was achieved by the synthesis of diamond modified triphosphates and phosphoramidites from brominated diamondoids. These artificial nucleotides were then incorporated into DNA in two ways, either using DNA polymerase or automated solid phase synthesis. Remarkably, the β -conformation of the DNA double helix tolerates the diamond-modified nucleotides.

4.4 Host-guest molecular recognition

Inclusion complexes of cyclodextrins (CDs) can form host-guest pairs whose stabilities are mainly determined by the shape and hydrophobicity of the guest molecules. Schreiner and Ravoo have reported the synthesis and characterization of inclusion complexes of water-soluble lower diamondoid carboxylic acids and their 5-aminoisophthalic acid derivatives (Scheme 16) into β - and γ -cyclodextrins (β -CD and γ -CD).⁸⁵ Due to their hydrophobicity and symmetry, it was expected that the cages of these diamondoids would be excellent guests for CDs, with the pendant



Scheme 16 Host-guest inclusion complexes in β -CD (top) and γ -CD (bottom) of derivatives of adamantane (**1**), diamantane (**2**), and triamantane (**3**) bearing a carboxylic acid or peptide side chain.

hydrophilic aromatic moieties (R) not included in the CDs cavity. Indeed, all diamondoids studied interact with β -CD. However, only the bulkiest ones (mainly triamantanes) interact with γ -CD. γ -CD is more flexible than β -CD, and in solution the cavity of γ -CD partially collapses. Therefore, its tendency to replace internal hydration water with a suitable hydrophobic guest is significantly reduced. The stoichiometry of host-guest complexes was found to be 1:1 and their interaction is endothermic in each case, with increasingly negative ΔH for the larger diamondoid acids.

From another approach of organohybrid design, Stoddart and Zink have built a nanocontainer based on an α -CD blocked by an adamantyl stopper (non-inclusive assembly). This container can encapsulate luminescent rhodamine B and controls its release by removal of its snap-top adamantyl ester motif *via* enzymatic esterase bond breaking.⁸⁶ The global system is a biocompatible controlled release system exploiting enzymatic specificity for controlled delivery of small encapsulated molecules (exemplified with rhodamine).

4.5 Polymer materials upgrading

1-Ethynyladamantane, 1,3-diethynyladamantane,⁸⁷ and 1,4-, 4,9- and 1,6-diethynyldiamantane⁸⁸ have been synthesized and polymerized or co-polymerized to give thermoset resins thermally stable above 400 °C. Diamondoids have also been incorporated as co-monomers that increase the rigidity and thermal stability of light-emitting polyolefins.⁸⁹ The incorporation of an adamantane unit in the repeating motif significantly increases the T_g and T_d of the polymers. The adamantane unit is an efficient π -conjugation interrupter and prevents interchain interactions. Blue or green light emission and low turn-on voltages were obtained from a single-layer LED fabricated from the polymers.

1,3,5,7-Tetrabromoadamantane has been employed to synthesize 1,3,5,7-tetrakis(4-aminophenyl)adamantane that was then used as a cross-linker for the incorporation of adamantane into a commercial epoxy resin network.⁹⁰ A new epoxy material obtained exhibited superior thermal properties with high glass transition temperatures and low dielectric constants in the GHz frequency range.

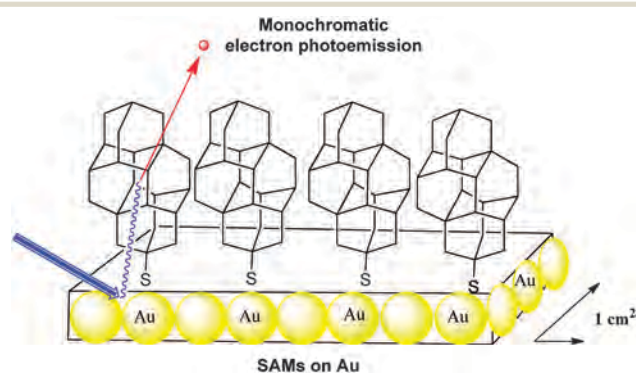
1-Adamantylacrylate, 1-vinyladamantane, 1-diamantylacrylate, and 4-diamantylmethacrylate have been employed to form polymers containing side-chain adamantane and diamantane motifs, from either atom-transfer radical-polymerization (ATRP), cationic, or free radical polymerization.⁹¹ Soluble colourless polymers of low molar masses exhibited an unusual combination of moderately high refractive index with low optical dispersion, making the polymers potentially applicable as thin film specialty optical plastics.

Diamondoids can be used as additives in polypropylene and polycarbonate polymer formulation, for which they can behave as plasticizers or antiplasticizers.⁹²

4.6 Photoemission from self-assembled monolayers (SAMs)

The functionalized diamondoid [121]tetramantane-6-thiol, which pertains to the family of thiolated diamondoid derivatives

(Scheme 10), has been used to form large area SAMs on silver and gold surfaces (Scheme 17).⁹³



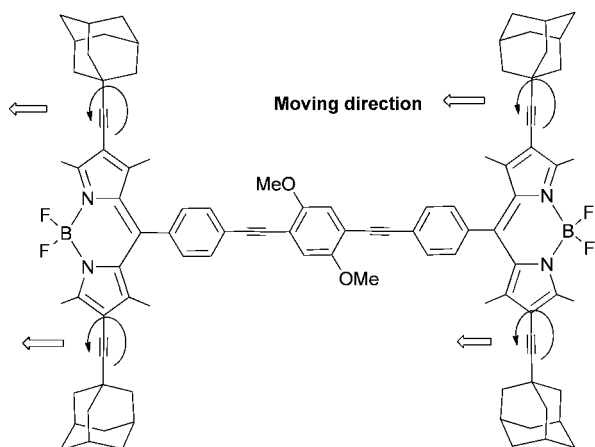
Scheme 17 Monochromatic electron photoemission from self-assembled monolayers of [121]tetramantane-6-thiol on gold.

Photoelectron spectra of the layers exhibited a peak at the low-kinetic energy threshold with up to 68% of all emitted electrons emitted within this single energy peak.⁹⁴ With a narrow energy distribution width of 0.3 electron volts, this source of monochromatic electrons might find application in technologies such as electron microscopy, electron beam lithography, and field-emission flat-panel displays. Comparatively, the spectrum of a [121]tetramantane film shows only a small peak at low kinetic energy.⁹³ The poor electron conductivity within the thicker films *versus* that through the SAMs, as well as the role that the thiol groups play within the samples could be the origin of this difference. Such strong electron emission does not occur exclusively from the diamondoid surface and the metal substrate is also involved in the process. Measurement of the mean free path for scattering demonstrates that such diamondoid SAMs do have a significantly short interaction length compared to the known related materials.

4.7 Molecular machines and rotors

Owing to their unique rigidity and sphericity diamondoid structures have provided decisive “mechanical” functions at the nanometer scale within the framework of organohybrid structures.

So-called “nanocars” are supramolecular structures that can translate on surfaces with some controlled directionality.⁹⁵ These “nanocars” incorporate wheels similar to their real-live models. The synthesis of fluorescent nanocars equipped with adamantane wheels has thus been reported (Scheme 18), and their behaviour was analysed by imaging using a method named single-molecule fluorescence microscopy (SMFM). The “nanocars” were imaged using 4,4-difluoro-4-bora-3a,4a-diaza-s-indacene (BODIPY) as the chromophore. A BODIPY moiety was rigidly incorporated into the molecule chassis *via* acetylenic cross-coupling. The mobility of the nanocars was determined from fluorescence images taken as a function of time. The adamantane four-wheeled nanocar showed a significant improvement in the percentage of moving nanocars over less-spherical carborane-wheeled nanocars having the same “chassis”. The interaction energy between the chosen wheels (diamondoid or carborane)

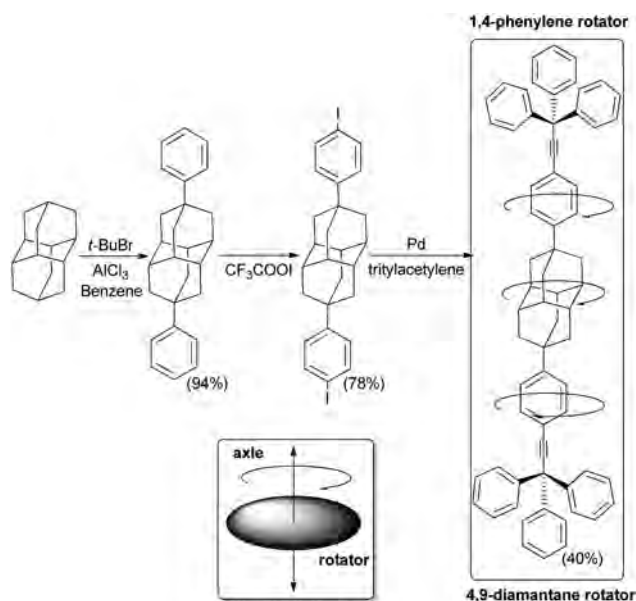


Scheme 18 Adamantane incorporated into a molecular machine: a mobile adamantane-wheeled fluorescent “nanocar”.

and the glass substrate determines the mobility of the nanocars (weak van der Waals forces or hydrogen bonding, respectively). The final results are consistent with a wheel-like rolling motion associated with the sphericity of adamantane.

Diamantane has been functionalized to serve as a rotator in a so-called “nanogyroscope” (Scheme 19).⁹⁶ This was achieved in three synthetic steps with an overall yield of 29%.⁹⁷

4,9-Diphenyldiamantane was first obtained from one-pot Lewis acidic catalysed bromination and subsequent phenylation. Iodination of the phenyl groups at the *para*-position of *ipso*-C followed by a palladium-catalysed arylation of tritylacetylene leads to a “nanogyroscope” in which both phenylene and diamantane rotating units are present (Scheme 19). The interest in controlling rotary dynamics at the molecular level within a rigid crystalline environment led to this construction, with the objective of introducing diamantane as a more cylindrical group with

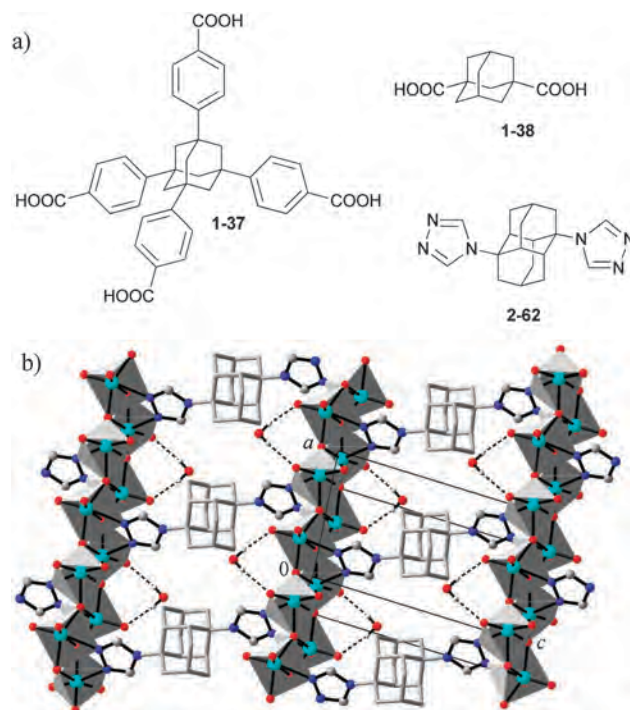


Scheme 19 Diamantane incorporated into a molecular “nanogyroscope” with a fast diamantane rotator within a rigid crystalline environment.

potentially low-energy rotational barriers. Solid state NMR studies have shown that the rotary dynamics of nanogyroscopes depend primarily on steric shielding. In general, while such structures ending with triptycyls are static, analogues with trityl groups can display 180° rotation with rates of *ca.* 500 Hz at 300 K.⁹⁷ Remarkably, at 300 K the diamantane group rotates 20 000 times faster than the connected phenylene groups, despite their proximity and close environment. These observations confirm that the more cylindrical high order rotators may have much higher rotational frequencies in solids.

4.8 Diamondoids as 3D building blocks for material chemistry

Functionalized diamondoids provide a unique combination of valuable features and properties for building new materials: multivalence, geometrically stiff structure, absence of π - π stacking interactions and great size of the molecular scaffold. In particular, their rigidity makes diamondoids valuable building blocks and platforms for crystal design and crystal engineering. Adamantane-1,3,5,7-tetracarboxylate (**1-7**, Scheme 5) is an ideal tetrahedral spacer, which was co-polymerized with $\text{Cu}(\text{NO}_3)_2$ ⁹⁸ or $\text{Zn}(\text{NO}_3)_2$ ⁹⁹ to form porous metal–organic framework (MOF) materials with a 3D channel system. Utilization of the expanded analogue of **1-7**, the adamantane-1,3,5,7-tetrabenzoate (derived from **1-37**, Scheme 20), retains the tetrahedral topology of MOF but comprises larger channels.¹⁰⁰ The MOFs based on adamantane-1,3-dicarboxylate (derived from **1-38**) usually also display the 3D structures.¹⁰¹ The condensations of **1-38** carboxylate



Scheme 20 The metal–organic framework building blocks based on adamantane and diamantane (a), and the molybdenum(vi) oxide–organic framework system based on 1,6-bis(1,2,4-triazol-4-yl)adamantane (**2-62**) (see (b) adapted from ref. 104).

derivative with different pyridyl-containing ligands give rise to various coordination architectures.¹⁰² A novel one-dimensional (1D) metal–organic nanotube has been synthesized and characterized presenting the first independent 1D metal–organic nanotube with mesohelical structure.¹⁰³

1,6-Bis(1,2,4-triazol-4-yl)diamantane (**2-62**) and other ditopic adamantane and diamantane based 1,2,4-triazole ligands were used in the preparation of metal oxide–organic frameworks (MOOFs) that complement and extend the general design approaches towards common MOFs (Scheme 20).¹⁰⁴

5. Conclusions

Diamondoids (molecular nanodiamonds) represent a unique class of chemical structures with largely untapped potential in chemistry, for the preparation of highly lipophilic pharmacologically active compounds, and as building blocks for novel carbon materials. Here we provide an overview of their origin as well as functionalization with typical chemical functional groups, and provide glimpses of applications that have come forward in the last few years.

Practically all bridgehead tertiary derivatives are available or can be synthesized by predictable routes with high chemical yields. Highly valuable halides, alcohols, acids, amines and aryl derivatives are now at the chemist's and materials scientist's disposal. Secondary derivatives are much more difficult to access and the only high-yielding route currently involves the oxidation to the respective ketones followed by subsequent functional group conversion.

Nanodiamonds complement the surging rise of carbon materials that are for the most part based on sp^2 -materials (e.g., fullerenes, nanotubes, graphenes) with largely different properties. Several fundamental studies on the electronic properties of functionalized nanodiamonds are highly promising in this respect as they show that many of the highly desirable properties of macroscopic diamond (hardness, electron emission, high chemical resistance, low toxicity, fluorescence, biocompatibility, etc.) are readily transferred to the nano scale with the added advantage of chemical functionalizability, purity and reproducibility.

Acknowledgements

The work in Dijon was supported by the “Conseil Régional de Bourgogne” (PhD grant for M. A. G. in project PARI-IME SMT08) and by CNRS from 3MIM P4-program. The diamondoid programme work in Germany was supported over the years by the Deutsche Forschungsgemeinschaft and the National Science Foundation of the USA (DFG-NSF Schr597/12-1), and in part by the Department of Energy, Office of Basic Energy Sciences, Division of Materials Science and Engineering, under contract DE-AC02-76SF00515.

Notes and references

- H. Schwertfeger, A. Fokin and P. R. Schreiner, *Angew. Chem., Int. Ed.*, 2008, **47**, 1022.
- A. Krueger, *Adv. Mater.*, 2008, **20**, 2445.

- V. N. Mochalin, O. Shenderova, D. Ho and Y. Gogotsi, *Nat. Nanotechnol.*, 2012, **7**, 11.
- A. T. Balaban and P. v. R. Schleyer, *Tetrahedron*, 1978, **34**, 3599. This definition prevents thus the inclusion of cyclohexane and other simple alkanes. In this reference various examples of non-polydiamond diamondoids are described.
- G. P. Moss, *Pure Appl. Chem.*, 1999, **71**, 513.
- J. Filik, Diamondoid Hydrocarbons, in *Carbon-Based Nanomaterials, Materials Science Foundations (monograph series)*, ed. N. Ali, A. Öchsner and W. Ahmed, Trans Tech, Switzerland, 2010.
- S. Landa and V. Machacek, *Collect. Czech. Chem. Commun.*, 1933, **5**, 1.
- S. Landa, S. Kriebel and E. Knobloch, *Chem. Listy*, 1954, **48**, 61.
- P. v. R. Schleyer, *J. Am. Chem. Soc.*, 1957, **79**, 3292.
- C. A. Cupas, P. v. R. Schleyer and D. J. Trecker, *J. Am. Chem. Soc.*, 1965, **87**, 917.
- T. Courtney, D. E. Johnston, M. A. McKerverey and J. J. Rooney, *J. Chem. Soc., Perkin Trans. 1*, 1972, 2691.
- S. Hala, S. Landa and V. Hanus, *Angew. Chem., Int. Ed. Engl.*, 1966, **5**, 1045.
- V. Z. Williams, P. v. R. Schleyer, G. J. Gleicher and L. B. Rodewald, *J. Am. Chem. Soc.*, 1966, **88**, 3862.
- W. Burns, T. Mitchell, M. McKerverey, J. Rooney, G. Ferguson and P. Roberts, *J. Chem. Soc., Chem. Commun.*, 1976, 893.
- P. v. R. Schleyer, My Thirty Years in Hydrocarbon Cages: From Adamantane to Dodecahedrane, in *Cage Hydrocarbons*, ed. G. A. Olah, John Wiley, New York, 1990.
- E. Osawa, A. Furusaki, N. Hashiba, T. Matsumoto, V. Singh, Y. Tahara, E. Wiskott, M. Farcasiu, T. Iizuka, N. Tanaka, T. Kan and P. v. R. Schleyer, *J. Org. Chem.*, 1980, **45**, 2985.
- R. Lin and Z. A. Wilk, *Fuel*, 1995, **74**, 1512.
- J. E. Dahl, J. M. Moldowan, K. E. Peters, G. E. Claypool, M. A. Rooney, G. E. Michael, M. R. Mello and M. L. Kohnen, *Nature*, 1999, **399**, 54.
- J. E. Dahl, S. Liu and R. M. K. Carlson, *Science*, 2003, **299**, 96.
- J. E. P. Dahl, J. M. Moldovan, Z. Wei, P. A. Lipton, P. Denisevich, R. Gatt, S.-G. Liu, P. R. Schreiner and R. M. K. Carlson, *Angew. Chem., Int. Ed.*, 2010, **49**, 9881.
- J. Reiser, E. McGregor, J. Jones, R. Enick and G. Holder, *Fluid Phase Equilib.*, 1996, **117**, 160.
- T. E. Jenkins and J. Lewis, *Spectrochim. Acta, Part A*, 1980, **36**, 259.
- J. E. P. Dahl, J. M. Moldowan, T. M. Peakman, J. C. Clardy, E. Lobkovsky, M. M. Olmstead, P. W. May, T. J. Davis, J. W. Steeds, K. E. Peters, A. Pepper, A. Ekuan and R. M. K. Carlson, *Angew. Chem., Int. Ed.*, 2003, **42**, 2040.
- For chloroadamantane, see: R. Jalal and R. Gallo, *Synth. Commun.*, 1989, **19**, 1697.
- For iodoadamantane, see: H. Stone and H. Shechter, *J. Org. Chem.*, 1950, **15**, 491.
- For fluoroadamantane, see: S. Hara and M. Aoyama, *Synthesis*, 2008, 2510.

- 27 G. L. Baughman, *J. Org. Chem.*, 1964, **29**, 238.
- 28 T. M. Gund and P. v. R. Schleyer, *Tetrahedron Lett.*, 1971, **19**, 1586.
- 29 T. M. Gund, P. v. R. Schleyer, G. D. Unruh and G. J. Gleicher, *J. Org. Chem.*, 1974, **39**, 2995.
- 30 A. A. Fokin, B. A. Tkachenko, P. A. Gunchenko, D. V. Gusev and P. R. Schreiner, *Chem.–Eur. J.*, 2005, **11**, 7091.
- 31 T. M. Gund, M. Nomura, V. Z. Williams Jr and P. v. R. Schleyer, *Tetrahedron Lett.*, 1970, **56**, 4875.
- 32 A. A. Fokin, B. A. Tkachenko, P. A. Gunchenko, D. V. Gusev and P. R. Schreiner, *Chem.–Eur. J.*, 2005, **11**, 7091.
- 33 (a) Methods have been early on developed for the conversion of diamantane into the three possible types of mono-functional derivatives: 1-(medial), 3-(secondary), 4-(apical), see synthetic details in ref. 48; (b) A. A. Fokin, T. S. Zhuk, A. E. Pashenko, P. O. Dral, P. A. Gunchenko, J. E. P. Dahl, R. M. K. Carlson, T. V. Koso, M. Serafin and P. R. Schreiner, *Org. Lett.*, 2009, **11**, 3068.
- 34 H. Schwertfeger, C. Würtele, H. Hausmann, J. E. P. Dahl, R. M. K. Carlson, A. A. Fokin and P. R. Schreiner, *Adv. Synth. Catal.*, 2009, **351**, 1041.
- 35 P. R. Schreiner, N. A. Fokina, B. A. Tkachenko, H. Hausmann, M. Serafin, J. E. P. Dahl, S. Liu, R. M. K. Carlson and A. A. Fokin, *J. Org. Chem.*, 2006, **71**, 6709.
- 36 N. A. Fokina, B. A. Tkachenko, A. Merz, M. Serafin, J. E. P. Dahl, R. M. K. Carlson, A. A. Fokin and P. R. Schreiner, *Eur. J. Org. Chem.*, 2007, 4738.
- 37 A. A. Fokin, P. R. Schreiner, N. A. Fokina, B. A. Tkachenko, H. Hausmann, M. Serafin, J. E. P. Dahl, S. Liu and R. M. K. Carlson, *J. Org. Chem.*, 2006, **71**, 8532.
- 38 Z. Cohen, E. Keinan, Y. Mazur and T. H. Varkony, *J. Org. Chem.*, 1975, **40**, 2141.
- 39 G. L. Baughman, *J. Org. Chem.*, 1964, **29**, 238.
- 40 S. Liu, J. Guo and D. Jia, *Pat. CN*, 1974515A, 2007.
- 41 H. Schwertfeger, C. Würtele, M. Serafin, H. Hausmann, R. M. K. Carlson, J. E. P. Dahl and P. R. Schreiner, *J. Org. Chem.*, 2008, **73**, 7789.
- 42 B. A. Tkachenko, N. A. Fokina, L. V. Chernish, J. E. P. Dahl, S. Liu, R. M. K. Carlson, A. A. Fokin and P. R. Schreiner, *Org. Lett.*, 2006, **8**, 1767.
- 43 (a) G. Molle, P. Bauer and J. E. Dubois, *J. Org. Chem.*, 1982, **47**, 4120; (b) J. E. Dubois, P. Bauer, G. Molle and J. Daza, *C. R. Acad. Sci., Paris Ser. IIC: Chim.*, 1977, **284**, 145.
- 44 G. Molle, P. Bauer and J. E. Dubois, *J. Org. Chem.*, 1983, **48**, 2975.
- 45 P. R. Schreiner, L. V. Chernish, P. A. Gunchenko, E. Yu. Tikhonchuk, H. Hausmann, M. Serafin, S. Schlecht, J. E. P. Dahl, R. M. K. Carlson and A. A. Fokin, *Nature*, 2011, **477**, 308.
- 46 A. A. Fokin, L. V. Chernish, P. A. Gunchenko, E. Yu. Tikhonchuk, H. Hausmann, M. Serafin, J. E. P. Dahl, R. M. K. Carlson and P. R. Schreiner, *J. Am. Chem. Soc.*, 2012, **134**, 13641.
- 47 H. Stetter, M. Schwarz and A. Hirschhorn, *Angew. Chem.*, 1959, **71**, 429–430.
- 48 T. M. Gund, M. Nomura and P. v. R. Schleyer, *J. Org. Chem.*, 1974, **39**, 2987.
- 49 N. A. Fokina, B. A. Tkachenko, J. E. P. Dahl, R. M. K. Carlson, A. A. Fokin and P. R. Schreiner, *Synthesis*, 2012, 259.
- 50 G. S. Lee, J. N. Bashara, G. Sabih, A. Oganessian, G. Godjoian, H. M. Duong, E. R. Marinez and C. Gutierrez, *Org. Lett.*, 2004, **6**, 1705.
- 51 A. A. Fokin, B. A. Tkachenko, N. A. Fokina, H. Hausmann, M. Serafin, J. E. P. Dahl, R. M. K. Carlson and P. R. Schreiner, *Chem.–Eur. J.*, 2009, **15**, 3851.
- 52 L. Wanka, K. Iqbal and P. R. Schreiner, *Chem. Rev.*, 2013, **113**, 3516.
- 53 A. A. Fokin, A. Merz, N. A. Fokina, H. Schwertfeger, S. L. Liu, J. E. P. Dahl, R. M. K. Carlson and P. R. Schreiner, *Synthesis*, 2009, 909.
- 54 H. Schwertfeger, C. Würtele and P. R. Schreiner, *Synlett*, 2010, 493.
- 55 J. R. Goerlich and R. Schmutzler, *Phosphorus, Sulfur Silicon Relat. Elem.*, 1995, **102**, 211.
- 56 A. Köllhofer and H. Plenio, *Chem.–Eur. J.*, 2003, **9**, 1416.
- 57 M. Beller, A. Ehrentraut, C. Fuhrmann and A. Zapf, *PCT Int. Appl.*, WO 2002010178 A1 20020207, 2002.
- 58 A. Zapf and M. Beller, *Chem. Commun.*, 2005, 431.
- 59 J. P. Stambuli, S. R. Stauffer, K. H. Shaughnessy and J. F. Hartwig, *J. Am. Chem. Soc.*, 2001, **123**, 2677.
- 60 M. Gouygou, G. Etemad-Moghadam and M. Koenig, *Synthesis*, 1987, 508.
- 61 G. A. Olah, O. Farooq, Q. Wang and A. Wu, *J. Org. Chem.*, 1990, **55**, 1224.
- 62 H. Duddeck, M. Hani, A. Elgamel and A. G. Hanna, *Phosphorus, Sulfur Silicon Relat. Elem.*, 1986, **28**, 307.
- 63 H. Schwertfeger, M. M. Machuy, C. Würtele, J. E. P. Dahl, R. M. K. Carlson and P. R. Schreiner, *Adv. Synth. Catal.*, 2010, **352**, 609.
- 64 A. A. Fokin, E. D. Butova, L. V. Chernish, N. A. Fokina, J. E. P. Dahl, R. M. K. Carlson and P. R. Schreiner, *Org. Lett.*, 2007, **9**, 2541.
- 65 (a) I. Tabushi and S. Kojo, *Tetrahedron Lett.*, 1973, **26**, 2329; (b) I. Tabushi, S. Kojo and K. Fukunishi, *J. Org. Chem.*, 1978, **43**, 2370.
- 66 J. A. Wright, M. J. Gaunt and J. B. Spencer, *Chem.–Eur. J.*, 2006, **12**, 949.
- 67 A. A. Fokin, E. D. Butova, A. V. Barabash, N. N. Huu, B. A. Tkachenko, N. A. Fokina and P. R. Schreiner, *Synth. Commun.*, 2013, **43**, 1772–1777.
- 68 I. Tabushi, S. Kojo, P. v. R. Schleyer and T. M. Gund, *J. Chem. Soc., Chem. Commun.*, 1974, 591.
- 69 A. A. Fokin, P. A. Gunchenko, A. A. Novikovskiy, T. E. Shubina, B. V. Chernyaev, J. E. P. Dahl, R. M. K. Carlson, A. G. Yurchenko and P. R. Schreiner, *Eur. J. Org. Chem.*, 2009, 5153.
- 70 (a) S. Samnick, S. Ametamey, K. L. Leenders, P. Vontobel, G. Quack, C. G. Parsons, H. Neu and P. A. Schubiger, *Nucl. Med. Biol.*, 1998, **25**, 323; (b) B. Reisberg, R. Doody, A. Stöffler, F. Schmitt, S. Ferris and H. J. Möbius, *N. Engl. J. Med.*, 2003, **348**, 1333.
- 71 (a) E. Ōsawa, Z. Majerski and P. v. R. Schleyer, *J. Org. Chem.*, 1971, **36**, 205; (b) G. Molle, J. E. Dubois and P. Bauer, *Can. J. Chem.*, 1987, **65**, 2428.

- 72 M. Aoyama and S. Hara, *Tetrahedron*, 2009, **65**, 3682.
- 73 (a) L. Bauer and K. K. Khullar, *J. Org. Chem.*, 1971, **36**, 3038; (b) J. M. Kokosa, L. Bauer and R. S. Egan, *J. Org. Chem.*, 1975, **40**, 3196; (c) P. A. Cahill, *Tetrahedron Lett.*, 1990, **31**, 5417.
- 74 P. R. Schreiner, A. A. Fokin, O. Lauenstein, Y. Okamoto, T. Wakita, C. Rinderspacher, G. H. Robinson, J. K. Vohs and C. F. Campana, *J. Am. Chem. Soc.*, 2002, **124**, 13348.
- 75 A. A. Fokin, O. Lauenstein, P. A. Gunchenko and P. R. Schreiner, *J. Am. Chem. Soc.*, 2001, **123**, 1842.
- 76 A. E. Lukach, A. N. Santiago and R. A. Rossi, *J. Org. Chem.*, 1997, **62**, 4260.
- 77 A. Tewari, M. Hein, A. Zapf and M. Beller, *Tetrahedron*, 2005, **61**, 9705.
- 78 G. Eastham, N. Tindale, *PCT Int. Appl.*, WO 2005079981 A1 20050901, 2005.
- 79 A. Köllhofer and H. Plenio, *Adv. Synth. Catal.*, 2005, **347**, 1295.
- 80 A. Köllhofer and H. Plenio, *Chem.–Eur. J.*, 2003, **9**, 1416.
- 81 C. E. Müller, L. Wanka, K. Jewell and P. R. Schreiner, *Angew. Chem., Int. Ed.*, 2008, **47**, 6180.
- 82 C. B. Shinisha and R. B. Sunoj, *Org. Lett.*, 2009, **11**, 3242.
- 83 W. Danysz, C. G. Parsons, J. Kornhuber, W. J. Schmidt and G. Quack, *Neurosci. Biobehav. Rev.*, 1997, **21**, 455.
- 84 Y. Wang, B. A. Tkachenko, P. R. Schreiner and A. Marx, *Org. Biomol. Chem.*, 2011, **9**, 7482.
- 85 J. Voskuhl, M. Waller, S. Bandaru, B. A. Tkachenko, C. Fregonese, B. Wibbeling, P. R. Schreiner and B. J. Ravoo, *Org. Biomol. Chem.*, 2012, **10**, 4524.
- 86 K. Patel, S. Angelos, W. R. Dichtel, A. Coskun, Y.-W. Yang, J. I. Zink and J. F. Stoddart, *J. Am. Chem. Soc.*, 2008, **130**, 2382.
- 87 T. G. Archibald, A. A. Malik and K. Baum, *Macromolecules*, 1991, **24**, 5261.
- 88 A. A. Malik, T. G. Archibald and K. Baum, *Macromolecules*, 1991, **24**, 5266.
- 89 S. Zheng, J. Shi and R. Mateu, *Chem. Mater.*, 2000, **12**, 1814.
- 90 Q. Wei, A. Lazzeri, F. Di Cuia, M. Scalari and E. Galoppini, *Macromol. Chem. Phys.*, 2004, **205**, 2089.
- 91 (a) D. R. Robello, *J. Appl. Polym. Sci.*, 2013, **127**, 96; (b) C. Sinkel, S. Agarwal, N. A. Fokina and P. R. Schreiner, *J. Appl. Polym. Sci.*, 2009, **114**, 2109.
- 92 A. Ghosh, S. F. Sciamanna, J. E. Dahl, S. Liu, R. M. K. Carlson and D. A. Schiraldi, *J. Polym. Sci., Polym. Chem. Ed.*, 2007, **45**, 1077.
- 93 W. L. Yang, J. D. Fabbri, T. M. Willey, J. R. I. Lee, J. E. Dahl, R. M. K. Carlson, P. R. Schreiner, A. A. Fokin, B. A. Tkachenko, N. A. Fokina, W. Meevasana, N. Mannella, K. Tanaka, X. J. Zhou, T. van Buuren, M. A. Kelly, Z. Hussain, N. A. Melosh and Z.-X. Shen, *Science*, 2007, **316**, 1460.
- 94 S. Roth, D. Leuenberger, J. Osterwalder, J. E. Dahl, R. M. K. Carlson, B. A. Tkachenko, A. A. Fokin, P. R. Schreiner and M. Hengsberger, *Chem. Phys. Lett.*, 2010, **495**, 102.
- 95 P.-L. E. Chu, L. Y. Wang, S. Khatua, A. B. Kolomeisky, S. Link and J. M. Tour, *ACS Nano*, 2013, **7**, 35.
- 96 Macroscopic gyroscopes are devices used for measuring or maintaining orientation, based on the principles of angular momentum. Gyroscopes consist of a spinning wheel or disk mounted on an axle, which is free to assume any orientation. Myriad of applications of these devices are found in navigation and stabilizing systems (planes, helicopters, space-crafts, remote control, guiding systems, mobile phones, motion capture systems, etc.).
- 97 S. D. Karlen, R. Ortiz, O. L. Chapman and M. A. Garcia-Garibay, *J. Am. Chem. Soc.*, 2005, **127**, 6554.
- 98 B. Chen, M. Eddaoudi, T. M. Reineke, J. W. Kampf, M. O'Keeffe and O. M. Yaghi, *J. Am. Chem. Soc.*, 2000, **122**, 11559.
- 99 N. L. Rosi, J. Kim, M. Eddaoudi, B. Chen, M. O'Keeffe and O. M. Yaghi, *J. Am. Chem. Soc.*, 2005, **127**, 1504.
- 100 J. Kim, B. Chen, T. M. Reineke, H. Li, M. Eddaoudi, D. B. Moler, M. O'Keeffe and O. M. Yaghi, *J. Am. Chem. Soc.*, 2001, **123**, 8239.
- 101 F. Millange, C. Serre, J. Marrot, N. Gardant, F. Pelle and G. Férey, *J. Mater. Chem.*, 2004, **14**, 642.
- 102 J. Jin, Y. Wang, W. Zhang, A. S. Lermontov, E. Kh. Lermontova and Q. Shi, *Dalton Trans.*, 2009, 10181.
- 103 J. Jin, Y. Wang, P. Liu, R. Liu, C. Ren and Q. Shi, *Cryst. Growth Des.*, 2010, **10**, 2029.
- 104 A. B. Lysenko, G. A. Senchyk, J. Lincke, D. Lassig, A. A. Fokin, E. D. Butova, P. R. Schreiner, H. Krautscheid and K. V. Domasevitch, *Dalton Trans.*, 2010, **39**, 4223.

Chapter 2: Vapor pressure measurements for vapor deposition of diamondoids as crystalline self-assemblies

2.1. Introduction

As shown in **Chapter 1**, the construction of organic materials and organohybrids based on functionalized diamondoids is an attractive challenge. Based on such edifices, carbon nucleation followed by growth may also pave the way to access continuous diamond thin films of better defined structure and surface.¹ Diamondoids may serve also as precursors in “bottom-up” strategies to build organohybrids,² and to devise diamond-like new structures under conditions that are milder than the chemical vapor deposition (CVD) conditions currently used for diamond growth.³

Methods have been reported akin to CVD that yielded higher diamondoids (more than four carbon fused-cages) and even diamond from diamondoid seeds.⁴ However, for applications of nanodiamonds-based materials built “bottom-up” there are still a need for better fundamental understanding and mastering of the conditions of nucleation, growth and self-assembly of diamondoids units.⁵

The construction of organohybrids by metal growth over functionalized diamondoids as substrates first requires depositing the diamondoids as well-defined crystalline edifices. Their assembly from a vapor phase would be innovative and convenient since some diamondoids are known to be rather volatile. However, knowledge of their vapor pressure and sublimation (or vaporisation) enthalpy is a prerequisite. Therefore, our first studies were devoted to accurately measuring sublimation enthalpies of pristine adamantane **1** and diamantane **10** for which different values have been reported.^{6,7} This was then followed by measuring the enthalpies of various functionalized derivatives.^{6b}

¹ Y.-C. Chen, L. Chang. *RSC Advances*, **2014**, 4, 18945-18950. Chemical vapor deposition of diamond on an adamantane-coated sapphire substrate.

² Few diamondoid-based hybrid compounds exist, see for cluster and MOOFs species: (a) A. B. Lysenko, G. A. Senchyk, J. Lincke, D. Lassig, A. A. Fokin, E. D. Butova, P. R. Schreiner, H. Krautscheid and K. V. Domasevitch. *Dalton Trans.*, **2010**, 39, 4223-4231. Metal oxide-organic frameworks (MOOFs), a new series of coordination hybrids constructed from molybdenum(VI) oxide and bitopic 1,2,4-triazole linkers. (b) B. E. K. Barth, B. A. Tkachenko, J. P. Eußner, P. R. Schreiner, S. Dehnen. *Organometallics*, **2014**, 33, 1678-1688. Diamondoid hydrazones and hydrazides: sterically demanding ligands for Sn/S cluster design.

³ S. Koizumi, C. Nebel and M. Nesladek. *Physics and Applications of CVD Diamond*, Wiley-VCH, Weinheim, Germany, **2008**.

⁴ J. E. P. Dahl, J. M. Moldovan, Z. Wei, P. A. Lipton, P. Denisevich, R. Gatt, S.-G. Liu, P. R. Schreiner, R. M. K. Carlson. *Angew. Chem. Int. Ed.*, **2010**, 49, 9881-9885. Synthesis of Higher Diamondoids and Implications for Their Formation in Petroleum.

⁵ J.-C. Arnault and H. A. Girard. in *Nanodiamond*, p. 221-252, Diamond Nucleation and Seeding Techniques, (Ed: O. A Williams), RSC, Cambridge, **2014**.

⁶ (a) T. Clark, T. Knox, M. A. McKervey, H. Mackle, J. J. Rooney. *J. Am. Chem. Soc.*, **1979**, 101, 2404-2410. Thermochemistry of bridged-ring substances. Enthalpies of formation of some diamondoid hydrocarbons and of perhydroquinacene. Comparisons with data from empirical force field calculations. (b) T. Clark, T. Knox, M. A. McKervey, H. Mackle. *J. Chem. Soc. Perkin Trans. 2*, **1980**, 1686-1689. Thermochemistry of bridged-ring substances. Enthalpies of formation of diamantan-1-, -3-, and -4-ol and of diamantanone.

2.2. Diamondoid volatility

The enthalpy of sublimation for adamantane has been studied and reported by various groups.⁸ Conversely, only one study of the enthalpy of diamantane was experimentally conducted by using two methods: TSGC (Temperature Scanning Gas Chromatography) and bomb calorimetry measurement.⁶ **Table 2.1** shows the ΔH_{sub} (kJ mol^{-1}) for adamantane, diamantane and derivatives. For functionalized diamondoids, only few studies of their vapor pressure exist. The reported values were found to be rather different depending on the methods used for the experimental measurement, or by computational studies.

Table 2.1. Enthalpy of sublimation of adamantane and diamantane derivatives.

Year	ΔH_{sub} (kJ mol^{-1})	Method	Author
<i>Adamantane 1:</i>			
1967	58.6±0.6 / 59.6/62.3	Dibutyl phthalate manometer	Cupas
1968	54.3		Florian
1970	59.3±0.16	Calorimetric determination	Westrum Jr.
1970	59.5		Blanchard
1971	59.3±0.2 / 60.5±1.3	Bourdon gauge	McNally
1971	53.6 / 54.8	Isotenoscope	Dows
1975	59.5		Slutsky
1975	59.7±0.8	TSGC	McKervey
1982	58.45	Calorimetric determination	Somsen
1987	55.3 / 59.7	Antoine & Clausius Clapeyron equations	Malanowski
1993	58.6		Liebman
1998	52.6	Combined correlation gas chromatography – differential scanning calorimetry (CGC-DSC)	Webb
2000	59.1		Zabransky
2000	58.3		Sevruk
<i>Diamantane 10:</i>			
1971	117.2±8 / 129.33	Calculation	McKervey, et al.

⁷ Concerning diamantane, enthalpy of sublimation $\Delta H^{\circ} = 117.2 \pm 8 \text{ kJ mol}^{-1}$ was reported that was calculated from the sum of the enthalpy of vaporization and the enthalpy of fusion, see: A. S. Carson, P. G. Laye, W. V. Steele, D. E. Johnston, M. A. McKervey. *J. Chem. Thermodyn.*, **1971**, 3, 915-918. Various other methods have been used which conversely gave for diamantane ΔH° values ranging between 73 and 97 kJ mol^{-1} .

⁸ J. S. Chikos, W. E. Acree, Jr. *J. Phys. Chem. Ref. Data*, **2002**, 31, 537-698. Enthalpies of Sublimation of Organic and Organometallic Compounds. 1910-2001.

1974	74.9	First-order calculation of the molecular-rotation potential	Fyfe, et al.
1975	95.96±0.80	TSGC	McKervey, et al.
1979	95.94±0.80	Bomb calorimetric	McKervey, et al.
2013	82.8 or 73.5	DFT calculations from molecular surface properties	Keshavarz, et al.
<i>Adamantan-1-ol 6:</i>			
1978	86.6±2.5	BG (Bourdon gauge)	Steele
<i>Diamantan-1-ol 30:</i>			
1975	118.0±0.6	Gas-saturation technique	McKervey, et al.
<i>Diamantan-4-ol 48:</i>			
1975	117.8±0.2	Gas-saturation technique	McKervey, et al.

For measuring the vapor pressure and enthalpy of sublimation of organic compounds, various methods have been reported:

1. ΔH was calculated from the sum of the enthalpy of vaporization at temperature T and the enthalpy of fusion at the melting point.⁶
2. Differential scanning calorimetry (DSC): DSC is a thermoanalytical technique in which the difference in the amount of heat required to increase the temperature of a sample and a reference is measured as a function of temperature. Both the sample and reference are maintained at nearly the same temperature throughout the experiment. Generally, the temperature program for a DSC analysis is designed such that the sample holder temperature increases linearly as a function of time. The reference sample should have a well-defined heat capacity over the range of temperatures to be scanned – the ΔH is deduced.⁹
3. Equilibrium state: the solid/liquid compound was placed under vacuum condition. It was brought to equilibrium by heating at given temperature then the vapor pressure was measured.¹⁰
4. Transpiration/vapor transport technique: an inert gas was passed through U-shaped tube containing the solid compound mixed with glass beads in order to provide a large surface for rapid equilibrium vapor-solid state at saturation equilibrium at each temperature; the transported gas was collected in a cold trap and the condensed product was weighed.^{11,12}

⁹ G. J. Kabo, A. V. Blokhin, M. B. Charapennikau, A. G. Kabo, V. M. Sevruc. *Thermochimica Acta*, **2000**, 345, 125-133. Thermodynamic properties of adamantane and the energy states of molecules in plastic crystals for some cage hydrocarbons.

¹⁰ O. E. May, J. F. T. Berliner, D. F. J. Lynch. *J. Am. Chem. Soc.*, **1927**, 1012-1016. Studies in vapor pressure. IV. The Naphthols.

¹¹ V. N. Emel'yanenko, S. P. Verevkin. *J. Chem. Thermodynamics*, **2008**, 40, 1661-1665. Thermodynamic properties of caffeine: Reconciliation of available experimental data.

5. Thermogravimetry (TG): the vapor pressure was determined by measuring the mass loss rates recorded by microbalance under isothermal/non-isothermal condition.¹³
6. Effusion: ΔH is obtained from measuring the amount of substance evaporated by weighing the mass before and after conditioning at certain time and constant temperature inside calorimeter.¹⁴
7. Gas-Liquid Chromatography: the vapor pressure at a given temperature was calculated from height of the chromatograph resultant peak of fixed volume samples of equilibrium liquid/vapor.¹⁵
8. Bomb calorimetric: ΔH was determined from heats of combustion by igniting a sample in a high pressure of oxygen in a sealed vessel and measuring the resulting rise in temperature.

2.3. Vapor pressure measurement of diamondoids

Because the volatility of some diamondoid derivatives was mostly unknown, we first decided to use a simple mass-loss method to determine it. This has been applied before to determine the vaporization enthalpy of volatile organometallic complexes.¹⁶

1. Mass-loss method

In a CVD apparatus we measured the flow of diamondoid vapors (Q_d) by monitoring precise mass-loss of volatile diamondoids heated between 20 and 80 °C for 5 minutes. The measurements were done with diamondoids **1**, **6**, **10**, **30**, and **49** (**Figure 2.1**) which are reported in **Table 2.2**. By processing Clausius-Clapeyron thermodynamic calculations, we obtained the vapor pressure of diamondoids from the treatment of the linear relationship obtained experimentally (**Figure 2.2**). The vapor pressure of diamondoids was related to temperature according to *eq. 4*. This curve could be obtained from molar fraction and total pressure by the equation (1, 2, and 3) below.

$$x = \frac{P_d}{P_T} = \frac{Q_d}{Q_{N_2}} \quad \dots \text{(eq. 1)} \quad \begin{array}{l} X : \text{molar fraction of diamondoids} \\ P_d : \text{vapor pressure of diamondoids} \end{array}$$

¹² R. Pankajavalli, C. Mallika, O. M. Sreedharan, M. Premila, P. Gopalan. *Thermochimica Acta*, **1998**, 316, 101-108. Vapour pressure of C60 by transpiration method using a horizontal thermobalance.

¹³ S. Vecchio. *Thermochimica Acta*, **2010**, 499, 27-33. Vapor pressures and standard molar enthalpies, entropies and Gibbs energies of sublimation of two hexachloro herbicides using a TG unit.

¹⁴ I. Wadsö. *Acta Chem. Scand.*, **1966**, 20, 536-543. A Heat of vaporization calorimeter for work at 25 °C and for small amounts of substances.

¹⁵ H. Mackle, R. T. B. McClean. *Trans. Faraday Soc.*, **1964**, 60, 817-821. Measurement of vaporization heats by the method of gas-liquid chromatography.

¹⁶ J.-C. Hierso, C. Satto, R. Feurer, P. Kalck. *Chem. Mater.*, **1996**, 8, 2481-2485. Organometallic chemical vapor deposition of palladium under very mild conditions of temperature in the presence of a low reactive gas partial pressure.

For each temperature of measurement :

$$P_d = \frac{Q_d}{Q_{N_2}} \cdot P_T \quad \dots \text{(eq. 2)}$$

Clausius-Clapeyron relation :

$$\ln P_d = -\frac{\Delta H^{sv}}{R} \frac{1}{T} + (R \cdot \Delta S) \quad \dots \text{(eq. 3)}$$

$$\ln P_d = -a \cdot \frac{1}{T} + b \quad \dots \text{(eq. 3)}$$

$$\rightarrow P_d = f\left(\frac{1}{T}\right) \quad \dots \text{(eq. 4)}$$

(Pascal)

P_T : total pressure (Pascal)

Q_d : flow of diamondoids

(mass loss per minute = mol.min⁻¹ =

(mass.Mw⁻¹.duration⁻¹)

Q_{N_2} : flow of N₂ (mol.min⁻¹) = L.h⁻¹.(60 x

22.4)⁻¹

T : Kelvin

R : 8.314 Pa.mol⁻¹.K⁻¹

From **Table 2.2**, adamantane **1** was surprisingly found less volatile than the functionalized analogue 1-hydroxyadamantane **6**. Similarly, 1-hydroxy **30** and di-hydroxy functions **49** on diamantane provided a better volatility than diamantane **10**.

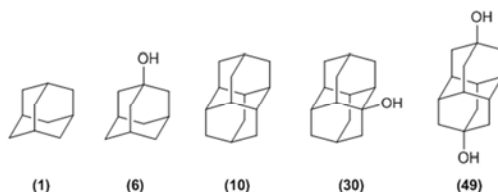


Figure 2.1. Adamantane **1**, diamantane **10**, and their hydroxylated derivatives (**6**, **30**, **49**).

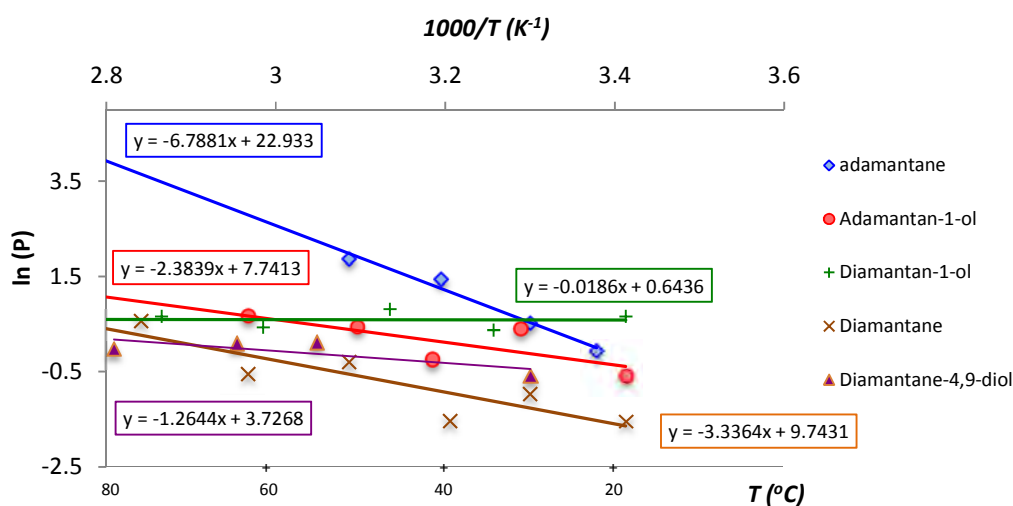


Figure 2.2. Vapor pressure of diamondoids as a function of temperature.

The volatility of 1-hydroxydiamantane **30** was surprisingly found quasi-unchanged between 20 and 80 °C and close to the one of 1-hydroxyadamantane **6**. A wrong value of enthalpy (0.2 kJ mol⁻¹) was found for

1-hydroxydiamantane **30** indicating a serious trouble in the methodology since this compound is visibly of moderate volatility.

Table 2.2. Enthalpy of diamondoids measured by mass-loss method.

No.	Diamondoids	ΔH_{exp} (kJ mol ⁻¹)	ΔH_{ref} (kJ mol ⁻¹)	m.p. (°C)
1	Adamantane	56.4	54.3-62.3	209-212
6	1-Hydroxyadamantane	19.8	86.6±2.5	247
10	Diamantane	27.7	95.94±0.8	250
30	1-Hydroxydiamantane	0.2	118.0±0.6	293
49	4,9-Dihydroxydiamantane	10.5	n. a.	299

Compared with values of reference (**Table 2.1**), the trends of these vapor pressure data were clearly not reliable. The apparatus used for mass-loss measurement was not adequate, so we reoriented our vapor measurements.

2. Measurement of vapor pressure at equilibrium state

In order to get reliable experimental data, we developed an alternative experimental method to measure the vapor pressure of functionalized diamondoids *at the solid/vapor thermodynamic equilibrium state*. Our choice was reinforced by the fact that our experiments using the mass-loss method gave inconsistent results (**Table 2.2**, **Figure 2.2**) possibly because measurements were not achieved at equilibrium state. Inspired by the method used for measuring the vapor pressure of liquids at liquid-vapor equilibrium state, we built a system for measuring the vapor pressure of finely divided diamondoid powders (**Figure 2.3**).

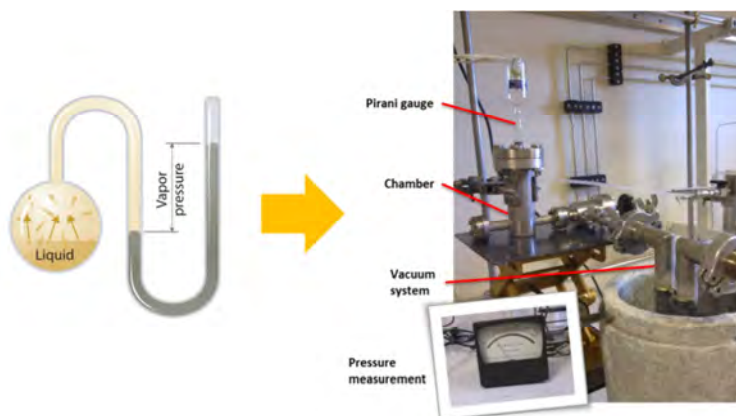


Figure 2.3. Vapor pressure measurement apparatus.

In this process, the diamondoids were brought into the sublimation regime in a chamber connected with a Pirani vacuum gauge ($\pm 1 \mu\text{m Hg}$) and the pressure was continuously monitored until the equilibrium state was reached. The time to reach the equilibrium state was long (about 4 h) so we fixed the duration of measurement to 7 h. The temperature dependence of the vapor pressure for the diamondoids followed the Clausius-Clapeyron equations (**Table 2.3**). The enthalpies of sublimation obtained from these equations are $\Delta H^0 = 60.0 \text{ kJ mol}^{-1}$ for **1**, 92.1 kJ mol^{-1} for **10**, $102.1 \text{ kJ mol}^{-1}$ for **30**, $108.8 \text{ kJ mol}^{-1}$ for **48**, and 96.4 kJ mol^{-1} for **25**. They indicate the highest volatility for adamantane, and the lowest for hydroxydiamantane derivatives.

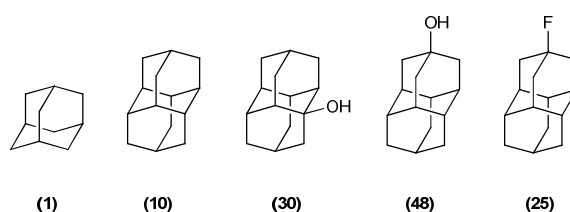


Table 2.3. Clausius-Clapeyron equations for the sublimation of diamondoids (pressure in Pa, T in K).

Diamondoid	Clausius-Clapeyron equations	r^2	ΔH^0 (kJ mol^{-1})
1	$\ln P = -7212.4/T + 26.869$	0.9991	60.0 ± 5
10	$\ln P = -11073/T + 37.172$	0.9992	92.1 ± 5
30	$\ln P = -12282/T + 39.589$	0.9960	102.1 ± 5
48	$\ln P = -13087/T + 42.196$	0.9983	108.8 ± 5
25	$\ln P = -11597/T + 38.335$	0.9965	96.4 ± 5

The enthalpy of sublimation obtained for adamantane **1** following equilibrium state pressure measurements, $\Delta H^0 = 60.0 \text{ kJ mol}^{-1}$ ($14.3 \text{ kcal mol}^{-1}$), was fully consistent with the values previously reported ($14.2 \pm 0.3 \text{ kcal mol}^{-1}$).^{6a} This was also the case for diamantane **10** measurements ($\Delta H^0 = 92.1 \text{ kJ mol}^{-1}$), with the values obtained using calorimetry bomb combustion,^{6a} and gas-saturation temperature scanning (95.9 kJ mol^{-1}).¹⁷ These measurements validated our vapor pressure measurement procedure. As expected, the fluorodiamantane **25** was found to be fairly volatile with a $\Delta H^0 = 96.4 \text{ kJ mol}^{-1}$ approaching the value we found for pristine diamantane **10**. Due to a noticeable hygroscopic behavior of the hydroxydiamantanes, their vapor pressure measurements were more delicate to achieve and required more precaution. Accordingly, the identical sublimation enthalpy values around $116\text{--}118 \text{ kJ mol}^{-1}$ reported for diamantan-1-ol, diamantan-3-ol and diamantan-4-ol,^{6b} were rather questionable and

¹⁷ T. Clark, T. Knox, H. Mackle, M. A. McKervey, J. J. Rooney. *J. Chem. Soc. Faraday Trans. 1*, **1975**, 71, 2107-2110. Heat of sublimation of some cage hydrocarbons by a temperature scanning technique.

might be overestimated according to our measurements. We observed that a good reproducibility required cautiously dried, finely divided, pure hydroxydiamantane powders to exclude water traces. Under these conditions it was determined that 1-hydroxydiamantane **30** ($\Delta H^0 = 102.1 \text{ kJ mol}^{-1}$) was significantly more volatile than 4-hydroxydiamantane **48** ($\Delta H^0 = 108.8 \text{ kJ mol}^{-1}$).¹⁸

DSC measurements of the melting points for **30** and **48** confirmed this tendency. It showed that the melting points for **30** and **48** also showed ΔH discrepancies with values substantially different for 1-hydroxydiamantane **30** and 4-hydroxydiamantane **48**: $137 \pm 1 \text{ }^\circ\text{C}$ and $177 \pm 1 \text{ }^\circ\text{C}$, respectively.

This difference between **30** and **48** correlates with an oxygen atom that is sterically more accessible to be involved in intermolecular hydrogen bondings for **48**, as confirmed by single crystal X-ray studies. In any case, a similar volatility for these hydroxydiamantanes was not experimentally observed, nor expected from their respective structures. DSC measurements on cooling were also achieved between $25 \text{ }^\circ\text{C}$ and $210 \text{ }^\circ\text{C}$ for determining crystallization peaks that gave single peaks excluding any polymorphism of **30** and **48**.

While the mass-loss method we first used is not reliable to measure the volatility of our functionalized diamondoids, the new apparatus and method developed was satisfactory.

3. Comparison with volatile organometallics

A comparison of the ΔH value measured for our diamantane-based diamondoids with the ones reported for organometallic precursors $[\text{Pd}(\eta^3\text{-allyl})\text{Cp}]$ and $[\text{Pt}(\eta^3\text{-allyl})(\text{hfacac})]$, hfacac = hexafluoroacetylacetonato, that we selected for CVD growth of hybrids (see **Chapters 3** and **5**) indicates that the complexes are more volatile, with values at 81 and 61 $\text{kJ}\cdot\text{mol}^{-1}$ (**Table 2.4**).¹⁶ These results validate the possibility to achieve a metal deposit on self-assemblies of diamondoid as substrate under the mild OMCVD conditions envisaged without detrimental vaporization of the diamondoids used as substrates.

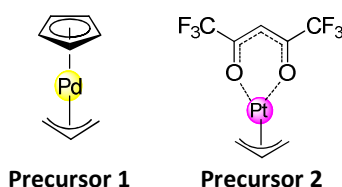


Figure 2.4. Palladium and platinum organometallic precursors selected for CVD deposition (**Chapters 3** and **5**).

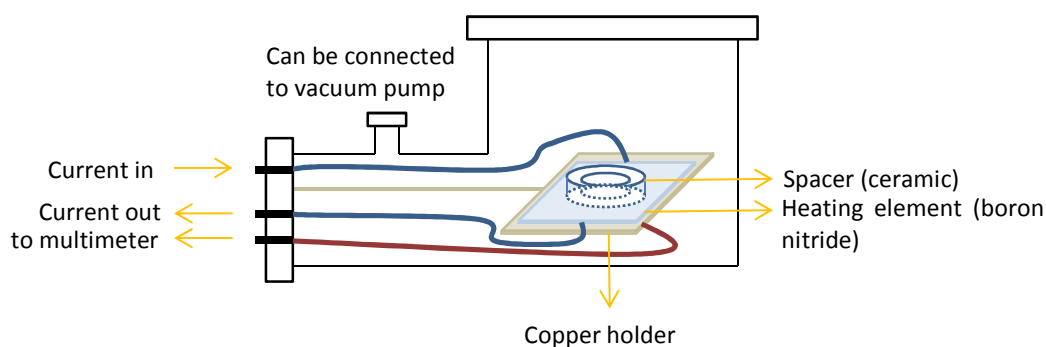
¹⁸ The identical sublimation enthalpy values reported at $116\text{--}118 \text{ kJ mol}^{-1}$ for diamantan-1-ol, diamantan-3-ol and diamantan-4-ol are questionable and may be overestimated according to our measurements (see reference 6).

Table 2.4. Vapor pressure of organometallic precursors.

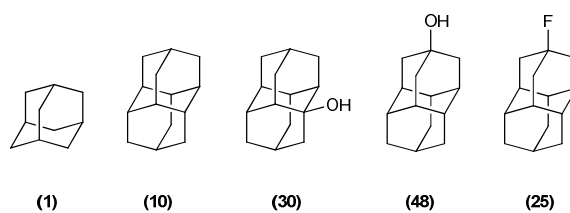
Entry	Compound	ΔH (kJ mol ⁻¹)
Precursor 1	[Pd(allyl)Cp]	81
Precursor 2	[Pt(allyl)(hfacac)]	61

2.4. Deposition of diamondoids as crystalline self-assemblies

To take profit of the suitable ΔH values of functionalized diamondoids we build a simple apparatus for running vapor phase deposition of diamondoids at atmospheric pressure on various supports, based on the sublimation of finely divided powders (**Figure 2.5**). Diamondoids for sublimation were placed in a DSC aluminum cup on a boron nitride element. Above this system, a planar substrate was placed on which the diamondoids vapor was re-condensed. Substrate and diamondoids were separated by a spacer of tunable size in ceramic.

**Figure 2.5.** Sublimation apparatus.

Deposits of diamondoids were achieved following conditions of **Table 2.5**.



Condition	T (°C)	Time
A	50	30 min
B	50	16 h
C	85	30 min

Table 2.5. Conditions used for diamondoids deposit.

In the growth process higher sublimation temperatures (condition C, 85 °C) favors nucleation in comparison to crystal growth. A good nucleation rate then will quickly generate numerous small crystals of critical size that will no longer disappear to serve as “nutrients” for growth of bigger crystals (Ostwald ripening).¹⁹ Conversely, lower-temperatures (A and B, 50 °C) allow the germination and important growth of only few sites.

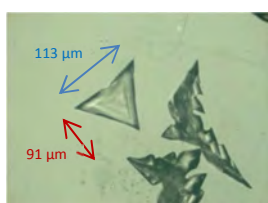
All deposits were first observed by optical microscopy from x16 to x500 enhancement, and we then focused our investigations on the most interesting samples in terms of ordered self-assembly. By SEM, the deposit morphology was observed at higher scale and EDX analysis was achieved *in-situ*. Optimization of the vapor deposition conditions was then conducted for the diamondoids that were found most suitable for generating well-defined crystal self-assembly from vapor deposition.

1. Vapor deposition under atmospheric pressure (P = 1 atm)

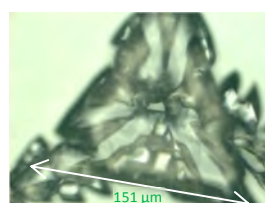
Optical microscopy of the deposits

a) Adamantane **1** vapor deposition

From the vapor deposition of **1**, few crystals of triangular shape can be observed by optical microscopy on a limited part of the mica substrate (about 113 μm). By substituting mica for silicon, only a single big crystal was deposited (**Figure 2.6**). The control of adamantane deposit is however difficult probably due to the high volatility of the compound.



Mica: 0.6 A, 50°C, 30 min (200x)



Silicon without evacuator: 0.8 A, 40 min (500x)

Figure 2.6. Adamantane **1** deposited on mica and Si.

The deposition of functionalized adamantanes was not found very satisfactory since for most of them the morphology of the resulting self-assembled crystals was rather unclear, hardly crystalline or badly reproducible (see the best examples below). We thus focused our efforts on the deposition of adamantane and adamantane derivatives for comparison.

¹⁹ F. Wang, V. N. Richards, S. P. Shields, W. E. Buhro. *Chem. Mater.*, **2014**, 26, 5-21. Kinetics and mechanisms of aggregative nanocrystal growth.

b) Diamantane 10 deposition

After deposition of **10** at 50 °C for 30 min on mica, only a few small crystals of triangular shape were observed in optical microscopy. Upon longer deposition time (16 h), some few crystals with an almost equilateral triangle shape appeared (390 μm) (**Figure 2.7**). However, despite their transparency these crystal self-assemblies were found too fragile to be used properly as substrates for metal deposition. Self-assemblies achieved at higher 80-85 °C temperature on mica and silicon conserved the same morphology of acute triangles.

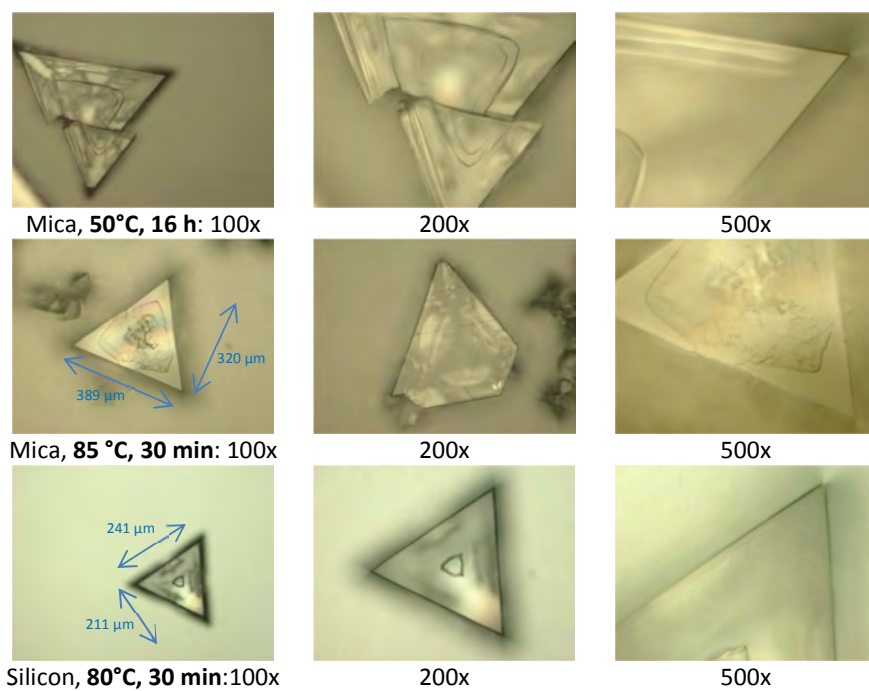


Figure 2.7. Diamantane **10** deposited on mica and Si.

c) 1-Hydroxydiamantane 30 deposition

From the deposition of **30**, crystals of hexagonal shapes with acute edges were observed both on mica and silicon (64x30 μm sizes) (**Figure 2.8**). The growth at 50 °C for 30 min was not visible by optical microscopy demonstrating, consistently with the ΔH measured, the lower volatility of this hydroxylated diamondoid. Crystallinity of the deposits appeared good if we referred to transparency and acute shapes of the hexagonal crystals.

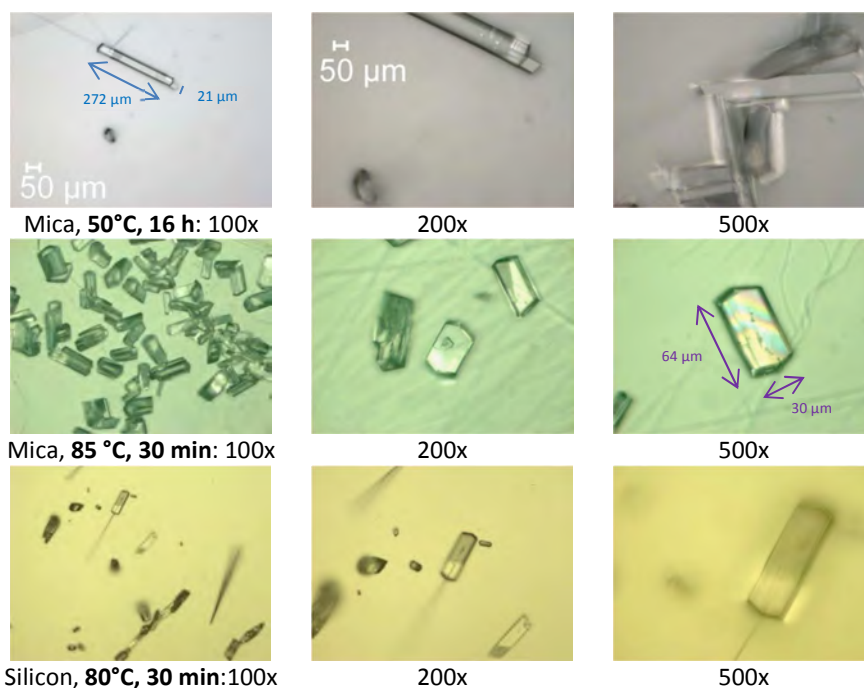
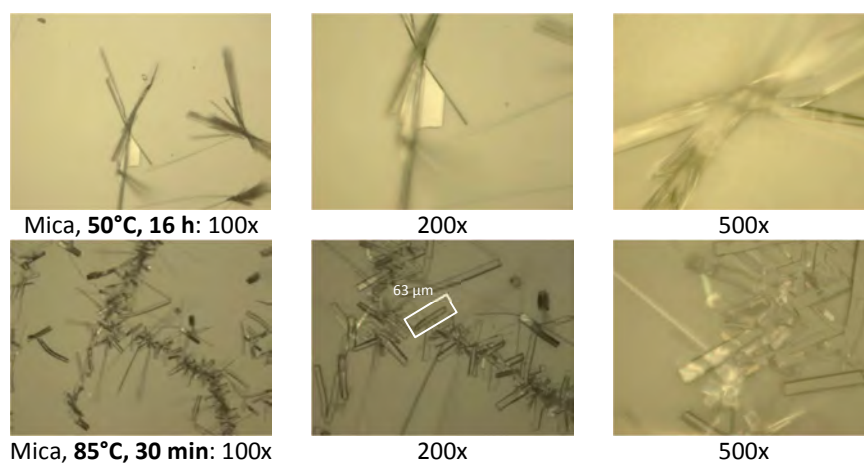


Figure 2.8. 1-Hydroxydiamantane **30** deposited on mica and Si.

*d) 4-Hydroxydiamantane **48** deposition*

Deposition of the isomeric 4-hydroxydiamantane **48** was found very different. Very few thin needles formed after 16 h of deposition at 50 °C on mica (nothing visible after 30 min). At 85 °C after 30 min on mica, a good dispersion of numerous of these thin sticks (63 μm) was obtained and some were arranged like “thorns of fir” branches. At 80 °C on silicon, similar morphology was observed for the deposits, although they were found thinner (**Figure 2.9**).



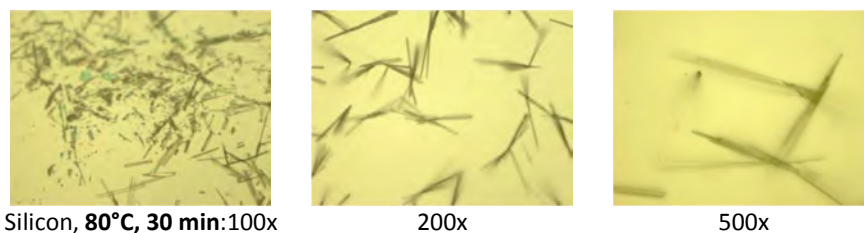
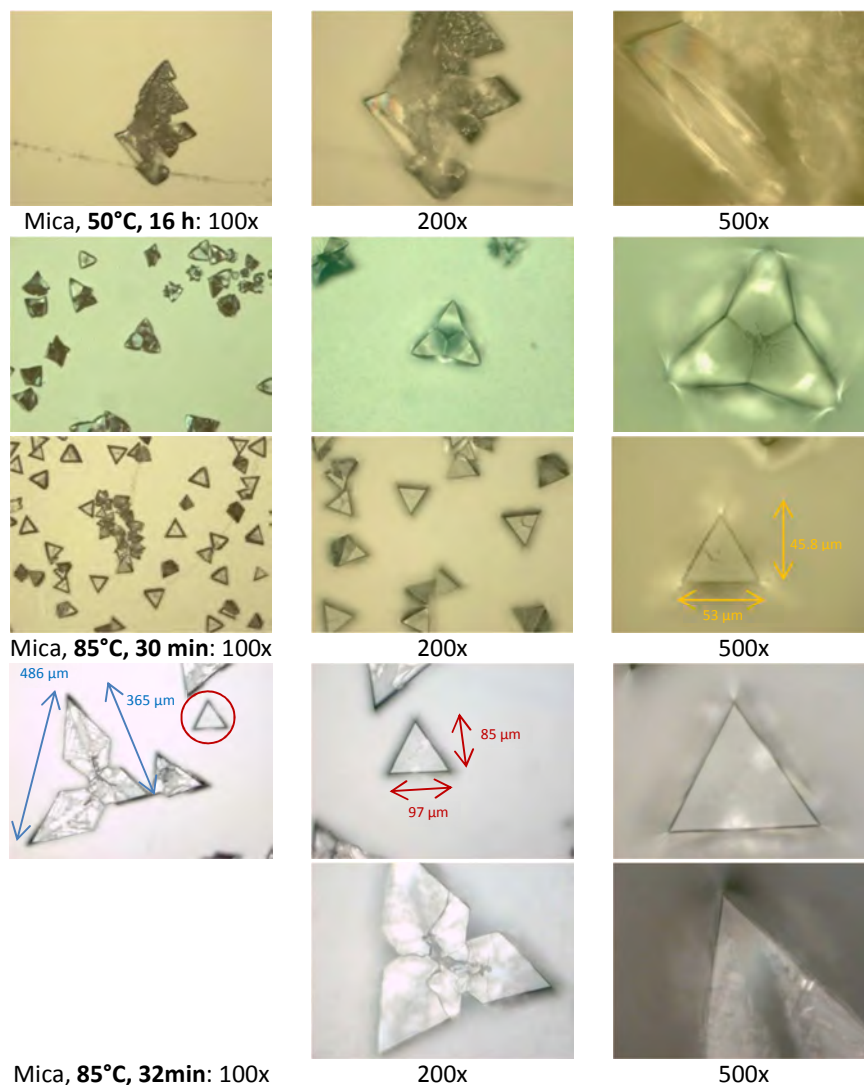


Figure 2.9. 4-Hydroxydiamantane **48** deposited on mica and Si.

e) 4-Fluorodiamantane 25 deposition

Deposition of 4-fluorodiamantane **25** appeared to be promising with discrete crystals of triangular shape obtained reproducibly. After 16 h deposition on mica, some big crystals were observed which were clearly polycrystalline aggregates of poorly-defined macrostructure (**Figure 2.10**).



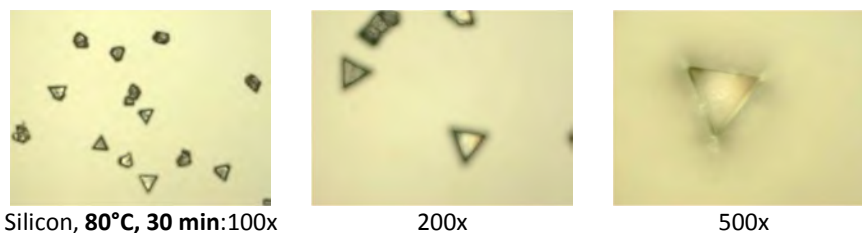


Figure 2.10. 4-Fluorodiamantane **25** deposits on mica and Si.

Deposition at 85 °C for 30 min on mica show an excellent dispersion of various particles of very well-defined geometry: some are perfectly regular equilateral triangles about 50 μm. From optical microscopy the 3-D polyhedral growth of the particles based on triangle motifs is visible, as schematized in **Figure 2.11**. Deposits on silicon were found very similar as shown in the selection of pictures.

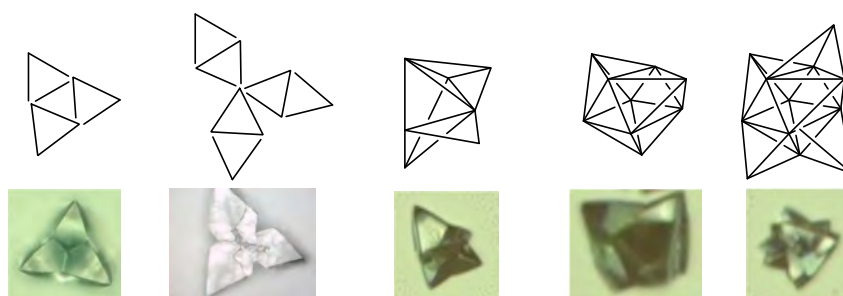


Figure 2.11. Triangle motifs of **25** on mica and Si.

In general, nice crystalline deposits of well-dispersed homogeneous microcrystals were obtained in less than one hour from the vapor deposition of hydroxyl- and fluoro-functionalized diamantanes. Not only the nature of the functionalization showed an overwhelming influence on the self-assembly and thus microstructure of the deposits, but also the position of the functional group on the cage. Thus, from the vapor deposition of **30**, **48**, **25**, hexagonal rod, rectangular needle, and triangular plate microcrystals were observed, respectively. The size of the crystals could be adjusted through the duration of the deposition with conservation of excellent dispersion and size homogeneity.

In order to investigate the extent of this deposition method to produce well-defined crystalline self-assemblies of diamondoids, some other adamantane and diamantane derivatives were deposited under similar conditions as exemplified below. However, for different structural and practical reasons they were not selected to further be used in hybrid construction by CVD metallization.

f) *1-Hydroxyadamantane 6* deposition

A rather good dispersion of this regular shape was formed at 85 °C on mica (**Figure 2.12**). Implementation on the silicon was not very satisfactory since from optical microscopy (x500) the degree of crystallinity appeared poorer than with **30** and **48**, with loss of transparency and light diffusion.

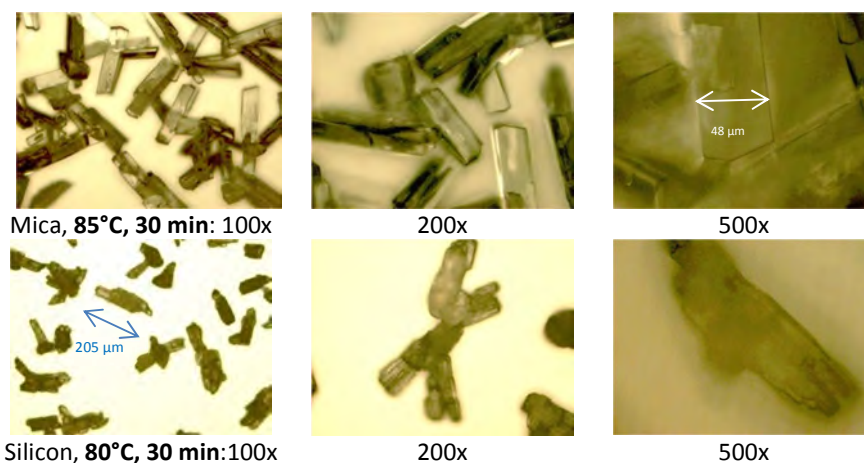


Figure 2.12. 1-Hydroxyadamantane **6** deposits on mica and Si.

g) *1-Adamantylidiphenylphosphinite 174* deposition

We observed on mica and silicon a distribution of small sized spheroidal particles with black spots in the center of each drop (**Figure 2.13**). However, this deposit much looked like liquid instead of solid deposit and was easily removed from the substrate. The absence of crystallinity was also manifested here. Therefore, deposit of this functionalized diamondoid did not seem suitable for CVD substrate.

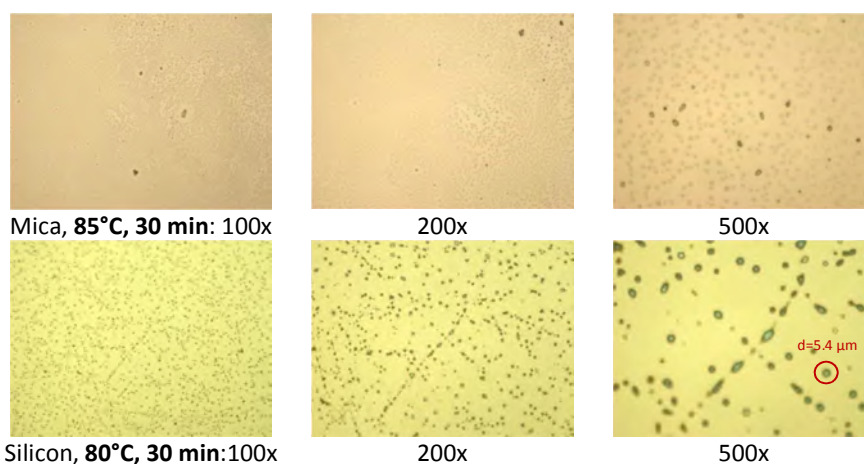


Figure 2.13. 1-Adamantylidiphenylphosphinite **174** deposits on mica and Si.

*h) 1-Aminoadamantane **64** deposition*

Deposition of this diamondoid at 85 °C on mica rapidly produced discrete particles of rather blur and imprecise triangular or hexagonal shape. Therefore deposits of this functionalized diamondoid did not seem suitable for further CVD metallization.

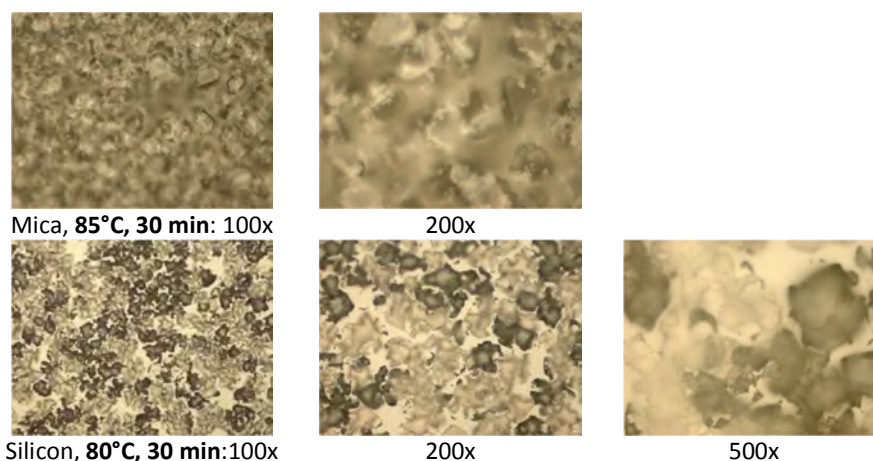


Figure 2.14. 1-Aminoadamantane **64** deposits on mica and Si.

*i) 4,9-Dihydroxydiamantane **49** deposition*

Deposition of 4,9-dihydroxydiamantane was troublesome in comparison to 4-hydroxydiamantane **48**. Indeed, after 30 min at 85 °C needles rather similar to the ones obtained with 4-hydroxydiamantane formed but in much lower amount. Therefore deposit of this difunctionalized diamondoid was also not selected.

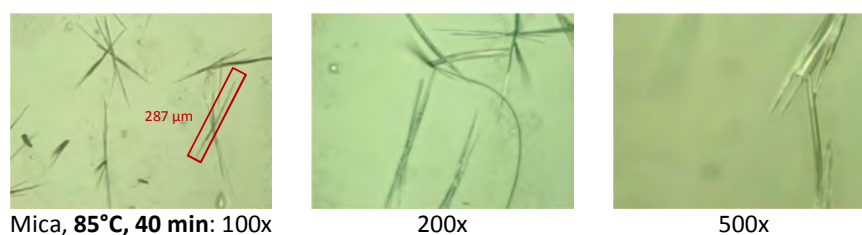


Figure 2.15. 4,9-Dihydroxydiamantane **49** deposits on mica and Si.

*j) 4,9-Difluorodiamantane **27** deposition*

The difunctionalized diamondoid **27** is deposited as polyhedral crystals on mica. The resulting self-assembly is, however, less crystalline than those obtained from 4-fluorodiamantane **25** with much less accurate shape and edges. On the silicon substrate a good distribution of seemingly more regular

triangular polyhedral particles was observed. In general, optical microscopy x500 evidenced for all these samples a polycrystallinity that is detrimental for well-oriented growth of the edifices. This polycrystallinity made **27** less attractive as substrate for metal deposition.

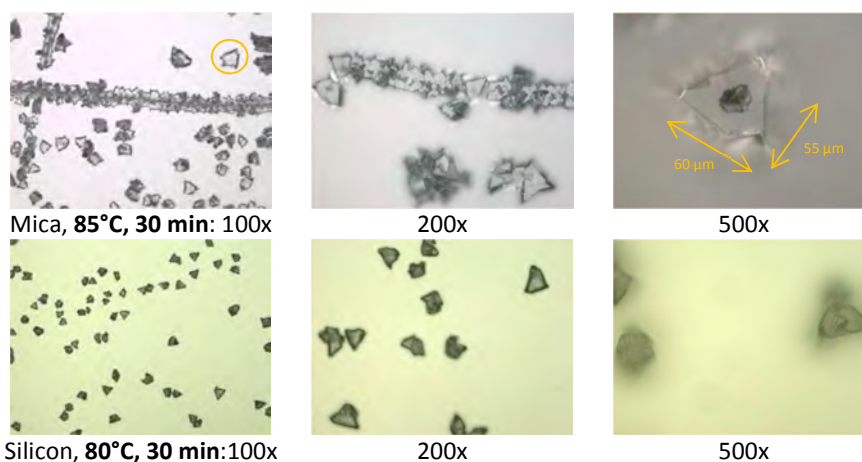


Figure 2.16. 4,9-Difluorodiamantane **27** deposits on mica and Si.

2. Scanning Electron Microscopy (SEM) of the deposits

Optical microscopy allowed us to determine the feasibility of generating self-assemblies from vapor deposition by observing the microstructure of particles around 50 μm . However, the analysis of the surface morphology and the observation of eventual smaller particles have to be done by scanning electron microscopy (SEM). Much to our surprise, the first SEM analyses (**Figure 2.17**, second from left) showed that the deposits hardly resist to the vacuum conditions imposed (10^{-6} mbar). We thus tried to protect diamondoid particles by covering them with a 15-20 nm small layer of gold before analysis, by using sputtering with high resolution ion beam coater (**Figure 2.17**, third from left). But, this metallization process was also achieved under high vacuum (10^{-5} mbar) and consequently the crystal morphology was modified before the gold layer could protect the deposit (see details below).

1) SEM of 1-hydroxydiamantane **30**

These samples appeared somewhat more resistant to SEM conditions, consistently with the lower volatility of **30**. However, SEM images showed drastic modifications of the crystal morphology. Microcrystals that appeared as well-defined hexagonal rods in optical microscopy (**Figure 2.17**, first from left) turned into hollow rectangular structures under the SEM conditions (**Figure 2.17**, second from left).

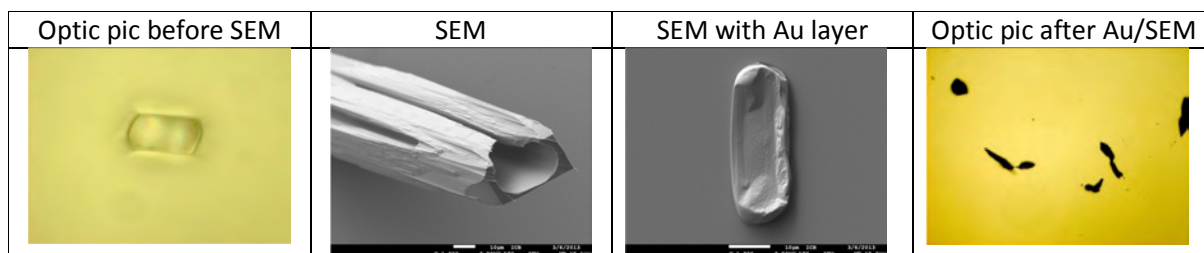


Figure 2.17. Optical and SEM images of **30**.

2) SEM of 4-hydroxydiamantane **48**

This self-assembly deposit which is made of rather thin needles has been found more resistant to SEM conditions than other deposits when it was protected with a gold layer (**Figure 2.18**). As we could see from the images below, the deposit was, however, porous and its shape was slightly changed, maybe due to some trapped gas which readily escaped under vacuum, giving somewhat deflated needles.

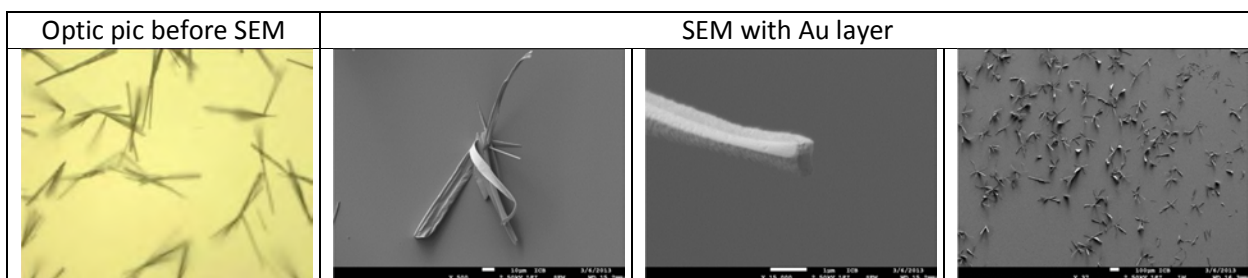


Figure 2.18. SEM images of **48**.

3) SEM of 4-fluorodiamantane **25**

An identical phenomenon of crystals “burst” occurred with 4-fluorodiamantane, as visible in the pictures below (**Figure 2.19**). EDX analysis indicated that the remaining traces contained only pure 4-fluorodiamantane.

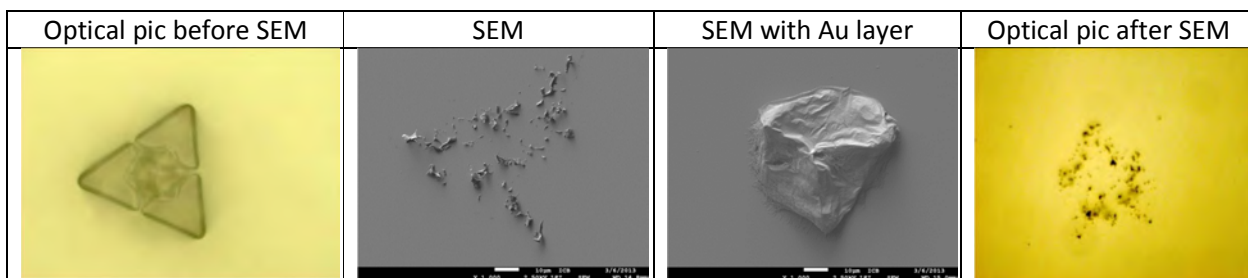


Figure 2.19. SEM images of **25**.

We hypothesized that vapor deposition of diamondoids under atmospheric pressure may trap some water, oxygen or other undesired gas inside the self-assembled crystals. We confirmed the instability of 1-hydroxydiamantane **30** crystal self-assembly by putting a sample in a Schlenk tube for 10 minutes under primary vacuum (10^{-2} mbar) at room temperature. We observed evaporation and/or destruction of the crystalline self-assembly, like in the case of SEM analysis. To further investigate this issue we performed a single crystal X-Ray analysis of the 1-hydroxydiamantane **30** deposited under atmospheric pressure (**Figure 2.20**). The analysis confirmed the high crystallinity of the deposits with a crystal arrangement in which were found discrete tetramers embedded in a cyclic network of O–H...O hydrogen bonding.²⁰ However, we did not find any evidence of small molecule trapping.

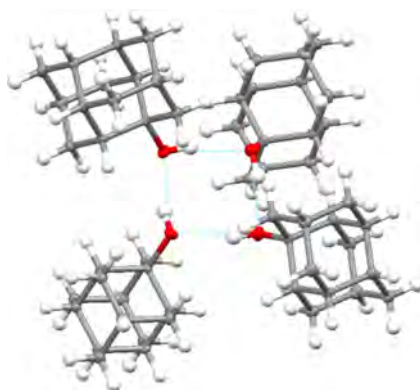


Figure 2.20. Molecular structure X-Ray of a 1-hydroxydiamantane **30** single crystal that was obtained by sublimation apparatus and determined by X-ray structure analysis.

A brief overview of the literature indicates that hollow micro- and nanostructures like the ones we observed are studied in areas which include catalysis, cosmetics, drug and gene delivery, hydrogen production and storage, photonics, photovoltaics, and rechargeable batteries.^{21,22,23,24} Mostly metal-based and ceramic hollow micro-/nanostructures have been prepared, commonly from template-removing procedures. To the best of our knowledge, the formation of non-polymeric hollow structures of pure hydrocarbons has not previously been documented.

²⁰ C. Y. Yu, Q. Li, L. B. Wang, H. W. Ma. *Acta Cryst. E: Structure Reports Online*, **2006**, 62, o2369-o2370. 1-Hydroxydiamantane.

²¹ X. W. Lou, L. A. Archer, Z. Yang. *Adv. Mater.*, **2008**, 20, 3987-4019. Hollow micro/nanostructures: synthesis and applications.

²² X. W. Lou, Y. Wang, C. Yuan, J. Y. Lee, L. A. Archer. *Adv. Mater.*, **2006**, 18, 2325-2329. Template-free synthesis of SnO₂ hollow nanostructures with high lithium storage capacity.

²³ H. J. Hah, J. S. Kim, B. J. Jeon, S. M. Koo, Y. E. Lee. *Chem. Commun.*, **2003**, 1712-1713. Simple preparation of monodisperse hollow silica particles without using templates.

²⁴ Y. Sun, B. Mayers, Y. Xia. *Adv. Mater.*, **2003**, 15, 641-646. Metal nanostructures with hollow interiors.

However, the overall cohesion strength of the crystalline self-assemblies was troublesome for our objective. We thus investigated further alternative methodologies for vapor deposition of the selected functionalized diamondoids as more robust self-assemblies.

3. Vapor deposition under primary vacuum ($P = 5$ mbar)

With the goal of growing crystals that would be resistant to the vacuum and high energy beam of SEM conditions, we modified the vapor deposition apparatus used under atmospheric pressure. Sublimation was then conducted under 5 mbar of reduced pressure. The deposition experiments were conducted either under static vacuum (initial pressure 5.3 mbar) or dynamic vacuum (5.3 mbar). We also investigated the deposition under 1 atm of argon. Temperature conditions ranging between 70 and 100 °C were applied. The **Figure 2.21** depicts the SEM analysis on a microcrystal as a function of the deposit conditions.

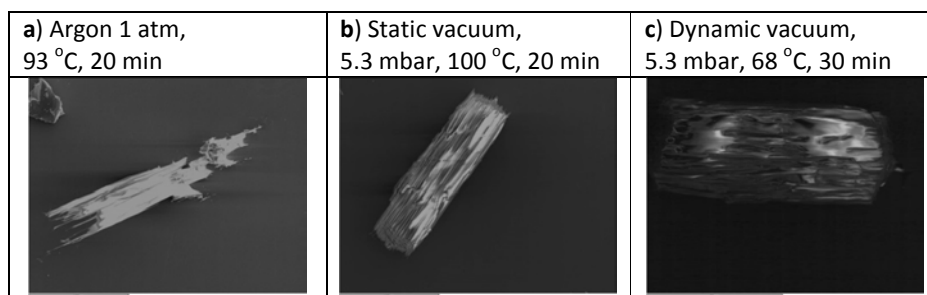


Figure 2.21. SEM images of crystals of 1-hydroxydiamantane **30** deposited under various conditions.

As illustrated in **Figure 2.21**, the deposition of microcrystals of **30** as rods of about 40 μm was achieved. These deposits were resistant to the vacuum conditions of SEM. The microscopy revealed three-dimensional structures fully consistent with the optical microscopy observations. This confirmed the necessity of a partial vacuum during diamondoids vapor deposition for getting a final stronger cohesion of self-assemblies. Conversely, the deposits realised under 1 atm of argon were not resistant to the vacuum conditions of SEM.

The EDX microanalysis conducted during the SEM experiments on various areas of the samples confirmed the elemental composition and the nature of the deposits. This is illustrated in **Figure 2.22** that presents a deposit of functionalized diamondoid **25** on silicon (area-Spect 3, EDX $C_{K\alpha 1} = 0.280$ keV,

$F_{K\alpha 1} = 0.532$ keV) and compares it to a pristine zone of the silicon substrate (area-Spect 2, EDX $Si_{K\alpha 1} = 1.739$ keV). Thus, consistently with the single crystal X-ray diffraction analysis that attested high crystallinity and purity of the deposits, the peaks corresponding to the electron binding energies $K_{\alpha 1}$ for C, and F (and Si substrate) were detected depending on the focus area of the beam. The size distribution in **Figure 2.22** (right) confirmed an average size of $40 \mu\text{m}$ with the major part of the particles having a size between 25 and $55 \mu\text{m}$. More than 90% of the visible aggregates had pyramidal and octahedral shapes, and less than 5% edifices experienced Ostwald ripening for reaching sizes above $60 \mu\text{m}$ (*small crystals or particles dissolve and redeposit onto larger crystals or particles because larger particles are more energetically favoured than smaller particles*).

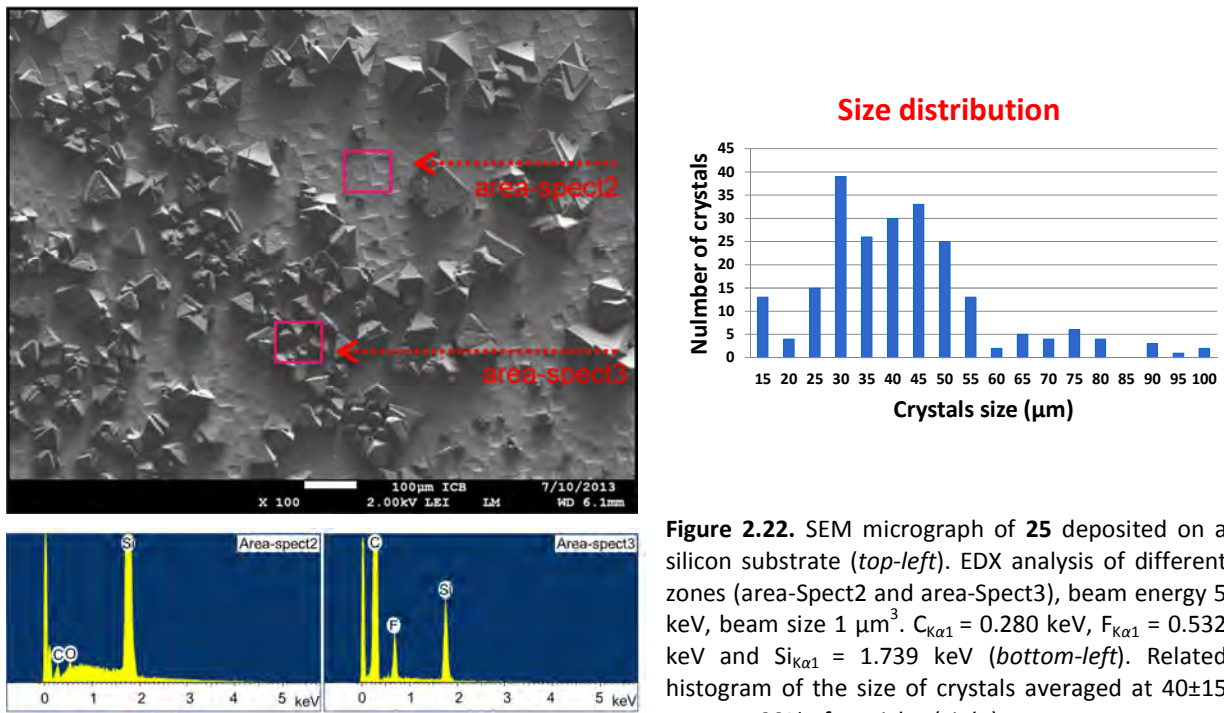


Figure 2.22. SEM micrograph of **25** deposited on a silicon substrate (*top-left*). EDX analysis of different zones (area-Spect2 and area-Spect3), beam energy 5 keV, beam size $1 \mu\text{m}^3$. $C_{K\alpha 1} = 0.280$ keV, $F_{K\alpha 1} = 0.532$ keV and $Si_{K\alpha 1} = 1.739$ keV (*bottom-left*). Related histogram of the size of crystals averaged at $40 \pm 15 \mu\text{m}$ on > 90% of particles (*right*).

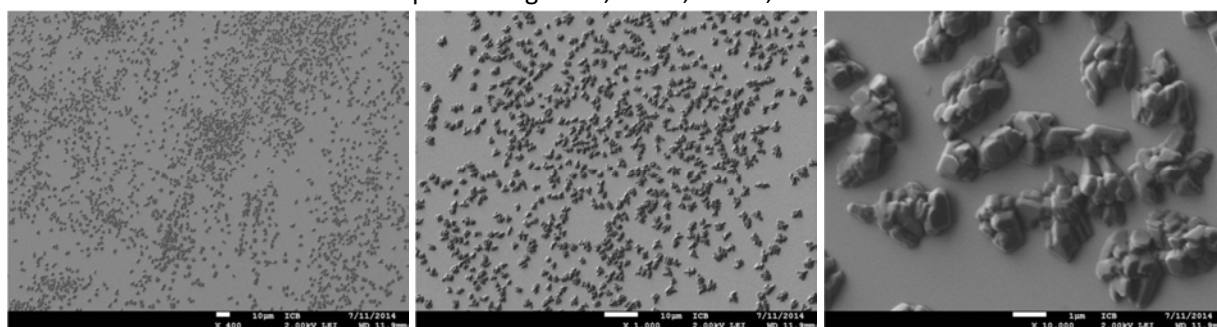
The optical microscopy images and SEM images for further functionalized (di and tetrafunctionalized) diamondoids that have been deposited under dynamic vacuum clearly illustrate the general interest of the self-assembly methodology we found. This is shown below:

a) 4,9-Dihydroxydiamantane **49**

The deposition of the difunctionalized hydroxydiamantane **49** under reduced pressure gave deposits with homogeneous distribution and uniform size (**Figure 2.23**). Surprisingly, large amounts of crystals with a different morphology were formed in comparison to the deposits that were conducted under atmospheric pressure (mostly needles in very low amount). The SEM images indicate the agglomeration of prisms into apparently polycrystalline heaps. These deposits are resistant to vacuum.



Optical images : Si, 2 min, 4 Torr, 80 °C



SEM images : Si, 2 min, 4 Torr, 80 °C

Figure 2.23. Optical and SEM images of 4,9-dihydroxydiamantane **49** deposited on Si.

b) 1,4,6,9-Tetrabromodiamantane **18**

The deposition of tetrafunctionalized tetrabromodiamantane at 80 °C for 2 minutes under reduced pressure gave also a unique “bacillus-like” motif very well distributed. The size of particles was varied, from 0.5 to 4 μm long (**Figure 2.24**).

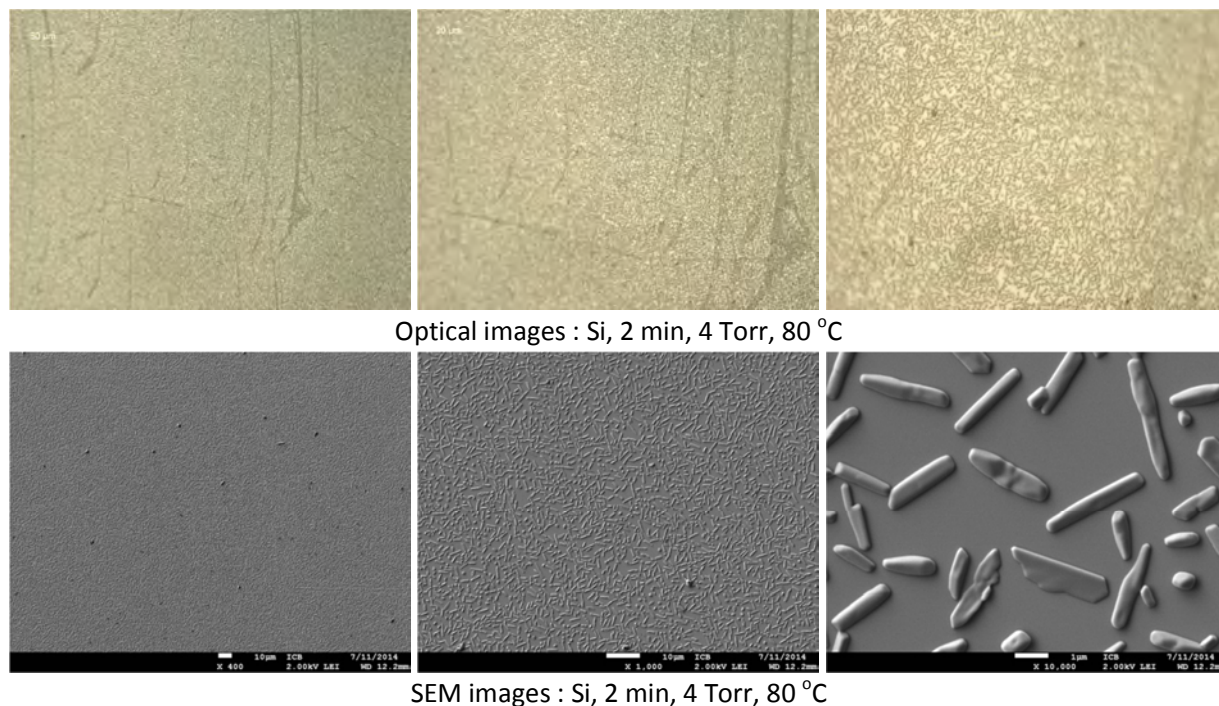
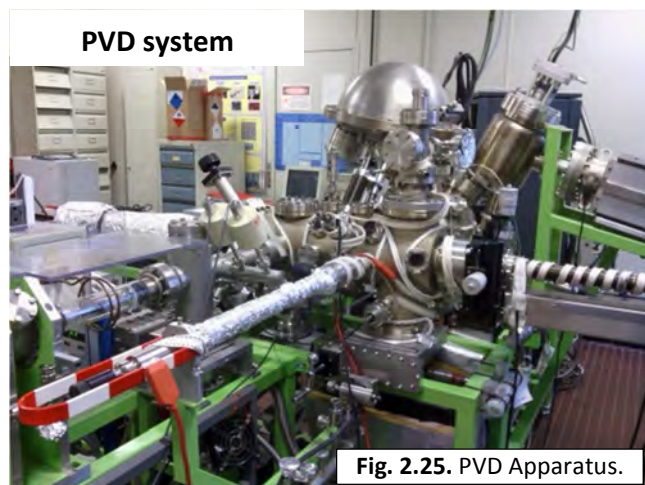


Figure 2.24. Optical and SEM images of 1,4,6,9-tetrabromodiamantane **18** deposited on Si.

While we focused our present investigations on lighter monofunctionalized diamondoids, the preliminary studies dedicated to the two last examples of heavier polyfunctionalized diamantanes clearly indicate that vapor deposition under partial vacuum is generalizable to these species.

In contrast, our attempts to generate accurate and reproducible self-assemblies such as obtained from vapor phases, but by crystallization from liquid phases in solution or suspension (dip-coating in dichloromethane or water) were unsuccessful, giving mainly large areas covered with isotropic and structurally poorly-defined coated material. Thus, this attractive vapor deposition method is simple and outperforms in terms of deposit quality dip-coating methods we used (not reported herein). This vapor phase deposition approach is expected to allow for an easy formation of diamondoid nanoobjects on different types of substrates.

2.5. Physical vapor deposition (PVD) under high-vacuum



After having determined practical vapor deposition conditions for growing well-dispersed self-assembly of diamondoids as microcrystals –with various shapes depending on the diamondoid functionalization and on the position of the function on the cage–, we addressed the more challenging task of growing crystals of *nanometer* size and under a very clean atmosphere by a similar vapor deposition technique.

A particularly pertinent issue was whether shapes and structures previously obtained from functionalized diamondoids vapor self-assembly would be conserved at the nanoscale. The very first step of the deposition process could not be controlled by the sublimation apparatus which was designed for fast and easy access to self-assembled microcrystal diamondoids. Instead we thus used a three-chamber high vacuum physical vapor deposition (PVD, 10^{-9} mbar) apparatus incorporating *in-situ* XPS analysis (details in Experimental Part). Diamondoid vapours were brought very close to the substrates through a heating tube placed at 2 mm distance. This apparatus was kindly loaned by Dr. B. Domenichini (LICB UMR CNRS-6302, Dijon), and he supervised the entire process conducted with M. Didier Poinot (**Figure 2.25**).

Table 2.6. Parameters of PVD.

Diamondoids	Substrate	Pressure Conditions	SEM observation
Adamantane 1	Si	1.5×10^{-6} mbar	-
1-Hydroxyadamantane 6	Si	3.6×10^{-6} mbar	-
Diamantane 10	Si	$(5-8) \times 10^{-6}$ mbar	-
1-Hydroxydiamantane 30	Si	1.4×10^{-6} mbar	Thickness 10-20 nm
4,9-Dihydroxydiamantane 49	Si	1.1×10^{-6} mbar	-

From five diamondoids (**Table 2.6**), 1-hydroxydiamantane **30** has been the only one giving satisfactory results in deposition. This was due to its adequate volatility (not too high for controlling deposition, not too low for getting a deposit within deposition time). Deposition on a silicon surface, treated following

RCA protocol (see experimental part) to remove carbon contamination, was achieved from 20 mg of **30** heated at 80 °C for 3 h under a low pressure of 1.4×10^{-6} mbar. Deposit was visible with naked eye as a white film. SEM images of the resulting deposits are provided in **Fig. 2.26**.

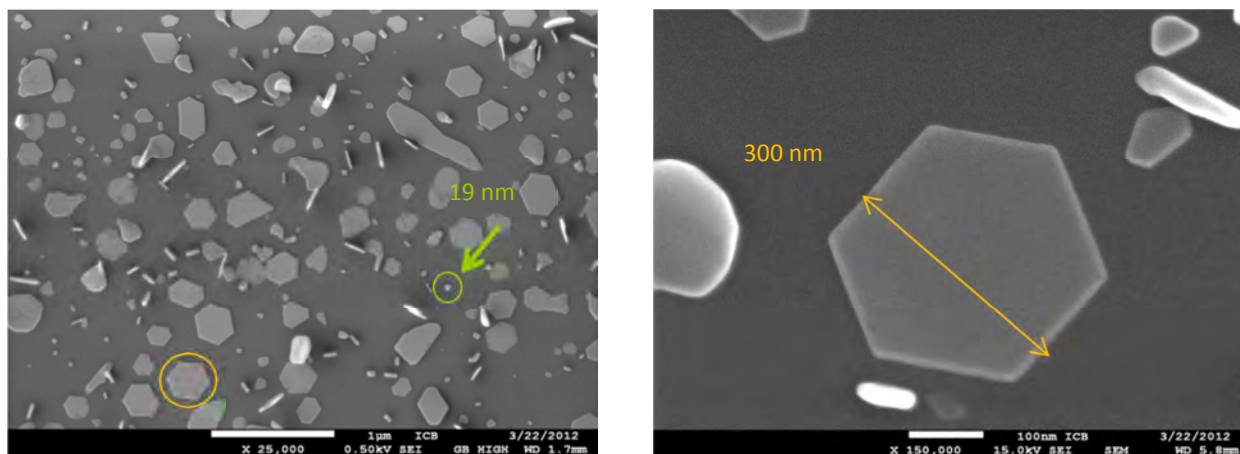
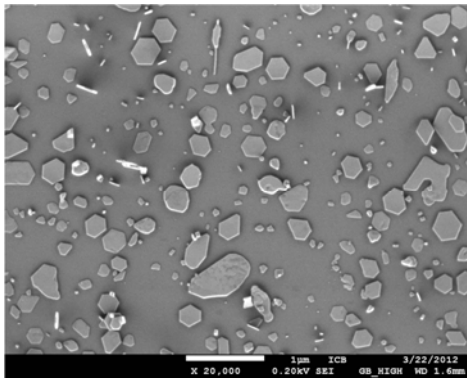


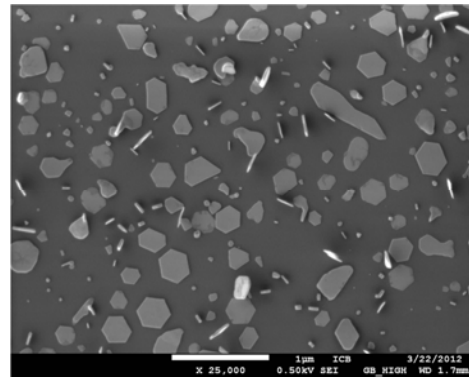
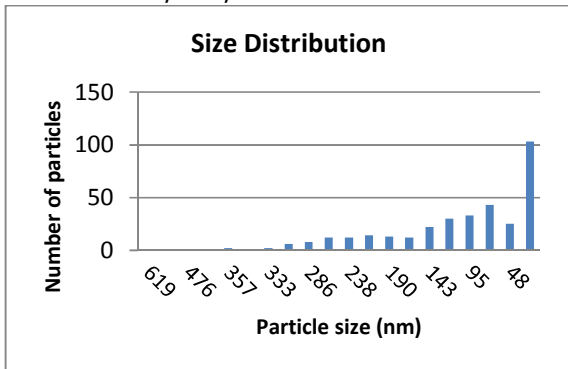
Figure 2.26. SEM images of 1-hydroxydiamantane **30** deposited by PVD.

As expected, these deposits were resistant to the SEM analysis conditions. Discrete 30–80 nm nanocrystals were obtained (>60% of the particles). **Figure 2.27** provides a representative histogram of the nanocrystals dispersion. Generally, sizes ranging between 20 and 600 nm were obtained under these conditions. We were pleased to observe that the self-assembly of **30** mostly exhibit hexagonal shapes with well-defined growth directions. These growth directions were not induced by the Si(111) substrate since an amorphous SiO₂ thin layer was always present at the surface of the substrate before deposition as confirmed by XPS at 532.5 eV (**Figure 2.29**). Accordingly, owing to non-preferentially oriented macroscopic growth of nanocrystals some were positioned perpendicularly to the surface.

In the SEM picture (**Figure 2.26**) these diamondoid particles could be easily identified and the images allowed measuring their thicknesses, which were remarkably regular around 20 nm. This regularity suggested a fairly homogeneous growth rate of the diamondoid particles. EDX analysis with a beam focusing on the edifices (beam energy 5 keV, size $1 \mu\text{m}^3$) showed that the deposit of **30** exclusively contained carbon and oxygen, in full agreement with the chemical nature of the deposit (**Figure 2.28**). We therefore demonstrated that particles of **30** of approximately 20 nm thickness and size could be deposited from a vapor phase under strictly anaerobic and low-pressure conditions (1.4×10^{-6} mbar), showing self-assembly into hexagonal structures similar to the microstructures formed at micrometer scale under few mbar pressure.



Histogram of particle size distribution for 1-hydroxydiamantane – Area 1



Histogram of particle size distribution for 1-hydroxydiamantane – Area 2

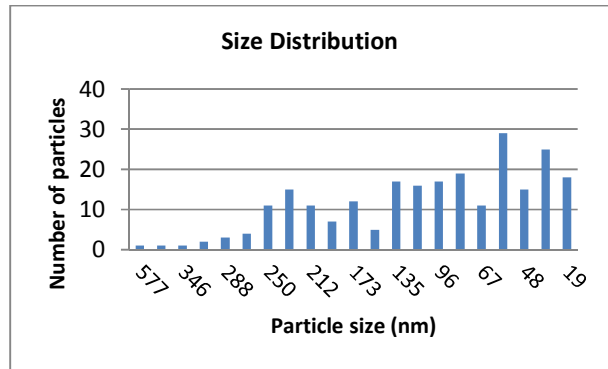
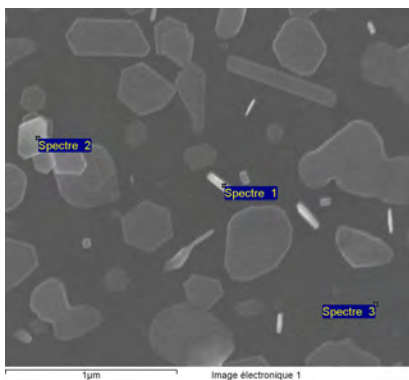


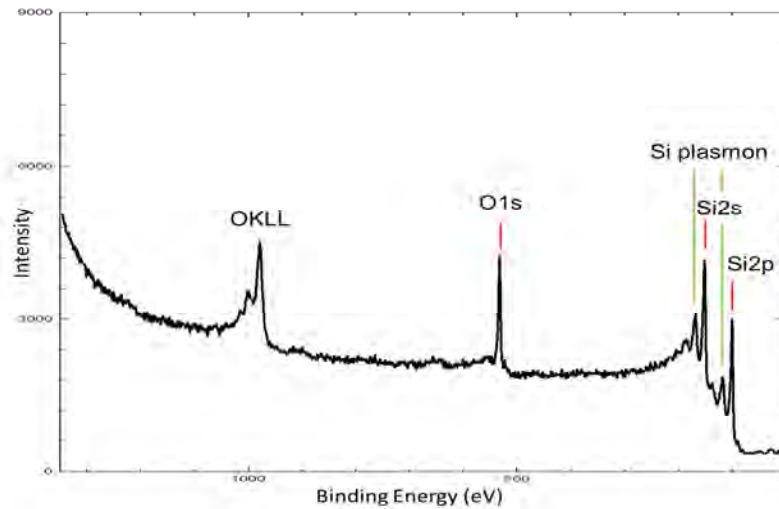
Figure 2.27. SEM pictures of two different areas.



Analyzed Elements (Normalized) : % wt

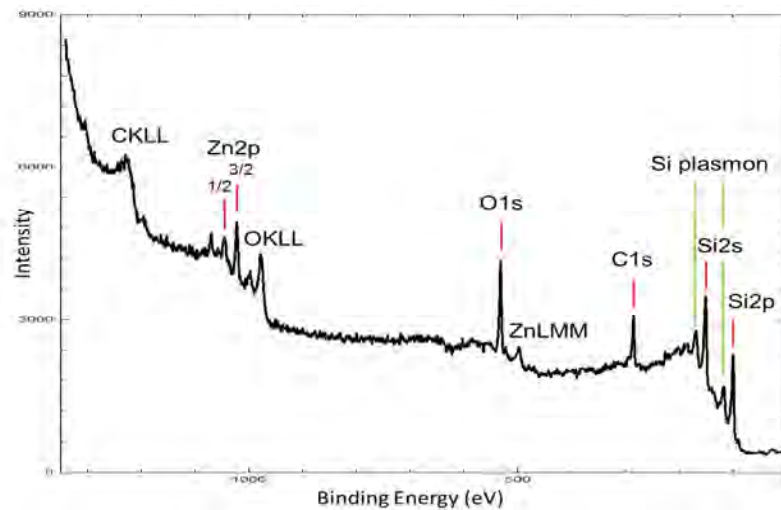
	C	O	Si
Spectre 1	13.15	1.95	84.90
Spectre 2	13.72	2.20	84.08
Spectre 3	28.94		71.06
Max.	28.94	2.20	84.90
Min.	13.15	1.95	71.06

Figure 2.28. EDX analysis of 1-hydroxydiamantane 30 deposited by PVD in Si(111).



$BE_{OKLL} = 978.3$ eV, $BE_{O1s} = 532.5$ eV, $BE_{Si\ plasmon} = 167.8$ eV, $BE_{Si2s} = 150.8$ eV, $BE_{Si\ plasmon} = 117.7$ eV, $BE_{Si2p} = 99.7$ eV

Figure 2.29. XPS analysis of Si(111) wafer after RCA protocol cleaning and heating 800 °C.



$BE_{CKLL} = 1229.7$ eV, $BE_{Zn2p1/2} = 1045.4$ eV, $BE_{Zn2p3/2} = 1022.4$ eV, $BE_{OKLL} = 978.3$ eV, $BE_{O1s} = 531.5$ eV, $BE_{ZnLMM} = 498.4$ eV, $BE_{C1s} = 284.0$ eV, $BE_{Si\ plasmon} = 167.8$ eV, $BE_{Si2s} = 150.8$ eV, $BE_{Si\ plasmon} = 117.7$ eV, $BE_{Si2p} = 99.7$ eV)

Figure 2.30. XPS analysis of 1-hydroxydiamntane deposit by PVD on Si(111) wafer after RCA protocol cleaning and heating 800 °C.

For now, the relation between the self-assemblies morphology and the functional groups in the molecular precursor is difficult to rationalize. This is related to the recognized general non-predictability of molecular structure and morphology of crystals. Accordingly, complexity in polymorphism of

functionalized diamondoids has been recently illustrated for adamantane halide derivatives.²⁵ Nevertheless, it is worth mentioning the excellent reproducibility which is obtained from this approach in the formation of robust well-defined self-assemblies.

2.6. Conclusion

Readily accessible processes for the mild vapor deposition of functionalized diamondoids provide previously unobserved self-assembly of organic micro- and nanocrystals. Key thermodynamic data including sublimation enthalpy of several diamondoid derivatives have been determined from a new measurement protocol at solid-vapor thermodynamic equilibrium state.

The conditions of pressure used for the depositions are crucial and if appropriately adjusted lead to deposits resistant to high vacuum and high energy beams. Vapor deposition under atmospheric pressure of air or argon lead to unprecedented assemblies that apparently capture gases, and turn to hollow edifices upon gas evacuation. Depending on the type of functional group and its position on the diamondoid, the general structure of the discrete deposits can vary dramatically and anisotropic structures such as rods, needles, triangles or truncated octahedra form. Self-assembled edifices of sizes ranging from 20 nm to several hundred micrometres can be obtained with conservation of a similar geometry for a given diamondoid.

In the following chapter, we describe the use of these diamondoid self-assemblies having reactive functions (OH, F) as supports and seeds for metal deposition towards organohybrid carbon-metal constructions.

²⁵ P. Negrier, M. Barrio, J. L. Tamarit, D. Mondieig. *J. Phys. Chem. B*, **2014**, 118, 9595-9603. Polymorphism in 2-X-adamantane derivatives (X = Cl, Br).

Cite this: *Nanoscale*, 2015, 7, 1956

The functionalization of nanodiamonds (*diamondoids*) as a key parameter of their easily controlled self-assembly in micro- and nanocrystals from the vapor phase†

Maria A. Gunawan,^{a,b} Didier Poinso,^a Bruno Domenichini,^c Céline Dirand,^c Sébastien Chevalier,^c Andrey A. Fokin,^{b,d} Peter R. Schreiner*^b and Jean-Cyrille Hierso*^{a,e}

We detail herein readily accessible processes to control previously unobserved robust self-assemblies of nanodiamonds (*diamondoids*) in micro- and nanocrystals from their mild vapor deposition. The chemical functionalization of uniform and discernible nanodiamonds was found to be a key parameter, and depending on the type of functional group (hydroxy, fluorine, etc.) and its position on the diamondoid, the structure of the discrete deposits can vary dramatically. Thus, well-defined anisotropic structures such as rod, needle, triangle or truncated octahedron shapes can be obtained, and self-assembled edifices of sizes ranging from 20 nm to several hundred micrometers formed with conservation of a similar structure for a given diamondoid. Key thermodynamic data including sublimation enthalpy of diamondoid derivatives are reported, and the SEM of the self-assemblies coupled with EDX analyses and XRD attest the nature and purity of nanodiamond crystal deposits. This attractive method is simple and outperforms in terms of deposit quality dip-coating methods we used. This vapor phase deposition approach is expected to allow for an easy formation of diamondoid nanoobjects on different types of substrates.

Received 3rd August 2014,
Accepted 7th December 2014

DOI: 10.1039/c4nr04442h

www.rsc.org/nanoscale

Introduction

Diamondoids are cage hydrocarbon molecules that can be described as fully hydrogen-terminated nanometer-sized diamonds.^{1,2} Adamantane (**1**) and diamantane (**2**) are the smallest diamondoids and their selective functionalization can be achieved with high efficiency at various positions of the hydrocarbon cage (Fig. 1).¹ Ultra-disperse detonation nanodiamond^{3–6} and diamondoids (also called *nanodiamonds*)⁷

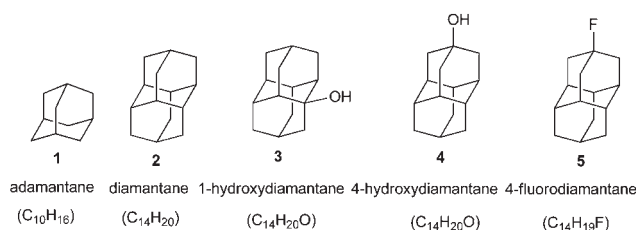


Fig. 1 Fully hydrogenated hydrocarbon cages adamantane **1** and diamantane **2**, and functionalized diamantane analogues **3–5**.

^aInstitut de Chimie Moléculaire de l'Université de Bourgogne (ICMUB), UMR-CNRS 6302, Université de Bourgogne, 9 avenue Alain Savary, 21078 Dijon Cedex, France. E-mail: hiersojc@u-bourgogne.fr

^bInstitut für Organische Chemie, Justus-Liebig-Universität, Heinrich-Buff-Ring 58, 35392 Giessen, Germany. E-mail: prs@uni-giessen.de

^cLaboratoire Interdisciplinaire Carnot de Bourgogne (LICB), UMR-CNRS 6303, Université de Bourgogne, 9 avenue Alain Savary, 21078 Dijon Cedex, France

^dDepartment of Organic Chemistry, Kiev Polytechnic Institute, Pr. Pobedy 37, 03056 Kiev, Ukraine

^eInstitut Universitaire de France (IUF), 103 Bd. Saint Michel, 75005 Paris Cedex 5, France

†Electronic supplementary information (ESI) available: Full details of vapor pressure measurements, vapor deposition of functionalized diamondoids, apparatus (including PVD) and all characterization for all functionalized diamondoids self-assemblies investigated from vapor phases and solution dip-coating. See DOI: 10.1039/c4nr04442h

have shown impressive success in the utilization of diamond properties in various areas that span the fields of nanomedicine,^{8–10} nanodevices for energy,^{11a} and molecular machines.^{12,13} For instance, large area self-assembled monolayers of thiolated diamondoids on gold surfaces exhibit intense monochromatic photoemission with an energy distribution width <0.5 eV, which is related to the negative electron affinity of the surface-attached nanodiamonds.¹¹

Another attractive and hitherto unmet challenge in this field is the construction of organic materials and organohybrids based on nano- and microcrystals of functionalized diamondoids. Based on such edifices, carbon nucleation followed by growth may also pave the way to access continuous



diamond thin films of better defined structure and surface.¹⁴ Diamondoids may also serve as precursors in “bottom-up” strategies to build organohybrids,¹⁵ and to devise diamond structures under conditions that are possibly milder than the chemical vapor deposition (CVD) conditions currently used for diamond growth.¹⁶ Methods have been reported akin to CVD that yielded higher diamondoids (more than four carbon fused-cages) and even diamond from diamondoid seeds.¹⁷

However, for applications of nanodiamond-based materials built “bottom-up” there is still a need for better fundamental understanding and mastering of the conditions of nucleation, growth and self-assembly of diamondoid units.¹⁸ Additionally, general interest in dispersed micro- and nanocrystals stems from the fact that their properties dramatically change with their size and shape,¹⁹ and many applications from optical (plasmon absorption) to medical (transportation through biological barriers) illustrate this point. We thus report on readily accessible processes for the mild vapor deposition of functionalized diamondoids that provide robust self-assembly of nanodiamonds micro- and nanocrystals. Key thermodynamic data including sublimation enthalpy of several diamondoid derivatives are reported from a new measurement protocol at solid–vapor thermodynamic equilibrium state. Easily accessible processes for self-assembled edifices of sizes ranging from 20 nm to several hundred micrometers are reported with remarkable conservation of the general geometry for a given diamondoid, chemical analysis with microscopy ascertaining the full preservation of the nature of nanodiamonds.

Results and discussion

Due to the volatility of adamantane (1) and diamantane (2) (Fig. 1), we envisioned that vapor deposition of functionalized diamondoids might be a general and convenient access to nanocrystals, microcrystals, and thin films of carbon-based materials. The control of a given vapor deposition process entails knowledge of the partial pressure of the source under the experimental conditions. Accordingly, enthalpies of sublimation are critical thermodynamic properties of the condensed phase in relationship with vapor pressure. Therefore, our vapor deposition studies were first devoted to measuring sublimation enthalpies of pristine adamantane and diamantane for which different values have been reported.^{20,21} Conversely, fundamental studies of the vapor pressure of functionalized diamondoids remain very limited.^{21b} We found significant differences in the reported values for the enthalpies of sublimation (see ESI†, Table 1S), depending on the measurement and calculation methods. Mainly destructive calorimetric measurements had been conducted using total combustion of the diamondoids in a bomb calorimeter.²² This prompted us to develop an alternative experimental method to measure the vapor pressure of functionalized diamondoids at the solid–vapor thermodynamic equilibrium state. In this process the diamondoids were brought into the sublimation regime in a chamber connected with a Pirani vacuum gauge at

Table 1 Thermodynamic data for sublimation of 1–5^a

	Clausius–Clapeyron equations	ΔH^0 (kJ mol ⁻¹)	r^2
1	$\ln P = -7212.4/T + 26.869$	60.0 ± 5	0.9991
2	$\ln P = -11\,073/T + 37.172$	92.1 ± 5	0.9992
3	$\ln P = -12\,282/T + 39.589$	102.1 ± 5	0.9960
4	$\ln P = -13\,087/T + 42.196$	108.8 ± 5	0.9983
5	$\ln P = -11\,597/T + 38.335$	96.4 ± 5	0.9965

^a Pressure in Pa, T in K (see ESI for measurement full details).

±0.13 Pa (*i.e.* ±1 μmHg) and the pressure was continuously monitored until the equilibrium state was reached. The temperature dependence of the vapor pressure for the diamondoids 1–5 follows the Clausius–Clapeyron equations given in Table 1.

The enthalpies of sublimation obtained from these equations are $\Delta H^0 = 60.0$ kJ mol⁻¹ for 1, 92.1 kJ mol⁻¹ for 2, 102.1 kJ mol⁻¹ for 3, 108.8 kJ mol⁻¹ for 4, and 96.4 kJ mol⁻¹ for 5, indicating the highest volatility for adamantane, and the lowest for hydroxydiamantane derivatives. The enthalpy of sublimation obtained for adamantane 1 following equilibrium state pressure measurements, $\Delta H^0 = 60.0$ kJ mol⁻¹ (14.3 kcal mol⁻¹), is consistent with the values previously reported (14.2 ± 0.3 kcal mol⁻¹).^{21a} This was also the case for diamantane 2 measurements ($\Delta H^0 = 92.1$ kJ mol⁻¹), with the values obtained using calorimetry bomb combustion,^{21a} and gas-saturation temperature scanning (95.9 kJ mol⁻¹).²³ As expected, the fluoro-diamantane 5 was found to be fairly volatile with a $\Delta H^0 = 96.4$ kJ mol⁻¹ approaching the one we found for pristine diamantane. Due to a noticeable hygroscopic behaviour of the hydroxydiamantanes a good reproducibility required cautiously dried finely divided pure hydroxydiamantane powders to exclude water traces. It was determined that 4-hydroxydiamantane 4 is significantly less volatile, $\Delta H^0 = 108.8$ kJ mol⁻¹, than 1-hydroxydiamantane 3, $\Delta H^0 = 102.1$ kJ mol⁻¹.²⁴

The vapor deposition of 1–5 was then conducted, under tuneable conditions of pressure and temperature, on silicon and mica substrates using a simple sublimation apparatus (see ESI†). The deposition experiments were conducted first under air or argon atmosphere 1.0 bar (10⁵ Pa), and then either under static vacuum (initial pressure 5.3 mbar) or dynamic vacuum (5.3 mbar). Temperature conditions ranging between 50 and 110 °C were investigated. Higher sublimation temperatures favour a higher vapor supersaturation regime, which in turn favours effective nucleation in comparison with crystal growth. A good nucleation rate, in comparison with growth rate, then will quickly generate numerous small crystals of critical size that will no longer disappear and serve as “nutrients” for the growth of bigger crystals (Ostwald ripening).²⁵ Deposition times were varied between a few minutes to 16 h. The vapor deposition of a wide variety of functionalized diamondoids was conducted (see ESI†), including compounds 1–5 (Fig. 2).

Other functionalized adamantane and diamantane derivatives, such as the 1-aminoadamantane, 1-adamantyl-diphenylphosphinite, 1-adamantyl-diphenyl-thiophosphinite, 1-ethynyl-



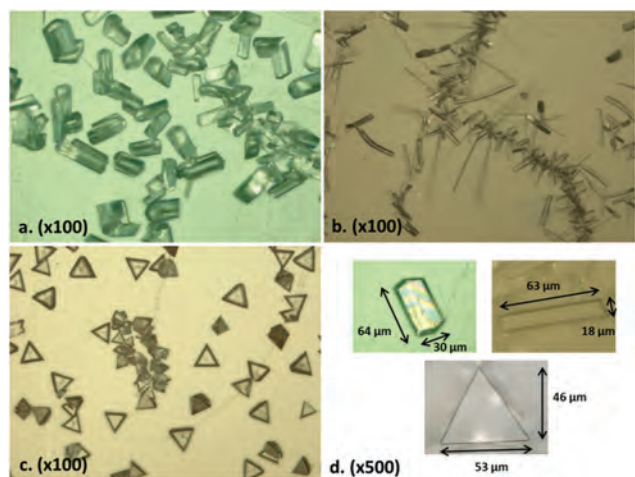


Fig. 2 Optical microscopy of deposits of functionalized diamondanes 3–5. Deposition at 85 °C on mica for 30 min: (a) 1-hydroxydiamantane 3; (b) 4-hydroxydiamantane 4; (c) 4-fluorodiamantane 5; (d) Enhancement from (a–c) micrographs of typical microcrystals of 3–5.

adamantane, 1-hydroxyadamantane, 4,9-dihydroxydiamantane, 4,9-difluorodiamantane were also deposited (see details in ESI†). Optical microscopy of the deposits was conducted for visual inspection of the obtained deposits. Optimization of the deposition conditions was conducted for the diamondoids that were found most suitable for generating from vapor deposition well-defined crystals self-assembly. As illustrated in Fig. 2, crystals of a micrometer size with very different shapes and structures grew depending on the nature of the diamondoid. The deposition of 1 was difficult due to the high volatility of this compound which easily re-evaporates after condensation. The vapor deposition of 2, although easier, resulted in very fragile assemblies that easily broke on handling (see microstructures in ESI†). Conversely, nice crystalline deposits of well-dispersed homogeneous microcrystals were obtained in less than one hour from the vapor deposition of hydroxyl- and fluoro-functionalized nanodiamonds 3–5. Interestingly, not only the nature of the functionalization shows an overwhelming influence on the self-assembly and thus microstructure of the deposits, but also the position of the functional group on the cage. Thus, from the vapor deposition of 3–5, hexagonal rod, rectangular needle, and triangular plate microcrystals were observed, respectively. The size of the crystals can be adjusted through the duration of the deposition with conservation of excellent dispersion and size homogeneity. The high crystallinity of the deposits was confirmed by successful single crystal X-ray diffraction analyses conducted on all these samples. For instance, the X-ray diffraction analysis of microcrystals of 3 (Fig. 17S in ESI†),²⁶ shows the presence of discrete tetramers for which the units are in a cyclic network of O–H...O hydrogen bonding. These tetramers are arranged in 1-D columns. A similar structure was found for 4.

Scanning electron microscopy (SEM) analysis was conducted to examine surface morphologies in further details (Fig. 3). Much to our surprise the SEM images showed that the

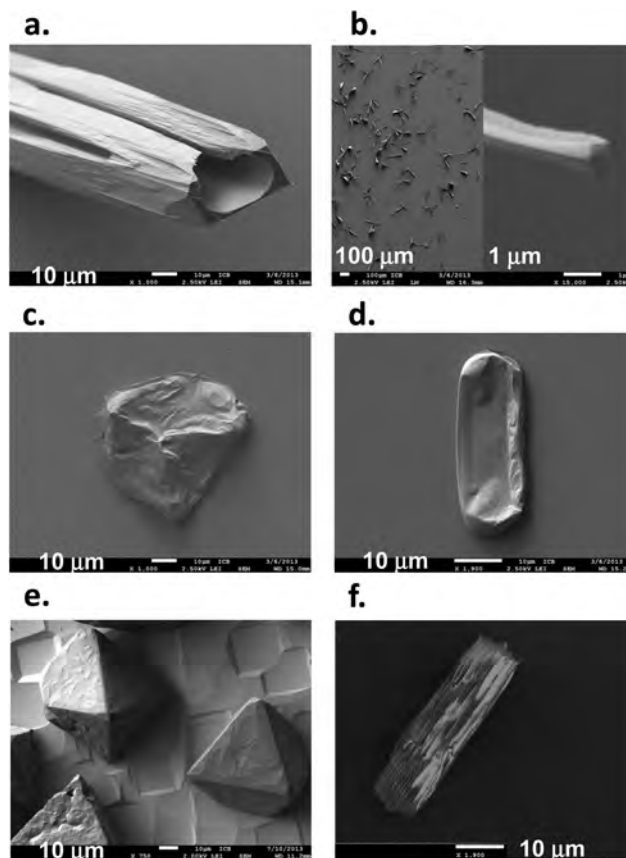


Fig. 3 SEM micrographs of self-assembled functionalized diamondanes deposited from the vapor phase: (a) hexagonal rod of 3 deposited at 1 bar (air or Ar); (b) needles of 4 deposited at 1 bar (air or Ar) protected by a gold layer before SEM analysis (enhancement of a hollow crystal, bottom right); (c) and (d) deposits of 5 and 3 protected by a gold layer before SEM analysis (as truncated octahedron and rod, respectively); (e) and (f) self-assembly of 5 and 3 deposited under 5.3 mbar dynamic vacuum.

first deposits elaborated under atmospheric pressure of air or argon do not tolerate the low pressure, 10^{-6} mbar, and the voltage imposed by SEM analysis. For instance, deposits of 5 were completely volatilized, and while self-assemblies of 3 and 4 were more resistant, they also showed a tendency toward shrinkage during the analysis. Microcrystals of 3 that appeared as well-defined hexagonal rods in optical microscopy turned into hollow rectangular structures under the SEM conditions (Fig. 3a). The formation of hollow needles for 4 is shown in the SEM micrographs (Fig. 3b) with shrinkage also evidenced for the needle crystals from collapsed edges shown in the enlarged picture (right). Hollow micro- and nanostructures are studied in areas which include catalysis, cosmetics, drug and gene delivery, hydrogen production and storage, photonics, photovoltaics, and rechargeable batteries.²⁷ Mostly metal-based and ceramic hollow micro-/nanostructures have been prepared, commonly from template-removing procedures. To the best of our knowledge, the formation of non-polymeric hollow structures of pure hydrocarbons has not previously



been documented. We hypothesized that their formation was either due to some unlikely selective internal volatilization and/or rearrangement of the self-assembly under the SEM conditions, or better to some gas capture – either air or argon – inside the structures during the growth process. To support the latter hypothesis, we tried to protect the diamondoid particles grown under atmospheric pressure by covering them with a 15–20 nm thin layer of gold metal before SEM analysis using sputtering by high resolution ion beam coater. This metallization was also achieved under high vacuum (10^{-5} mbar) and consequently the crystal morphologies were modified before the gold layer could fully protect the deposit. However, these experiments established that during the vapor deposition process under atmospheric pressure some gas was trapped inside the self-assembly of diamondoids. As shown in Fig. 3c and d respectively, shrinkage of the polyhedral particles based on triangle motifs for 5, and hexagonal rods for 3 were observed, while the gold protective layer roughly conserved the original shape of the edifices.

With the goal of growing crystals in which no gas trapping occurs and that would also be resistant to the SEM conditions, we modified the vapor deposition apparatus used under atmospheric pressure to allow sublimation under 5 mbar reduced pressure (Fig. 16S in ESI†). We were delighted to confirm the success of this strategy. As illustrated in Fig. 3e and f, the deposition of microcrystals of about $40\ \mu\text{m}$ was achieved, with the SEM revealing three-dimensional structures fully consistent with the optical microscopy observations. The triangular shapes observed in optical microscopy thus correspond to the faces of regular octahedra which result from the self-assembly from the vapor phase of fluorinated diamondoid 5. The hexagonal rods observed for hydroxylated diamantane 3 revealed an apparent surface roughness that was not observed for 5. EDX microanalysis conducted during the SEM experiments on various areas of the deposited samples confirmed elemental composition and nature of the deposits. This is illustrated in Fig. 4 that presents a deposit of 5 on silicon (area-Spect 3, EDX $C_{K\alpha 1} = 0.280\ \text{keV}$, $F_{K\alpha 1} = 0.532\ \text{keV}$) and compares it to a pristine zone of the silicon substrate (area-Spect 2, EDX $Si_{K\alpha 1} = 1.739\ \text{keV}$). Thus, consistent with the single crystal X-ray diffraction analysis that attested high crystallinity and purity of the deposits, the peaks corresponding to the electron binding energies $K_{\alpha 1}$ for C, F and Si were detected depending on the focus area of the beam. The size distribution in Fig. 4 confirmed an average size of $40\ \mu\text{m}$ with the major part of the particles having a size between 25 and $55\ \mu\text{m}$. More than 90% of the visible aggregates have pyramidal and octahedral shapes, and less than 5% edifices experienced intense Ostwald ripening for reaching sizes above $60\ \mu\text{m}$.

Heavier plasma-hydrogenated detonation nanodiamond developed by Arnault and co-workers have shown a tendency to self-assembling as aggregates in water solution, depending on counter ions present.²⁸ Our attempts to generate accurate and reproducible self-assemblies such as obtained from vapor phases, but by crystallization from our functionalized diamondoids in solution (dip-coating, dichloromethane, water)

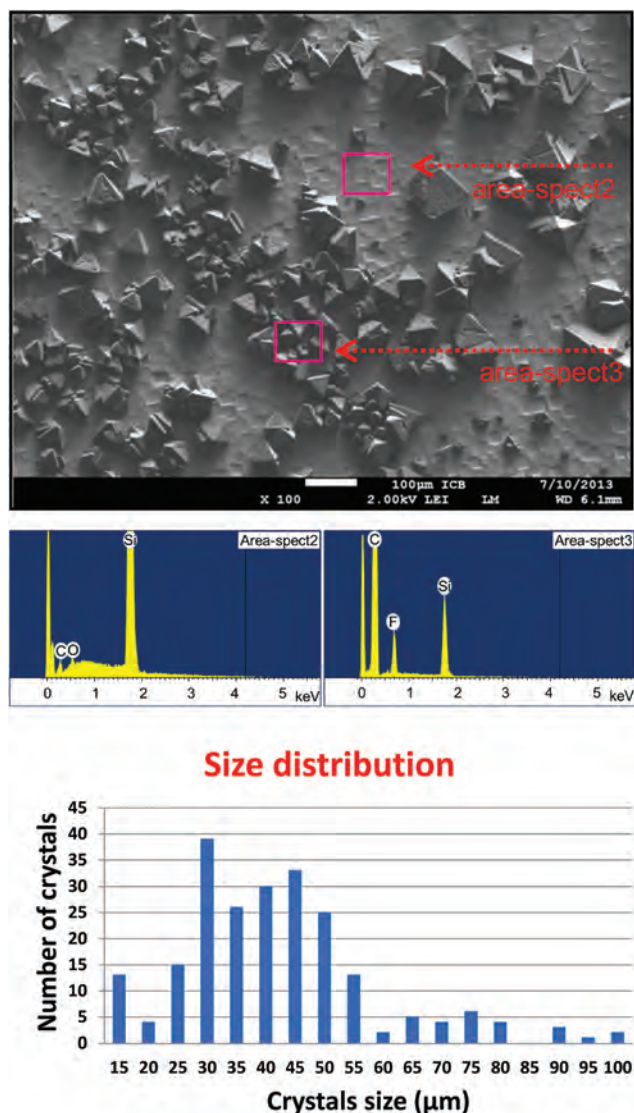


Fig. 4 SEM micrograph of 5 deposited on a silicon substrate (top). EDX analysis of different zones (area-Spect2 and area-Spect3), beam energy 5 keV, a beam size $1\ \mu\text{m}^3$. $C_{K\alpha 1} = 0.280\ \text{keV}$, $F_{K\alpha 1} = 0.532\ \text{keV}$ and $Si_{K\alpha 1} = 1.739\ \text{keV}$ (middle). Related histogram of the size of crystals averaged at $40 \pm 15\ \mu\text{m}$ on >90% of particles (bottom).

were unsuccessful, giving mainly a large area covered with isotropic structurally poorly-defined coated material (see optical microscopy and SEM images in ESI†).

After having determined practical vapor deposition conditions for growing well-dispersed self-assembly of diamondoids as microcrystals – with various shapes depending on the diamondoid functionalization and on the position of the function on the cage – we addressed the more challenging task of growing crystals of nanometer size by a similar vapor deposition technique. A particularly pertinent issue was whether shapes and structures previously obtained from functionalized diamondoids vapor self-assembly would be conserved at the nanoscale. The very first step of deposition process could not be controlled by the simple evaporation apparatus we designed



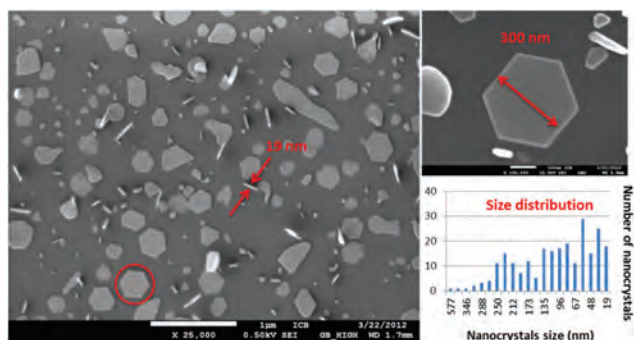


Fig. 5 SEM micrograph of nanocrystals of 1-hydroxydiamantane **3** deposited on Si(111)/SiO₂ by PVD under a pressure 1.4×10^{-6} mbar of argon (left). Magnification on a typical hexagonal-shaped nanocrystal (top right) and related histogram of the size of nanocrystals (bottom right).

for fast and easy self-assembly of diamondoids as microcrystals. Instead we thus used a three-chamber high vacuum physical vapor deposition (PVD, 10^{-9} mbar) apparatus incorporating *in situ* XPS analysis (see Fig. SXPS2 in ESI† from **3** a typical C 1s peak at 284.0 eV appears). The vapor deposition of **3** under suitable vapor pressure was performed using this PVD apparatus, and led to the growth of well-defined crystalline hexagonal rods. Diamondoid vapours were brought very close to the substrates through a heating tube placed at 2 mm distance. Deposition on a silicon surface that was treated following a RCA protocol to remove carbon contamination was achieved from 20 mg of **3** heated at 100 °C for 3 h under a low pressure of 1.4×10^{-6} mbar. SEM images of the resulting deposits are provided in Fig. 5. As expected, these deposits were resistant to the SEM analysis conditions. Fig. 5 (bottom right) provides a representative histogram of the nanocrystals dispersion. Generally, sizes ranging between 20 and 600 nm were obtained under these conditions. Discrete 30–100 nm nanocrystals were obtained in majority (>70% of the particles). We were glad to observe that the self-assembly of **3** mostly exhibits hexagonal shapes with well-defined growth directions. These growth directions were not induced by the Si(111) substrate since an amorphous SiO₂ thin layer is always present at the surface of the substrate before deposition as confirmed by XPS (with O 1s peak of SiO₂ found at 532.5 eV, see Fig. SXPS1 in ESI†). Accordingly, owing to non-preferentially oriented macroscopic growth of nanocrystals some were positioned perpendicularly to the surface.

In the SEM picture Fig. 5 (left) these diamondoid particles can be easily identified and the images allowed measuring their thicknesses, which were remarkably regular around 20 nm. This regularity suggests a fairly homogeneous growth rate of the diamondoid particles. EDX analysis with a beam focusing on the edifices (beam energy 5 keV, size $1 \mu\text{m}^3$) showed that the deposit of **3** exclusively contains carbon and oxygen, in full agreement with the chemical nature of the deposit (see Fig. SEDX1 in ESI†). We therefore demonstrated that particles of **3** of approximately 20 nm thickness and size

can be deposited from a vapor phase under strictly anaerobic and low-pressure conditions (1.4×10^{-6} mbar), showing self-assembly into hexagonal structures similar to the microstructures formed at micrometer scale under few mbar pressure. This could be straightforwardly extended to the other nanodiamonds **4** and **5**.

The relation between the self-assemblies morphology and the functional groups in the molecular precursor is for now difficult to rationalize. This is related to the recognized general non-predictability of molecular structure and morphology of crystals. Accordingly, complexity in polymorphism of functionalized diamondoids has been recently illustrated for adamantane halide derivatives.²⁹ Nevertheless, it is worth mentioning the excellent reproducibility which is obtained from this approach in the formation of robust well-defined self-assemblies. This attractive method is very simple and in our case outperforms in terms of quality dip-coating popular methods (see ESI†). Accordingly, this mild temperature vapor phase deposition approach is expected to allow for an easy formation of diamondoid nanoobjects on different types of substrates, including sensitive ones.

Conclusions

In summary, we report here on readily accessible processes for the mild vapor deposition of functionalized nanodiamonds to provide previously unobserved self-assembly of organic micro- and nanocrystals. Key thermodynamic data including sublimation enthalpy of several diamondoid derivatives are reported from a new measurement protocol at solid–vapor thermodynamic equilibrium state. The conditions of pressure used for the depositions are crucial and if appropriately adjusted lead to deposits resistant to high vacuum and high energy beams. Vapor deposition under atmospheric pressure of air or argon led to unprecedented assemblies that apparently capture gases, and turn to hollow edifices upon gas evacuation. Finally, depending on the type of functional group and its position on the diamondoid, the general structure of the discrete deposits can vary dramatically and anisotropic structures such as rods, needles, triangles or in truncated octahedra form. Self-assembled edifices of sizes ranging from 20 nm to several hundred micrometers can be obtained with conservation of a similar geometry for a given diamondoid. Our ongoing work aims at using these diamondoid self-assemblies having reactive functions (OH, F) as supports and seeds for metal deposition and organohybrid diamond constructions.

Experimental

General

Pristine adamantane and diamantane were prepared and purified by sublimation before use.² 1-Aminoadamantane and 1-hydroxyadamantane were obtained from commercial sources. 1-Hydroxydiamantane, 4-hydroxydiamantane, and 4,9-



dihydroxydiamantane were synthesized from diamantane;³⁰ 4-fluorodiamantane and 4,9-difluorodiamantane were prepared from its hydroxyl derivatives.³¹ Syntheses of other functionalized nanodiamonds were from literature reports. Full details of vapor pressure measurements, vapor deposition of functionalized diamondoids, apparatus, including PVD, and all characterization are described in the ESI.†

Mild controlled self-assembly of functionalized nanodiamonds from vapor phases. A functionalized diamondoid (1–5) was placed in a DSC cup on a boron nitride heating element. The substrate was placed above this DSC cup and separated by a ceramic spacer. The whole system was sealed using copper gasket and a valve that was connected to either vacuum line (5 mbar pressure), or argon (1 atm), or air (1 atm). With the vacuum line the inner gas was removed by pumping for 5 min, and then sublimation was started by adjusting the intensity of the current and duration of deposition. After adjusting the intensity of the applied current the deposition started. The temperature setting was also monitored as a function of time. After the deposition time, the source was switched off allowing the system to cool. Once the temperature dropped below 30 °C, the system was opened, the substrate on which the deposit was made was characterized by optical microscopy and by scanning electron microscopy (SEM), EDX and additionally by X-ray diffraction. To avoid tampering samples were stored sealed in a freezer at 4 °C.

Physical vapor deposition. Typically a Si(111) wafer $1 \times 1 \text{ cm}^2$ was cleaned from carbon-based contamination with RCA clean (see ESI†) and kept inside the heating chamber of a PDV apparatus. An amorphous SiO₂ thin layer forms, the Si(111)/SiO₂ then were heated by induction at 800 °C for 12 min, and then moved into the main vacuum deposition chamber with an initial pressure of 1.6×10^{-8} mbar. A glass tube containing 1-hydroxydiamantane (3) was purged before the connection valve was opened and then heated with heating wire at around 80 °C for 3 h; the pressure increased to about 1.4×10^{-6} mbar. *In situ* XPS analysis allowed monitoring of the deposition process. After cooling, the sample was removed from the PVD apparatus, and to avoid its altering it was stored sealed in a freezer at 4 °C.

Acknowledgements

This work was supported by the “Conseil Régional de Bourgogne” (18 months PhD grant for M. A. G. in project PARI-IME SMT08) and by the CNRS through 3MIM P4-program on *nanodiamonds functionalization for biological applications*. The work in Giessen was in part supported by the Department of Energy, Office of Basic Energy Sciences, Division of Materials Science and Engineering, under contract DE-AC02-76SF00515. Thanks are due to Frederic Herbst (LICB, Dijon), Claire-Hélène Bra-chais (ICMUB, Dijon), and Philippe Richard (ICMUB, Dijon), for their assistance with EDX, DSC, and XRD measurements, respectively.

Notes and references

- M. A. Gunawan, J.-C. Hierso, D. Poinso, A. A. Fokin, N. A. Fokina, B. A. Tkachenko and P. R. Schreiner, *New J. Chem.*, 2014, **38**, 28.
- H. Schwertfeger, A. Fokin and P. R. Schreiner, *Angew. Chem., Int. Ed.*, 2008, **47**, 1022.
- V. N. Mochalin, O. Shenderova, D. Ho and Y. Gogotsi, *Nat. Nanotechnol.*, 2012, **7**, 11.
- A. Krueger, *Adv. Mater.*, 2008, **20**, 2445.
- Ultrananocrystalline Diamond: Synthesis, Properties and Applications*, ed. O. Shenderova and D. Gruen, William-Andrew Publishing, Norwich, NY, USA, 2006.
- A. Krueger and D. Lang, *Adv. Funct. Mater.*, 2012, **22**, 890.
- We reserve “nanodiamond” as a generic name for mixtures of compounds (mostly originating from CVD or detonation methods), and in singular form because it is a class of materials. The term “nanodiamonds” used for diamondoids on the other hand implies, because of plural, that the individual entities can be counted, that is, they have to be uniform and discernible nanometer sized molecules.
- L. Moore, E. K.-H. Chow, E. Osawa, J. M. Bishop and D. Ho, *Adv. Mater.*, 2013, **25**, 3532.
- O. Faklaris, V. Joshi, T. Irinopoulou, P. Tauc, M. Sennour, H. Girard, C. Gesset, J.-C. Arnault, A. Thorel, J. P. Boudou, P. A. Curmi and F. Treussart, *ACS Nano.*, 2009, **3**, 3955.
- A. Krueger, *Chem. – Eur. J.*, 2008, **14**, 1382.
- (a) W. L. Yang, J. D. Fabbri, T. M. Willey, J. R. I. Lee, J. E. Dahl, R. M. K. Carlson, P. R. Schreiner, A. A. Fokin, B. A. Tkachenko, N. A. Fokina, W. Meevasana, N. Mannella, K. Tanaka, X. J. Zhou, T. van Buuren, M. A. Kelly, Z. Hussain, N. A. Melosh and Z.-X. Shen, *Science*, 2007, **316**, 1460; (b) W. A. Clay, Z. Liu, W. Yang, J. D. Fabbri, J. E. Dahl, R. M. K. Carlson, Y. Sun, P. R. Schreiner, A. A. Fokin, B. A. Tkachenko, N. A. Fokina, P. A. Pianetta, N. Melosh and Z. X. Shen, *Nano Lett.*, 2009, **9**, 57.
- P.-L. E. Chu, L. Y. Wang, S. Khatua, A. B. Kolomeisky, S. Link and J. M. Tour, *ACS Nano.*, 2013, **7**, 35.
- S. D. Karlen, R. Ortiz, O. L. Chapman and M. A. Garcia-Garibay, *J. Am. Chem. Soc.*, 2005, **127**, 6554.
- Y.-C. Chen and L. Chang, *RSC Adv.*, 2014, **4**, 18945.
- Few diamondoid-based hybrid compounds exist, see for cluster and MOOFs species: (a) A. B. Lysenko, G. A. Senchyk, J. Lincke, D. Lassig, A. A. Fokin, E. D. Butova, P. R. Schreiner, H. Krautscheid and K. V. Domasevitch, *Dalton Trans.*, 2010, **39**, 4223; (b) B. E. K. Barth, B. A. Tkachenko, J. P. Eußner, P. R. Schreiner and S. Dehnen, *Organometallics*, 2014, **33**, 1678.
- Physics and Applications of CVD Diamond*, ed. S. Koizumi, C. Nebel and M. Nesladek, Wiley-VCH, Weinheim, Germany 2008, pp. 13–93.
- J. E. P. Dahl, J. M. Moldovan, Z. Wei, P. A. Lipton, P. Denisevich, R. Gatt, S.-G. Liu, P. R. Schreiner and R. M. K. Carlson, *Angew. Chem., Int. Ed.*, 2010, **49**, 9881.



- 18 J.-C. Arnault and H. A. Girard, in *Nanodiamond, Diamond Nucleation and Seeding Techniques*, ed. O. A. Williams, RSC, Cambridge, 2014, pp. 221–252.
- 19 C. Burda, X. Chen, R. Narayanan and M. A. El-Sayed, *Chem. Rev.*, 2005, **105**, 1025.
- 20 J. S. Chickos and W. E. Acree Jr., *J. Phys. Chem. Ref. Data*, 2002, **31**, 537.
- 21 (a) T. Clark, T. Knox, H. Mackle, M. A. McKervey, H. Mackle and J. J. Rooney, *J. Am. Chem. Soc.*, 1979, **101**, 2404; (b) T. Clark, T. Knox, M. A. McKervey and H. Mackle, *J. Chem. Soc., Perkin Trans. 2*, 1980, 1686.
- 22 Concerning diamantane, enthalpy of sublimation $\Delta H^0 = 117.2 \pm 8 \text{ kJ mol}^{-1}$ was reported (see ref. 18) that was calculated from the sum of the enthalpy of vaporization and the enthalpy of fusion, see: A. S. Carson, P. G. Laye, W. V. Steele, D. E. Johnston and M. A. McKervey, *J. Chem. Thermodyn.*, 1971, **3**, 915. Various other methods have been used which conversely gave for diamantane ΔH^0 values ranging between 73 and 97 kJ mol^{-1} (see also ESI†).
- 23 T. Clark, T. Knox, H. Mackle, M. A. McKervey and J. J. Rooney, *J. Chem. Soc., Perkin Trans. 1*, 1975, **71**, 2107.
- 24 The identical sublimation enthalpy values reported at 116–118 kJ mol^{-1} for diamantan-1-ol, diamantan-3-ol and diamantan-4-ol are questionable and may be overestimated according our measurements (see ref. 21). Accordingly, DSC measurements of the melting points for **3** and **4** also showed ΔH discrepancies with values substantially different for 1-hydroxydiamantane and 4-hydroxydiamantane: $137 \pm 1 \text{ }^\circ\text{C}$ and $177 \pm 1 \text{ }^\circ\text{C}$, respectively. DSC measurements on cooling were also achieved for determining crystallization peaks that gave single peak excluding polymorphism of **3** and **4** between 25 and 210 $^\circ\text{C}$.
- 25 (a) J.-C. Hierro, R. Feurer and P. Kalck, *Chem. Mater.*, 2000, **12**, 390; (b) P. Serp, J.-C. Hierro and P. Kalck, in *Topics in Organometallic Chemistry: Precursor Chemistry of Advanced Materials: CVD, ALD and Nanoparticles*, 2005, vol. 9, pp. 147–171; (c) J.-C. Hierro, C. Satto, R. Feurer and P. Kalck, *Chem. Mater.*, 1996, **8**, 2481.
- 26 C. Y. Yu, Q. Li, L. B. Wang and H. W. Ma, *Acta Crystallogr., Sect. E: Struct. Rep. Online*, 2006, **62**, o2369.
- 27 (a) X. W. Lou, L. A. Archer and Z. Yang, *Adv. Mater.*, 2008, **20**, 3987; (b) X. W. Lou, Y. Wang, C. Yuan, J. Y. Lee and L. A. Archer, *Adv. Mater.*, 2006, **18**, 2325; (c) H. J. Hah, J. S. Kim, B. J. Jeon, S. M. Koo and Y. E. Lee, *Chem. Commun.*, 2003, 1712; (d) Y. Sun, B. Mayers and Y. Xia, *Adv. Mater.*, 2003, **15**, 641.
- 28 T. Petit, H. A. Girard, A. Trouvé, I. Batonneau-Gener, P. Bergonzo and J.-C. Arnault, *Nanoscale*, 2013, **5**, 8958.
- 29 P. Negrier, M. Barrio, J. L. Tamarit and D. Mondieig, *J. Phys. Chem. B.*, 2014, **118**, 9595 and references therein.
- 30 N. A. Fokina, B. A. Tkachenko, A. Merz, M. Serafin, J. E. P. Dahl, R. M. K. Carlson, A. A. Fokin and P. R. Schreiner, *Eur. J. Org. Chem.*, 2007, 4738.
- 31 H. Schwertfeger, C. Würtele, H. Hausmann, J. E. P. Dahl, R. M. K. Carlson, A. A. Fokin and P. R. Schreiner, *Adv. Synth. Catal.*, 2009, **351**, 1041.



Chapter 3: Chemical vapor deposition of palladium on functionalized diamantanes

Vapor pressure and deposition of diamondoids developed in **Chapter 2** demonstrated the general volatility of functionalized diamondoids and their propensity to form well-defined self-assembled deposits on various substrates. With these crystalline ordered deposits in hand, we intend to deposit metal on it, as nanoparticles or thin films, and thus generate new hybrid materials by OMCVD.

OMCVD is a powerful method to deposit noble metals onto surfaces, it allows using: mild temperature conditions, complex substrate shapes, and thermally sensitive materials. Selective nucleation is possible and thus subsequent area selective growth compared with other methods, such as PVD.¹ In recent literature, the presence of hydroxyl groups on TiO₂ and SiO₂ inorganic substrates has been reported as being responsible for creating new nucleation sites for palladium deposition.² Surface functional groups with organic thiol monolayers can also control the growth of the Pd and Au metal deposits.³ By using hydroxylated diamantanes as a substrate, we expect to control palladium growth specifically on these organic substrates, and thereby uncover properties of novel organohybrid materials.

3.1. Introduction to vapor phase deposition techniques

Several methods exist to produce thin layers by metal deposition. These processes can be distinguished on the basis of the nature of the operating phase for deposition (solid, liquid, or gas). Depositions from gaseous phases (vapor deposition) can be distinguished as physical or chemical vapor deposition, as follows (**Figure 3.1**):

1. Physical Vapor Deposition (PVD)

Physical vapor deposition (PVD) describes a variety of vacuum deposition methods used to deposit thin films by the condensation of a vaporized form of the desired film material onto various workpiece surfaces (e.g., onto semiconductor wafers). The coating method involves purely physical processes such as high-temperature vacuum evaporation with subsequent condensation, or plasma sputter

¹ L. Valade, F. Teyssandier. *L'Actualité Chimique* no. 2, **1999**, 14-21. Précurseurs « métallo-organiques » et dépôt chimique à partir d'une phase gazeuse.

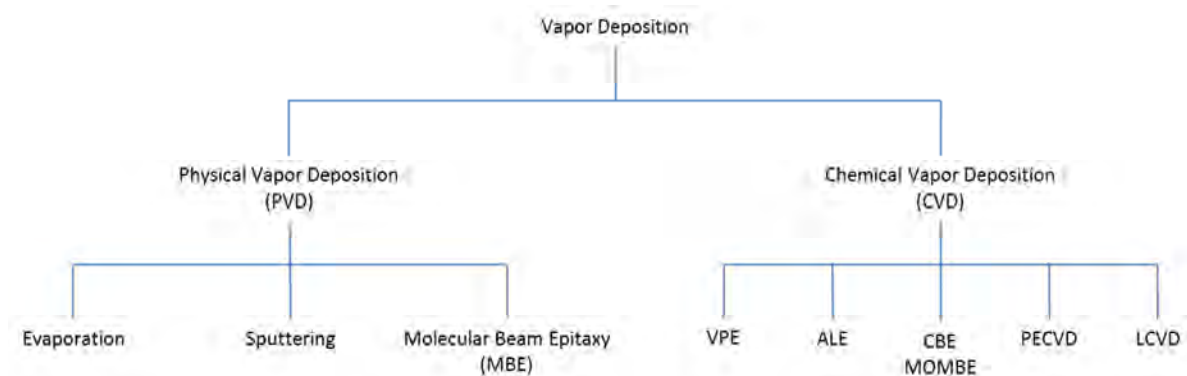
² A. Binder, M. Seipenbusch, G. Kasper. *Chem. Vap. Deposition*, **2011**, 17, 54-57. Observation of structure-sensitive decomposition of [Cp(allyl)Pd] on Pd Nanodots formed by MOCVD.

³ R. A. Fischer, U. Weckenmann, C. Winter, J. Käshammer, V. Scheumann, S. Mittler. *J. Phys. IV France*, **2001**, 11, Pr3-1183-Pr3-1190. Area selective OMCVD of gold and palladium on self-assembled organic monolayers: control of nucleation sites.

bombardment rather than involving a chemical reaction at the surface to be coated as in chemical vapor deposition.

2. Chemical Vapor Deposition (CVD)

CVD is a chemical process used to produce high quality, high-performance, solid materials (ceramics, oxides, metals, etc.). The process is often used in the semiconductor industry to produce thin films. In typical CVD, the wafer (substrate) is exposed to one or more volatile precursors, which react and/or decompose on the substrate surface to produce the desired deposit. Frequently, volatile by-products are also produced, which are removed by gas flow through the reaction chamber. Organometallic chemical vapor deposition (OMCVD) allows making thin layers of metals from gaseous precursors by chemical reactions occurring during the deposition. Organometallic/metallo-organic precursors are used as a starting compound. The vapor of the precursor is injected to the furnace/reactor to deposit a thin layer of metal on the substrate. This technique is very powerful and used in industry because it allows covering substrates of complex shape with uniform layer thickness (cavity, concave surfaces, powder, etc.). Chemical vapor deposition processes are distinguished as several specific technical modes (**Figure 3.1**), such as: vapor phase epitaxy (VPE), atomic layer epitaxy (ALE), as well as plasma and laser enhanced chemical vapor deposition (PECVD, LECVD).



VPE = Vapor Phase Epitaxy

ALE = Atomic Layer Epitaxy

CBE = Chemical Beam Epitaxy or MOMBE = Metal-Organic Molecular Beam Epitaxy

PECVD = Plasma enhanced CVD or PACVD = Plasma Assisted CVD

LCVD = Laser Assisted CVD or LECVD = Laser Enhanced CVD

Figure 3.1. Classification of vapor deposition modes.

The mechanisms operating in chemical vapor deposition are described in **Figure 3.2**:

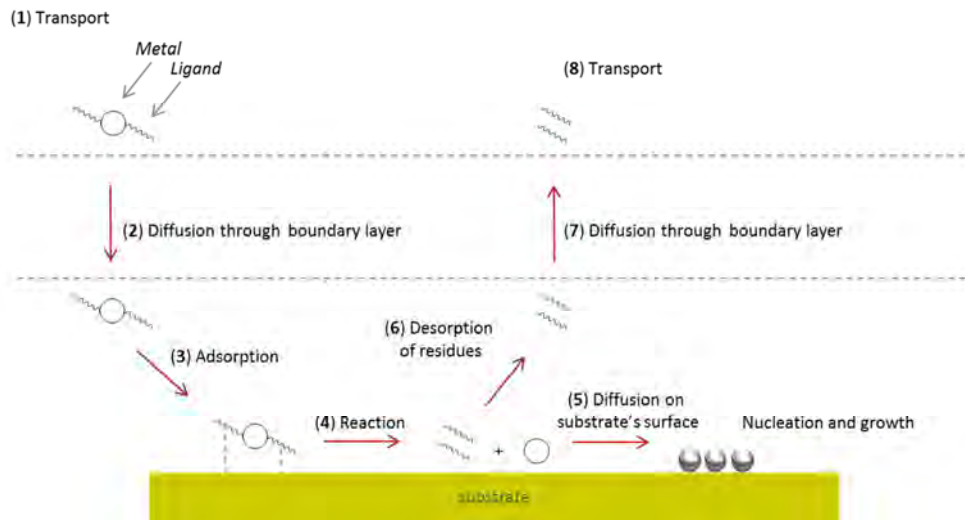


Figure 3.2. Mechanism of CVD.

Step 1: Introduction of the precursor into the vapor phase near the substrate by convection (pumping).

Step 2: Diffusion of the precursor through boundary layer to the substrate surface.

Step 3: Adsorption of the precursor to the substrate surface by chemisorption or physisorption.

Step 4: Chemical reaction (with or without reactive gas, at the temperature of furnace) of the precursor on the substrate surface.

Step 5: Diffusion of metallic atoms to the preferential sites: nucleation followed by growth of the film.

Step 6: Desorption of the residual volatiles from the substrate surface.

Step 7: Diffusion of the residual volatiles through boundary layer to gas phase.

Step 8: Volatiles evacuation and/or trapping (nitrogen trap).

A simplified vision of CVD mechanism can be described as follows: vapor of precursors is delivered by carrier inert gas from the reactor's entrance to the substrate surface by convection to the boundary layer followed by adsorption to substrate surface. The vapor of precursors is then possibly mixed with reactive gas into a homogeneous phase. On the surface, the mixed gas is adsorbed by chemisorption or physisorption. It dissociates and the ligands desorb from the surface to the vapor phase. The formed metals then diffuse to the surface for making nucleation and growing a film.

3. Organometallic precursors and essential features

The chemical reaction of the precursors is a key step of thin film production, with decisive issues concerning growth rate and final purity. A good choice of precursors is thus required. The ideal parameters for precursors^{1,4,5} are described below:

A good precursor should have a high volatility with more particularly vapor pressure ≥ 0.1 Torr at 100 °C. It has been observed empirically that the volatility of organometallic complexes is increased by the presence of various organic ligands such as allyl, halides, cyclopentadienyl, CO, β -diketonato or hydride.⁶ But very polar species or those carrying an anionic or cationic charge are generally much less volatile due to strong molecular interactions. In the solid, polymers, adducts or compounds having hydrogen bonds also have a reduced volatility. It should be able to decompose to the desired material under a suitable temperature regime and give a clean decomposition, avoiding the contamination of the resulting material. It should have an adequate thermal stability especially during the vaporization, gas-phase transport steps, and ideally during the storage. In addition, its synthesis should be preferably high yield with high purity, and cheap. Finally, it must be non-toxic, non-corrosive, and non-pyrophoric.

OMCVD precursor has the general advantage of reactivity and decomposition at relatively low temperature below 200 °C. All the necessary atoms can be provided in a single molecule, and it can be purified by sublimation, recrystallization or distillation.

[Pd(η^3 -allyl)Cp] has been reported to decompose at 260 °C in the gas phase in the absence of reactive gas such as oxygen or hydrogen.⁵ In this work, we selected [Pd(η^3 -allyl)Cp] as organometallic precursor because the temperature of decomposition could be lowered to 30 °C in the presence of H₂ gas.⁵ The deposition of this precursor under various conditions and applications have been extensively studied.^{2,3,7,8,9,10} Beside lowering the temperature, the hydrogen gas also increased the purity of the deposit with less than 3% of native carbon contamination.

⁴ F. Maury. *J. Phys. IV France*, **1995**, c5-449-c5-463. Recent trends in the selection of metal-organic precursors for MOCVD process.

⁵ J.-C. Hierro, R. Feurer, P. Kalck. *Coordination Chemistry Reviews*, **1998**, 178-180, 1811-1834. Platinum, palladium and rhodium complexes as volatile precursors for depositing materials.

⁶ T. T. Kostas, M. J. Hampden-Smith. *Chem. Met. CVD*, **1994**, 329-355. Chemical vapor deposition of platinum, palladium and nickel.

⁷ Q.-H. Wu, M. Gunia, T. Strunskus, G. Witte, M. Muhler, C. Wöll. *Chem. Vap. Deposition*, **2005**, 11, 355-361. Deposition of palladium from a cyclopentadienyl-allyl-palladium precursor on Si-based substrates with various pretreatments: the role of surface Si-OH and Si-H species studied by X-ray photoelectron spectroscopy.

⁸ A. Niklewski, T. Strunskus, G. Witte, C. Wöll. *Chem. Mater.*, **2005**, 17, 861-868. Metal-organic chemical vapor deposition of palladium: spectroscopic study of cyclopentadienyl-allyl-palladium deposition on a palladium substrate.

⁹ C. Dossi, R. Psaro, A. Bartsch, E. Brivio, A. Galasco, P. Losi. *Catalysis Today*, **1993**, 17,527-535. Organometallics-chemical vapor deposition: a new technique for the preparation of non-acidic, zeolite-supported Pd and Pt catalysts.

3.2. Metal deposition on diamondoids by CVD at very low temperature

The deposition was conducted in a hand-made CVD apparatus, depicted in **Figure 3.3**. A quartz cylinder was used as a reactor. The hydrogen gas was introduced into the reactor through small metal tubing. The substrate was placed at a distance about 5 mm from the hydrogen's metal tip. The metal precursor in a small glass cup was placed inside the furnace at about 15 cm distance from the substrate with self-assembled diamondoid crystals. Argon carrier gas was used to dilute the hydrogen gas (1/100). The reactor was connected with a liquid nitrogen trap.

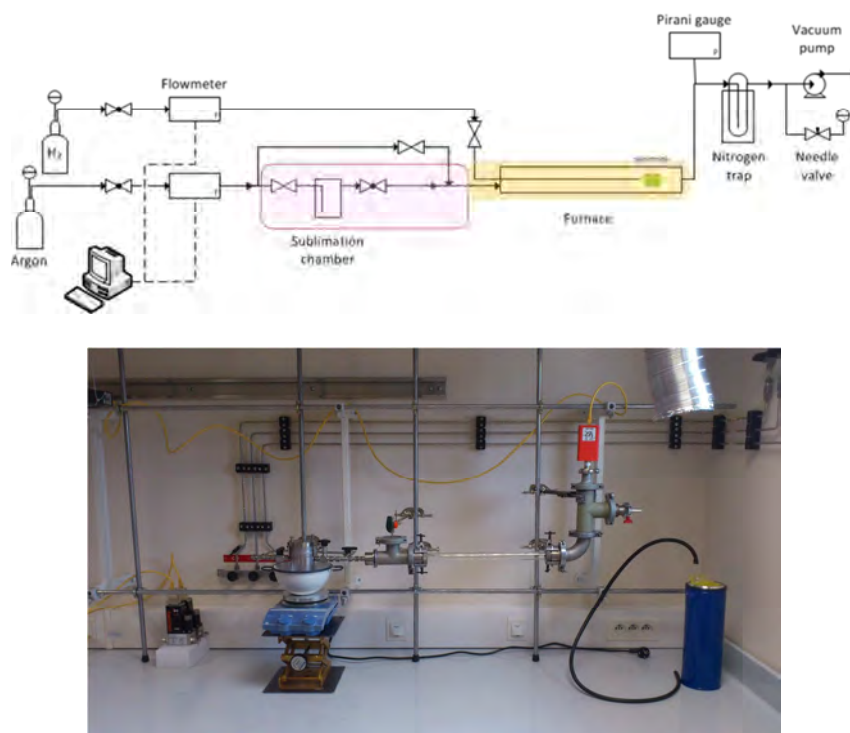


Figure 3.3. Experimental set-up for OMCVD.

1. Palladium CVD on 1-hydroxydiamantane (**30**) and 4-fluorodiamantane (**25**) at 65 °C

1-Hydroxydiamantane **30** deposit that was made by vapor deposition under reduced pressure at 80 °C was used as substrate in the CVD of palladium. The deposition of $[\text{Pd}(\eta^3\text{-allyl})\text{Cp}]$ (**precursor 1**) was done under the following conditions: 51 Torr pressure, 65 °C, 30 min, argon flow = 80 mL/min and H_2 flow = 1.6 mL/min. The same condition was used for 4-fluorodiamantane **25**. The resulting deposits were observed with SEM and in-situ EDX analysis (**Figure 3.4** and **3.5**, respectively).

¹⁰ C. Liang, W. Xia, H. Soltani-Ahmadi, O. Schlüter, R. A. Fischer, M. Muhler. *Chem. Commun.*, **2005**, 282-284. The two-step chemical vapor deposition of Pd(allyl)Cp as an atom-efficient route to synthesize highly dispersed palladium nanoparticles on carbon nanofibers.

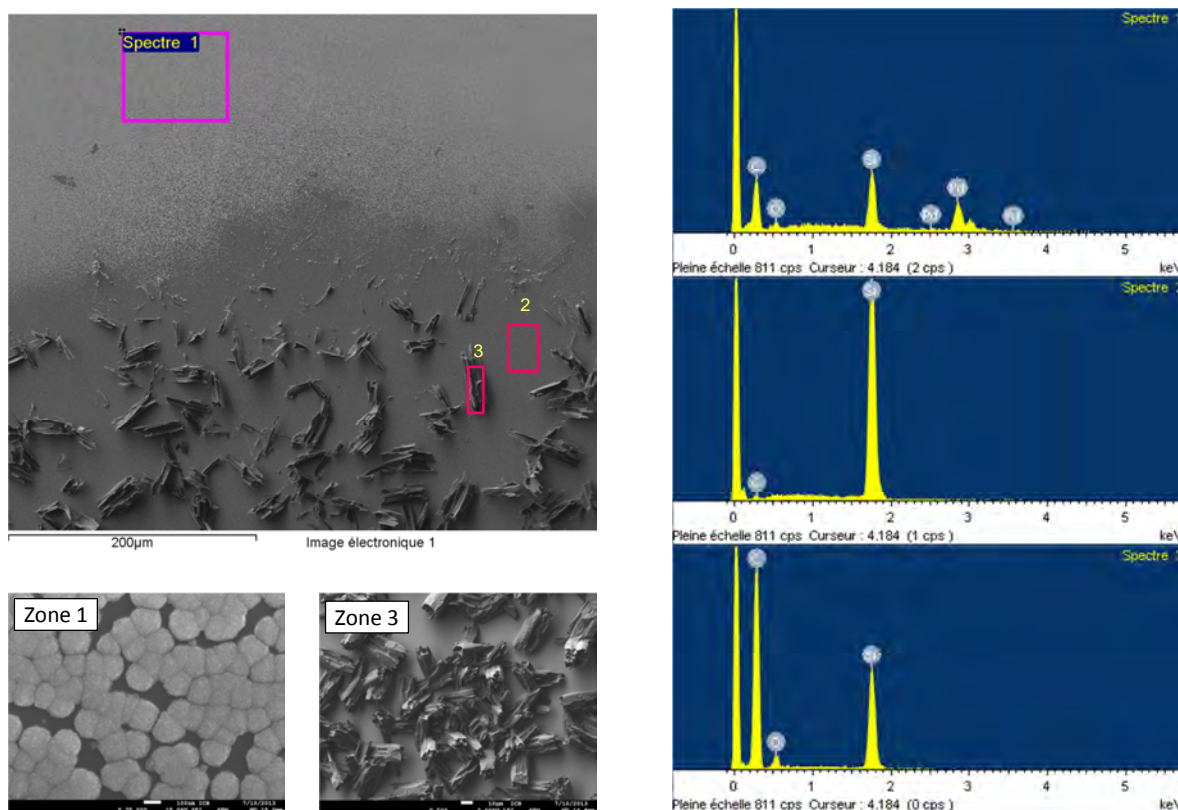


Figure 3.4. Left: Deposit of **30** on Si (dynamic vacuum, 4 Torr, 80 °C, 2 min) followed by CVD of palladium (65 °C, 51 Torr, using **precursor 1**) with enhancement (zone 1 for spectra 1, and zone 3). Right: EDX spectra for zone 1, 2, and 3.

Palladium deposition mainly occurred on the inner wall of the quartz furnace and on the back of the Si wafer (zone 1). The scanning electron microscopy of these deposits showed that Pd deposits include cauliflower-like grain agglomerations having a size ranging from 100 to 160 nm (zone 1, **Figure 3.4**). Metal growth on the quartz wall was similarly observed by several groups for CVD using $[\text{Pd}(\eta^3\text{-allyl})\text{Cp}]^{10}$ or platinum precursors $[\text{PtMe}_2(\eta^4\text{-C}_8\text{H}_{12})]$,¹¹ $[\text{PtMe}_3(\eta^5\text{-C}_5\text{H}_4\text{Me})]$,¹² and low amounts of anchoring sites on the substrates was proposed to be at the origin of such a phenomenon.^{10,12} Additionally, the presence of hydroxyl groups as a thin layer on as-received Si wafers may also explain the palladium deposition on the back of the Si wafer. This result reminded one of experiments reported by the Wöll's group for which using as-received Si wafer was more effective for metal deposition of palladium than using clean Si.⁷

¹¹ P. Serp, R. Feurer, Y. Kihn, P. Kalck, J. L. Faria, J. L. Figueiredo. *J. Mater. Chem.*, **2001**, 11, 1980-1981. Novel carbon supported material: highly dispersed platinum particles on carbon nanospheres.

¹² T. Ngo, L. Brandt, R. S. Williams, H. D. Kaesz. *Surf. Sci.*, **1993**, 291, 411-417. Scanning tunneling microscopy study of platinum deposited on graphite by metalorganic chemical vapor deposition.

Conversely, and much to our surprise and disappointment, we found that the palladium deposition almost did not occur on the diamondoids self-assembly. EDX analysis focused on the hydroxylated diamondoid particles (zone 3, **Figure 3.4**), confirmed the presence of peaks that exclusively corresponds to the diamondoid substrates (C and O at 0.3 eV and 0.55 eV), and the absence of any Pd peak expected at 2.85 eV (see Spectre 1, left **Figure 3.4**). We observed a similar phenomenon of palladium deposit segregation avoiding the area specifically covered with the fluorodiamantane **25** (**Figure 3.5**, Spectre 3) to clearly nucleate over outside areas (**Figure 3.5**, Spectre 1).

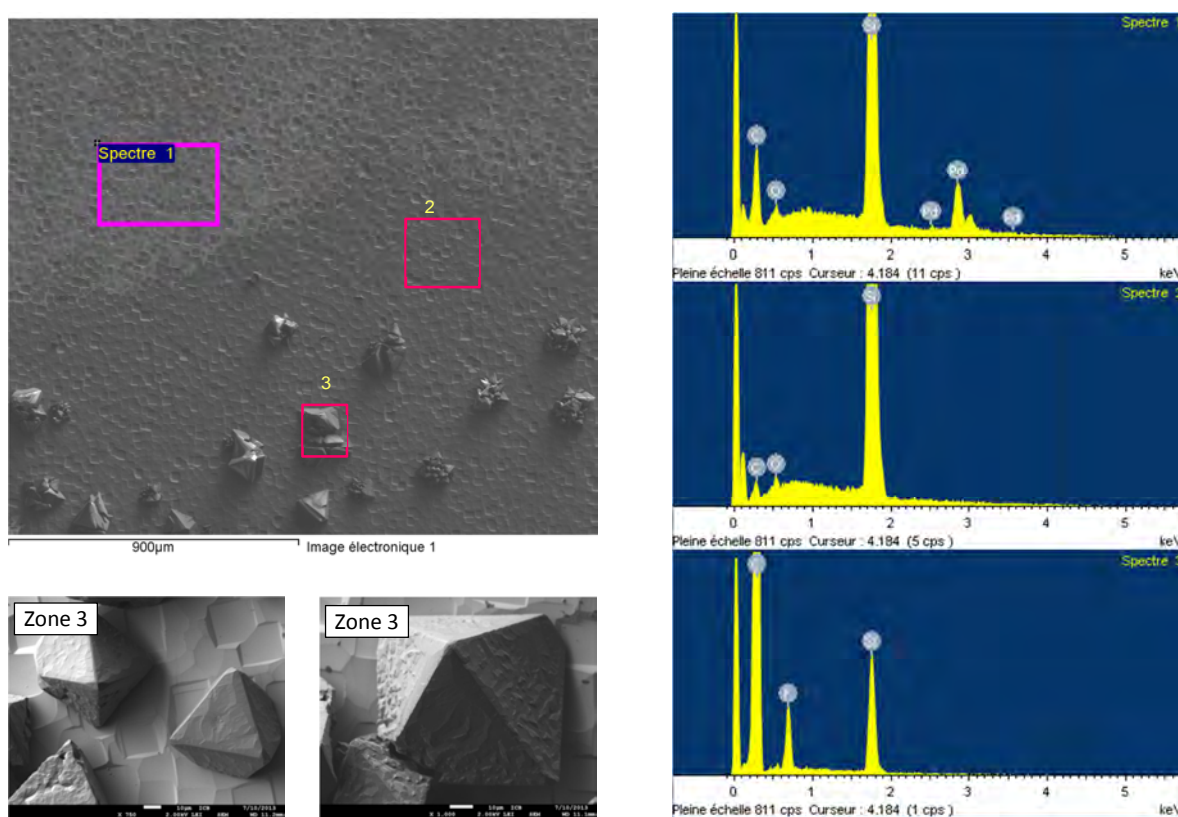


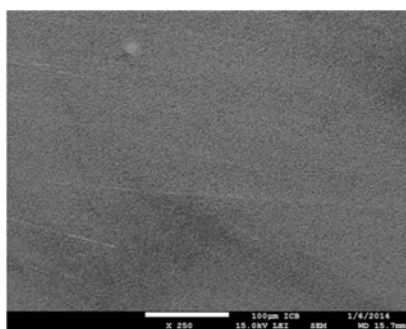
Figure 3.5. Left: deposit of **25** on Si (dynamic vacuum, 4 Torr, 80 °C, 2 min) followed by CVD (65 °C, 51 Torr, using **precursor 1**) and enhancement (zone 3). Right: EDX spectra for zone 1, 2, and 3.

The palladium deposition which occurs preferentially not onto the diamondoids crystallites was not fitting our expectations and we further investigated the OMCVD conditions relating to temperature.

2. Palladium CVD on 1-hydroxydiamantane (**30**) at 30 °C

The temperature of CVD deposition was reduced to 30 °C, and the duration for deposition was increased to 2 h and up to 5 h. The resulting deposit was observed with SEM and EDX analysis as shown

in **Figure 3.6**. Over these long periods of time, thick Pd deposits occurred as layers and the initial diamondoid deposits were thus hardly discernible. Again, the expected use of the hydroxy function on diamondoids as preferential sites for metal growing was clearly not demonstrated by this long-time low temperature approach.



Spectre	C	O	Si	Pd	Pd/O
Spectre 1	48.88	1.96	40.77	8.39	4.3
Moyenne	48.88	1.96	40.77	8.39	
Ecart type	0.00	0.00	0.00	0.00	
Max.	48.88	1.96	40.77	8.39	
Min.	48.88	1.96	40.77	8.39	

Figure 3.6. SEM image of Pd deposit thick layers over **30** and corresponding EDX analysis (% atomic).

The metal deposition using **Precursor 2** [Pt(η^3 -allyl)(hfacac)] is not realized in this work since the study of Pt deposition at low temperature (under 65 °C) has not been optimized yet. Thus, we devoted our effort exclusively to the Pd precursor [Pd(η^3 -allyl)Cp].

3.3. Conclusion

Our first approach for building hybrid carbon-metal ordered structures was based on the two steps self-assembly of functionalized diamondoids on silicon by vapor phase, followed by palladium deposition using low-temperature OMCVD promoted at 65 °C in the presence of H₂ reactive gas. This approach clearly failed. By lowering the temperature and extending the duration of deposition, we forced the deposition of palladium, but without specific selectivity or ordering over the substrates. As a consequence, thick uniform Pd layers were observed. Apparently the affinity of palladium with the Si surface (partially oxidized or with OH surface groups) is stronger than with the hydroxylated or fluorinated diamantanes. The reported studies of the influence of functional groups on the surface have shown that the presence of hydrogen/hydroxyl-terminated surface initiated the Pd decomposition.^{7,10,13,14} But in our case, the presence of H and OH at the surface of diamantane cages did not produce enough affinity to palladium.

¹³ C. P. Mehnert, D. W. Weaver, J. Y. Ying. *J. Am. Chem. Soc.*, **1998**, 120, 12289-12296. Heterogeneous heck catalysis with palladium-grafted molecular sieves.

To solve this issue, we changed our approach and decided to generate strong covalent bonding between the functionalized diamondoids and the transition metal. Concerning palladium, its affinity with phosphorus is well-known. Therefore, we anticipated that forming hybrids might be facilitated by introducing phosphino groups onto the diamondoids. The idea would be then to strongly coordinate the first palladium units that may in turn initiate nucleation of nanoparticles and growth of new hybrid edifices. The synthesis of a variety of original diamondoids functionalized with P-containing groups is the subject of **Chapter 4**.

¹⁴ X. Mu, U. Bartmann, M. Guraya, G. W. Busser, U. Weckenmann, R. Fischer, M. Muhler. *Applied Catal. A: General*, **2003**, 248, 85-95. The preparation of Pd/SiO₂ catalysts by chemical vapor deposition in fluidized-bed reactor.

Chapter 4: Functionalization of diamondoid phosphines

The synthesis of diamondoids having two different reactive functions is a requirement for their use as building blocks for the preparation of organohybrids based on the reactivity differences of the two functions. We thus found it rather surprising that to date no studies have been devoted to the unequal functionalization of adamantyl- and diamantylphosphines despite the high potential of such structures. In our present case we anticipated that difunctionalized diamondoids, bearing both a phosphino group and another reactive function (hydroxy, halide) would be of general interest beyond the present objective of carbon-metal hybrid construction. The main problem we anticipated was the conservation of sufficient volatility for efficient ordering as self-assembly. However, regarding the good volatility demonstrated in **Chapter 2** for hydroxylated diamantanes, it appears reasonable to think that, on this basis, some volatile functionalized diamondoid phosphines may be generated, for instance by tuning the substituents onto phosphorus.

4.1. Short review of the synthesis and applications of diamondoid phosphines

As discussed in **Chapter 1**, diamondoid phosphines were firstly accessible from adamantane or 1-bromo/hydroxyadamantane. The **Schemes 4.1** and **4.2** complement the general results reviewed in **Chapter 1** (shown here *in grey*) with further details on the state-of-the-art concerning diamondoid phosphine synthesis.

The 1-adamantylphosphonic dichloride **126** can be prepared from 1-bromoadamantane **2** with an excess of AlBr_3 in PCl_3 ^{1,2} via a complex $[(1\text{-Ad})\text{PCl}_3^+\text{AlBr}_4^-]$ and also from 1-hydroxyadamantane **6** with PCl_3 in warm concentrated sulfuric acid.³ The primary adamantylphosphine **129** is obtained in three steps from **126** through reaction with $(p\text{-CH}_3\text{OC}_6\text{H}_4\text{PS}_2)_2$ (a.k.a. Lawesson's reagent), sulfide reduction with PPh_3 followed by reduction with LiAlH_4 .⁴ This synthetic pathway can be shortened to a single step by direct

¹ H. Stetter, W. –D. Last. *Chem. Ber.*, **1969**, 102, 3364-3366. Über Adamantan-phosphonsäure-(1)-dichlorid.

² 1-Adamantylphosphonic dibromide from reflux 1-bromoadamantane with 21 eq. of PBr_3 and 1.5 eq. of AlBr_3 for 3 h, 24% yield: H. Duddeck, M. H. A. Elgamal, A. G. Hanna. *Phosphorus and Sulfur*, **1986**, 28, 307-314. Synthesis and Mass Spectra of Adamantylphosphoryl Derivatives.

³ I. K. Moiseev, N. V. Makarova, M. N. Zemtsova. *Russian Chem. Rev.*, **1999**, 68, 1001-1020. Reactions of adamantanes in electrophilic media.

⁴ M. Gouygou, G. Etemad-Moghadam, M. Koenig. *Synthesis*, **1987**, 5, 508-509. A Convenient Method for the Synthesis of 1-Adamantyl-dichlorophosphine.

reduction of **126** with LiAlH_4 in THF under mild conditions to get **129**. This route has been developed by Stetter¹ and patented by Eastham.⁵

Reduction of **116** with HSiCl_3 or with LiAlH_4 gives the secondary phosphine **117**.^{6,7} The di-1-adamantyl phosphinic chloride **116** can be prepared by refluxing adamantane **1** in 5 eq. of PCl_3 with 1 eq. of AlCl_3 .^{5,7} The di-1-adamantylphosphine **117** treated with COCl_2 and DBU leads to di-1-adamantylchlorophosphine **118** that is a valuable starting materials in organophosphorus chemistry.^{7,8} Alternatively, the compound **118** can also be achieved from refluxing the Grignard reagent **60** in diethyl ether with an excess of PCl_3 .⁹ The cousin organophosphorus compounds *tert*-butyl-1-adamantylchlorophosphine **159** and 1-adamantyl phenylphosphonic chloride **160** can also be synthesized from **60** by reaction with 1 equivalent of *t*-Bu PCl_2 and PhPCl_2 , respectively.^{10,11} The oxide of *tert*-butyl-1-adamantylchlorophosphine **161** is formed from reaction between 1-hydroxyadamantane **6** or 1-bromoadamantane **2** with PCl_2Ph in sulfuric acid.^{12,13}

The alkylphosphines **124** and **125** can be prepared from **60**.¹⁴ Another route in order to get the tertiary phosphine **120** is using chlorinated secondary phosphine **118** with a Grignard reagent and CuBr .⁸ Brown *et al.* used 1-bromoadamantane **2** with silver triflate, HPPH_2 and hydrogen peroxide to yield oxide phosphine **126**.¹⁵

⁵ G. R. Eastham, P. A. Cameron, R. P. Tooze, K. J. Cavell, P. G. Edwards, D. L. Coleman. PCT Int. Appl. (2004), WO 2004014552 A1 20040219. Preparation of an aryl-bridged adamantylphosphine catalytic system for carbonylation of olefins.

⁶ HSiCl_3 : (a) H. Fritzsche, U. Hasserodt, F. Korte. *Chem. Ber.*, **1965**, 98, 1681-1687. Reduction of organic compounds of pentavalent phosphorus to phosphines. III. Preparation of primary and secondary phosphines with silanes. (b) J. R. Goerlich, R. Schmutzler. *Phosphorus, Sulfur, and Silicon*, **1993**, 81, 141-148. Di-1-adamantylphosphine, a highly sterically hindered phosphine. Preparation and reactions.

⁷ J. R. Goerlich, R. Schmutzler. *Phosphorus, Sulfur, and Silicon*, **1995**, 102, 211-215. Organophosphorus Compounds with Tertiary alkyl substituents. VI: A convenient Method for the Preparation of di-1-adamantylphosphine and di-1-adamantylchlorophosphine.

⁸ CCl_4 : A. Köllhofer, H. Plenio. *Chem. Eur. J.*, **2003**, 9, 1416-1425. Homogeneous Catalysts Supported on Soluble Polymers: Biphase Sonogashira Coupling of Aryl Halides and Acetylenes Using MeOPEG-Bound Phosphine-Palladium Catalysts for Efficient Catalyst Recycling.

⁹ S. L. Buchwald, D. W. Old, P. J. Wolfe, M. Palucki, K. Kamikawa. U. S. Patent (2001), US 6307087 B1 20011023. Ligands for metals and improved metal-catalyzed processes based thereon.

¹⁰ *t*Bu PCl_2 : M. Su, S. L. Buchwald. *Angew. Chem. Int. Ed.*, **2012**, 51, 4710-4713. A Bulky Phosphine Ligand Allows for Palladium-Catalyzed amidation of Five-Membered Heterocycles as Electrophiles.

¹¹ PhPCl_2 : S. Torker, A. Müller, R. Sigrüst, P. Chen. *Organometallics*, **2010**, 29, 2735-2751. Tuning the Steric Properties of a Metathesis Catalyst for Copolymerization of Norbornene and Cyclooctene toward Complete Alternation.

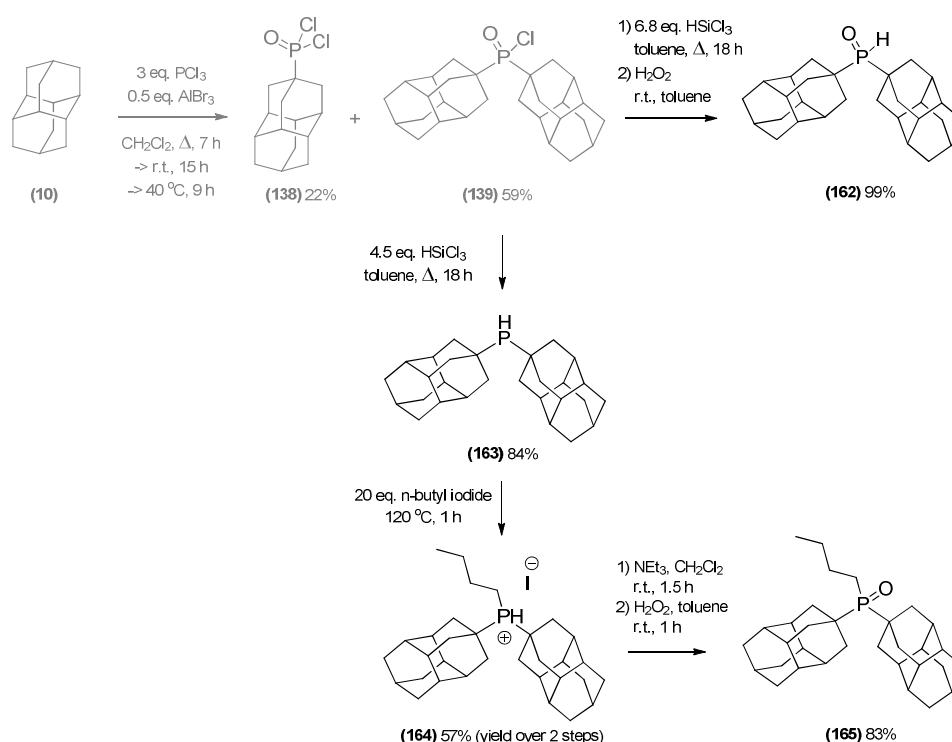
¹² R. I. Yurchenko, L. P. Peresyphkina. *Zhurnal Obshchei Khimii*, **1992**, 62, 2389-2390. Acid dichlorides of phosphonous acids in synthesis of R-(1-adamantyl)chlorophosphinates.

¹³ R. I. Yurchenko, L. P. Peresyphkina, V. V. Miroshnichenko, A. G. Yurchenko. *Zhurnal Obshchei Khimii*, **1993**, 63, 1534-1539. Phosphorylated adamantanes. XV. Phosphorylation of adamantane by trivalent phosphorus acid chloride in sulfuric acid.

¹⁴ J. P. Stambuli, S. R. Stauffer, K. H. Shaughnessy, J. F. Hartwig. *J. Am. Chem. Soc.*, **2001**, 123, 2677-2678. Screening of Homogeneous Catalysts by Fluorescence Resonance Energy Transfer. Identification of Catalysts for Room-Temperature Heck Reactions.

¹⁵ AgOTf: J. Prabagar, A. R. Cowley, J. M. Brown. *Synlett*, **2011**, 16, 2351-2354. Electrophilic Routes to Tertiary Adamantyl and Diamantyl Phosphonium Salts.

The first phosphorylation of adamantane was reported by Olah *et al.* by mixing the adamantane **10** with PCl_3 and AlCl_3 to lead to 1-adamantylphosphonic dichloride.¹⁶ The Schreiner group found that the isomer 4-adamantylphosphonic dichloride **138** was obtained instead (**Scheme 4.2**). Diadamantylphosphinic chloride **139** was also formed in this reaction. The synthesis of secondary and tertiary adamantyl and triadamantyl phosphines was also reported.¹⁷ Reduction of **139** with HSiCl_3 gave the corresponding phosphine **163** in 84% yield. The tertiary phosphine oxide **165** could be prepared *via* the phosphonium salt of di-adamantylphosphine **164** formed from phosphine **163**.



Scheme 4.2. Phosphorylated adamantane derivatives.

The main applications of diamondoid phosphines have been their use as ligands for transition metal catalysis. Adamantylphosphines used in catalysis has been early on investigated by the Buchwald group.^{9,18} The electron-rich, bulky biaryl-di-1-adamantylphosphine ligand **170** (**Scheme 4.3**) was used in the palladium-catalyzed formation of diaryl ethers (**Scheme 4.3, a**). Phosphine **170** was synthesized from

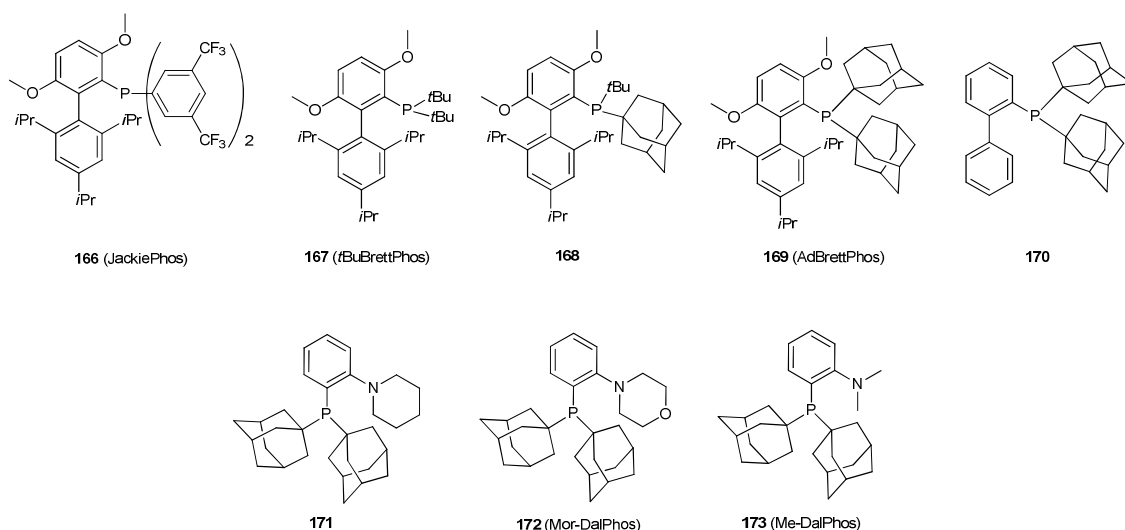
¹⁶ G. A. Olah, O. Farooq, Q. Wang, A. H. Wu. *J. Org. Chem.*, **1990**, 55, 1224-1227. AlCl_3 -Catalyzed Dichlorophosphorylation of Saturated Hydrocarbons with PCl_3 in Methylene Chloride Solution.

¹⁷ H. Schwertfeger, M. M. Machuy, C. Würtele, J. E. P. Dahl, R. M. K. Carlson, P. R. Schreiner. *Adv. Synth. Catal.*, **2010**, 352, 609-615. Diamondoid Phosphines – Selective Phosphorylation of Nanodiamonds.

¹⁸ S. L. Buchwald, X. Huang, D. Zim. U. S. Patent (**2004**), US 20040171833 A1 20040902. Ligands for metals and improved metal-catalyzed processes based thereon.

chlorophosphine **118** and an adequate Grignard reagent (**Scheme 4.1**).¹⁹ The Beller group used diadamantyl-*n*-butylphosphane **123** for Suzuki coupling reactions (**Scheme 4.3**, b) and palladium-catalyzed α -arylations of ketones (**Scheme 4.3**, c) that later on was commercialized as cataCXium®.^{20,21} A similar ligand with a benzyl group was described by Plenio for Sonogashira coupling reactions (**Scheme 4.3**, d).²² In 2012, Buchwald synthesized a series of ligands, including JackiePhos **166**, tBuBrettPhos **167**, ligand **168**, and AdBrettPhos **169** (**Scheme 4.3**). Phosphine **168** was used in palladium-catalyzed amidation of 4-bromo-1-methylimidazole (**Scheme 4.3**, e). They also used the bulkier ligand AdBrettPhos **169** with two adamantyl groups (**Scheme 4.3**, e).¹⁰ They showed also the performance of **169** in palladium-catalyzed coupling of five-membered heterocyclic bromide with amides in 62-94% yield (**Scheme 4.3**, f).¹⁰

Other pertinent examples of phosphine ligands were developed by the Stradiotto group, and several P,N-ligands bearing diadamantylphosphines were designed (**Scheme 4.3**). Mor-DalPhos **172**, is air-stable and suitable for large scale palladium-catalyzed cross-coupling reactions of aryl chlorides and tosylates with hydrazine (**Scheme 4.3**, g)²³ and ammonia (**Scheme 4.3**, h).²⁴



¹⁹ A. Aranyos, D. W. Old, A. Kiyomori, J. P. Wolfe, J. P. Sadighi, S. L. Buchwald. *J. Am. Chem. Soc.*, **1999**, 121, 4369-4378. Novel Electron-Rich Bulky Phosphine Ligands Facilitate the Palladium-Catalyzed Preparation of Diaryl Ethers.

²⁰ A. Zapf, A. Ehrentraut, M. Beller. *Angew. Chem. Int. Ed.*, **2000**, 39, 4153-4155. A new Highly Efficient Catalyst System for the coupling of Nonactivated and Deactivated Aryl Chlorides with Arylboronic Acids.

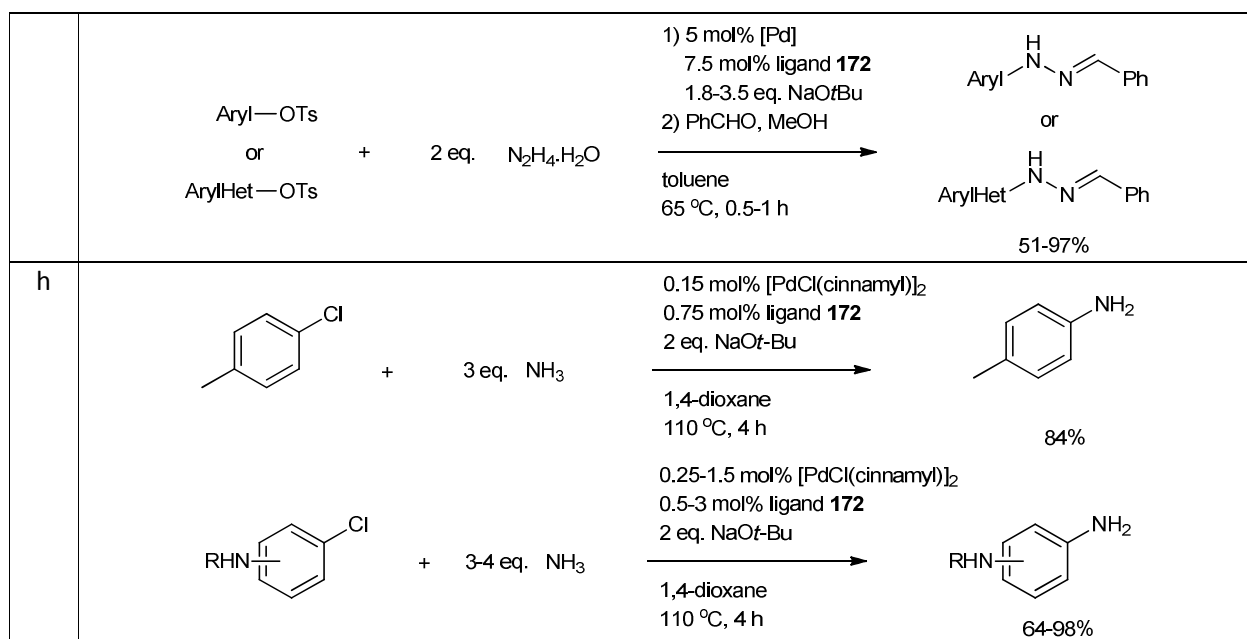
²¹ A. Ehrentraut, A. Zapf, M. Beller. *Adv. Synth. Catal.*, **2002**, 344, 209-217. Progress in the Palladium-Catalyzed α -Arylation of Ketones with Chloroarenes.

²² A. Köllhofer, T. Pullmann, H. Plenio. *Angew. Chem. Int. Ed.*, **2003**, 42, 1056-1058. A Versatile Catalyst for the Sonogashira Coupling of Aryl Chlorides.

²³ R. J. Lundgren, M. Stradiotto. *Angew. Chem. Int. Ed.*, **2010**, 49, 8686-8690. Palladium-Catalyzed Cross-Coupling of Aryl Chlorides and Tosylates with Hydrazine.

²⁴ R. J. Lundgren, B. D. Peters, P. G. Alsabeh, M. Stradiotto. *Angew. Chem. Int. Ed.*, **2010**, 49, 4071-4074. A P,N-Ligand for Palladium-Catalyzed Ammonia Arylation: Coupling of Deactivated Aryl Chlorides, Chemoselective Arylations, and Room Temperature Reactions.

a		<p>2 mol% Pd(OAc)₂ 3 mol% ligand 170 2 eq. K₃PO₄</p> <p>3 mL toluene 100 °C, 14-26 h</p> <p>73%</p>
b		<p>0.005 mol% Pd(OAc)₂ 0.01 mol% ligand 123 (n-Bu) 2 eq. K₃PO₄</p> <p>6 mL toluene 100 °C, 20 h</p> <p>100%</p>
c		<p>0.05 mol% Pd(dba)₂ 0.05 mol% ligand 123 (n-Bu) 2.2 eq. NaOt-Bu</p> <p>5 mL toluene 80 °C, 20 h</p> <p>97%</p>
d		<p>2 mol% NaPdCl₄ 4 mol% ligand 123 (Bn) 1.5 mol% CuI Na₂CO₃</p> <p>3 mL DMSO/toluene/xylene 100 °C, 4-14 h</p> <p>54-96%</p>
e		<p>0.75 mol% [PdCl(allyl)]₂ 3 mol% ligand 168 / 169 2 eq. Cs₂CO₃</p> <p>2 mL 2-methyl-2-butanol 90 °C, 21 h</p> <p>24% for 168 83% for 169</p>
f		<p>0.75 mol% [PdCl(allyl)]₂ 3 mol% ligand 169 2 eq. Cs₂CO₃</p> <p>2 mL 2-methyl-2-butanol 90 °C, 21 h</p> <p>62-94%</p>
g		<p>1) 5 mol% [Pd] 7.5 mol% ligand 172 1.8-2 eq. NaOtBu 2) PhCHO, MeOH</p> <p>toluene 90 °C, 1 h</p> <p>50-97%</p>



Scheme 4.3. Phosphine ligands bearing adamantyl groups and their reaction conditions in catalysis.

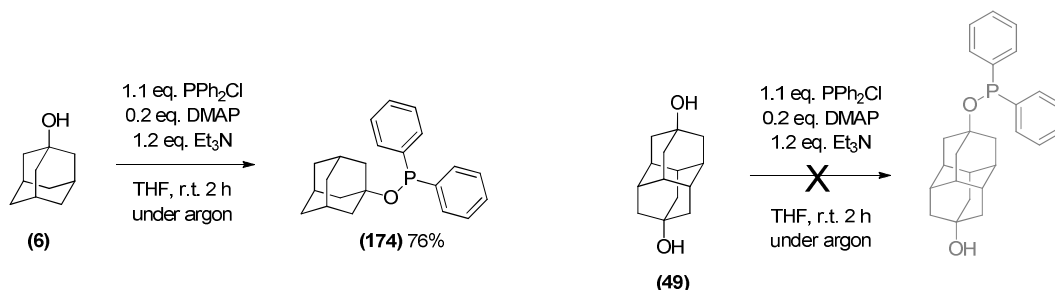
4.2. Synthesis of functionalized diamondoid phosphines and derivatives

Before starting our work in 2011, no studies had been reported concerning the direct functionalization of adamantane and diamantane phosphines. In addition, proper syntheses for diamondoid primary phosphines had been reported only for 1-adamantylphosphine **129** but diamantyl-containing analogs were notably absent. Yet, such primary phosphines could be important intermediates for further tuning the substituents on diamondoid phosphines.

We envisioned that diamondoid phosphines with a supplementary functional group (hydroxyl, halide, *etc.*) could be ideal candidates for anchoring strongly stabilized self-assemblies on chosen substrates. The most serious limitation we anticipated was the unknown resulting volatility of the rather heavy diamondoid derivatives obtained. However, the studies in **Chapter 2** revealed the volatility of hydroxylated diamondoids. Thus, we focused our synthetic work on the formation of novel hydroxylated diamondoid phosphines based on adamantane and diamantane frameworks.

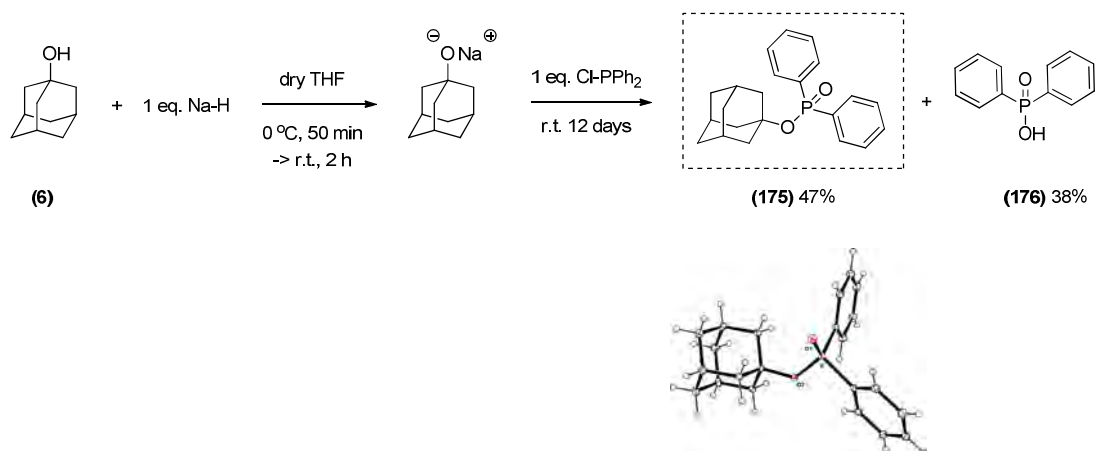
The adamantane scaffold was used as starting material to disclose conditions that may be afterwards transferred to functionalized diamantanes. Based on the reported bibliography we first investigated the synthesis of phosphinite derivatives, since they ought to be more air-stable than phosphines. The

adamantylidiphenylphosphinite **174** was prepared in 76% yield following the literature procedure.^{25,26} However, similar conditions applied to dihydroxydiamantane **49** failed to provide the expected hydroxylated adamantylphosphinite (**Scheme 4.4**).



Scheme 4.4. Synthetic attempts to get phosphinite diamondoids.

We then changed the conditions and attempted to synthesize **174** via deprotonation of **6** (NaH) followed by addition of ClPPh₂. We mainly obtained the oxide of adamantylidiphenylphosphinite **175** (47%, **Scheme 4.5**).²⁷ Since these conditions did not straightforwardly give the expected phosphinite targets, we changed our strategy to investigate direct phosphorylation.



Scheme 4.5. Synthesis of adamantyl diphenylphosphinate.

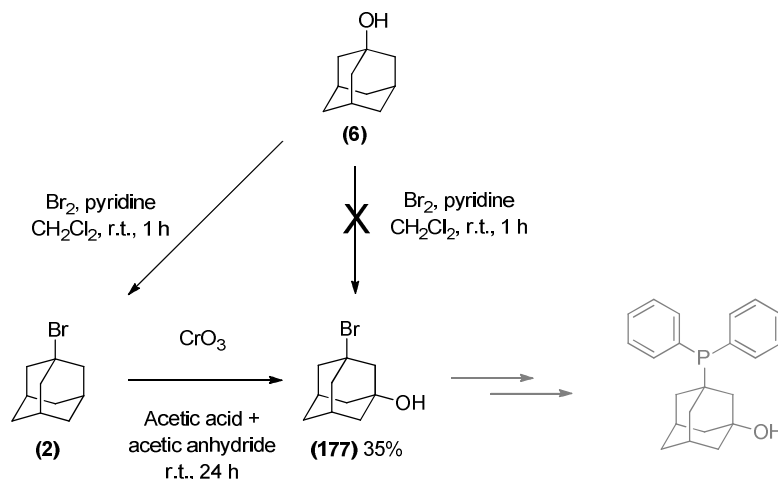
²⁵ K. Ikegai, W. Pluemanupat, T. Mukaiyama. *Bull. Chem. Soc. Jpn.*, **2006**, 79, 780-790. Stereospecific C-S bond formation from chiral tertiary alcohols by quinone-mediated oxidation-reduction condensation using alkyl diphenylphosphinites and its application to the synthesis of a chiral tertiary thiol.

²⁶ K. Kuroda, Y. Hayashi, T. Mukaiyama. *Tetrahedron*, **2007**, 63, 6358-6364. Conversion of tertiary alcohols to tert-alkyl azides by way of quinone-mediated oxidation-reduction condensation using alkyl diphenylphosphinites.

²⁷ For X-Ray data, please see the Experimental Part.

1. Phosphorylation and hydroxylation of diamondoids

Direct bromination of 1-hydroxyadamantane **6** in view of making 3-bromo-adamantan-1-ol **177** failed and 1-bromoadamantane **2** was obtained instead (**Scheme 4.6**). Preparing **177** by hydroxylation of 1-bromoadamantane **2** using chromic oxide was successful, giving a moderate 35% yield.²⁸

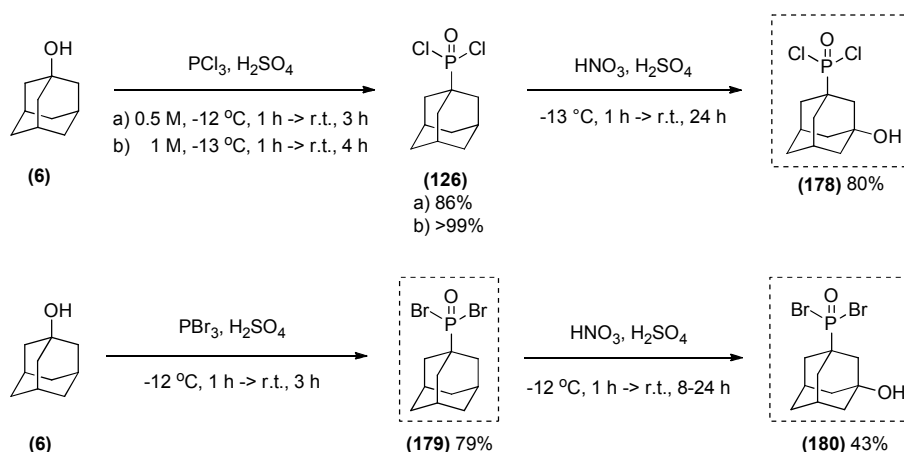


Scheme 4.6. Bromination and hydroxylation of adamantane.

The same conditions were employed with diamantane **10**, showing that chromium trioxide is mainly reactive toward medial position of diamantane, and thus gave 1-hydroxydiamantane **30**. Since we preferentially aimed at functionalizing the apical positions for steric reason related to organohybrid formation, these conditions were not further optimized.

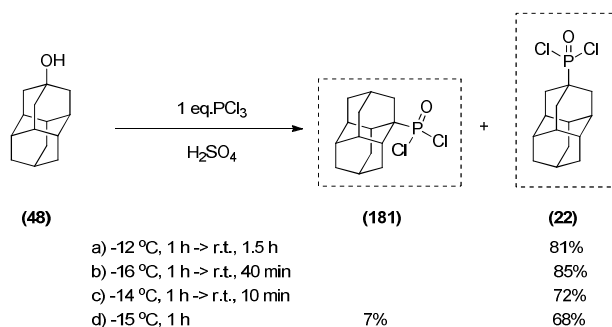
Adamantylphosphonic dichloride **126** ($\delta_p = 65.1$ ppm) was prepared by reaction of 1-hydroxyadamantane **6** with PCl_3 in sulfuric acid (**Scheme 4.7**). Compound **126** was obtained in quantitative yield without further purification needed using concentrated H_2SO_4 . Direct phosphorylation of widely available adamantane **1** using the same conditions unfortunately failed. Straightforward hydroxylation of **126** with nitric acid and sulfuric acid was found the fastest way to get (3-hydroxyadamant-1-yl)phosphonic dichloride **178** ($\delta_p = 62.2$ ppm). Analogous phosphorylation and hydroxylation reactions using PBr_3 gave 1-adamantylphosphonic dibromide **179** ($\delta_p = 52.3$ ppm) and (3-hydroxyadamant-1-yl)phosphonic dibromide **180** ($\delta_p = 47.6$ ppm) although in slightly reduced yields (**Scheme 4.7**).

²⁸ a) A. E. Lukash, A. N. Santiago, R. A. Rossi. *J. Org. Chem.*, **1997**, 62, 4260-4265. Reactions of 1,3-Dihaloadamantanes with Carbanions in DMSO: Ring-Opening Reactions to Bicyclo [3.3.1]nonane Derivatives by the $\text{S}_{\text{RN}}1$ Mechanism.; b) A. E. Lukash, A. N. Santiago, R. A. Rossi. *J. Phys. Org. Chem.*, **1994**, 610-614. Reactions of 1,3-Dihaloadamantanes with diphenylphosphide ions by the $\text{S}_{\text{RN}}1$ mechanism. Competition between intermolecular and intramolecular electron transfer reactions.



Scheme 4.7. Phosphorylation and hydroxylation of 1-hydroxyadamantane **6**.

We then used these conditions with 4-hydroxyadamantane **48** and pleasingly the reaction went very smoothly to give **22** in good yields ($\delta_{\text{p}} = 66.1\text{ ppm}$) (**Scheme 4.8**).

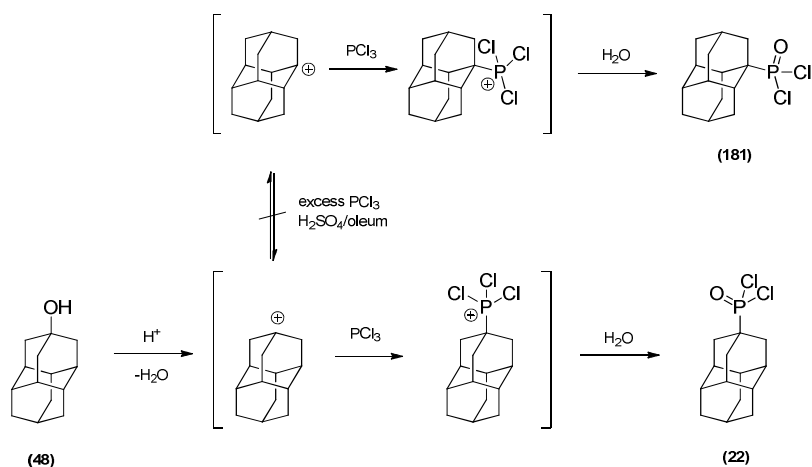


Scheme 4.8. Phosphorylation of 4-hydroxyadamantane **48**.

When the reaction time was reduced to only 1 hour at $-15\text{ }^\circ\text{C}$, the formation of 1-diamantylphosphonic dichloride **181** as byproduct ($\delta_{\text{p}} = 65.8\text{ ppm}$) was evidenced, and confirmed by an X-Ray structure determination.

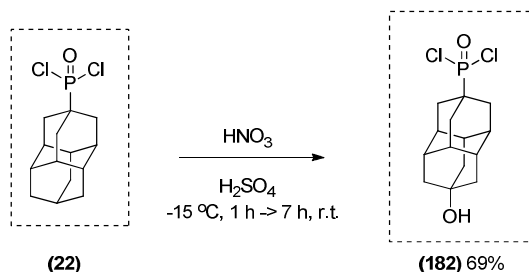
The group of Pr. A. A. Fokin succeeded in optimizing reaction conditions that give exclusively **22**, by using 5 equivalents of PCl_3 in a mixture of sulfuric acid with oleum, and heating at $50\text{ }^\circ\text{C}$ for 30 min. Thereby the formation of phosphonic dichloride isomer **181** (**Scheme 4.9**) is avoided. The compound **22** could also be synthesized in 75% yield from the corresponding hydroxyl derivative **48** reacted with PCl_3 in trifluoroacetic acid.²⁹

²⁹ A. A. Fokin, R. I. Yurchenko, B. A. Tkachenko, N. A. Fokina, M. A. Gunawan, D. Poinot, J. E. P. Dahl, R. M. K. Carlson, M. Serafin, H. Cattey, J.-C. Hierso, P. R. Schreiner. *J. Org. Chem.*, **2014**, 79, 5369-5373. Selective Preparation of Diamondoid Phosphonates.



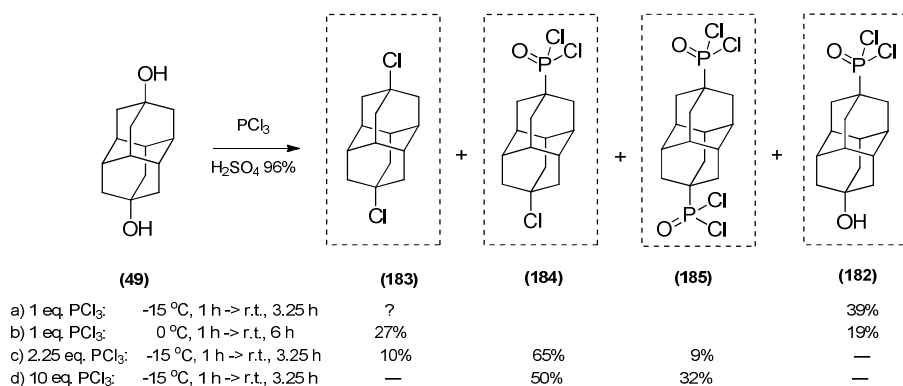
Scheme 4.9. Regioselectivity issues in the medial and apical phosphorylation of 4-hydroxydiamantane.

The hydroxylation of 4-diamantylphosphonic dichloride **22** (**Scheme 4.10**) was achieved to give in high yield hydroxylated diamantane derivative **182** ($\delta_p = 65.3$ ppm). The reaction is regioselective at the apical position, which confirmed our expectation that longer reaction times favor the functionalization at the apical position as it was observed for direct hydroxylation of diamantane (**Scheme 4.8**).



Scheme 4.10. Hydroxylation of 4-diamantylphosphonic dichloride regioselective at the apical position.

With the view to reduce the number of steps to produce **182**, we investigated the direct phosphorylation of 4,9-dihydroxydiamantane **49** under various conditions (**Scheme 4.11**). The best conditions afforded **182** in 39% yield after purification. When longer reaction times at higher temperature were applied, the formation of 4,9-dichlorodiamantane **183** was favored.

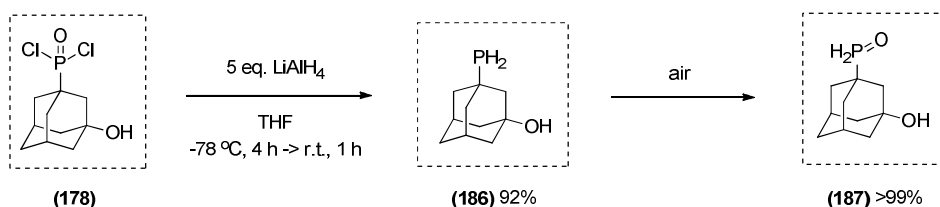


Scheme 4.11. Direct phosphorylation of 4,9-dihydroxydiamantane **49**.

In order to get (diamant-4,9-diyl)diphosphonic dichloride **185**, we increased the quantity of PCl₃ from 1 to 2.5 equiv. Unequally difunctionalized (9-chlorodiamant-4-yl)phosphonic dichloride **184** ($\delta_p = 64.9$ ppm) was obtained as the major product in 65% yield. 4,9-Dichlorodiamantane **183** and (diamant-4,9-diyl)diphosphonic dichloride **185** ($\delta_p = 64.0$ ppm) were also obtained in 10 and 9% yield respectively. By using 10 equivalents of PCl₃ we got a 50% yield of **184** as a major product and all the dichlorodiamantane **183** was converted to **185** (32%). These conditions were found convenient to break the symmetry of the bi-apical diamantane derivatives without any protection/deprotection sequence.

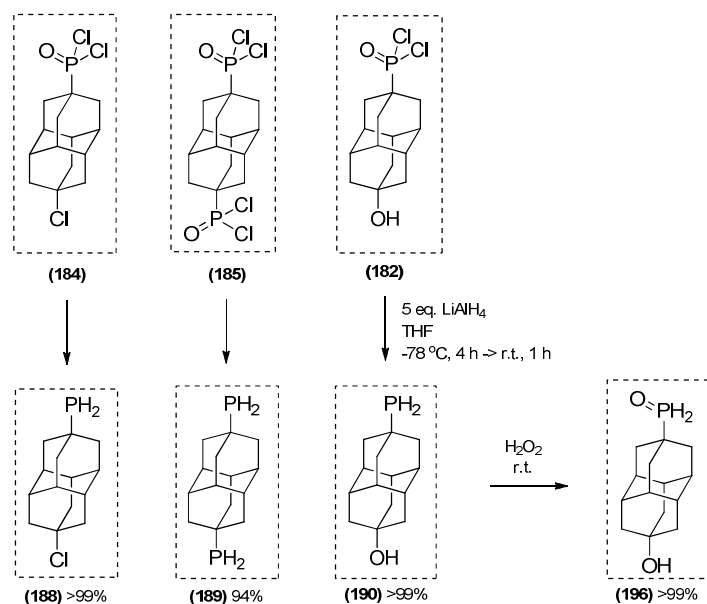
2. Reduction of phosphorylated diamondoids

In order to get rather light weight phosphino groups with a minor impact on the good volatility of hydroxylated diamondoids, we reduced the phosphorylated diamondoids with LiAlH₄. Reduction of **178** with excess LiAlH₄ in THF quantitatively led to **186** (Scheme 4.12). The resulting primary phosphine **186** ($\delta_p = -86.0$ ppm, $^1J_{PH} = 188$ Hz)³⁰ is very air-sensitive and completely oxidized under air in 5 min, giving the oxide **187** ($\delta_p = 25.7$ ppm, $^1J_{PH} = 452$ Hz).



Scheme 4.12. Reduction of phosphorylated adamantane derivative.

³⁰ Hydroxyadamantylphosphine **186** has a ³¹P chemical shift consistent with the reported adamantylphosphine **129** ($\delta_p = -83.6$ ppm, $^1J_{PH} = 189$ Hz).



Scheme 4.13. Reduction of phosphorylated adamantane derivatives.

The reduction of **182** with LiAlH_4 at $-80\text{ }^\circ\text{C}$ selectively and quantitatively yields hydroxylated primary phosphine **190** ($\delta_{\text{P}} = -85.7\text{ ppm}$, $^1J_{\text{PH}} = 192\text{ Hz}$, $^{\text{TS}}J_{\text{PH}} = 6\text{ Hz}$). In the synthesis of **190** the control of low temperature is essential since at higher temperature a cleavage of the phosphino group may occur, giving 4-hydroxyadamantane **48** as the main product. The primary phosphine **190** is air-stable for several days in the solid state. In solution, phosphine **190** slowly undergoes phosphine oxidation to **196** ($\delta_{\text{P}} = 27.6\text{ ppm}$, $^1J_{\text{PH}} = 450\text{ Hz}$) over several days. A complete oxidation is obtained by addition of H_2O_2 at rt. Such air stability was not observed for the adamantyl analog **186**. Actually, few air stable primary phosphines are known (**Figure 4.1**),^{31,32} however, they have frameworks that are all very different from the present diamondoid phosphine.

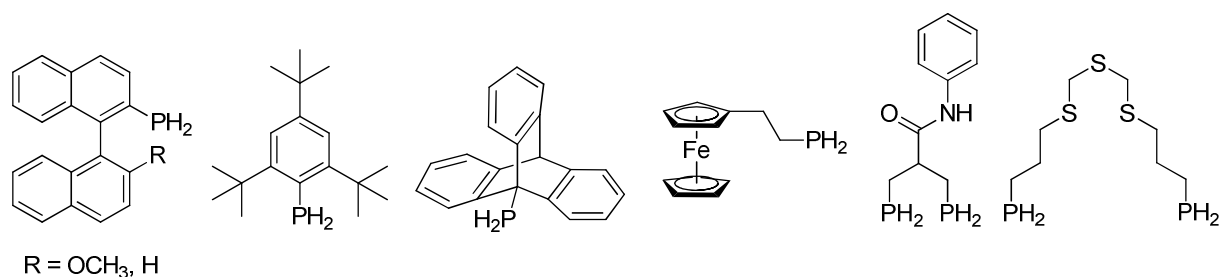


Figure 4.1. Air-stable primary phosphines.

³¹ B. Stewart, A. Harriman, L. J. Higham. *Organometallics*, **2011**, 30, 5338-5343. Predicting the Air Stability of Phosphines.

³² L. H. Davies, B. Stewart, L. J. Higham. *Organomet. Chem.*, **2014**, 39, 51-71. Air-stable, fluorescent primary phosphines.

The mechanism of phosphine oxidation by elemental oxygen has not been fully elucidated, but the formation of the radical cation corresponding to the primary phosphine is a postulated pathway to its oxidation via a radical mechanism.³¹ Primary phosphines which have an extended π -electron structural motif (naphthyl, binaphthyl, triptyceny) possess a HOMO with no significant phosphorus character and are those which usually demonstrate stability to air oxidation.³¹ Steric hindrance has been also claimed as important in stabilizing an otherwise sensitive phosphine, as well as the incorporation in the framework of sufficient conjugation/heteroatom in the molecular skeleton. Obviously, none of these structural features applies to **190** and can explain its air stability compared with cousin compounds **186** and **189**. Analysis of the HOMO orbital for **190** and the SOMO for its corresponding radical cation may be helpful for further understanding.

The reduction of chlorophosphonic dichloride **184** with LiAlH_4 also quantitatively led to the corresponding primary diamantylphosphine, the 4-chloro-9-phosphinodiamantane (**188**, $\delta_p = -85.9$ ppm, $^1J_{\text{PH}} = 193$ Hz, **Scheme 4.13**). The chloro-functionalized diamantylphosphine **188**, similarly to **190**, is air stable for several days in the solid state and in solution (34% after 19 days).

Figures 4.2 and **4.3** illustrate the monitoring in time of oxidation of the functionalized diamantylphosphine **188**, evidencing a very slow kinetic.

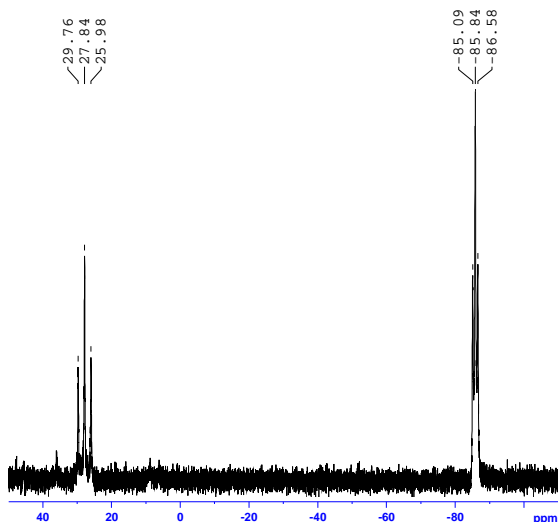


Figure 4.2. ^{31}P NMR (600 MHz, CDCl_3) after 19 days (left is the oxide of **188** at 27.84 ppm and right is the phosphine **188**).

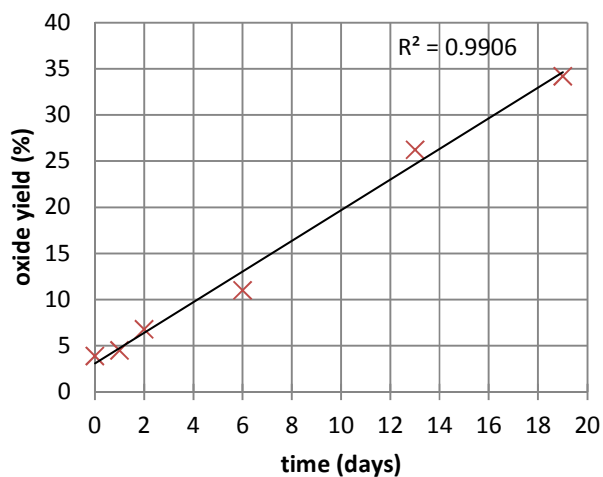
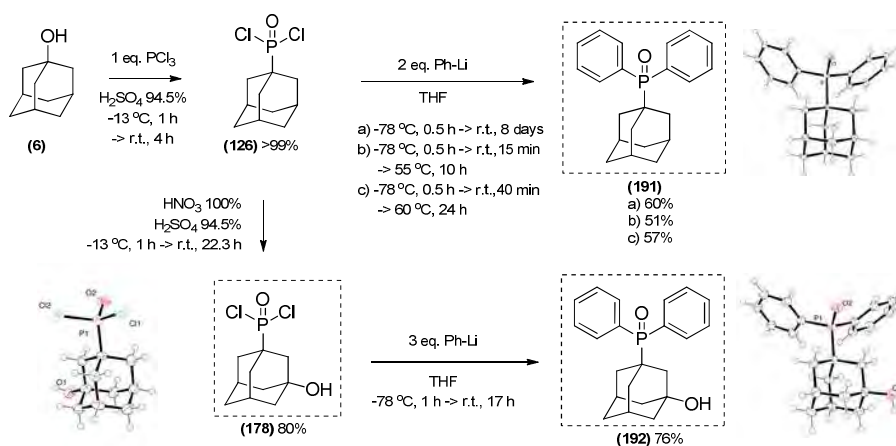


Figure 4.3. Formation of phosphine oxide **188** over time monitored by ^{31}P NMR.

3. Arylation and benzylation of phosphorylated diamondoids

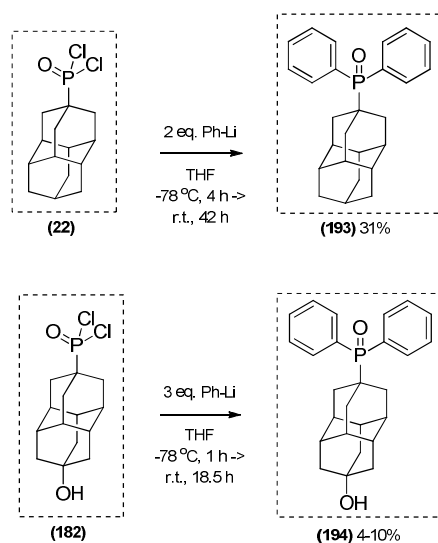
With the phosphorylated diamondoids in our hand, we first tried to prepare tertiary phosphines containing aryl groups. Aryl phosphines are generally more stable compared to alkyl phosphines. Alkyl phosphines, containing a hydrocarbon backbone only, are more electron-rich and more prone to air oxidation.³³ The arylation of adamantylphosphinic chloride **126** with phenyllithium in THF provided modest yield of **191** ($\delta_p = 34.3$ ppm) (**Scheme 4.14**). Using three equivalents of phenyllithium and treatment with water on **178** give straightforwardly **192**, and avoid any protection/deprotection sequences. This pathway thus reduces the number of synthetic steps to get **192** by phenylation ($\delta_p = 33.8$ ppm).



Scheme 4.14. Synthetic route of arylation of phosphorylated adamantyl compounds (X-ray crystal structures for **191** and **192**, showing mostly identical arrangement, are provided).

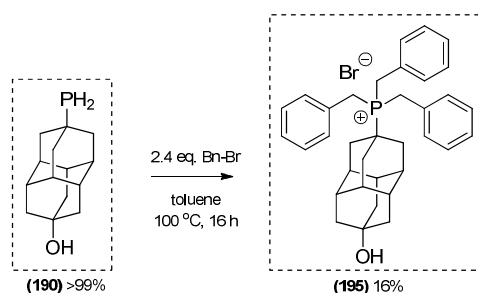
Similar reaction conditions using milder temperature were applied on diamantane derivatives **22** and **182** to respectively form the cousin diamantylphosphine oxides **193** ($\delta_p = 35.0$ ppm) and **194** ($\delta_p = 36.0$ ppm). These syntheses provided lower yields due to repeated delicate purification by crystallization (**Scheme 4.15**).

³³ C. A. Busacca, R. Raju, N. Grinberg, N. Haddad, P. James-Jones, H. Lee, J. C. Lorenz, A. Saha, C. H. Senanayake. *J. Org. Chem.*, **2008**, 73, 1524-1531. Reduction of tertiary phosphine oxides with DIBAL-H.



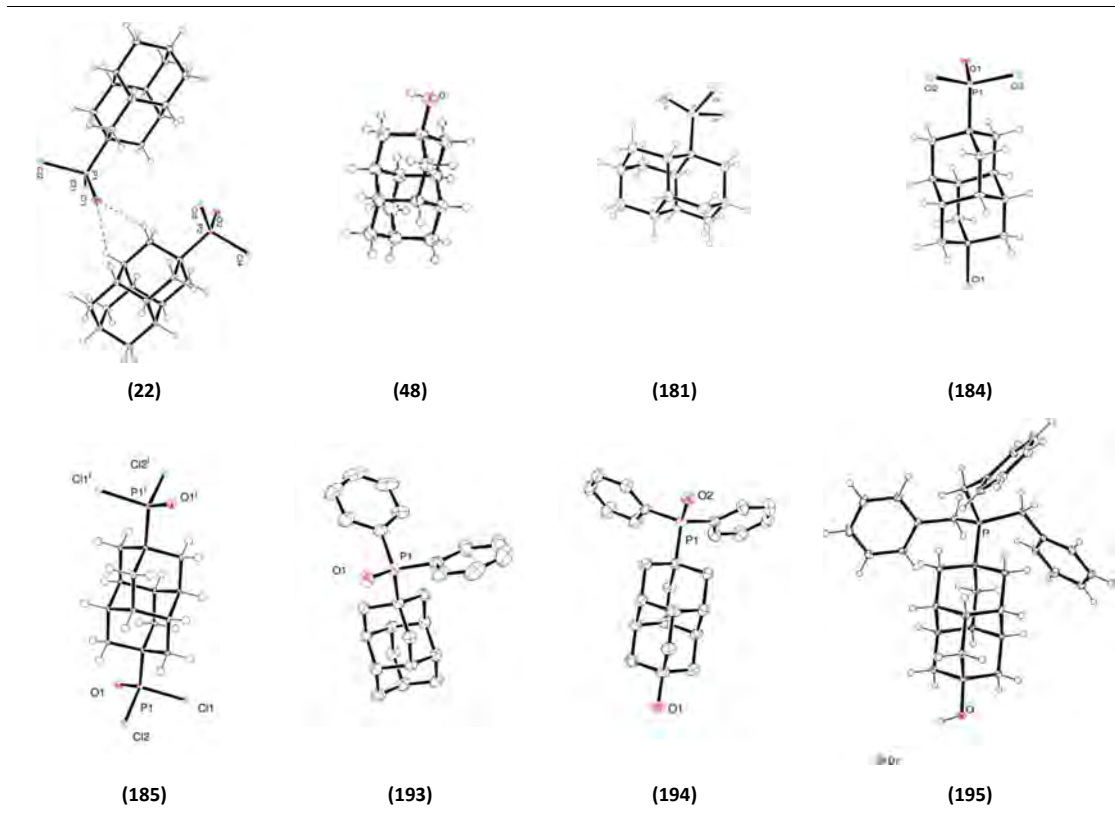
Scheme 4.15. Arylation of phosphorylated diamantyl derivatives.

Benzylation of hydroxyphosphine **190** by with benzyl bromide in toluene for 16 h under reflux (**Scheme 4.16**) gave the phosphonium salt **195** ($\delta_p = 27.5$ ppm) in low yield, while we tried to synthesize a hydroxylated analogue of the adamantylphosphine efficient catalyst cataCXium **123** (**Scheme 4.1**).



Scheme 4.16. Benzylation of phosphorylated diamantyl compounds.

The molecular structures of single crystals of the new diamantane derivatives obtained by X-ray structure analysis are presented in **Figure 4.4**. Typical P...O bond lengths for **22**, **181**, **184**, **185**, **193**, and **194** were observed within the range 1.453-1.500 Å, and phosphonium salt **195** indicates a weak interaction between the hydroxyl group and the bromide O-H...Br.



22: $d(\text{P-O})=1.461(4) \text{ \AA}$; **48:** $d(\text{C-O})=1.4428(16) \text{ \AA}$; **181:** $d(\text{P-O})=1.458(3) \text{ \AA}$; **184:** $d(\text{P-O})=1.453(3) \text{ \AA}$, $d(\text{C-Cl})=1.825(4) \text{ \AA}$; **185:** $d(\text{P-O})=1.463(2) \text{ \AA}$; **193:** $d(\text{P-O})=1.5001(17) \text{ \AA}$; **194:** $d(\text{P-O})=1.4963(15) \text{ \AA}$, $d(\text{C-O})=1.437(2) \text{ \AA}$; **195:** $d(\text{C-O})=1.429(2) \text{ \AA}$, $d(\text{O-Br}) = 3.4239(15) \text{ \AA}$, angle $\text{O-H-Br} = 162.6^\circ$.

Figure 4.3. X-ray crystal structures of diamondane derivatives and some typical bondings.

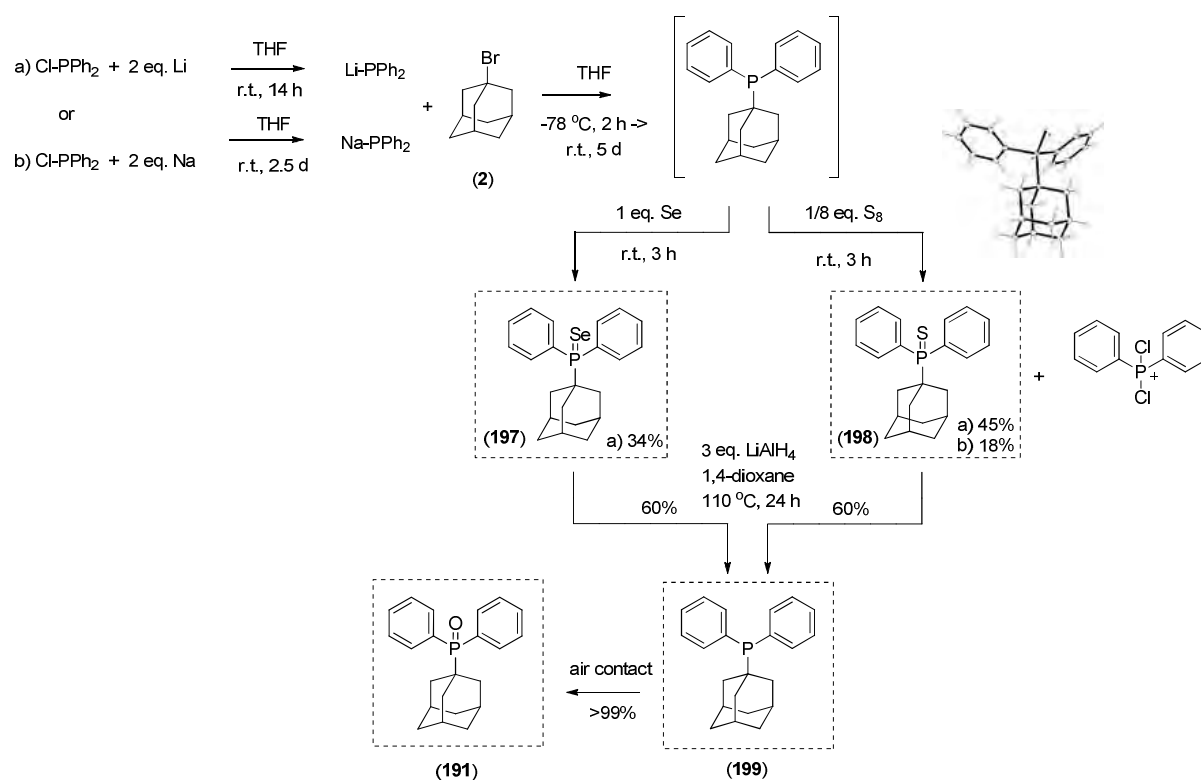
4. Reduction of diamondoid phosphine oxide/selenide/sulfide

After having prepared tertiary diamondoid phosphine oxides, we tried to find the right conditions to reduce the oxide. The isolation of pure phosphine product was found rather challenging. Under most of the reported conditions, the tertiary phosphines have not been isolated, or should be protected in-situ with a borane.³⁴ We investigated the reduction mode of diamondoid phosphine oxides starting with the adamantane derivative **191**. Reduction of **191** with LiAlH_4 in THF and 1,4-dioxane under various conditions failed. To overcome this difficulty, we introduced $-\text{P}(\text{E})\text{Ph}_2$ fragments (where $\text{E} = \text{S}, \text{Se}$), with sulfur or selenium, directly on adamantyl. Instead of starting with adamantyllithium and ClPPh_2 , we started with LiPPh_2 (synthesized from ClPPh_2 and Li) and 1-bromoadamantane **2**, which are technically easier to prepare than the adamantyllithium (**Scheme 4.17**). Changing the lithium base for sodium base gave a lower yield of **198** (**Scheme 4.17**). The photochemical reaction using 1,3-dichloroadamantane and

³⁴ See reference 17, 33, and therein.

Ph_2P^- ion in liquid ammonia by the Rossi group^{28b} is the only reported way to prepare adamantyldiphenylphosphine **199** as a by-product that has been isolated only as its oxide **191**.

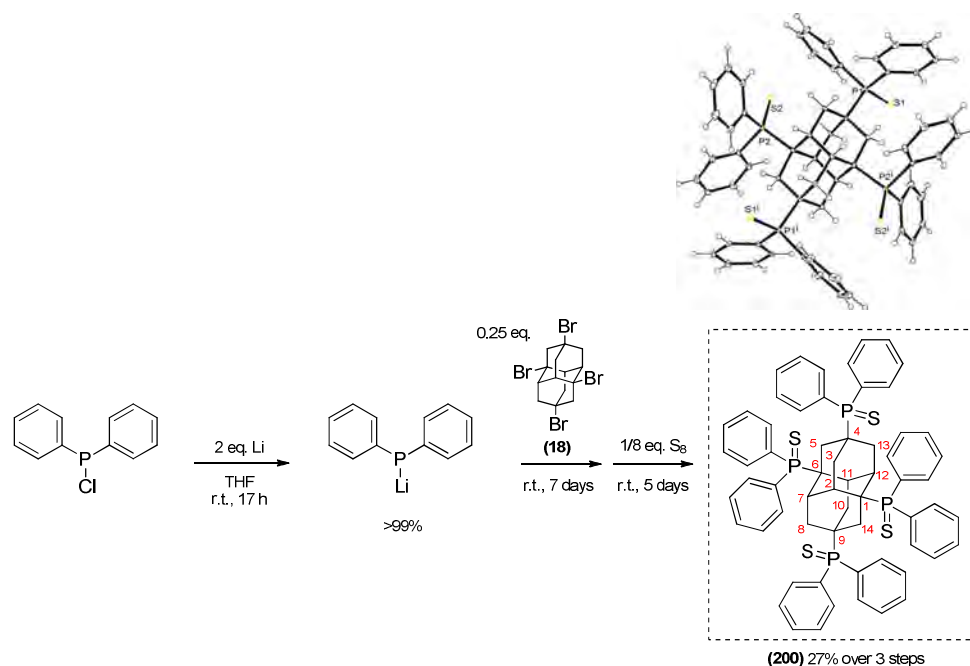
Protection of the phosphine **199** with sulfur and selenium effectively made the purification process easier. Then, a reduction of sulfide and selenide compounds **198** ($\delta_{\text{p}} = 56.3$ ppm) and **197** ($\delta_{\text{p}} = 53.7$ ppm)³⁵ with excess LiAlH_4 in distilled 1,4-dioxane yielded phosphine **199** quantitatively ($\delta_{\text{p}} = 16.3$ ppm). This diarylalkylphosphine is indeed very air-sensitive and was quantitatively oxidized upon short contact with air.



Scheme 4.17. Synthesis of tertiary phosphine **199** and corresponding molecular structure obtained from X-Ray structure analysis (**198**: $d(\text{P-S})=1.9717(7)$ Å).

A similar method was used to prepare the new tetrakis(diphenylphosphine) sulfide **200** from the starting polyfunctionalized tetrabromodiamantane **18** (Scheme 4.18). Due to the low solubility of **18** in THF, long term reaction was necessary to give **200** ($\delta_{\text{p}} = 27.6$ ppm) in 27% yield over 3 steps.

³⁵ The $^1J_{\text{P-Se}}$ for **197** is equal to 712 Hz, as expected slightly inferior to the $^1J_{\text{P-Se}}$ benchmark value for triphenylphosphine selenide (Se=PPh_3 , 730 Hz). This is consistent with the electron-donating effect of the adamantyl alkyl group, and thus the higher basicity of **197** compared to PPh_3 .



Scheme 4.18. Synthesis of tetradiphenylphosphine sulfide **200** and its molecular structure obtained from X-ray structure analysis ($d(\text{P}_1\text{-S}_1)=1.9697(8)$ Å, $d(\text{P}_2\text{-S}_2)=1.9520(8)$ Å, $d(\text{P}_3\text{-S}_3)=1.9609(8)$ Å, $d(\text{P}_4\text{-S}_4)=1.9571(8)$ Å).

After the compound **200** has been crystallized in a mixture DCM and methanol, the colorless crystals formed have very low solubility in the solvents we used (chloroform, DCM, methanol), so further deprotection was not yet achieved for testing its air sensitivity. X-ray structure **200** showed classical P=S bond lengths very similar to that in compound **198** (Scheme 4.17).

4.3. Conclusion

We synthesized a full set of unprecedented functionalized diamondoid phosphines based on adamantyl and diamantyl frameworks. Our approach was to first investigate synthetic pathways on the unfunctionalized and easily accessible adamantyl backbone, then to transfer these conditions to diamantane derivatives. We delivered synthetic routes to functionalized diamondoid phosphines and primary phosphines (**186**, **188**, **190**) (Scheme 4.13) based on adamantane and diamantane frameworks. Brønsted acids have a great potential for phosphorylations of diamondoids allowing dissymmetrization of symmetric substrate like **49** (Scheme 4.11).

Facile unequal difunctionalization of these diamondoids was possible avoiding tedious sequences of protection/deprotection for hydroxylated and chlorinated diamondoid phosphines (**186**, **188**, **190**). In the

course of our investigations we also synthesized various tertiary phosphines (**199**, **Scheme 4.17**) with their pentavalent oxides (**191**, **192**, **193**, **194**), sulfides (**198**), selenides (**197**) and phosphonium salt (**195**), as well as other difunctionalized derivatives for which synthetic protocols and characterizations are reported (**Scheme 4.14**, **4.15**, **4.16**, and **4.17**). Unexpected air-stability of some primary diamondoid phosphines (**188**, **190**, **Scheme 4.13**) was observed. The air-stability of these compounds is remarkable regarding their donating alkyl substituents. This discovery allowed us to use **188** and **190** preferentially for preparing hybrid material by chemical vapor deposition of organometallic complexes as described in **Chapter 5**.

Selective Preparation of Diamondoid Phosphonates

Andrey A. Fokin,^{*,#,‡} Raisa I. Yurchenko,[#] Boryslav A. Tkachenko,[‡] Natalie A. Fokina,[‡] Maria A. Gunawan,^{‡,§} Didier Poinsoot,[§] Jeremy E. P. Dahl,^{||} Robert M. K. Carlson,^{||} Michael Serafin,[⊥] H el ene Cattey,[§] Jean-Cyrille Hierso,^{*,§} and Peter R. Schreiner^{*,‡}

[#]Department of Organic Chemistry, Kiev Polytechnic Institute, pr. Pobedy 37, 03056 Kiev, Ukraine

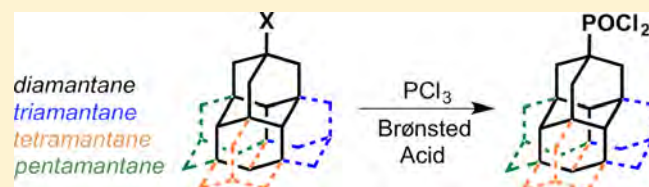
[‡]Institute of Organic Chemistry and [⊥]Institute of Inorganic Chemistry, Justus-Liebig University, Heinrich-Buff-Ring 58, 35392 Giessen, Germany

[§]Institut de Chimie Mol culaire de l'Universit  de Bourgogne (ICMUB), UMR CNRS 6302, Universit  de Bourgogne, 9 avenue Alain Savary, 21078 cedex, Dijon, France

^{||}Stanford Institute for Materials & Energy Science, Stanford University, 476 Lomita Mall, Stanford, California 94305, United States

Supporting Information

ABSTRACT: We present an effective sequence for the preparation of phosphonic acid derivatives of the diamondoids diamantane, triamantane, [121]tetramantane, and [1(2,3)4]pentamantane. The reactions of the corresponding diamondoid hydroxy derivatives with PCl₃ in sulfuric or trifluoroacetic acid give mono- as well as didichlorophosphorylated diamondoids in high preparative yields.



The family of naturally occurring diamondoids, which are nanometer-sized hydrocarbons resembling subunits of the cubic diamond lattice,^{1–3} have been shown to be highly useful in a variety of applications^{4–7} by mimicking many properties of natural H-terminated diamond. For example, diamondoid thiol self-assembled monolayers (SAMs) on metal surfaces reproduce the negative electron affinity (NEA) of bulk diamond.⁸ While such SAMs with extraordinary monochromatic photoemission properties are useful for the construction of novel cathodes, their long-term stability is low as a result of the weakness of the metal–sulfur bonds. Even though cesium bromide can be added as a protective layer to increase overall device stability,⁹ the weak linkage problem remains unsolved. Very recently¹⁰ we demonstrated that covalent attachment of phosphonic acid dichloride of diamantane (**1**, Figure 1) to tungsten (oxide) surfaces displays a characteristic monochromatic NEA peak and provides a material that exhibits remarkable thermal stability (>300 °C). Considering that the photoemission efficiency increases with an increase of the diamondoid cage size,⁸ it is important to note that higher diamondoids¹¹ are effective dispersion energy donors (DEDs), a property that also increases the stability of SAMs.¹² This is crucial for the construction of nanometer-scale devices,¹³ whose properties are strongly affected by intermolecular van der Waals interactions.¹⁴

Preparative methods for the functionalizations of triamantane (**2**),¹⁵ [121]tetramantane (**3**),¹⁵ and [1(2,3)4]pentamantane (**4**)¹⁶ with radical and oxidative reagents allow their selective C–H-bond functionalizations. However, direct phosphorylation of **1** and **2**,¹⁷ in contrast to parent adamantane,^{18,19} gives mixtures and is low-yielding; the monophosphorylation of **1** in the AlCl₃/PCl₃/CH₂Cl₂ system²⁰ was difficult to reproduce¹⁷

as didiamantane-phosphinic acid chloride derivatives form as the main products. Ditriramantane-phosphinic acid chloride was the only product of the reaction of **2** with AlCl₃/PCl₃/CH₂Cl₂.¹⁷ Hence, this makes the selective C–H-bond phosphorylation of diamondoids problematic in the presence of strong Lewis acids. The phosphorylation of haloadamantanes with AlBr₃/PCl₃ is the well-known Clay–Kinnear–Perren reaction²¹ that, however, requires large amounts of reagents and strongly depends on the quality of the employed AlBr₃.²²

Diamondoidyl cations can easily be generated from the corresponding halogen or hydroxy derivatives in the presence of strong Brønsted acids. Previously one of us discovered the dichlorophosphorylation of 1-bromoadamantane with PCl₃ in concentrated sulfuric acid with >95% preparative yield,^{22–24} revealing effective trapping of the 1-adamantyl cation with nucleophilic PCl₃ in *protic* solvents. Trifluoroacetic acid (TFA) can also be used and provides adamantyl phosphonic dichloride in 69% preparative yield from 1-hydroxy adamantane with PCl₃.²⁵ We have recently found that both methods are applicable to the preparation of diamantane 1-phosphonic dichloride (**5**) from the 1-bromo derivative (**6**).¹⁰ As we found substantial discrepancies between our and previously published spectral data,²⁰ the structure of **5** was additionally confirmed by an X-ray crystal structure analysis (Figure 2).

The fact that 4-phosphonic dichloride (**8**) did not form in this reaction is somewhat surprising as the 1- and 4-diamantyl cations equilibrate in H₂SO₄.²⁶ Presumably PCl₃ rapidly traps the 1-diamantyl cation, thus preventing isomerization (Figure

Received: April 8, 2014

Published: May 9, 2014

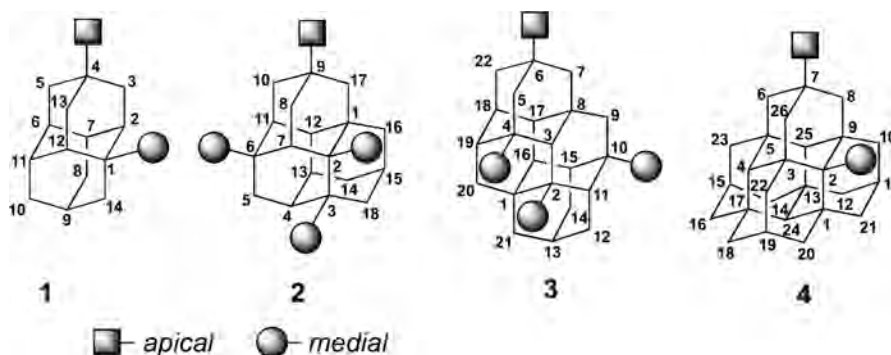


Figure 1. Diamantane (1), triamantane (2), [121]tetramantane (3), and [1(2,3)4]pentamantane (4), with numbering of carbon atoms and their apically as well as medially substituted derivatives.

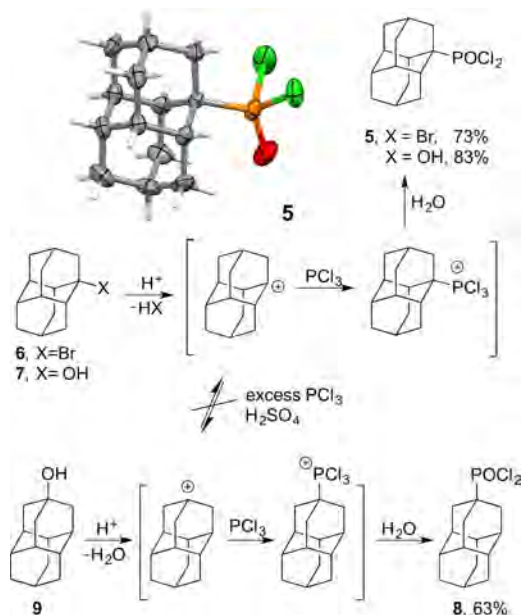


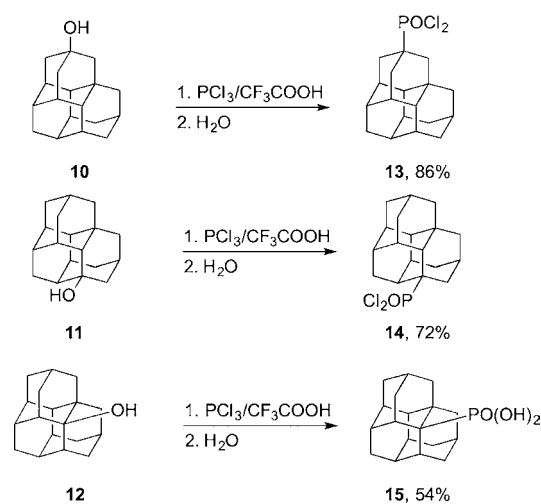
Figure 2. Phosphorylations of diamantane derivatives in sulfuric acid (yields are preparative) and the X-ray crystal structure of dichlorophosphonate 5.

2). This was confirmed by a separate experiment in the $\text{PCl}_3/\text{H}_2\text{SO}_4$ system where 4-hydroxydiamantane (9) gave 8¹⁷ exclusively with a 5 equiv excess of PCl_3 (Figure 2). In contrast, with only 1 equiv of PCl_3 already ca. 10% of isomerized dichloride 5 forms, together with 8 as the main product.

We also found that the preparative yield slightly increases for 1-hydroxydiamantane (7) when TFA is used for the phosphorylation.¹⁰ The 4-hydroxy derivative 9 gave 8 in 75% preparative yield under these conditions. Thus, for the phosphorylations of larger diamondoids we employed the PCl_3/TFA system, which additionally provides higher solubility of the starting material. We first tested various triamantane hydroxy derivatives 10–12 that are available through the nitroxylation/hydrolysis of 2.¹⁵

The phosphorylation of alcohols 10 and 11 in the PCl_3/TFA system provides the phosphoryl derivatives 13 and 14 in high preparative yields (Scheme 1). In contrast, the sterically congested alcohol 12 gave a complex mixture under these conditions, from which we were able to isolate phosphonic acid 15 in only moderate yield due to its low solubility in organic solvents. The behavior of 12 is in line with the low selectivities

Scheme 1. Phosphorylation of Triamantane Derivatives in Trifluoroacetic Acid (Yields Are Preparative)



of the functional group transformations of 2-triamantyl derivatives in electrophilic media.²⁷

As higher diamondoid derivatives larger than 2 demonstrate enhanced potential in the construction of electron-emitting devices,⁸ we extended our phosphorylation protocol to the apical derivatives of [121]tetramantane (16) and [1(2,3)4]pentamantane (18). The apical dichloro phosphoryl derivatives 17 and 19 were isolated in high preparative yields, and their structures were confirmed by X-ray crystal structure analyses (Figure 3).

In contrast to other alkanes, whose already poor electron conductivity exponentially decreases with chain length,²⁸ diamondoids are superior semiconductors as their band gap narrows with increasing molecule size.²⁹ As we have shown that the POCl_2 group provides strong attachment to metal-oxide surfaces,¹⁰ double-phosphorylated diamondoids are potentially useful as saturated spacers in molecule/metal oxide molecular electronic junctions.^{30–33} Previous attempts to attach two phosphoryl groups to 1,3-adamantane derivatives in sulfuric acid gave mixtures of monophosphorylated products only. This is due to the presence of the highly electron-withdrawing trichlorophosphonium group in the positively charged intermediates.³⁴ More distant substituents in the diamondane cage allow for double phosphorylation. The readily available dihydroxy diamantanes 20³⁵ and 21³⁶ that are typically poorly soluble in polar media are highly soluble in the TFA/PCl_3 system and give the desired dichloro phosphonates 22 and 23

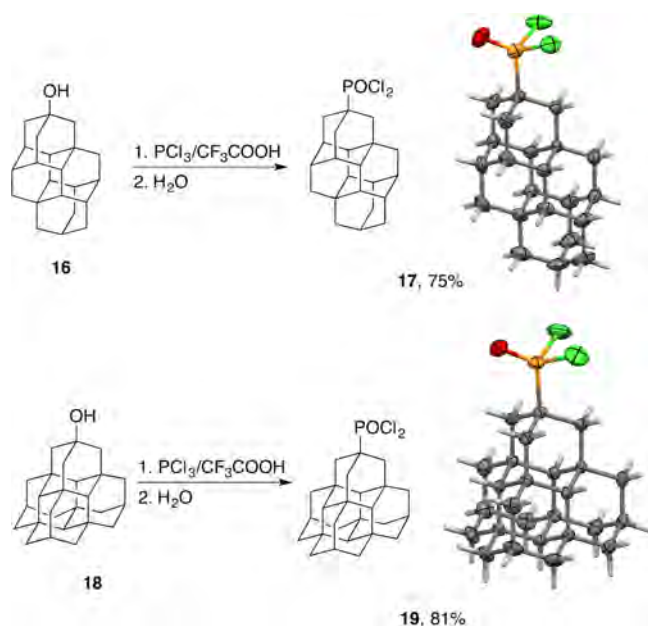
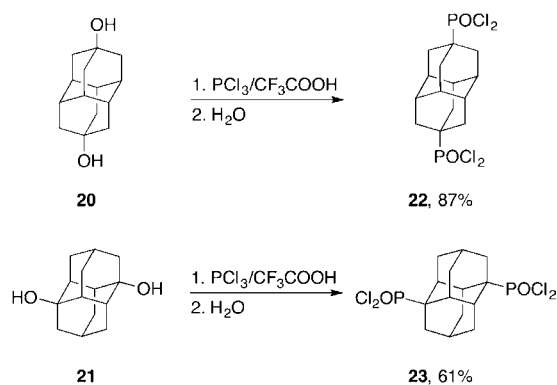


Figure 3. Phosphorylations of the apical [121]tetramantane (**16**) and [1(2,3)4]pentamantane (**18**) derivatives (yields are preparative) and the X-ray crystal structures of dichlorophosphonates **17** and **19**.

in high preparative yields (Scheme 2). These compounds are characterized by exceptionally high thermal stabilities and high

Scheme 2. Double Phosphorylations of Diamantane Derivatives in Trifluoroacetic Acid (Yields Are Preparative)



melting points. For instance, dichloro phosphonate **23** melts without decomposition at 360 °C and may be useful for high-temperature deposition on metal oxide surfaces.

In summary, we have developed a Brønsted acid catalyzed protocol for the phosphorylation of diamondoids with PCl_3 . Highly nucleophilic PCl_3 effectively traps the intermediate cations, thereby avoiding the rearrangements that usually complicate transformations of diamondoids. Thus, this method is superior to previously reported Lewis acid catalyzed phosphorylations. The resulting dichlorophosphoryl diamondoid derivatives have high potential not only in nanoelectronics for surface oxide modifications¹⁰ but also for the preparation of highly sterically demanding building blocks for catalysis.

EXPERIMENTAL SECTION

General Information. NMR spectra were recorded on 400 and 600 MHz (^1H) spectrometers with TMS as internal standard. High-resolution mass spectra (HRMS) were recorded using electron impact

ionization on a focusing sector-type mass spectrometer. Products were purified by chromatography on 100–160 mesh silica gel. All melting points were determined without correction. Commercially available reagents and solvents were used without further purification.

General Procedure for the Phosphorylation of Diamondoid Derivatives in Sulfuric Acid. The diamondoid derivative (bromo or hydroxy, 0.0024 mol) was added to a cooled mixture (ice bath) of 100 mL of 96% sulfuric acid and 30 mL of 20% oleum (0.0024 mol), followed by addition of 1.4 mL (0.017 mol) of phosphorus trichloride at 7–10 °C. The reaction mixture was stirred for 1.5 h at room temperature and 0.5 h at 45–55 °C, cooled, and then poured onto ice. The reaction mixture was filtered, and the precipitate was washed with water and dried over sodium sulfate. The crude product was purified by column chromatography on silica gel (pentane/ether = 5:1).

General Procedure for the Phosphorylation of Diamondoid Derivatives in Trifluoroacetic Acid. To a mixture of 3 g (0.015 mol) of the corresponding hydroxy diamondoid and 50 mL of trifluoroacetic acid was added 7 mL (0.08 mol) of phosphorus trichloride, and the reaction mixture was refluxed for 3.5 h and then poured onto ice. The reaction mixture was extracted three times with CH_2Cl_2 , washed with brine, and dried over sodium sulfate. The resulting crude product was purified as above.

1-Dichlorophosphoryldiamantane (5). Obtained from 150 mg (0.73 mmol) of 1-hydroxydiamantane (**7**) as a colorless solid through the phosphorylation in trifluoroacetic acid, yield 186 mg (83%). Mp = 98–100 °C. ^1H NMR (δ , 400 MHz, CDCl_3): 1.58 (d, $J = 12$ Hz, 2H), 1.70–1.80 (m, 7H), 1.92 (bs, 1H), 1.90–2.10 (m, 5H), 2.30 (d, $J = 8$ Hz, 2H), 2.74 (d, $J = 12$ Hz, 2H). ^{13}C NMR (δ , 100 MHz, CDCl_3): 24.7 (CH), 26.1 (CH, d, $J_{\text{CP}} = 15$ Hz), 34.0 (CH_2), 36.7 (CH, d, $J_{\text{CP}} = 2$ Hz), 36.8 (CH_2 , d, $J_{\text{CP}} = 3$ Hz), 37.0 (CH, d, $J_{\text{CP}} = 2$ Hz), 38.4 (CH_2), 38.8 (CH_2 , d, $J_{\text{CP}} < 1$ Hz), 38.9 (CH, d, $J_{\text{CP}} = 16$ Hz), 56.3 (C, d, $J_{\text{CP}} = 73$ Hz). ^{31}P NMR (δ , 162 MHz, CDCl_3): 66.1. EI-HRMS (m/z): found 304.0564, calcd for $\text{C}_{14}\text{H}_{19}\text{Cl}_2\text{OP}$ 304.0551. Anal. Calcd for $\text{C}_{14}\text{H}_{19}\text{Cl}_2\text{OP}$ C 55.10, H 6.28. Found C 55.34, H 6.26.

9-Dichlorophosphoryltriadamantane (13). Obtained from 150 mg (0.58 mmol) of 9-hydroxytriadamantane (**10**) as a colorless solid through the phosphorylation in trifluoroacetic acid, yield 179 mg (86%). Mp = 142–143 °C. ^1H NMR (δ , 400 MHz, CDCl_3): 1.36 (d, $J = 2.9$ Hz, 2H), 1.51 (bs, 2 H), 1.60 (d, $J = 8$ Hz, 2 H), 1.64–1.80 (m, 10 H), 1.86–1.96 (m, 3 H), 1.96–2.11 (m, 4 H). ^{13}C NMR (δ , 100 MHz, CDCl_3): 27.5 (CH), 33.5 (C), 33.7 (d, $J_{\text{CP}} = 2.2$ Hz, CH), 34.4 (CH), 35.6 (d, $J_{\text{CP}} = 3.8$ Hz, CH_2), 37.2 (d, $J_{\text{CP}} = 16$ Hz, CH), 37.4 (d, $J_{\text{CP}} = 2.2$ Hz, CH), 37.5 (d, $J_{\text{CP}} = 2.7$ Hz, CH_2), 37.6 (CH_2), 42.1 (d, $J_{\text{CP}} = 4.4$ Hz, CH_2), 44.6 (CH_2), 45.3 (d, $J_{\text{CP}} = 2.2$ Hz, CH), 48.5 (d, $J_{\text{CP}} = 88$ Hz, C). ^{31}P NMR (δ , 162 MHz, CDCl_3): 65.1. MS (m/z): 356 (<1), 239 (100), 183 (2), 157 (4), 143 (8), 129 (5). EI-HRMS (m/z): found 356.0846, calcd for $\text{C}_{18}\text{H}_{23}\text{Cl}_2\text{OP}$ 356.0864.

3-Dichlorophosphoryltriadamantane (14). Obtained from 150 mg (0.58 mmol) of 3-hydroxytriadamantane (**11**) through the phosphorylation in trifluoroacetic acid as a colorless solid, yield 150 mg (72%). Mp = 135–136 °C. ^1H NMR (δ , 600 MHz, CDCl_3): 1.26–1.35 (m, 2 H), 1.40 (s, 2 H), 1.47–1.55 (m, 2 H), 1.65–1.81 (m, 8 H), 1.82–1.91 (m, 2 H), 1.96–2.09 (m, 4 H), 2.18–2.25 (m, 1 H), 2.67–2.76 (m, 2 H). ^{13}C NMR (δ , 151 MHz, CDCl_3): 26.9 (CH), 27.4 (d, $J_{\text{CP}} = 16$ Hz, CH), 33.2 (CH), 33.9 (CH), 34.4 (d, $J_{\text{CP}} = 15$ Hz, C), 34.7 (CH_2), 34.74 (d, $J_{\text{CP}} = 2.2$ Hz, CH), 36.6 (d, $J_{\text{CP}} = 3$ Hz, CH_2), 37.3 (CH_2), 37.4 (CH), 37.5 (CH_2), 38.99 (d, $J_{\text{CP}} = 0.9$ Hz, CH_2), 39.0 (d, $J_{\text{CP}} = 17$ Hz, CH), 44.2 (d, $J_{\text{CP}} = 3$ Hz, CH_2), 45.3 (d, $J_{\text{CP}} = 3$ Hz, CH_2), 45.9 (d, $J_{\text{CP}} = 2.3$ Hz, CH), 46.2 (d, $J_{\text{CP}} = 3$ Hz, CH), 57.4 (d, $J_{\text{CP}} = 72$ Hz, C). ^{31}P NMR (δ , 162 MHz, CDCl_3): 65.7. MS (m/z): 358 (<1), 356 (<1), 239 (100), 167 (16), 143 (9), 129 (7). EI-HRMS (m/z): found 356.0851, calcd for $\text{C}_{18}\text{H}_{23}\text{Cl}_2\text{OP}$ 356.0864.

2-Triadamantane Phosphonic Acid (15). Obtained from 150 mg (0.58 mmol) of 2-hydroxytriadamantane (**12**) through the phosphorylation in trifluoroacetic acid. The reaction mixture was filtered, and the precipitate was washed with water, ether, chloroform and dried in vacuum, yield 101 mg (54%) of white solid (mp = 342–343 °C). ^1H NMR (δ , 400 MHz, $\text{DMSO}-d_6$): 0.93 (d, $J = 12$ Hz, 2 H), 1.24 (d, $J = 13$ Hz, 2 H), 1.37 (bs, 1 H), 1.53–1.71 (m, 10 H), 1.77 (bs, 2 H), 1.90 (bs, 2 H), 2.35 (d, $J = 12$ Hz, 2 H), 3.08 (d, $J = 12$ Hz, 2 H). ^{13}C NMR

(δ , 100 MHz, DMSO- d_6): 27.1 (CH), 34.1 (CH₂), 35.5 (C), 36.6 (d, J_{CP} = 11 Hz, CH), 37.5 (CH), 37.9 (CH₂), 38.4 (CH), 39.1 (CH₂), 40.4 (CH₂), 47.9 (d, J_{CP} = 129 Hz, C), 49.9 (d, J_{CP} = 12 Hz, CH). ³¹P NMR (δ , 162 MHz, DMSO- d_6): 30.2. MS (m/z): 320 (2), 239 (100), 197 (2), 183 (1), 143 (9), 129 (12). EI-HRMS (m/z): found 320.1524, calcd for C₁₈H₂₅O₃P 320.1541.

6-Dichlorophosphoryl[121]tetramantane (17). Obtained from 80 mg of 9-hydroxytriamentane (0.26 mmol) (16) as a colorless solid through the phosphorylation in trifluoroacetic acid, yield 80 mg (75%). Mp = 175–176 °C. ¹H NMR (δ , 600 MHz, CDCl₃): 1.30 (d, J = 3 Hz, 2 H), 1.32 (d, J = 2.9 Hz, 2 H), 1.34 (d, J = 3 Hz, 2 H), 1.44 (bs, 2 H), 1.47 (bs, 2 H), 1.64 (d, J = 8 Hz, 2 H), 1.67–1.72 (m, 6 H), 1.72–1.77 (m, 2 H), 1.86–1.90 (m, 1 H), 1.90–1.95 (m, 2 H), 2.00–2.05 (m, 4 H). ¹³C NMR (δ , 151 MHz, CDCl₃): 27.6 (CH), 30.9 (C), 31.6 (d, J_{CP} = 16 Hz, C), 35.43 (d, J_{CP} = 3.7 Hz, CH₂), 35.45 (CH), 36.6 (d, J_{CP} = 1.3 Hz, CH), 37.26 (d, J_{CP} = 16 Hz, CH), 37.6 (CH₂), 37.8 (CH), 41.3 (d, J_{CP} = 4.4 Hz, CH₂), 43.9 (CH₂), 44.7 (d, J_{CP} = 2.5 Hz, CH₂), 45.0 (CH₂), 45.8 (d, J_{CP} = 2.3 Hz, CH), 46.5 (d, J_{CP} = 1.9 Hz, CH), 48.6 (d, J_{CP} = 88 Hz, C). ³¹P NMR (δ , 243 MHz, CDCl₃): 65.1. MS (m/z , %): 408 (1), 404 (1), 325 (1), 305 (2), 292 (100), 155 (11), 141 (8). EI-HRMS (m/z): found 408.1174, calcd for C₂₂H₂₇Cl₂OP 408.1177.

7-Dichlorophosphoryl[1(2,3)4]pentamantane (19). Obtained from 50 mg of 7-hydroxy[1(2,3)4]pentamantane (0.14 mmol) (18) as a colorless solid through the phosphorylation in trifluoroacetic acid, yield 52 mg (81%). Mp = 330–331 °C. ¹H NMR (δ , 600 MHz, CDCl₃): 1.00 (s, 4 H), 1.28–1.38 (m, 12 H), 1.38–1.43 (m, 6 H), 1.63 (d, J = 8 Hz, 6 H), 1.87–1.98 (m, 3 H). ¹³C NMR (δ , 151 MHz, CDCl₃): 28.2 (CH), 32.8 (C), 33.4 (d, J_{CP} = 15 Hz, C), 41.7 (d, J_{CP} = 5 Hz, CH₂), 44.2 (CH₂), 44.4 (CH₂), 49.1 (d, J_{CP} = 85 Hz, C), 52.2 (d, J_{CP} = 2 Hz, CH), 52.9 (CH). ³¹P NMR (δ , 243 MHz, CDCl₃): 64.1. MS (m/z , %): 461 (<1%), 343 (100), 230 (2), 181 (2), 171 (5), 141 (1) ESI-HRMS (m/z + Na): found 483.1378, calcd for C₂₆H₃₁Cl₂OPNa 483.1387.

4,9-Bis(dichlorophosphoryl)diamantane (22). Obtained from 120 mg (0.54 mmol) of 4,9-dihydroxydiamantane (20) as a colorless solid through the phosphorylation in trifluoroacetic acid, yield 200 mg (87%). Mp = 340–341 °C. ¹H NMR (δ , 400 MHz, CDCl₃): 2.05 (bs, 6 H), 2.08–2.16 (m, 12 H). ¹³C NMR (δ , 100 MHz, CDCl₃): 35.03 (CH), 35.07 (dd; J_{CP} = 17, 3 Hz; CH₂), 46.0 (d, J_{CP} = 93 Hz, C). ³¹P NMR (δ , 162 MHz, CDCl₃): 64.0. MS (m/z , %): 305 (70), 303 (100), 185 (38), 157 (2), 143 (4), 129 (12). Anal. Calcd for C₁₄H₁₈Cl₄O₂P₂ C 39.84, H 4.30. Found C 39.49, H 4.32.

1,6-Bis(dichlorophosphoryl)diamantane (23). Obtained from 110 mg (0.50 mmol) of 1,6-dihydroxydiamantane (21) as a colorless solid through the phosphorylation in trifluoroacetic acid, yield 128 mg (61%). Mp = 360–361 °C. ¹H NMR (δ , 400 MHz, CDCl₃): 1.61 (d, J = 13.5 Hz, 4 H), 2.09 (bs, 4 H), 2.14–2.23 (m, 2 H), 2.47 (bs, 4 H), 2.85 (d, J = 13.3 Hz, 4 H). ¹³C NMR (δ , 100 MHz, CDCl₃): 24.8 (t, J_{CP} = 7 Hz, CH), 32.8 (CH₂), 38.5 (t, J_{CP} = 8 Hz, CH), 39.3 (CH₂), 55.4 (d, J_{CP} = 76 Hz, C). ³¹P NMR (δ , 162 MHz, CDCl₃): 63.5. MS (m/z , %): 305 (50), 303 (62), 185 (100), 143 (10), 129 (30). Anal. Calcd for C₁₄H₁₈Cl₄O₂P₂ C 39.84, H 4.30. Found C 40.05, H 4.27.

ASSOCIATED CONTENT

Supporting Information

Copies of NMR spectra and selected X-ray crystallographic data. This material is available free of charge via the Internet at <http://pubs.acs.org>.

AUTHOR INFORMATION

Corresponding Authors

*E-mail: aaf@xtf.kpi.ua.

*E-mail: Jean-Cyrille.Hierso@u-bourgogne.fr.

*E-mail: prs@uni-giessen.de.

Notes

The authors declare no competing financial interest.

ACKNOWLEDGMENTS

This work was supported by the Ukrainian Basic Research Foundation, Ministry of Science and Education of Ukraine and in part by the Department of Energy, Office of Basic Energy Sciences, Division of Materials, Science and Engineering under Contract DE-AC-76SF00515.

REFERENCES

- (1) Dahl, J. E.; Moldowan, J. M.; Peters, K. E.; Claypool, G. E.; Rooney, M. A.; Michael, G. E.; Mello, M. R.; Kohnen, M. L. *Nature* **1999**, *399*, 54–57.
- (2) Dahl, J. E. P.; Moldowan, J. M.; Peakman, T. M.; Clardy, J. C.; Lobkovsky, E.; Olmstead, M. M.; May, P. W.; Davis, T. J.; Steeds, J. W.; Peters, K. E.; Pepper, A.; Ekuon, A.; Carlson, R. M. K. *Angew. Chem., Int. Ed.* **2003**, *42*, 2040–2044.
- (3) Dahl, J. E.; Liu, S. G.; Carlson, R. M. K. *Science* **2003**, *299*, 96–99.
- (4) Ishiwata, H.; Acremann, Y.; Scholl, A.; Rotenberg, E.; Hellwig, O.; Dobisz, E.; Doran, A.; Tkachenko, B. A.; Fokin, A. A.; Schreiner, P. R.; Dahl, J. E. P.; Carlson, R. M. K.; Melosh, N.; Shen, Z. X.; Ohldag, H. *Appl. Phys. Lett.* **2012**, *101*, 163101.
- (5) Schwertfeger, H.; Fokin, A. A.; Schreiner, P. R. *Angew. Chem., Int. Ed.* **2008**, *47*, 1022–1036.
- (6) Lysenko, A. B.; Senchyk, G. A.; Lincke, J.; Lassig, D.; Fokin, A. A.; Butova, E. D.; Schreiner, P. R.; Krautscheid, H.; Domasevitch, K. V. *J. Chem. Soc., Dalton Trans.* **2010**, *39*, 4223–4231.
- (7) Sinkel, C.; Agarwal, S.; Fokina, N. A.; Schreiner, P. R. *J. Appl. Polym. Sci.* **2009**, *114*, 2109–2115.
- (8) Yang, W. L.; Fabbri, J. D.; Willey, T. M.; Lee, J. R. I.; Dahl, J. E.; Carlson, R. M. K.; Schreiner, P. R.; Fokin, A. A.; Tkachenko, B. A.; Fokina, N. A.; Meevasana, W.; Mannella, N.; Tanaka, K.; Zhou, X. J.; van Buuren, T.; Kelly, M. A.; Hussain, Z.; Melosh, N. A.; Shen, Z. X. *Science* **2007**, *316*, 1460–1462.
- (9) Clay, W. A.; Maldonado, J. R.; Pianetta, P.; Dahl, J. E. P.; Carlson, R. M. K.; Schreiner, P. R.; Fokin, A. A.; Tkachenko, B. A.; Melosh, N. A.; Shen, Z. X. *Appl. Phys. Lett.* **2012**, *101*, 241605.
- (10) Li, F. H.; Fabbri, J. D.; Yurchenko, R. I.; Mileskin, A. N.; Hohman, J. N.; Yan, H.; Yuan, H.; Tran, I. C.; Willey, T. M.; Bagge-Hansen, M.; Dahl, J. E. P.; Carlson, R. M. K.; Fokin, A. A.; Schreiner, P. R.; Shen, Z.-X.; Melosh, N. A. *Langmuir* **2013**, *29*, 9790–9797.
- (11) Schreiner, P. R.; Chernish, L. V.; Gunchenko, P. A.; Tikhonchuk, E. Y.; Hausmann, H.; Serafin, M.; Schlecht, S.; Dahl, J. E. P.; Carlson, R. M. K.; Fokin, A. A. *Nature* **2011**, *477*, 308–311.
- (12) Grimme, S.; Huenerbein, R.; Ehrlich, S. *ChemPhysChem* **2011**, *12*, 1258–1261.
- (13) Kergeris, C.; Bourgoin, J. P.; Palacin, S.; Esteve, D.; Urbina, C.; Magoga, M.; Joachim, C. *Phys. Rev. B* **1999**, *59*, 12505–12513.
- (14) Nerngchamngong, N.; Yuan, L.; Qi, D. C.; Li, J.; Thompson, D.; Nijhuis, C. A. *Nat. Nanotechnol.* **2013**, *8*, 113–118.
- (15) Schreiner, P. R.; Fokina, N. A.; Tkachenko, B. A.; Hausmann, H.; Serafin, M.; Dahl, J. E. P.; Liu, S. G.; Carlson, R. M. K.; Fokin, A. A. *J. Org. Chem.* **2006**, *71*, 6709–6720.
- (16) Fokin, A. A.; Schreiner, P. R.; Fokina, N. A.; Tkachenko, B. A.; Hausmann, H.; Serafin, M.; Dahl, J. E. P.; Liu, S. G.; Carlson, R. M. K. *J. Org. Chem.* **2006**, *71*, 8532–8540.
- (17) Schwertfeger, H.; Machuy, M. M.; Wurtele, C.; Dahl, J. E. P.; Carlson, R. M. K.; Schreiner, P. R. *Adv. Synth. Catal.* **2010**, *352*, 609–615.
- (18) Goerlich, J. R.; Fischer, A.; Jones, P. G.; Schmutzler, R. Z. *Naturforsch. B* **1994**, *49*, 801–811.
- (19) No, B. I.; Zotov, Y. L.; Karev, V. N. *Zh. Obshch. Khim.* **1982**, *52*, 933–934.
- (20) Olah, G. A.; Farooq, O.; Wang, Q.; Wu, A. H. *J. Org. Chem.* **1990**, *55*, 1224–1227.
- (21) Stetter, H.; Last, W. D. *Chem. Ber. Recl.* **1969**, *102*, 3364–3366.
- (22) Yurchenko, R. I.; Peresyphina, L. P. *Zh. Obshch. Khim.* **1991**, *61*, 1019–1019.
- (23) Yurchenko, R. I.; Peresyphina, L. P. *Zh. Obshch. Khim.* **1994**, *64*, 1564–1564.

- (24) Yurchenko, R. I.; Peresyphina, L. P.; Miroshnichenko, V. V.; Yurchenko, A. G. *Zh. Obshch. Khim.* **1993**, *63*, 1534–1539.
- (25) Erokhina, E. V.; Shokova, E. A.; Luzikov, Y. N.; Kovalev, V. V. *Synthesis (Stuttgart)* **1995**, 851–854.
- (26) Gund, T. M.; Nomura, M.; Schleyer, P. v. R. *J. Org. Chem.* **1974**, *39*, 2987–2994.
- (27) Fokina, N. A.; Tkachenko, B. A.; Dahl, J. E. P.; Carlson, R. M. K.; Fokin, A. A.; Schreiner, P. R. *Synthesis (Stuttgart)* **2012**, *44*, 259–264.
- (28) Wold, D. J.; Frisbie, C. D. *J. Am. Chem. Soc.* **2001**, *123*, 5549–5556.
- (29) Fokin, A. A.; Schreiner, P. R. *Mol. Phys.* **2009**, *107*, 823–830.
- (30) Kalakodimi, R. P.; Nowak, A. M.; McCreery, R. L. *Chem. Mater.* **2005**, *17*, 4939–4948.
- (31) Kolipaka, S.; Aithal, R. K.; Kuila, D. *Appl. Phys. Lett.* **2006**, *88*, 233104.
- (32) Lenfant, S.; Krzeminski, C.; Delerue, C.; Allan, G.; Vuillaume, D. *Nano Lett.* **2003**, *3*, 741–746.
- (33) Selzer, Y.; Salomon, A.; Cahen, D. *J. Phys. Chem. B* **2002**, *106*, 10432–10439.
- (34) Yurchenko, R. I.; Voitsekhovskaya, O. M.; Verpovskaya, I. N.; Kudryavtsev, A. A. *Zh. Obshch. Khim.* **1992**, *62*, 589–592.
- (35) Fokina, N. A.; Tkachenko, B. A.; Merz, A.; Serafin, M.; Dahl, J. E. P.; Carlson, R. M. K.; Fokin, A. A.; Schreiner, P. R. *Eur. J. Org. Chem.* **2007**, 4738–4745.
- (36) Burns, W.; McKervey, M. A.; Mitchell, T. R. B.; Rooney, J. J. *J. Am. Chem. Soc.* **1978**, *100*, 906–911.

Chapter 5: Palladium CVD under mild conditions on functionalized diamondoid phosphines

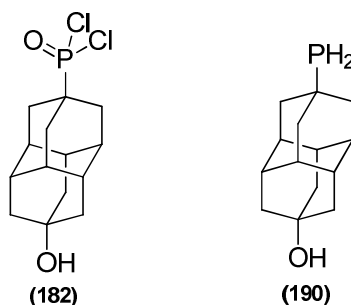
5.1. Introduction

Our first results devoted to palladium deposition by OMCVD from $[\text{Pd}(\eta^3\text{-allyl})\text{Cp}]$ on hydroxylated and fluorinated diamondoids, reported in **Chapter 3**, indicated that short duration deposition (below 30 min) at 65 °C in the presence of H_2 was not selectively achieved on the diamondoid substrate as we expected, but rather mainly deposited on the silica substrates that support the diamondoid. This was a major obstacle to our building of hybrid materials. Further experiments then conducted over a longer period of time (2-5 h) at lower temperature (30 °C) lead to the homogeneous deposition of Pd layers (particle size around 250-865 nm from SEM). While the deposition of palladium layers that was achieved may be of interest and could be further explored as “carbon-doped” metal layers (conductivity, catalytic properties, emission, *etc.*), this was not our initial objective devoted to produce discernible individual hybrid edifices.

As explained in **Chapter 3**, to solve this issue, we thought about generating covalent bonding between functionalized diamondoids and transition metals. Concerning group 10 transition metals, and in particular palladium (but also platinum and nickel), their affinity with phosphorus is well-known. Therefore, we introduced phosphino groups onto the diamondoids, as described in **Chapter 4**. To the best of our knowledge, this present approach of substrate functionalization with phosphines for metallization has not been previously reported in the CVD literature. However, it is worth mentioning a study from the group of Senkevich *et al.* They reported that “*the ability to modify the dielectric or barrier layer surface with an atomic layer of phosphorus (deposited) via a PH_3/He plasma (255 °C) allows favorable interaction to occur,(...) favorable interaction ultimately allows metals like Pd or Cu to “wet” the dielectric surface, improving adhesion, and ultimately leading to superior properties of the metal deposit ($[\text{Pd}(\text{hexafluoropentanedionate})_2]$, 180 °C). Such interface engineering should improve metallization via techniques like ALD, CVD, ELD, and ECD.*”¹ Phosphorus atomic layer deposition from PH_3 is conceptually and technically fairly different from our intended diamondoid hybrid construction. Nevertheless, this approach assumes that metal complexes have only weak interactions with oxide and polymeric (carbon) surfaces and that a phosphorus atomic layer can improve this “interaction” to allow high quality metal deposit. Interestingly, this approach is thus somewhat related to our own hypothesis.

¹ J. J. Senkevich, G.-R. Yang, T.-M. Lu, T. S. Cale, C. Jezewski, W. A. Landford. *Chem. Vap. Deposition*, **2002**, 8, 189-192. Phosphorus atomic layers promoting the chemisorption of highly polarizable transition metallorganics.

As detailed in **Chapter 2**, the prerequisite for using diamondoid phosphine derivatives as support for palladium growth is the formation of an adequate robust self-assembly from vapor deposition. Therefore, volatility of functionalized diamondoid phosphines is essential in our choice of diamondoid substrates. We also considered in priority air-stable difunctionalized compounds since several experimental preparations are achieved under normal atmosphere. The new difunctionalized diamantane derivatives depicted in **Scheme 5.1** were thus investigated.



Scheme 5.1. (9-Hydroxydiamant-4-yl)phosphonic dichloride **182** and 9-phosphinodiamantan-4-ol **190**.

5.2. Palladium-diamantane phosphine hybrids construction by vapor deposition

1. Self-assembly of (9-Hydroxydiamant-4-yl)phosphonic dichloride (**182**)

Gratifyingly, the self-assembly of the selected diamondoids **182** on Si wafer was successfully achieved, validating the method described in **Chapter 2** with monofunctionalized diamondoids. Vapor deposition was performed under dynamic vacuum (3 Torr) for 2 min at 85 °C. Due to the limited quantity that has been prepared for **182** and **190**, the enthalpy of sublimation could not be measured, and will be a priority of follow-up work.

As shown in the optical microscopy and SEM observation reported in **Figure 5.1**, self-assembly of diamondoid **182** is easily achieved and is very different from the previously observed crystal self-assemblies of fluoro- and hydroxy-diamantane **25** and **30** (**Chapter 2**). Optical microscopy indicated a good distribution on the Si wafer where the crystal growth resembled “pine leaves”. SEM images showed that mostly the diamondoid particles grew as regular parallelepiped platelets with a remarkable unity of shape and size. The typical platelets’ shape is depicted in **Figure 5.2**, having an average size of 2.4 μm x 0.5 μm and a thickness around 0.24 μm . The mutual arrangement of the pellets cover large areas without notable preferential orientation. The conditions used for vapor deposition of **182** led to self-assemblies which are found fully resistant to SEM conditions (vacuum and energy beam).

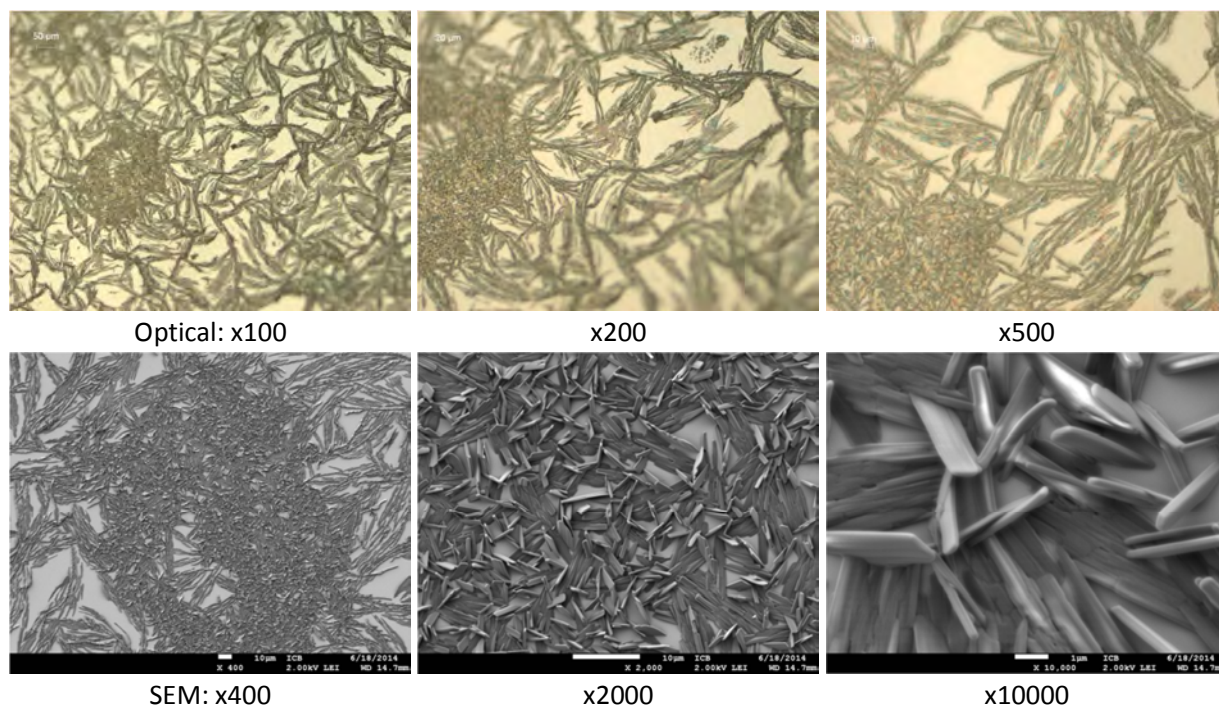


Figure 5.1. Optical and SEM images of of **182** self-assembly by vapor deposition.

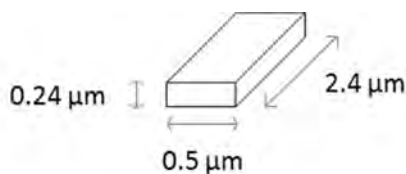


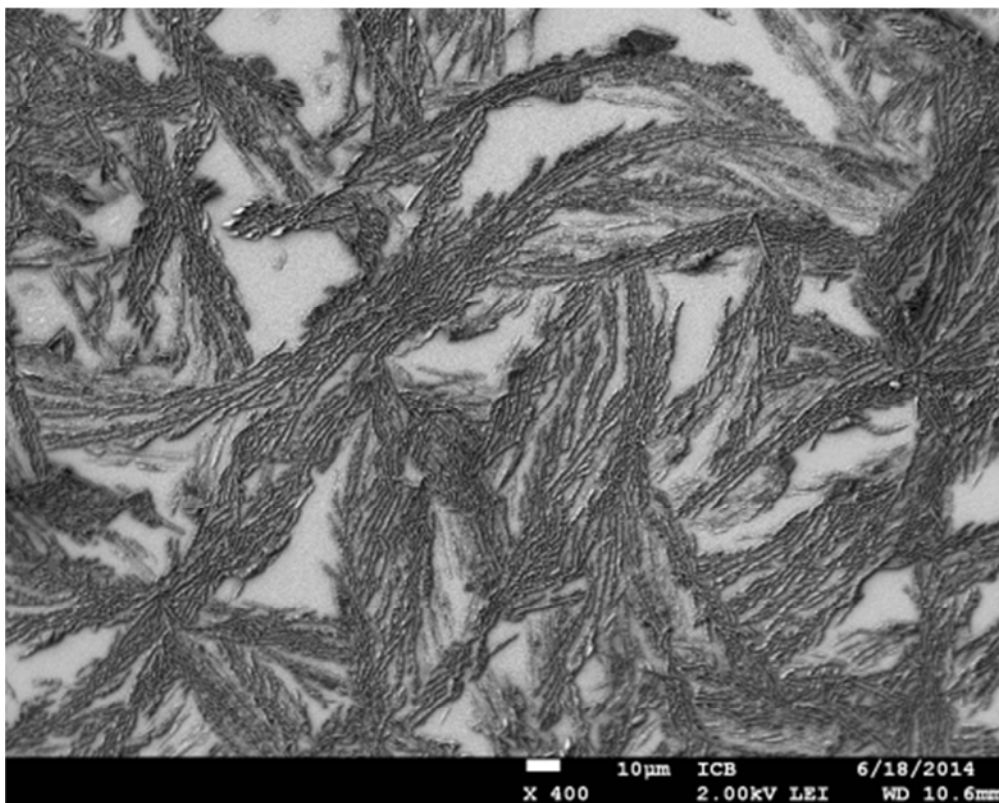
Figure 5.2. Typical self-assemblies of **182** as dispersed regular platelets.

2. Palladium CVD on (9-hydroxydiamant-4-yl)phosphonic dichloride (**182**)

Palladium deposition on the self-assembled crystals of **182** using $[\text{Pd}(\eta^3\text{-allyl})\text{Cp}]$ was achieved at 51 Torr and 30 °C using 3.2 mL/min of H_2 as reactive gas, and 80 mL/min of argon as carrier gas, for various deposition times.

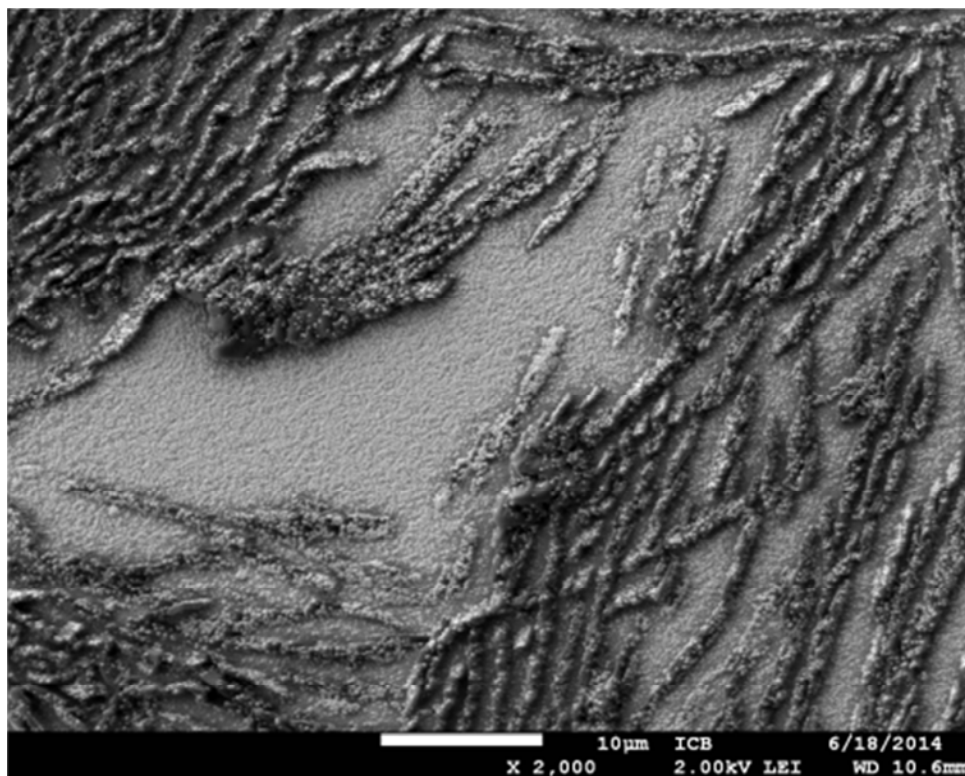
Observation in SEM of the resulting Pd deposit after 6 h is shown in **Figure 5.3**. A very significant covering with palladium is observed all over the substrate (**Figure 5.3(a)**) both on the platelets of **182** and on the naked silicon area remaining between the diamondoid platelet arrangement. Enhancement of microscope photography (**Figure 5.3(b)** and **(c)**) confirmed the absence of selectivity in the Pd-covering; however the presence of diamondoid platelet is still clearly visible. The palladium deposition

mode is classical,² forming roughly spherical cauliflower-like particles of size ranging between 30 and 300 nm.

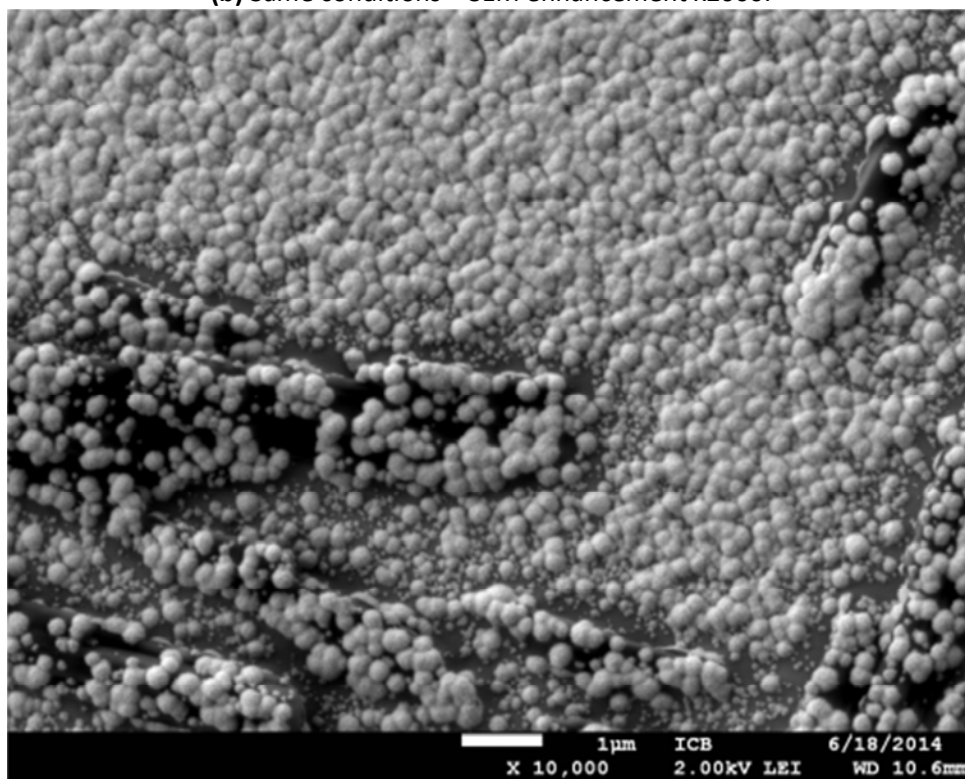


(a) CVD of $[\text{Pd}(\eta^3\text{-allyl})\text{Cp}]$ on **182** self-assembly, 6 h run – SEM enhancement x400.

² J.-C. Hierro, C. Satto, R. Feurer, P. Kalck. *Chem. Mater.*, **1996**, *8*, 2481-2485. Organometallic chemical vapor deposition of palladium under very mild conditions of temperature in the presence of a low reactive gas partial pressure.



(b) Same conditions – SEM enhancement x2000.



(c) Same conditions – SEM enhancement x10000.

Figure 5.3. CVD of $[\text{Pd}(\eta^3\text{-allyl})\text{Cp}]$ on **182** self-assembly, 6 h run with various enhancements.

Since the diamondoid platelets are still discernible on the deposits, EDX analyses were conducted with focus on various areas, and also compared with EDX analyses of the non-metallized self-assembly of **182** (Figure 5.4).

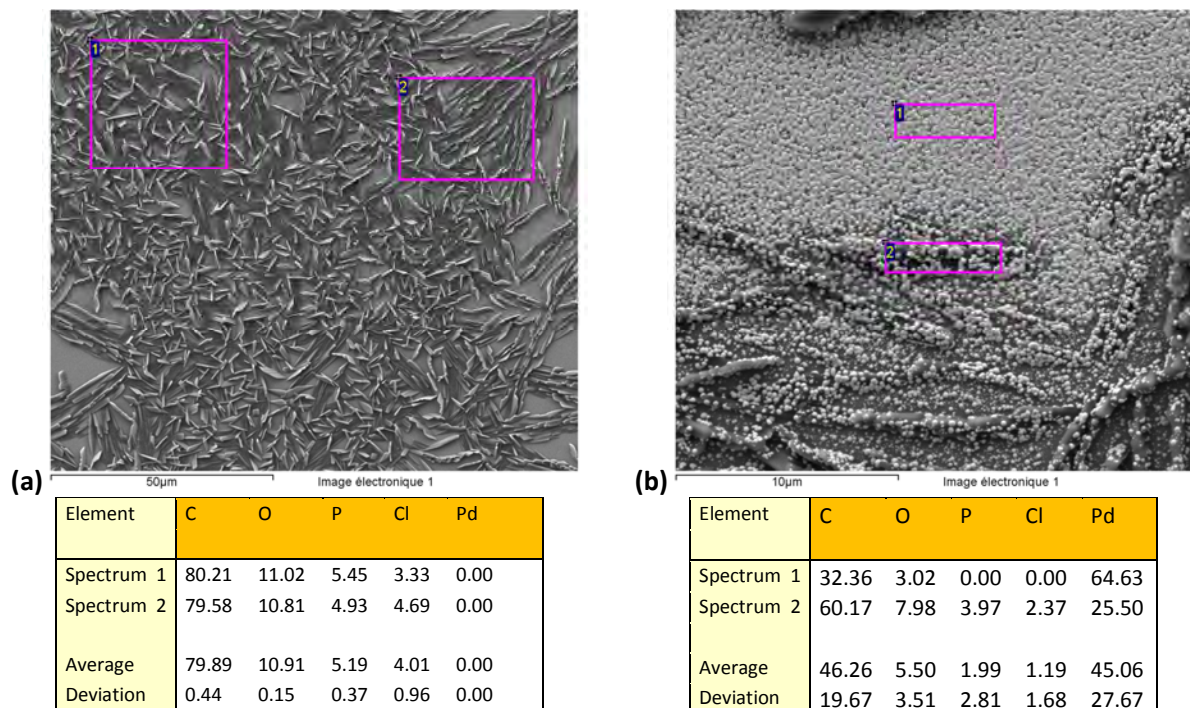


Figure 5.4. SEM picture (top) and EDX analysis (bottom) of “naked” self-assemblies of **182** (left) and Pd deposition over the self-assembly (right).

EDX analysis of the self-assembly of **182** indicates the presence, over various areas of analysis (Figure 5.4(a) Spectrum 1 and 2) of consistent amounts of C (80%), O (11%), P (5%) and Cl (4%). The excess in C and O (compared to the elemental analysis of pure diamondoid) is attributed to predictable surface contamination of the Si wafer since this one was not specifically treated (pollution post deposit being also current). EDX analysis of the samples was achieved after the palladium deposition. Two typical areas are distinguishable, one for which a signature of the diamondoid **182** is clearly present (Figure 5.4(b) Spectrum 2: C, 60.17%, O, 7.98%, P, 3.97%, Cl, 2.37%) together with palladium (25.5%). The other areas (Figure 5.4(b) Spectrum 1) are mainly covered with palladium (64.63%) while carbon (32.36%) and oxygen (3.02%) contamination is also detected but not phosphorus. Therefore, the EDX measurements are in full agreement with the SEM observation strongly suggesting unselective Pd covering.

By using self-assemblies of **182** as support for CVD of Pd, the growth of palladium “layers” covers the Si wafer and the platelets of difunctionalized diamondoid without apparent distinction or special selectivity. This result was not a genuine surprise since our initial objective of building a covalent P–Pd bond between the diamondoid and atomic palladium, to serve as a seed for hybrids construction, is hardly possible from a P(V) phosphine oxide dichloride lacking a lone-pair for coordinating Pd. These experiments were nevertheless attempted with the hope of partially reducing the ($-\text{Cl}_2\text{P}=\text{O}$) groups from the joint action of H_2 and Pd. If this reaction occurs, it clearly does not conduct to the preferential growth of palladium over the diamondoid. Accordingly the palladium deposit that was formed during CVD is not influenced in any manner by the original morphology of the diamondoid self-assembly. We therefore focused our efforts on the diamondoid phosphine **190**.

3. Self-assembly of 9-Phosphinodiamantan-4-ol (**190**)

The self-assembly of **190** on Si wafer was successfully achieved under dynamic vacuum (3 Torr) for 2 min at 85 °C. Optical microscopy revealed a well-dispersed self-assembly with an apparent morphology of rods very different from **182**.

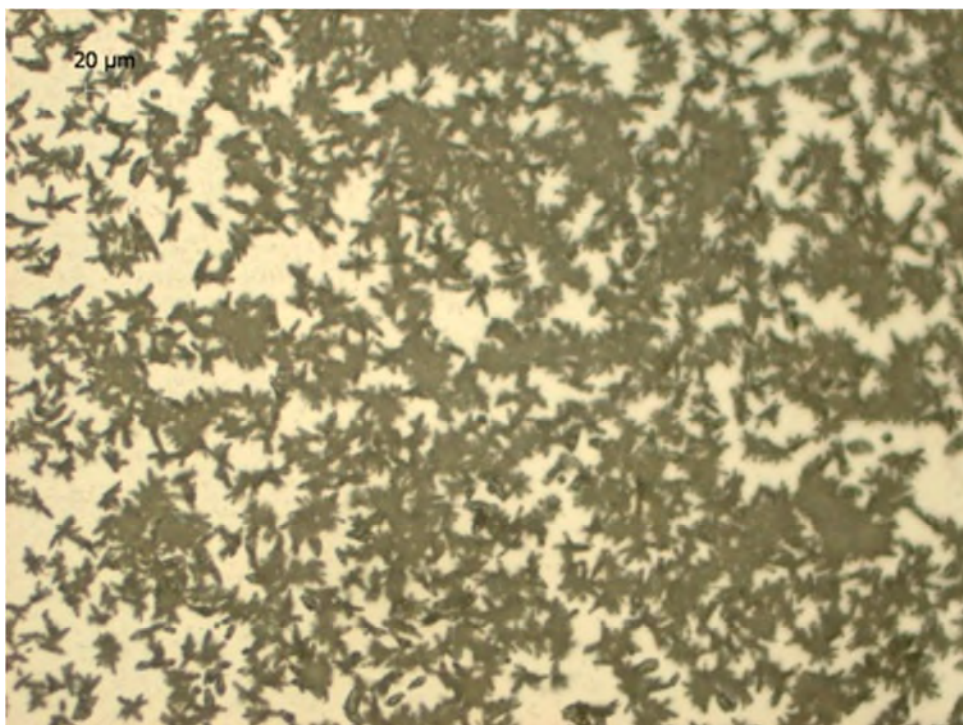
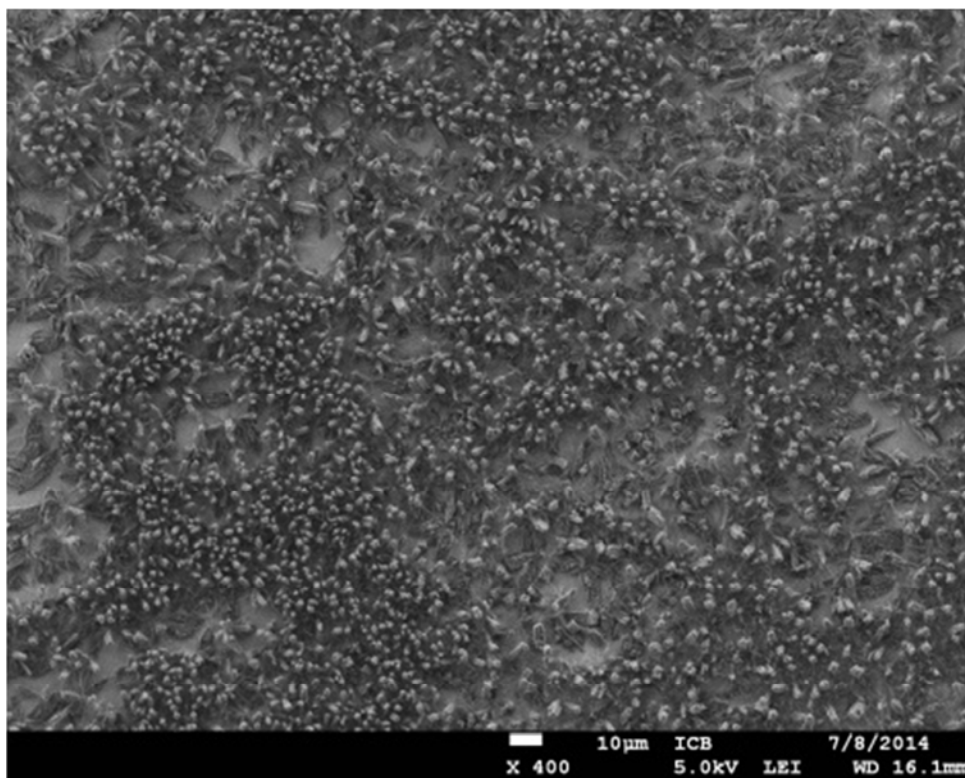
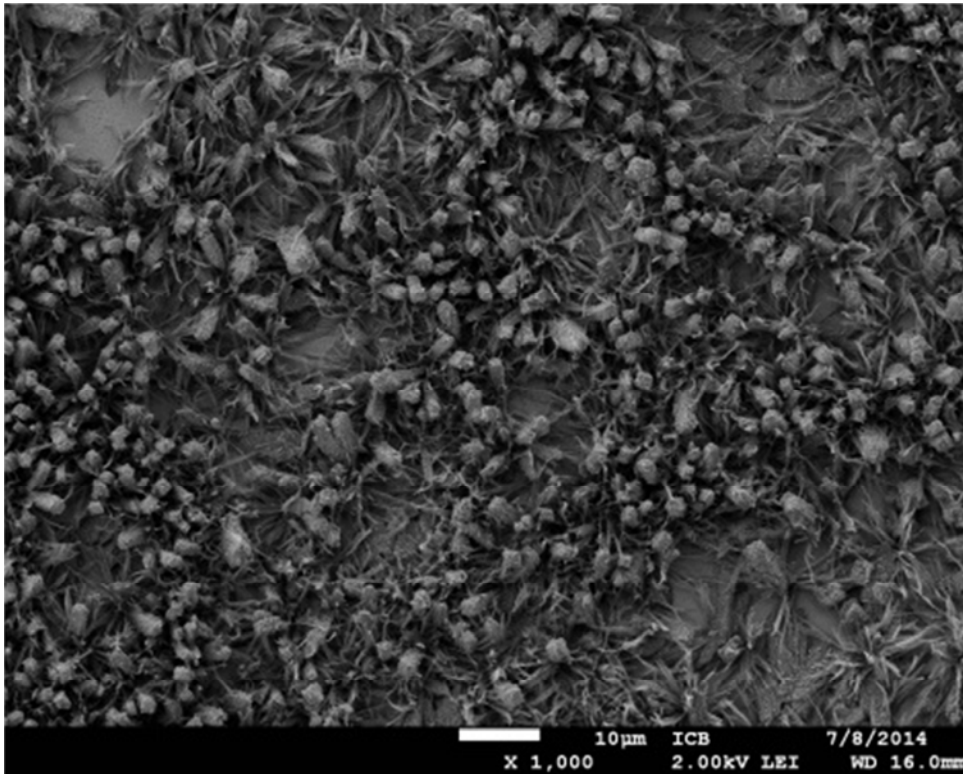


Figure 5.5. Optical microscopy of self-assembled rods of **190**.

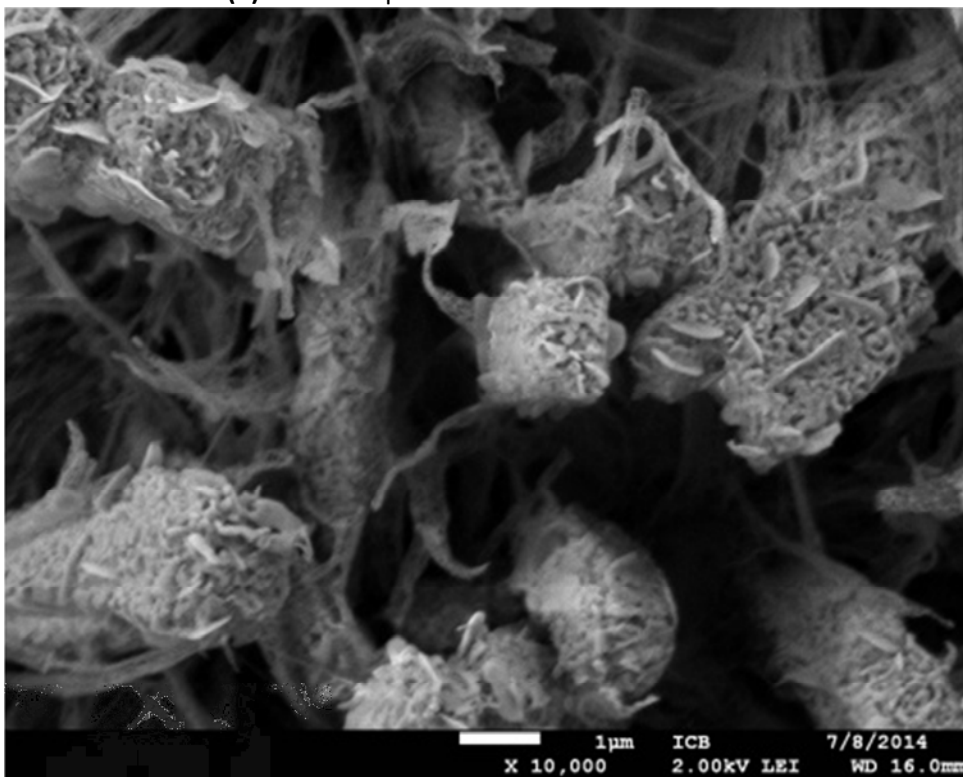
SEM photographs of the self-assembly of diamondoid hydroxyphosphine **190** (**Figure 5.6, (a)-(c)**), give a clearer picture of the unusual morphology obtained, which is indeed very different from all the other self-assemblies observed up to now (see **Chapter 2** and previous section). The Si wafer substrate was almost entirely covered with a dense intermingling of two types of structures. The better ordered crystals are seemingly compact columnar edifices mostly positioned *perpendicular to the original surface* (as vertical “pillar”, see depiction **Figure 5.6(d)**). These edifices present a rather homogenous size with a square top of about $1.4\ \mu\text{m} \times 1.4\ \mu\text{m}$. The determination of their height from SEM micrographs is difficult due to their vertical growth. From enlargement **Figure 5.6(c)**, a very high porosity of the compact edifices is visible at their surface. These *porous compact pillars* are embedded in a network of *entangled thin sheets*. The enhancement (picture **Figure 5.6(c)**) suggests that the *pillars* are formed from compacted *thin sheets* since many of these latter are visibly emerging from the columnar edifices. The self-assembly by vapor deposition under vacuum was conducted several times and, as it is usually found using our vapor deposition method, a consistent reproducibility of the edifices formed and of their size was obtained. Satisfyingly, the quality and reproducibility of the images obtained certify that both the compact pillar edifices and the network of entangled thin sheet are resistant to SEM conditions. The self-assembly was conserved for a full week under normal conditions, in air, without visible alteration.



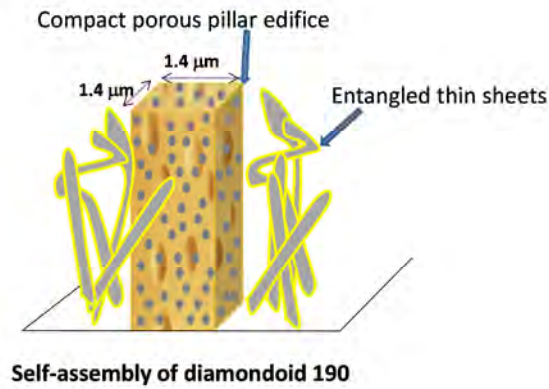
(a) SEM picture of diamondoid **190** self-assembly by vapor deposition.



(b) Same sample – SEM enhancement x1000.

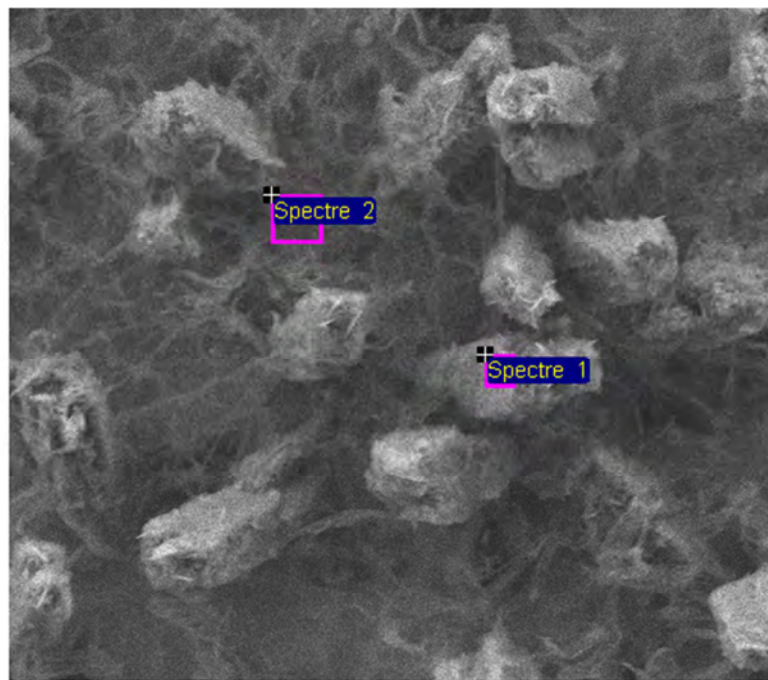


(c) Same sample – SEM enhancement x10000.



(d) Representation of diamondoid phosphine **190** self-assembly.

Figure 5.6. SEM analysis of **190** self-assembly and representation.



10μm		Image électronique 1			
Element	C	O	P	Pd	
Spectrum 1	79.19	8.97	11.83	0.00	
Spectrum 2	82.91	9.50	7.58	0.00	
Average	81.05	9.24	9.71	0.00	
Ecart type	2.63	0.37	3.00	0.00	

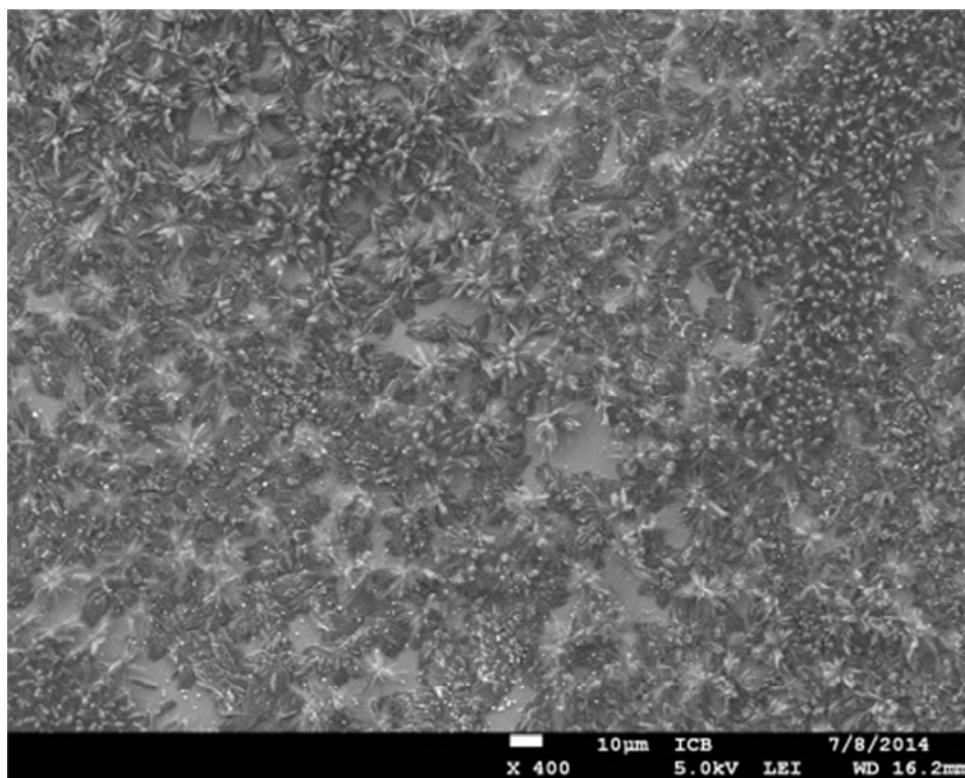
Figure 5.7. EDX analysis of self-assembly of **190**.

EDX analysis on self-assembly of **190** (**Figure 5.7**) over the two different areas (Spectrum 1 and 2) clearly indicated the expected presence of carbon (average 81.05%), oxygen (9.24%), and phosphorus

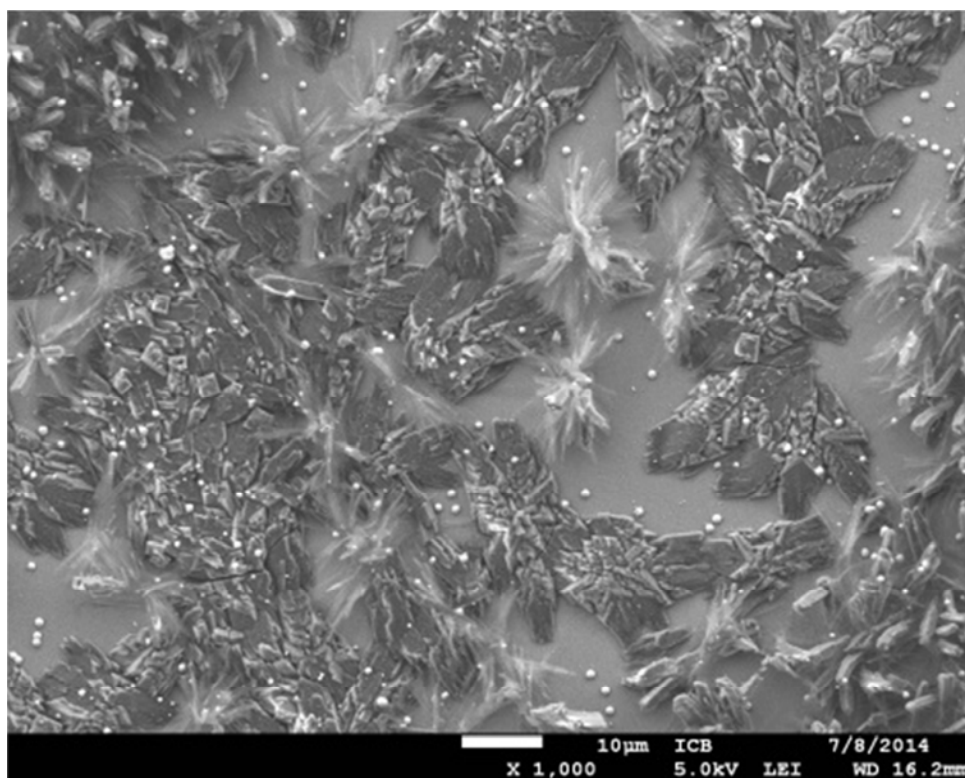
(9.71%). Interestingly, EDX confirmed the consistent nature of the deposit whatever the area observed (pillar or thin sheets), but also the fact that columnar edifices (Spectrum 1) are, as supposed from the micrographs, more compact than the network of thin sheets (Spectrum 2), with superior P content (12%). Therefore, for pillars self-assembly (C (79.19%) and O (8.97%)) the detection of (C, O) contamination from the Si support is minored by about 5% compared with the thin sheet network: C (82.91%) and O (9.50%). Here again the EDX measurements are in excellent agreement with the SEM observation.

4. Palladium CVD on 9-Phosphinodiamantan-4-ol (**190**)

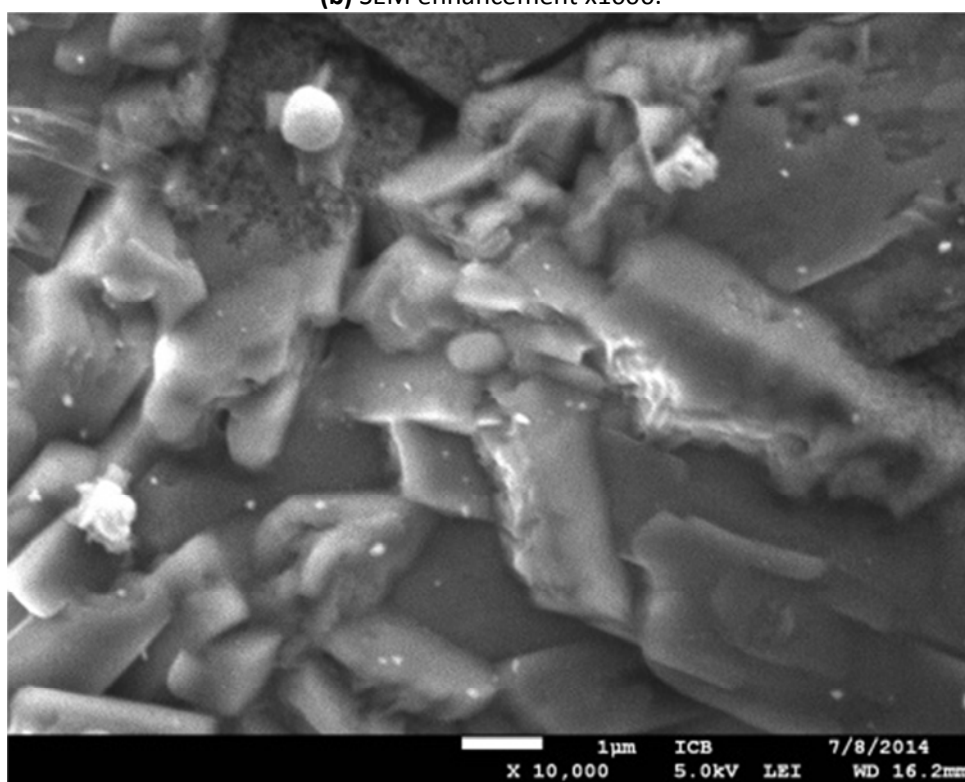
Palladium was deposited on the self-assembly of **190** by chemical vapor deposition conducted at 30 °C and 51 Torr using the precursor $[\text{Pd}(\eta^3\text{-allyl})\text{Cp}]$ with 3.2 mL/min of H_2 as reactive gas and 80 mL/min of argon as carrier gas. CVD deposition time was varied from 1 h to 7.5 h. The resulting deposits were analyzed by SEM and EDX. **Figure 5.8** below corresponds to CVD conducted for 1 h.



(a) CVD of Pd on **190** self-assembly, 1 h run – SEM enhancement x400.



(b) SEM enhancement x1000.



(c) SEM enhancement x10000.

Figure 5.8. CVD of $[\text{Pd}(\eta^3\text{-allyl})\text{Cp}]$ on **190** self-assembly, 1 h run with various enhancements.

SEM observation indicated two major changes in comparison with the non-metallized self-assembly. While the compact columnar edifices were still clearly discernible, surprisingly their porosity appeared to be less pronounced. In addition, on the sample were observed spherical particles with sizes ranging between 100 to 700 nm deposited mainly on the network of entangled thin sheets or on the Si support not covered with diamondoid. Such spherical particles (nodules) were hardly found on the diamondoids pillar assembly. The EDX analysis (**Figure 5.9**) over various areas of the sample indicated that the nodules incorporate palladium (45.56%, Spectrum 4) with the presence of phosphorus (3.77%) suggesting an interaction with diamondoids. However, after 1 h of chemical vapor deposition, with the exception of the nodules, palladium is hardly detectable by EDX on most of the sample, either on the diamondoid self-assembly (Spectrum 1 and 2) or on the Si support not covered with diamondoid (Spectrum 3).

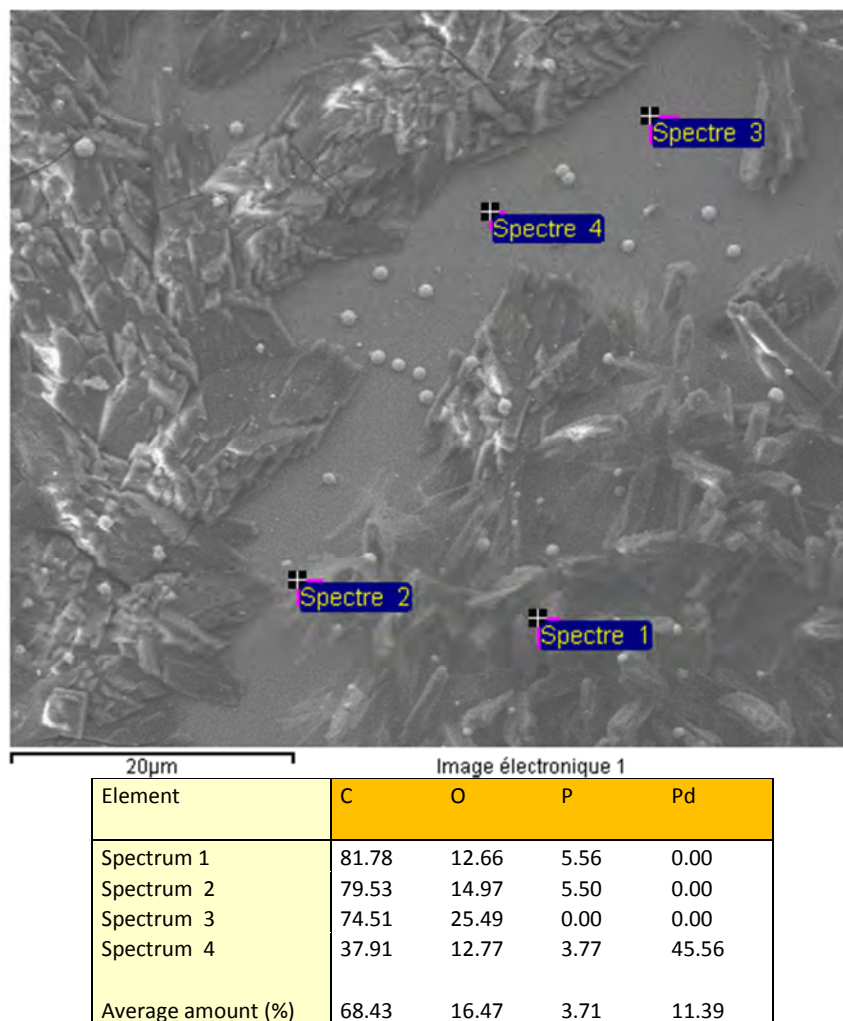
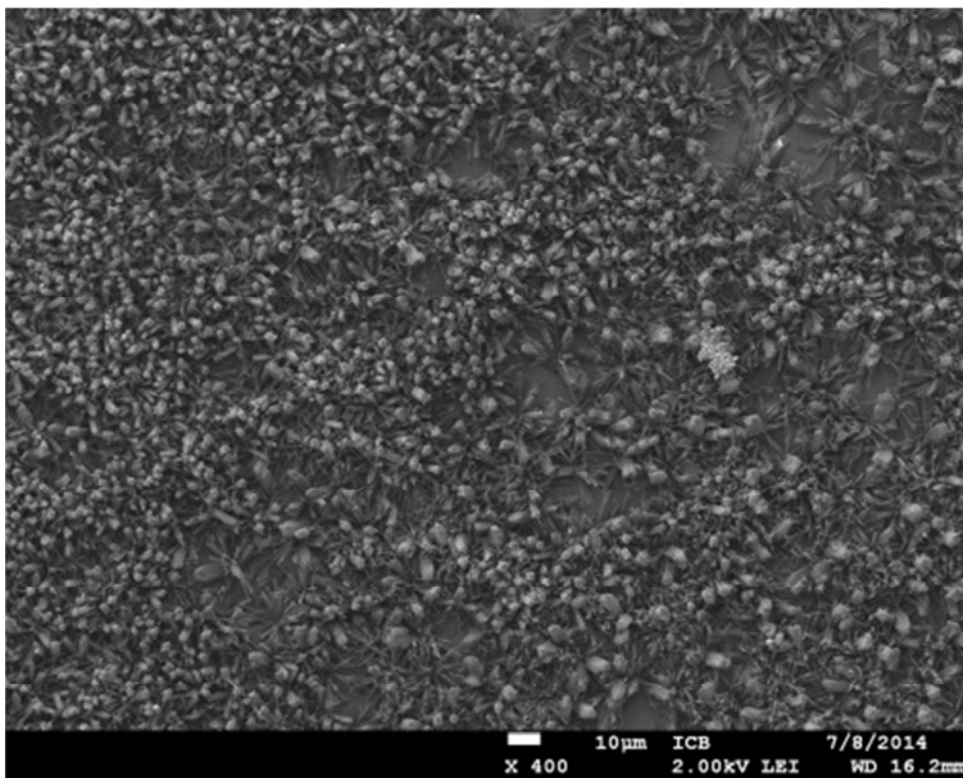
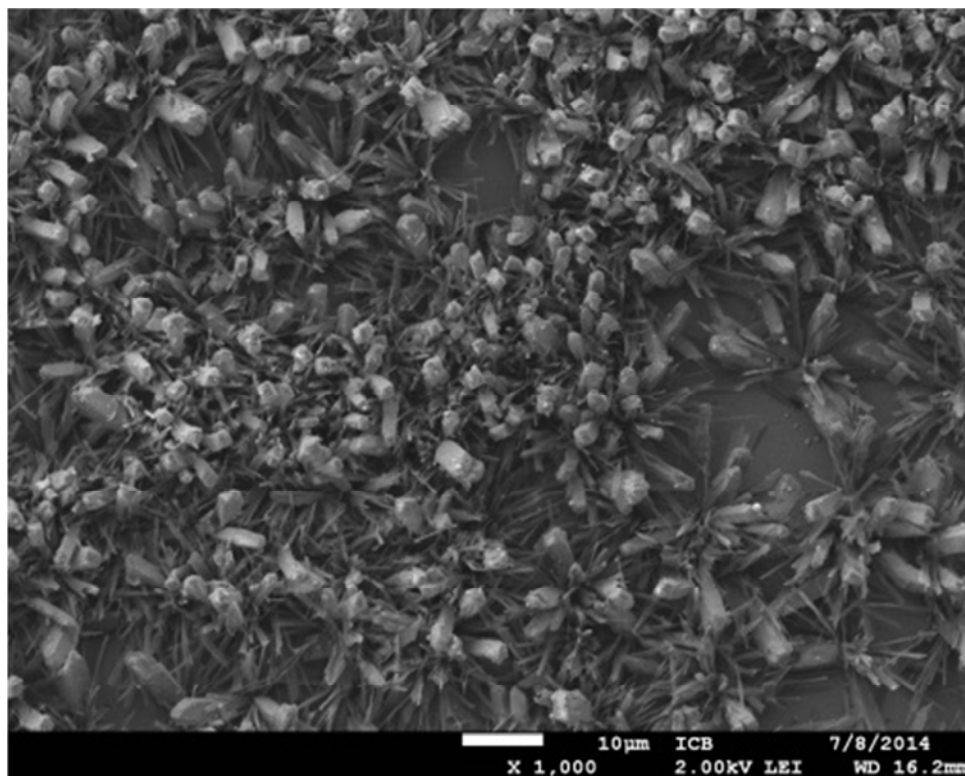


Figure 5.9. EDX analysis of Pd deposited on **190** self-assembly, 1 h run.

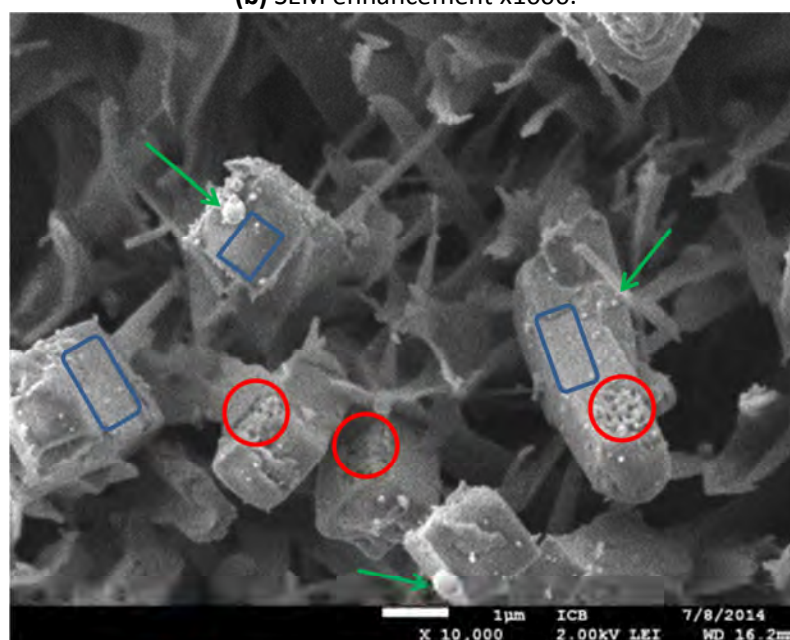
The surface modification of the columnar diamondoid self-assembly was largely confirmed after 3 h of Pd deposition as shown in **Figure 5.10(a)-(c)**. The enhancement photograph x10000 clearly shows (**Figure 5.10(c)**) that a very thin layer is now covering the porous surface of the self-assembly, while the rectangular pillar remained mostly of same size with square surfaces about $1.4\ \mu\text{m} \times 1.4\ \mu\text{m}$. On this photograph is visible, depending on the area, both the original porosity of the diamondoid “pillars” (red circles) and the new smooth layer (blue rectangle) which appear very thin from comparison with a nearby porous area. The detectable nodules have a size between 100 and 400 nm and are dispersed all over the sample. However, these nodules remain fairly rare and the detection of palladium by EDX from non-focused global analysis is difficult.



(a) CVD of Pd on **190** self-assembly, 3 h run – SEM enhancement x400.



(b) SEM enhancement x1000.

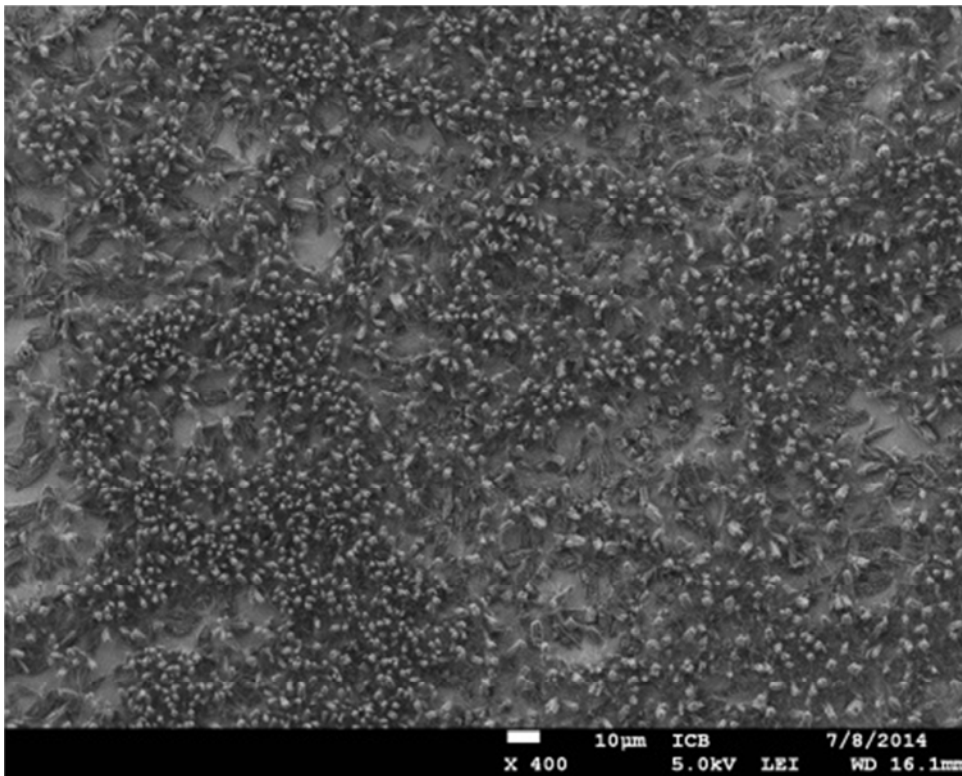


-  Porous surface on columnar self-assembly
-  New layer covering the assembly
-  Palladium spherical particles

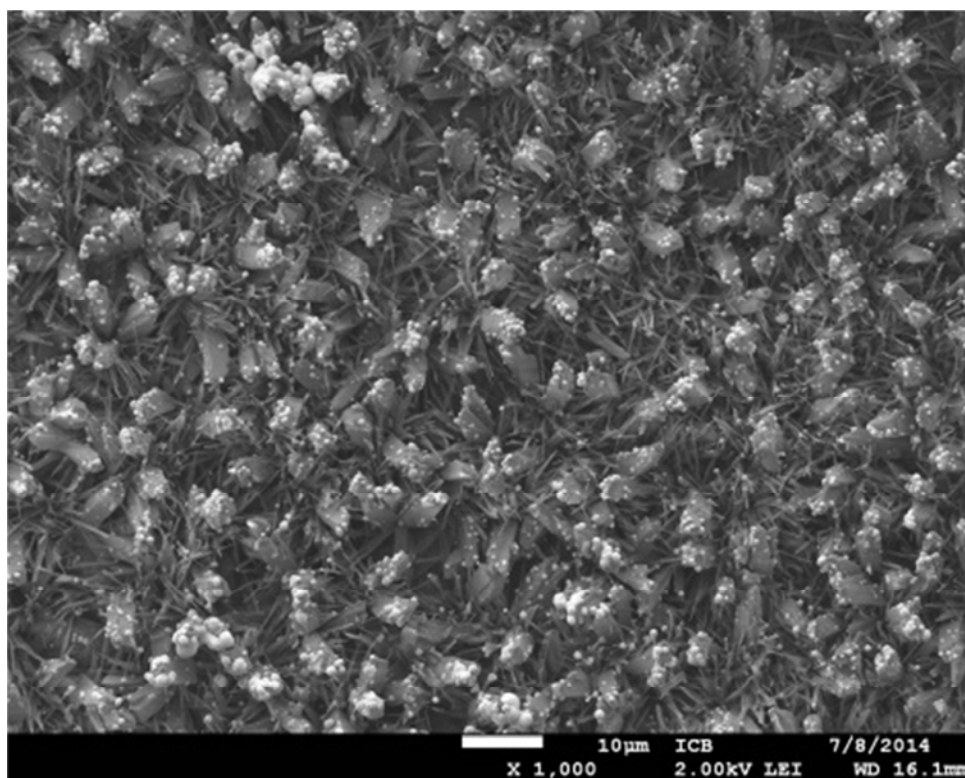
(c) SEM enhancement x10000.

Figure 5.10. CVD of $[\text{Pd}(\eta^3\text{-allyl})\text{Cp}]$ on **190** self-assembly, 3 h run.

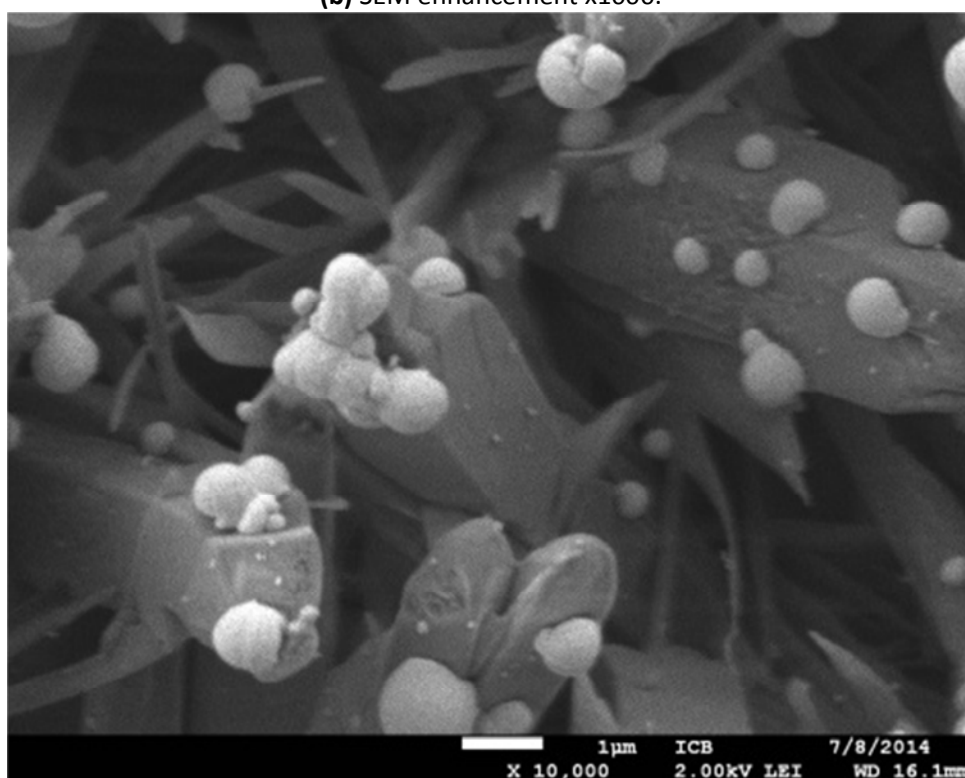
Pictures from deposition experiments conducted for 5.5 h (**Figure 5.11(a)-(c)**) confirmed that in addition to the smooth covering formed over the columnar self-assembly, a good dispersion of nodules (with a size distribution centered around 350 to 800 nm, as reported in **Figure 5.12**) is observed all over the sample. The distribution of nodules appears very homogeneous with most of them about 700 nm, and enhancement indicates that under these conditions both compact pillars and thin sheets are indeed supporting the nodules (**Figure 5.11(c)**).



(a) CVD of Pd on **190** self-assembly, 5.5 h run – SEM enhancement x400.



(b) SEM enhancement x1000.



(c) SEM enhancement x10000.

Figure 5.11. CVD of $[\text{Pd}(\eta^3\text{-allyl})\text{Cp}] \text{Pd}$ on **190** self-assembly, 5.5 h run.

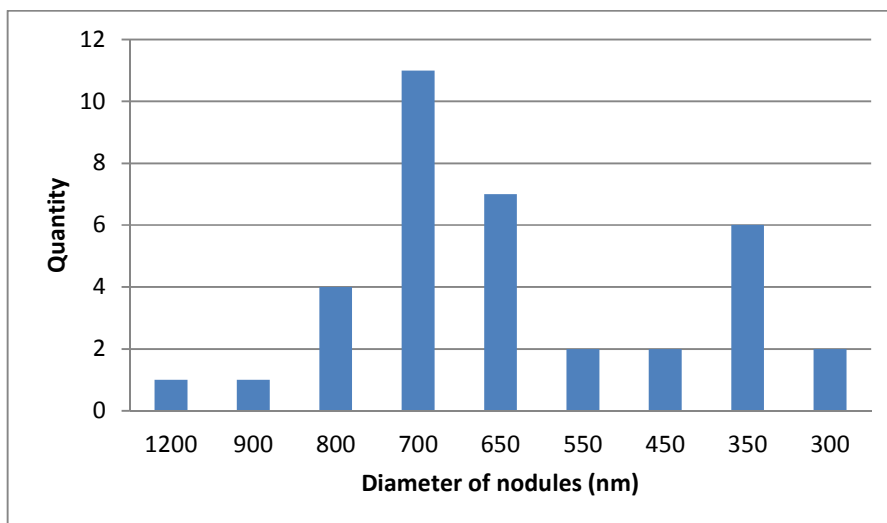


Figure 5.12. Histogram of 190 self-assembly, 5.5 h run.

A longer palladium deposition time of 7.5 h confirmed the previous trends, and magnification of the SEM observation further supports that the smooth layer covering the self-assembly is a palladium metal deposition leading to the formation of a hybrid with a previously unseen core-shell carbon-palladium structure (see **Figure 5.13**). Indeed, on this micrograph the layer is clearly visible and from the scale of the picture is estimated at less than 20 nm (measured difference of a stairs between porous and smooth area). Beside the clear coating aspect, “metallic” brilliance appeared at SEM observation may be attributed to a smooth surface of insulating materials that gives electron charge to the surface and induces a brilliant effect under SEM measurement. Another noticeable feature is that some nodules of large size ranging from 500 nm to 1 μm are visible, and that these nodules are often found at proximity of areas of the diamondoid self-assembly which have not been coated (**Figure 5.14**, red circle). This feature is consistent with Ostwald ripening phenomenon which expresses the diffusion of smaller condensate to larger ones. After a critical size reached for nodules, the system tries to lower its overall energy, and fragments on the surface of a smaller (energetically unfavorable) particle will tend to detach and diffuse from proximal areas and then attach to the surface of larger particle, therefore “...as larger crystals grow the area around them is depleted of smaller crystals...”³

³ J. B. Hannon, S. Kodambaka, F. M. Ross, R. M. Tromp. *Nature*, **2006**, 440, 69-71. The influence of the surface migration of gold on the growth of silicon nanowires.

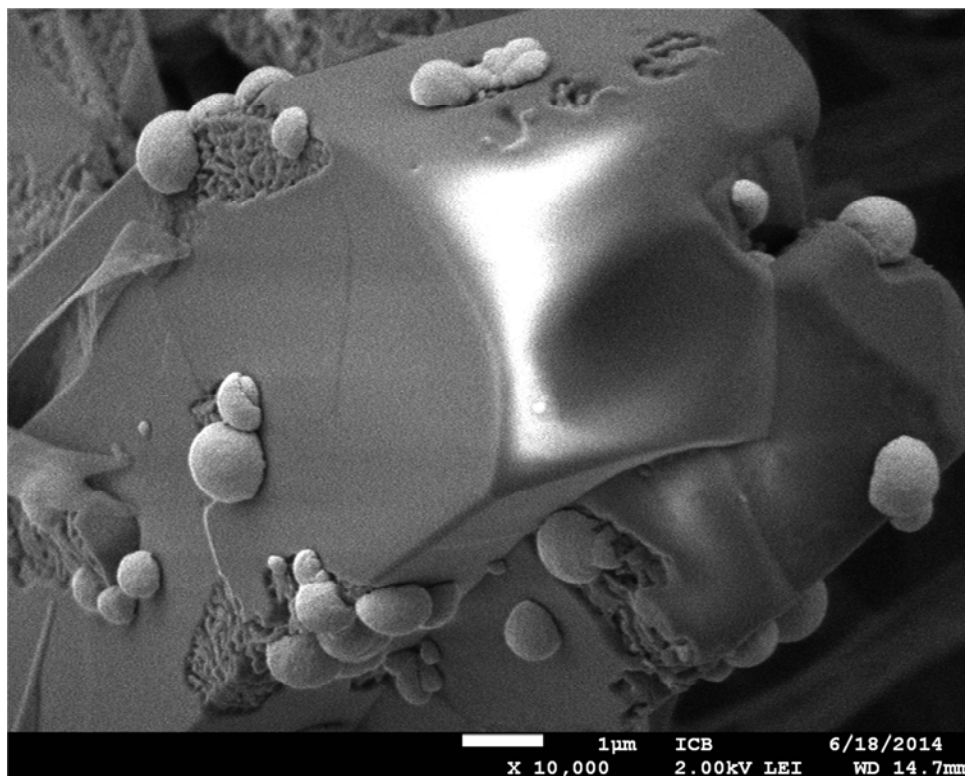


Figure 5.13. CVD of $[\text{Pd}(\eta^3\text{-allyl})\text{Cp}]$ Pd on **190** self-assembly, 7.5 h run – SEM x10000.

EDX analysis of the samples after 7.5 h of palladium chemical vapor deposition is given in **Figure 5.15**. The analysis was purposefully focused for Spectrum 1 on a single compact columnar edifice of the diamondoid phosphine (over about $1.5 \mu\text{m}^2$, C, 89.26%, O, 6.62%, P, 3.22%). The compact nature of the self-assembly is supported by the low detection of Si substrate signature (0.72%). The analysis confirmed the presence of palladium (0.18%) and the low amount detected is in agreement with the presence of only a thin layer of the elemental palladium. The EDX in Spectrum 2 is focused on a more extended area (over $30 \mu\text{m}^2$), encompassing in majority the network of entangled thin sheets with spherical nodules of palladium. Accordingly the detection of phosphorus (5.15%), Si from support (1.73%) and palladium (0.37%) was much increased. Spectrum 3 was focused on a large area over a $200 \mu\text{m}^2$ giving an estimation of the average composition of the deposit which was indeed found intermediate (averaged) between the analyses on the two previous areas.

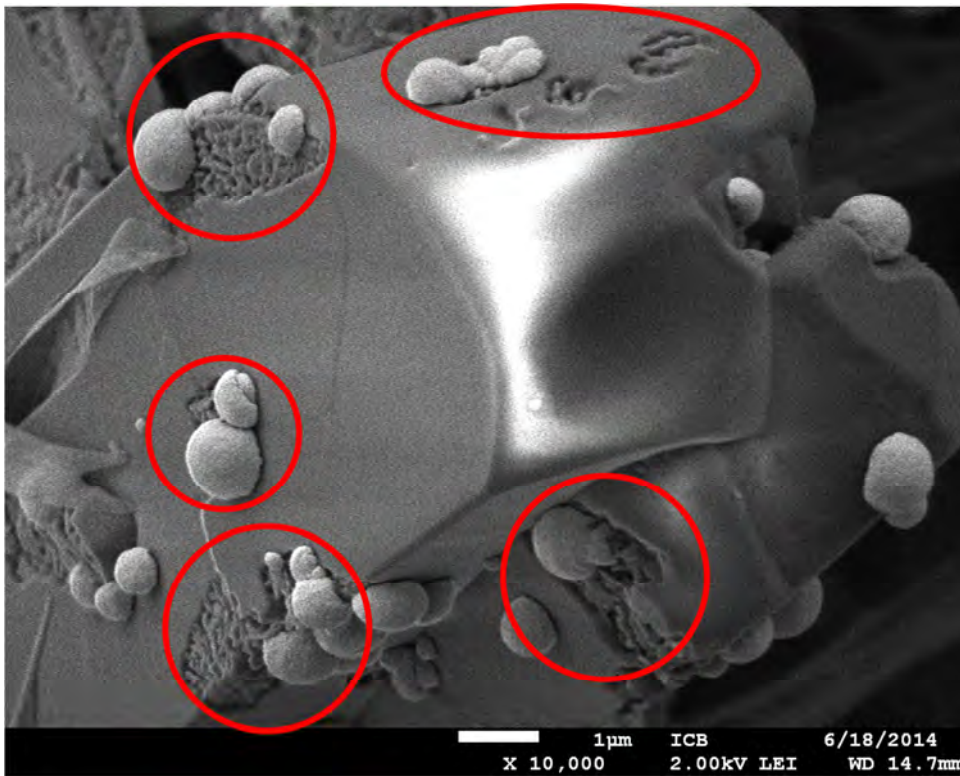
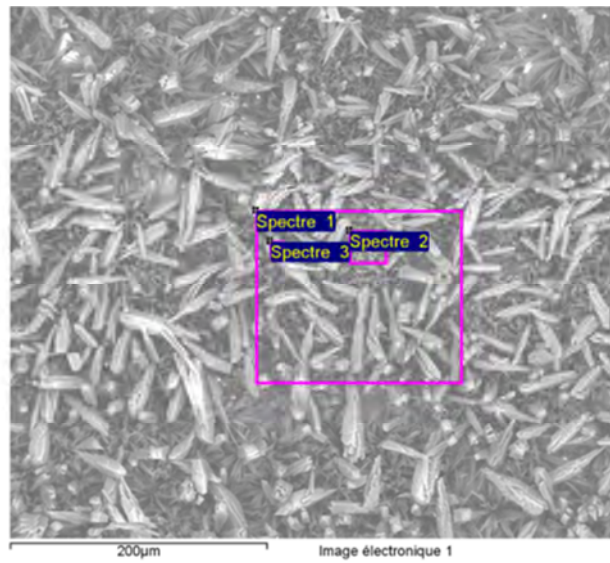


Figure 5.14. Pd nodules growth at proximity of uncovered diamondoid areas.



Element	C	O	Si	P	Pd
Spectre 1	89.26	6.62	0.72	3.22	0.18
Spectre 2	88.17	4.57	1.73	5.15	0.37
Spectre 3	91.17	3.33	1.80	3.44	0.27
Average	89.53	4.84	1.42	3.94	0.27
Standard deviation	1.52	1.66	0.60	1.06	0.10

Figure 5.15. EDX analysis of 190 deposits on sample after 7.5 h Pd deposition.

The EDX analysis is again consistent with the SEM observations and further confirmed both the global palladium metallization and the formation of hybrid columnar compact pillars covered with a thin layer of palladium, while other areas mainly supported palladium spherical nodules.

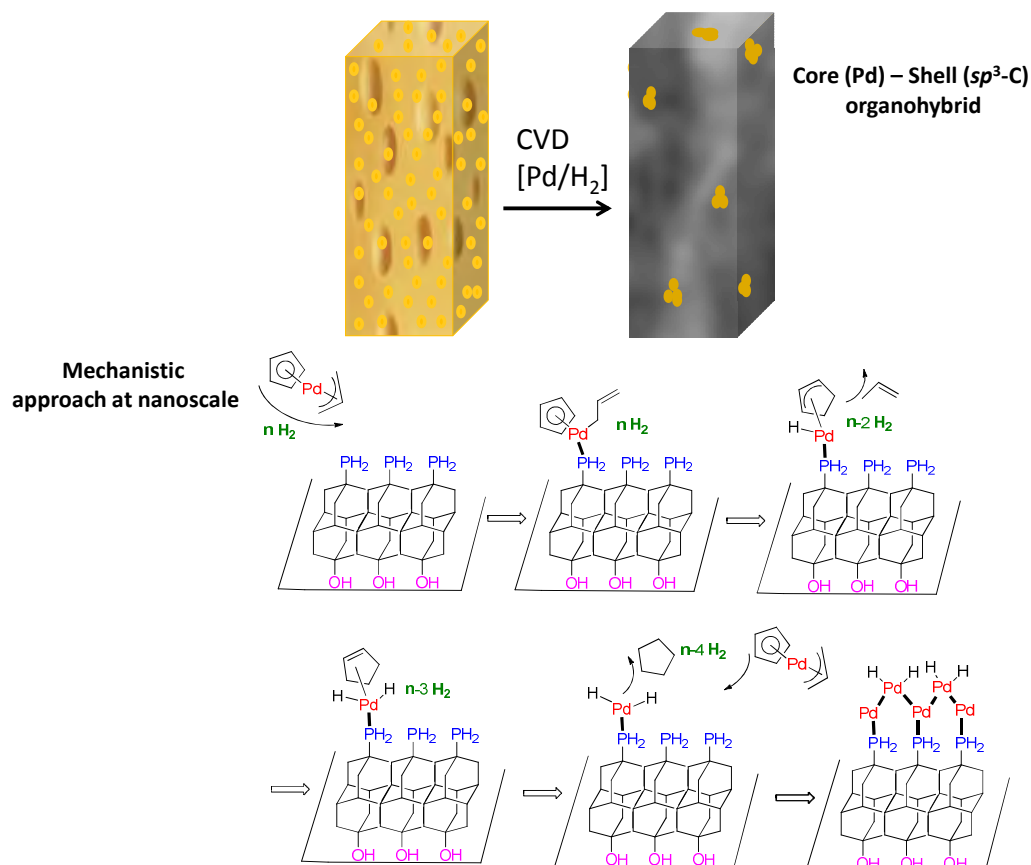


Figure 5.16. Pd covering of columnar self-assembly of diamondoid **190** and mechanism proposed.

In **Figure 5.16** (bottom) is proposed a general mechanism for the thin layer formation under the palladium CVD conditions. By comparison with diamondoid phosphine oxide **182**, the presence of air-stable phosphino PH₂ groups in a compact arrangement would allow stabilizing palladium molecular species for which the easy hydrogenation of ligands can occur in the coordination sphere of Pd(II)/Pd(0) species. Autocatalytic hydrogenation using [Pd(allyl)Cp] in CVD has been early on demonstrated by Hierso in the Kalck group from the analysis of the gaseous effluent by mass-spectrometry in operando conditions.² In the presence of 1% vol/vol H₂, the major effluent formed are hydrogenated products of the ligands (cyclopentane, propane, cyclopentene, etc.) from [Pd(η^3 -allyl)Cp]. The high density of phosphino groups on the surface of the compact pillars self-assembly would be at the origin of the dense

metallization on the surface of the edifice. This behavior makes a clear difference to all the functionalized diamondoid self-assemblies studied before in palladium CVD (hydroxy and fluoro in **Chapter 3** and phosphine oxide **182** in the present chapter). *It appears now clearly to us that the opportunity to create a strong P–Pd covalent bond with the metal is a decisive feature of diamondoids for any metallization.* This finding opens the way to further metal deposition such as nickel or platinum. In addition, amino and sulfur diamondoids may be also very interesting candidates for deposition of copper and gold for instance, in line with their recognized mutual affinity from coordination chemistry (HSAB Pearson theory).

The kind of organohybrid **Pd@PH₂-Diam-OH** we designed here is unique to date. A crucial point is the identification of the P–Pd covalent bond near the surface of these edifices. This seems possible at the very first stage of CVD deposition. Such kind of characterization with Raman and infrared are envisioned in the near future. It is thus necessary to further support the formation/existence of these organohybrids, and to characterize these new materials in comparison with the existing supported palladium species. This was achieved by careful XPS measurements and high resolution TEM (Transmission electron microscopy) analysis, as described in the next section.

5. XPS analysis of the organohybrid **Pd@PH₂-Diam-OH**

X-ray photoelectron spectroscopy (XPS) is a surface-sensitive quantitative spectroscopic technique that measures the elemental composition at the parts per thousand range, empirical formula, chemical state and electronic state of the elements that exist within a material (**Figure 5.17**). XPS spectra are obtained by irradiating a material with a monochromatic beam of X-rays (here 1486.6 eV) while simultaneously measuring the kinetic energy and number of electrons that escape from the top 2 to 5 nm of the material being analyzed. XPS requires high vacuum. XPS is thus used to identify the elements within 2-5 nm surface depth. Based on the measurement of an apparent binding energy, this technique allows identifying the chemical environment of an analyzed element through the shift in energy observed in the spectra.

XPS experiments were conducted on three different samples: *sample 1* results from the self-assembly of **190**; *sample 2* results from a Pd CVD long run of 7.5 h over the self-assembly of **190**, and *sample 3* results from a Pd CVD short run of 1 h over the self-assembly of **190** (thus at the very beginning of Pd deposition). These samples were scanned first with a low energetic resolution over a range of binding energy (BE) 0–1350 eV that is called here “Survey”.

All the deposits were analyzed precisely on the center of the samples where both diamondoid self-assembly and Pd coating was homogeneously visible. Supplementary XPS analysis at the edge of the support was used as standard since there only pure metallic palladium nodules were present (areas free of diamondoid **190** self-assembly). More precise analysis with focused scans were recorded for specifically analyzing the elements O, C, Pd, and P separately, in order to examine rigorously energy shifts in signals (called here “high resolution spectra”).

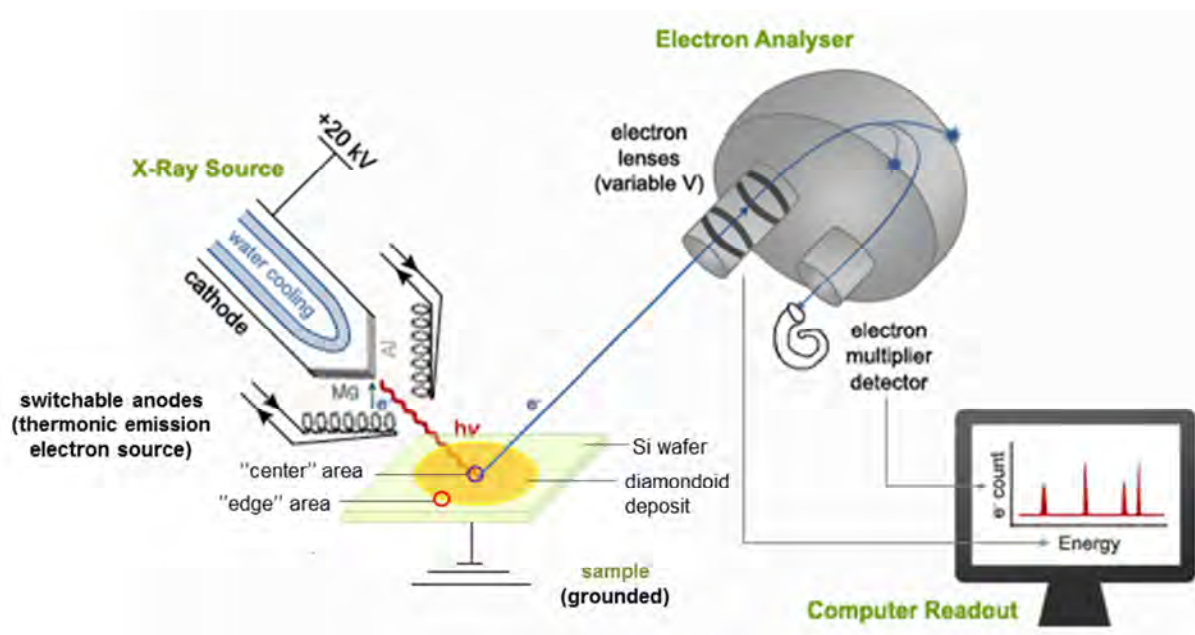


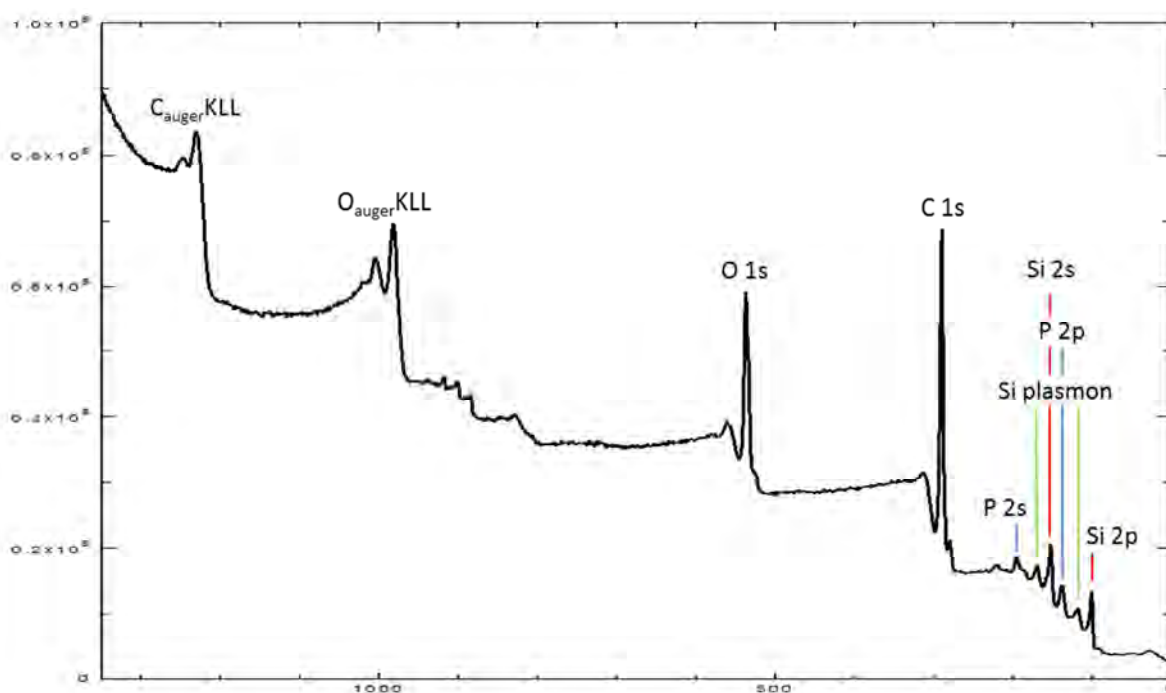
Figure 5.17. Diagram of an X-ray photoelectron spectrometer.

The spectra were calibrated to get the corrected binding energy by the following formula: $BE^* = BE + 0.0018 \cdot BE - 1.3838$. The charge effect was calculated for Sample 2: the metallic palladium $3d_{5/2}$ peak was used for calibration (335.5 eV).⁴ After the XPS spectrum was calibrated to the correct BE, we obtained the peak C 1s of the diamondoid at 289.3 eV. This peak was then used as reference to calibrate the Samples 1 and 3.

⁴ F. Boekman, A. Gogoll, L. G. M. Pettersson, O. Bohman, H. O. G. Siegbahn. *Organometallics*, **1992**, 11, 1784-1788. Electronic structure of catalytically important palladium complexes studied by photoelectron spectroscopy.

a) Sample 1 (center) – self-assembly of **190**

XPS analysis of **190** self-assembly is depicted in **Figure 5.18** (see **Figure 5.6** for SEM images). The C 1s peak of diamondoid was found at binding energies (BE) of 289.3 eV. The Si peaks, Si 2s at 152.1 eV and Si 2p at 100.0 eV could be observed even though the deposit was seemingly very covering on SEM images (**Figure 5.6**). This meant that the self-assembly did not fully cover the Si wafer in particular due to the space existing between the non-compact thin sheets network. The expected peaks of O 1s, C 1s, P 2s, and P 2p from **190** were present and are detailed at higher resolution in the following.



$BE_{C_{KLL}} = 1230.0$ eV, $BE_{O_{KLL}} = 981.6$ eV, $BE_{O_{1s}} = 536.8$ eV, $BE_{C_{1s}} = 289.3$ eV, $BE_{P_{2s}} = 195.1$ eV, $BE_{Si_{plasmon}} = 169.1$ eV, $BE_{Si_{2s}} = 152.1$ eV, $BE_{P_{2p}} = 138.0$ eV, $BE_{Si_{plasmon}} = 118.0$ eV, $BE_{Si_{2p}} = 100.0$ eV.

Figure 5.18. XPS survey of **190** self-assembly: Sample 1 (center).

Figure 5.19 showed more precise BE for O 1s peak. With this scan enhancement for oxygen, two peaks of O 1s at 536.7 eV (left) and 533.2 eV (right) were observed. The O 1s at 533.2 eV belongs to SiO₂ (SiO₂ 532.9 eV).⁵ The SiO₂ came from the native thin oxide layer on Si wafer since we used such supports without further treatment. Accordingly, the peak at 536.7 eV was attributed as O 1s from hydroxyphosphine **190**.

⁵ T. L. Barr. *J. Vac. Sci. Technol A*, **1991**, 9, 1793-1805. Recent advances in x-ray photoelectron spectroscopy studies of oxides.

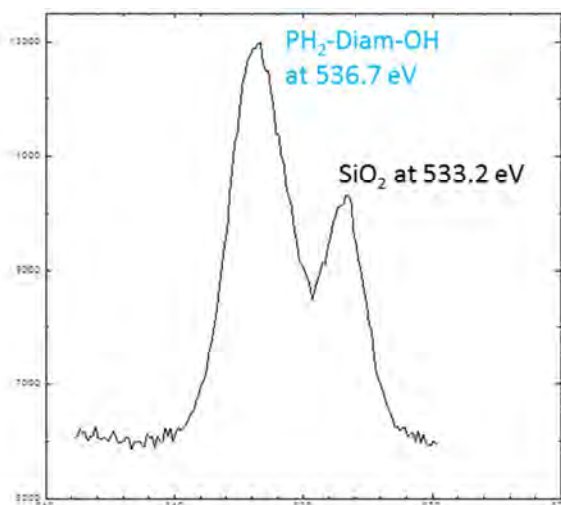


Figure 5.19. XPS spectrum O 1s for **190** self-assembly: Sample 1 (center).

For the carbon element (**Figure 5.20**), only a single peak C 1s at 289.3 eV was obtained and this peak corresponded to the carbon sp^3 of the diamondoid phosphine **190**. This value is in the range of reported values: diamond sp^3 (pure from JEOL) is 290.45 eV,⁶ adamantane is 290.0 eV,⁷ sp^3 hybridized carbon (on Si support) is 285.2 eV,⁸ diamantane-4-thiol (SAM on Au(111) support) is 284.0 eV.⁹ Schreiner's group showed that the presence of functional groups such as thiol on adamantane shifted the BE to higher BE. "This shift is due to the transfer of electron density from the parent molecule to the highly electronegative thiol group."⁷

⁶ C 1s BE for sp^3 hybridized carbon was 290.45 eV and for ion-bombarded diamond was 285.35 eV: J. C. Lascovich, R. Giorgi, S. Scaglione. *Appl. Surf. Sci.*, **1991**, 47, 17-21. Evaluation of the sp^2/sp^3 ratio in amorphous carbon structure by XPS and XAES.

⁷ C 1s BE for adamantane was 290.0 eV and for adamantane-1-thiol 290.2 eV: L. Landt, M. Staiger, D. Wolter, K. Klünder, P. Zimmermann, T. M. Willey, T. van Buuren, D. Brehmer, P. R. Schreiner. *J. Chem. Phys.*, **2010**, 132, 024710/1-024710/7. The influence of a single thiol group on the electronic and optical properties of the smallest diamondoid adamantane.;

⁸ C 1s BE for diamond sp^3 was 285.2 eV: P. Mérel, M. Tabbal, M. Chaker, S. Moisa, J. Margot. *Appl. Surf. Sci.*, **1998**, 136, 105-110. Direct evaluation of the sp^3 content in diamond-like carbon films by XPS.

⁹ (a) C 1s BE for adamantanethiol, diamantane-1-thiol, diamantane-4-thiol on Au(111) supports were 284.2 eV, 284.0 eV, and 284.2 eV, respectively. T. M. Willey, J. D. Fabbri, J. R. I. Lee, P. R. Schreiner, A. A. Fokin, B. A. Tkachenko, N. A. Fokina, J. E. P. Dahl, R. M. K. Carlson, A. L. Vance, W. Yang, L. J. Terminello, T. van Buuren, N. A. Melosh. *J. Am. Chem. Soc.*, **2008**, 130, 10536-10544. Near-edge X-ray absorption fine structure spectroscopy of diamondoid thiol monolayers on gold. (b) C 1s BE for for adamantane-1-thiol on Au(111) support was 284.2 eV: A. A. Dameron, T. J. Mullen, R. W. Hengstebeck, H. M. Saavedra, P. S. Weiss. *J. Phys. Chem. C*, **2007**, 111, 6747-6752. Origins of displacement in 1-adamantanethiolate self-assembled monolayers.

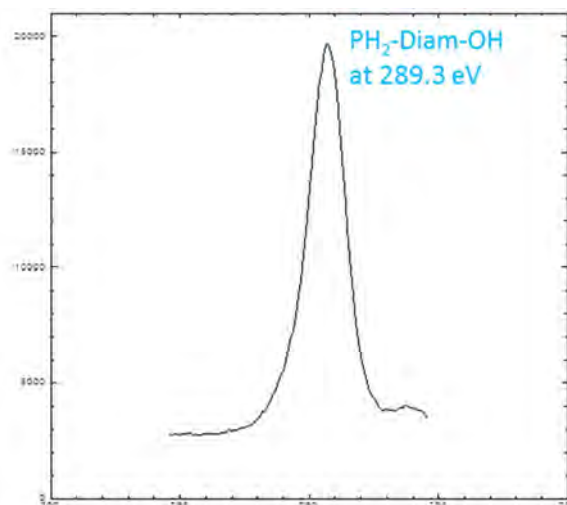


Figure 5.20. XPS spectrum of C 1s for **190** self-assembly: Sample 1 (center).

The XPS for phosphorus area (**Figure 5.21**) indicated two peaks. Peak on the left at 138.3 eV was attributed to the hydroxyphosphine oxide **196** from hydroxyphosphine **190** that is slowly oxidized in air. The presence of this P=O peak on the surface came from the oxidation of the sample when contacted with air before measurement. But this intense peak is probably not representative of the bulk deposit because the oxidation mainly happened on the surface around. This was confirmed by supplementary experiments of vapor deposition of hydroxyphosphine oxide **196** (that was synthesized independently, see **Chapter 4**) with typical conditions: 85 °C for 4 min on Si wafer. The XPS spectrum P 2p of this **196** self-assembly is given in **Figure 5.22**. The peak attribution at 138.3 eV was thus confirmed by direct XPS of **196**. The presence of P 2p at 135.2 eV (right) (**Figure 5.21**) was attributed to PH₂ of hydroxyphosphine **190**, and indicated that the primary phosphine at the surface deposit was not completely oxidized (after overnight before XPS measurement) and is unchanged during the handling in air.

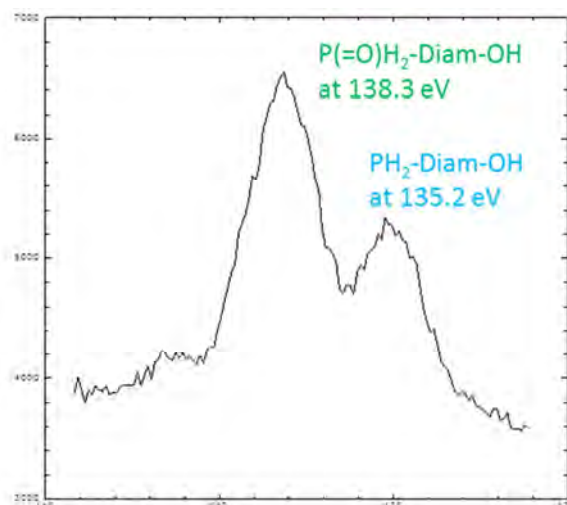


Figure 5.21. XPS spectrum of P 2p for **190** self-assembly: Sample 1 (center).

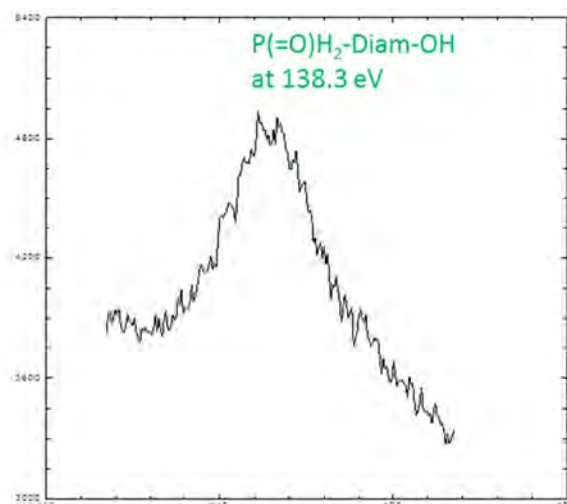
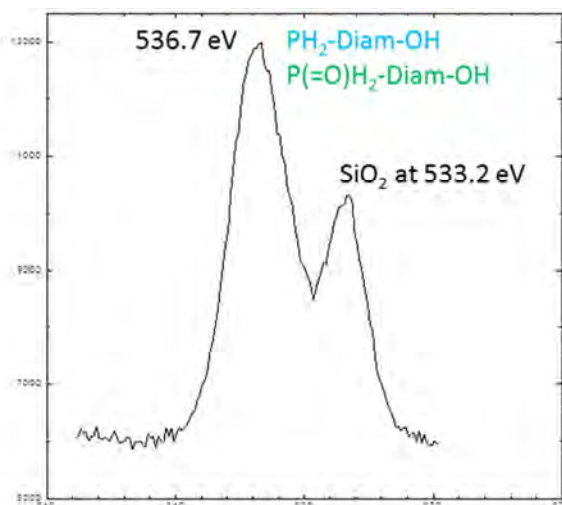
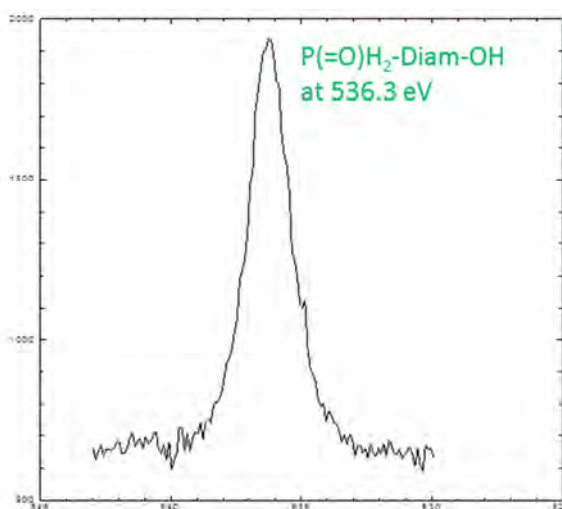


Figure 5.22. Comparative XPS spectrum of P 2p for **196** self-assembly (center).

The presence of the phosphine oxide **196** at the surface of our deposit led us to refine the attribution of O 1s for diamondoid phosphine in **Figure 5.19** (**Figure 5.23**). The O 1s of P=O is also present at the same BE at 536.7 eV. The oxygenated species OH of **190** (536.7 eV), and P=O and OH of **196** (536.3 eV) have very close BE and cannot be easily distinguished on the basis of our XPS data.



(a) XPS spectrum O 1s for **190** self-assembly: Sample 1 (center). (or **Figure 5.19**)



(b) XPS spectra of O 1s for **196** self-assembly (center).

Figure 5.23. XPS spectrum of O 1s for self-assembly of **190** and **196** (center).

b) Sample 2 (edge) – metallic palladium nodules

The analysis of Sample 2 considered areas where metallic palladium nodules are concentrated in **Figure 5.24** with very dark contrast. Optical images of this edge area (yellow circle) showed mostly metallic palladium. Eventually, some very few diamondoid small deposits are observed at the edge of metallic nodules.

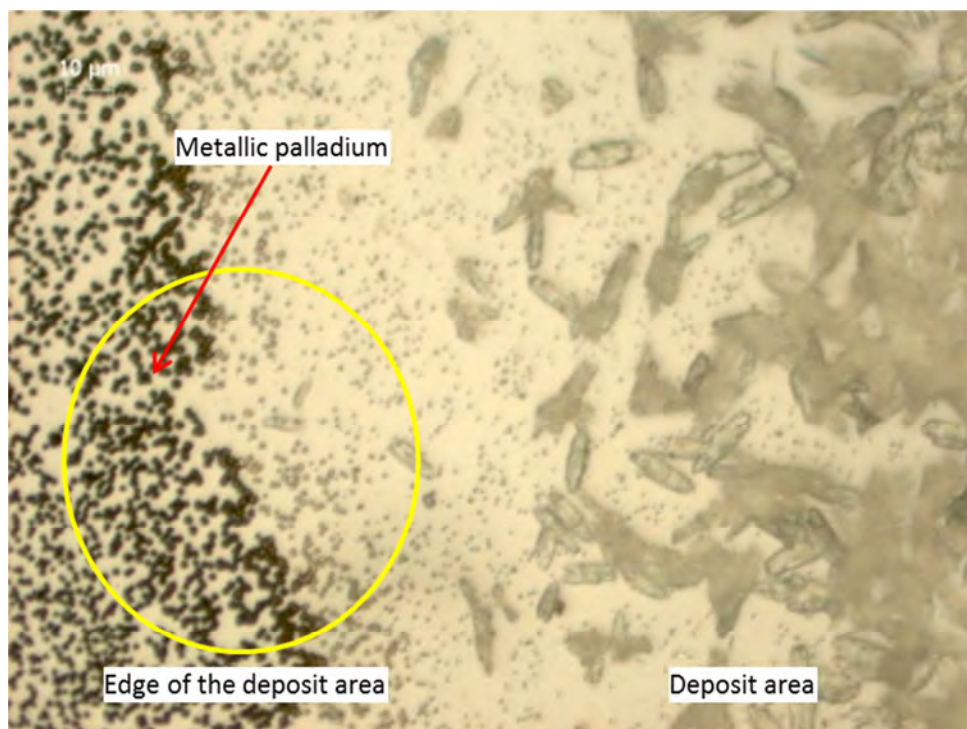
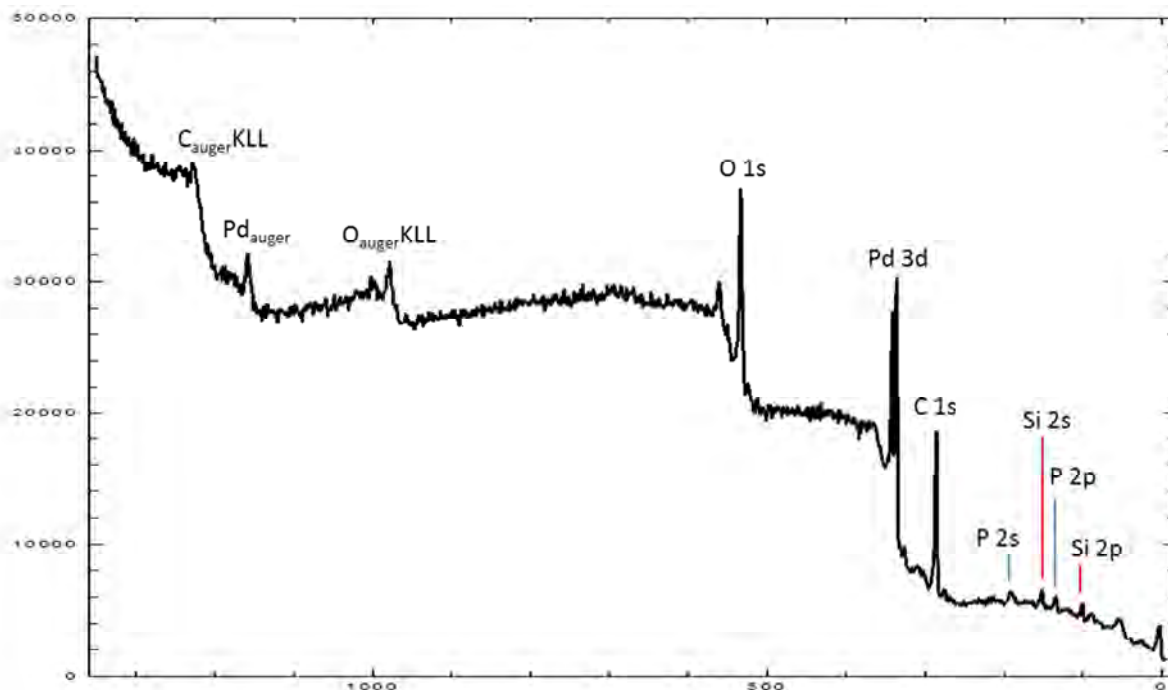


Figure 5.24. Optical image of Pd deposition on **190** self-assembly (Sample 2).

The XPS survey of this area confirmed that indeed only traces of the diamondoid could be detected in this edge area (**Figure 5.25**, peak P 2s and P 2p at 191.3 eV and 133.2 eV respectively).



$BE_{CKLL} = 1228.2$ eV, $BE_{Pd\ augeter} = 1158.1$ eV, $BE_{OKLL} = 977.8$ eV, $BE_{O1s} = 533.0$ eV, $BE_{Pd3d} = 340.6$ eV, $BE_{Pd3d} = 335.5$ eV, $BE_{C1s} = 284.9$ eV, $BE_{P2s} = 191.3$ eV, $BE_{Si2s} = 151.3$ eV, $BE_{P2p} = 133.2$ eV, $BE_{Si2p} = 100.2$ eV.

Figure 5.25. XPS survey of Pd deposition on **190** self-assembly: Sample 2 (edge).

Figure 5.26 shows the single O 1s peak of SiO₂ at 533.2 eV. This peak of SiO₂ confirmed the attribution in Sample 1 (**Figure 5.19**).

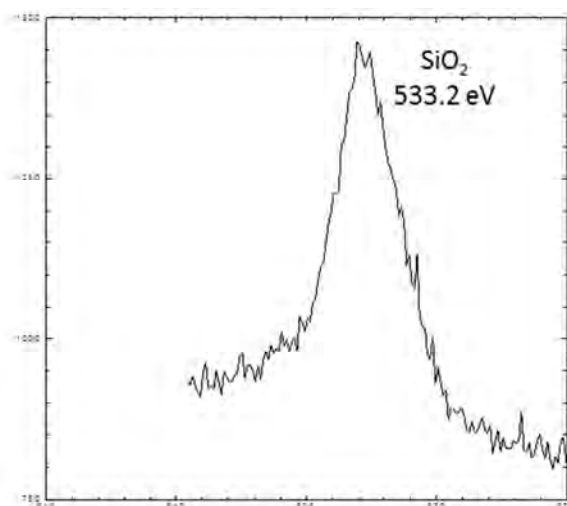


Figure 5.26. XPS spectrum O 1s for Pd deposition on **190** self-assembly: Sample 2 (edge).

For XPS C 1s (**Figure 5.27**), the peak at 284.9 eV was the mainly evidence and the signature of C pollution on the surface. This pollution is mainly due to C-(H)_n species adsorbed or graphitic carbon.¹⁰ Senkevich reported that such peak was observed during Pd deposition using [Pd(allyl)Cp], and they used it for spectra calibration.¹ At 289.3 eV, a trace of diamondoid is visible from sp³ C. In contrast, P 2p was not detected due to its very low concentration (**Figure 5.28**). These data confirmed that further Pd XPS analysis will concern deposit free from diamondoids.

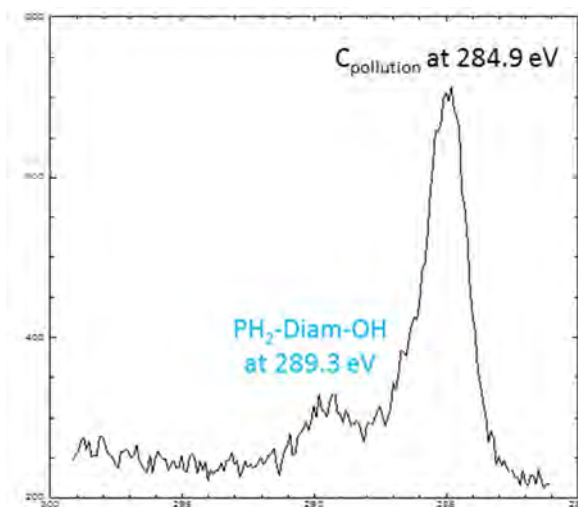


Figure 5.27. XPS spectrum C 1s for Pd deposition on **190** self-assembly: Sample 2 (edge).

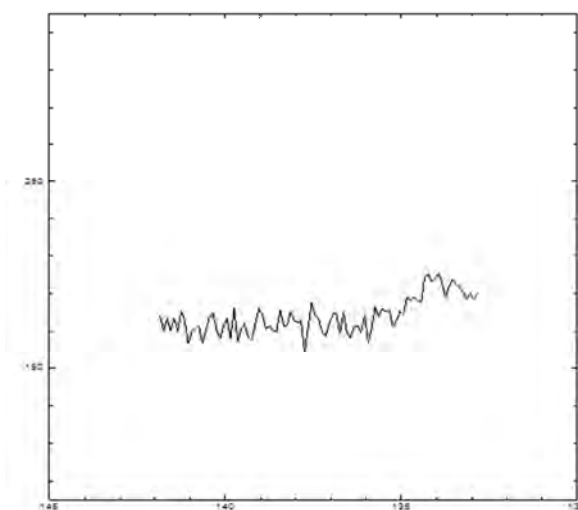


Figure 5.28. XPS spectrum P 2p for Pd deposition on **190** self-assembly: Sample 2 (edge).

¹⁰ *Handbook of X-Ray Photoelectron Spectroscopy*, Perkin-Elmer Corp., 1992.

The signals of the Pd 3d peak at 341.0 eV ($3d_{3/2}$) and 335.5 eV ($3d_{5/2}$) (**Figure 5.29**) is characteristic metallic palladium from elemental Pd(0) deposit.¹¹ No palladium oxide is noted indicating the clean separation of the ligands from the metal, and the absence of remaining precursor.

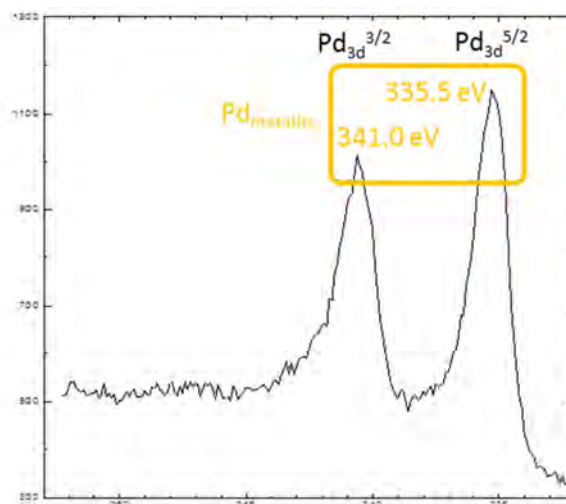
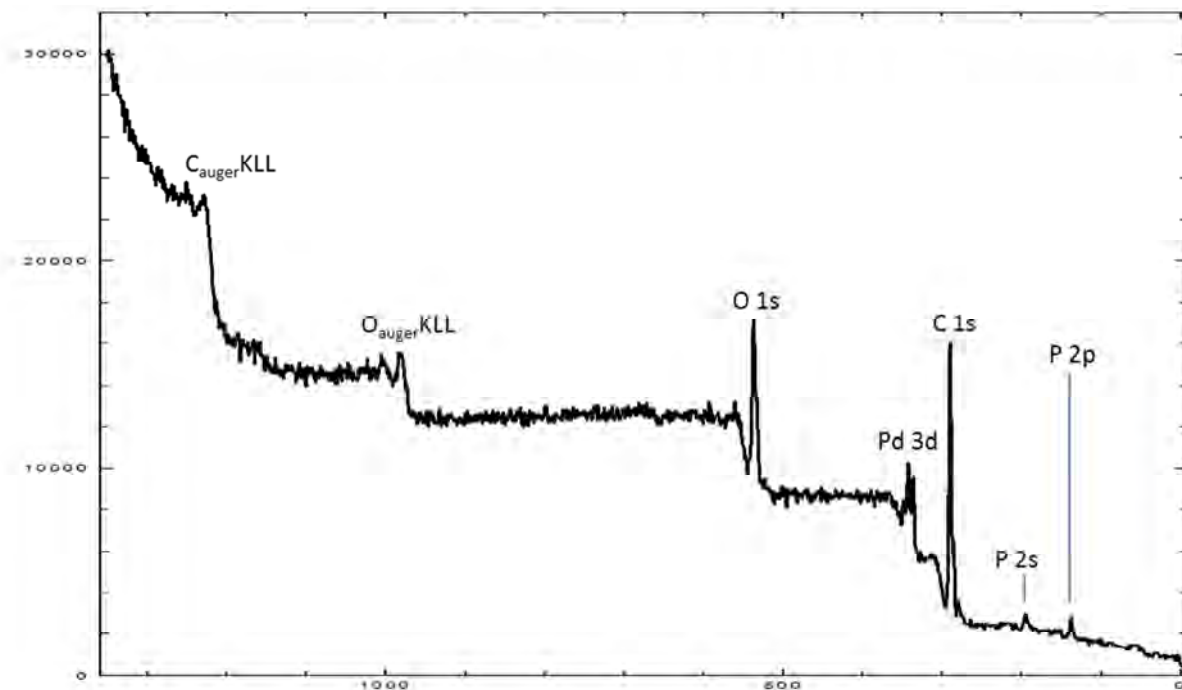


Figure 5.29. XPS spectrum Pd 3d for Pd deposition on **190** self-assembly: Sample 2 (edge).

Sample 2 (center) – Pd CVD long run of 7.5 h over the self-assembly of 190

Figure 5.30 illustrates the XPS measurement after palladium CVD on self-assembly **190** for 7.5 h, focusing in the center of the sample. The Si peaks are not observed due to the thickness of the deposit. The peak of O 1s, Pd 3d, C 1s, and P 2s, and P 2p that correspond to the **Pd@PH₂-Diam-OH** hybrid are observed together with additional elemental Pd peaks. These new signals clearly highlight the interaction existing now between the diamondoid and palladium, and they are discussed at high resolution in the following. The most significant information is the presence of two kinds of palladium on the surface.

¹¹ XPS BE of metallic Pd at 340.8 eV ($3d_{3/2}$) and 335.6 eV ($3d_{5/2}$) were reported by: J. E. Gozum, D. M. Pollina, J. A. Jensen, G. S. Girolami. *J. Am. Chem. Soc.*, **1988**, 110, 2688-2689. "Tailored" organometallics as precursors for chemical vapor deposition of high-purity palladium and platinum thin films.



$BE_{CKLL} = 1228.2$ eV, $BE_{OKLL} = 983.8$ eV, $BE_{O1s} = 537.0$ eV, $BE_{Pd3d} = 348.6$ eV, $BE_{Pd3d} = 341.6$ eV, $BE_{Pd3d} = 335.6$ eV, $BE_{C1s} = 289.5$ eV, $BE_{P2s} = 194.3$ eV, $BE_{P2p} = 137.2$ eV.

Figure 5.30. XPS survey of Pd deposition on **190** self-assembly: Sample 2 (center).

High resolution XPS for oxygen (**Figure 5.31**) indicates two peaks at 536.7 eV and 533.2 eV, with SiO_2 from Si wafer at 533.2 eV. The peak at 536.7 eV was attributed to O 1s for hydroxyphosphine and phosphine oxide as seen in Sample 1 (**Figure 5.23**).

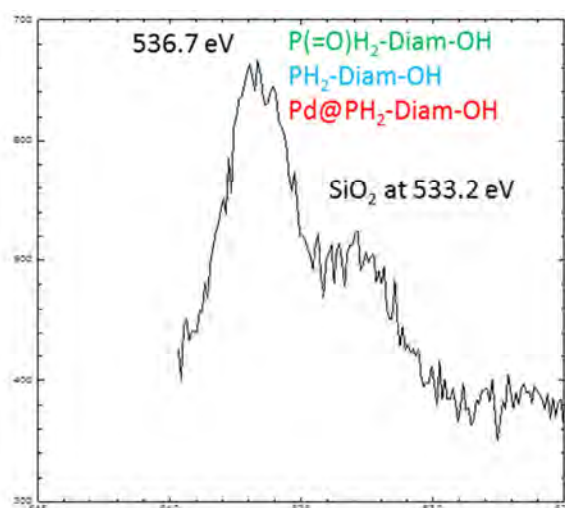


Figure 5.31. XPS spectrum O 1s for Pd deposition on **190** self-assembly: Sample 2 (center).

The peak of C 1s at 289.3 eV corresponds to C sp³ of the diamondoid similarly to the self-assembly in Sample 1. The C 1s pollution is minored and detected at 284.9 eV (**Figure 5.32**).

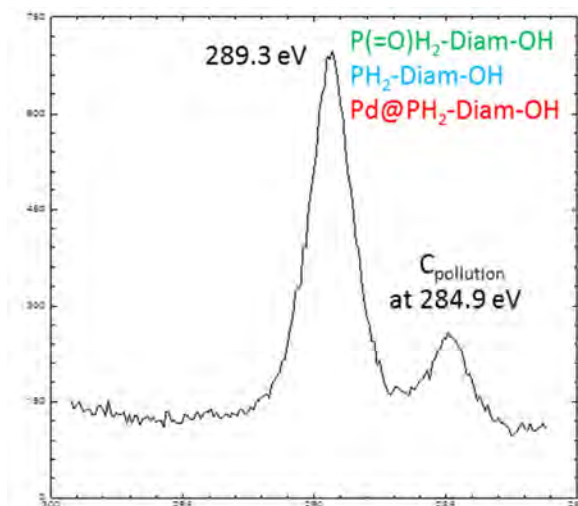


Figure 5.32. XPS spectrum C 1s for Pd deposition on **190** self-assembly sample 2 (center).

The presence of metallic Pd was observed with two signals at 341.0 eV and 335.5 eV (**Figure 5.33**, peaks on the right), that are attributed respectively to Pd 3d_{3/2} and Pd 3d_{5/2} for elemental Pd(0) in XPS table,¹¹ similarly to metallic Pd nodules on SiO₂ at the edge of the substrate (**Figure 5.29**). Consistently with observation on “Survey” mode (**Figure 5.30**), we observed two other intense Pd 3d_{3/2} and 3d_{5/2} signals at much higher energy at 347.7 eV and 342.3 eV, respectively.

To assign these signals, we further examined literature reports and XPS Handbook. The BE of Pd 3d_{5/2} at lower energy is the signal usually used to characterize the nature of palladium deposits or surfaces. The peaks observed at high energy (Pd 3d_{5/2} = 342.3 eV) were clearly not assignable to any kind of Pd oxide assigned in the literature (Pd(II) 3d_{5/2} = 336.1 eV) and also not [Pd(allyl)Cp] (Pd²⁺ 3d_{5/2} 337.6 eV and Pd²⁺ 3d_{3/2} 342.9 eV).^{5,12} This peak did not even get close to P–Pd(0) in phosphine Pd(PPh₃)₄ that was assigned Pd 3d_{5/2} = 336.2 eV,¹³ nor Pd–P with phosphorus may bond through Si–P bonding on SiO₂ support 335.8 eV.¹

¹² A. Niklewski, T. Strunskus, G. Witte, C. Wöll. *Chem. Mater.*, **2005**, *17*, 861-868. Metal-organic chemical vapor deposition of palladium: spectroscopic study of cyclopentadienyl-allyl-palladium deposition on palladium substrate.

¹³ V. I. Nefedov, YA. V. Salyn, I. Moiseev, A. P. Sadovskii, A. S. Berenbljum, A. G. Knizhnik, S. L. Mund. *Inorg. Chim. Acta*, **1979**, *35*, L343-L344. ESCA and X-Ray spectral study of Pd(0), Pd(I) and Pd(II) compounds with triphenylphosphine ligands.

This result must be analyzed differently. High shift towards higher binding energy can also be observed when the charge effect is present.^{14,15,16} Such a phenomenon occurs in the case of insulator material (or metal is on the top of an insulator, it acts like an insulator because charges cannot reach the ground due to interfacial insulator) where the positive charges created by the photoemission process cannot be evacuated to the ground.¹⁴⁻¹⁶ The resulting positive electric field then reduced the kinetic energy of emitted electrons, and thus their apparent binding energy. In other words, the Pd 3d_{5/2} peak at 342.3 eV is a signature for a novel insulator material formed during the deposition. This signature is a convincing spectroscopic evidence of the formation of an unprecedented hybrid edifice **Pd@PH₂-Diam-OH** with strong P–Pd interaction deeply altering its surface properties.

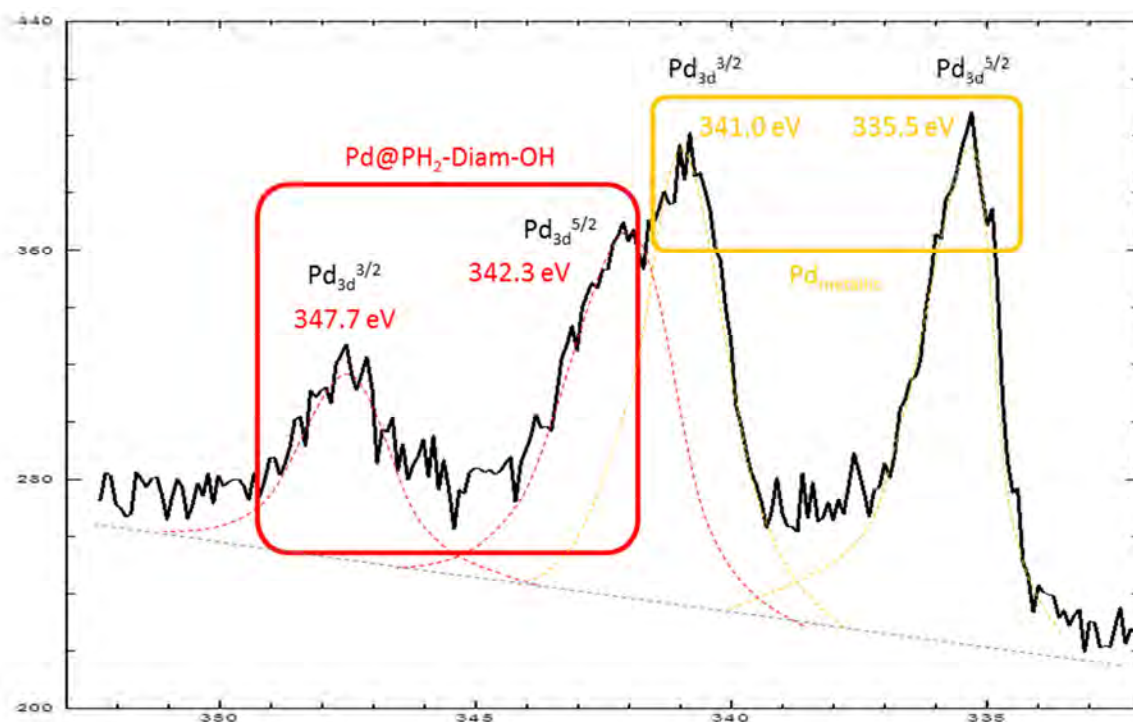


Figure 5.33. XPS spectrum Pd 3d for Pd deposition on **190** self-assembly: Sample 2 (center).

Consistently, we found for P 2p a low intensity peak shifted at 136.0 eV on **Figure 5.34** and thus experiencing also the charge effect mentioned previously. The previously observed value for P 2p at

¹⁴ A. Cros. *J. Electron Spectrosc. Relat. Phenom.*, **1992**, 59, 1-14. Charging effects in X-ray photoelectron spectroscopy.

¹⁵ M. Dubey, I. Gouzman, S. L. Bernasek, J. Schwartz. *Langmuir*, **2006**, 22, 4649-4653. Characterization of self-assembled organic films using differential charging in X-ray photoelectron spectroscopy.

¹⁶ T. Ichinose, H. Monjushiro, H. Watarai. *Analytical Sciences*, **1996**, 12, 43-47. Charge-up phenomena of insulated metals in X-ray photoelectron spectroscopy.

135.2 eV originating from PH₂-Diam-OH (**Figure 5.21**) completely disappeared and a signal at 136.0 eV, slightly shifted to higher energy is consequently attributed to the hybrid emission of **Pd@PH₂-Diam-OH**.

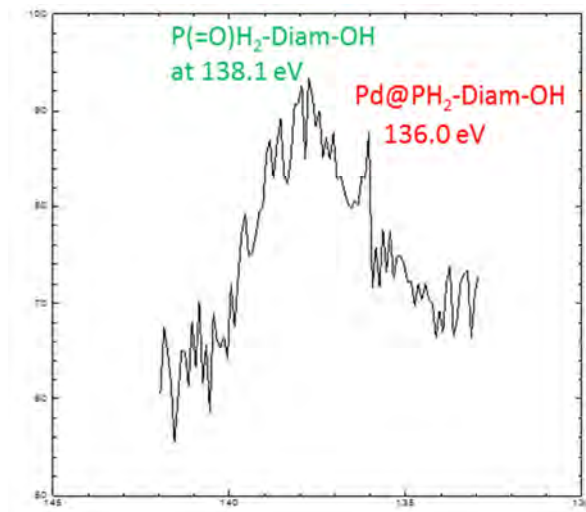
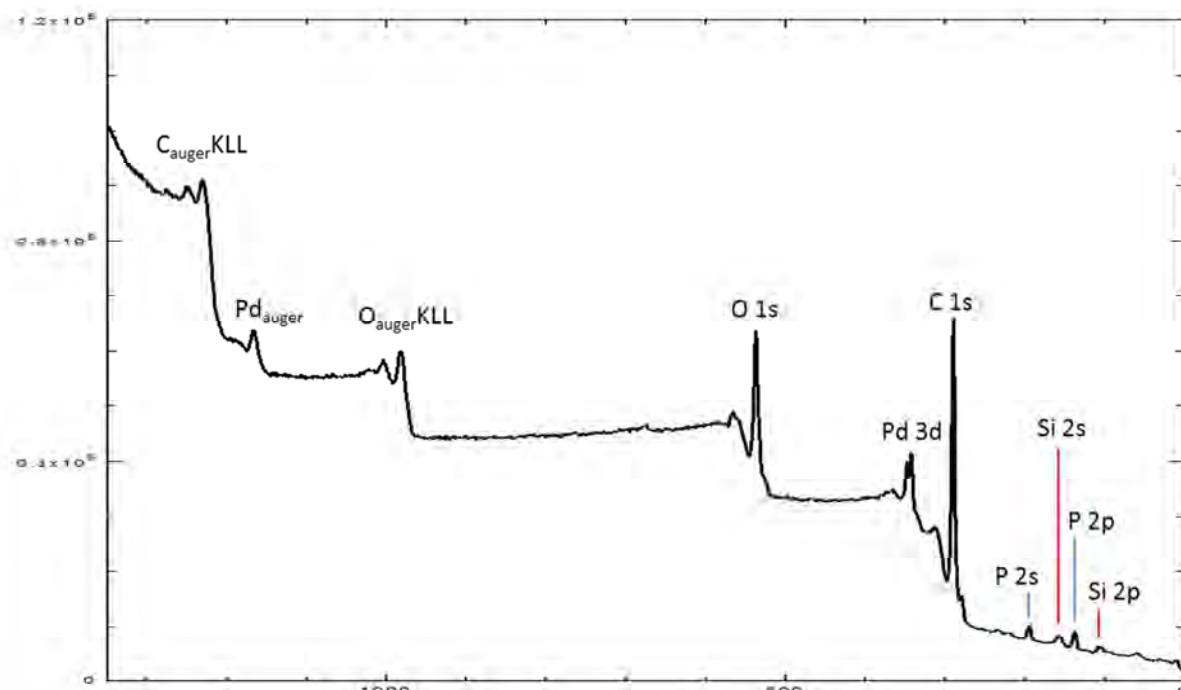


Figure 5.34. XPS spectrum P 2p for Pd deposition on **190** self-assembly: Sample 2 (center).

Sample 3 (center) – Pd CVD short run of 1 h over the self-assembly of 190

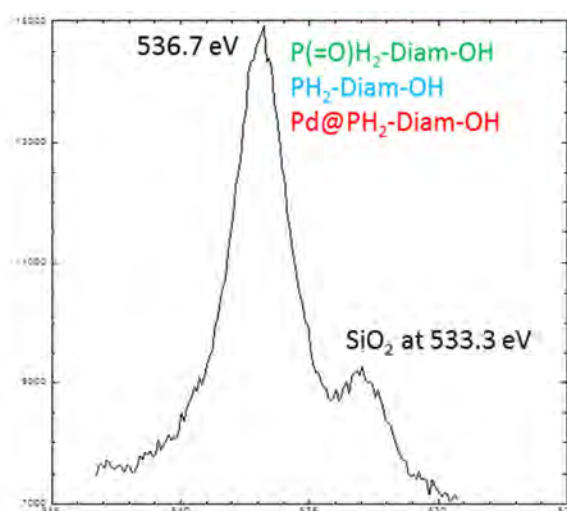
With the view to analyze the very beginning of Pd deposition process by OMCVD on diamondoid **190** self-assembly (SEM image **Figure 5.8**), we also deposited Sample 3, that mainly contained organohybrid **Pd@PH₂-Diam-OH** and only very few Pd metallic nodules. Consistently, the XPS survey measurement **Figure 5.35** provided almost similar spectrum to longer run 7.5 h (**Figure 5.30**) but how we expected specifically lacking the Pd 3d_{5/2} at 335.5 eV attributed to the dispersion of metallic Pd(0) nodule.



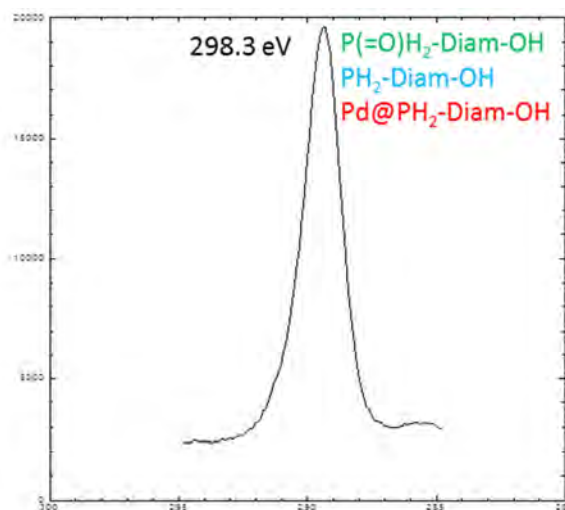
$BE_{CKLL} = 1230.0$ eV, $BE_{Pd\ augeter} = 1166.9$ eV, $BE_{OKLL} = 982.6$ eV, $BE_{O1s} = 536.8$ eV, $BE_{Pd3d} = 347.4$ eV, $BE_{Pd3d} = 342.4$ eV, $BE_{C1s} = 289.3$ eV, $BE_{P2s} = 194.1$ eV, $BE_{Si2s} = 158.1$ eV, $BE_{P2p} = 137.0$ eV, $BE_{Si2p} = 103.0$ eV.

Figure 5.35. XPS survey of Pd deposition on **190** self-assembly: Sample 3 (center).

All the high resolution spectra of O 1s and C 1s confirmed the presence of hydroxydiamondoid phosphine (**Figure 5.36(a)-(b)**).



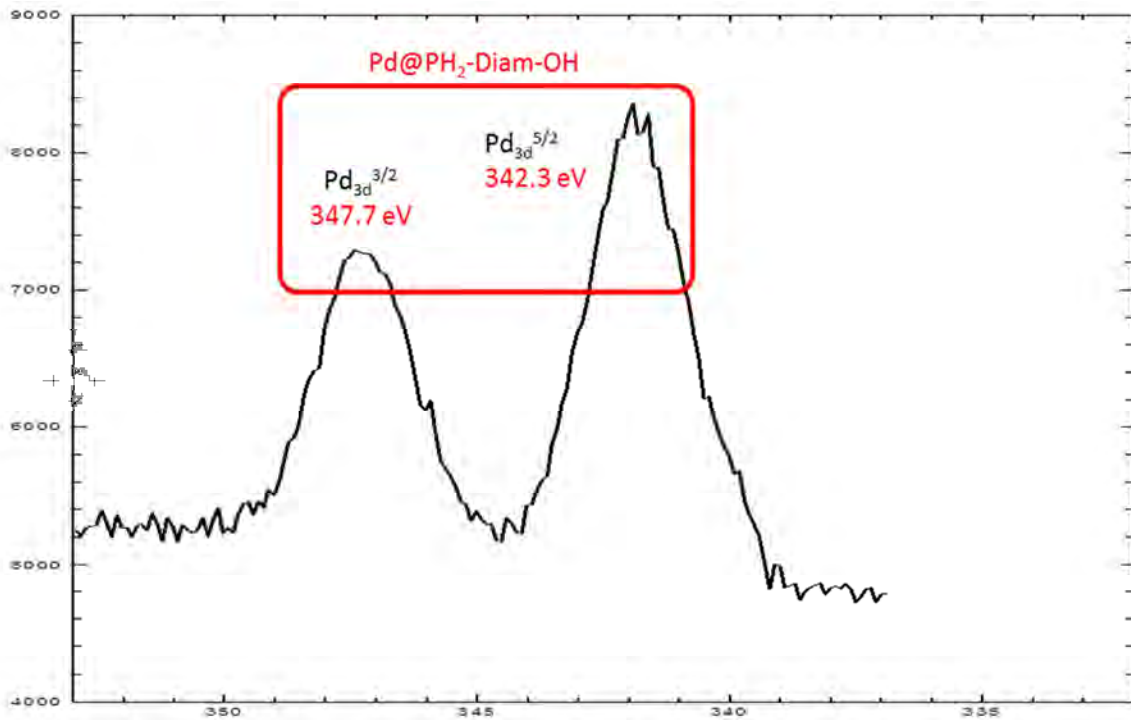
(a) XPS spectrum O 1s for Pd deposition on **190** self-assembly: Sample 3 (center).



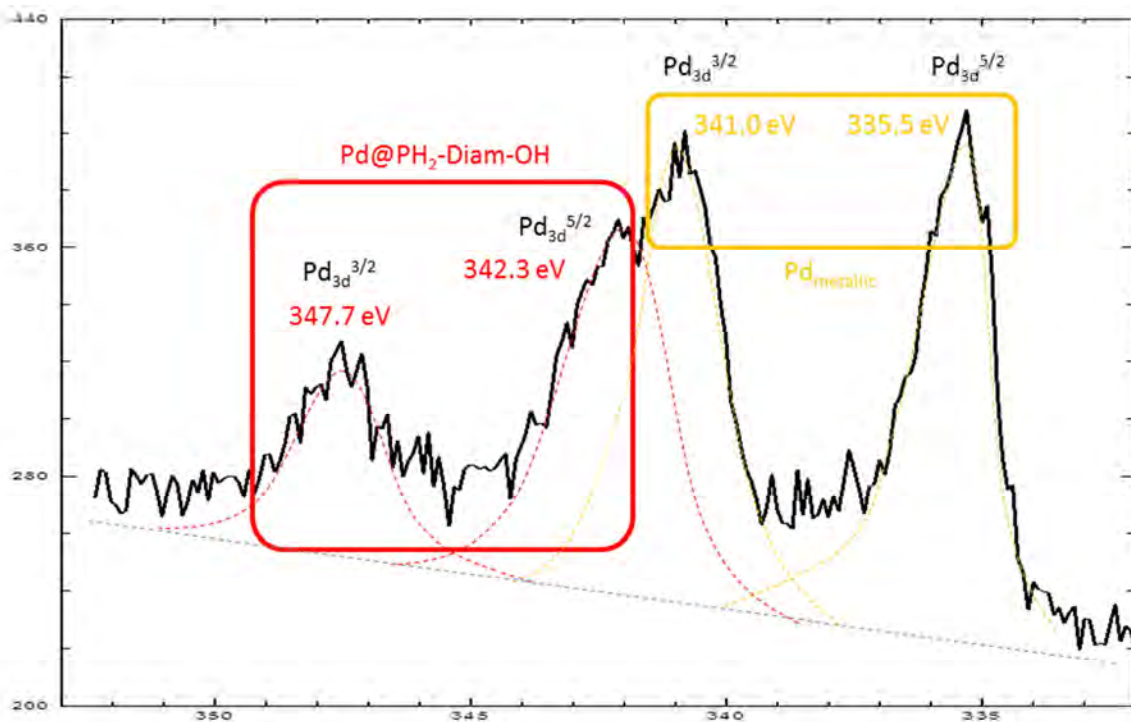
(b) XPS spectrum C 1s for Pd deposition on **190** self-assembly: Sample 3 (center).

Figure 5.36. XPS spectra O 1s and C 1s for Pd deposition on **190** self-assembly: Sample 3 (center).

Interestingly, here only the two Pd $3d_{3/2}$ and Pd $3d_{5/2}$ peaks at BE 347.7 eV and 342.3 eV were observed (no metallic palladium at 341.0 eV and 335.5 eV) (**Figure 5.37(a)**). The high BE signals observed previously were confirmed, indicating that **Pd@PH₂-Diam-OH** layer emission corresponds to insulator properties. The quasi absence of Pd(0) metallic nodules seems to indicate that the formation of the hybrid occurs at the very first stage of the deposition, and then could be in competition with nucleation and growth of the nodules (or rearrangement of the surface deposition in nodules).



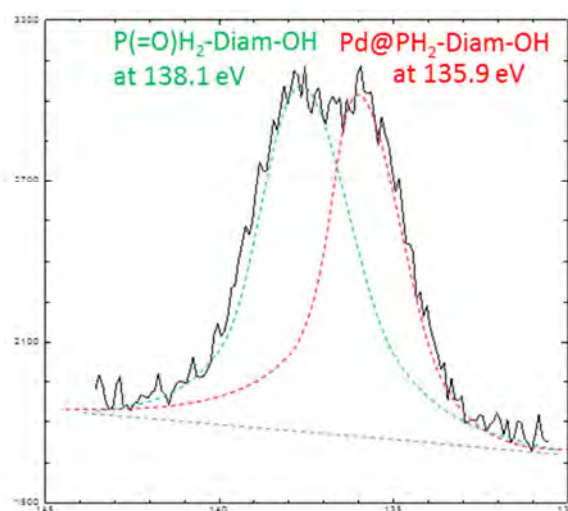
(a) XPS spectrum Pd 3d for Pd deposition on **190** self-assembly: Sample 3 (center).



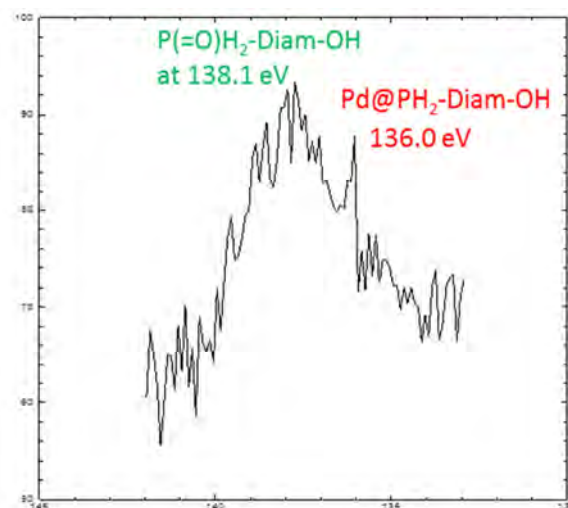
(b) XPS spectrum Pd 3d for Pd deposition on **190** self-assembly: Sample 2 (center) (or **Figure 5.33**).

Figure 5.37. XPS spectra Pd 3d for Pd deposition on **190** self-assembly: Sample 3 vs Sample 2.

From **Figure 5.38(a)**, the interaction P–Pd in the hybrid **Pd@PH₂-Diam-OH** was confirmed by the clear presence of P 2p peak at 135.9 eV that is similar to observation in Sample 2 (**Figure 5.38(b)**) but far more intense. This is probably due to the thinner layer of Pd deposited on the diamondoid. The fact that the signal at 138.1 eV from P=O was not shifted means that no reaction occurred between the phosphine oxide **196** and palladium. This observation also confirmed our hypothesis that the construction of hybrid edifice is not obtained with **196**, certainly due to the lack of a lone-pair for coordinating palladium. This was also shown in the case of Pd deposition on hydroxydiamantylphosphonic dichloride **182**.



(a) XPS spectrum P 2p for Pd deposition on **190** self-assembly: Sample 3 (center).



(b) XPS spectrum P 2p for Pd deposition on **190** self-assembly: Sample 2 (center) (or **Figure 5.34**).

Figure 5.38. XPS spectra P 2p for Pd deposition on **190** self-assembly: Sample 2 vs 3 (center).

All the spectra that have been discussed previously are collected in **Figure 5.39** for the purpose of comparison. XPS data clearly indicated typical binding energy signals related to the formation of a novel edifice for which Pd $3d_{5/2}$, Pd $3d_{3/2}$ and P 2p are different from the mixture of metallic Pd(0) deposit and pure diamondoid phosphine. The organohybrid efficiently forms in the very first time of CVD (1 h Pd deposition) and preclude nodular Pd metallic formation. The **Pd@PH₂-Diam-OH** hybrid was further characterized by TEM.

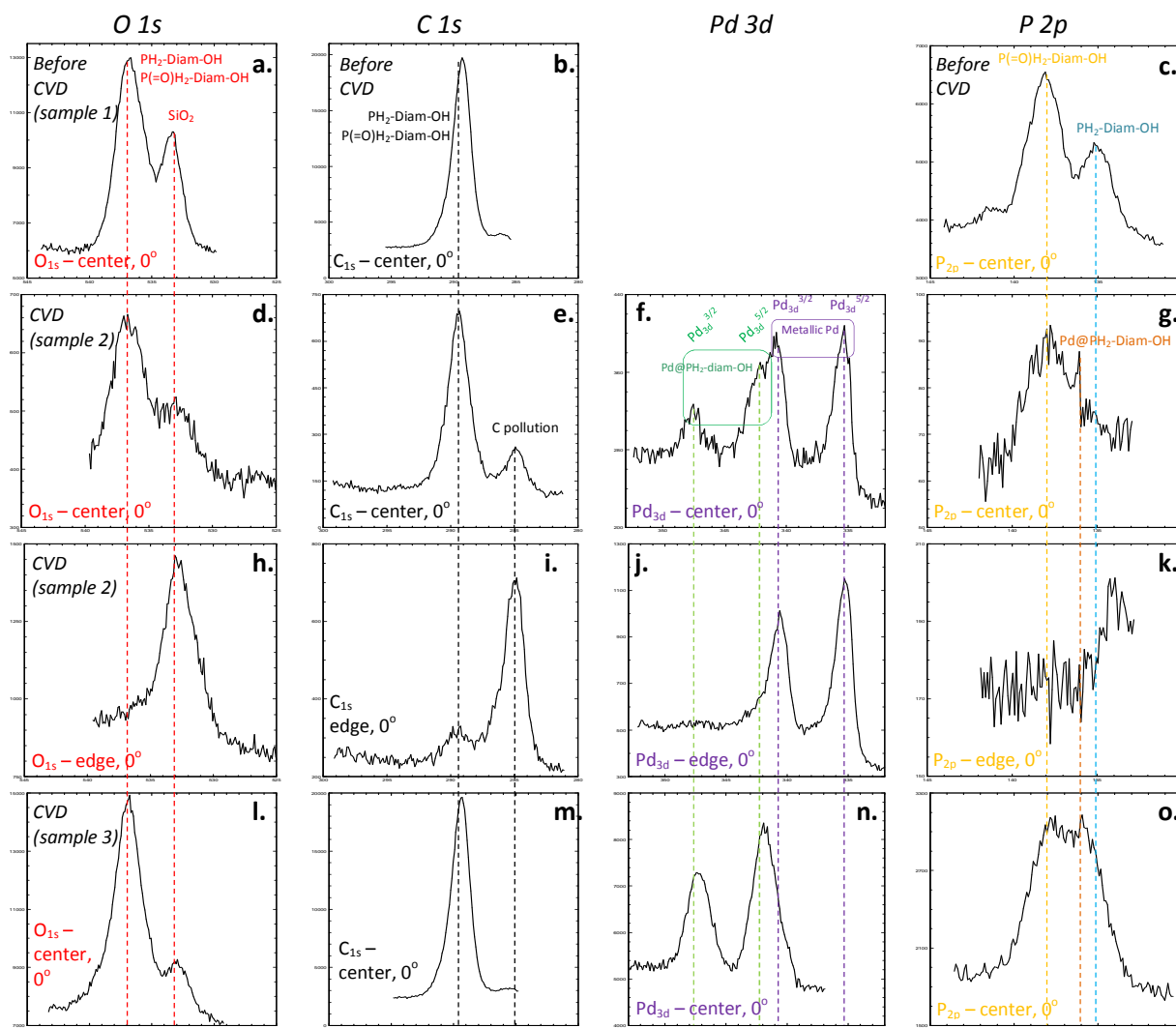


Figure 5.39. XPS for O 1s, C 1s, Pd 3d and P 2p: *first row* is Sample 1 for self-assembly hydroxyphosphine **190**; *second row* is after CVD (Sample 2) at the center of deposit; *third row* is Sample 2 at the edge of the deposit; *fourth row* is Sample 3 at the center of deposit.

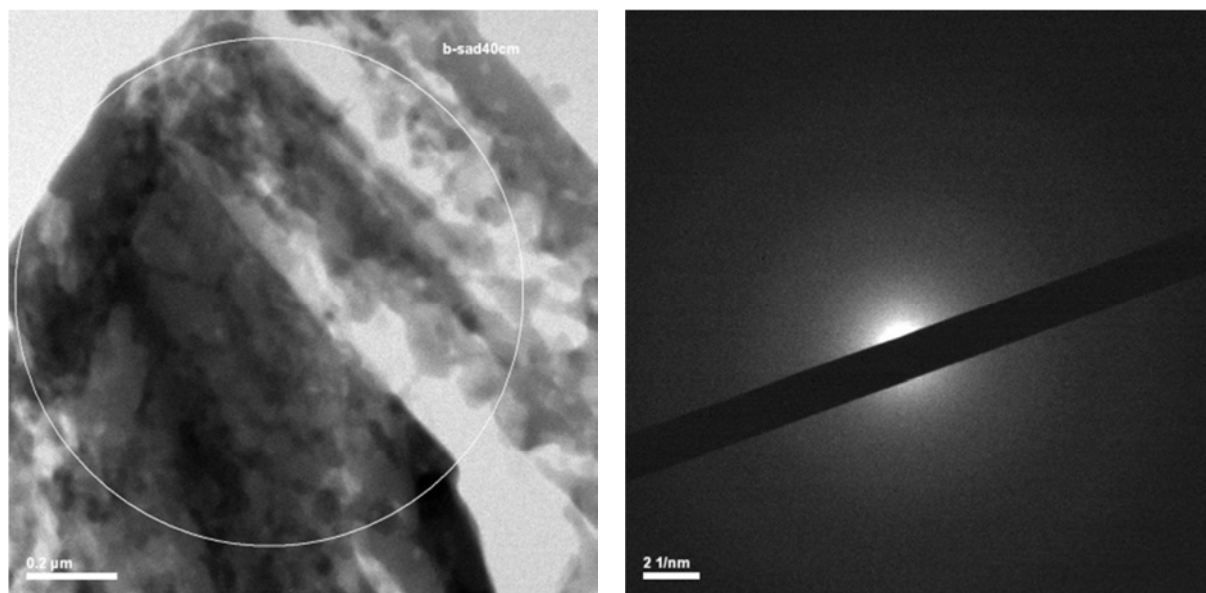
6. TEM analysis of the organohybrid Pd@PH₂-Diam-OH

To go deeply into the understanding of the hybrid construction, further characterization was performed by Transmission Electron Microscopy (TEM). A TEM copper grid covered with an amorphous carbon membrane was used as a substrate. The exact conditions used for previous diamondoid self-assembly by vapor deposition, followed by Pd OMCVD, were achieved on the TEM grid. The conditions for the vapor deposition of **190** were 2 min, 85 °C, and the Pd OMCVD time was fixed to 1.5 h; with the aim to analyze the beginning of growth of the hybrid **Pd@PH₂-Diam-OH**. Several images were taken using different modes: TEM, Scanning Transmission Electron Microscopy (STEM), Energy-Dispersive X-Ray Spectroscopy (EDX), and Selected Area Electron Diffraction (SAED). TEM is a microscopy technique in which a beam of electrons is transmitted through an ultra-thin specimen, interacting with the specimen as it passes through. An image is formed from the interaction of the electrons transmitted through the specimen; the image is magnified and focused onto an imaging device, such as a fluorescent screen, on a layer of photographic film, or to be detected by a sensor such as a CCD camera. STEM is a type of TEM with focusing the electron beam into a narrow spot which is scanned over the sample in a raster. EDX is an analytical technique used for the elemental analysis or chemical characterization of a sample. It relies on an interaction of some source of X-ray excitation and a sample. A high-energy beam of charged particles such as electrons or protons, or a beam of X-rays, is focused into the sample then the number and energy of the X-rays emitted from a specimen is measured. SAED is a crystallographic experimental technique that can be performed inside a transmission electron microscope (TEM).

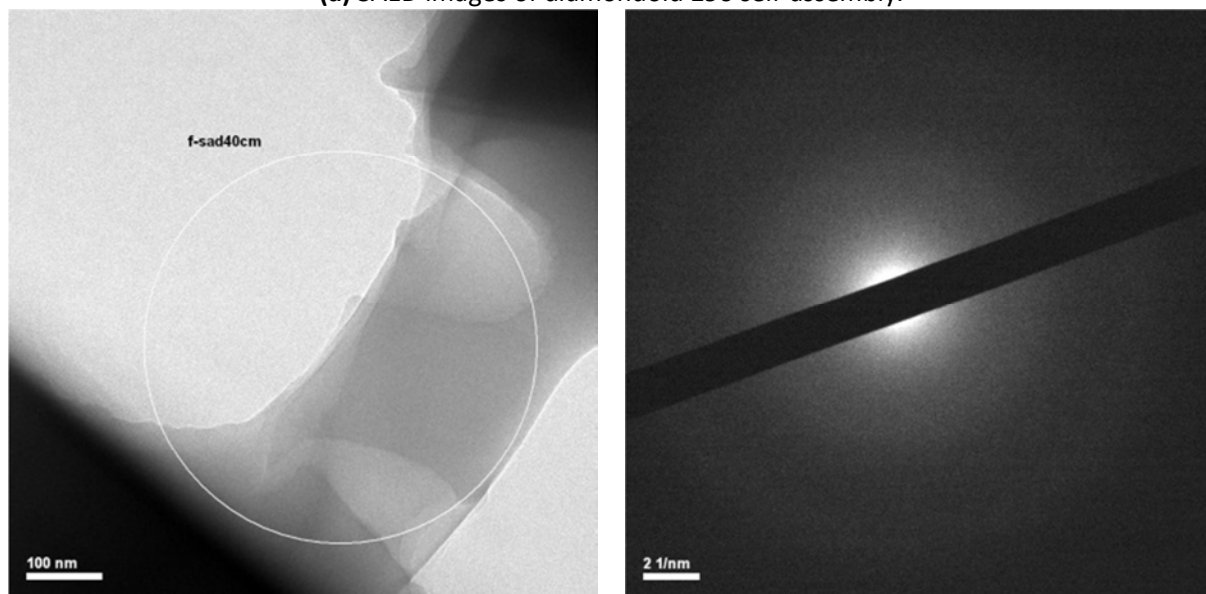
Figure 5.40 illustrates the SAED measurement. No diffraction circle or spot was visible, indicating that both hydroxyphosphine and hybrid material were not diffracting and as such were non-crystalline edifices. This SAED measurement without any diffraction signature illustrates also that the contrast in the TEM and STEM images are mainly due to differences of thickness in the sample observed.

Figure 5.41(a) shows the diamondoid on the grid. Images show the rectangular self-assembly deposit, with multiple grey colors due to the porosity on the deposit. The obtained images showed also that the deposit resisted under TEM conditions (10^{-6} mbar and 200 keV energy electron beam) which are much harsher conditions than SEM. The size of the self-assembly pillars on amorphous carbon membrane was found slightly smaller than deposits on Si substrate, sizing around 0.850 μm versus 1.4 μm for Si wafer. This is probably due to the difference of substrate. Difference in temperature during the vapor deposition process (due to heat capacity of the support) may also influence the self-assembly size with higher nucleation rate of smaller edifices at higher temperature. **Figure 5.41(b)** shows the same deposit after 48 h in the electronic microscope under reduced pressure 10^{-6} mbar. Only a minor part of the

deposit sublimated, the self-assembly being still present on the substrate without major changes of size and structure. This observation further evidenced the excellent robustness of the self-assembly.



(a) SAED images of diamondoid **190** self-assembly.



(b) SAED images of Pd@PH₂-Diam-OH.

Figure 5.40. SAED images of **190** self-assembly and Pd@PH₂-Diam-OH.

Pd deposition was achieved by OMCVD (1.5 h at 35 °C), and images reported in **Figure 5.41(c)** showed the surface modification of the original hydroxydiamondoid phosphine self-assembly into darker columnar deposit. The porosity entirely disappeared and the rectangular deposits looked smooth.

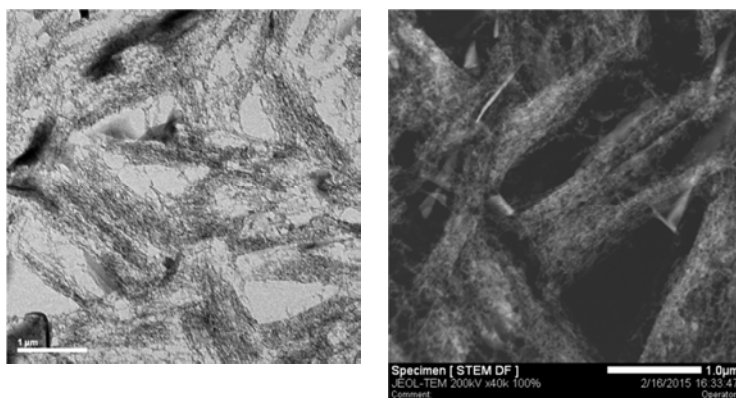


Optical image x500

TEM-bright field x5000

STEM-dark field x20000

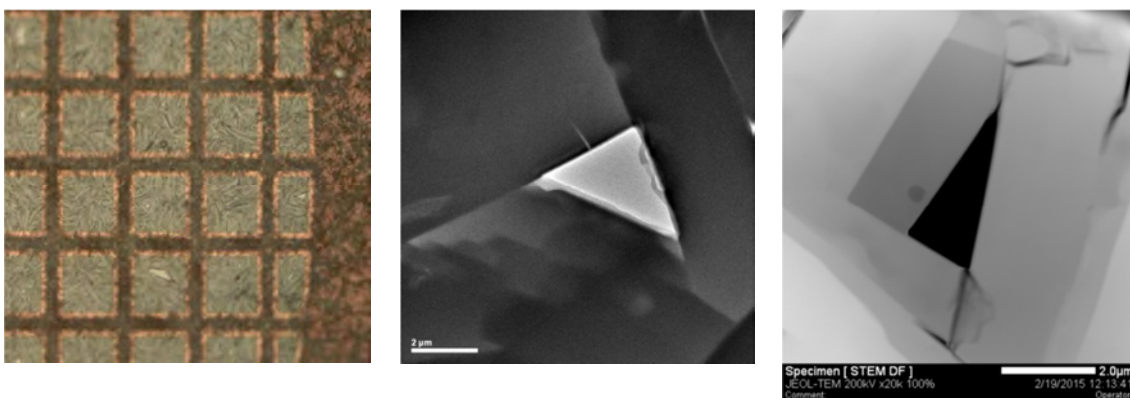
(a) images of diamondoid **190** self-assembly



TEM-bright field x4000

STEM-dark field x40000

(b) images of diamondoid **190** self-assembly after 48 h inside the TEM



Optical image x200

TEM-bright field x2000

STEM-dark field x20000

(c) images of Pd@PH₂-Diam-OH.

Figure 5.41. Optical images (*left*), TEM-bright field (*middle*), and STEM-dark field (*right*) of **190** deposited on amorphous carbon film: (a) diamondoid **190** self-assembly (85 °C, 2 min); (b) diamondoid **190** self-assembly after 48 h inside TEM apparatus; (c) Pd@PH₂-Diam-OH (Pd CVD at 35 °C, 1.5 h).

The contrast in bright field being very dark clearly indicated the formation of a layer with heavier atom. This confirmed the observations of SEM images (**Figure 5.13**), and the thin smooth layer covered the columnar deposits.

The EDX measurement (**Figure 5.42**) shows the different elements analyzed in the deposit. Copper peak came from the grid, and chromium traces from the objective lens. Satisfactorily, for self-assembly of hydroxydiamondoid phosphine **190** (**Figure 5.42**), the oxygen and phosphorous content were found similar and consistent with the EDX-SEM measurements (**Figure 5.7**).

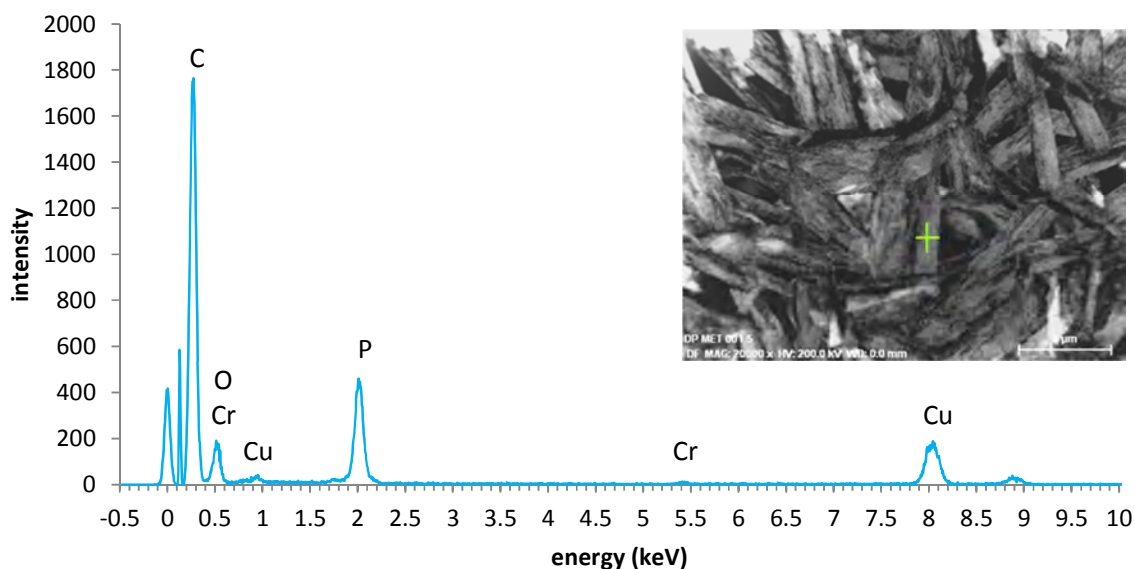


Figure 5.42. EDX-TEM analysis **190** self-assembly with ratio (O : P) = (48.34 : 51.66) in atomic %.

Unfortunately, for the hybrid **Pd@PH₂-Diam-OH** (**Figure 5.43(a)**), EDX spectra did not detect the presence of palladium; this was also the case for SEM-EDX and is attributed to the very thin layer of Pd we anticipated (Pd was detected clearly by XPS). On a spherical particle visible on the image **Figure 5.43(b)**, which is similar to the nodule particles visible in SEM images (**Figure 5.14**), the presence of Pd is detected in high concentration (or content).

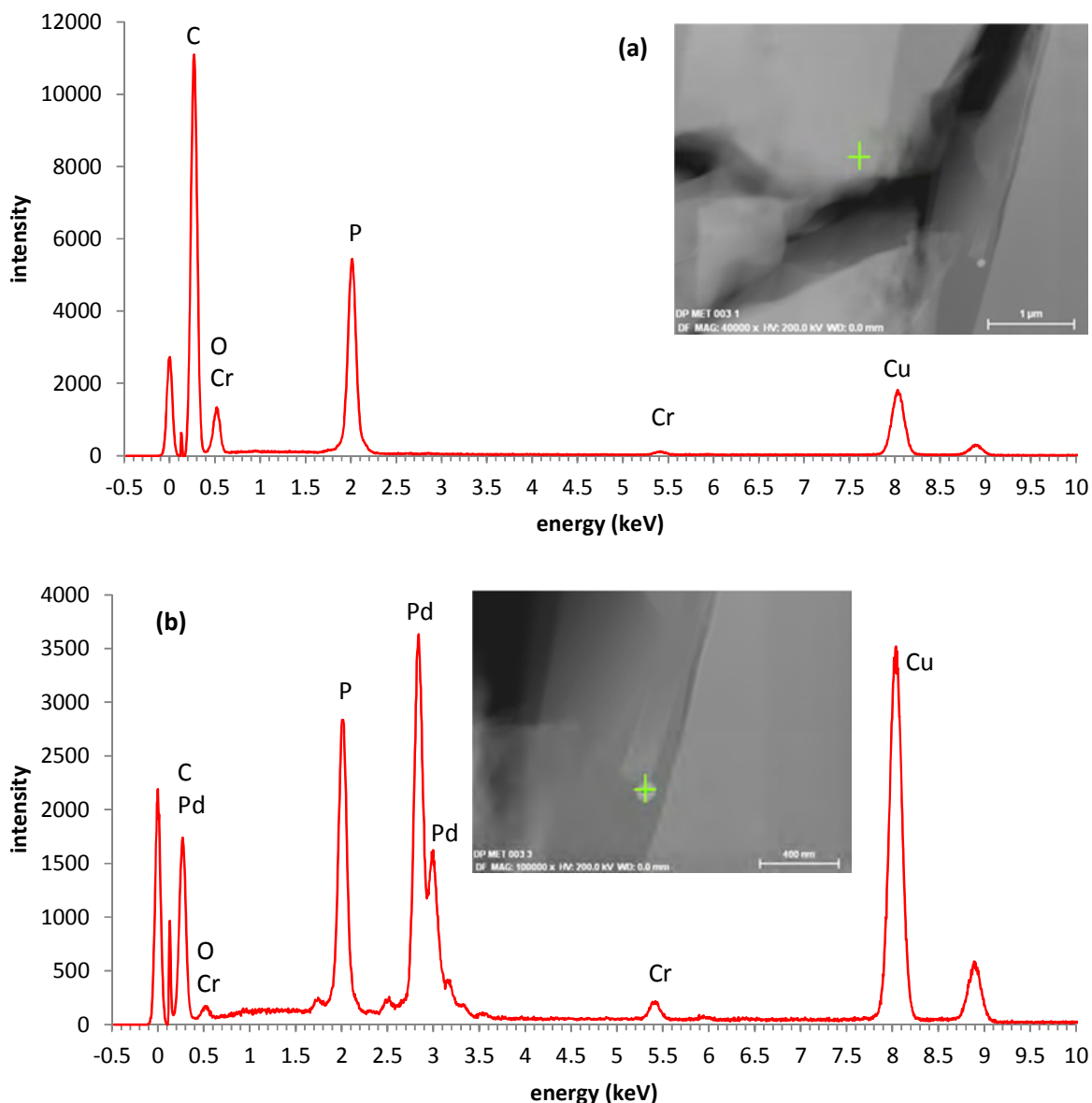


Figure 5.43. EDX-TEM analysis Pd@PH₂-Diam-OH in various areas of the sample.

A cartography of the different element distribution was then done for the **190** self-assembly and hybrid Pd@PH₂-Diam-OH (**Figures 5.44** and **5.45**), by scanning the same area that was previously observed by TEM. The corresponding EDX spectrum was recorded for each spot. Chemical composition is determined by comparing the intensities of characteristic X-rays from the sample material with intensities from known composition (standards). Counts from the sample must be corrected for matrix effects (depth of production of the X-rays, absorption and secondary fluorescence) to yield quantitative chemical compositions. The resulting chemical information is gathered in textural context. The

cartography of C (red), O (green), and P (blue) element confirmed that these elements are located at the exact same place; thus they exclusively come from the diamondoid **190**. The palladium (turquoise-blue) map proved the presence of this element. It shows that Pd was dispersed in all hybrid deposit, certainly in too low and very dispersed content to be clearly detected with an EDX spot analysis. This was coherent with EDX–SEM analysis (**Figure 5.15**, 7.5 h) which measured percentages of Pd around 0.27 % after 7.5 h of OMCVD deposit, compared here with 1.5 h for our TEM measurements. The layer **Pd@PH₂-Diam-OH** is certainly thinner than on the sample we reported in **Figure 5.14**. The layer seems to begin growing everywhere, but the map showed clearly that it concentrates on the edge of the parallelepiped edifices. These areas are shown with circles (white colored) on **Figure 5.45**.

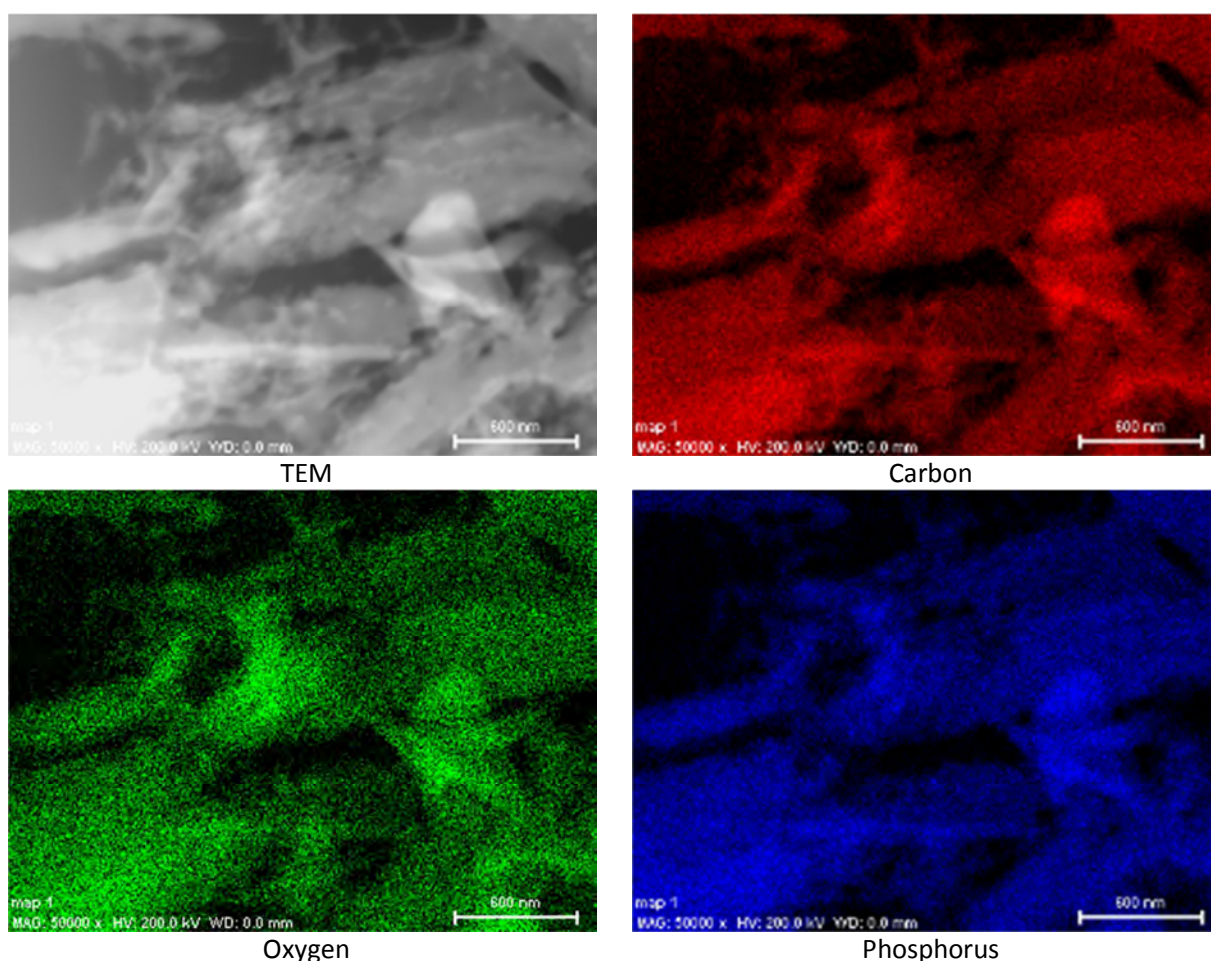


Figure 5.44. Cartography of element distribution (C, O, P) of self-assembly **190**.

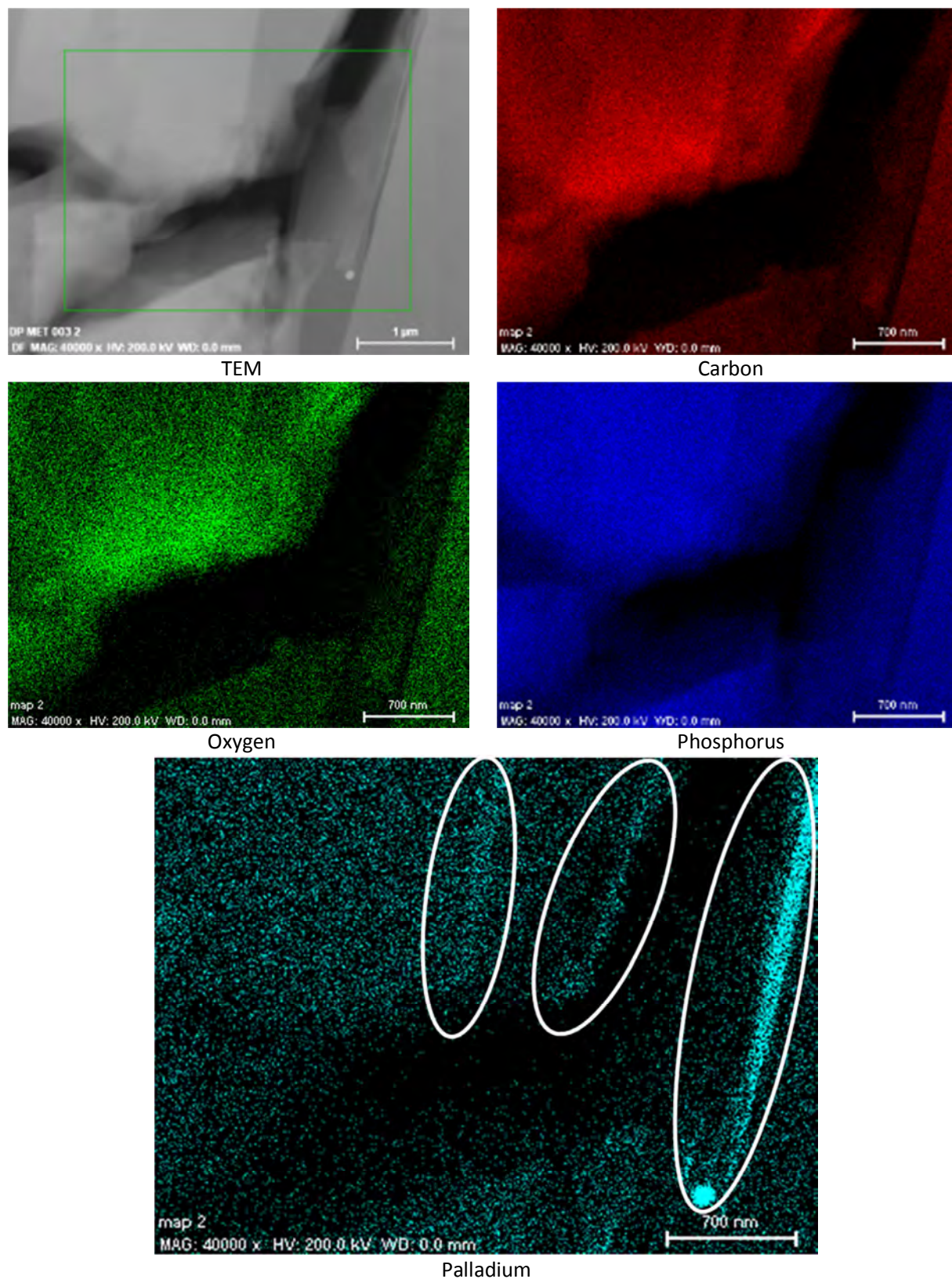


Figure 5.45. Cartography of element distribution (C, O, P, Pd) of hybrid Pd@PH₂-Diam-OH.

These TEM analyses mainly confirmed XPS characterization and further demonstrate the formation of the hybrid **Pd@PH₂-Diam-OH**, for which the layer surface has been recognized. A competition with the formation of Pd metallic nodules growth is also detected. But in the very beginning of CVD this phenomenon is clearly minored in comparison with the hybrid formation. This is confirmed by the Pd cartography we achieved. The first follow-up experiments will concern the TEM observation of **Pd@PH₂-Diam-OH** formation over longer time of CVD deposition (due to the limited access to TEM, this has not been carried out yet).

5.3. Conclusion

Our first attempt to build hybrid Pd-diamondoid on **Chapter 3** using hydroxydiamantane showed that palladium growth by CVD had no specific selectivity towards diamondoids. Changing the hydroxy group with P(V) phosphonic dichloride **182** could not increase the affinity and did not conduct the preferential growth of palladium over the diamondoid. However, by switching the strategy and using P(III) phosphine as anchoring sites, hybrid material **Pd@PH₂-Diam-OH** was achieved. By varying the duration of palladium deposition by CVD, we could control the growth of the palladium. At a shorter time (1 h run), SEM analysis showed the metallic Pd nodules grew preferentially on Si support. XPS and TEM confirmed that the hybrid was present since the first one hour. After 3 h run, the SEM analysis showed that a new smooth layer appeared, covering the columnar self-assembly **190**, and nodules formed with a size of 100-400 nm that are dispersed all over the sample. And after more than 5 h run, the smooth layer was clearly visible by SEM, covering the columnar self-assembly and the size of nodules increased with most of them about 700 nm. XPS measurement showed that an insulator material **Pd@PH₂-Diam-OH** formed during the CVD deposition with P-Pd interaction, deeply altering its surface properties. These characterizations revealed that the formation of the hybrid occurs at the very first stage of the deposition, and then could be in competition with nucleation and growth of the nodules (or rearrangement of the surface deposition in nodules).

Chapter 6: Experimental part

6.1. Clausius-Clayperon calculation for vapor pressure of diamondoids

1. General conditions

Pristine adamantane **1** and diamantane **10** were prepared in the Giessen group and were purified by sublimation before use. 1-Aminoadamantane **64** and 1-hydroxyadamantane **6** were obtained from Alfa Aesar and Aldrich. 1-Hydroxydiamantane **30**, 4-hydroxydiamantane **48**, and 4,9-dihydroxydiamantane **49** were synthesized from diamantane;¹ 4-fluorodiamantane and 4,9-difluorodiamantane were prepared from its hydroxyl derivatives.² The melting points reported for diamondoids were measured by DSC TA instrument 2920 modulated with a temperature calibrated by an Indium reference and at heat of 10 °C/min under nitrogen flow.

2. Vapor pressure measurements of diamondoids and thermodynamic data

In order to accurately measure the vapor pressure of finely divided diamondoid powders a system inspired by the method used for measuring the vapor pressure of liquids at liquid-vapor equilibrium state was developed (**Figures 6.1 and 6.2**).



Figure 6.1. General method for the measurements of liquid vapor pressure.

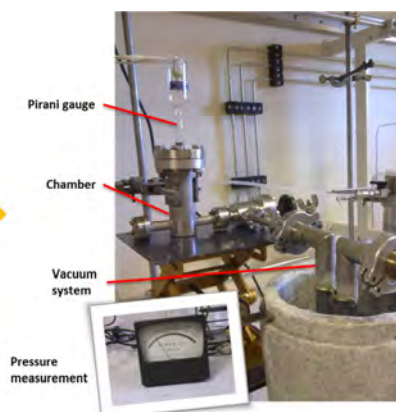


Figure 6.2. Experimental setup for measurement of functionalized diamondoids vapor pressures.

¹ N. A. Fokina, B. A. Tkachenko, A. Merz, M. Serafin, J. E. P. Dahl, R. M. K. Carlson, A. A. Fokin, P. R. Schreiner. *Eur. J. Org. Chem.*, **2007**, 4738-4745. Hydroxy Derivatives of Diamantane, Triamantane, and [121]Tetramantane: Selective Preparation of Bis-Apical Derivatives

² H. Schwertfeger, C. Würtele, H. Hausmann, J. E. P. Dahl, R. M. K. Carlson, A. A. Fokin, P. R. Schreiner. *Adv. Synth. Catal.*, **2009**, 351, 1041-1054. Selective Preparation of Diamondoid Fluorides.

A closed sublimation chamber connected with a calibrated Pirani gauge was used, which allows measuring the vapor pressure for diamondoid reaching its solid-vapor equilibrium state at a given temperature. The whole system is made of temperature-resistant glass and metal pieces, including the Pirani gauge, the joints, and gauge cable. For degassing and cleaning purpose this sublimation chamber was rinsed with ethanol then heated in an oven at a temperature over 70 °C for >5 h while connected to a vacuum pump protected by a cold trap using liquid nitrogen. The oven was also conditioned at a given temperature for 16 h before use, for insuring a homogeneous and stable temperature. The purity of synthesized diamondoids was verified by GC-MS. Adamantane **1**, diamantane **10** and naphthalene were purified by sublimation. Diamondoids (about 300 mg) were grinded before being placed into a small glass flacon and weighted with a precision balance. The sample was put inside the sublimation chamber which was connected with a calibrated Pirani gauge (precision $\pm 1\mu\text{mHg}$, $\pm 0.13\text{ Pa}$). To dry the diamondoids powder, four cycles of primary vacuum / heating at 70 °C / cooling at room temperature were applied before measurements. Then, the chamber was put under vacuum during 5 minutes, to reach the lowest pressure (*caution* this value varies with the type of diamondoid, for example adamantane 100–118 μmHg , diamantane 11.5–15 μmHg , and naphthalene 90–181 μmHg). A valve positioned between the chamber and vacuum system was closed. After the chamber was disconnected from the vacuum system, it was put inside the oven that has been set up at a specific temperature (for instance 60 °C) and the pressure inside the chamber was measured with a manometer until it reached an equilibrium state (usually every 1 to 5 min, and then every hour, during 8 h). The entire system, the chamber and the measuring gauge were placed inside the oven. The temperature of the oven was controlled with a thermocouple connected to a multimeter. The thermocouple was calibrated by measuring the boiling point of distilled water and the melting point of ice. Comparing these values with its theoretical boiling point and melting point at local pressure (local pressure data was recorded from Dijon's official national Weather Station). The pressure was measured with a manometer in the scale 0–1000 μmHg . This method was repeated for various temperatures ranging from 20 to 75 °C. For room temperature, the system was placed in the oven turned-off.

Accurate calibration of the Pirani gauge was done with an appropriate standard product of known vapor pressure. Naphthalene was used for calibration of the gauge for temperatures between 20 and 55 °C, because of technical limitation an exponential extrapolation was operated for temperatures between 55 and 75 °C with r^2 fitting > 0.999 . Vapor pressures of naphthalene measured at different temperatures with our system are given in **Figure 6.3**.

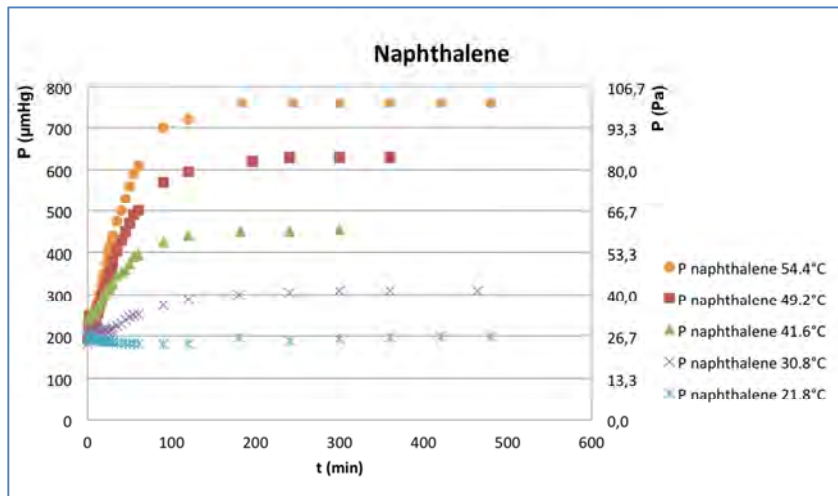


Figure 6.3. Monitoring of naphthalene vapor pressure at various temperatures.

Calibration of the gauge as a function of the temperature was achieved by calculating the invert ratio of the vapor pressure of naphthalene that was measured at equilibrium state (Figure 6.4, after 4 h experiments) over the reported references values (Figure 6.5),³ as reported in Table 6.1.

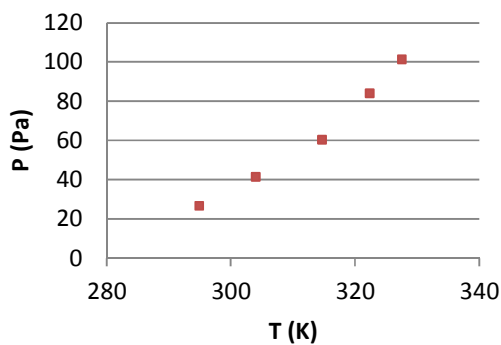


Figure 6.4. Saturated vapor pressure of naphthalene as a function of temperature.

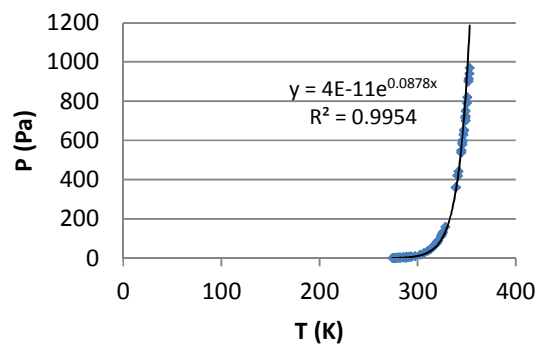


Figure 6.5. Saturated vapor pressure of naphthalene from literature data.

Table 6.1. Calibration of the Pirani gauge from naphthalene measurement and ref. 3.

T_{exp} (°C)	T_{exp} (K)	P_{ref} (Pa)	P_{exp} (Pa)	$P_{\text{ref}} / P_{\text{exp}}$ ratio
54.40	327.55	123.5627	101.3080	1.2197
49.20	322.35	78.2719	83.9790	0.9320
41.55	314.70	39.9856	60.2072	0.6641
30.85	304.00	15.6279	41.3230	0.3782
21.80	294.95	7.0602	26.5267	0.2662

³ C. G. De Kruif, T. Kuipers, J. C. V. Miltenburg, R. C. F. Schaake, G. Stevens. *J. Chem. Thermodynamics*, **1981**, 13, 1081. The vapor pressure of solid and liquid naphthalene.

The calibration curve in **Figure 6.6** was obtained by plotting [$P_{\text{ref}} / P_{\text{exp}}$ ratio] as a function of the temperature [T] (K).

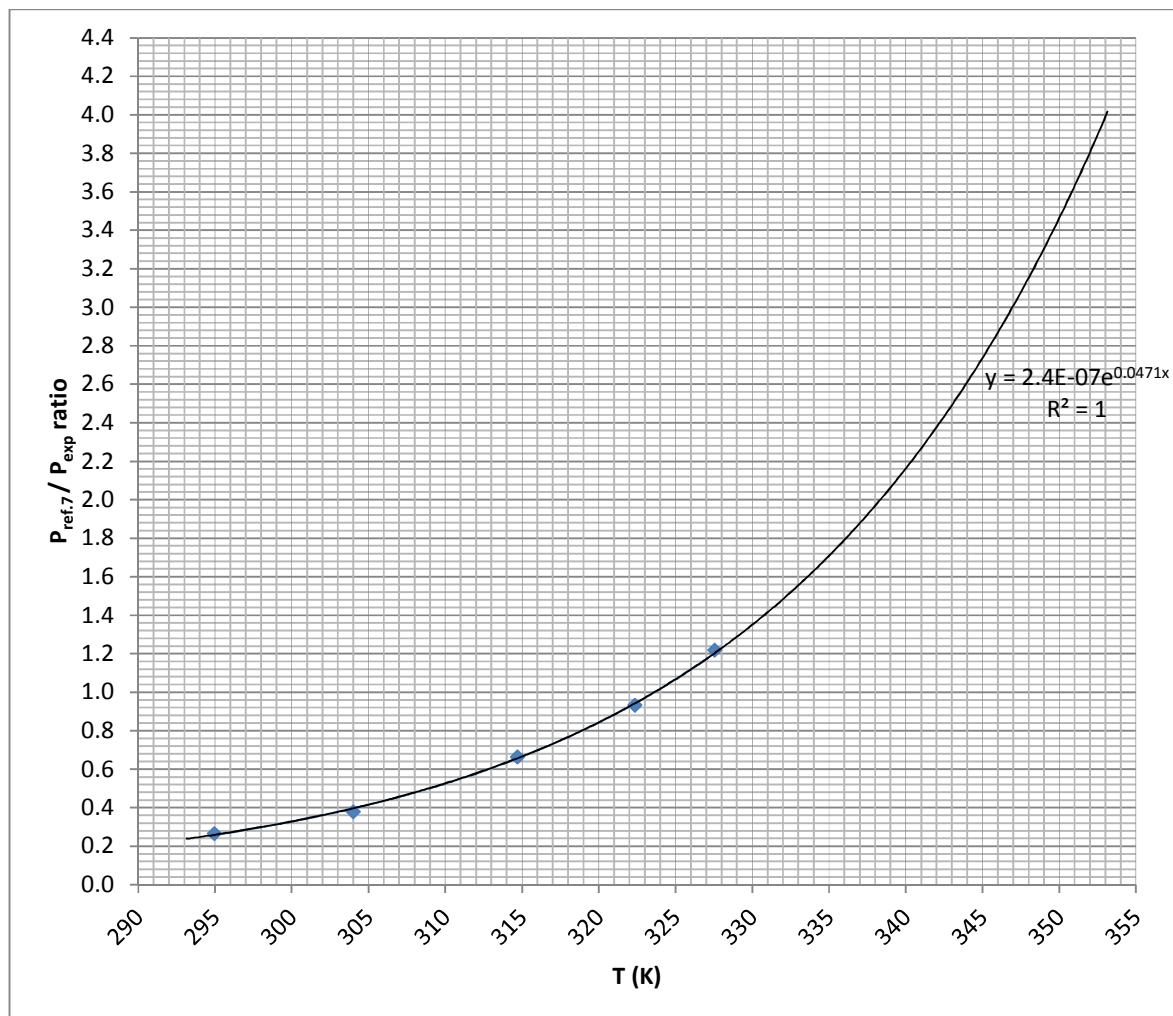


Figure 6.6. Naphtalene vapor pressure calibration curve.

The calibration curve in **Figure 6.6** was used to calculate the vapor pressure of diamondoids from our measurements by correction of the pressure ratio for a given temperature. This is illustrated below for five different diamondoids: adamantane **1**, diamantane **10**, 1-hydroxydiamantane **30**, 4-hydroxydiamantane **48**, and 4-fluorodiamantane **25**.

a) Adamantane

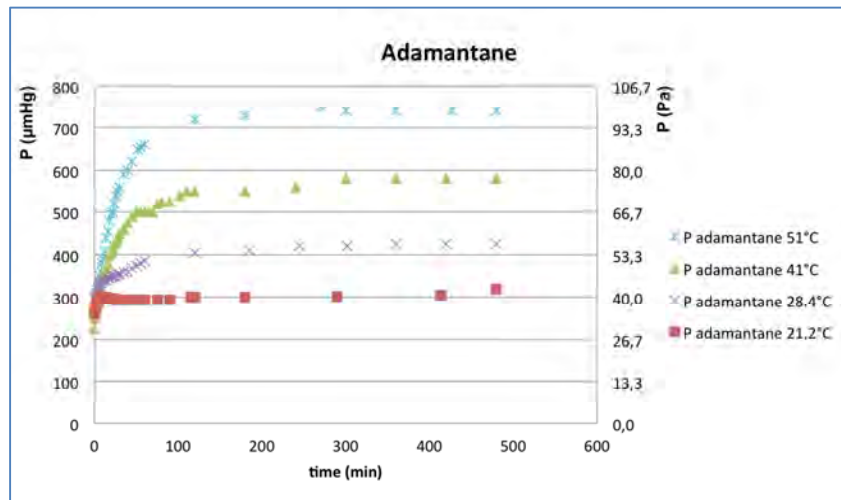


Figure 6.7. Vapor pressure measurement for adamantane.

Table 6.2. Experimental vapor pressure and corrections for adamantane.

T_{exp} (K)	P_{exp} (Pa)	P_{ref}/P ratio	$P_{\text{corrected}}$	$1/T$	$\ln(P_{\text{corrected}})$
294.38	41.1897	0.2523	10.3918	$3.397 \cdot 10^{-3}$	2.3410
301.58	56.4859	0.3540	19.9963	$3.316 \cdot 10^{-3}$	2.9955
314.18	77.3140	0.6408	49.5455	$3.183 \cdot 10^{-3}$	3.9029
324.23	98.6420	1.0288	101.4806	$3.084 \cdot 10^{-3}$	4.6199

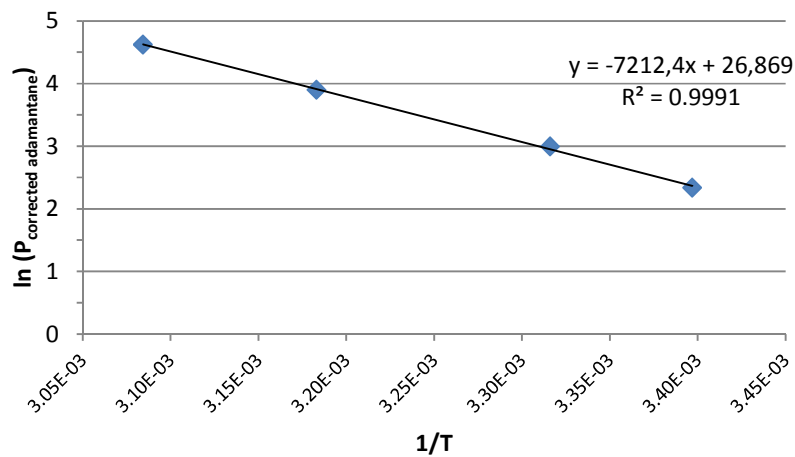


Figure 6.8. Clausius-Clapeyron plot for adamantane.

Clausius-Clapeyron equation allows determining ΔH :

$$\ln P = -\frac{\Delta H^{sv}}{R} \frac{1}{T} + \left(\frac{\Delta S^{sv}}{R}\right)$$

The enthalpy of sublimation of adamantane is $\Delta H = 60.0 \pm 5$ kJ/mol.

b) Diamantane

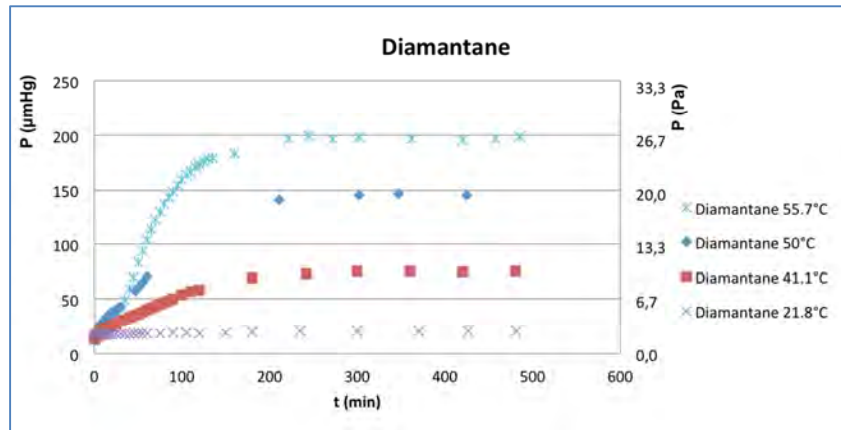


Figure 6.8. Vapor pressure measurement for diamantane.

Table 6.3. Experimental vapor pressure and corrections for diamantane.

T_{exp} (K)	P_{exp} (Pa)	P_{ref}/P ratio	$P_{\text{corrected}}$	$1/T$	$\ln(P_{\text{corrected}})$
294.98	2.7365	0.2594	0.7099	$3.390 \cdot 10^{-3}$	-0.3426
314.28	10.0508	0.6439	6.4713	$3.182 \cdot 10^{-3}$	1.8674
323.18	19.4391	0.9795	19.0410	$3.094 \cdot 10^{-3}$	2.9466
328.89	26.2774	1.2816	33.6765	$3.041 \cdot 10^{-3}$	3.5168

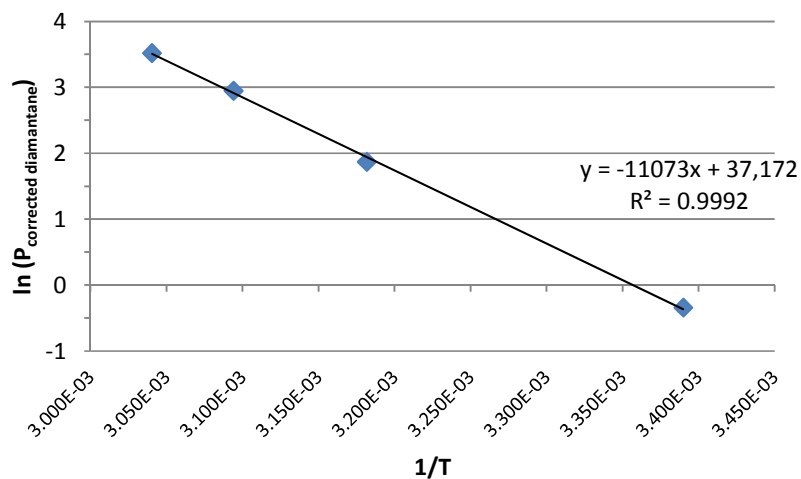


Figure 6.9. Clausius-Clapeyron plot for diamantane.

The enthalpy of sublimation of diamantane is $\Delta H = 92.1 \pm 5$ kJ/mol.

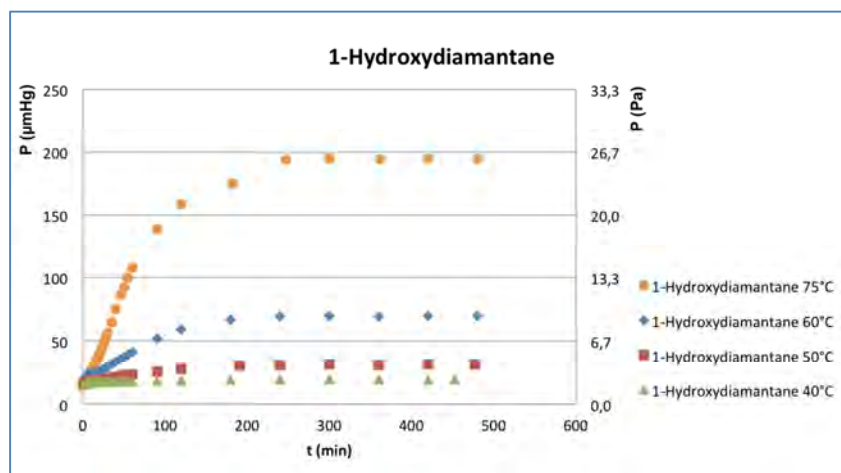
c) 1-Hydroxydiamantane

Figure 6.10. Vapor pressure measurement for 1-hydroxydiamantane.

Table 6.4. Experimental vapor pressure and corrections for 1-hydroxydiamantane.

T_{exp} (K)	P_{exp} (Pa)	P_{ref}/P ratio	$P_{\text{corrected}}$	$1/T$	$\ln(P_{\text{corrected}})$
313.00	2.6139	0.6063	1.5849	$3.195 \cdot 10^{-3}$	0.4605
322.60	4.1892	0.9530	3.9922	$3.100 \cdot 10^{-3}$	1.3843
333.20	9.3577	1.5700	14.6918	$3.001 \cdot 10^{-3}$	2.6873
348.85	25.9546	3.2812	85.1622	$2.867 \cdot 10^{-3}$	4.4446

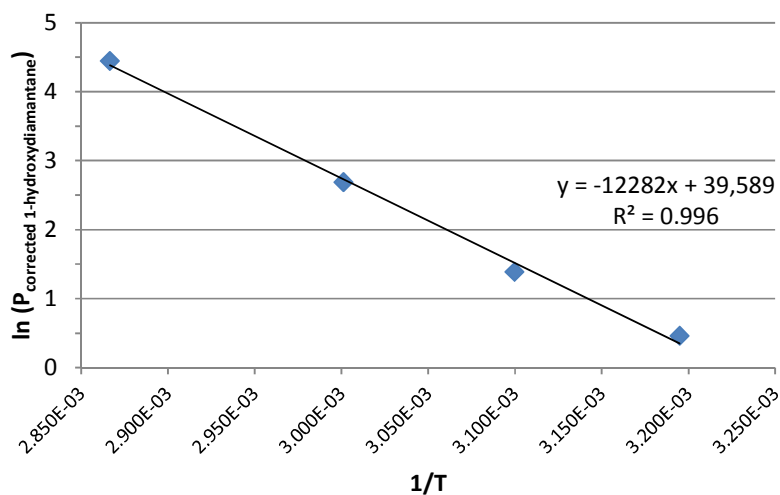


Figure 6.11. Clausius-Clapeyron plot for 1-hydroxydiamantane.

The enthalpy of sublimation of 1-hydroxydiamantane is $\Delta H = 102.1 \pm 5$ kJ/mol.

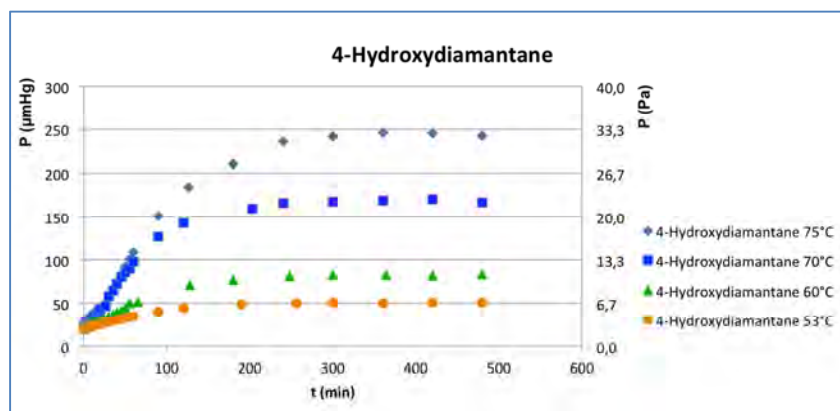
d) 4-Hydroxydiamantane

Figure 6.12. Vapor pressure measurement for 4-hydroxydiamantane.

Table 6.5. Experimental vapor pressure and corrections for 4-hydroxydiamantane.

T_{exp} (K)	P_{exp} (Pa)	P_{ref}/P ratio	$P_{\text{corrected}}$	$1/T$	$\ln(P_{\text{corrected}})$
326.05	6.7832	1.1211	7.6048	$3.067 \cdot 10^{-3}$	2.0288
331.55	11.0654	1.4526	16.0740	$3.016 \cdot 10^{-3}$	2.7772
343.55	22.4611	2.5563	57.4182	$2.911 \cdot 10^{-3}$	4.0504
348.20	32.5052	3.1823	103.4402	$2.872 \cdot 10^{-3}$	4.6390

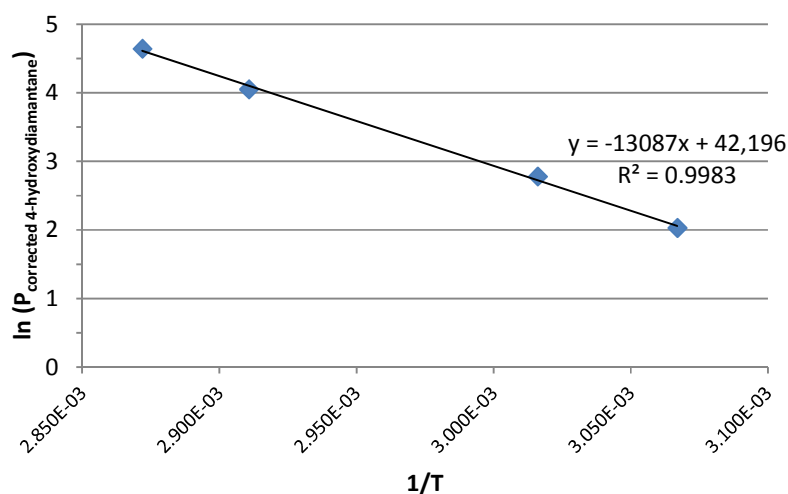


Figure 6.13. Clausius-Clapeyron plot for 4-hydroxydiamantane.

The enthalpy of sublimation of 4-hydroxydiamantane is $\Delta H = 108.8 \pm 5$ kJ/mol.

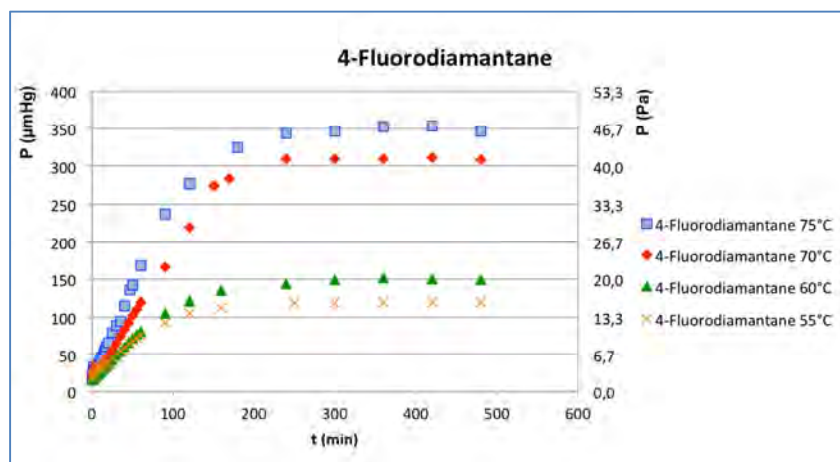
e) 4-Fluorodiamantane

Figure 6.14. Vapor pressure measurement for 4-fluorodiamantane.

Table 6.6. Experimental vapor pressure and corrections for 4-fluorodiamantane.

T_{exp} (K)	P_{exp} (Pa)	P_{ref}/P ratio	$P_{\text{corrected}}$	$1/T$	$\ln(P_{\text{corrected}})$
327.65	15.9360	1.2089	19.2646	$3.052 \cdot 10^{-3}$	2.9583
332.60	20.0234	1.5263	30.5613	$3.007 \cdot 10^{-3}$	3.4197
343.65	41.2146	2.5684	105.8562	$2.910 \cdot 10^{-3}$	4.6621
348.55	46.6133	3.2352	150.8014	$2.869 \cdot 10^{-3}$	5.0160

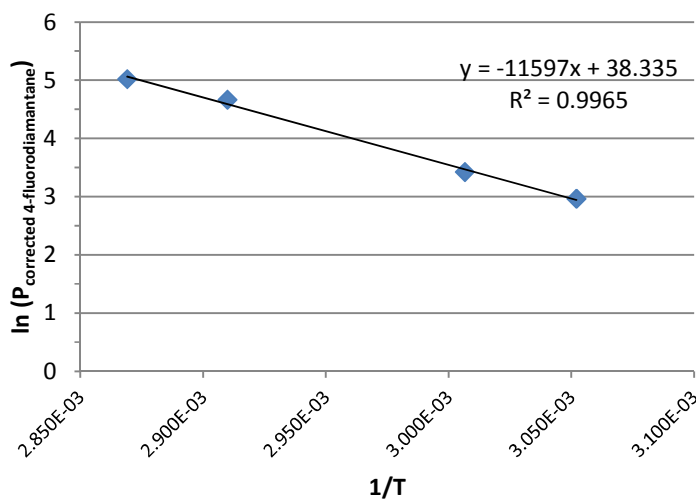


Figure 6.15. Clausius-Clapeyron plot for 4-fluorodiamantane.

The enthalpy of sublimation of 4-fluorodiamantane is $\Delta H = 96.4 \pm 5$ kJ/mol.

6.2. Vapor deposition conditions and apparatus

1. Deposition at atmospheric pressure or low vacuum

A sublimation apparatus was designed for running vapor deposition of diamondoids at atmospheric pressure on various supports (**Figure 6.16**). Diamondoids for sublimation were placed in a DSC aluminum cup on a boron nitride element. Above this system was placed a planar substrate on which the diamondoids vapor will re-condense. Substrate and diamondoids were separated by a spacer of tunable size in ceramic. A boron nitride element was used as a heating element and was attached to a copper holder with tungsten clips in its corners. A thermocouple type K was fixed to a hole on the side of holder to get the approximate temperature of the heating element measured with a multimeter apparatus. The heating element itself was connected to the power supply. The power supply was tuned based on its voltage and current. The heating was obtained by the Joule effect by means of a generator and the temperature was monitored using a multimeter equipped with a thermocouple. For a given intensity the temperature of the system is higher under vacuum than under atmospheric air or argon. The system was sealed using copper gasket and a valve. It was connected to a vacuum ramp/argon, itself connected to a vane pump. Vacuum was measured with a vacuum manometer (± 1 mmHg). The work atmosphere was either air, argon or a primary vacuum was established (5 mbar). Whatever the atmosphere in the chamber, a pump cycle was operated for a period of 10 min. Depending on the conditions the valve was closed to achieve a static vacuum, or the vacuum ramp was used for slow introduction of argon. Then, the valve was closed for establishing a static atmosphere, or the valve remained open for dynamic vacuum operating conditions. After adjusting the intensity of the applied current the deposition could start. The temperature setting was also monitored as a function of time. After the deposition time, the source was switched off allowing the system to cool. Once the temperature dropped below 30 °C, the system was opened, the substrate on which the deposit was made was characterized by optical microscopy and by scanning electron microscopy (SEM), EXD and additionally X-ray diffraction. To avoid tampering of the sample, it was stored sealed in a freezer at 4 °C.

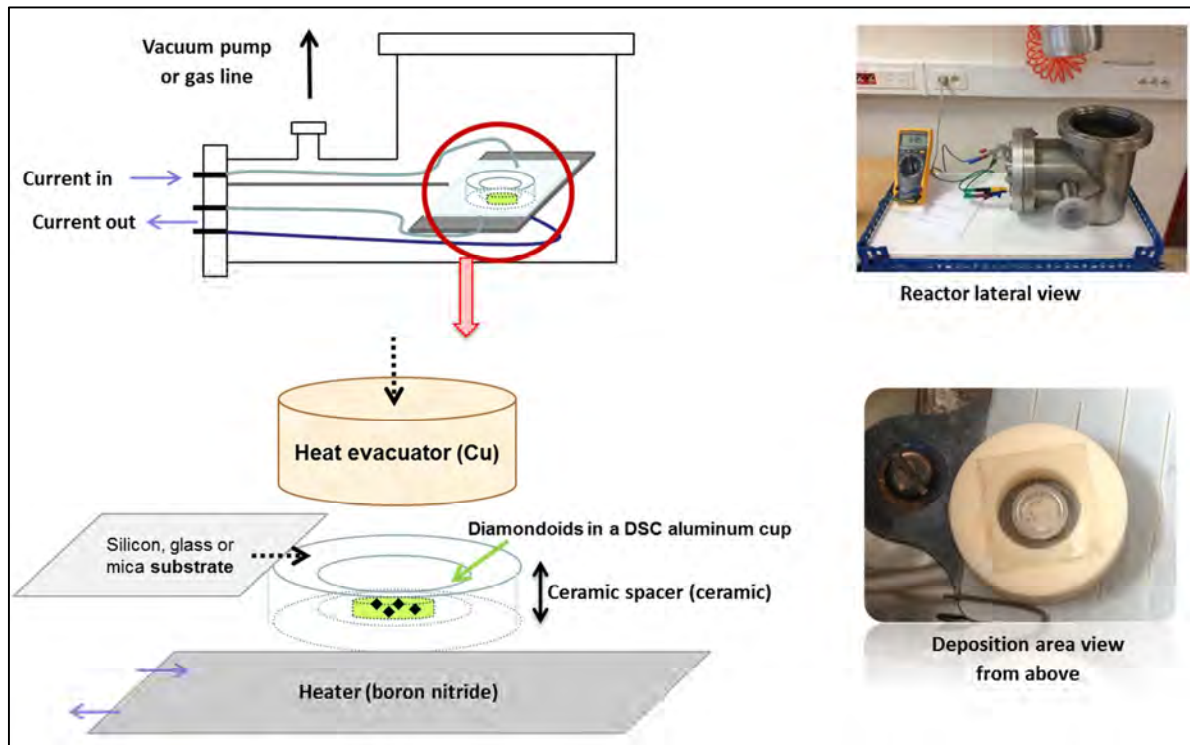


Figure 6.16. Reactor for vapor deposition of diamondoids under controlled atmosphere.

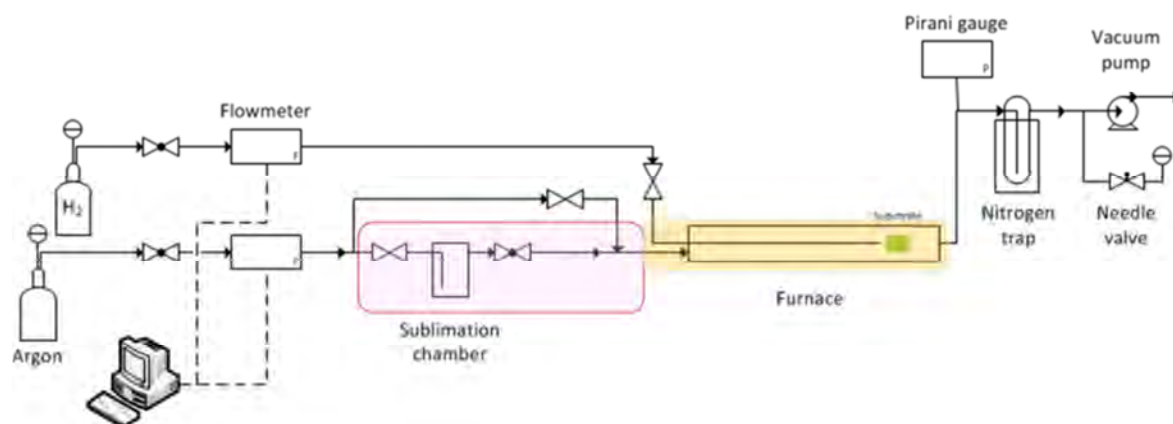
The substrates we used were cleaved mica, or silicon (111) from wafers. The substrates were placed on the top of the spacer. Deposits of diamondoids were achieved following various conditions (*vide infra* part 3), and all deposits were observed by optical microscopy (X16 to X500 size) before SEM analysis.

2. Vapor deposition apparatus for experiments under high vacuum (PVD)

Before exposure, silicon substrates Si(111) wafer pieces, *ca.* 1 cm², were cleaned out of carbon residue according to a RCA process (*Radio Corporation of America* is a standard set of wafer cleaning steps for high-temperature processing steps (*oxidation, diffusion, CVD, PVD, etc.*) of silicon wafers in semiconductor manufacturing: *i*) the silicon was immersed in a solution of distilled water: NH₄OH : H₂O₂ = 5 : 1 : 1 at 75–80 °C for 10 min; *ii*) it was then immersed in a solution of HF: distilled water = 1:100 or 1:50 at 25 °C for 15 s; *iii*) the silicon wafer was immersed in a solution of distilled water/HCl/H₂O₂ = 5:1:1 at 75–80 °C for 10 min; *iv*) the substrate was submersed in distilled water and dried with argon flushed when it was put inside the main chamber.

Following a fast entry procedure, the treated Si substrates were introduced in a first chamber, mainly built in silica and insuring a low pressure of *ca.* 10^{-7} Pa (10^{-9} mbar). At this stage a small layer of amorphous SiO₂ inevitably forms at the surface (as confirmed by XPS in **Figure 6.17**). The wafers were heated at 800 °C by an induction oven for 12 min to complete the surface cleaning. Such treatment allowed removal of remaining contaminants such as atmospheric carbon and oxygen species. After cooling, the substrate was transferred into the deposition chamber that was previously baked out and maintained under vacuum with a turbo pump and an ionic pump. The diamondoids were held in a silica ampoule that was independently evacuated at room temperature for purification. The ampoule was connected to the deposition chamber through a stainless steel pipe. Through a linear translator, the pipe can reach up to 3 cm the silicon surface. During exposure, the ampoule and the pipe are heated at 80 °C or more with the help of a heater tape and a thermocoax wire in order to generate a *ca.* 10^{-1} Pa (10^{-3} mbar) partial pressure of diamondoids inside the ampoule which also avoids cold spots. Diamondoid vapors were then introduced into the vacuum chamber via a leak valve to control the pressure. During exposures, the silicon sample was kept at a temperature below 40 °C controlled by a thermocouple. During exposure, the pressure in the chamber increased slowly from 3.5×10^{-5} Pa up to 1.5×10^{-4} Pa for exposure times longer than 15 min. A third chamber, connected to the two other ones, allows recording *in-situ* X-ray photoelectron spectroscopy (XPS) spectra, using a VG Microtech CLAM4 MCD analyzer system. These experiments were carried out with a non-monochromatised Al K α radiation with detection normal to the surface.

6.3. CVD conditions and apparatus



Position of substrates bearing diamondoids at surface / H₂ arrival

Figure 6.17. Experimental set-up for OMCVD

The deposition was conducted in a hand-made CVD apparatus (**Figure 6.17**). A quartz cylinder with a length 30 cm was used as a reactor. It was washed with acetone, flushed with compressed air, and heated before use. The temperature of the furnace was observed with a thermocouple connected to multimeter. The hydrogen gas was introduced into the reactor by a small metal tubing. The substrate was placed at a distance about 5 mm from the hydrogen's metal tip. The system was purged and filled with argon before use, then 100 mg of [Pd(η^3 -allyl)Cp] was placed inside the furnace and followed by the

substrate as fast as possible. Once the furnace was closed, it was covered with heating band and a thermocouple was connected on the outer wall of the furnace.

The argon flow was fixed at 80 mL/min. Then the vacuum pump was turned on and the pressure was fixed at 50 Torr using a needle valve connected to the manometer. The valve of hydrogen gas was opened and the flow was fixed at 3.2 mL/min then the heating band was set at 30 °C with the duration of deposition was about 6-7 h.

To stop the process, the flow of H₂ was fixed at 0 mL/min and valve of H₂ was closed and continued with turned off the vacuum pump. The system was left until it reaches 1 atm. It was done in similar way for argon. The substrate deposit was removed and kept in a closed vial for the characterization.

6.4. Synthesis of diamondoid phosphines and precursors

1. General information

The synthesis of sensitive products was done using Schlenk techniques. Glassware was dried in an oven at 110°C before use.

The tetrahydrofuran (THF) and diethyl ether solvents were distilled under argon using sodium (Na) and benzophenone mixture; dichloromethane (DCM) was purified by distillation under argon using CaH₂; 1,4-dioxane was purified by stirring with LiAlH₄ under argon overnight and distillation under argon (b.p. = 101 °C); CDCl₃ was dried over activated 4 Å molecular sieves under argon.¹ The other solvents were obtained directly from the manufacture or distilled from technical grade.

TLC was done on 0.2 mm silica gel with a fluorescent indicator (pre-coated polyester sheets UV₂₅₄ from Macherey-Nagel) or TLC Silica gel 60 F₂₅₄ on aluminum sheets (from Merck).

Column chromatography was done on silica gel (40-63 μm/230-400 mesh from Sigma-Aldrich or 0.063-0.2 mm/70-230 mesh from Macherey-Nagel).

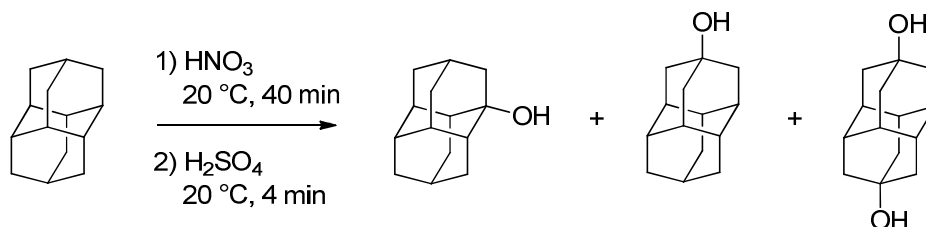
NMR spectra were recorded at 300 MHz Bruker Avance (in Dijon), 400 MHz Bruker Avance (in Giessen), 500 MHz (in Dijon), and 600 MHz (in Dijon and Giessen) spectrometers. ¹H and ¹³C NMR assignments were confirmed by DEPT-135/JMOD and two-dimensional ¹H-¹³C NMR experiments.

Adamantane and diamantane were obtained from the Giessen group. 1-Hydroxyadamantane **6** was purchased from Aldrich. 1-Aminoadamantane **64** and 1-bromoadamantane were purchased from Alfa Aesar. They were used directly without prior purification.

2. Procedures

a) 1-Hydroxydiamantane (**30**), 4-hydroxydiamantane (**48**), and 4,9-dihydroxydiamantane (**49**)

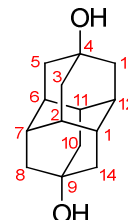
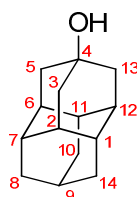
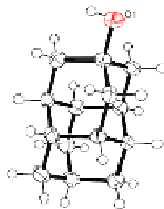
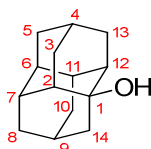
Hydroxydiamantane derivatives were prepared according to the literature.²



¹ D. B. G. Williams, M. Lawton. *J. Org. Chem.*, **2010**, 75, 8351-8354. Drying of Organic Solvents: Quantitative Evaluation of the Efficiency of Several Desiccants.

² N. A. Fokina, B. A. Tkachenko, A. Merz, M. Serafin, J. E. P. Dahl, R. M. K. Carlson, A. A. Fokin, P. R. Schreiner. *Eur. J. Org. Chem.*, **2007**, 4738-4745. Hydroxy Derivatives of Diamantane, Triamantane, and [121]Tetramantane: Selective Preparation of Bis-Apical Derivatives.

Two batches were prepared (total 12 g of diamantane, 63.72 mmol) and gave:



1-hydroxydiamantane

 $C_{14}H_{20}O$

Mw: 204.31

20% (ref.2: 24%)

2.572 g

4-hydroxydiamantane

 $C_{14}H_{20}O$

Mw: 204.31

31% (ref.2: 44%)

4.087 g

4,9-dihydroxydiamantane

 $C_{14}H_{20}O_2$

Mw: 220.15

28% (ref.2: 22%)

3.921 g

Analytical data are identical with the literature.²

1-Hydroxydiamantane (30):

1H NMR (600 MHz, 300 K, $CDCl_3$): δ =2.16 (d, J =12.6 Hz, 2H; CH_2), 2.08-2.04 (m, 1H; CH), 1.96 (s, 2H; CH), 1.76-1.71 (m, 1H; CH), 1.68-1.61 (m, 11H; CH_2 & CH), 1.48-1.43 (m, 2H; CH_2), 1.38 (s, 1H; OH) ppm.

^{13}C NMR (151 MHz, 300 K, $CDCl_3$): δ =70.89 (s, 1C; C_q), 46.49 (s, 1C; CH_2), 43.49 (s, 2C; CH), 40.05 (s, 2C; CH), 38.08 (s, 1C; CH_2), 37.62 (s, 2C; CH_2), 36.83 (s, 1C; CH), 32.64 (s, 2C; CH_2), 30.54 (s, 1C; CH), 25.39 (s, 1C; CH) ppm.

4-Hydroxydiamantane (48):

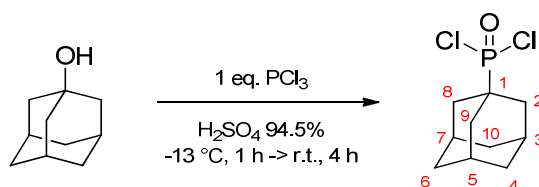
1H NMR (600 MHz, 300 K, $CDCl_3$): δ =1.96-1.92 (m, 3H; CH; H-2,6,12), 1.81-1.77 (m, 1H; CH; H-9), 1.77-1.73 (t, 6H; CH_2 ; H-3,5,13), 1.73-1.70 (m, 3H; CH; H-1,7,11), 1.70-1.67 (m, 6H; CH_2 ; H-8,10,14), 1.26 (br s, 1H; OH) ppm.

^{13}C NMR (151 MHz, 300 K, $CDCl_3$): δ =67.67 (s, 1C; C_q ; C-4), 45.82 (s, 3C; CH_2 ; C-8,10,14), 40.01 (s, 3C; CH; C-2,6,12), 37.34 (s, 3C; CH_2 ; C-3,5,13), 36.52 (s, 3C; CH; C-1,7,11), 25.77 (s, 1C; CH; C-9) ppm.

4,9-Dihydroxydiamantane (49):

^1H NMR (400 MHz, 270 K, CDCl_3): $\delta=1.93$ (s, 6H; CH; H-1,2,6,7,11,12), 1.75 (s, 12H; CH_2 ; H-3,5,8,10,13,14), 1.41 (br s, 2H; OH) ppm.

^{13}C NMR (101 MHz, 271 K, CDCl_3): $\delta=67.35$ (s, 1C; C_q ; C-4 or 9), 44.72 (s, 6C; CH_2 ; C-3,5,8,10,13,14), 38.81 (s, 6C; CH; C-1,2,6,7,11,12) ppm.

b) 1-Adamantylphosphonic dichloride (126)

In a 100-mL round bottom flask, 40 mL of H_2SO_4 94.5% was cooled with a salt-ice bath at $-13\text{ }^\circ\text{C}$. 1-Hydroxyadamantane (6.090 g, 40.0 mmol) was added and followed by PCl_3 (3.49 mL, 40.0 mmol, 1 eq.). The mixture was stirred for 1 h at the same temperature ($-13\text{ }^\circ\text{C}$) and for 4 h at r.t.

Workup:

The colorless solution was slowly poured onto 600 g of crushed ice. The white precipitate formed was then filtered, rinsed with distilled water, and dried in air. Pure 1-adamantylphosphonic dichloride was obtained as a white solid (10.124 g, 99%).

Mw: 253.11.

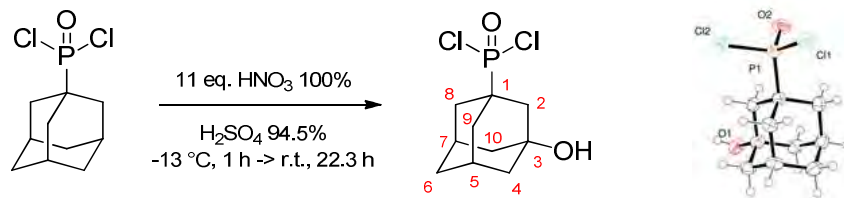
^1H NMR (400 MHz, 300 K, CDCl_3): $\delta=2.24$ -2.12 (m, 3H; CH; H-3,5,7), 2.07 (dd, $J=7.7$, 2.6 Hz, 6H; CH_2 ; H-2,8,9), 1.88-1.70 (m, 6H; CH_2 ; H-4,6,10) ppm.

^{31}P NMR (162 MHz, 300 K, CDCl_3 , H_3PO_4 external standard): $\delta=65.14$ ppm.

^{13}C NMR (101 MHz, 300 K, CDCl_3): $\delta=48.67$ (d, $^1J(\text{C},\text{P})=88.2$ Hz, 1C; C_q ; C-1), 35.95 (d, $^4J(\text{C},\text{P})=3.0$ Hz, 3C; CH_2 ; C-4,6,10), 35.07 (d, $^2J(\text{C},\text{P})=4.4$ Hz, 3C; CH_2 ; C-2,8,9), 27.61 (d, $^3J(\text{C},\text{P})=15.2$ Hz, 3C; CH; C-3,5,7) ppm.

HR-MS: m/z (%): calc. for $\text{C}_{10}\text{H}_{15}\text{Cl}_2\text{OP}$: 252.024; found: 252.022.

Elem. Analysis: calc.: C 49.46, H 6.41; found: C 47.49, H 5.99.

c) (3-Hydroxyadamant-1-yl)phosphonic dichloride (**178**)

In a 10-mL round bottom flask, 3 mL of H₂SO₄ 94.5% was cooled with a salt-ice bath until $-13\text{ }^{\circ}\text{C}$. 1-Adamantylphosphonic dichloride (1.658 g, 6.5 mmol) was added and stirred until it completely dissolved. Then HNO₃ 100% (3 mL, 72.0 mmol, 11 eq.) was slowly added. The colorless solution turned into white cloudy and viscous. It was stirred for 1 h at $-13\text{ }^{\circ}\text{C}$ and for 22 h and 20 min at r.t. When the solution reached r.t., it turned colorless.

Workup:

The colorless solution was slowly poured onto 15 g of crushed ice. 100 mL of DCM was added and the mixture was stirred at r.t. Solid NaHCO₃ was added in small portions until no more bubbles appeared. The aqueous phase turned clear yellow. It was extracted with DCM several times (total 225 mL of DCM) and diethyl ether (total 125 mL). It was dried over MgSO₄ and the solvent was evaporated and gave a yellowish sticky compound.

Purification:

Purification by column chromatography on silica gel using diethyl ether 100% (R_f: 0.3) gave pure (3-hydroxyadamant-1-yl)phosphonic dichloride as a white solid (1.417 g, 80%).

Mw: 269.10.

¹H NMR (400 MHz, 300 K, CDCl₃): δ =2.50-2.36 (m, 2H; CH; H-5,7), 2.04-1.94 (m, 6H; CH₂; H-2,4,10), 1.78-1.69 (m, 5H; CH₂, OH; H-3,8,9), 1.69-1.57 (m, 2H; CH₂; H-6) ppm.

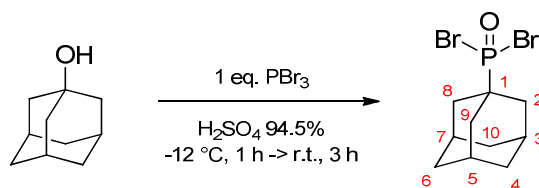
³¹P NMR (162 MHz, 300 K, CDCl₃, H₃PO₄ external standard): δ =62.21 ppm.

¹³C NMR (101 MHz, 300 K, CDCl₃): δ =68.09 (d, ³J(C,P)=19.4 Hz, 1C; C_q; C-3), 51.04 (d, ¹J(C,P)= 91.3 Hz, 1C; C_q; C-1), 43.91 (d, ²J(C,P)=2.5 Hz, 2C; CH₂; C-8,9), 42.61 (d, ²J(C,P)=4.6 Hz, 1C; CH₂; C-2), 34.53 (d, ⁴J(C,P)=2.8 Hz, 1C; CH₂; C-6), 34.03 (d, ⁴J(C,P)=3.8 Hz, 2C; CH₂; C-4,10), 30.07 (d, ³J(C,P)=17.6 Hz, 2C; CH; C-5,7) ppm.

HR-MS: m/z (%): calc. for C₁₀H₁₅Cl₂O₂P:268.019; found: 268.016.

Elem. Analysis: calc.: C 44.63, H 5.62; found: C 44.15, H 5.59.

d) 1-Adamantylphosphonic dibromide (179)



In a 50-mL round bottom flask, 10 mL of H_2SO_4 94.5% was cooled with a salt-ice bath at $-12\text{ }^\circ\text{C}$. PBr_3 (0.24 mL, 2.5 mmol) was added, followed by 1-hydroxyadamantane (0.761 g, 5.0 mmol), and at the end another portion of PBr_3 (0.24 mL, 2.5 mmol, *note: total PBr_3 was 1 eq.*). It was stirred for 1 h at the same temperature ($-12\text{ }^\circ\text{C}$) and for 3 h at r.t..

Workup:

The colorless solution was slowly poured onto 150 g of crushed ice. The white precipitate was then filtered, rinsed with distilled water, and dried in air. Pure 1-adamantylphosphonic dibromide was obtained as a white solid (1.352 g, 79%).

Mw: 342.01.

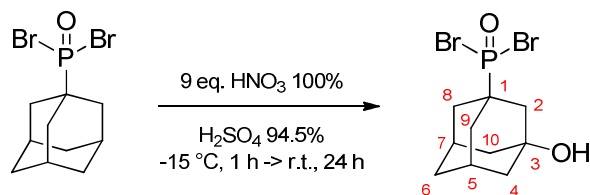
^1H NMR (400 MHz, 300 K, CDCl_3): $\delta=2.30\text{--}2.13$ (m, 3H; CH; H-3,5,7), 2.07 (dd, $J=8.4, 3.0$ Hz, 6H; CH_2 ; H-2,8,9), 1.81-1.68 (m, 6H; CH_2 ; H-4,6,10) ppm.

^{31}P NMR (162 MHz, 300 K, CDCl_3 , H_3PO_4 external standard): $\delta=52.34$ ppm.

^{13}C NMR (101 MHz, 300 K, CDCl_3): $\delta=53.13$ (d, $^1J(\text{C,P})=63.5$ Hz, 1C; C_q ; C-1), 36.02 (d, $^4J(\text{C,P})=3.1$ Hz, 3C; CH_2 ; C-4,6,10), 35.39 (d, $^2J(\text{C,P})=4.4$ Hz, 3C; CH_2 ; C-2,8,9), 28.01 (d, $^3J(\text{C,P})=15.6$ Hz, 3C; CH; C-3,5,7) ppm.

HR-MS: m/z (%): calc. for $\text{C}_{10}\text{H}_{15}\text{Br}_2\text{OP}$: 339.923; found: 339.918.

Elem. Analysis: calc.: C 37.11, H 4.81; found: C 34.97, H 4.82.

e) (3-Hydroxyadamant-1-yl)phosphonic dibromide (**180**)

In a 10-mL round bottom flask, 2 mL of H₂SO₄ 94.5% was cooled with a salt-ice bath until $-15\text{ }^{\circ}\text{C}$. 1-Adamantylphosphonic dibromide (0.342 g, 1.0 mmol) was added and stirred until it completely dissolved. Then HNO₃ 100% (0.38 mL, 9.0 mmol, 9 eq.) was slowly added. The colorless solution turned into orange slurry. It was stirred for 1 h at $-15\text{ }^{\circ}\text{C}$ and for 24 h at r.t.

Workup:

The colorless solution was slowly poured onto 10 g of crushed ice. 20 mL of DCM was added and stirred at r.t. Solid NaHCO₃ was added in small portions until no more bubbles formed. It was extracted with DCM several times (total 60 mL of DCM). It was dried over MgSO₄ and the solvent was evaporated to give a yellowish sticky compound. 10 mL of pentane were added into the flask containing the compound, and was stirred at r.t. overnight. A yellow powder was formed. Pentane solvent was removed with a pipette to let dry the powder in air. A yellow powder was obtained (0.276 g).

Purification:

Purification by column chromatography on silica gel with ether 100% (*R_f*: 0.4) gave pure (3-hydroxyadamant-1-yl)phosphonic dibromide (0.155 g, 43%).

Mw: 358.01.

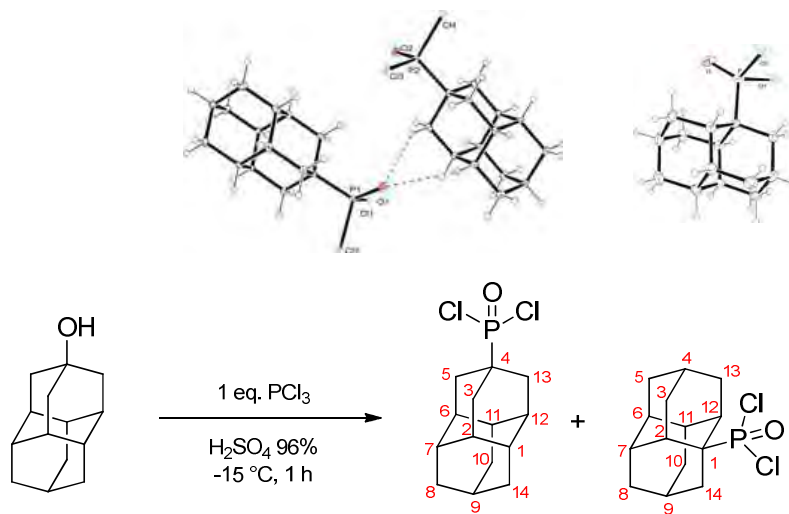
¹H NMR (400 MHz, 300 K, CDCl₃) δ =2.49-2.37 (m, 2H; CH; H-5,7), 2.09-1.91 (m, 6H; CH₂; H-2,4,10), 1.82-1.70 (m, 5H; CH₂, OH; H-3,8,9), 1.70-1.56 (m, 2H; CH₂; H-6) ppm.

³¹P NMR (162 MHz, 300 K, CDCl₃, H₃PO₄ external standard): δ =47.58 ppm.

¹³C NMR (101 MHz, 300 K, CDCl₃): δ =68.40 (d, ³*J*(C,P)=19.9 Hz, 1C; C_q; C-3), 55.04 (d, ¹*J*(C,P)=66.5 Hz, 1C; C_q; C-1), 43.94 (d, ²*J*(C,P)=2.6 Hz, 2C; CH₂; C-8,9), 42.88 (d, ²*J*(C,P)=4.6 Hz, 1C; CH₂; C-2), 34.58 (d, ⁴*J*(C,P)=3.0 Hz, 1C; CH₂; C-6), 34.31 (d, ⁴*J*(C,P)=4.0 Hz, 2C; CH₂; C-4,10), 30.19 (d, ³*J*(C,P)=17.6 Hz, 2C; CH; C-5,7) ppm.

HR-MS: *m/z* (%): calc. for C₁₀H₁₅Br₂O₂P: 355.918; found: 355.914.

Elem. Analysis: calc.: C 33.55, H 4.22; found: C 33.32, H 4.17.

f) 4-Diamantylphosphonic dichloride (**22**) and 1-diamantylphosphonic dichloride (**181**)

Concentrated sulfuric acid (96%, 5 mL) was cooled to $-15\text{ }^\circ\text{C} < T < -12\text{ }^\circ\text{C}$ in a 50 mL-round bottom flask equipped with magnetic stirring bar using a salt-ice bath. PCl_3 half portion (0.11 mL, 1.25 mmol) was added, followed by 4-hydroxyadamantane (0.511 g, 2.5 mmol) and another half portion of PCl_3 (0.11 mL, 1.25 mmol, *note: total PCl_3 was 1 eq.*). It was stirred for 1 h at the same temperature.

Workup:

The reaction mixture was poured onto 60 g of crushed ice and left for several hours. White precipitate then was filtered with a glass filter with frit size 3, rinsed with distilled water and dried in air.

Purification:

It was purified by column chromatography with silica gel using pentane:diethyl ether (19:1), and afforded 1-diamantylphosphonic dichloride (0.053 g, 7%). Slow evaporation of the solvent gave colorless crystals characterized by X-Ray diffraction analysis.

Changing the eluent with pentane:diethyl ether (9:1) gave 4-diamantylphosphonic dichloride (0.518 g, 68%). Slow evaporation of the solvent gave colorless crystals that we characterized by X-Ray diffraction analysis.

1-Diamantylphosphonic dichloride (181):

Mw: 305.18.

^1H NMR (600 MHz, 298 K, CDCl_3): $\delta=2.73$ (d, $J=13.3$ Hz, 2H; CH_2 ; H-14), 2.28 (d, $J=8.3$ Hz, 2H; CH; H-2,12), 2.08-2.01 (m, 1H; CH; H-9), 2.01-1.98 (m, 2H; CH; H-7,11), 1.98-1.93 (m, 2H; CH_2 ; H-13), 1.93-1.87 (m,

1H; CH; H-4), 1.80-1.75 (m, 1H; CH; H-6), 1.75-1.69 (m, 6H; CH₂; H-8,10), 1.58 (d, $J=13.3$ Hz, 2H; CH₂; H-5) ppm.

³¹P NMR (243 MHz, 298 K, CDCl₃, H₃PO₄ external standard): $\delta=65.78$ ppm.

¹³C NMR (151 MHz, 298 K, CDCl₃): $\delta=56.40$ (d, $^1J(C,P)=73.1$ Hz, 1C; C_q; C-1), 38.49 (d, $^3J(C,P)=16.0$ Hz, 2C; CH; C-7,11), 38.92 (s, 1C; CH₂; C-13), 38.54 (s, 1C; CH₂; C-10), 37.16 (d, $^4J(C,P)=3.0$ Hz, 1C; CH; C-6), 36.99 (d, $^4J(C,P)=3.1$ Hz, 2C; CH₂; C-8,10), 36.82 (d, $^2J(C,P)=2.1$ Hz, 2C; CH; C-2,12), 34.09 (s, 2C; CH₂; C-5,14), 26.18 (d, $^3J(C,P)=15.1$ Hz, 1C; CH; C-9), 24.84 (s, 1C; CH; C-4) ppm.

HR-MS: m/z (%): calc. for C₁₄H₁₉Cl₂OP: 304.055; found: 304.055.

Elem. Analysis: calc.: C 55.10, H 6.28; found: C 55.11, H 6.30.

4-Diamantylphosphonic dichloride (**22**):

Mw: 305.18.

¹H NMR (600 MHz, 298 K, CDCl₃): $\delta=2.04$ (d, $J=7.6$ Hz, 6H; CH₂; H-3,5,13), 1.99 (br s, 3H; CH; H-2,6,12), 1.86-1.81 (m, 1H; CH; H-9), 1.80-1.71 (m, 9H, H-1,7,8,10,11,14) ppm.

³¹P NMR (243 MHz, 298 K, CDCl₃, H₃PO₄ external standard): $\delta=66.14$ ppm.

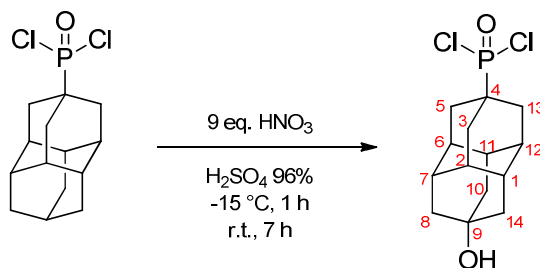
¹³C NMR (151 MHz, 298 K, CDCl₃): $\delta=47.22$ (d, $^1J(C,P)=89.3$ Hz, 1C; C_q; C-4), 37.41 (d, $^5J(C,P)=3.5$ Hz, 3C; CH₂; C-8,10,14), 36.76 (d, $^3J(C,P)=17.2$ Hz, 3C; CH; C-2,6,12), 36.16 (s, 3C; CH; C-1,7,11), 36.06 (d, $^2J(C,P)=4.0$ Hz, 3C; CH₂; C-3,5,13), 25.27 (s, 1C; CH; C-9) ppm.

HR-MS: m/z (%): calc. for C₁₄H₁₉Cl₂OP: 304.054; found: 304.054.

Elem. Analysis: calc.: C 55.10, H 6.28; found: C 55.06, H 6.28.

g) (9-Hydroxydiamant-4-yl)phosphonic dichloride (**182**)

Method A:



Concentrated sulphuric acid 96% (2.25 mL) was placed in a 5-mL round bottom flask and was cooled to -15°C with a salt-ice bath. 4-Diamantylphosphonic acid dichloride (0.332 g, 1.1 mmol) was added and

followed by HNO_3 100% (0.41 mL, 9.8 mmol, 9 eq.). The reaction mixture was stirred for 1 h at the same temperature ($-15\text{ }^\circ\text{C}$) and for 7 h at r.t.

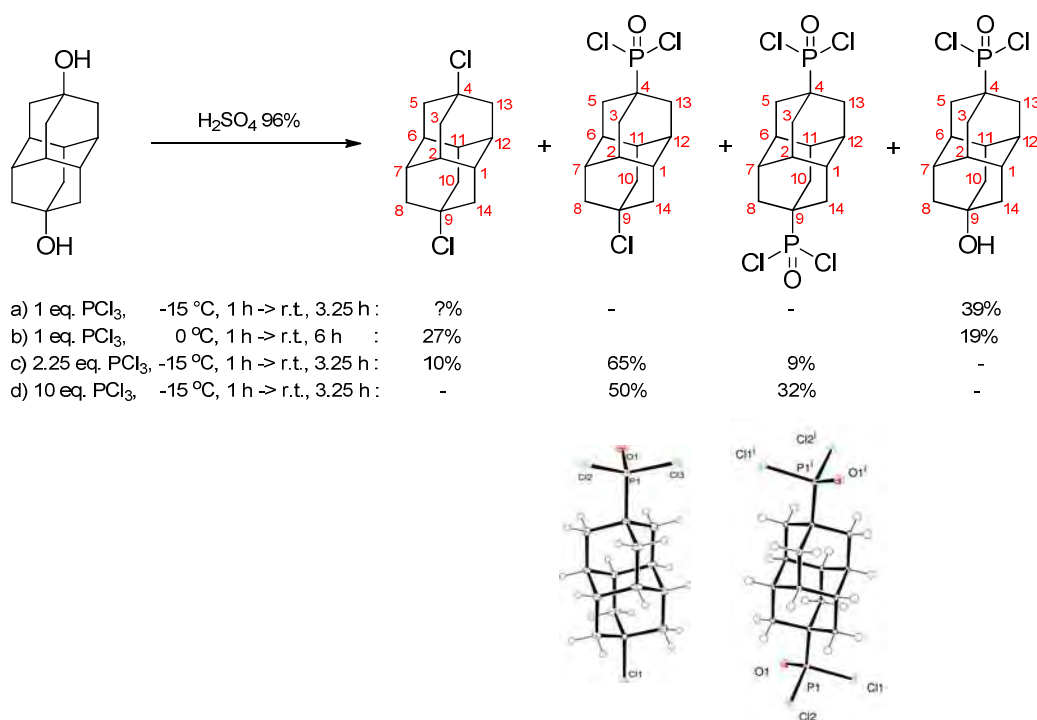
Workup:

The reaction mixture was slowly poured onto 38 g of crushed ice. 40 mL of DCM was added and followed by NaHCO_3 in portions until a neutral pH is reached and the aqueous phase turned clear yellow. It was extracted with DCM (110 mL) and dried over MgSO_4 . The solvent was evaporated to get 0.325 g of crude product.

Purification:

It was purified by column chromatography on silica gel using DCM:diethylether 1:1 (R_f : 0.3) to afford (9-hydroxydiamant-4-yl)phosphonic dichloride (0.242 g, 69% yield) as a white solid.

Method B:



Concentrated sulphuric acid 96% (a. 5 mL; b. 7.5 mL; c. 5 mL) was placed in a round bottom flask and was cooled to temperatures ranging between 0 to $-15\text{ }^\circ\text{C}$, depending on the conditions a, b, or c (see Scheme above) with an ice-salt bath. 4,9-Dihydroxydiamantane (a. 0.551 g, 2.5 mmol; b. 1.102 g, 5 mmol; c. 0.331 g, 1.5 mmol) was added and followed by PCl_3 (a. 1 eq., 0.22 mL, 2.5 mmol; b. 1 eq., 0.44 mL, 5

mmol; c. 2.25 eq., 0.33 mL, 3.75 mmol). The reaction mixture was stirred for 1 h at the same temperature and for 3 to 6 h at r.t., depending on the conditions a, b, or c (see Scheme above).

Workup:

The reaction mixture was slowly poured onto crushed ice. White precipitate appeared and it was left for overnight. The white precipitate was filtered with sintered glass Buchner funnel and rinsed with distilled water. The solid was dried in air.

Purification:

Purification by column chromatography on silica gel with pentane:diethyl ether (3:1) afforded 4,9-dichlorodiamantane (R_f : 0.88) and (9-chloro-diamant-4-yl)phosphonic dichloride (R_f : 0.28). Changing the eluent with DCM:diethyl ether (3:1) give (4,9-diamantyl)diphosphonic dichloride (R_f : 0.76). Changing the ratio of the same eluent to 1:1 afforded (9-hydroxydiamant-4-yl)phosphonic dichloride (R_f : 0.22) as a white solid.

4,9-Dichlorodiamantane (183):

Mw: 257.20.

^1H NMR (600 MHz, 298 K, CDCl_3): δ =2.13 (s, 12H; CH_2 ; H-3,5,8,10,13,14), 1.98 (s, 6H; CH; H-1,2,6,7,11,12) ppm.

^{13}C NMR (151 MHz, 298 K, CDCl_3): δ =66.41 (s, 2C; C_q ; C-4,9), 46.93 (s, 6C; CH_2 ; C-3,5,8,10,13,14), 38.99 (s, 6C; CH; C-1,2,6,7,11,12) ppm.

HR-MS: m/z (%): calc. for $\text{C}_{14}\text{H}_{18}\text{Cl}_2$: 256.079; found: 256.078.

Elem. Analysis: calc.: C 65.38, H 7.05; found: C 65.29, H 7.10.

(9-Chlorodiamant-4-yl)phosphonic dichloride (184):

Mw: 339.62.

^1H NMR (600 MHz, 291 K, CDCl_3): δ =2.17 (d, J =3.4 Hz, 6H; CH_2 ; H-8,10,14), 2.11-2.06 (dd, 6H; CH_2 ; H-3,5,13), 2.06-2.01 (m, 3H; CH; H-2,6,12), 2.01-1.06 (m, 3H; CH; H-1,7,11) ppm.

^{31}P NMR (243 MHz, 291 K, CDCl_3): δ =64.85 ppm.

^{13}C NMR (151 MHz, 291 K, CDCl_3): δ =65.65 (s, 1C; C_q ; C-9), 47.13 (d, $^5J(\text{C},\text{P})$ =3.1 Hz, 3C; CH_2 ; C-8,10,14), 46.51 (d, $^1J(\text{C},\text{P})$ =92.8 Hz, 1C; C_q ; C-4), 39.13 (d, $^4J(\text{C},\text{P})$ =2.6 Hz, 3C; CH; C-1,7,11), 35.15 (d, $^3J(\text{C},\text{P})$ =16.7 Hz, 3C; CH; C-2,6,12), 34.97 (d, $^2J(\text{C},\text{P})$ =3.3 Hz, 3C; CH_2 ; C-3,5,13) ppm.

(4,9-Diamantyl)diphosphonic dichloride (185):

Mw: 422.05.

^1H NMR (600 MHz, 291 K, CDCl_3): $\delta=2.16\text{--}2.09$ (d, $J=7.4$ Hz, 12H; CH_2 ; H-3,5,8,10,13,14), 2.09–2.01 (m, 6H; CH; H-1,2,6,7,11,12) ppm.

^{31}P NMR (243 MHz, 291 K, CDCl_3): $\delta=63.97$ ppm.

^{13}C NMR (151 MHz, 291 K, CDCl_3): $\delta=46.26$ (d, $^1J(\text{C,P})=94.0$ Hz, 2C; C_q ; C-4,9), 35.37 (d, $^3J(\text{C,P})=2.4$ Hz, 3C; CH; C-2,6,12), 35.25 (s, 9C; $\text{CH}\&\text{CH}_2$; C-1,3,5,7,8,10,11,13,14) ppm.

(9-Hydroxydiamant-4-yl)phosphonic dichloride (182):

Mw: 321.18.

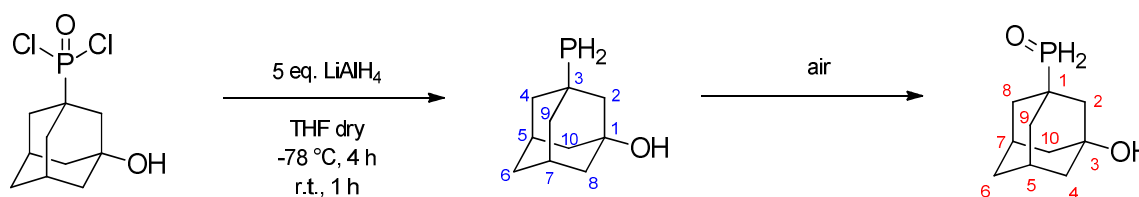
^1H NMR (600 MHz, 298 K, CDCl_3): $\delta=2.14\text{--}2.02$ (m, 6H; CH_2 ; H-8,10,14), 1.98 (br s, 6H; CH; H-1,2,6,7,11,12), 1.82–1.68 (m, 6H; CH_2 ; H-3,5,13), 1.51 (br s, 1H; OH) ppm.

^{31}P NMR (243 MHz, 300 K, CDCl_3): $\delta=65.29$ ppm.

^{13}C NMR (151 MHz, 298 K, CDCl_3): $\delta=66.79$ (s, 1C; C_q ; C-9), 46.77 (d, $^1J(\text{C,P})=91.6$ Hz, 1C; C_q ; C-4), 44.76 (d, $^2J(\text{C,P})=3.2$ Hz, 3C; CH_2 ; C-3,5,13), 38.47 (d, $^4J(\text{C,P})=2.3$ Hz, 3C; CH; C-1,7,11), 35.60 (d, $^3J(\text{C,P})=16.6$ Hz, 3C; CH; C-2,6,12), 35.04 (d, $^5J(\text{C,P})=3.1$ Hz, 3C; CH_2 ; C-8,10,14) ppm.

HR-MS: m/z (%): calc. for $\text{C}_{14}\text{H}_{19}\text{Cl}_2\text{O}_2\text{P}$: 320.050; found: 320.046.

Elem. Analysis: calc.: C 52.35, H 5.96; found: C 48.19, H 5.97.

h) 3-Phosphinoadamantan-1-ol (186) and (3-Hydroxyadamant-1-yl)phosphine oxide (187)

(3-Hydroxyadamant-1-yl)phosphonic dichloride (0.054 g, 0.2 mmol) was placed in a 5-mL-flask under argon. 1 mL of dry THF was added. The solution was cooled to -78 °C and LiAlH_4 solution (1 mL, 1 M in THF, 1 mmol, 5 eq.) was slowly added at -78 °C. The colourless solution was stirred for 4 h at -78 °C and for 1 h at r.t..

Workup:

1 mL of distilled water was added carefully drop by drop, and the colourless solution turned into a viscous white liquid. It was extracted with 10 mL of DCM and dried over MgSO_4 . The solvent was

evaporated to get a pure white air sensitive solid compound of hydroxyphosphine **186** (0.034 g, 92%) that was conserved under argon to avoid phosphine oxidation.

When contacted with air for 5 minutes, the product was quantitatively oxidized.

3-Phosphinoadamantan-1-ol (**186**):

Mw: 184.22.

^1H NMR (600 MHz, 300 K, C_6D_6): $\delta=2.70$ (d, $^1J(\text{H,P})=188.0$ Hz, 2H; PH_2), 1.91-1.83 (m, 2H; CH; H-5,7), 1.59 (d, $J=4.2$ Hz, 2H; CH_2 ; H-2), 1.53-1.4 (m, 8H; CH_2 ; H-4,8,9,10), 1.32-1.23 (m, 2H; CH_2 ; H-6), 1.16 (s, 1H; OH) ppm.

^{31}P NMR (243 MHz, 300 K, C_6D_6): $\delta=-85.97$ (t, $^1J(\text{P,H})=188.5$ Hz) ppm.

^{13}C NMR (151 MHz, 300 K, C_6D_6): $\delta=67.79$ (d, $^3J(\text{C,P})=8.7$ Hz, 1C; C_q ; C-1), 52.76 (d, $^2J(\text{C,P})=7.8$ Hz, 1C; CH_2 ; C-2), 44.33 (s, 2C; CH_2 ; C-8,9), 43.61 (d, $^2J(\text{C,P})=8.8$ Hz, 2C; CH_2 ; C-4,10), 35.00 (s, 1C; CH_2 ; C-6), 31.62 (d, $^3J(\text{C,P})=8.4$ Hz, 2C; CH; C-5,7), 31.52 (d, $^1J(\text{C,P})=4.8$ Hz, 1C; C_q ; C-3) ppm.

(3-Hydroxyadamant-1-yl)phosphine oxide (**187**):

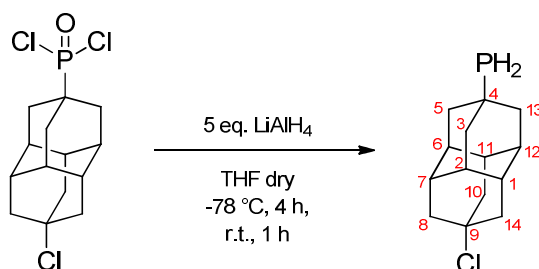
Mw: 200.21.

^1H NMR (600 MHz, 300 K, CDCl_3): $\delta=7.15$ (d, $^1J(\text{H,P})=452.8$ Hz, 2H; PH_2), 2.40-2.34 (m, 2H; CH; H-5,7), 1.95-1.67 (m, 13H; CH_2 , OH; H-2,4,6,8,9,10) ppm.

^{31}P NMR (243 MHz, 303 K, CDCl_3): $\delta=25.71$ (t, $^1J(\text{P,H})=452.8$ Hz) ppm.

^{13}C NMR (151 MHz, 303 K, CDCl_3): $\delta=67.71$ (d, $^3J(\text{C,P})=15.7$ Hz, 1C; C_q ; C-3), 44.45 (s, 2C; CH_2), 42.11 (s, 1C; CH_2), 36.81 (d, $^1J(\text{C,P})=72.7$ Hz, 1C; C_q ; C-1), 35.06 (d, $^2J(\text{C,P})=2.2$ Hz, 1C; CH_2), 33.59 (s, 2C; CH_2), 30.03 (d, $^3J(\text{C,P})=13.4$ Hz, 2C; CH; C-5,7) ppm.

i) (9-Chlorodiamant-4-yl)phosphine (**188**)



(9-Chlorodiamant-4-yl)phosphonic dichloride (0.051 g, 0.15 mmol) was placed in a 5-mL-flask under argon. The LiAlH_4 solution (0.75 mL, 1 M in THF, 0.75 mmol, 5 eq.) was slowly added at -78°C . The colourless solution was stirred for 4 h at -78°C and for 1 h at r.t.

Workup:

0.75 mL of distilled water was added drop by drop with a pipette and the colourless solution turned into a viscous white liquid. It was extracted with 10 mL of DCM and dried over MgSO_4 . The solvent was evaporated to get a pure white solid product **188** (0.036 g, 99%) that was conserved under argon to avoid the phosphine group oxidation.

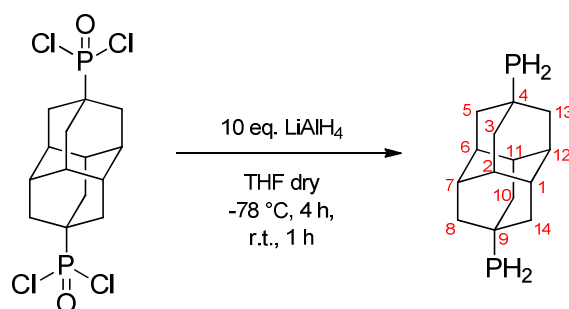
Mw: 254.74.

^1H NMR (600 MHz, 300 K, CDCl_3): $\delta=2.70$ (d, $^1J(\text{H,P})=192.8$ Hz, 2H; PH), 2.14-2.08 (m, 6H; CH_2 ; H-8,10,14), 1.86 (AB_q, 6H, $\Delta\delta_{\text{AB}}=0.11$, $J_{\text{AB}}=30$ Hz; CH; H-1,2,6,7,11,12), 1.80-1.78 (t, 4H; CH_2 ; H-5,13), 1.74-1.71 (t, 2H; CH_2 ; H-3) ppm.

^{31}P NMR (243 MHz, 300 K, CDCl_3): $\delta=-85.92$ (t, $^1J(\text{P,H})=194.9$ Hz, $^{3\text{T}5}J(\text{P,H})=6.8$ Hz) ppm.

^{13}C NMR (151 MHz, 300 K, CDCl_3): $\delta=67.28$ (s, 1C; C_q; C-9), 48.30 (s, 1C; CH_2 ; C-10), 47.70 (s, 2C; CH_2 ; C-8,14), 44.46 (d, $^2J(\text{C,P})=8.7$ Hz, 2C; CH_2 ; C-5,13), 40.80 (s, 1C; CH; C-11), 39.48 (s, 2C; CH; C-1,7), 37.15 (s, 1C; CH_2 ; C-3), 36.61 (d, $^3J(\text{C,P})=7.9$ Hz, 2C; CH; C-6,12), 36.02 (s, 1C; CH; C-2), 26.65 (d, $^1J(\text{C,P})=3.2$ Hz, 1C; C_q; C-4) ppm.

j) 4,9-Diamantylidiphosphine (**189**)



(4,9-Diamantyl)diphosphonic dichloride (0.042 g, 0.1 mmol) was placed into a 5-mL-flask under argon. The LiAlH_4 solution (1 mL, 1 M in THF, 1.0 mmol, 10 eq.) was slowly added at -78°C . The colourless solution was stirred for 4 h at -78°C and for 1 h at r.t.

Workup:

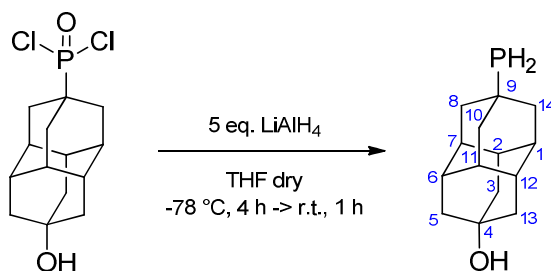
1 mL of distilled water was added carefully drop by drop with a pipette and colourless solution turned into a viscous white liquid. It was extracted with 10 mL of DCM and dried over MgSO_4 . The solvent was evaporated to get 0.025 g of mixture products difficult to separate (94% of 4,9-diamantylphosphine and 6% of 4-diamantylphosphine) that was conserved under argon to avoid phosphine groups oxidation.

Mw: 252.27.

^1H NMR (600 MHz, 300 K, CDCl_3): δ =2.69 (d, $^1J(\text{H},\text{P})=192.0$ Hz, 4H; PH), 1.77 (d, $J=4.1$ Hz, 12H; CH_2 ; H-3,5,8,10,13,14), 1.72 (br s, 6H; CH; H-1,2,6,7,11,12) ppm.

^{31}P NMR (243 MHz, 300 K, CDCl_3): δ =-85.56 (t, $^1J(\text{P},\text{H})=192.0$ Hz, $^{3\text{T}5}J(\text{P},\text{H})=5.2$ Hz) ppm.

^{13}C NMR (151 MHz, 300 K, CDCl_3): δ =45.20 (d, $^2J(\text{C},\text{P})=8.9$ Hz, 6C; CH_2 ; C-3,5,8,10,13,14), 37.03 (d, $^3J(\text{C},\text{P})=8.2$ Hz, 6C; CH; C-1,2,6,7,11,12), 26.87 (d, $^1J(\text{C},\text{P})=3.0$ Hz, 2C; C_q ; C-4,9) ppm.

k) 9-Phosphinodiamantan-4-ol (**190**)

(9-Hydroxydiamant-4-yl)phosphonic dichloride (0.032 g, 0.1 mmol) was placed in a 5-mL-flask under argon. A LiAlH_4 solution (0.5 mL, 1 M in THF, 0.5 mmol, 5 eq.) was added at -78 °C slowly. The resulting colourless solution was stirred for 4 h at -78 °C and for 1 h at r.t.

Workup:

0.5 mL of distilled water was added carefully drop by drop with a pipette and the colourless solution turned into a viscous white liquid. It was extracted with 10 mL of DCM and dried over MgSO_4 . The solvent was evaporated to get a pure product (0.024 g, 99%) that was conserved under argon to avoid the oxidation.

Mw: 236.29.

^1H NMR (600 MHz, 300 K, CDCl_3): δ =2.70 (d, $^1J(\text{H,P})=192.0$ Hz, 2H; PH), 1.95-1.91 (m, 1H; CH; H-2), 1.91-1.87 (m, 2H; CH; H-6,12), 1.83-1.80 (m, 4H; CH_2 ; H-8,14), 1.78-1.75 (m, 2H; CH; H-1,7), 1.75-1.73 (m, 2H; CH_2 ; H-10), 1.73-1.68 (m, 7H; CH & CH_2 ; H-3,5,11,13), 1.43 (s, 1H; OH) ppm.

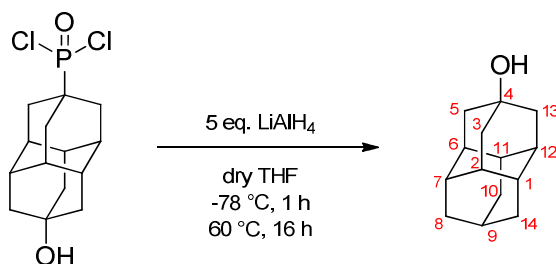
^{31}P NMR (243 MHz, 300 K, CDCl_3): δ =-85.70 (t, $^1J(\text{P,H})=192.0$ Hz) ppm.

^{13}C NMR (151 MHz, 300 K, CDCl_3): δ =67.34 (s, 1C; C_q ; C-4), 45.83 (s, 1C; CH_2 ; C-3), 45.27 (s, 2C; CH_2 ; C-5,13), 44.65 (d, $^2J(\text{C,P})=8.6$ Hz, 2C; CH_2 ; C-8,14), 40.02 (s, 1C; CH; C-2), 38.74 (s, 2C; CH; C-6,12), 37.35 (s, 1C; CH_2 ; C-10), 37.12 (d, $^3J(\text{C,P})=8.2$ Hz, 2C; CH; C-1,7), 36.52 (s, 1C; CH; C-11), 26.89 (d, $^1J(\text{C,P})=3.3$ Hz, 1C; C_q ; C-9) ppm.

HR-MS: m/z (%): calc. for $\text{C}_{14}\text{H}_{21}\text{OP}$: 236.133; found: 236.133.

Elem. Analysis: calc.: C 71.16, H 8.96; found: C 71.85, H 8.89.

l) 4-Hydroxydiamantane (48)



(9-Hydroxydiamant-4-yl)phosphonic dichloride (0.080 g, 0.25 mmol) was placed in a 5-mL-flask under argon equipped with a reflux system. The LiAlH_4 solution (1.25 mL, 1 M in THF, 1.25 mmol, 5 eq.) was slowly added at -78 °C. The colourless solution was stirred for 1 h at -78 °C and for 16 h at 60 °C.

Workup:

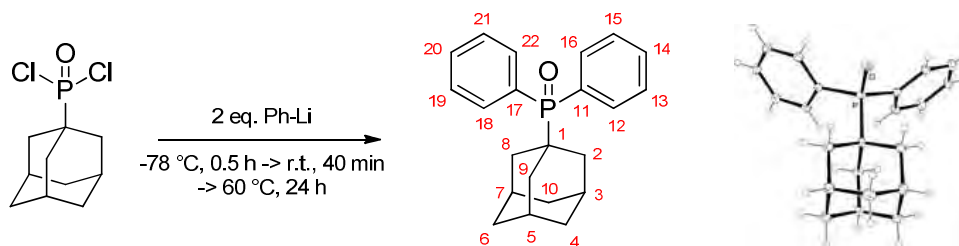
1.2 mL of distilled water was added carefully drop by drop with a pipette and all colourless solution turned into a viscous white liquid. It was extracted with 25 mL of DCM and dried over MgSO_4 . The solvent was evaporated to get a pure 1-hydroxydiamantane (0.051 g, 99%).

Mw: 204.31

^1H NMR (600 MHz, 298 K, CDCl_3) δ =1.96-1.91 (m, 3H; CH; H-2,6,12), 1.81-1.77 (m, 1H; CH; H-9), 1.77-1.73 (t, 6H; CH_2 ; H-3,5,13), 1.73-1.65 (m, 9H; CH, CH_2 ; H-1,7,8,10,11,14), 1.38 (br s, 1H; OH) ppm

^{13}C NMR (151 MHz, 298 K, CDCl_3): δ =67.69 (s, 1C; C_q ; C-4), 45.80 (s, 3C; CH_2 ; C-8,10,14), 39.99 (s, 3C; CH; C-2,6,12), 37.33 (s, CH_2 ; 3C; C-3,5,13), 36.49 (s, 3C; CH; C-1,7,11), 25.76 (s, 1C; CH; C-9) ppm.

HR-MS: m/z (%): calc. for $\text{C}_{14}\text{H}_{20}\text{O}$: 204.151; found: 204.152.

m) 1-Adamantyldiphenylphosphine oxide (**191**)

1-Adamantyldiphosphonic dichloride (1.012 g, 4.0 mmol) and 15 mL of freshly distilled dry THF were placed under argon in a 50 mL-flask equipped with a reflux system. It was cooled to $-78\text{ }^{\circ}\text{C}$ and phenyllithium (4.5 mL, 1.8 M in dibutyl ether, 8.0 mmol, 2 eq.) was slowly added with a syringe and stirred for 0.5 h at the same temperature, for 40 min at r.t., and for 24 h at $60\text{ }^{\circ}\text{C}$.

Workup:

10 mL of distilled water was carefully added with a pipette and two phases were obtained. The water phase was extracted with diethyl ether (3x20 mL) and DCM (3x20 mL). The combined organic phases were dried over MgSO_4 . The solvent was evaporated to get a white solid crude product.

Purification:

Purification by column chromatography on silica gel was performed first with pentane eluent, and then diethyl ether:ethanol (9:1). A second column chromatography on silica gel was done with diethyl ether:methanol (9:1) that unfortunately failed to remove all the impurities. Phosphine oxide **191** was then recrystallized in warm methanol at $60\text{ }^{\circ}\text{C}$ to give pure 1-adamantyldiphenylphosphine oxide (0.772 g, 57%).

Mw: 336.41.

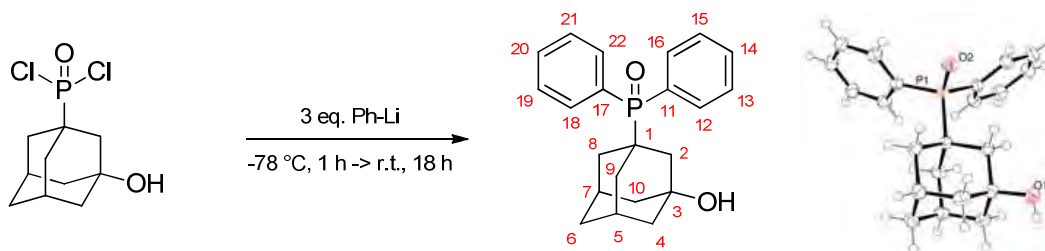
^1H NMR (400 MHz, 296 K, CDCl_3): δ =8.06-7.91 (m, 4H; CH; H-12,16,18,22), 7.63-7.43 (m, 6H; CH; H-13,14,15,19,20,21), 2.03-1.88 (m, 9H; CH, CH_2 ; H-2,3,5,7,8,9), 1.80-1.60 (m, 6H; CH_2 ; H-4,6,10) ppm.

^{31}P NMR (162 MHz, 296 K, CDCl_3 , H_3PO_4 external standard): δ =34.30 ppm.

^{13}C NMR (75 MHz, 300 K, CDCl_3): δ =132.42 (d, $^2J(\text{C,P})=7.9$ Hz, 4C; CH; C-12,16,18,22), 131.52 (d, $^4J(\text{C,P})=2.6$ Hz, 2C; CH; C-14,20), 130.75 (d, $^1J(\text{C,P})=90.0$ Hz, 1C; C_q ; C-11/17), 128.35 (d, $^3J(\text{C,P})=10.9$ Hz, 4C; CH; C-13,15,19,21), 37.16 (d, $^1J(\text{C,P})=72.5$ Hz, 1C; C_q ; C-1), 36.57 (d, $^4J(\text{C,P})=1.3$ Hz, 3C; CH_2 ; C-4,6,10), 35.50 (d, $^2J(\text{C,P})=1.8$ Hz, 3C; CH_2 ; C-2,8,9), 27.66 (d, $^3J(\text{C,P})=10.3$ Hz, 3C; CH; C-3,5,7) ppm.

HR-MS: m/z (%): calc. for $\text{C}_{22}\text{H}_{25}\text{PO}$: 336.164; found: 336.164.

Elem. Analysis: calc.: C 78.55, H 7.49; found: C 78.44, H 7.58.

n) (3-Hydroxyadamant-1-yl)diphenylphosphine oxide (**192**)

(3-Hydroxyadamant-1-yl)phosphonic dichloride (0.269 g, 1.0 mmol) and 9 mL of freshly distilled dry THF were placed under argon in a 2-neck-25 mL-flask. It was cooled to -78°C and phenyllithium (1.7 mL, 1.8 M in dibutyl ether, 3.0 mmol, 3 eq.) was slowly added with a syringe. The mixture was stirred for 1 h at the same temperature, and for 18 h at r.t. The clear yellow solution turned into dark brown solution after several minutes. At the end of reaction, the reaction mixture has turned brown cloudy.

Workup:

4.5 mL of distilled water was added carefully with a pipette and two clear phases were obtained. The water phase was extracted with 30 mL of diethyl ether and 30 mL of DCM. The combined organic phases were dried over MgSO_4 , and the solvent was evaporated. A yellow sticky crude compound (0.3020 g) was obtained.

Purification:

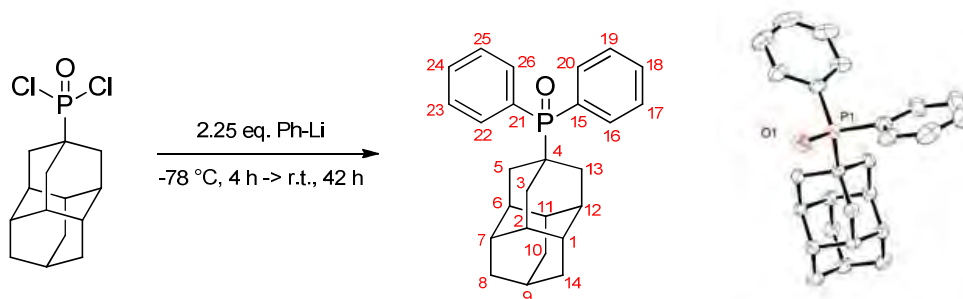
Phosphine oxide **192** was recrystallized in DCM/hexane (2:1) for overnight to get crystals and sticky impurities that could not be separated (0.269 g, 76%).

Mw: 352.41.

^1H NMR (600 MHz, 294 K, CDCl_3): δ =7.98-7.93 (m, 4H; CH; H-12,16,18,22), 7.56-7.51 (m, 2H; CH; H-14,20), 7.51-7.45 (m, 4H; CH; H-13,15,19,21), 2.28-2.21 (m, 2H; CH; H-5,7), 1.96 (s, 1H; OH), 1.89 (d, J =5.4 Hz, 2H; CH_2 ; H-2), 1.87-1.75 (m, 4H; CH_2 ; H-4,10), 1.66 (AB_q , 4H, $\Delta\delta_{\text{AB}}$ =0.03, J_{AB} =12 Hz; CH_2 ; H-8,9), 1.55 (s, 2H; CH_2 ; H-6) ppm.

^{31}P NMR (243 MHz, 294 K, CDCl_3): δ = 32.38 ppm.

^{13}C NMR (151 MHz, 294 K, CDCl_3): δ =132.35 (d, $^2J(\text{C},\text{P})$ =8.4 Hz, 4C; CH; C-12,16,18,22), 131.74 (d, $^4J(\text{C},\text{P})$ =2.9 Hz, 2C; CH; C-14,20), 130.33 (d, $^1J(\text{C},\text{P})$ =91.1 Hz, 2C; C_q ; C-11,17), 128.49 (d, $^3J(\text{C},\text{P})$ =11.1 Hz, 4C; CH; C-13,15,19,21), 68.12 (d, $^3J(\text{C},\text{P})$ =12.5 Hz, 1C; C_q ; C-3), 44.39 (s, 2C; CH_2 ; C-8,9), 43.13 (s, 1C; CH_2 ; C-2), 40.37 (d, $^1J(\text{C},\text{P})$ =72.0 Hz, 1C; C_q ; C-1), 35.05 (s, 1C; CH_2 ; C-6), 34.31 (s, 2C; CH_2 ; C-4,10), 30.25 (d, $^3J(\text{C},\text{P})$ =11.3 Hz, 2C; CH; C-5,7) ppm.

o) 4-Diamantylidiphenylphosphine oxide (**193**)

4-Diamantylphosphonic dichloride (0.122 g, 0.4 mmol) and 1.5 mL of freshly distilled dry THF were placed under argon in a 5 mL-flask. It was cooled to $-78\text{ }^{\circ}\text{C}$ and phenyllithium (0.5 mL, 1.8 M in dibutyl ether, 0.9 mmol, 2.25 eq.) was slowly added with a syringe. The mixture was stirred for 4 h at the same temperature, and for 42 h at r.t.

Workup:

1 mL of distilled water was added carefully with a pipette, 3 mL of saturated NH_4Cl , and 10 mL of diethyl ether. The water phase was extracted with diethyl ether (2x10 mL) and DCM (3x10 mL). The combined organic phases were dried over MgSO_4 and the solvent was evaporated.

Purification:

It was recrystallized in warm methanol at $60\text{ }^{\circ}\text{C}$ to give a pure 4-diamantylidiphenylphosphine oxide (0.042 g, 31%).

Mw: 338.48.

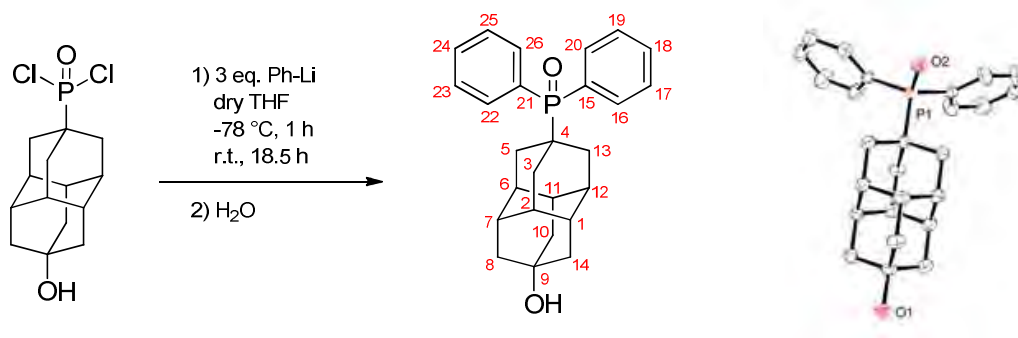
^1H NMR (400 MHz, 295 K, CDCl_3): δ =8.03-7.91 (m, 4H; CH; H-16,20,22,26), 7.58-7.42 (m, 6H; CH; H-17,18,19,23,24,25), 2.00-1.85 (m, 6H; CH_2 ; H-3,5,13), 1.80 (br s, 3H; CH; H-2,6,12), 1.75 (m, 1H; CH_3 ; H-9), 1.72-1.55 (m, 9H; CH, CH_2 ; H-1,7,8,10,11,14) ppm.

^{31}P NMR (162 MHz, 296 K, CDCl_3 , H_3PO_4 external standard): δ =35.02 ppm.

^{13}C NMR (101 MHz, 296 K, CDCl_3): δ =132.38 (d, $^2J(\text{C},\text{P})=8.1$ Hz, 4C; CH; C-16,20,22,26), 131.56 (d, $^4J(\text{C},\text{P})=2.6$ Hz, 2C; CH; C-18,24), 130.68 (d, $^1J(\text{C},\text{P})=73.1$ Hz, 1C; C_q ; C-15/21), 128.35 (d, $^3J(\text{C},\text{P})=10.8$ Hz, 4C; CH; C-17,19,23,25), 37.71 (d, $^2J(\text{C},\text{P})=1.5$ Hz, 3C; CH_2 ; C-3,5,13), 36.84 (d, $^3J(\text{C},\text{P})=11.3$ Hz, 3C; CH; C-2,6,12), 36.44 (s, 6C; CH, CH_2 ; C-1,7,8,10,11,14), 35.22 (d, $^1J(\text{C},\text{P})=72.8$ Hz, 1C; C_q ; C-4), 25.48 (s, 1C; CH; C-9) ppm.

HR-MS: m/z (%): calc. for $\text{C}_{22}\text{H}_{25}\text{PO}$: 388.196; found: 388.194.

Elem. Analysis: calc.: C 80.38, H 7.52; found: C 77.55, H 7.66.

p) (9-Hydroxydiamant-4-yl)diphenylphosphine oxide (**194**)

(9-Hydroxydiamant-4-yl)phosphonic dichloride (0.161 g, 0.5 mmol) and 4.5 mL of freshly distilled dry THF were placed under argon in a 2-neck-50 mL-flask. It was cooled to -78°C and phenyllithium (0.84 mL, 1.8 M in dibutyl ether, 1.5 mmol, 3 eq.) was slowly added with a syringe. The mixture was stirred for 1 h at the same temperature, and for 18.5 h at r.t. The clear brown solution turned into reddish brown slurry when it reached r.t. At the end of reaction, the reaction mixture had turned ivory slurry.

Workup:

4 mL of distilled water was added carefully with a pipette and two clear phases were obtained. The water phase was extracted with 40 mL of diethyl ether and 40 mL of DCM. The combined organic phases were dried over MgSO_4 and the solvent was removed. A white solid crude product was obtained.

Purification:

The purification with column chromatography failed and recrystallization in warm MeOH at 60°C was achieved. The crystals were rinsed with cold MeOH, we got colourless crystals (0.008 g, 4%). Repeated the experiment with the same condition improved the yield (0.020 g, 10%).

Mw: 404.48.

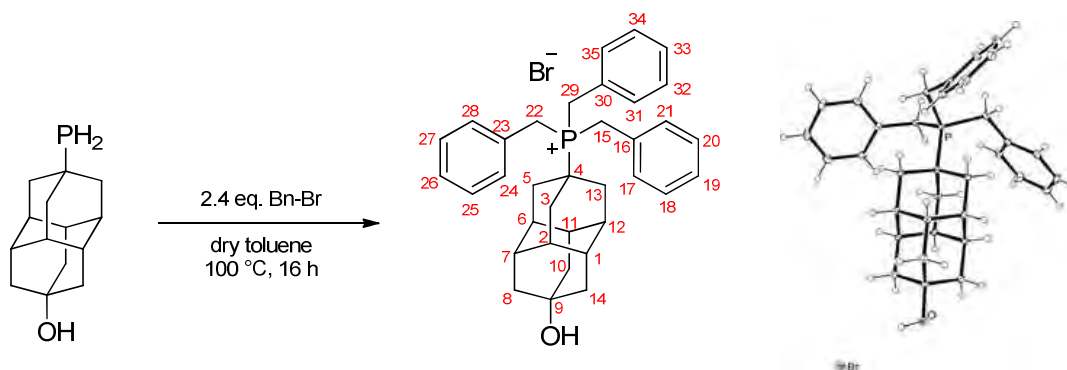
^1H NMR (400 MHz, 270 K, CDCl_3): δ =8.20-7.86 (m, 4H; CH; H-16,20,22,26), 7.71-7.42 (m, 6H; CH; H-17,18,19,23,24,25), 2.05 (br s; OH), 2.01-1.92 (m, 6H; CH_2 ; H-8,10,14), 1.88 (br s, 3H; CH; H-1,7,11), 1.81 (br s, 3H; CH; H-2,6,12), 1.77-1.59 (m, 6H; CH_2 ; H-3,5,13) ppm.

^{31}P NMR (162 MHz, 270 K, CDCl_3): δ =35.96 ppm.

^{13}C NMR (101 MHz, 270 K, CDCl_3): δ =132.39 (d, $^2J(\text{C,P})=8.1$ Hz, 4C; CH; C-16,20,22,26), 131.90 (d, $^4J(\text{C,P})=2.5$ Hz, 2C; CH; C-18,24), 128.54 (d, $^3J(\text{C,P})=11.0$ Hz, 4C; CH; C-17,19,23,25), 67.11 (s, 1C; C_q ; C-4/9), 45.07 (s, 3C; CH_2 ; C-3,5,13), 38.76 (s, 3C; CH; C-1,7,11), 35.65 (d, $^3J(\text{C,P})=11.2$ Hz, 3C; CH; C-2,6,12), 35.35 (s, 3C; CH_2 ; C-8,10,14) ppm.

HR-MS: m/z (%): calc. for $C_{26}H_{29}O_2P$: 404.191; found: 404.190.

q) *Tribenzyl(9-hydroxydiamant-4-yl)phosphonium bromide (195)*



9-Phosphinodiamantan-4-ol (0.050 g, 0.21 mmol) and dry toluene (2 mL) were placed under argon in a 5-mL-flask equipped with a reflux system. Benzylbromide (0.06 mL, 0.5 mmol, 2.4 eq.) was slowly added at r.t. The resulting colourless solution was heated at 100 °C for 16 h. A white precipitate appeared.

Workup:

The white precipitate was filter, rinsed with toluene and diethyl ether, and dried in air.

Purification:

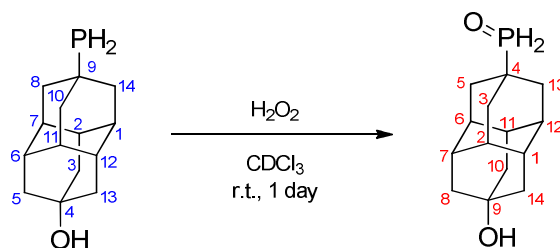
Purification by column chromatography on silica gel with eluent diethyl ether:methanol (3:1) gave tribenzyl(9-hydroxydiamantan-4-yl)phosphonium bromide (0.020 g, 16%). The crystals were grown in ethanol.

Mw: 587.57.

1H NMR (600 MHz, 300 K, MeOD) δ =7.43-7.37 (m, 9H; CH; H-18,19,20,25,26,27,32,33,34), 7.22-7.17 (m, 6H; CH; H-17,21,24,28,31,35), 3.84 (d, J =13.3 Hz, 6H; CH_2 ; H-15,22,29), 1.99-1.94 (m, 6H; CH_2 ; H-8,10,14), 1.94-1.90 (m, 3H; CH; H-1,7,11), 1.88-1.83 (m, 3H; CH; H-2,6,12), 1.69 (d, J =2.7 Hz, 6H; CH_2 ; H-3,5,13) ppm.

^{31}P NMR (243 MHz, 300 K, MeOD): δ =27.51 ppm.

^{13}C NMR (151 MHz, 300 K, MeOD): δ =132.08 (d, $^3J(C,P)$ =4.8 Hz, 6C; CH; C-17,21,24,28,31,35), 130.72 (d, $^4J(C,P)$ =2.3 Hz, 6C; CH; C-18,20,25,27,32,34), 129.81 (d, $^5J(C,P)$ =3.1 Hz, 3C; CH; C-19,26,33), 129.73 (d, $^2J(C,P)$ =8.2 Hz, 2C; Cq; C-16,23 or 30), 66.87 (s, 1C; Cq; C-9), 45.29 (s, 3C; CH_2 ; C-3,5,13), 39.40 (s, 3C; CH; C-1,7,11), 36.76 (d, $^3J(C,P)$ =10.3 Hz, 3C; CH; C-2,6,12), 35.49 (s, 3C; CH_2 ; C-8,10,14), 25.06 (d, $^1J(C,P)$ =41.3 Hz, 3C; CH_2 ; C-15,22,29) ppm.

r) (9-Hydroxydiamant-4-yl)phosphine oxide (**196**)

9-Phosphinodiamantan-4-ol (0.005 g, 0.02 mmol) was placed in NMR tube with CDCl_3 . One drop of H_2O_2 30% was added at r.t. and shaken gently. It was then leaved for overnight.

Workup:

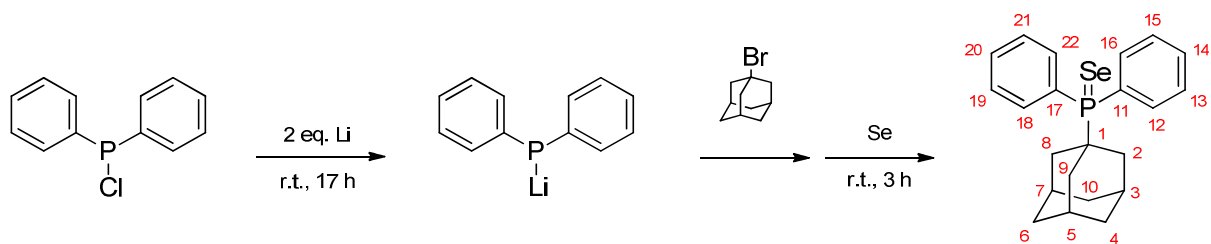
Distilled water (0.5 mL) was added with a pipette. It was extracted with 0.5 mL of CDCl_3 and dried over MgSO_4 . It was filtered to get colourless solution containing the pure compound **196**.

Mw: 252.29.

^1H NMR (600 MHz, 300 K, CDCl_3): δ =6.67 (d, $^1J(\text{H},\text{P})=450.0$ Hz, 2H; PH), 2.01-1.96 (m, 2H; CH; H-1,7), 1.96-1.91 (m, 3H; CH; H-6,11,12), 1.90-1.85 (dd, 4H; CH_2 ; H-8,14), 1.81-1.78 (m, 1H; OH), 1.78-1.76 (d, $J=3.6$ Hz, 4H; CH_2 ; H-5,13), 1.76-1.73 (t, 2H; CH_2 ; H-10), 1.73-1.70 (m, 1H; CH; H-2), 1.70-1.68 (dd, 2H; CH_2 ; H-3) ppm.

^{31}P NMR (243 MHz, 300 K, CDCl_3): δ =27.60 (t, $^1J(\text{P},\text{H})=450.0$ Hz) ppm.

^{13}C NMR (126 MHz, 300 K, CDCl_3): δ =66.99 (s, 1C; C_q ; C-9), 45.84 (s, 1C; CH_2 ; C-3), 45.17 (d, $^2J(\text{C},\text{P})=2.0$ Hz, 2C; CH_2 ; C-5,13), 40.04 (s, 1C; CH; C-11), 39.01 (d, $^4J(\text{C},\text{P})=1.5$ Hz, 2C; CH; C-1,7), 37.36 (s, 1C; CH_2 ; C-10), 36.55 (s, 1C; CH; C-2), 35.26 (d, $^3J(\text{C},\text{P})=13.3$ Hz, 2C; CH; C-6,12), 34.59 (s, 2C; CH_2 ; C-8,14), 31.61 (d, $^1J(\text{C},\text{P})=74.6$ Hz, 1C; C_q ; C-4) ppm.

s) 1-Adamantyldiphenylphosphine selenide (**197**)

In 2-neck-100-mL-flask containing dry THF (20 mL) and lithium metal (0.090 g), distilled chlorodiphenylphosphine (0.9 mL, 5.0 mmol) was added under argon at r.t. for 17 h. The reaction mixture turned clear orange solution lithiumdiphenylphosphanide (Li-PPh₂) which is air sensitive. The remaining Li (0.020 g) was removed with a forcep. Two equivalents (0.070 g, 2.0 mmol) of Li were consumed during the reaction.

The 1-bromoadamantane (1.076 g, 5.0 mmol) in 20 mL of dry THF was slowly added (1 drop/second) during 20 min using addition funnel into reaction mixture at $-78\text{ }^{\circ}\text{C}$ and stirred for 1 h at the same temperature and for 7 days at r.t.

Selenium powder (0.3945 g, 5.0 mmol) was added at r.t. and the clear orange solution turned into clear black. The mixture was stirred under argon for 3 h.

Workup:

The solvent was evaporated. Distilled water was added. It was extracted three times with DCM, dried over MgSO₄, then was filtered. The solvent was evaporated to get 1.948 g of light yellow oil.

Purification:

5 mL of diethyl ether was added and a white solid appeared. The solid was separated, rinsed with pentane, and dried in air (0.679 g, 34%). After several days it turned into a reddish brown solid without alteration.

Mw: 399.37

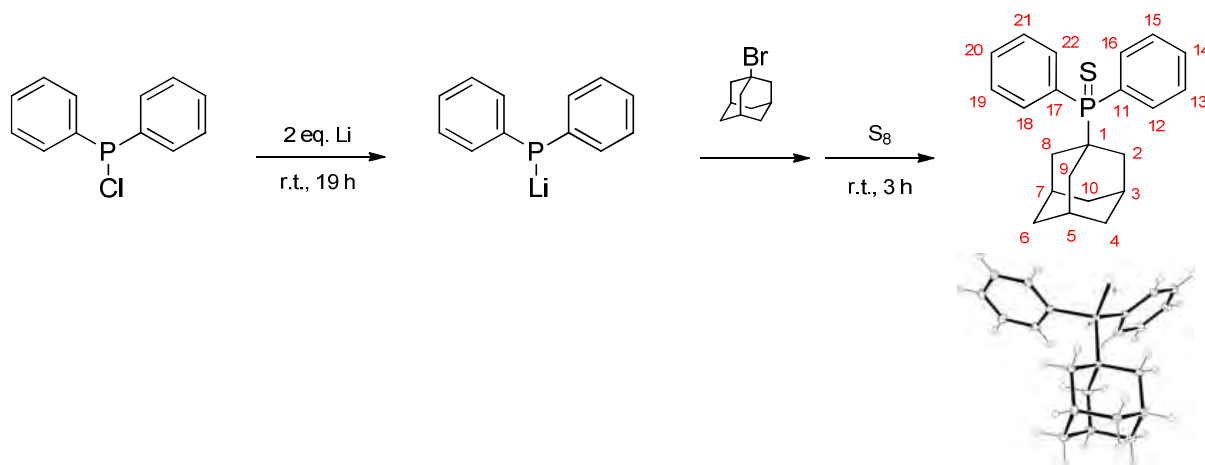
¹H NMR (300 MHz, 297 K, CDCl₃): δ =8.10-7.96 (m, 4H; CH; H-12,16,18,22), 7.55-7.38 (m, 6H; CH; H-13,14,15,19,20,21), 2.09-1.96 (m, 9H; CH, CH₂; H-2,3,5,7,8,9), 1.76-1.59 (m, 6H; CH₂; H-4,6,10) ppm.

³¹P NMR (121 MHz, 297 K, CDCl₃, H₃PO₄ external standard): δ =53.66 (t, ¹J_{P-Se} = 712.3 Hz) ppm.

¹³C NMR (75 MHz, 297 K, CDCl₃): δ =134.05 (d, ²J(C,P)=8.9 Hz, 4C; CH; C-12,16,18,22), 131.32 (d, ⁴J(C,P)=2.9 Hz, 2C; CH; C-14,20), 129.29 (d, ¹J(C,P)=65.7 Hz, 2C; C_q; C-11,17), 128.24 (d, ³J(C,P)=11.3

Hz, 4C; CH; C-13,15,19,21), 38.70 (d, $^1J(\text{C,P})=40.6$ Hz, 1C; C_q; C-1), 36.85 (s, 3C; CH₂; C-2,8,9), 36.36 (s, 3C; CH₂; C-4,6,10), 28.32 (d, $^3J(\text{C,P})=10.4$ Hz, 3C; CH; C-3,5,7) ppm.

t) 1-Adamantyldiphenylphosphine sulphide (**198**)



In 2-neck-100-mL-flask containing 20 mL of dry THF and lithium metal (0.240 g), distilled chlorodiphenylphosphine (0.9 mL, 5.0 mmol) was added under argon at r.t. for 19 h. The reaction mixture turned clear orange solution lithiumdiphenylphosphanide (Li-PPh₂) which is air sensitive. The remaining Li (0.170 g) was removed with a forcep. Two equivalents (0.070 g, 2.0 mmol) of Li were consumed during the reaction.

The 1-bromoadamantane (1.076 g, 5.0 mmol, 1 eq.) in dry THF (10 mL) was added slowly (1 drop/second) during 20 min using addition funnel into reaction mixture at -78 °C and stirred for 2 h at the same temperature and for 5 days at r.t.

Sulfur powder (0.160 g, 5.0 mmol, 1 eq.) was added at r.t. and the clear orange solution turned into clear yellow. It was keep stirred under argon for 3 h.

Workup:

The solvent was evaporated. 60 mL of diethyl ether was added, followed with distilled water to remove lithium halide. The mixture was extracted three times with DCM, dried over MgSO₄, then was filtered. White crystals appeared (0.793 g, 45%). It was characterized by X-Ray diffraction analysis.

(Note: using the sodium metal, first step for 2.5 days, in place of lithium metal afford 18% of pure compound.)

Mw: 352.47.

^1H NMR (300 MHz, 300 K, CDCl_3): δ =8.12-7.99 (m, 4H; CH; H-12,16,18,22), 7.55-7.39 (m, 6H; CH; H-13,14,15,19,20,21), 2.08-1.95 (m, 9H; CH, CH_2 ; H-2,3,5,7,8,9), 1.76-1.59 (m, 6H; CH_2 ; H-4,6,10) ppm.

^{31}P NMR (121 MHz, 300 K, CDCl_3 , H_3PO_4 external standard): δ = 56.33 (t, $^1J(\text{P,C})=35.7$ Hz) ppm.

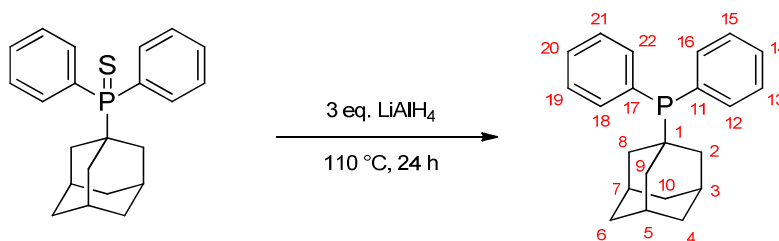
^{13}C NMR (75 MHz, 300 K, CDCl_3): δ =133.51 (d, $^2J(\text{C,P})=8.86$ Hz, 4C; CH; C-12,16,18,22), 131.29 (d, $^4J(\text{C,P})=2.9$ Hz, 2C; CH; C-14,20), 130.38 (d, $^1J(\text{C,P})=73.1$ Hz, 1C; C_q ; C-11/17), 128.23 (d, $^3J(\text{C,P})=11.2$ Hz, 4C; CH; C-13,15,19,21), 39.20 (d, $^1J(\text{C,P})=50.2$ Hz, 1C; C_q ; C-1), 36.42 (s, 6C; CH_2 ; C-2,4,6,8,9,10), 28.24 (d, $^3J(\text{C,P})=10.6$ Hz, 3C; CH; C-3,5,7) ppm.

HR-MS: m/z (%): calc. for $\text{C}_{22}\text{H}_{25}\text{PS}$: 352.142; found: 352.140.

Elem. Analysis: calc. C 74.97, H 7.15; found: C 74.89, H 7.06.

u) 1-Adamantyldiphenylphosphine (199)

Method A:

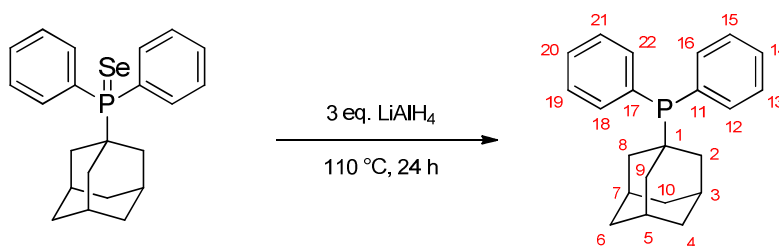


1-Adamantyldiphenylphosphine sulfide (0.053 g, 0.15 mmol), LiAlH_4 (0.017 g, 0.45 mmol, 3 eq.) and dry 1,4-dioxane (6 mL) were placed under argon in a Schlenk tube equipped with a reflux system. The mixture was heated under reflux for 24 h.

Workup:

The reaction mixture was cooled. It was filtered under argon using filter paper and rinsed with 3 mL of dry 1,4-dioxane to get a colourless filtrate. The solvent was evaporated. A very air sensitive white solid was obtained (0.029 g, 60%). Any contact with air oxidizes this 1-adamantyldiphenylphosphine to 1-adamantyldiphenylphosphine oxide.

Method B:



1-Adamantyldiphenylphosphine selenide (0.060 g, 0.15 mmol), LiAlH_4 (0.017 g, 0.45 mmol, 3 eq.) and dry 1,4-dioxane (6 mL) were placed under argon in a Schlenk tube equipped with a reflux system. The mixture was heated under reflux for 24 h.

Workup:

The reaction mixture was cooled. It was filtered under argon using filter paper and rinsed with 3 mL of dry 1,4-dioxane to get colourless filtrate. The solvent was evaporated. A very air sensitive white solid was obtained (0.029 g, 60%). Any contact with air oxidizes this 1-adamantyldiphenylphosphine to 1-adamantyldiphenylphosphine oxide.

Mw: 320.41.

^1H NMR (400 MHz, 270 K, CDCl_3): δ =7.66-7.57 (m, 4H; CH; H-12,16,18,22), 7.39-7.30 (m, 6H; CH; H-13,14,15,19,20,21), 1.99-1.91 (m, 3H; CH; H-3,5,7), 1.88-1.79 (t, 6H; CH_2 ; H-2,8,9), 1.75-1.61 (m, 6H; CH_2 ; H-4,6,10) ppm.

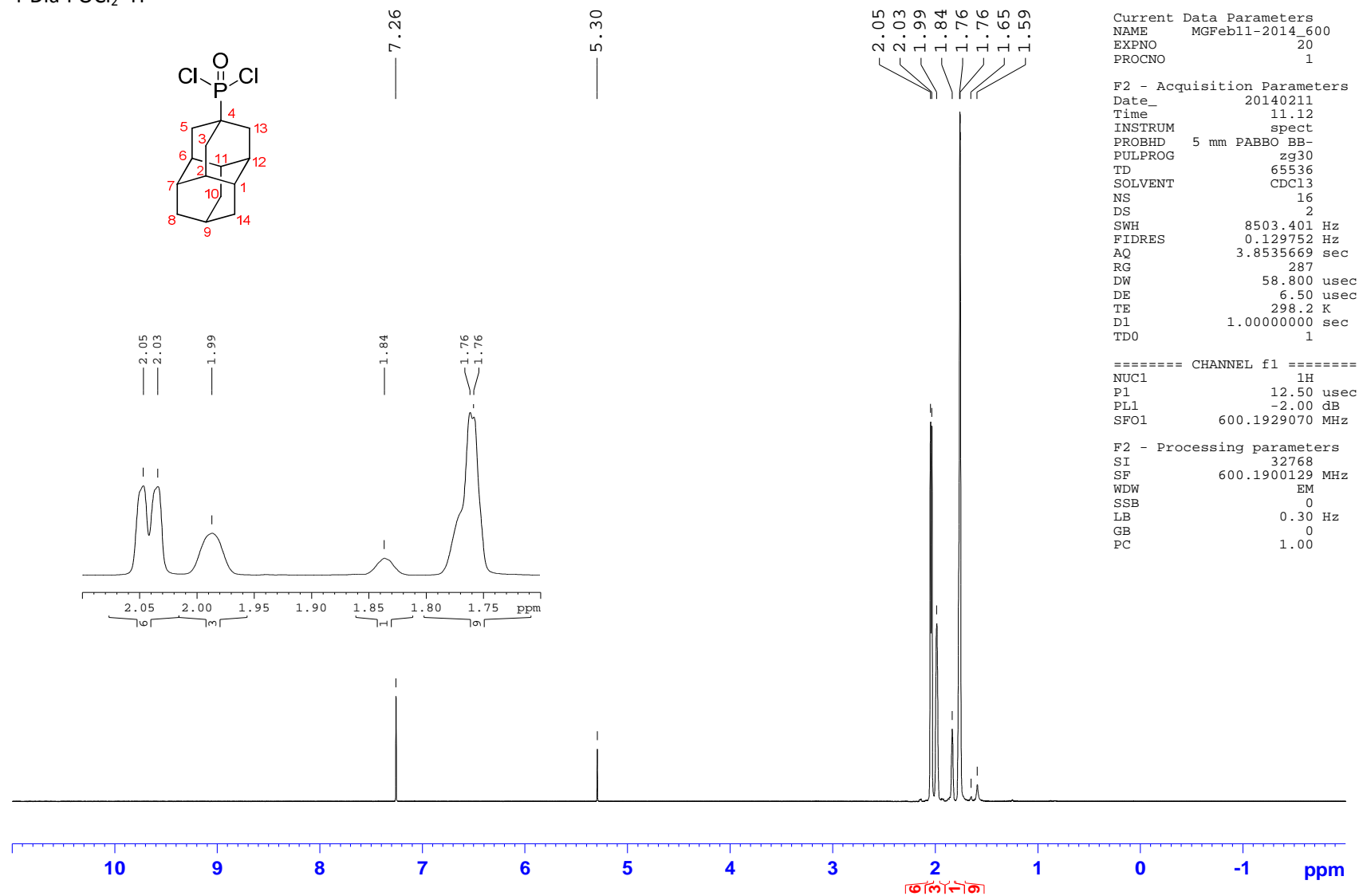
^{13}C NMR (101 MHz, 270 K, CDCl_3): δ =135.73 (d, $^1J(\text{C,P})=17.5$ Hz, 1C; C_q ; C-11/17), 135.14 (d, $^2J(\text{C,P})=20.0$ Hz, 4C; CH; C-12,16,18,22), 128.61 (s, 2C; CH; C-14,20), 128.08 (d, $^3J(\text{C,P})=7.2$ Hz, 4C; CH; C-13,15,19,21), 39.93 (d, $^2J(\text{C,P})=11.3$ Hz, 3C; CH_2 ; C-2,8,9), 36.92 (s, 3C; CH_2 ; C-4,6,10), 34.60 (d, $^1J(\text{C,P})=14.2$ Hz; 1C; C_q ; C-1), 28.79 (d, $^3J(\text{C,P})=9.0$ Hz, 3C; CH; C-3,5,7) ppm.

^{31}P NMR (162 MHz, 270 K, CDCl_3): δ =16.25 ppm.

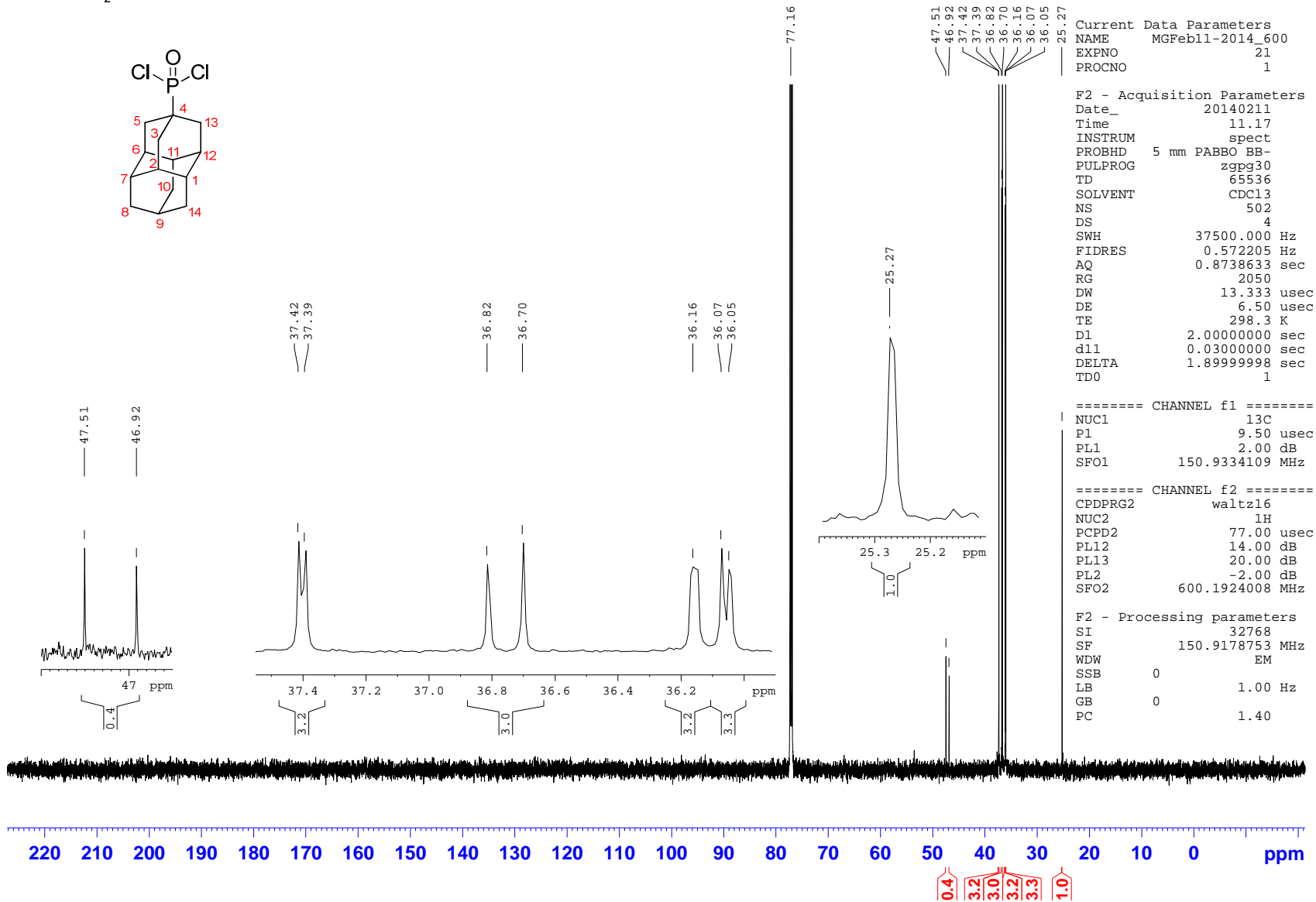
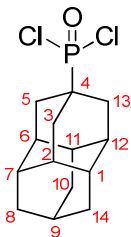
3. NMR Spectra

a) 4-Diamantylphosphonic acid dichloride (**22**)

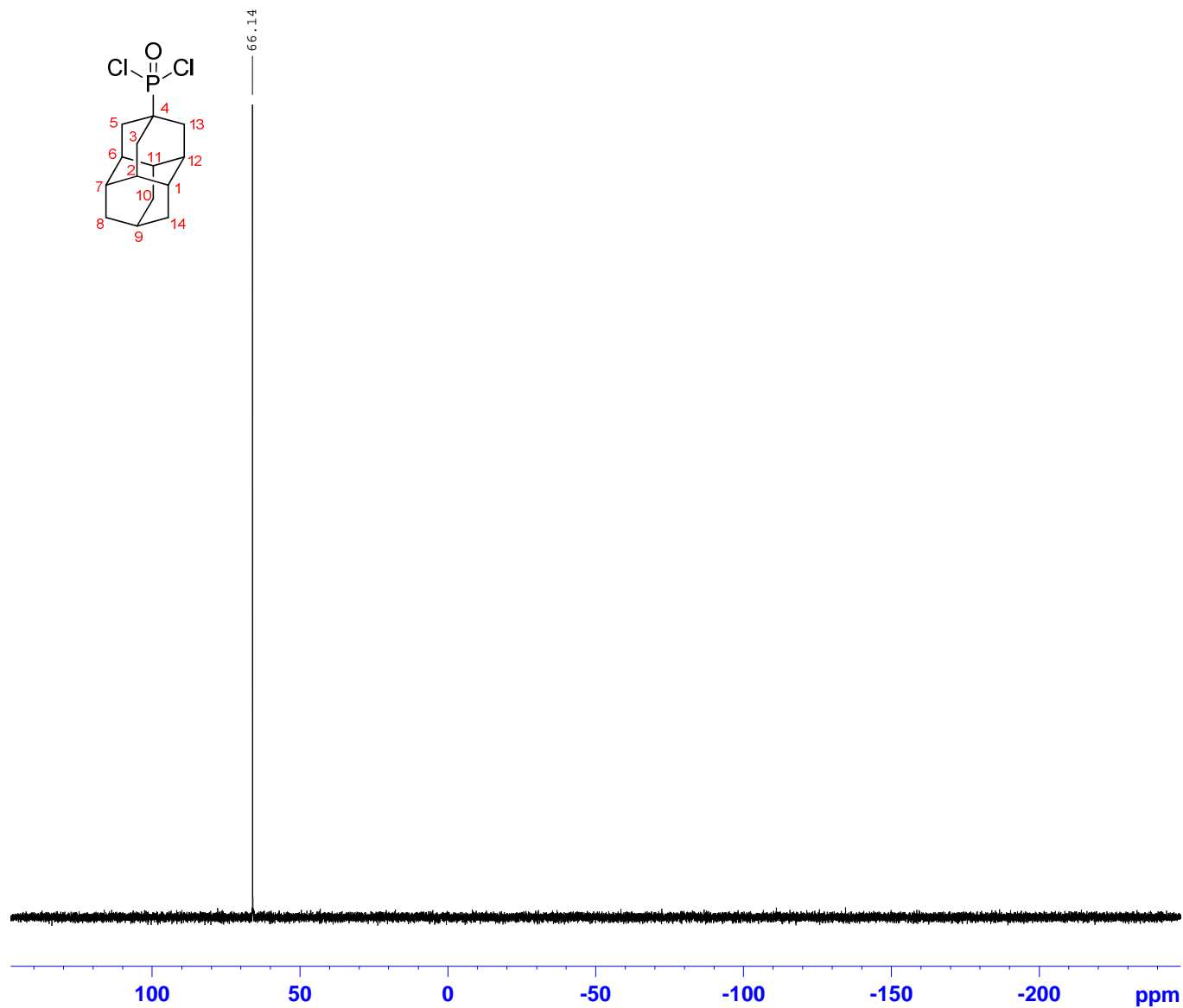
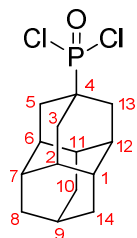
4-Dia-POCl₂ ¹H



4-Dia-POCl₂ ¹³C



4-Dia-POCl₂ ³¹P



```

Current Data Parameters
NAME      MGFeb11-2014_600
EXPNO     22
PROCNO    1

F2 - Acquisition Parameters
Date_     20140211
Time      11.45
INSTRUM   spect
PROBHD    5 mm PABBO BB-
PULPROG   zgpg30
TD         65536
SOLVENT   CDCl3
NS         16
DS         4
SWH        96153.844 Hz
FIDRES     1.467191 Hz
AQ         0.3408372 sec
RG         2050
DW         5.200 usec
DE         6.50 usec
TE         298.2 K
D1         2.00000000 sec
d11        0.03000000 sec
DELTA     1.89999998 sec
TDO        1

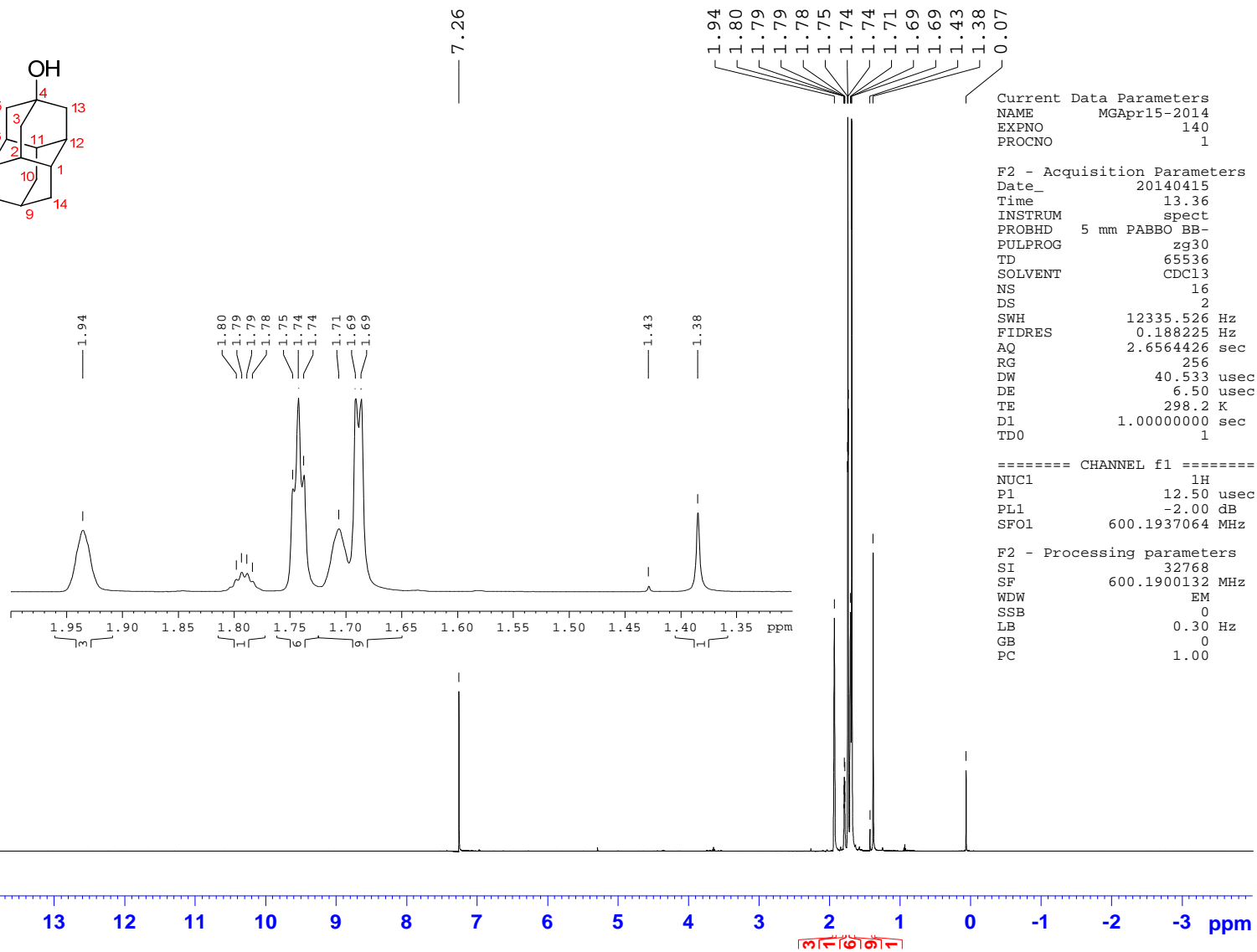
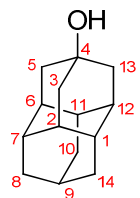
===== CHANNEL f1 =====
NUC1       31P
P1         11.00 usec
PL1        2.00 dB
SFO1       242.9492173 MHz

===== CHANNEL f2 =====
CPDPRG2    waltz16
NUC2       1H
PCPD2      77.00 usec
PL12       14.15 dB
PL13       20.00 dB
PL2        -2.00 dB
SFO2       600.1924008 MHz

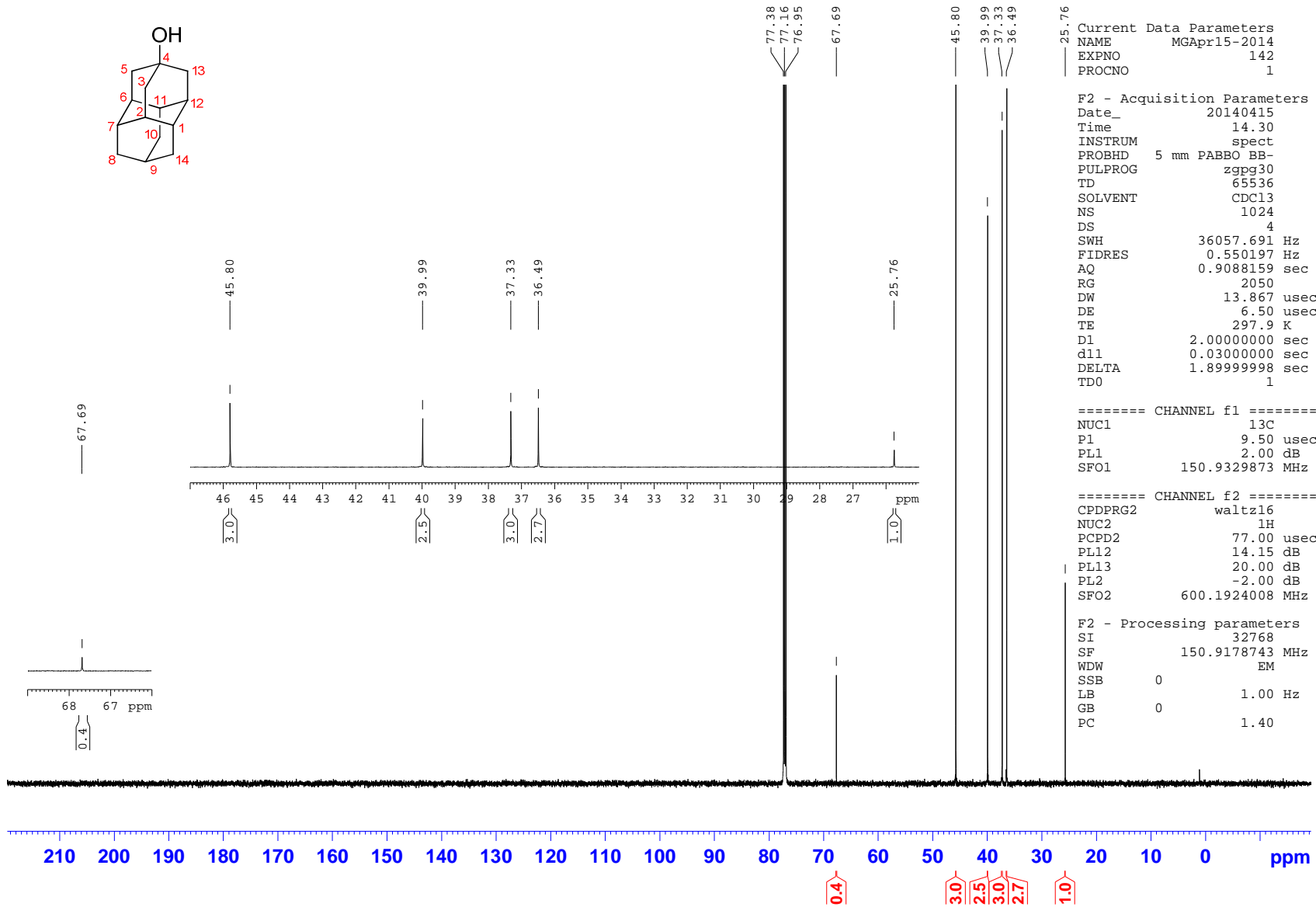
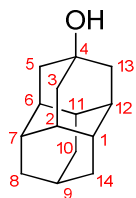
F2 - Processing parameters
SI         32768
SF         242.9613650 MHz
WDW        EM
SSB        0
LB         1.00 Hz
GB         0
PC         1.40
    
```

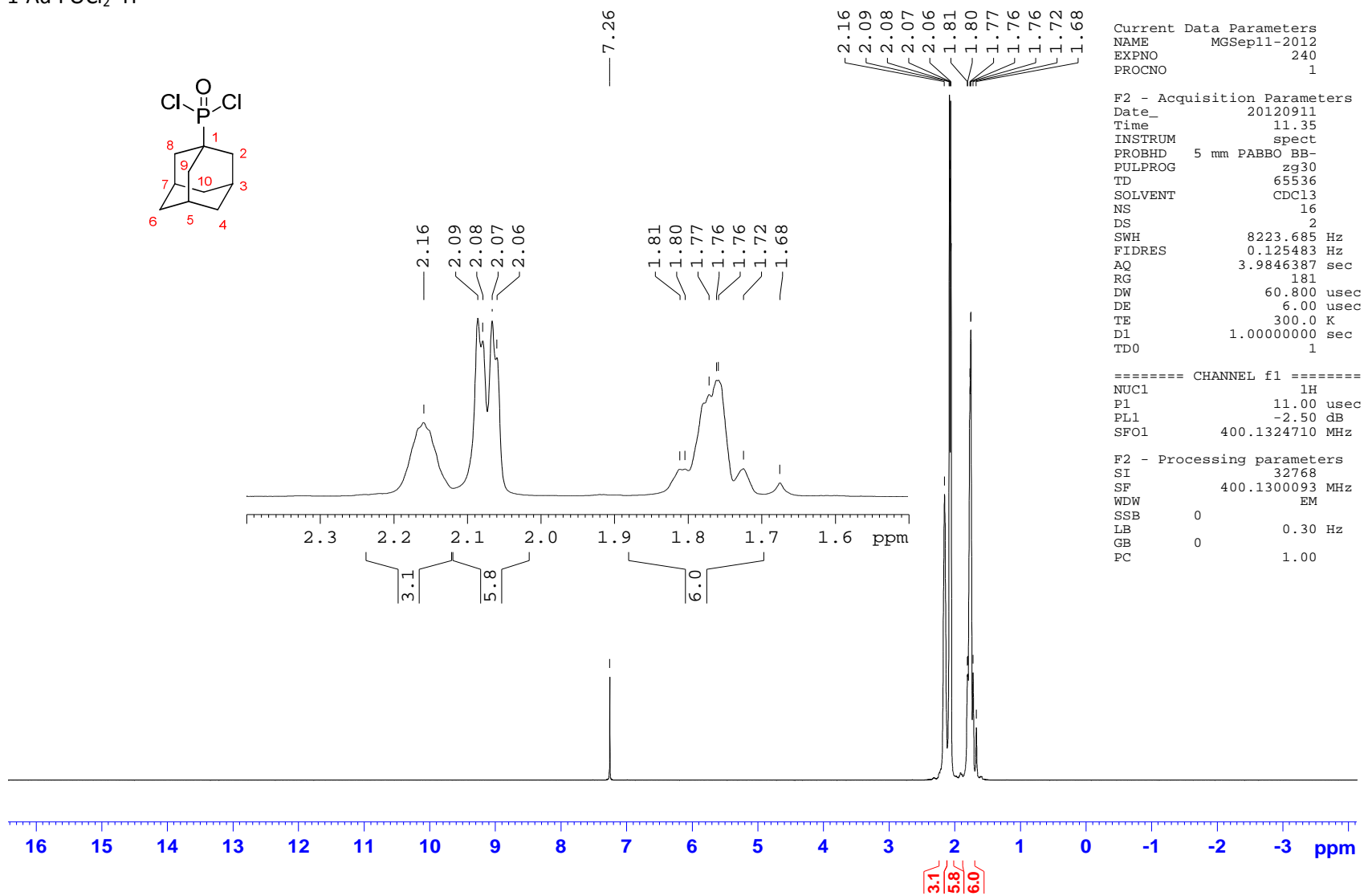
b) 4-Hydroxydiamantane (**48**)

4-OH-dia ¹H

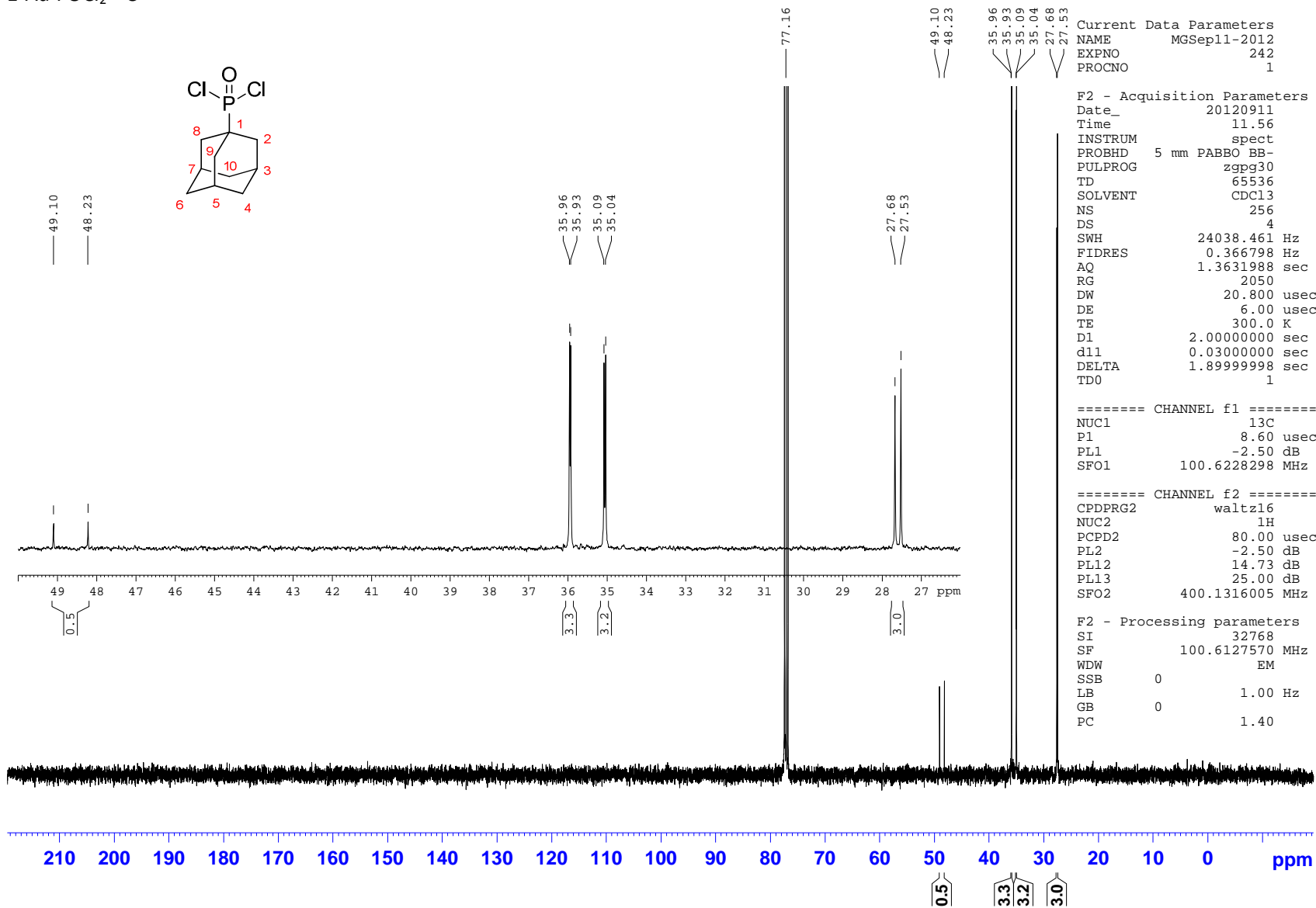


4-OH-dia ¹³C

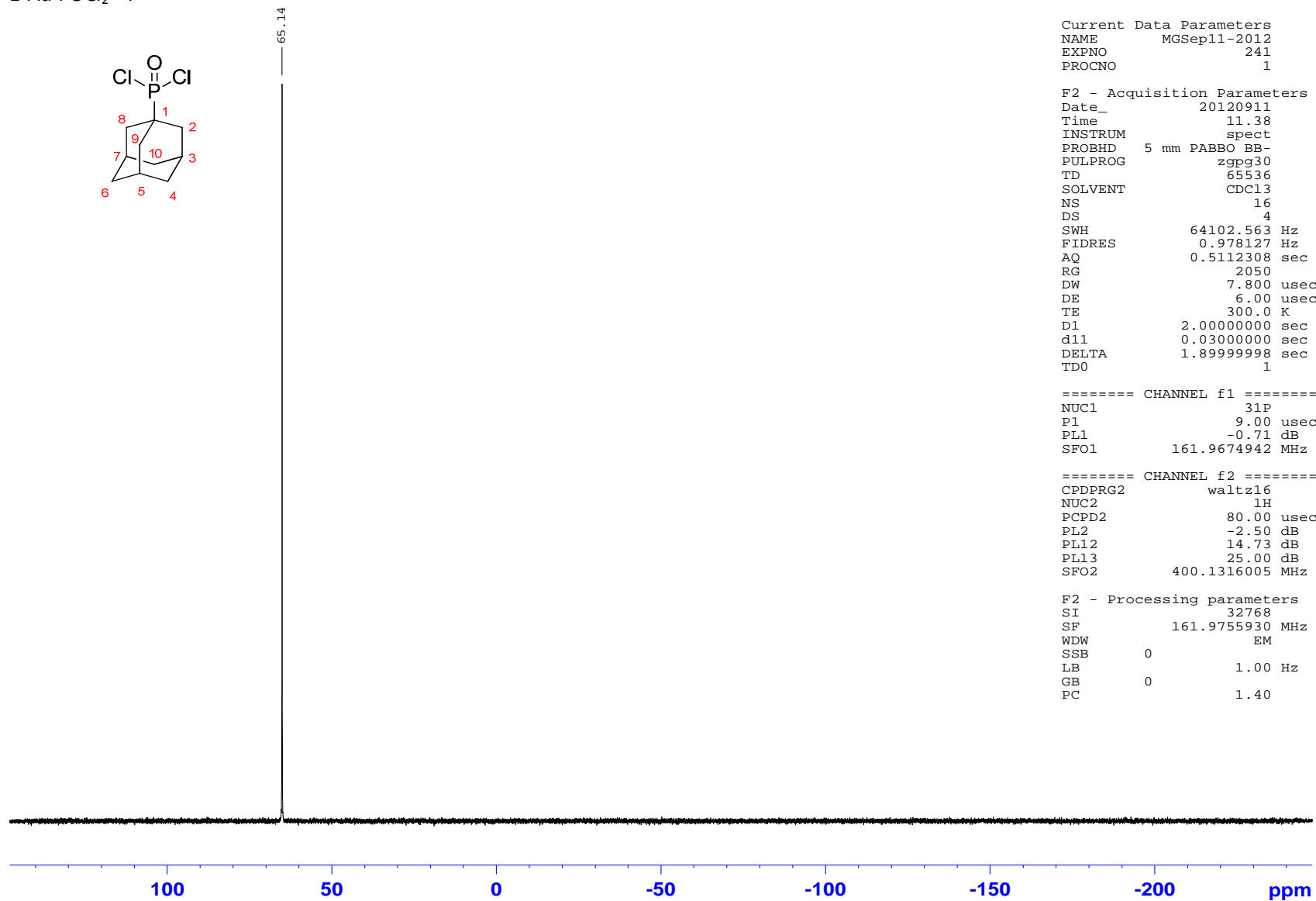
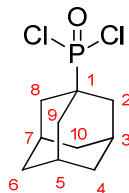


c) 1-Adamantylphosphonic dichloride (**126**)1-Ad-POCl₂ ¹H

1-Ad-POCl₂ ¹³C



1-Ad-POCl₂ ³¹P



```

Current Data Parameters
NAME      MGSep11-2012
EXPNO     241
PROCNO    1

F2 - Acquisition Parameters
Date_     20120911
Time      11.38
INSTRUM   spect
PROBHD    5 mm PABBO BB-
PULPROG   zgpg30
TD         65536
SOLVENT   CDCl3
NS         16
DS         4
SWH        64102.563 Hz
FIDRES     0.978127 Hz
AQ         0.5112308 sec
RG         2050
DW         7.800 usec
DE         6.00 usec
TE         300.0 K
D1         2.00000000 sec
d11        0.03000000 sec
DELTA     1.89999998 sec
TDO        1

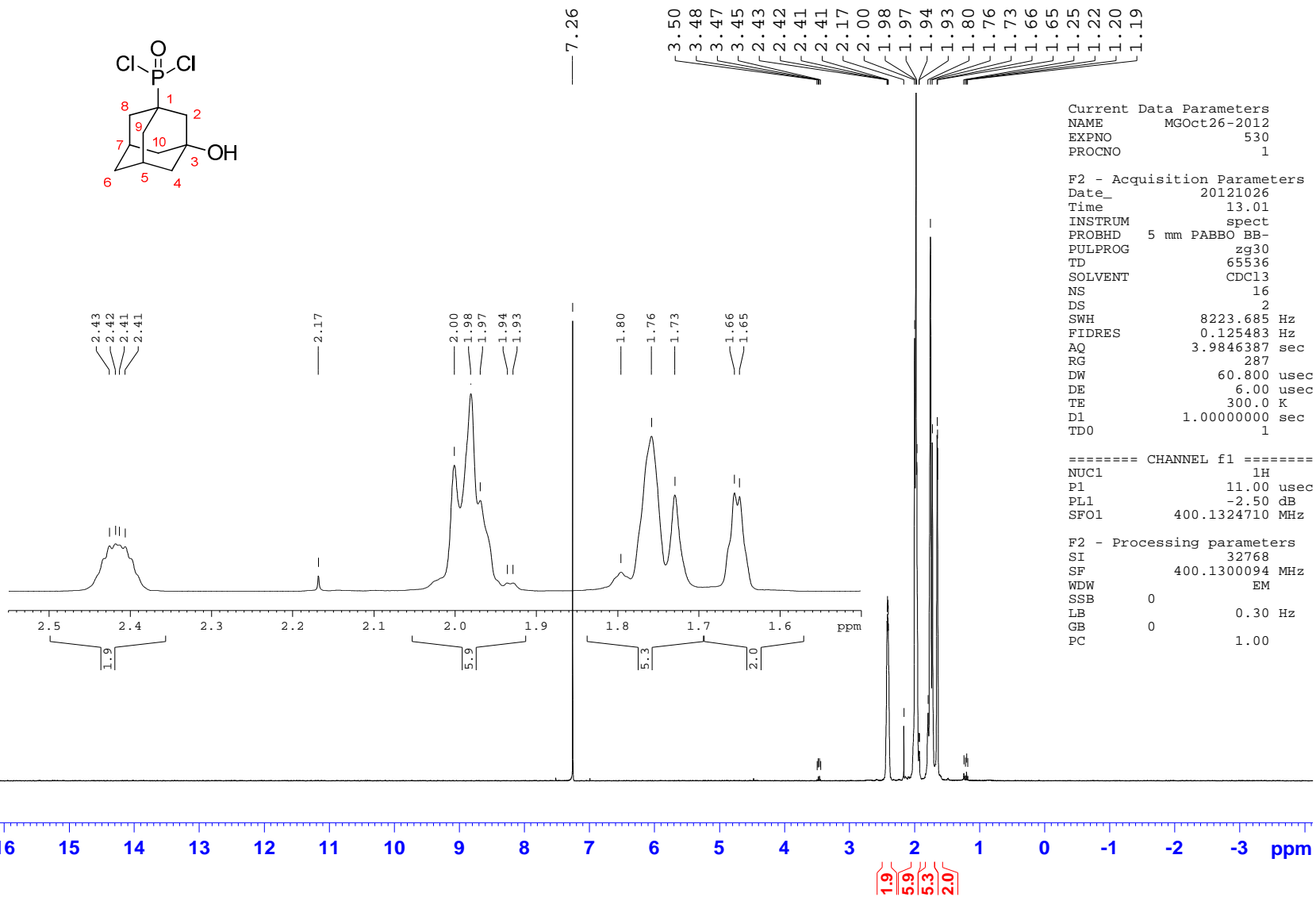
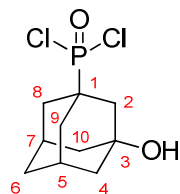
===== CHANNEL f1 =====
NUC1       31P
P1         9.00 usec
PL1        -0.71 dB
SFO1       161.9674942 MHz

===== CHANNEL f2 =====
CPDPRG2    waltz16
NUC2       1H
PCPD2      80.00 usec
PL2        -2.50 dB
PL12       14.73 dB
PL13       25.00 dB
SFO2       400.1316005 MHz

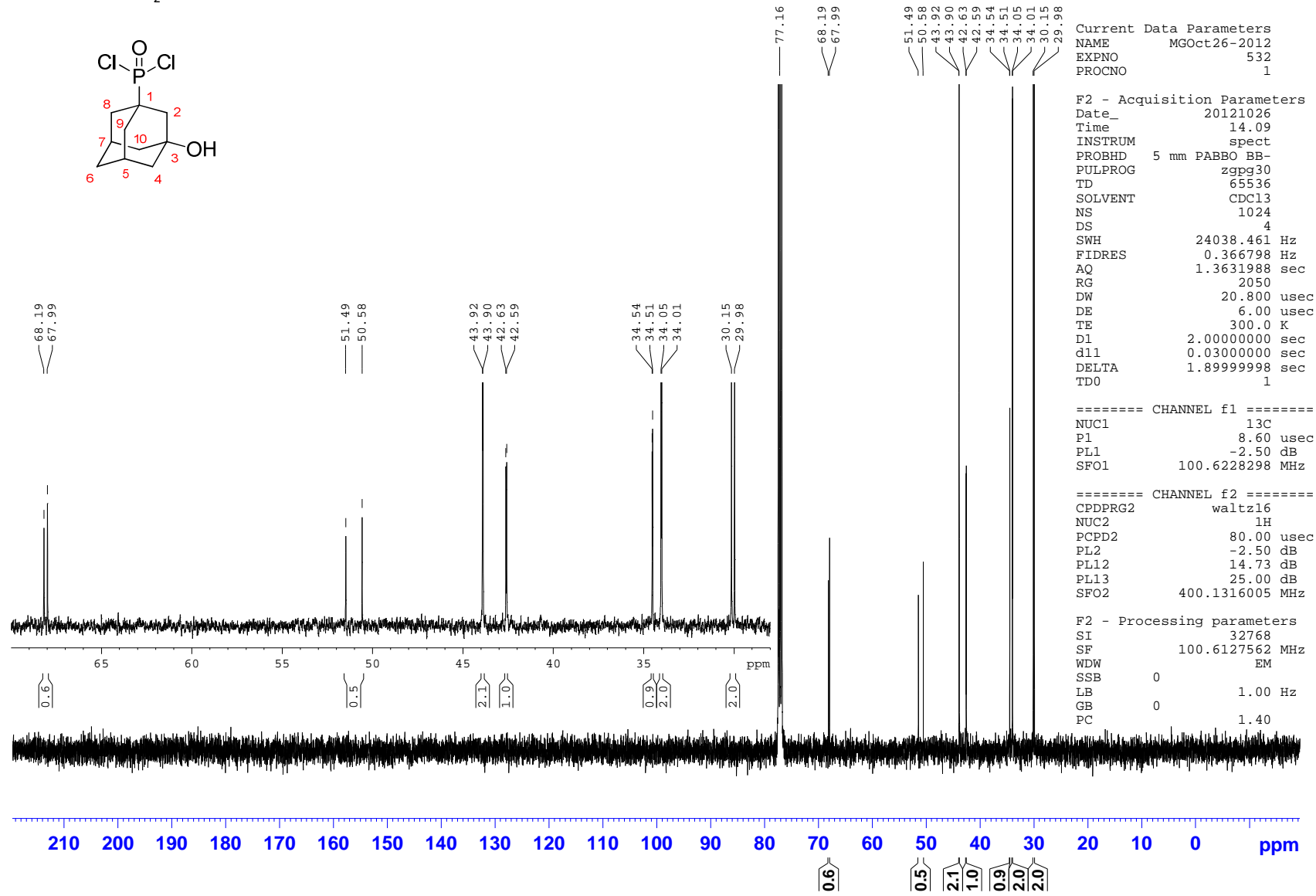
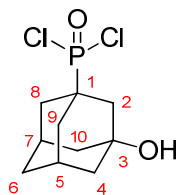
F2 - Processing parameters
SI         32768
SF         161.9755930 MHz
WDW        EM
SSB        0
LB         1.00 Hz
GB         0
PC         1.40
    
```

d) (3-Hydroxyadamant-1-yl)phosphonic dichloride (**178**)

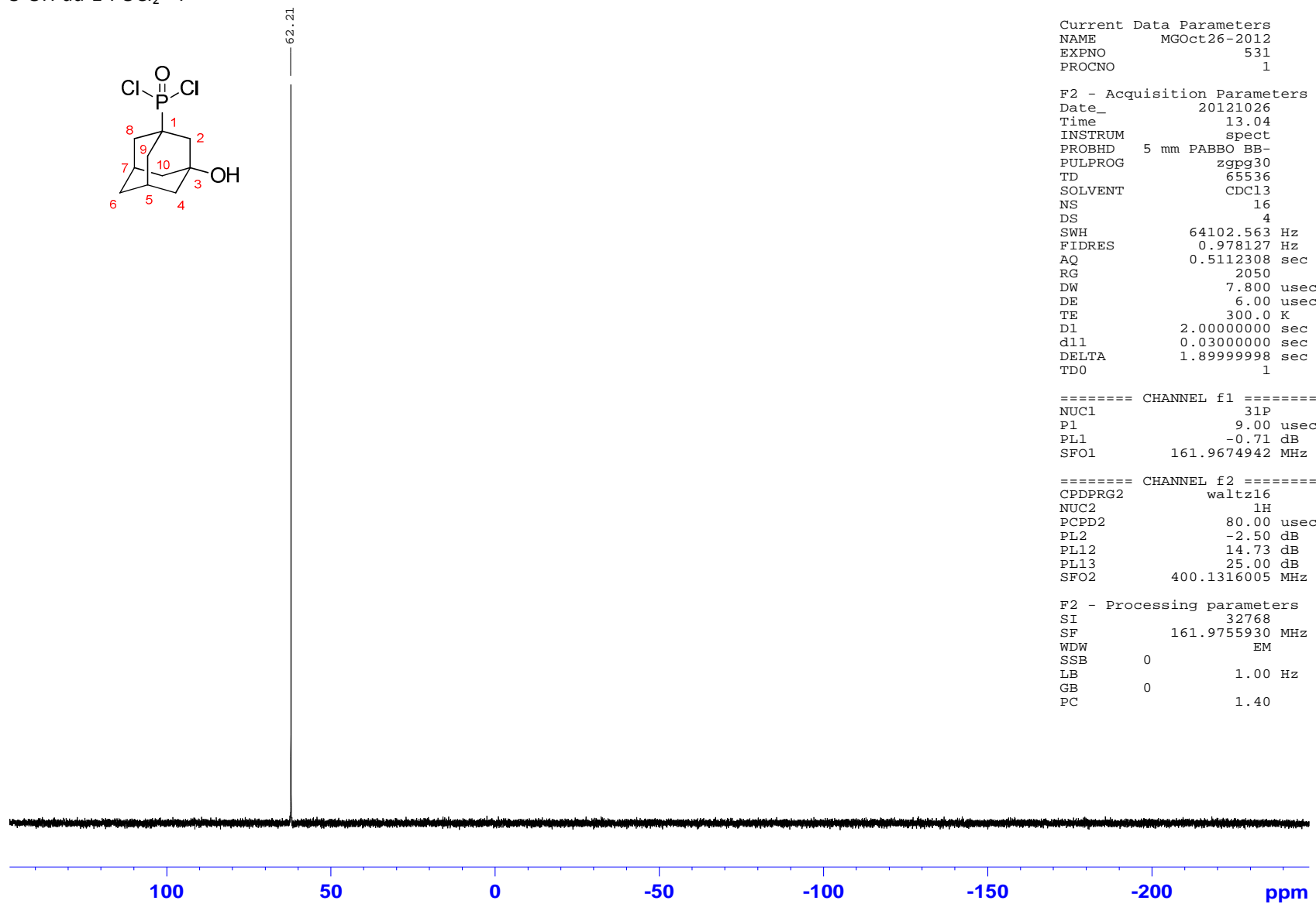
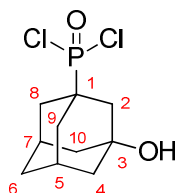
3-OH-ad-1-POCl₂ ¹H



3-OH-ad-1-POCl₂ ¹³C



3-OH-ad-1-POCl₂ ³¹P



```

Current Data Parameters
NAME          MGOct26-2012
EXPNO         531
PROCNO        1

F2 - Acquisition Parameters
Date_         20121026
Time          13.04
INSTRUM       spect
PROBHD        5 mm PABBO BB-
PULPROG       zgpg30
TD            65536
SOLVENT       CDCl3
NS            16
DS            4
SWH           64102.563 Hz
FIDRES        0.978127 Hz
AQ            0.5112308 sec
RG            2050
DW            7.800 usec
DE            6.00 usec
TE            300.0 K
D1            2.00000000 sec
d11           0.03000000 sec
DELTA         1.89999998 sec
TD0           1

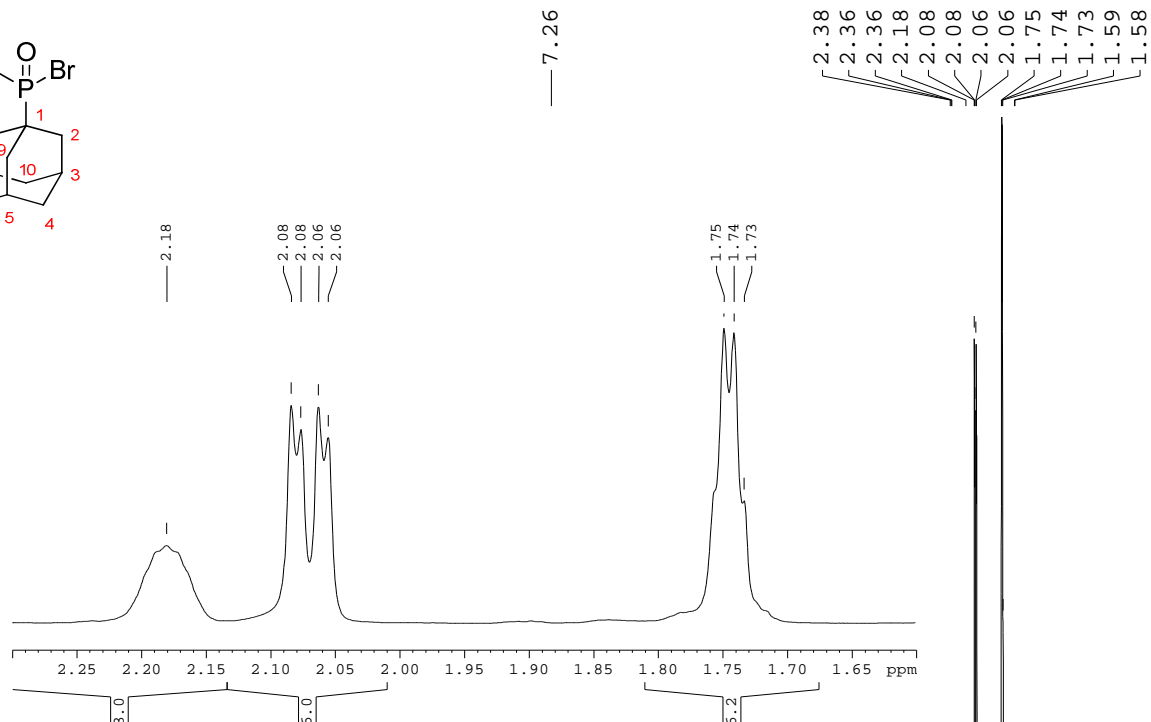
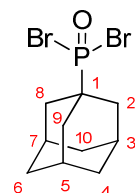
===== CHANNEL f1 =====
NUC1           31P
P1             9.00 usec
PL1            -0.71 dB
SFO1           161.9674942 MHz

===== CHANNEL f2 =====
CPDPRG2       waltz16
NUC2           1H
PCPD2          80.00 usec
PL2            -2.50 dB
PL12           14.73 dB
PL13           25.00 dB
SFO2           400.1316005 MHz

F2 - Processing parameters
SI             32768
SF            161.9755930 MHz
WDW            EM
SSB            0
LB             1.00 Hz
GB            0
PC             1.40
    
```

e) 1-Adamantylphosphonic dibromide (**179**)

1-Ad-POBr₂ ¹H

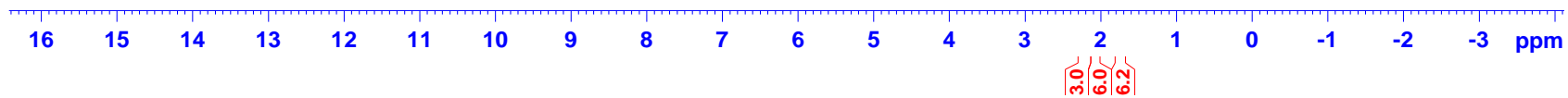


Current Data Parameters
 NAME MGSep10-2012
 EXPNO 11
 PROCNO 1

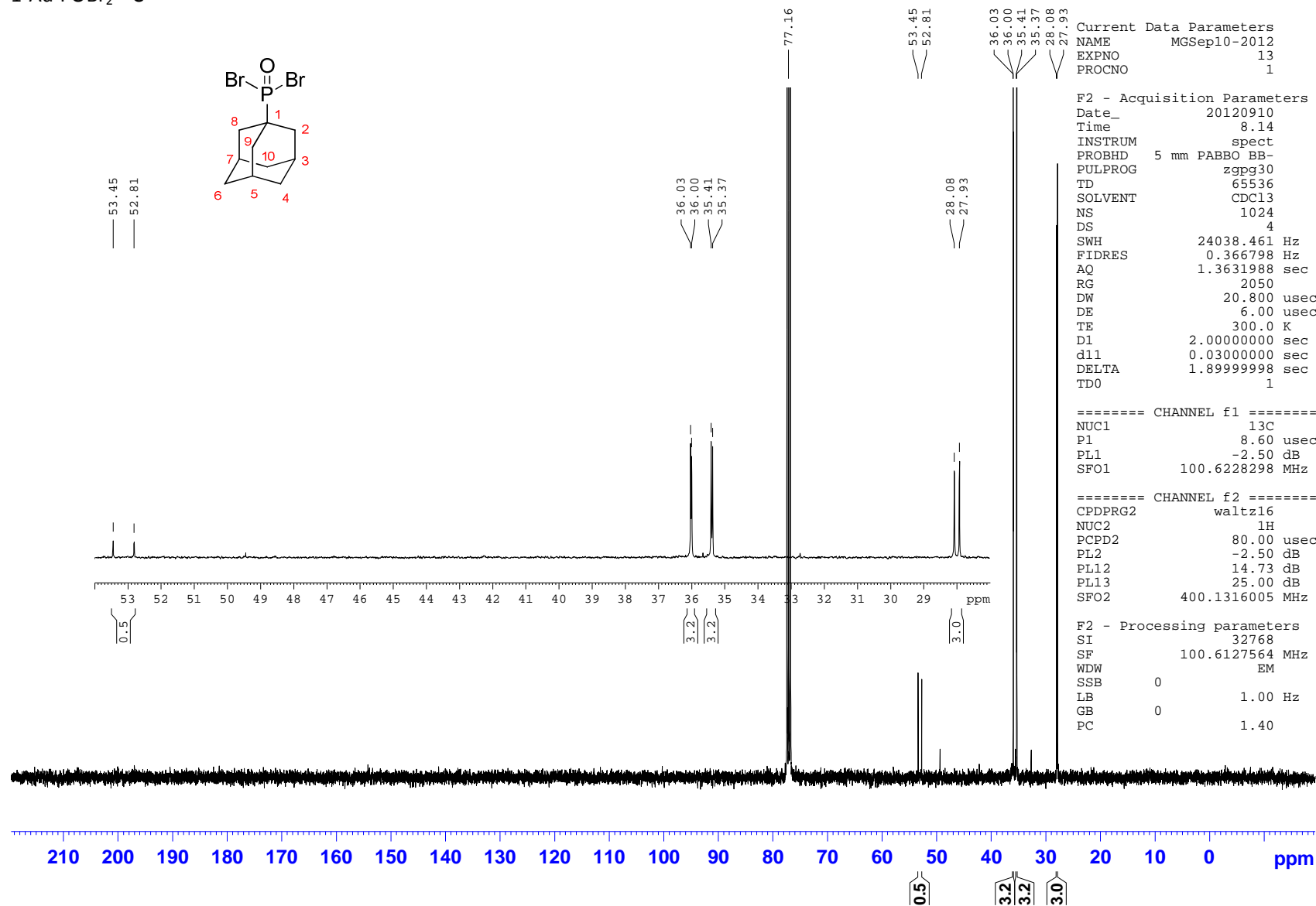
F2 - Acquisition Parameters
 Date_ 20120910
 Time 7.05
 INSTRUM spect
 PROBHD 5 mm PABBO BB-
 PULPROG zg30
 TD 65536
 SOLVENT CDCl3
 NS 16
 DS 2
 SWH 8223.685 Hz
 FIDRES 0.125483 Hz
 AQ 3.9846387 sec
 RG 228
 DW 60.800 usec
 DE 6.00 usec
 TE 300.0 K
 D1 1.00000000 sec
 TD0 1

===== CHANNEL f1 =====
 NUC1 1H
 P1 11.00 usec
 PL1 -2.50 dB
 SFO1 400.1324710 MHz

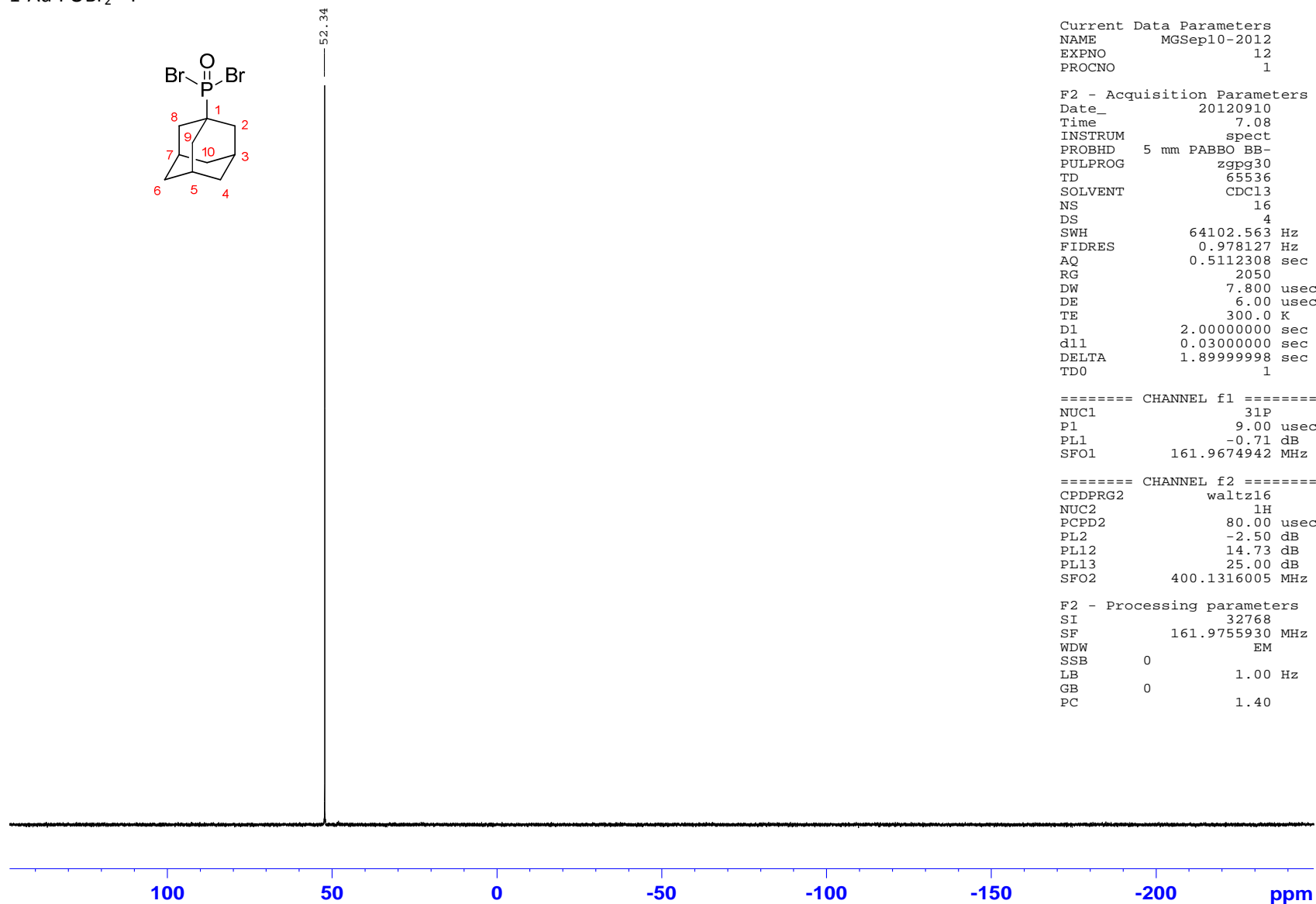
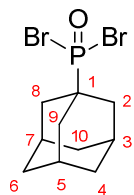
F2 - Processing parameters
 SI 32768
 SF 400.1300095 MHz
 WDW EM
 SSB 0
 LB 0.30 Hz
 GB 0
 PC 1.00



1-Ad-POBr₂ ¹³C



1-Ad-POBr₂ ³¹P



```

Current Data Parameters
NAME          MGSep10-2012
EXPNO         12
PROCNO        1

F2 - Acquisition Parameters
Date_         20120910
Time          7.08
INSTRUM       spect
PROBHD        5 mm PABBO BB-
PULPROG       zgpg30
TD            65536
SOLVENT       CDCl3
NS            16
DS            4
SWH           64102.563 Hz
FIDRES        0.978127 Hz
AQ            0.5112308 sec
RG            2050
DW            7.800 usec
DE            6.00 usec
TE            300.0 K
D1            2.00000000 sec
d11           0.03000000 sec
DELTA         1.89999998 sec
TD0           1

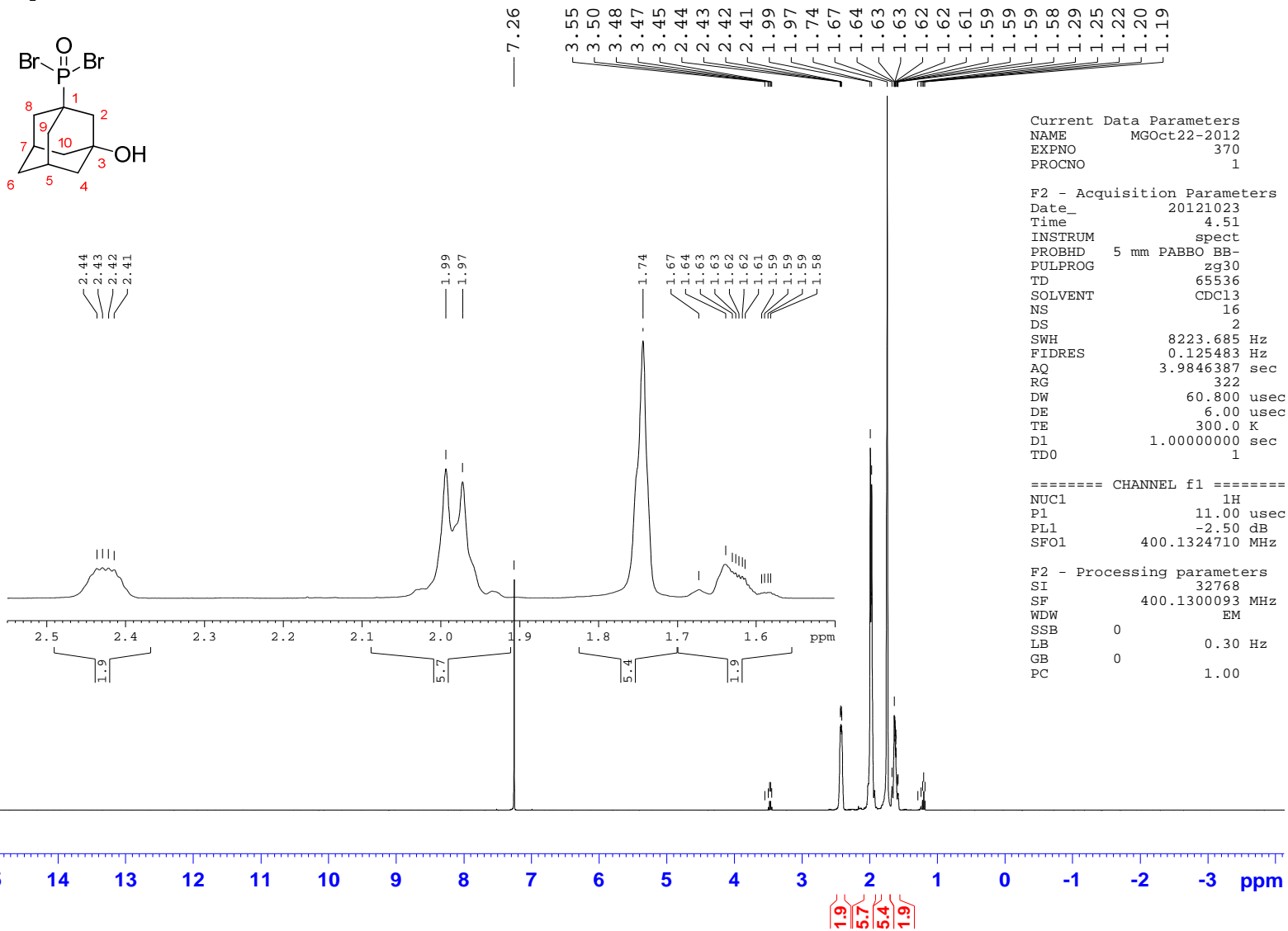
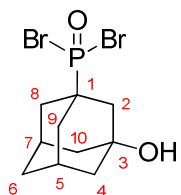
===== CHANNEL f1 =====
NUC1           31P
P1             9.00 usec
PL1            -0.71 dB
SFO1           161.9674942 MHz

===== CHANNEL f2 =====
CPDPRG2       waltz16
NUC2           1H
PCPD2          80.00 usec
PL2            -2.50 dB
PL12           14.73 dB
PL13           25.00 dB
SFO2           400.1316005 MHz

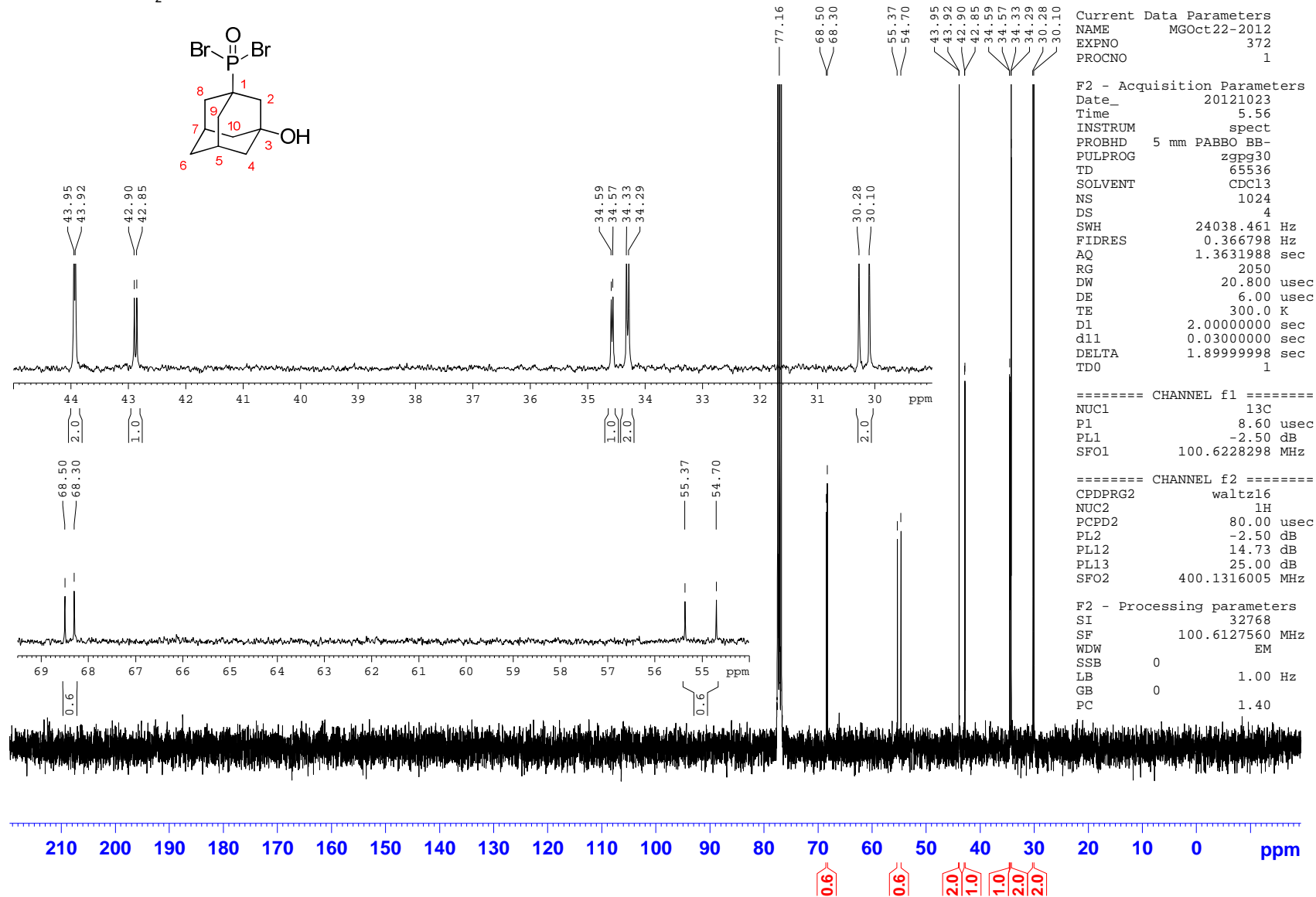
F2 - Processing parameters
SI             32768
SF             161.9755930 MHz
WDW            EM
SSB            0
LB             1.00 Hz
GB             0
PC             1.40
    
```

f) (3-Hydroxyadamant-1-yl)phosphonic dibromide (**180**)

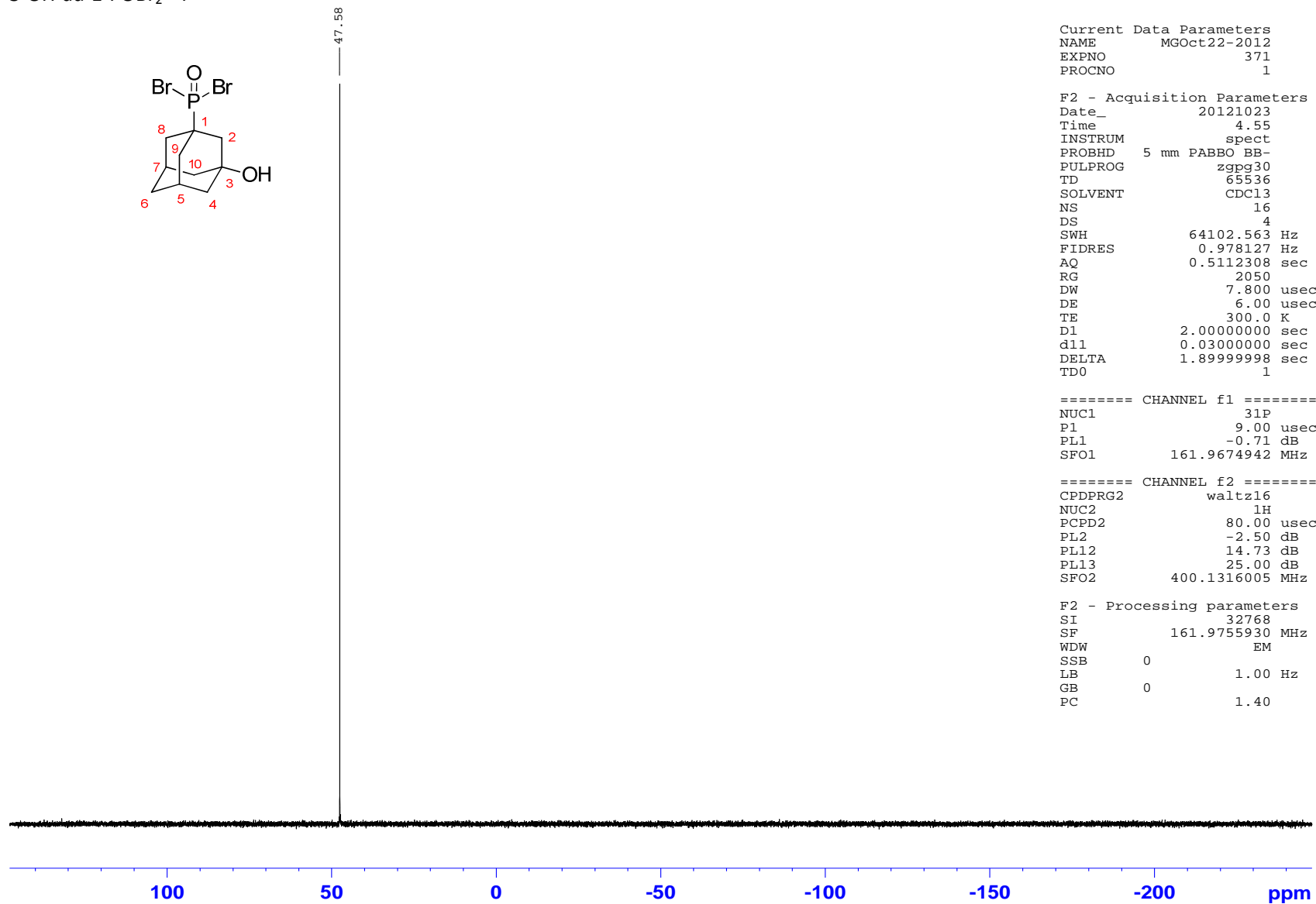
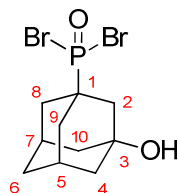
3-OH-ad-POBr₂ ¹H



3-OH-ad-1-POBr₂ ¹³C



3-OH-ad-1-POBr₂ ³¹P



```

Current Data Parameters
NAME      MGOct22-2012
EXPNO     371
PROCNO    1

F2 - Acquisition Parameters
Date_     20121023
Time      4.55
INSTRUM   spect
PROBHD    5 mm PABBO BB-
PULPROG   zgpg30
TD         65536
SOLVENT   CDCl3
NS         16
DS         4
SWH        64102.563 Hz
FIDRES     0.978127 Hz
AQ         0.5112308 sec
RG         2050
DW         7.800 usec
DE         6.00 usec
TE         300.0 K
D1         2.00000000 sec
d11        0.03000000 sec
DELTA     1.89999998 sec
TD0        1

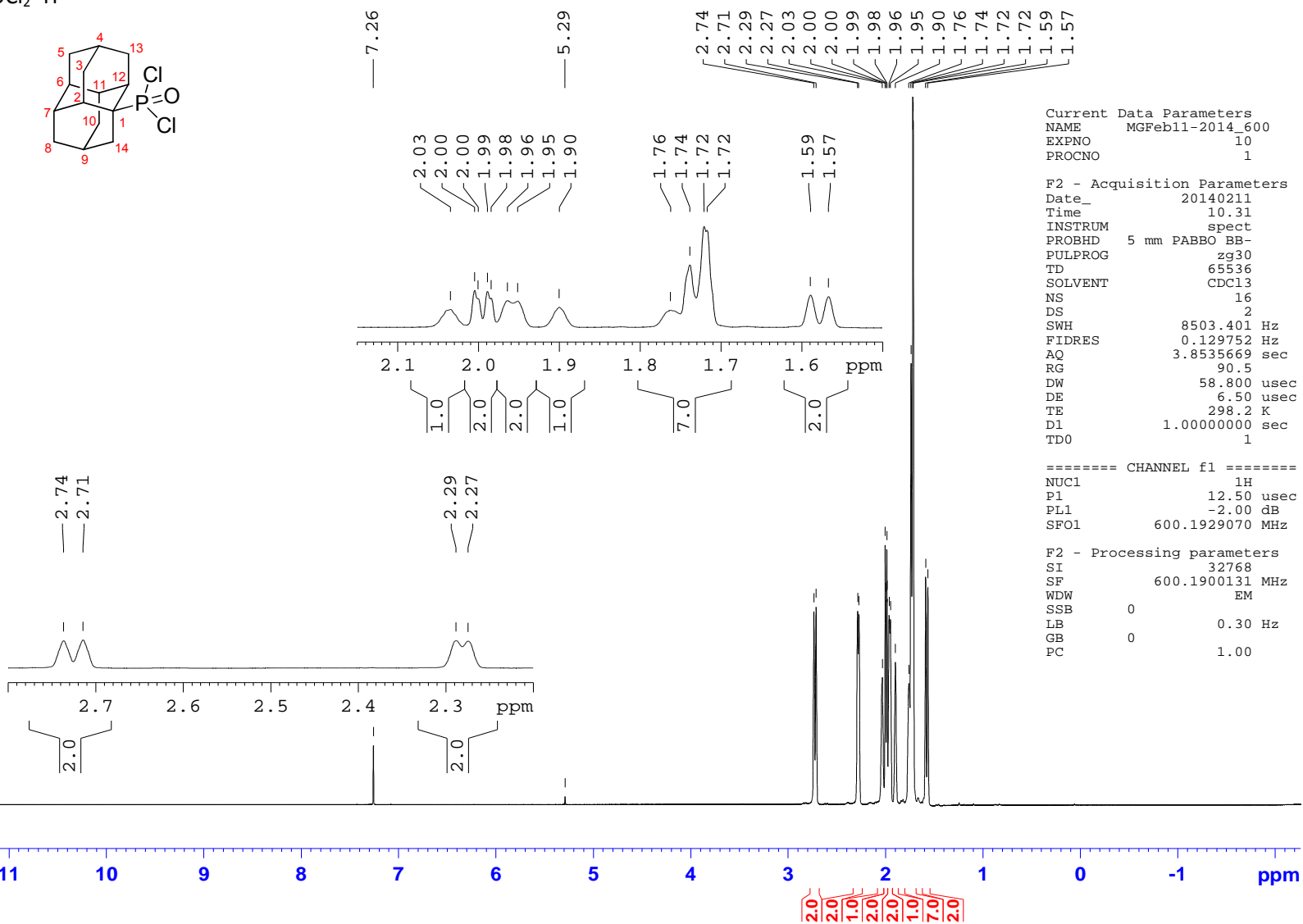
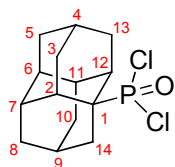
===== CHANNEL f1 =====
NUC1       31P
P1         9.00 usec
PL1        -0.71 dB
SFO1       161.9674942 MHz

===== CHANNEL f2 =====
CPDPRG2    waltz16
NUC2        1H
PCPD2       80.00 usec
PL2         -2.50 dB
PL12        14.73 dB
PL13        25.00 dB
SFO2        400.1316005 MHz

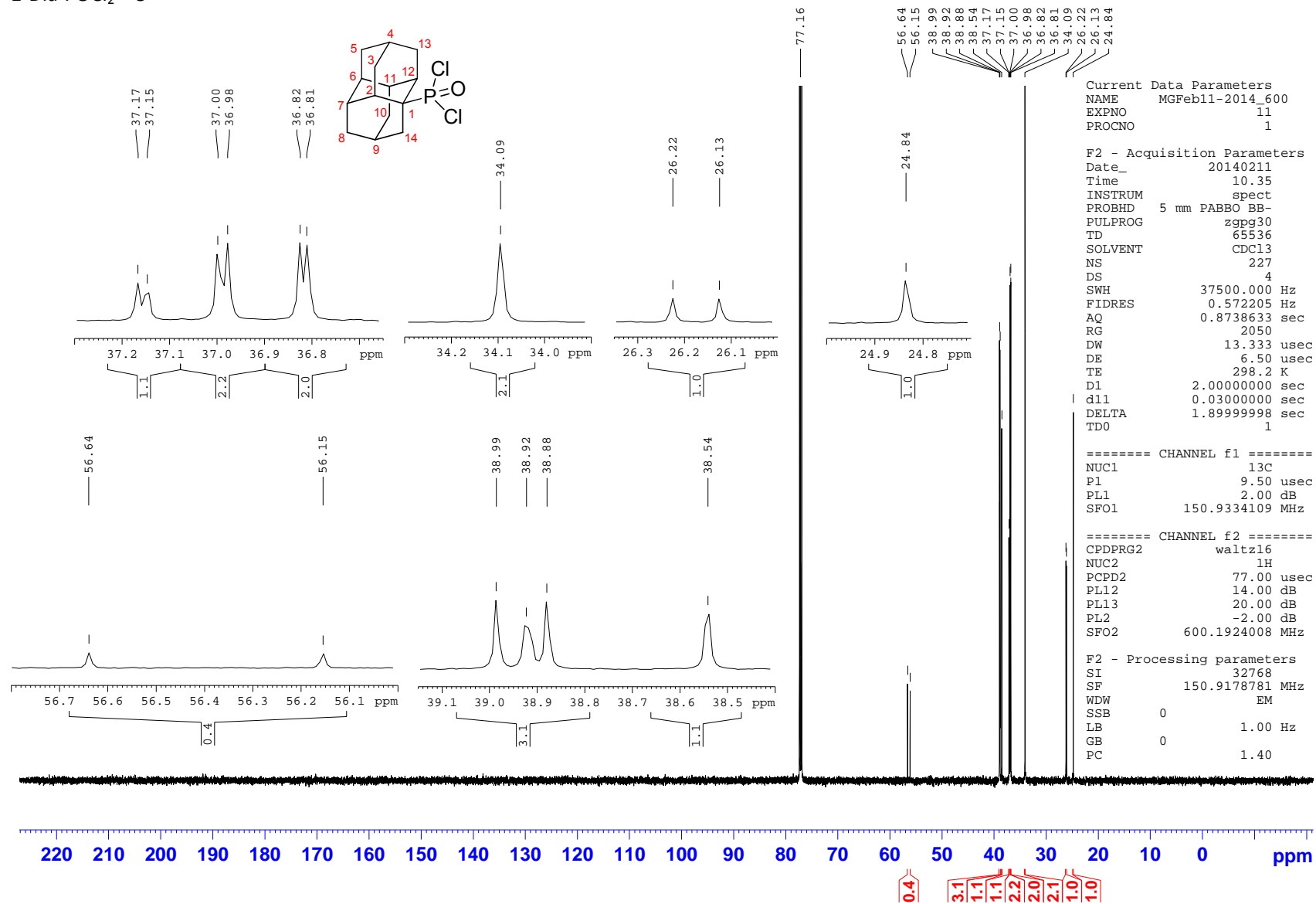
F2 - Processing parameters
SI          32768
SF          161.9755930 MHz
WDW         EM
SSB         0
LB          1.00 Hz
GB          0
PC          1.40
    
```

g) 1-Diamantylphosphonic acid dichloride (**181**)

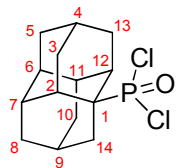
1-Dia-POCl₂ ¹H



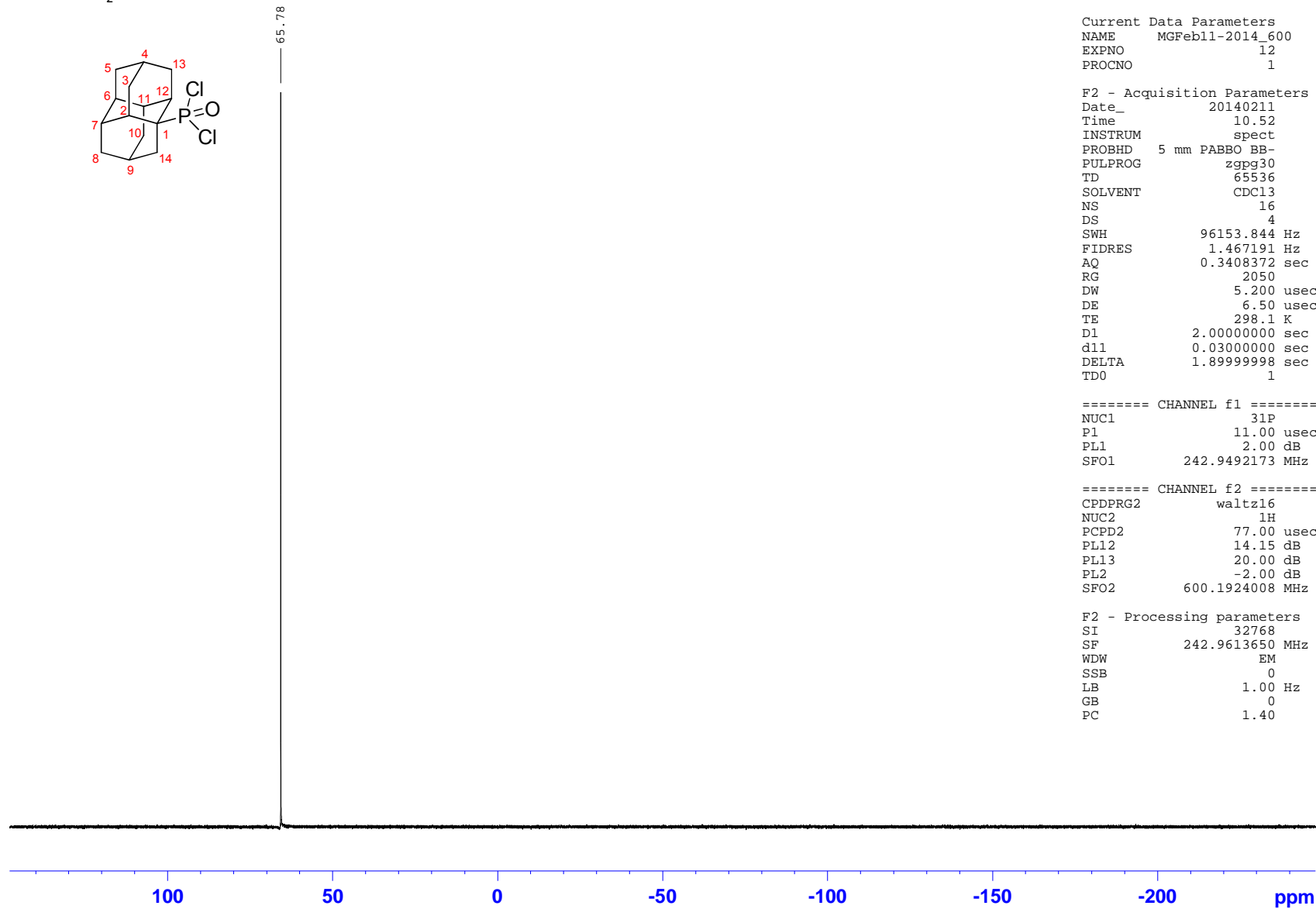
1-Dia-POCl₂ ¹³C



1-Dia-POCl₂ ³¹P



65.78



```

Current Data Parameters
NAME      MGFeb11-2014_600
EXPNO     12
PROCNO    1

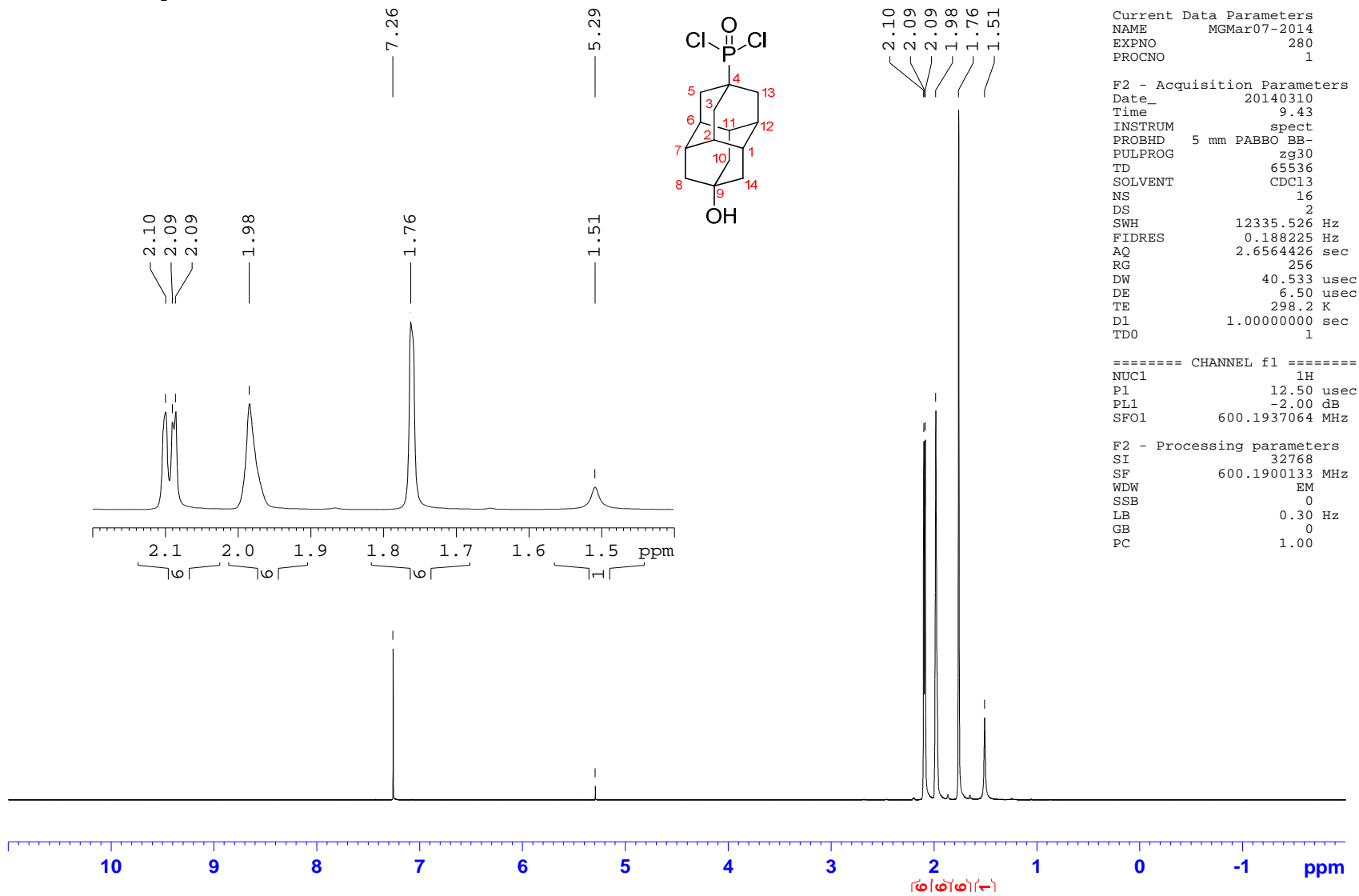
F2 - Acquisition Parameters
Date_     20140211
Time      10.52
INSTRUM   spect
PROBHD    5 mm PABBO BB-
PULPROG   zgpg30
TD        65536
SOLVENT   CDC13
NS         16
DS         4
SWH        96153.844 Hz
FIDRES     1.467191 Hz
AQ         0.3408372 sec
RG         2050
DW         5.200 usec
DE         6.50 usec
TE         298.1 K
D1         2.00000000 sec
d11        0.03000000 sec
DELTA     1.89999998 sec
TD0        1

===== CHANNEL f1 =====
NUC1       31P
P1         11.00 usec
PL1        2.00 dB
SFO1       242.9492173 MHz

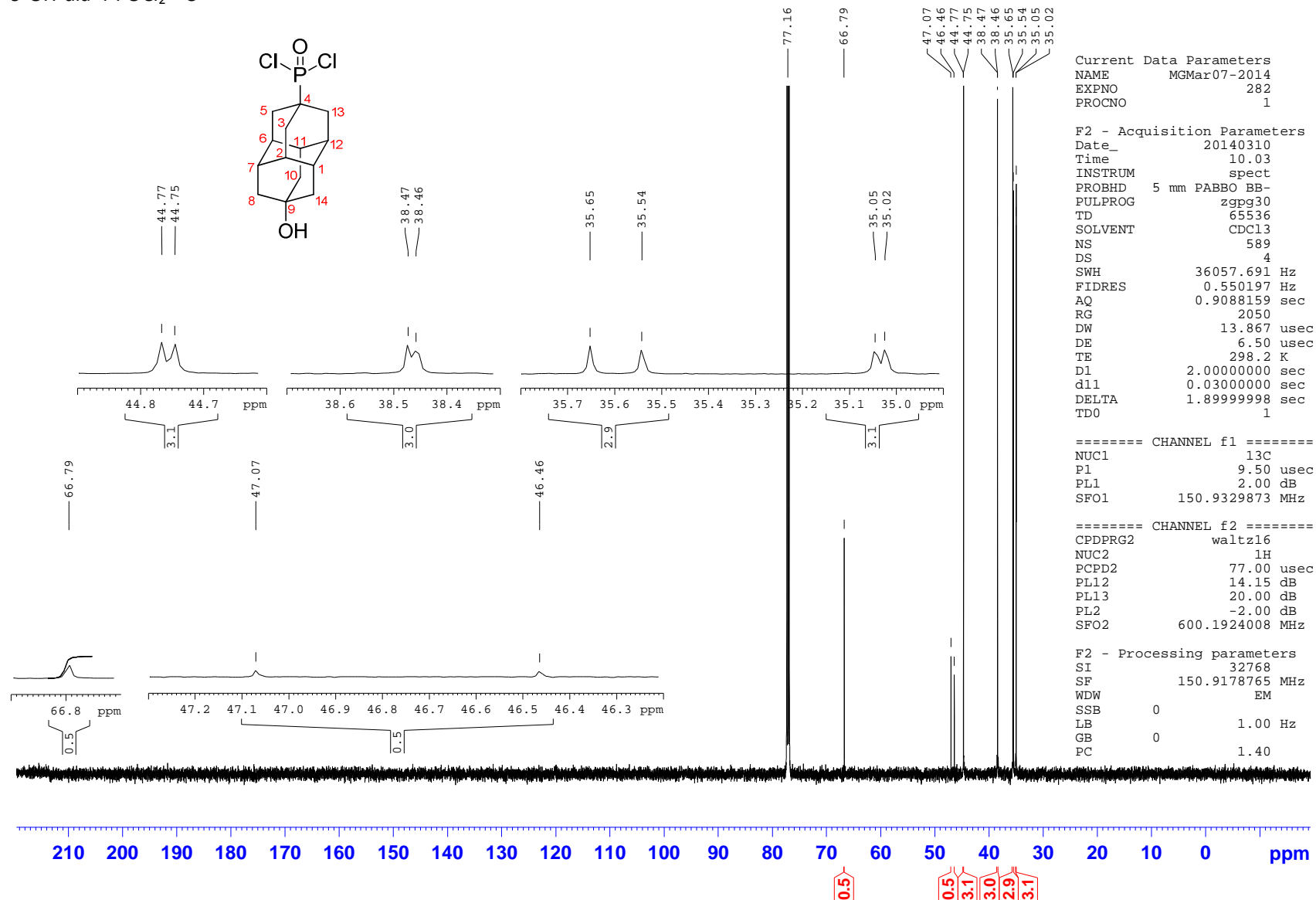
===== CHANNEL f2 =====
CPDPRG2    waltz16
NUC2        1H
PCPD2      77.00 usec
PL12       14.15 dB
PL13       20.00 dB
PL2        -2.00 dB
SFO2       600.1924008 MHz

F2 - Processing parameters
SI         32768
SF         242.9613650 MHz
WDW        EM
SSB        0
LB         1.00 Hz
GB         0
PC         1.40
    
```

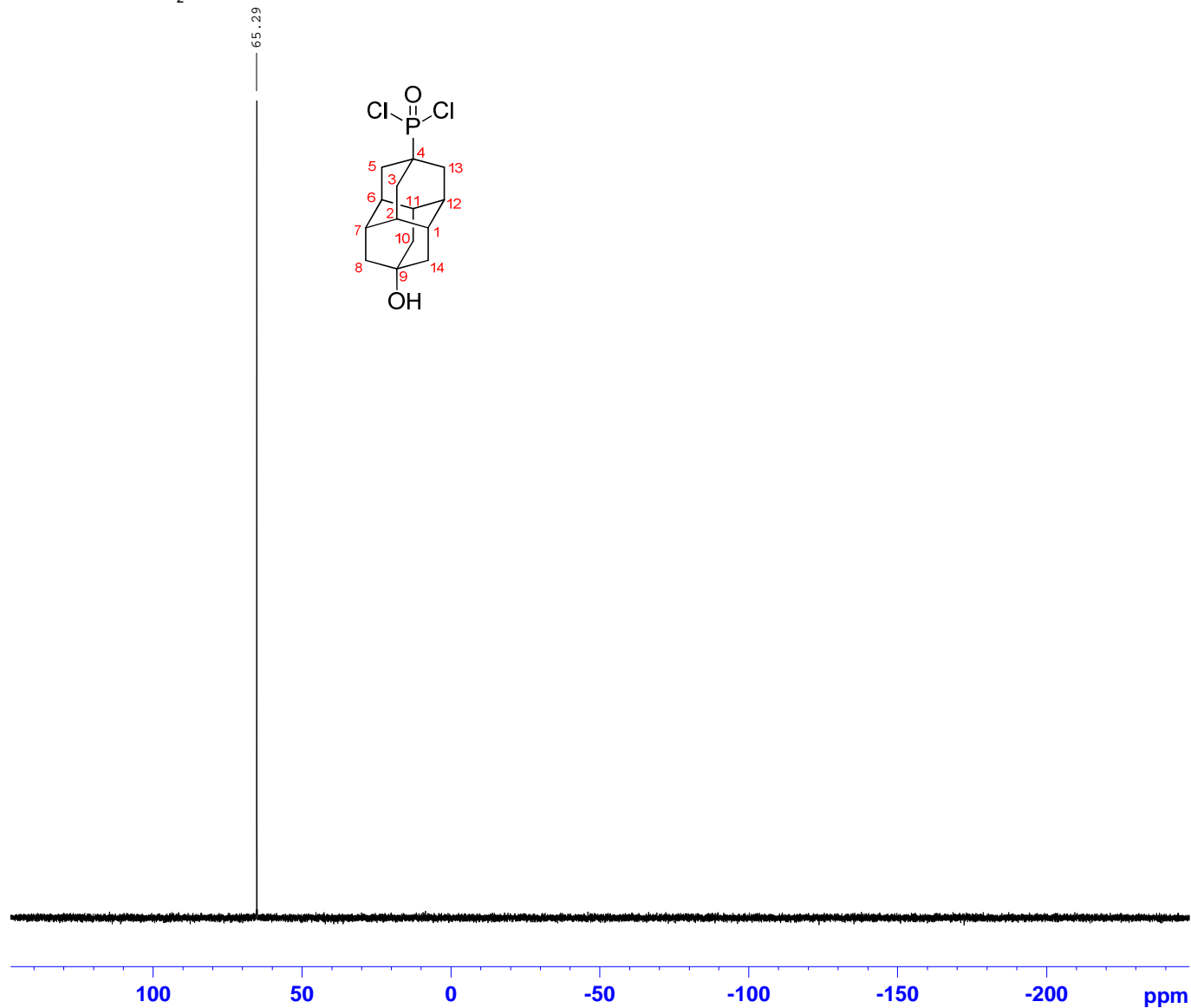
h) (9-Hydroxydiamant-4-yl)phosphonic dichloride (182)
 9-OH-dia-4-POCl₂ ¹H



9-OH-dia-4-POCl₂ ¹³C



9-OH-dia-4-POCl₂ ³¹P



```

Current Data Parameters
NAME      MGMar07-2014
EXPNO    281
PROCNO    1

F2 - Acquisition Parameters
Date_    20140310
Time     9.46
INSTRUM  spect
PROBHD   5 mm PABBO BB-
PULPROG  zgpg30
TD       65536
SOLVENT  CDC13
NS       16
DS       4
SWH      96153.844 Hz
FIDRES   1.467191 Hz
AQ       0.3408372 sec
RG       2050
DW       5.200 usec
DE       6.50 usec
TE       298.1 K
D1       2.00000000 sec
d11      0.03000000 sec
DELTA    1.89999998 sec
TD0      1

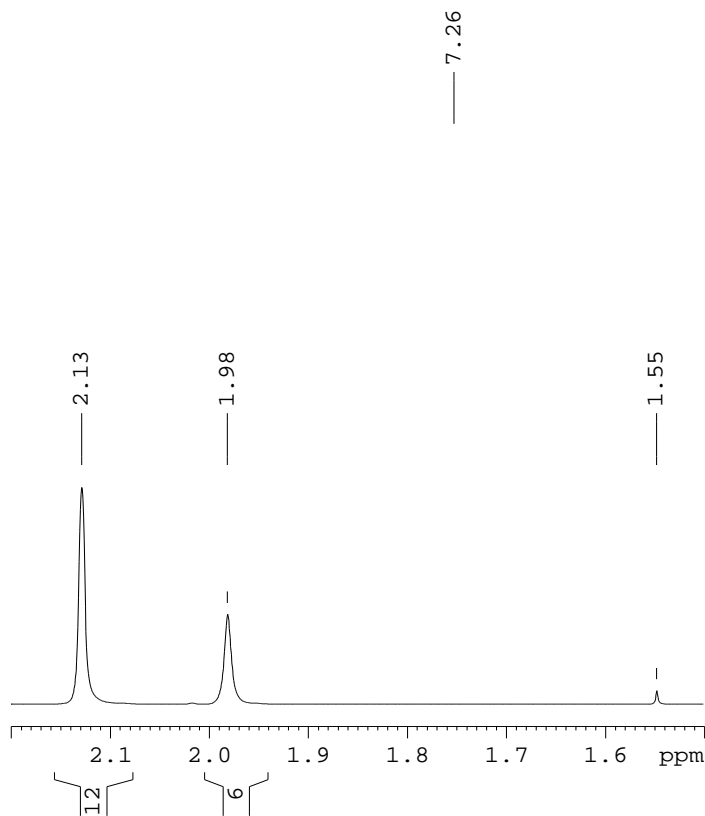
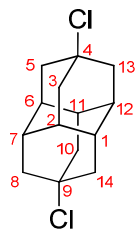
===== CHANNEL f1 =====
NUC1      31P
P1        11.00 usec
PL1       2.00 dB
SFO1     242.9492173 MHz

===== CHANNEL f2 =====
CPDPRG2   waltz16
NUC2      1H
PCPD2     77.00 usec
PL12      14.15 dB
PL13      20.00 dB
PL2       -2.00 dB
SFO2     600.1924008 MHz

F2 - Processing parameters
SI        32768
SF        242.9613650 MHz
WDW       EM
SSB       0
LB        1.00 Hz
GB        0
PC        1.40
    
```

i) 4,9-Dichlorodiamantane (**183**)

4,9-Dia-Cl₂ ¹H

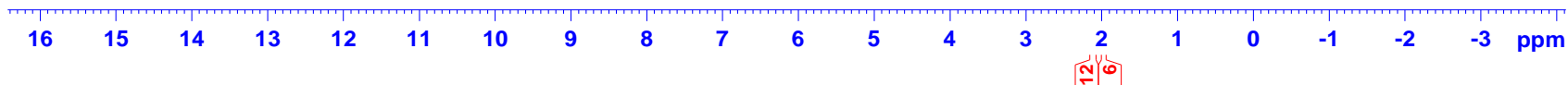


Current Data Parameters
 NAME MGApr23-2014
 EXPNO 370
 PROCNO 1

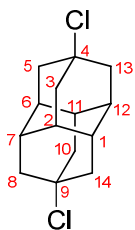
F2 - Acquisition Parameters
 Date_ 20140423
 Time 12.10
 INSTRUM spect
 PROBHD 5 mm PABBO BB-
 PULPROG zg30
 TD 65536
 SOLVENT CDCl3
 NS 16
 DS 2
 SWH 12335.526 Hz
 FIDRES 0.188225 Hz
 AQ 2.6564426 sec
 RG 203
 DW 40.533 usec
 DE 6.50 usec
 TE 298.2 K
 D1 1.00000000 sec
 TD0 1

==== CHANNEL f1 =====
 NUC1 1H
 P1 12.50 usec
 PL1 -2.00 dB
 SFO1 600.1937064 MHz

F2 - Processing parameters
 SI 32768
 SF 600.1900135 MHz
 WDW EM
 SSB 0
 LB 0.30 Hz
 GB 0
 PC 1.00



4,9-Dia-Cl₂ ¹³C



```

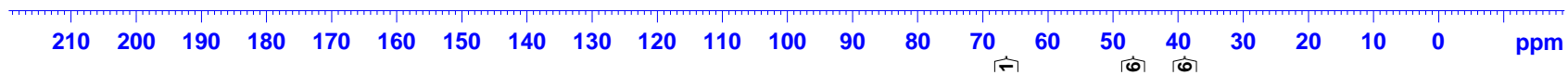
Current Data Parameters
NAME      MGApr23-2014
EXPNO    371
PROCNO   1

F2 - Acquisition Parameters
Date_    20140423
Time     13.02
INSTRUM  spect
PROBHD   5 mm PABBO BB-
PULPROG  zgpg30
TD       65536
SOLVENT  CDCl3
NS       1024
DS       4
SWH      36057.691 Hz
FIDRES   0.550197 Hz
AQ       0.9088159 sec
RG       2050
DW       13.867 usec
DE       6.50 usec
TE       298.1 K
D1       2.0000000 sec
d11      0.03000000 sec
DELTA    1.89999998 sec
TD0      1

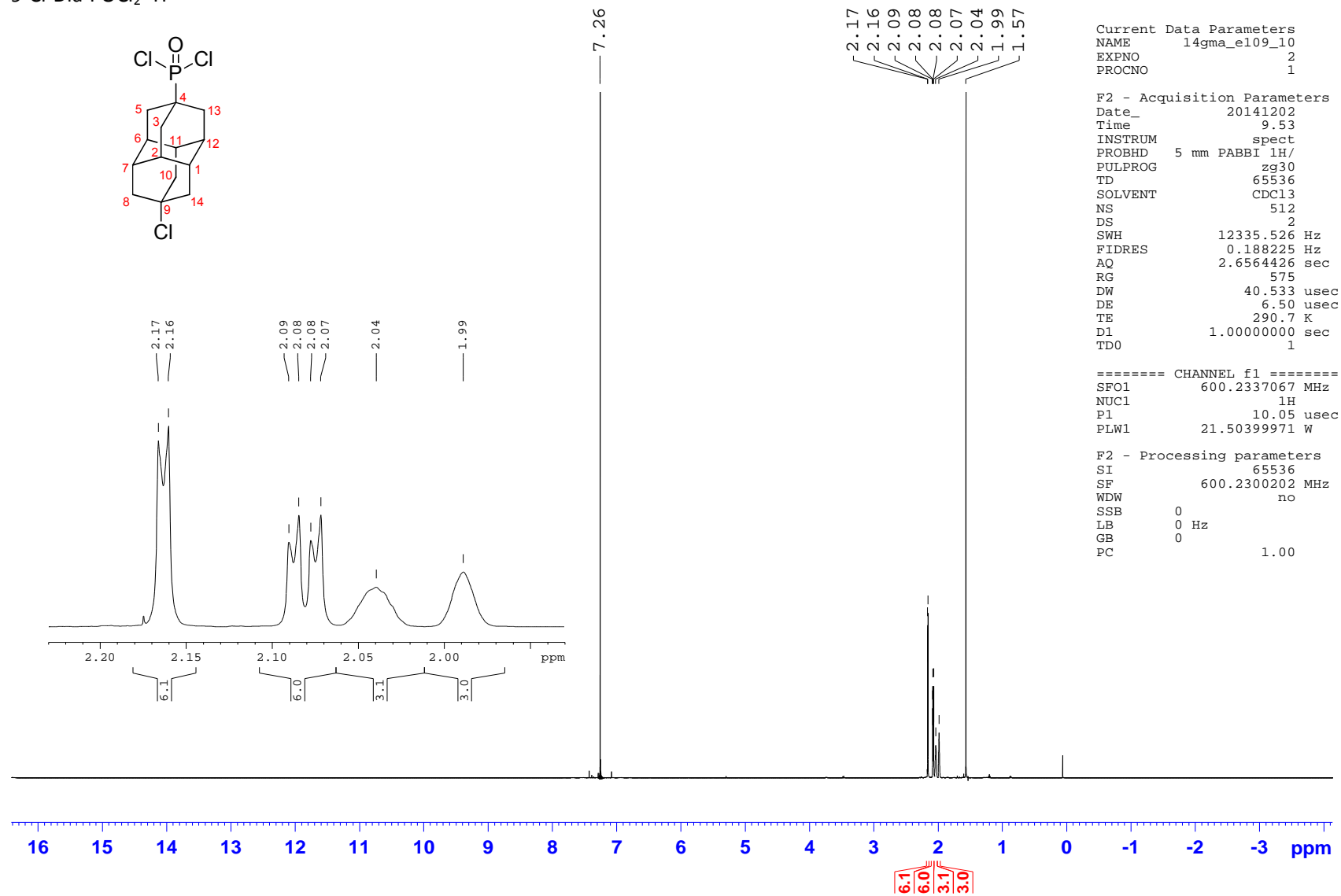
===== CHANNEL f1 =====
NUC1     13C
P1       9.50 usec
PL1      2.00 dB
SFO1     150.9329873 MHz

===== CHANNEL f2 =====
CPDPRG2  waltz16
NUC2     1H
PCPD2    77.00 usec
PL12     14.15 dB
PL13     20.00 dB
PL2      -2.00 dB
SFO2     600.1924008 MHz

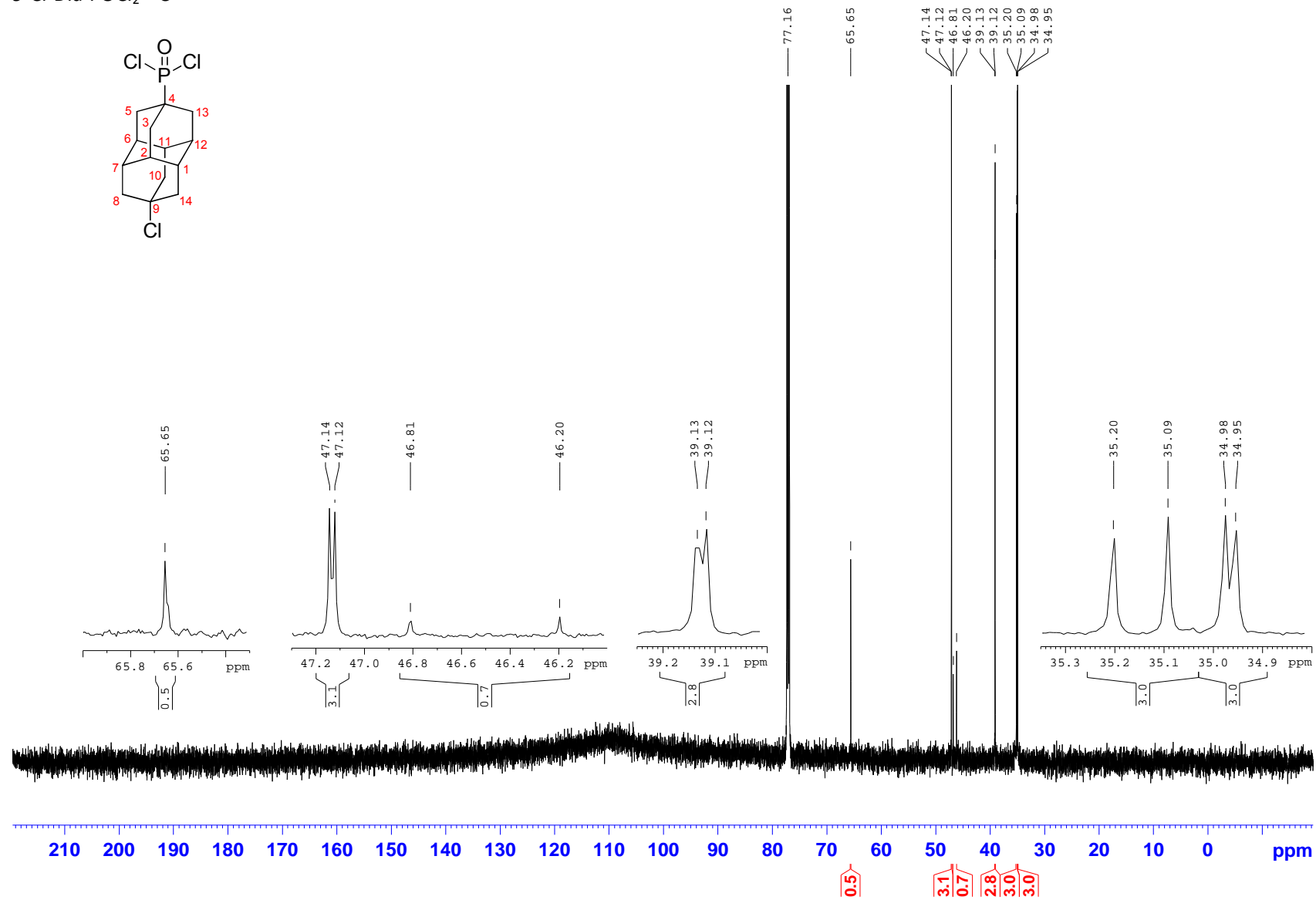
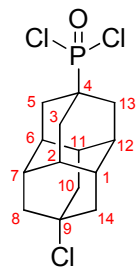
F2 - Processing parameters
SI       32768
SF       150.9178757 MHz
WDW      EM
SSB      0
LB       1.00 Hz
GB       0
PC       1.40
    
```



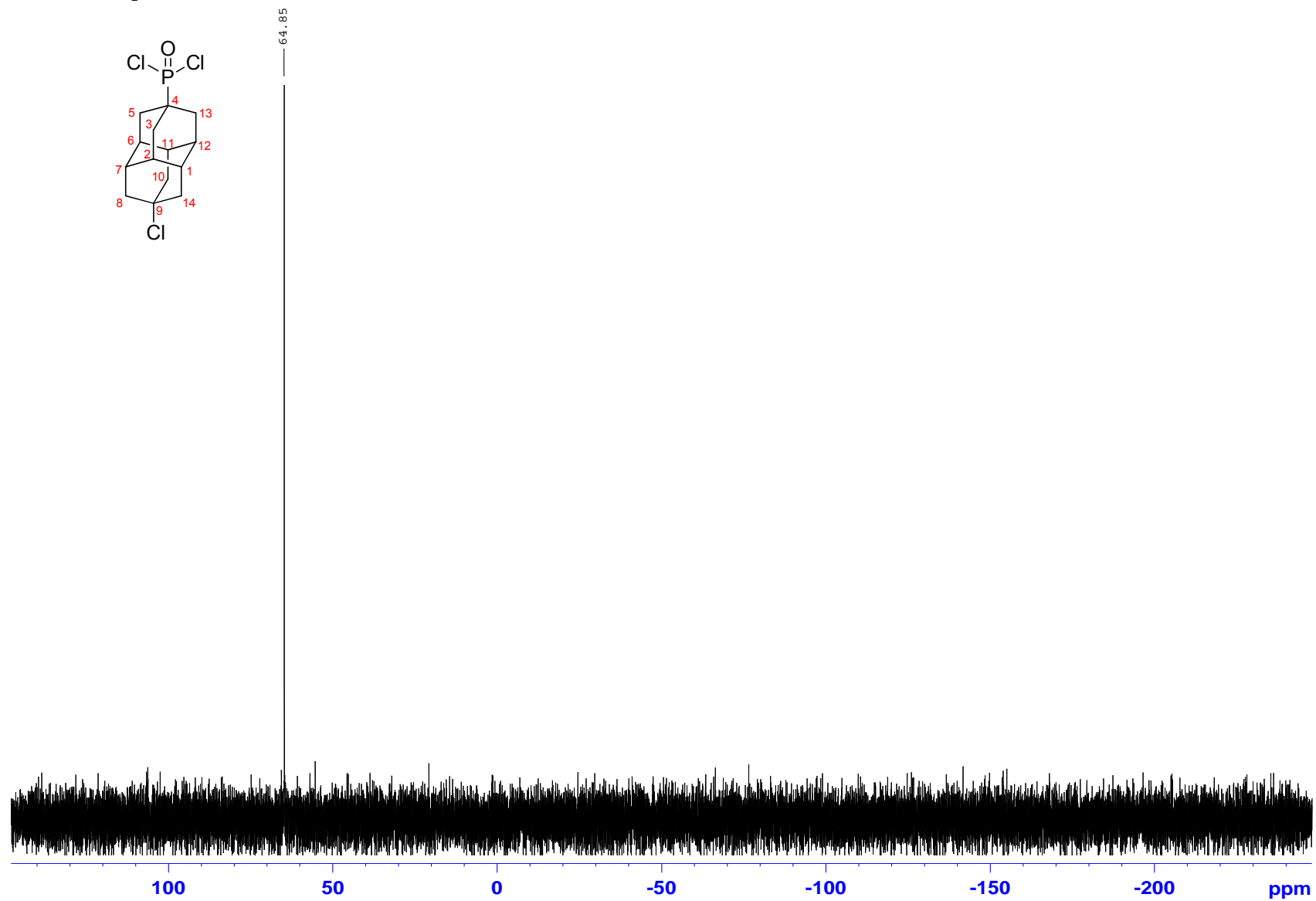
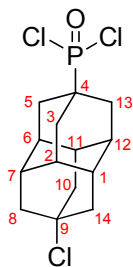
j) (9-Chlorodiamant-4-yl)phosphonic dichloride (**184**)
 9-Cl-Dia-POCl₂ ¹H



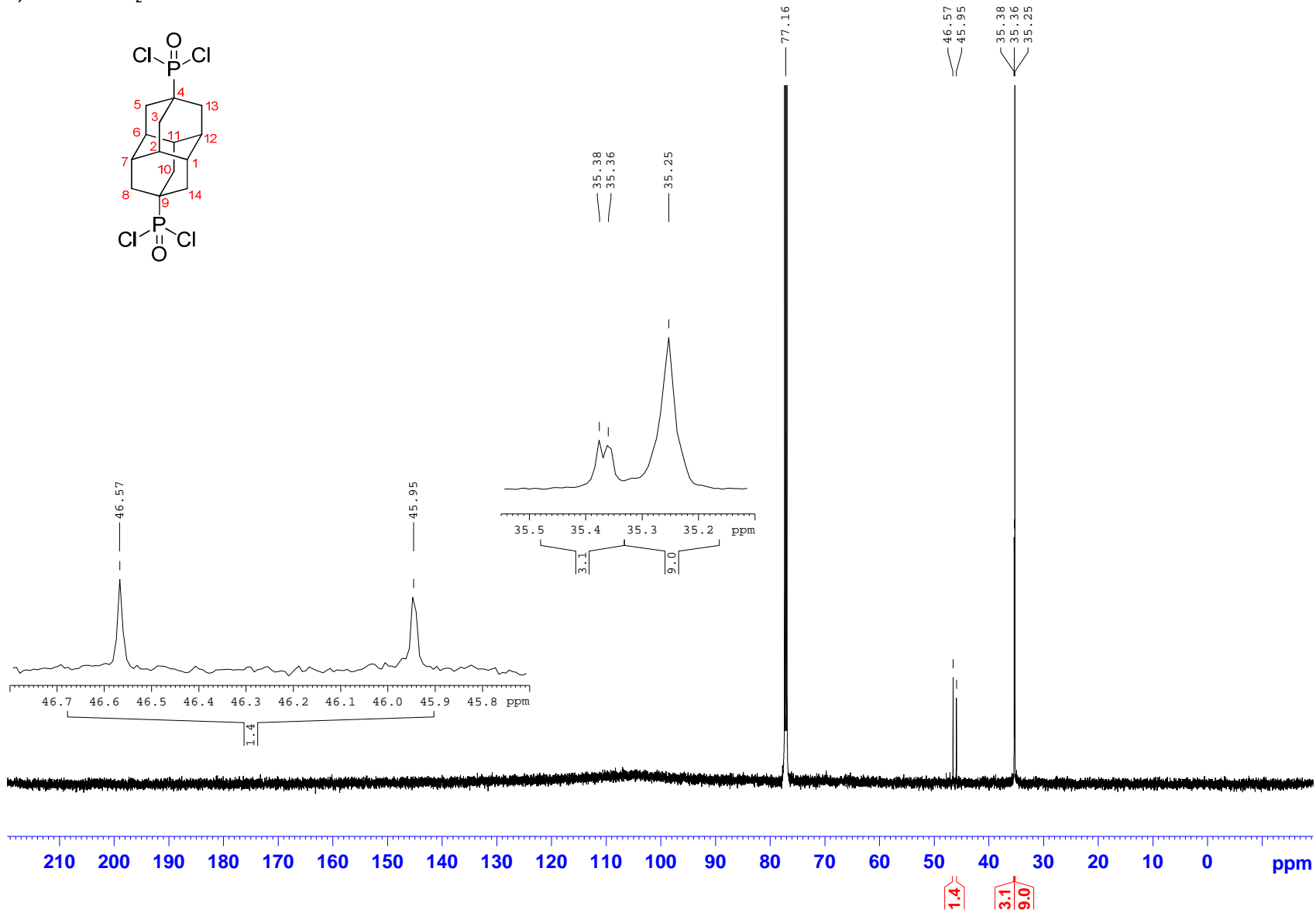
9-Cl-Dia-POCl₂ ¹³C



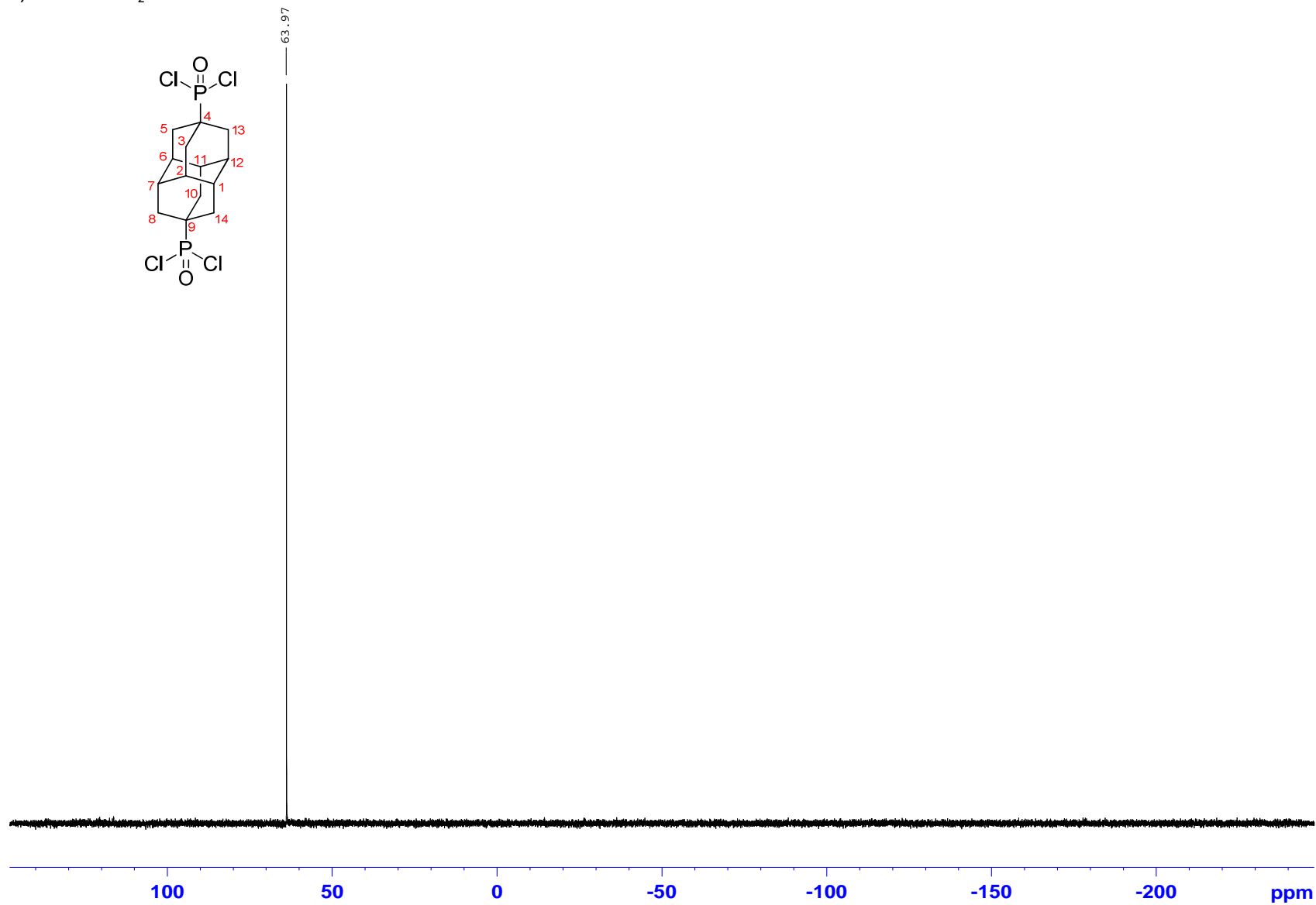
9-Cl-Dia-POCl₂ ³¹P



4,9-dia-diPOCl₂ ¹³C

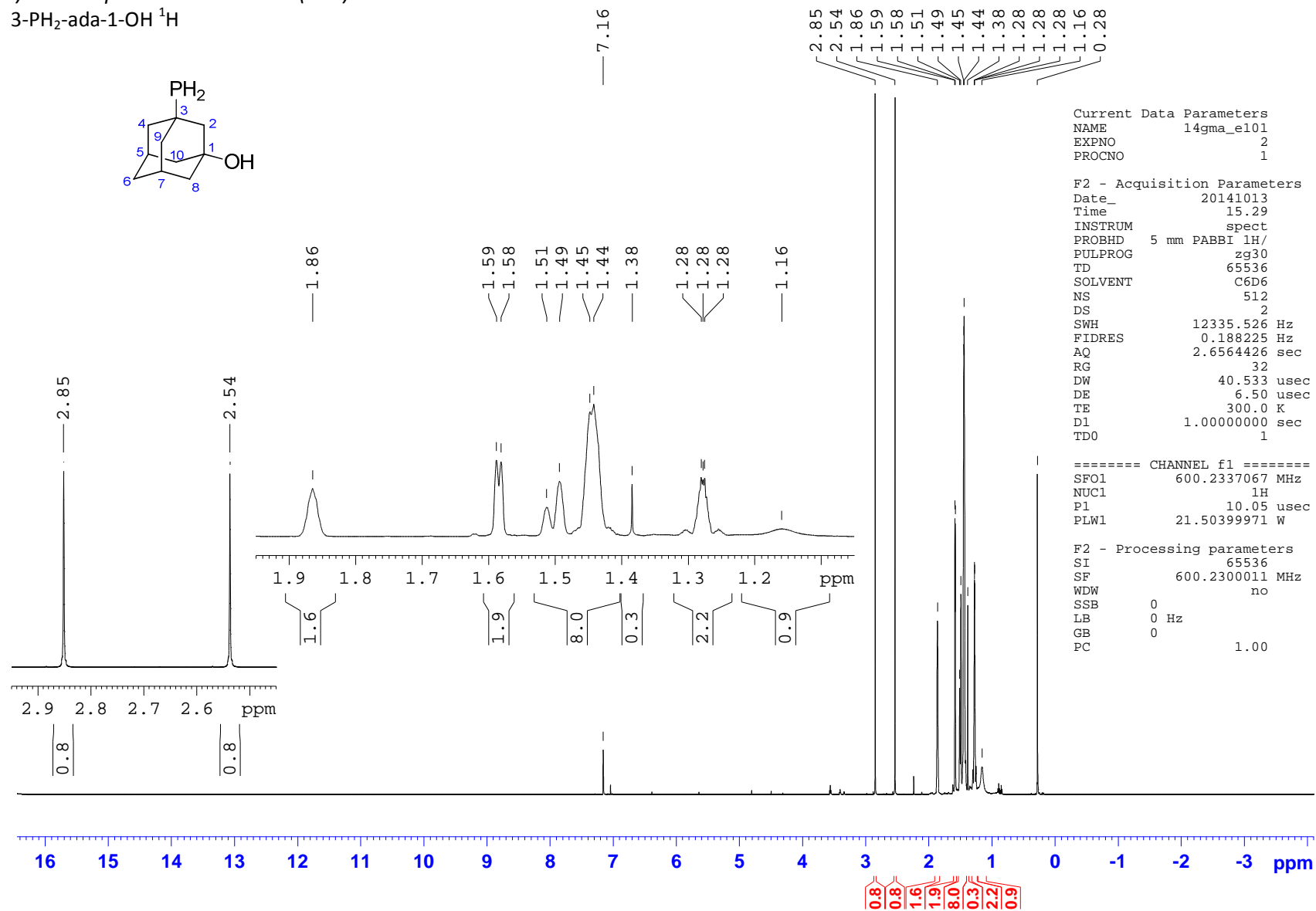
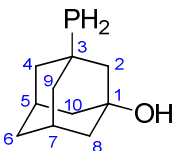


4,9-dia-diPOCl₂ ³¹P

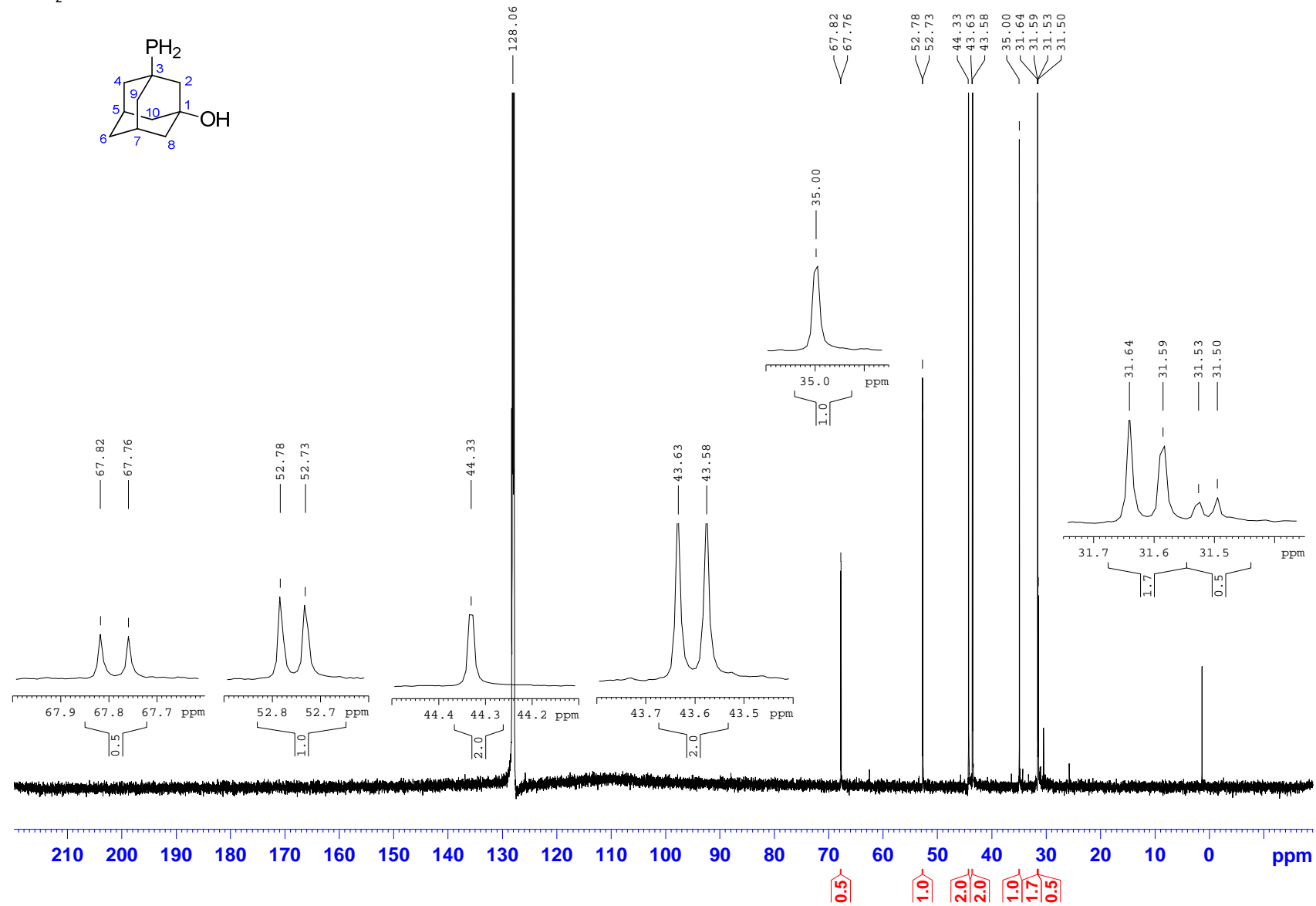


l) 3-Phosphinoadamant-1-ol (**186**)

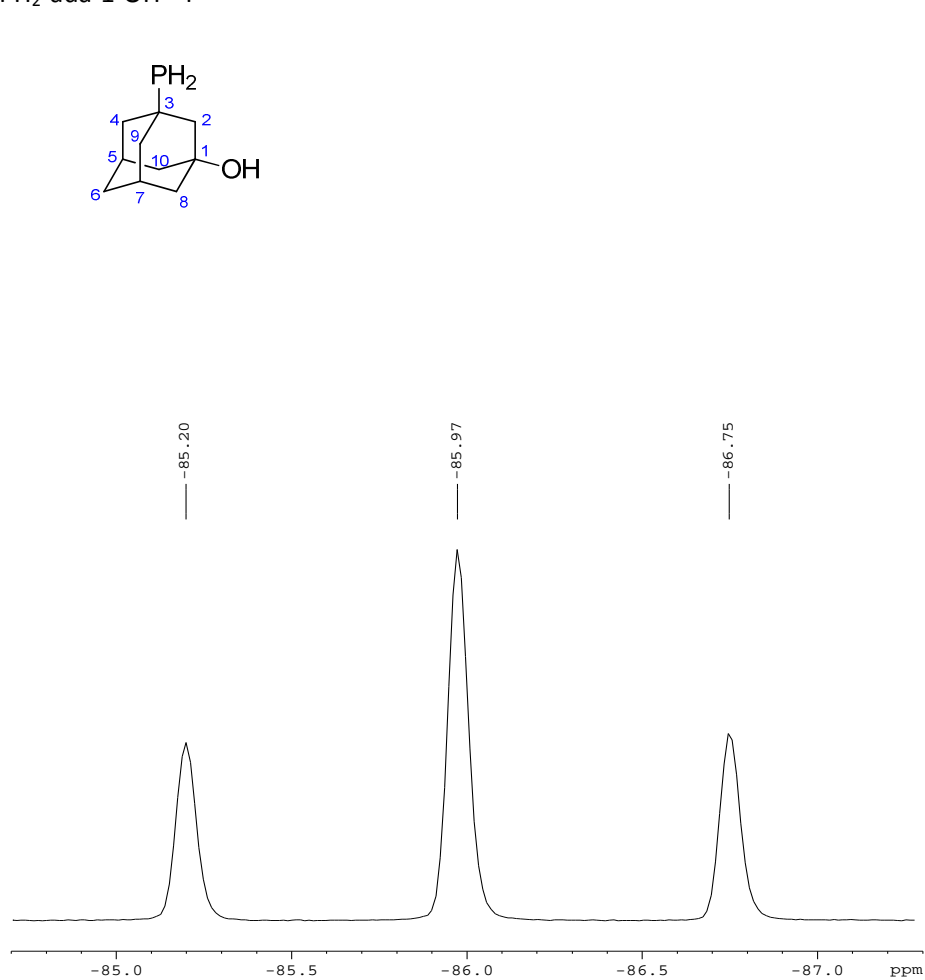
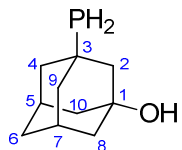
3-PH₂-ada-1-OH ¹H



3-PH₂-ada-1-OH ¹³C



3-PH₂-ada-1-OH ³¹P



```

Current Data Parameters
NAME      14gma_e101
EXPNO     1
PROCNO    1

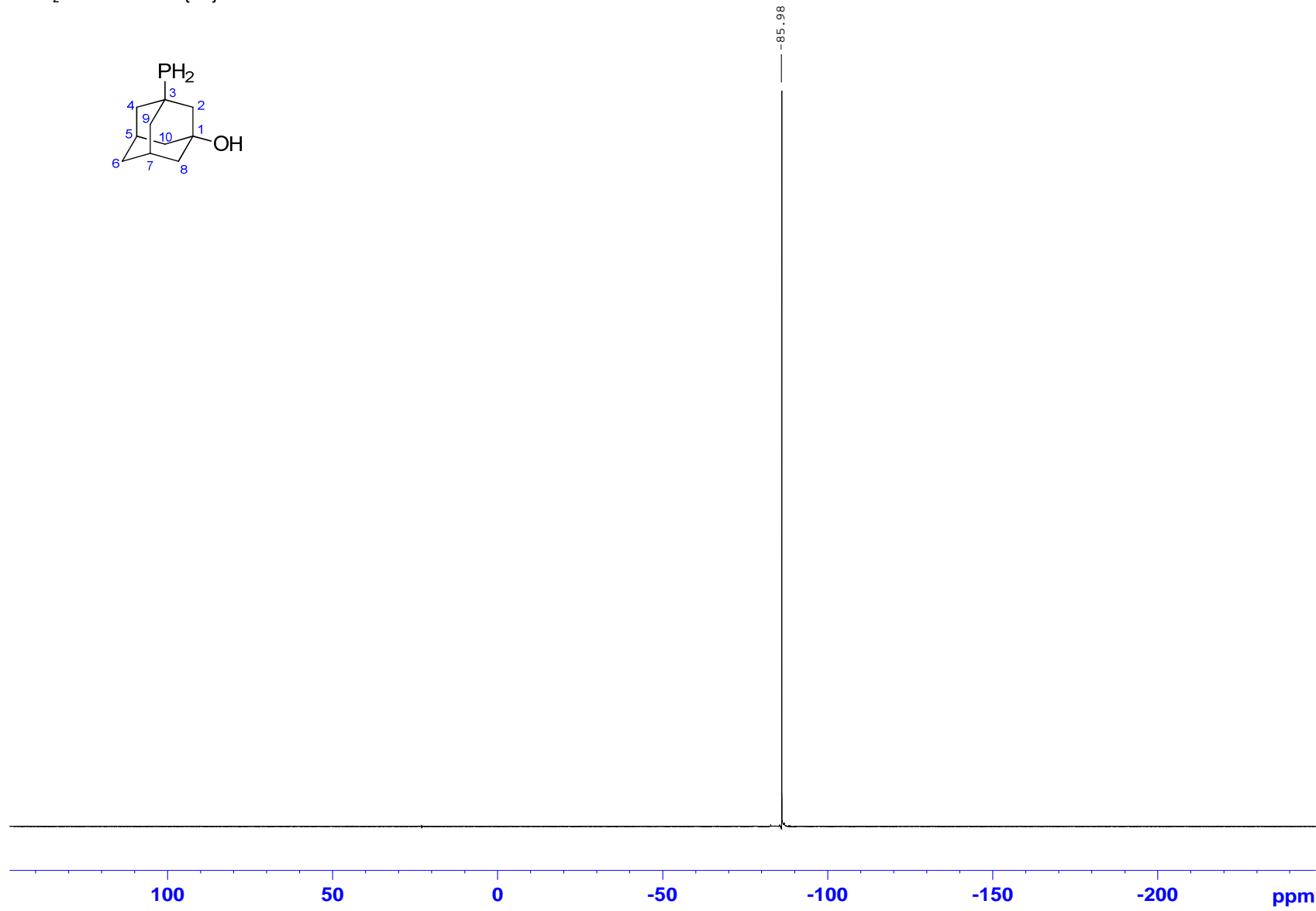
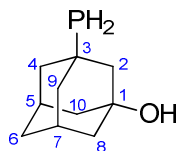
F2 - Acquisition Parameters
Date_     20141013
Time      14.45
INSTRUM   spect
PROBHD    5 mm PABBI 1H/
PULPROG   zg30
TD         65536
SOLVENT   C6D6
NS         512
DS         4
SWH        96153.844 Hz
FIDRES     1.467191 Hz
AQ         0.3408372 sec
RG         2050
DW         5.200 usec
DE         6.50 usec
TE         300.0 K
D1         2.00000000 sec
TD0        1

===== CHANNEL f1 =====
SF01      242.9654088 MHz
NUC1       31P
P1         22.50 usec
PLW1       49.08300018 W

F2 - Processing parameters
SI         32768
SF         242.9775580 MHz
WDW        EM
SSB        0
LB         1.00 Hz
GB         0
PC         1.40
    
```

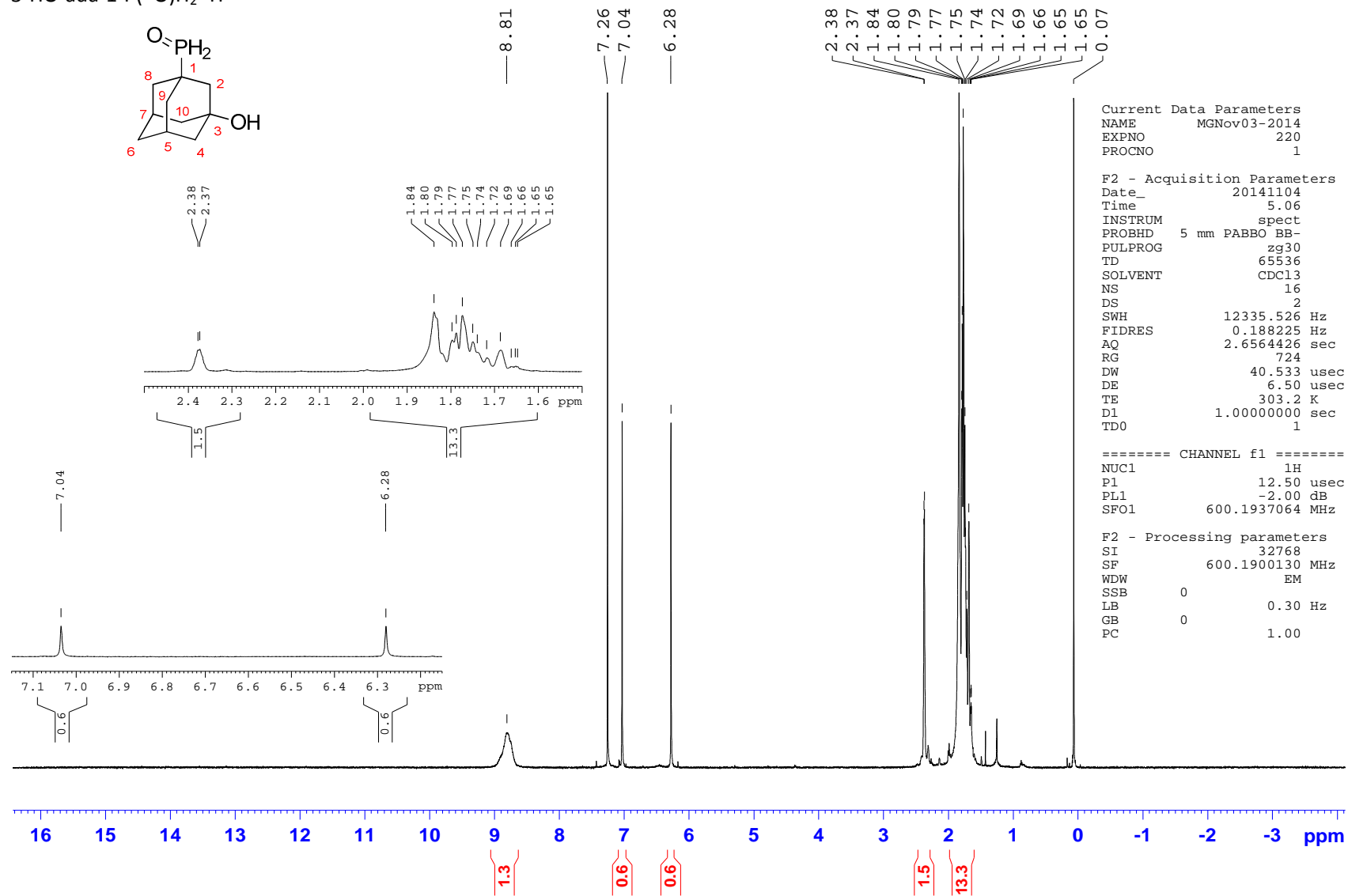


3-PH₂-ada-1-OH ³¹P{¹H}

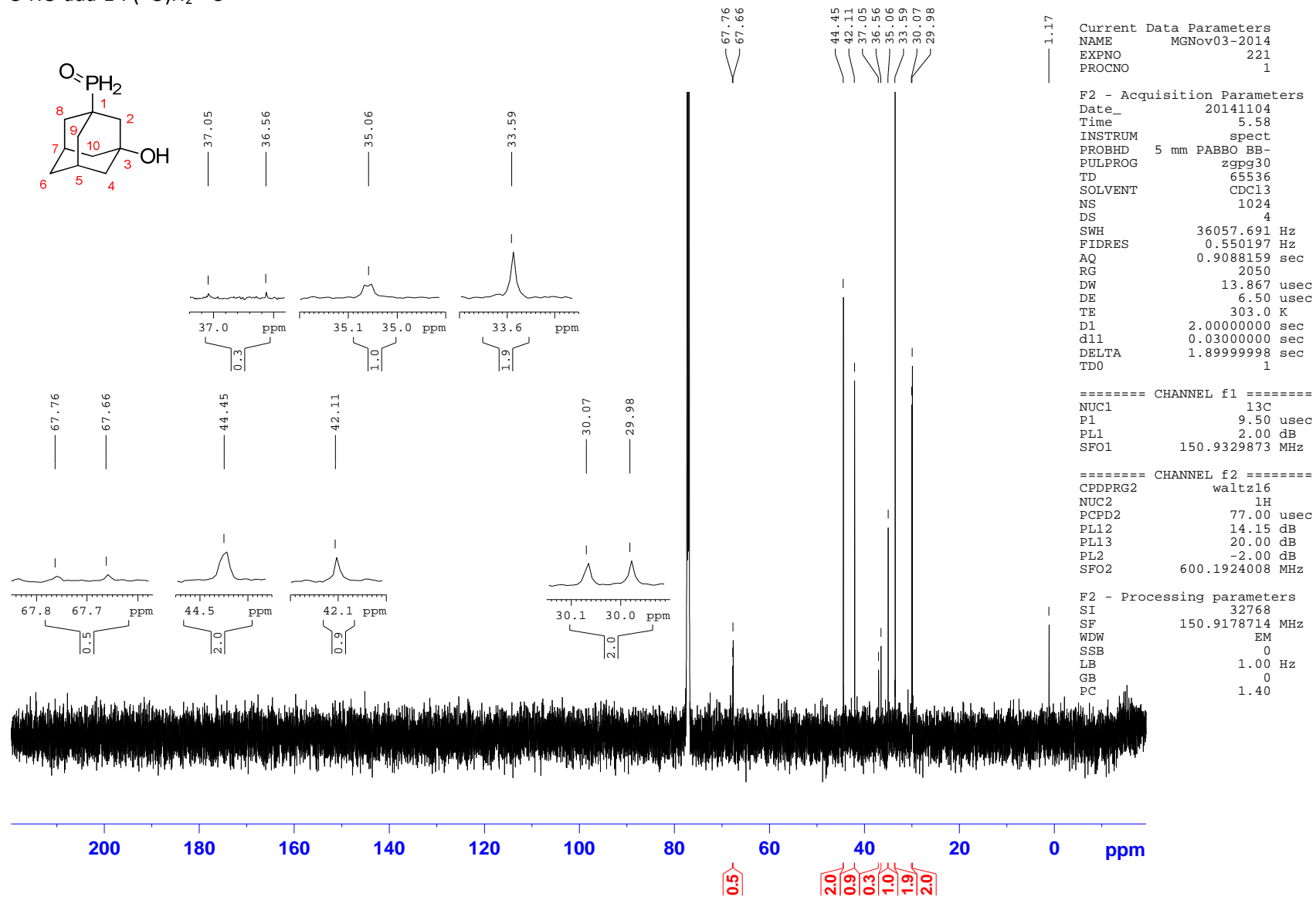


m)-(3-Hydroxyadamantan-1-yl)phosphine oxide (**187**)

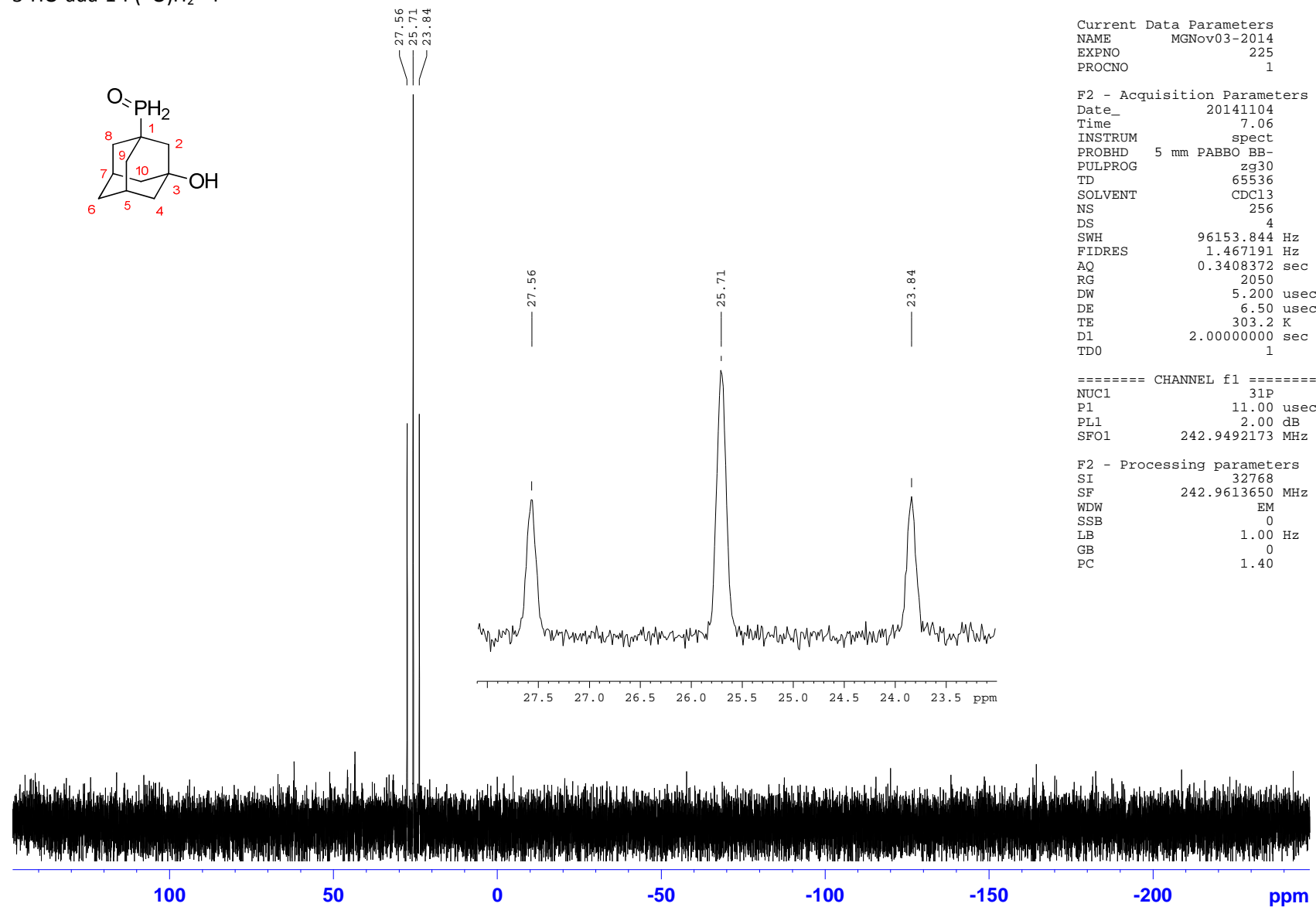
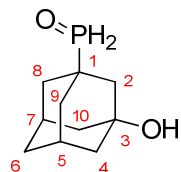
3-HO-ada-1-P(=O)H₂ ¹H



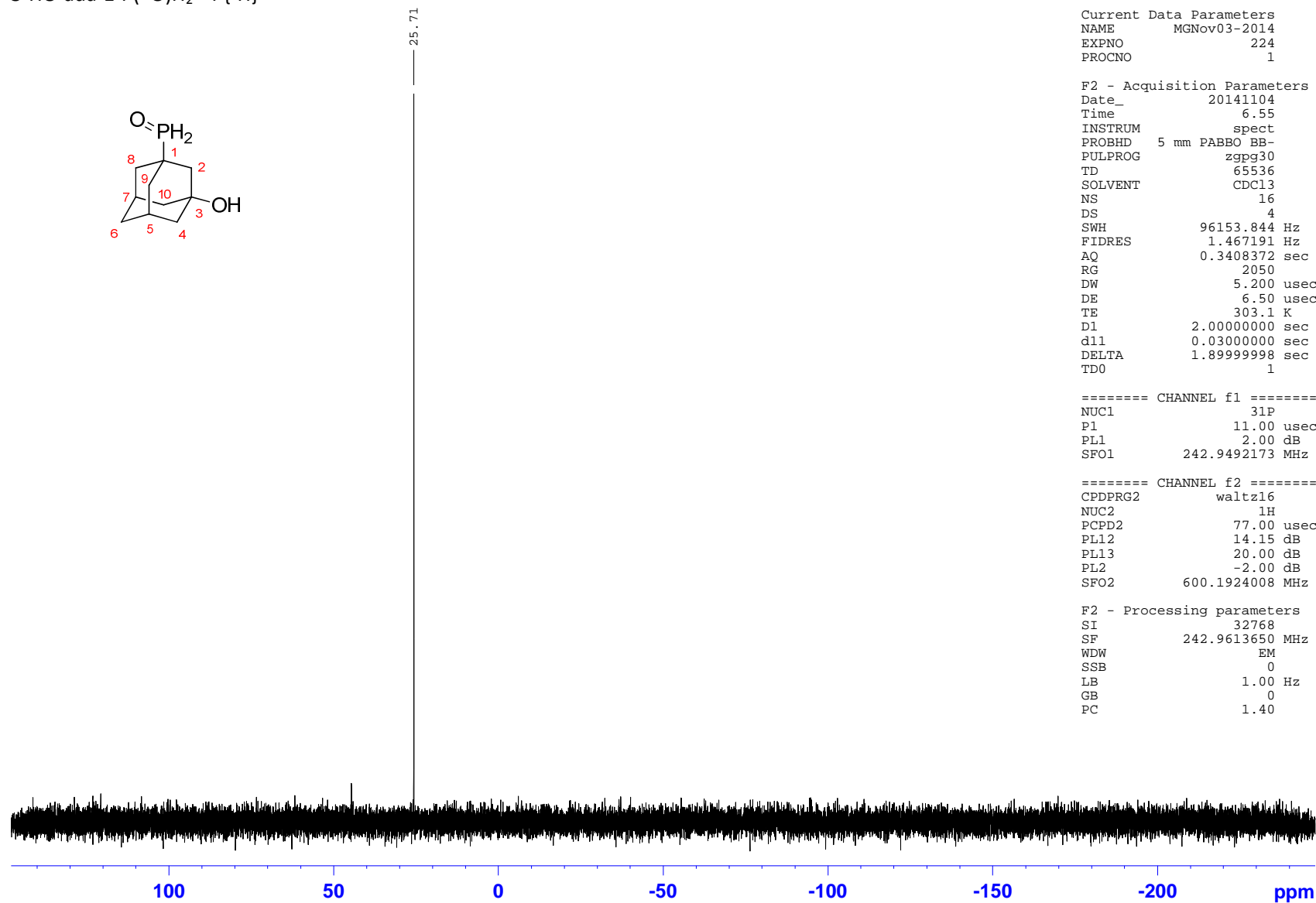
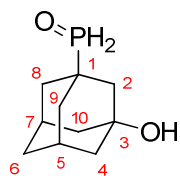
3-HO-ada-1-P(=O)H₂ ¹³C



3-HO-ada-1-P(=O)H₂ ³¹P



3-HO-ada-1-P(=O)H₂ ³¹P{¹H}



```

Current Data Parameters
NAME      MGNov03-2014
EXPNO     224
PROCNO    1

F2 - Acquisition Parameters
Date_     20141104
Time      6.55
INSTRUM   spect
PROBHD    5 mm PABBO BB-
PULPROG   zgpg30
TD         65536
SOLVENT   CDC13
NS         16
DS         4
SWH        96153.844 Hz
FIDRES     1.467191 Hz
AQ         0.3408372 sec
RG         2050
DW         5.200 usec
DE         6.50 usec
TE         303.1 K
D1         2.00000000 sec
d11        0.03000000 sec
DELTA     1.89999998 sec
TD0        1

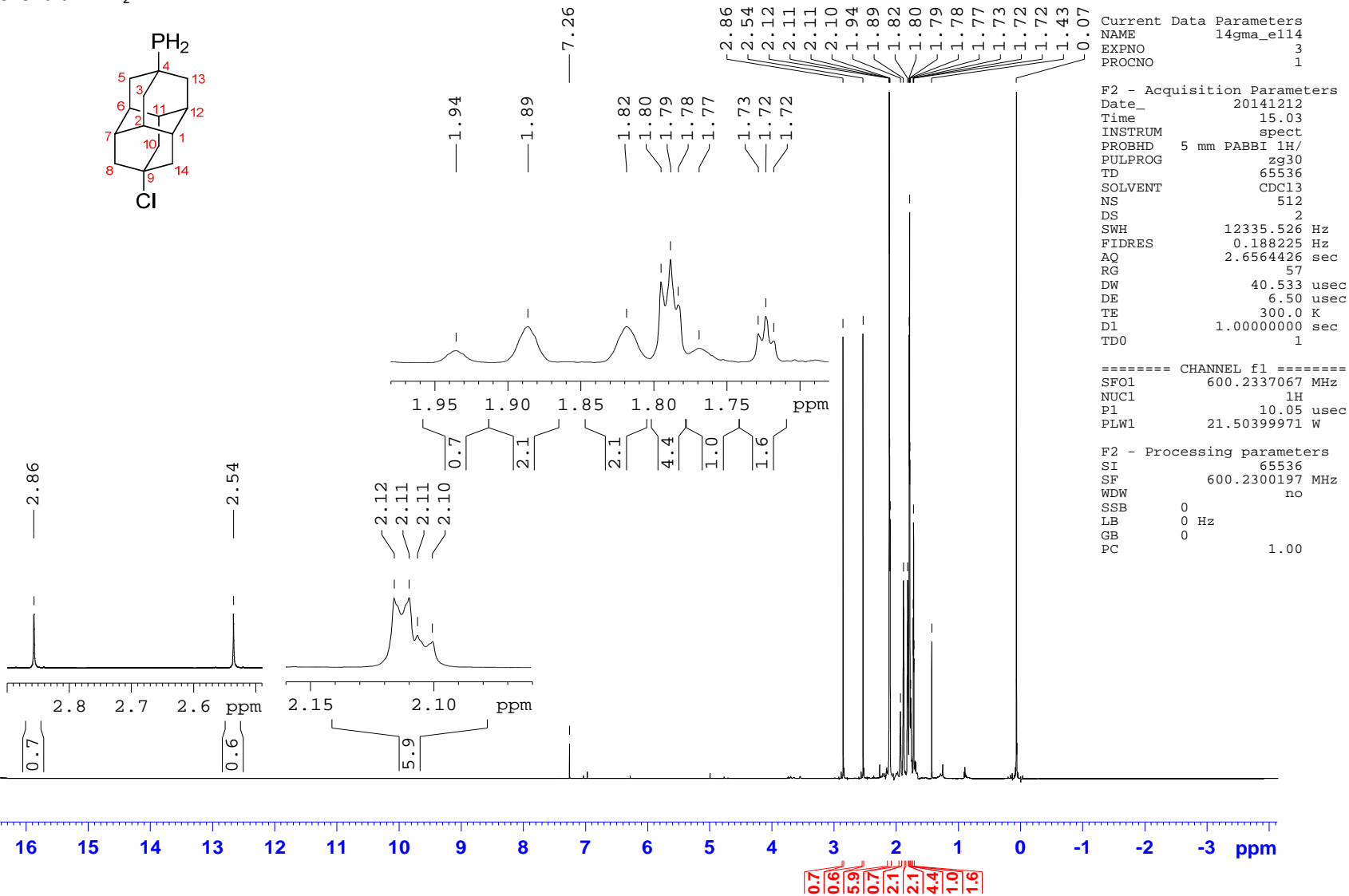
===== CHANNEL f1 =====
NUC1       31P
P1         11.00 usec
PL1        2.00 dB
SFO1       242.9492173 MHz

===== CHANNEL f2 =====
CPDPRG2    waltz16
NUC2       1H
PCPD2      77.00 usec
PL12       14.15 dB
PL13       20.00 dB
PL2        -2.00 dB
SFO2       600.1924008 MHz

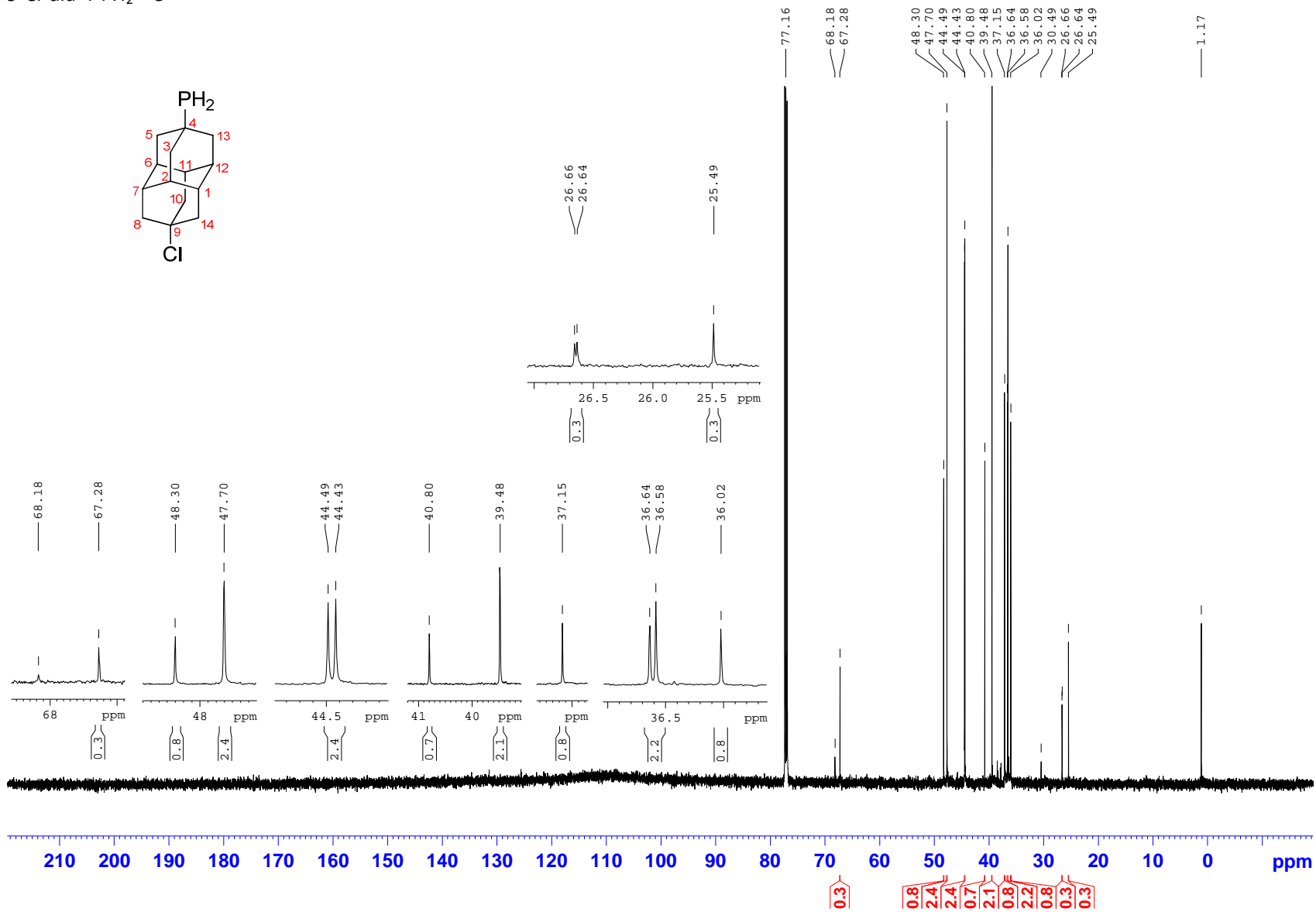
F2 - Processing parameters
SI         32768
SF         242.9613650 MHz
WDW        EM
SSB        0
LB         1.00 Hz
GB         0
PC         1.40
    
```

n) (9-Chlorodiamant-4-yl) phosphine (**188**)

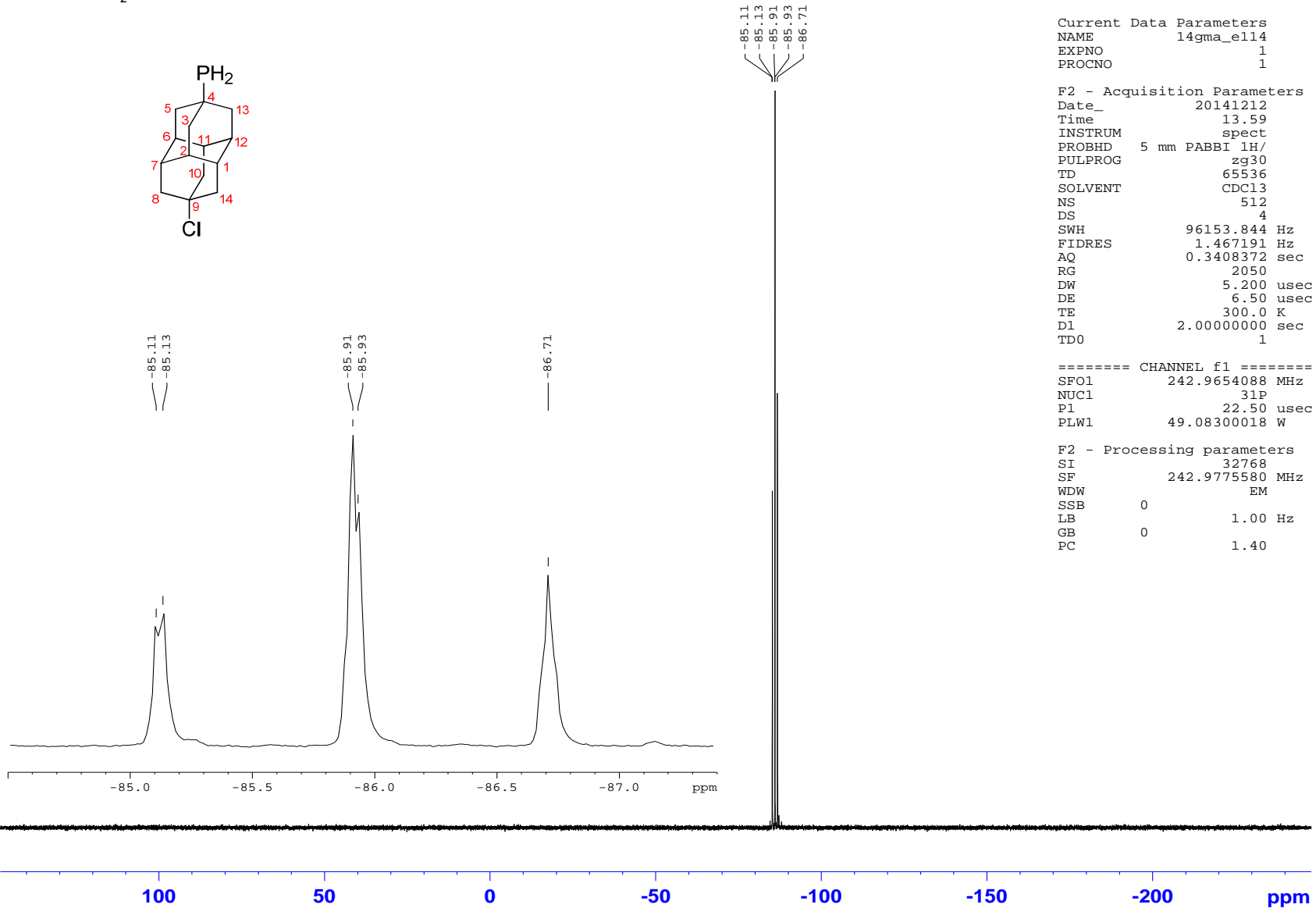
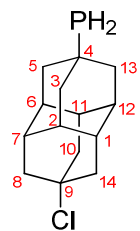
9-Cl-dia-4-PH₂ ¹H



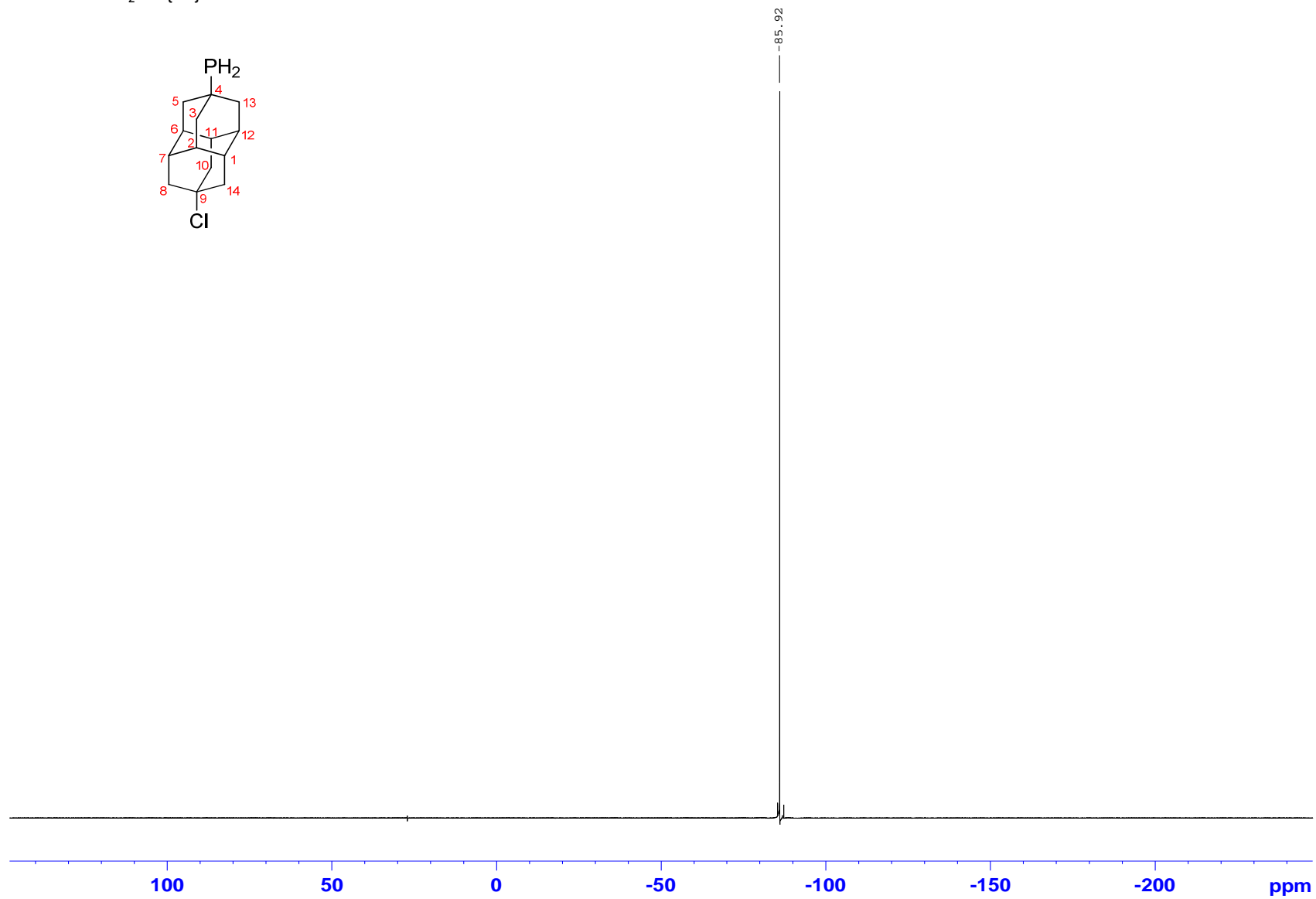
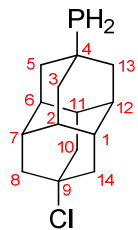
9-Cl-dia-4-PH₂ ¹³C



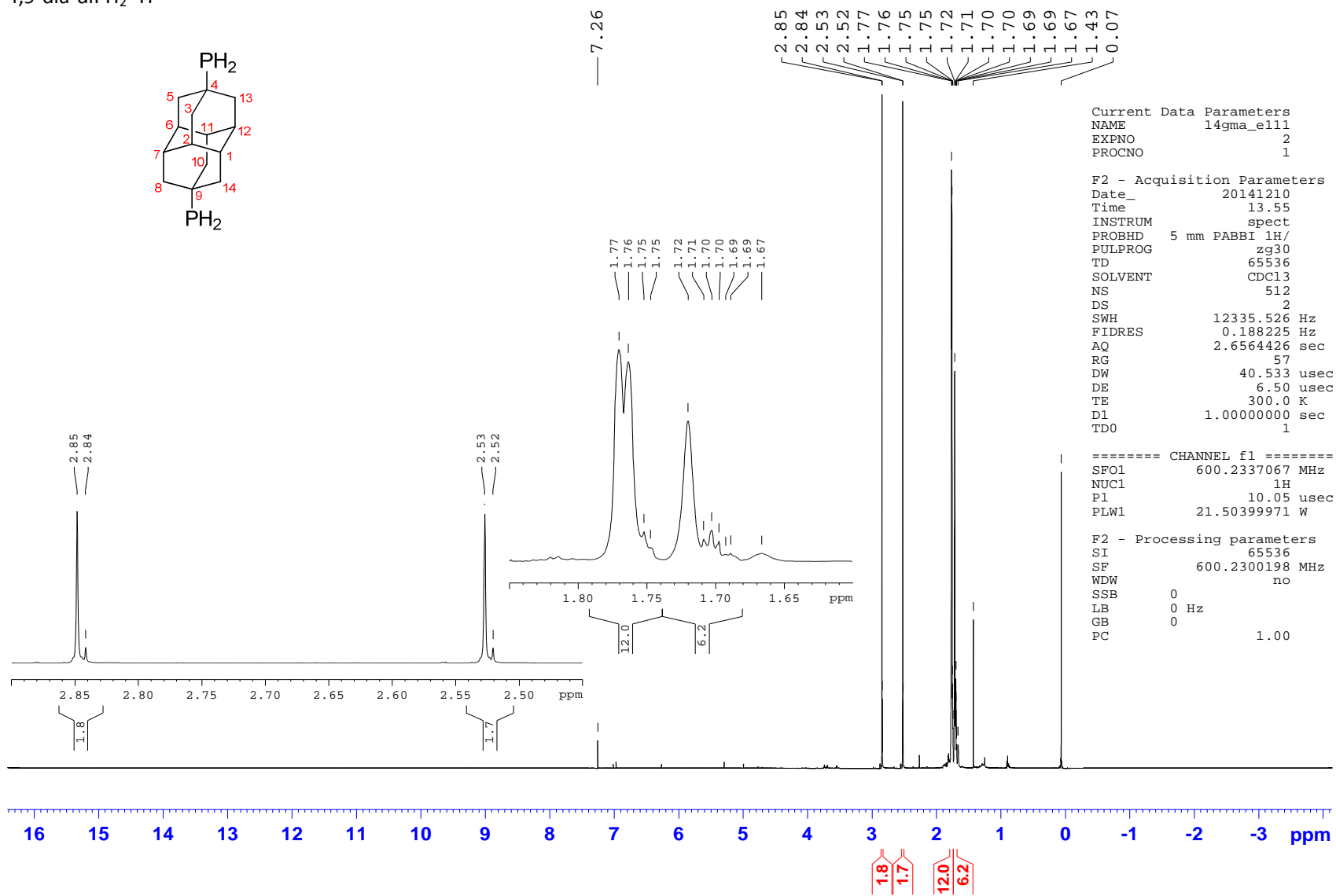
9-Cl-dia-4-PH₂ ³¹P



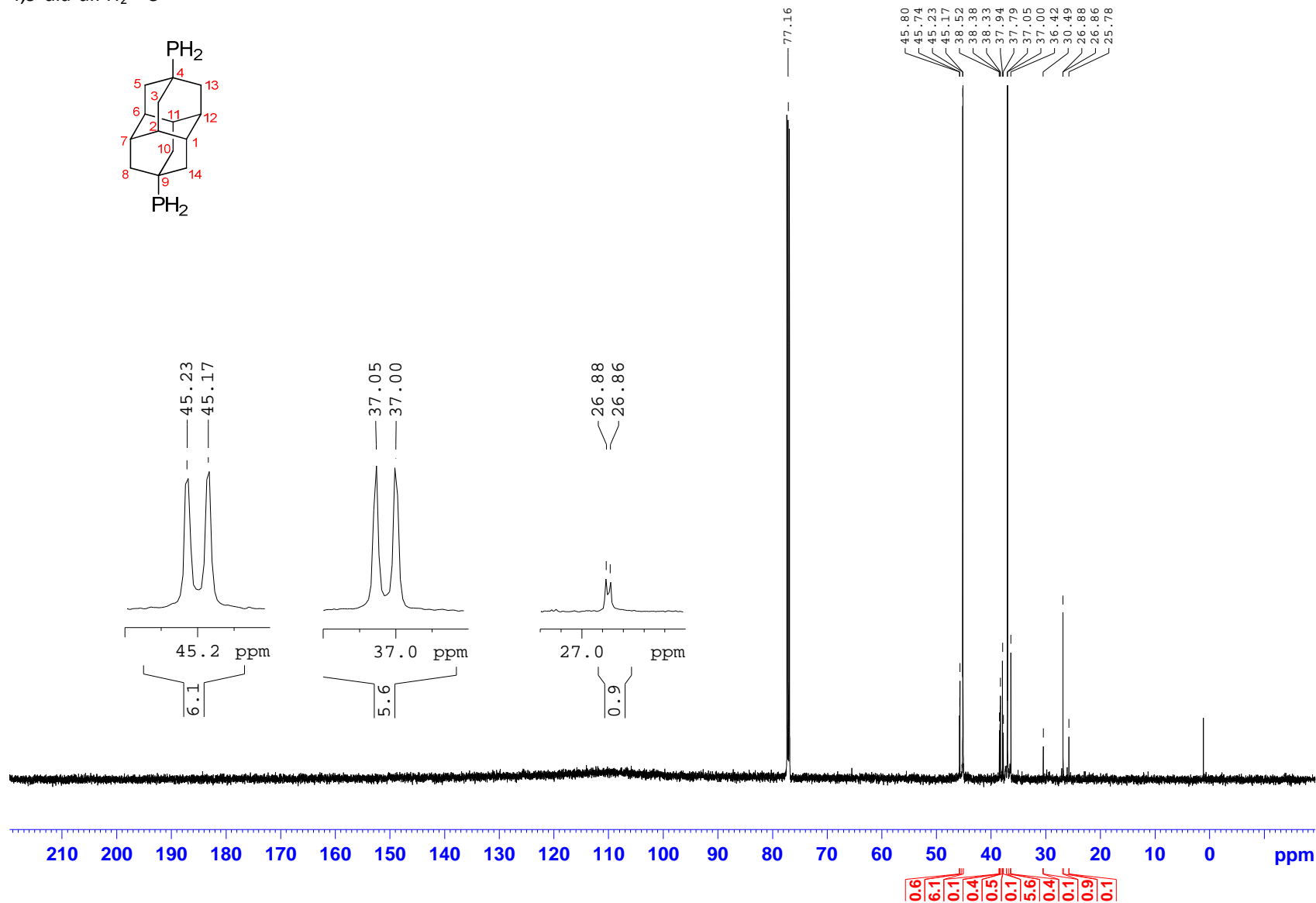
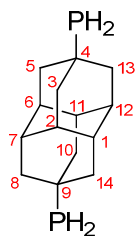
9-Cl-dia-4-PH₂ ³¹P{¹H}



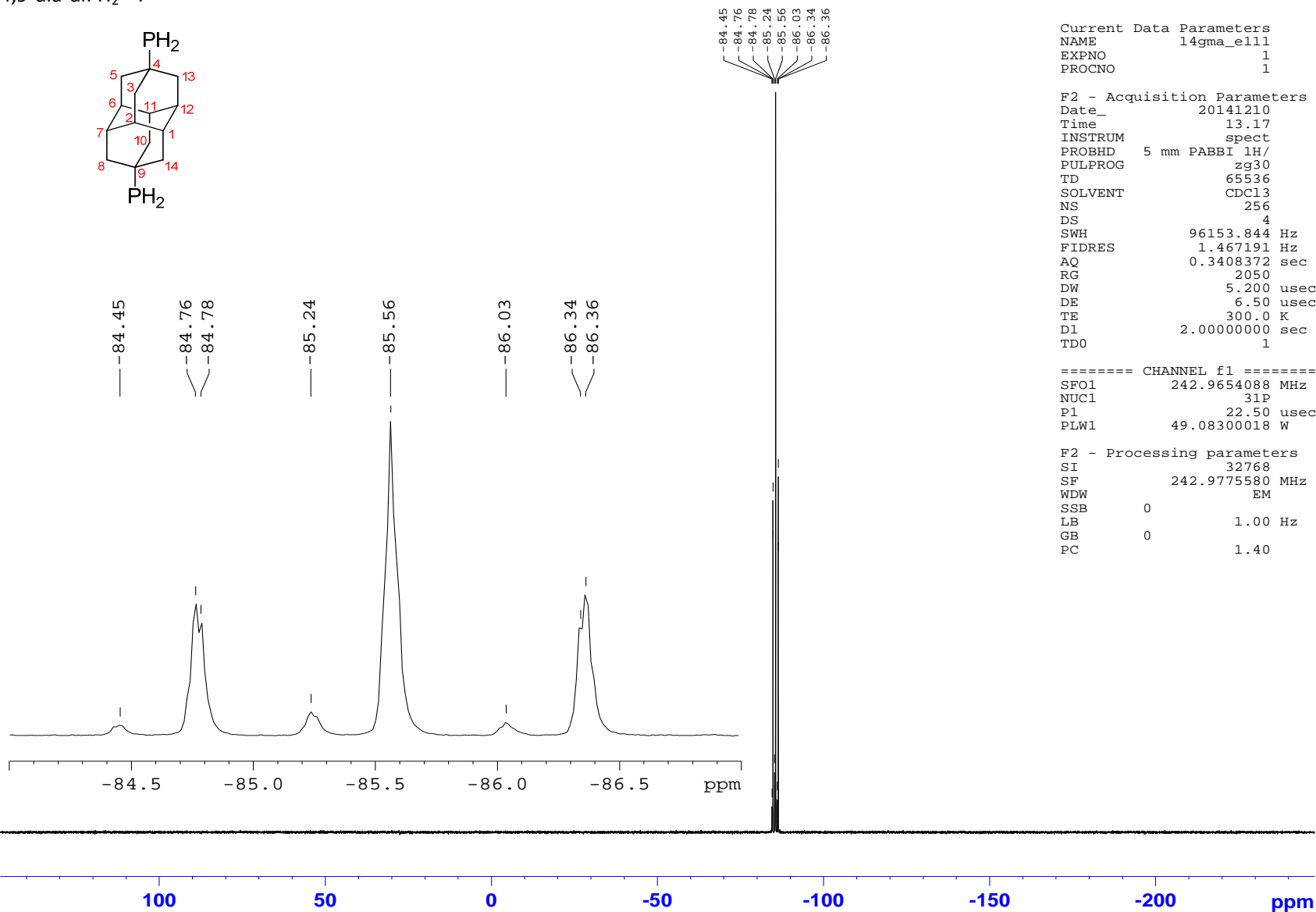
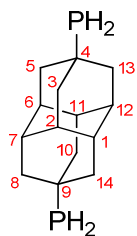
o) (4,9-Diamantyl)diphosphine (**189**)
4,9-dia-diPH₂¹H



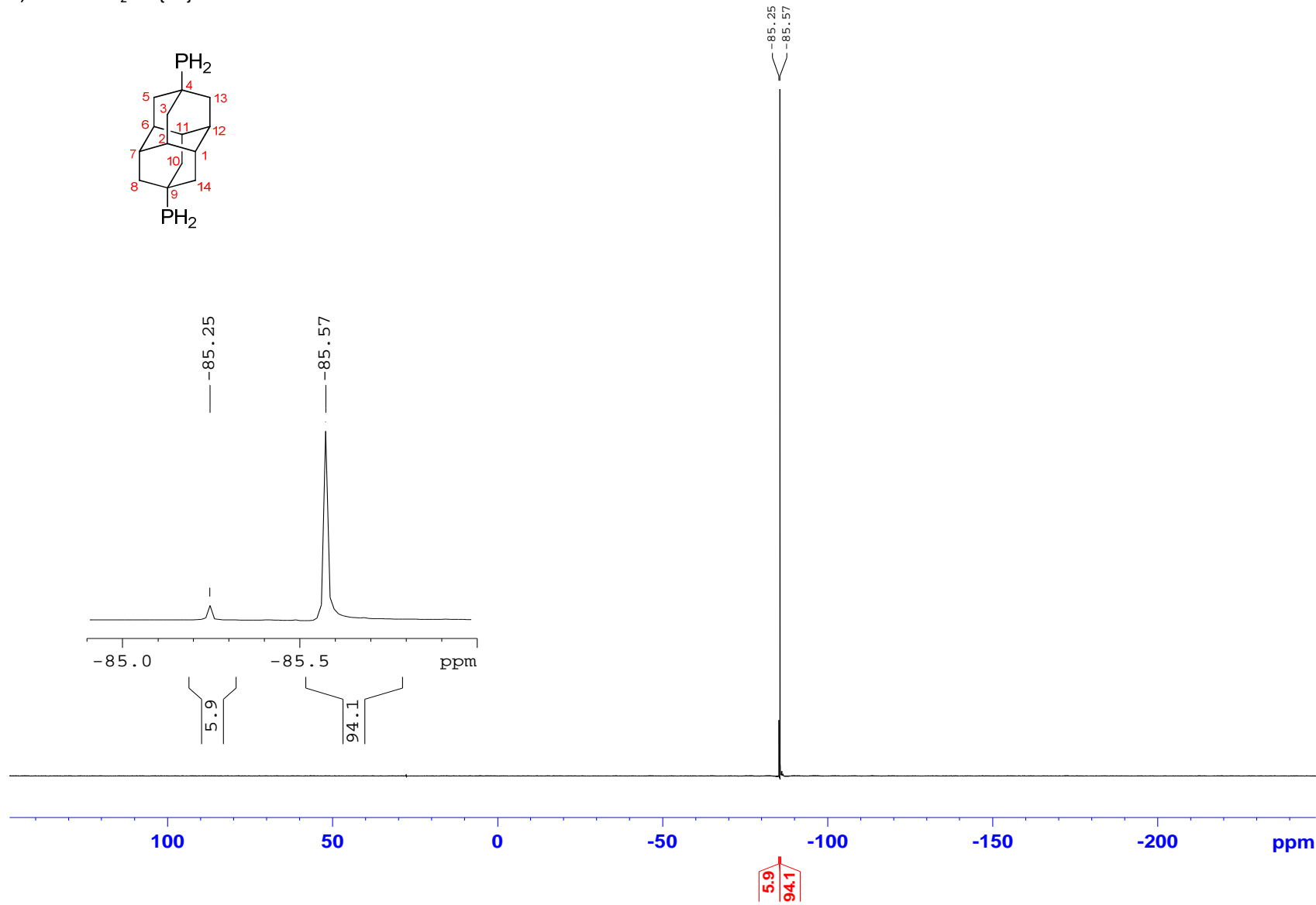
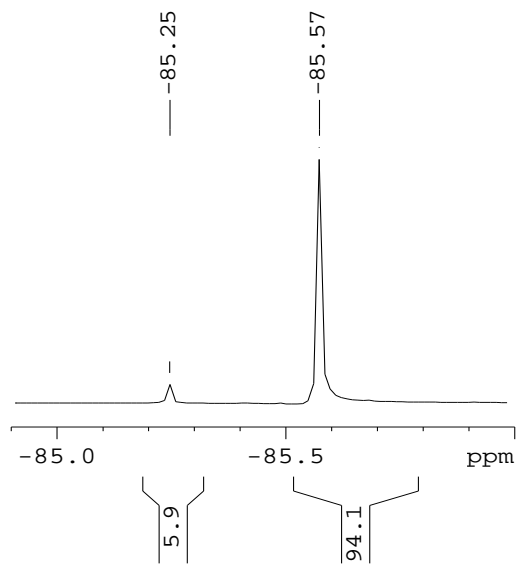
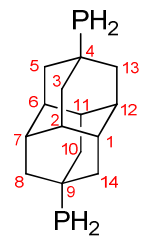
4,9-dia-diPH₂ ¹³C



4,9-dia-diPH₂ ³¹P

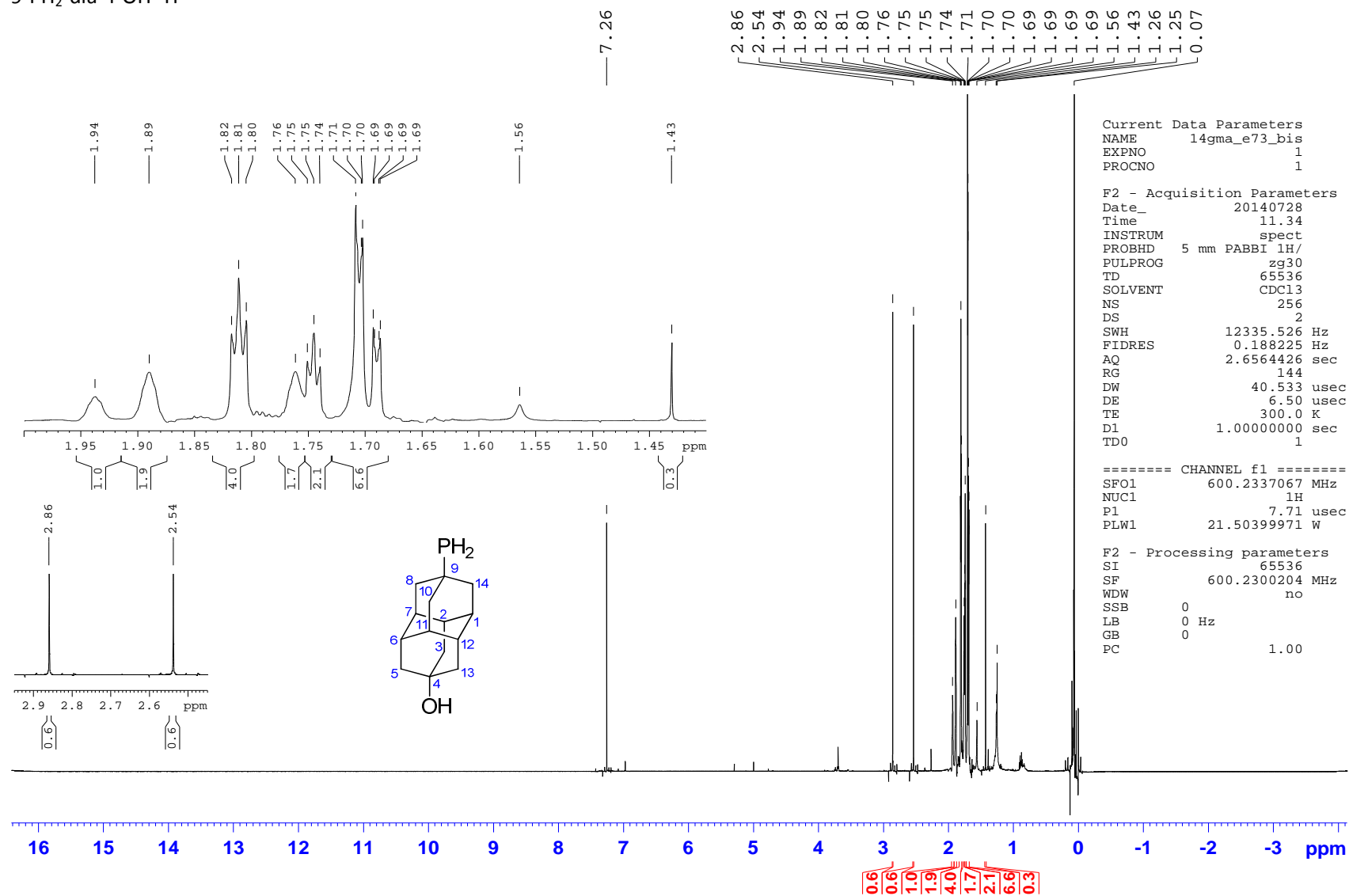


4,9-dia-diPH₂ ³¹P{¹H}

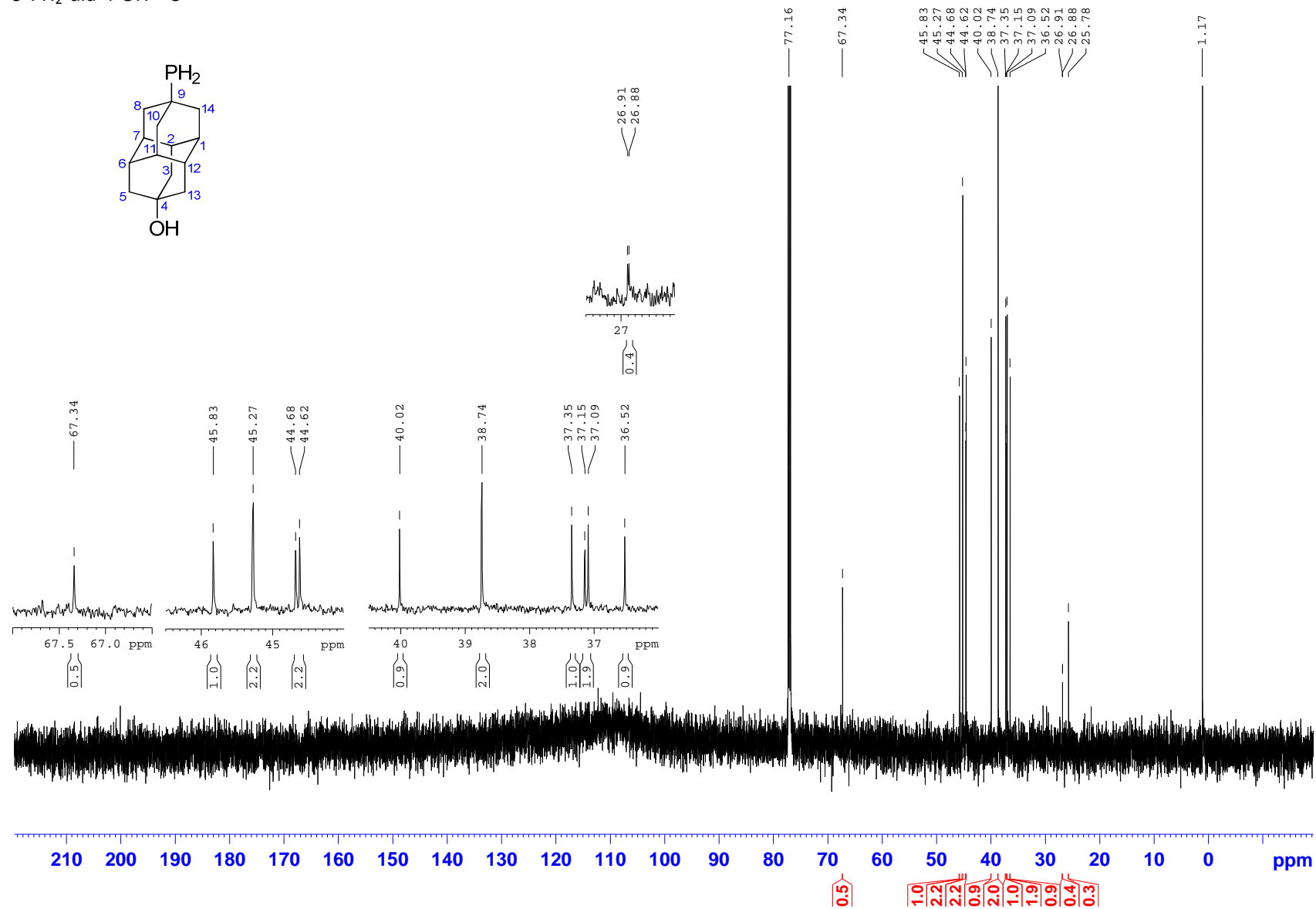
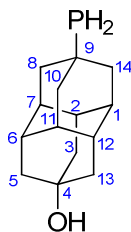


p) 9-Phosphinodiamantan-4-ol (**190**)

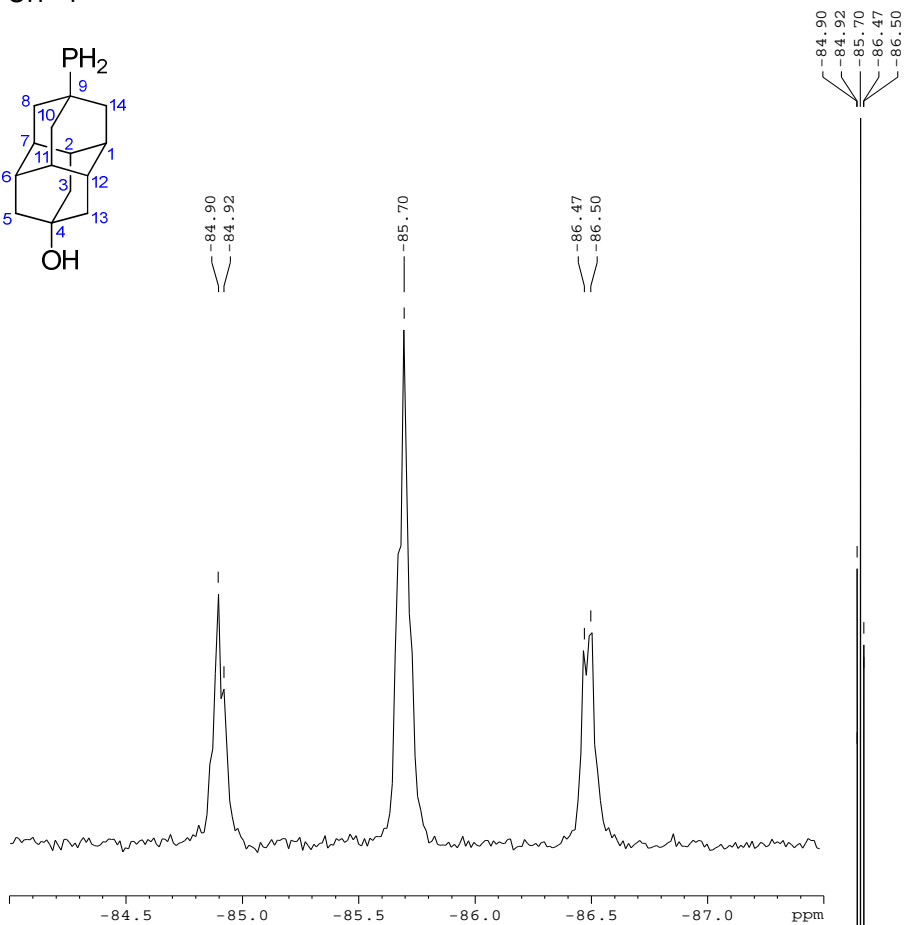
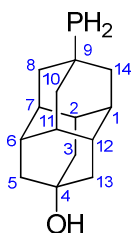
9-PH₂-dia-4-OH ¹H



9-PH₂-dia-4-OH ¹³C



9-PH₂-dia-4-OH ³¹P



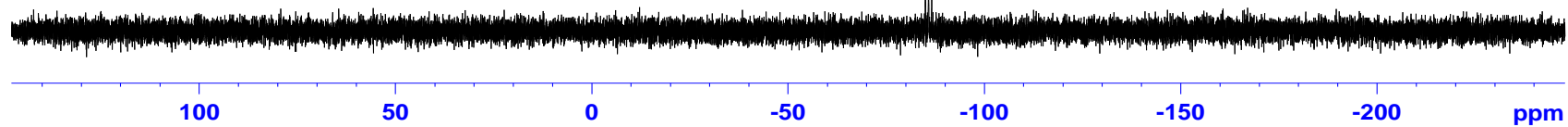
```

Current Data Parameters
NAME      14gma_e73_bis
EXPNO     3
PROCNO    1

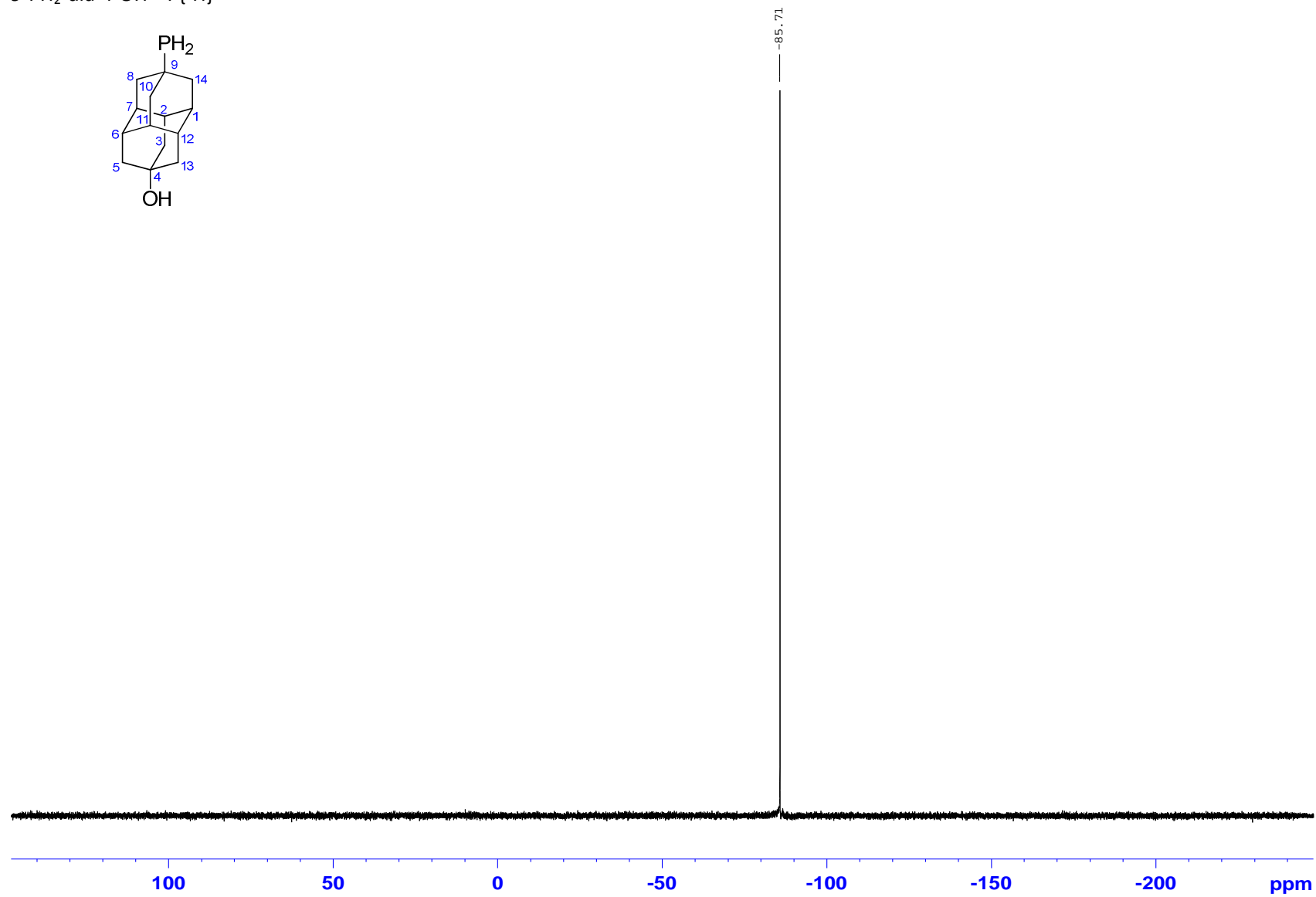
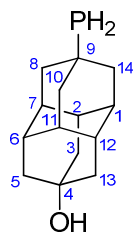
F2 - Acquisition Parameters
Date_     20140728
Time      12.18
INSTRUM   spect
PROBHD    5 mm PABBI 1H/
PULPROG   zg30
TD        65536
SOLVENT   CDCl3
NS        256
DS        4
SWH       96153.844 Hz
FIDRES    1.467191 Hz
AQ        0.3408372 sec
RG        2050
DW        5.200 usec
DE        6.50 usec
TE        300.0 K
D1        2.00000000 sec
TD0       1

===== CHANNEL f1 =====
SFO1      242.9654088 MHz
NUC1      31P
P1        22.50 usec
PLW1      49.08300018 W

F2 - Processing parameters
SI        32768
SF        242.9775580 MHz
WDW       EM
SSB       0
LB        1.00 Hz
GB        0
PC        1.40
    
```

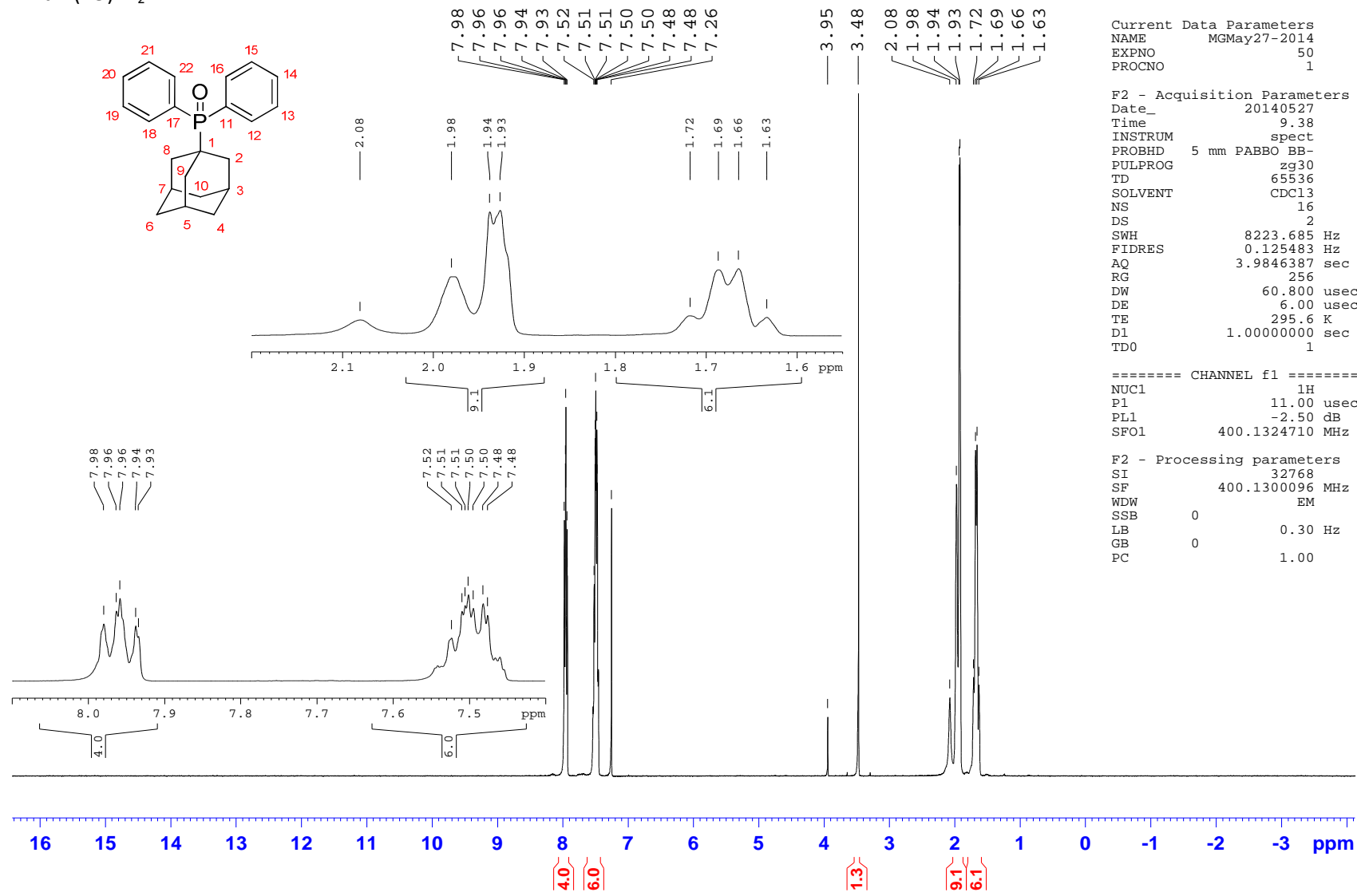


9-PH₂-dia-4-OH ³¹P{¹H}

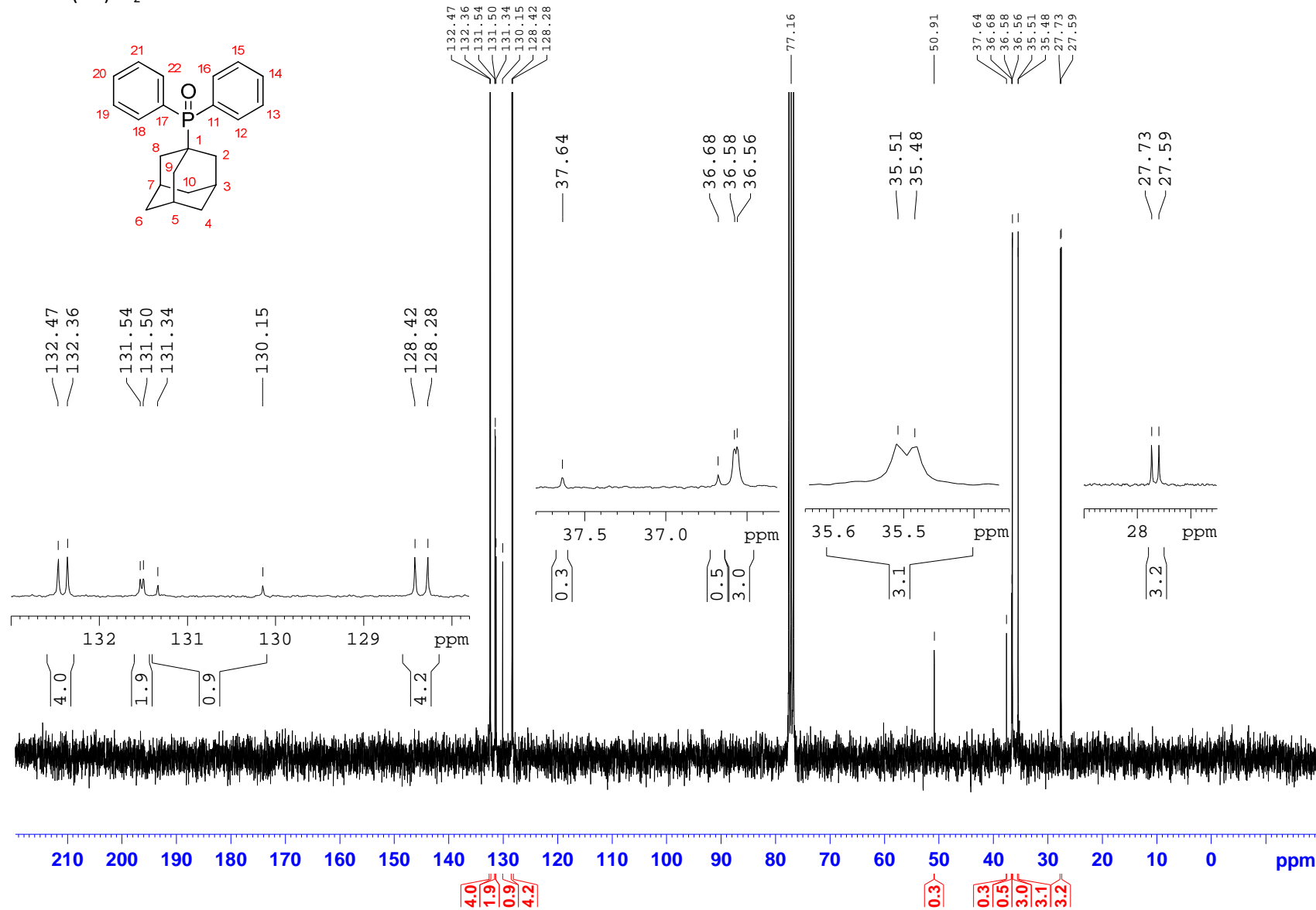


q) 1-Adamantylidiphenylphosphine oxide (**191**)

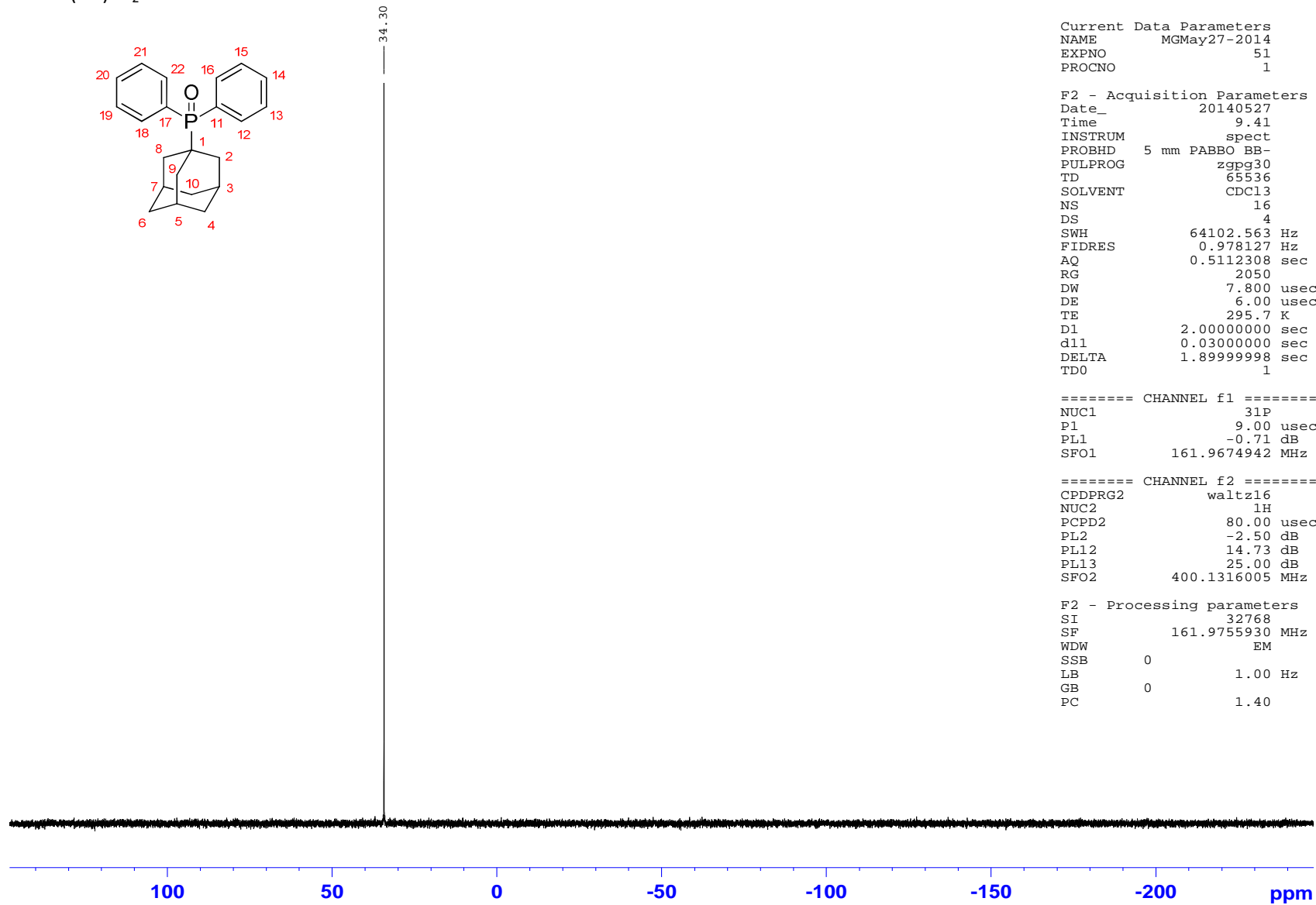
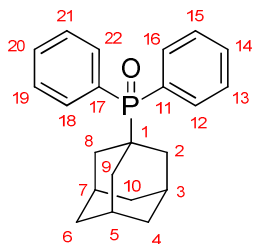
1-Ad-P(=O)Ph₂¹H



1-Ad-P(=O)Ph₂ ¹³C



1-Ad-P(=O)Ph₂ ³¹P



```

Current Data Parameters
NAME      MGMay27-2014
EXPNO     51
PROCNO    1

F2 - Acquisition Parameters
Date_     20140527
Time      9.41
INSTRUM   spect
PROBHD    5 mm PABBO BB-
PULPROG   zgpg30
TD         65536
SOLVENT   CDCl3
NS         16
DS         4
SWH        64102.563 Hz
FIDRES     0.978127 Hz
AQ         0.5112308 sec
RG         2050
DW         7.800 usec
DE         6.00 usec
TE         295.7 K
D1         2.00000000 sec
d11        0.03000000 sec
DELTA     1.89999998 sec
TD0        1

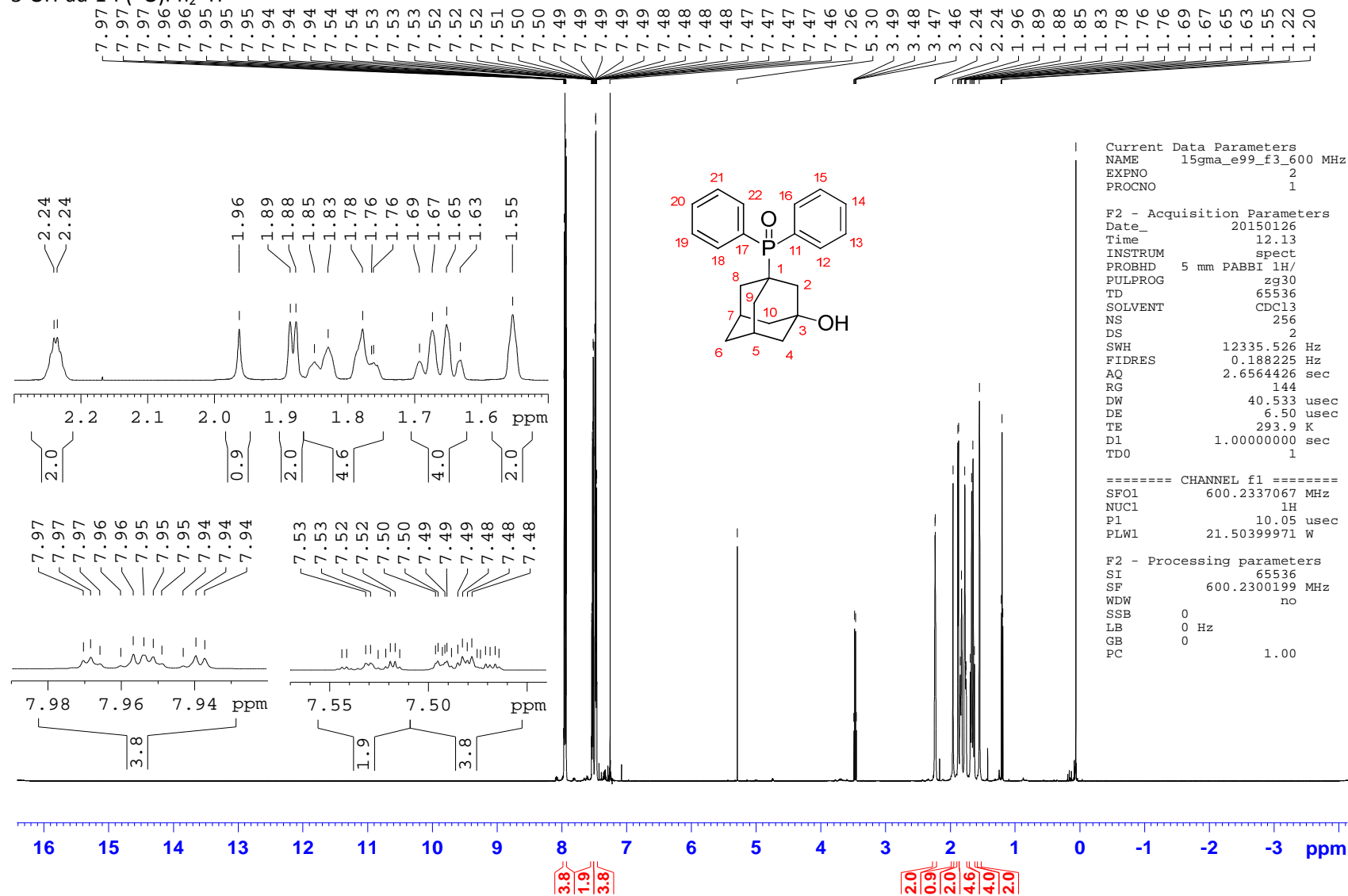
===== CHANNEL f1 =====
NUC1       31P
P1         9.00 usec
PL1        -0.71 dB
SFO1       161.9674942 MHz

===== CHANNEL f2 =====
CPDPRG2    waltz16
NUC2       1H
PCPD2      80.00 usec
PL2        -2.50 dB
PL12       14.73 dB
PL13       25.00 dB
SFO2       400.1316005 MHz

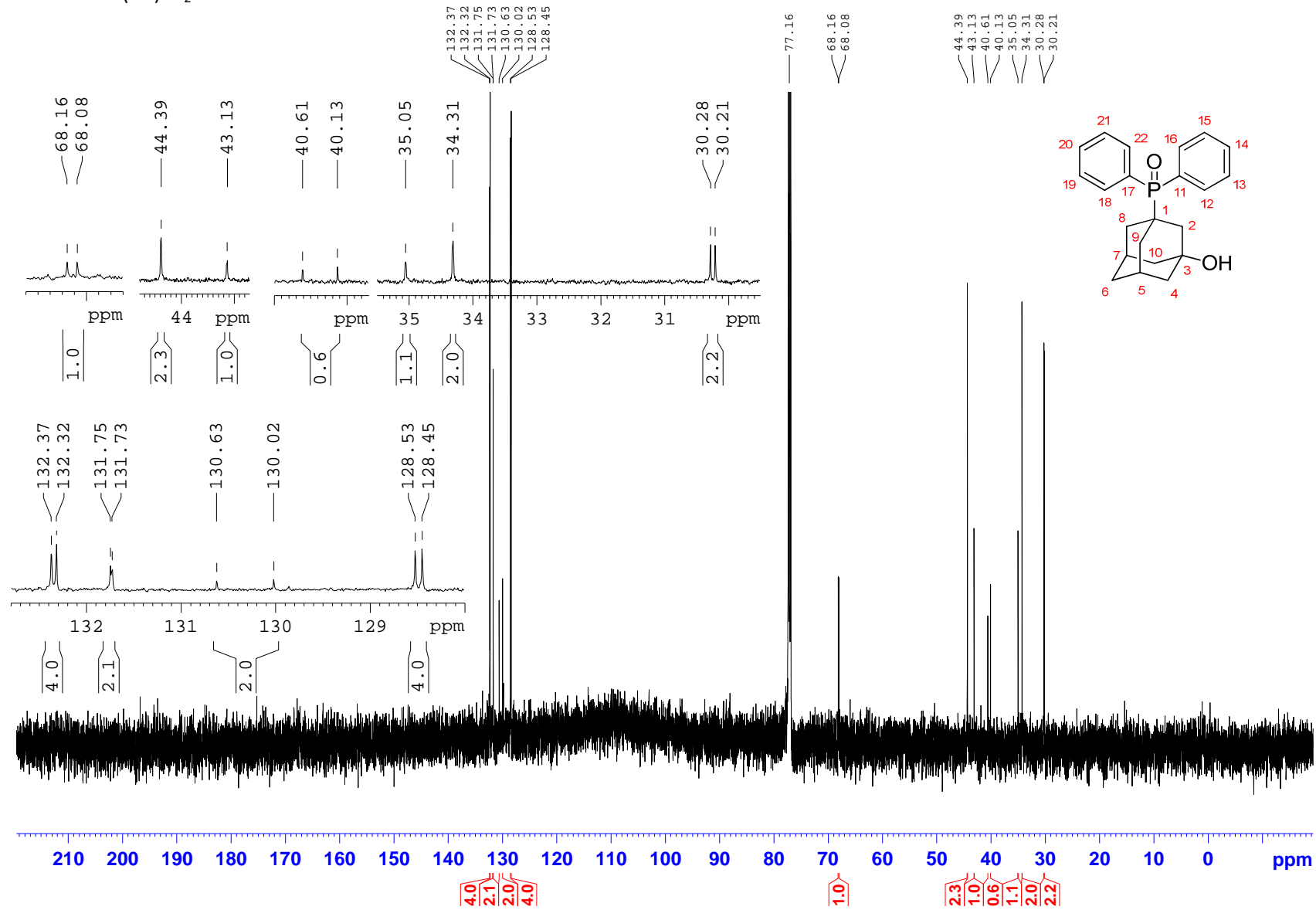
F2 - Processing parameters
SI         32768
SF         161.9755930 MHz
WDW        EM
SSB        0
LB         1.00 Hz
GB         0
PC         1.40
    
```

r) (3-Hydroxyadamant-1-yl)diphenylphosphine oxide (**192**)

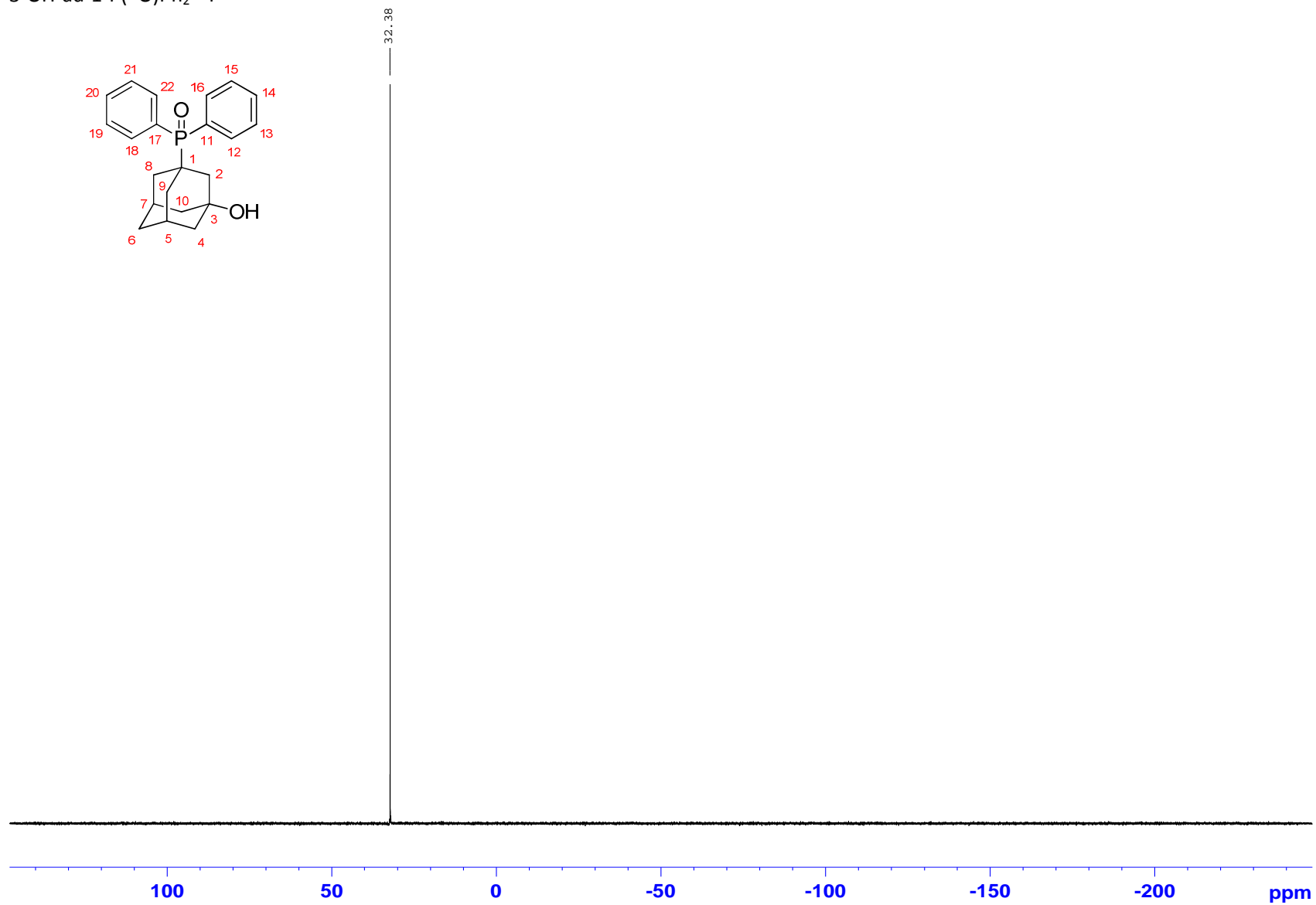
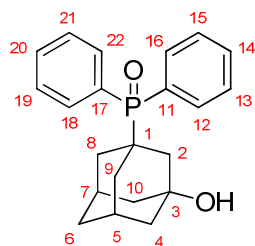
3-OH-ad-1-P(=O)Ph₂ ¹H



3-OH-ad-1-P(=O)Ph₂ ¹³C

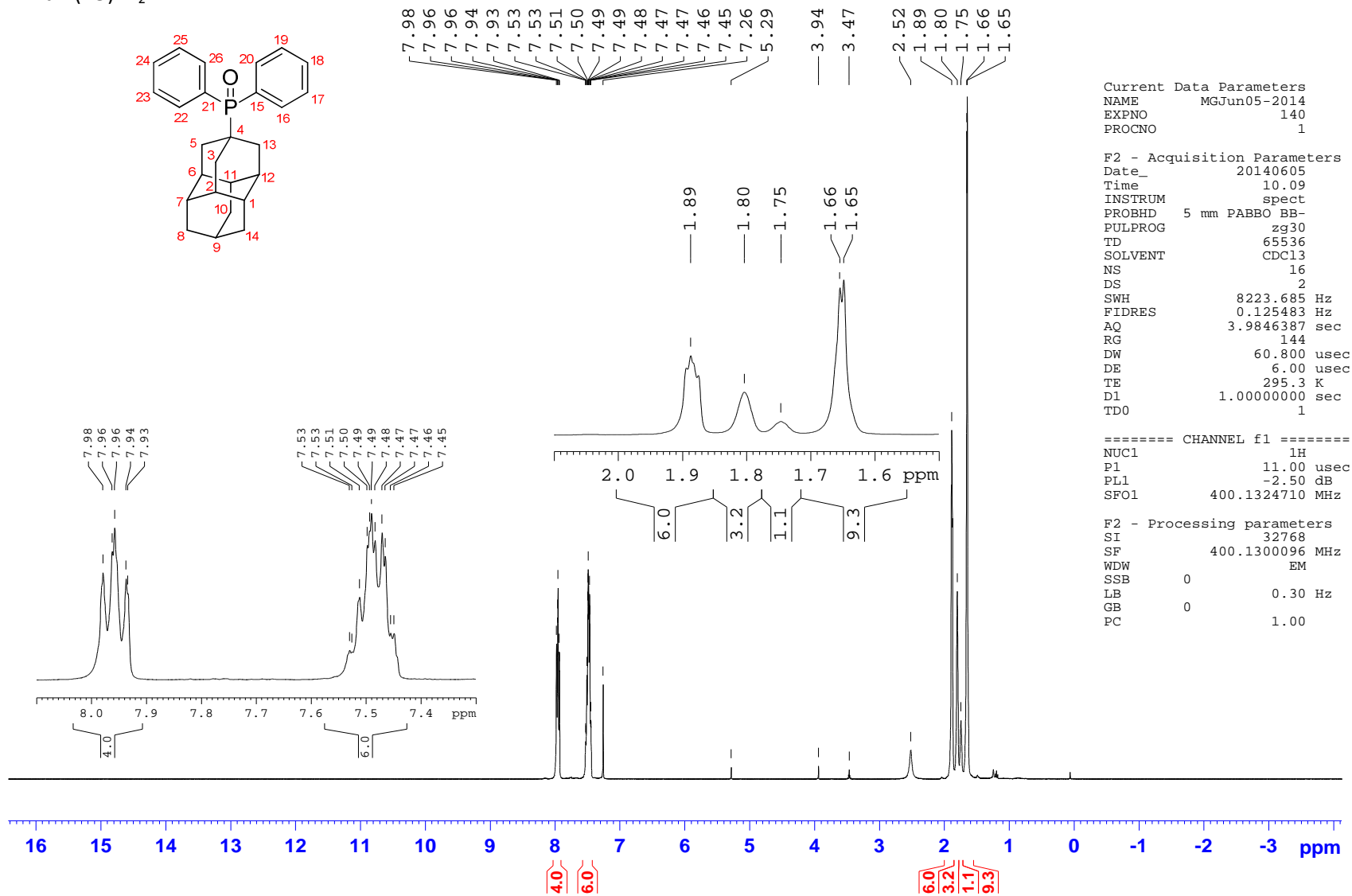


3-OH-ad-1-P(=O)Ph₂ ³¹P

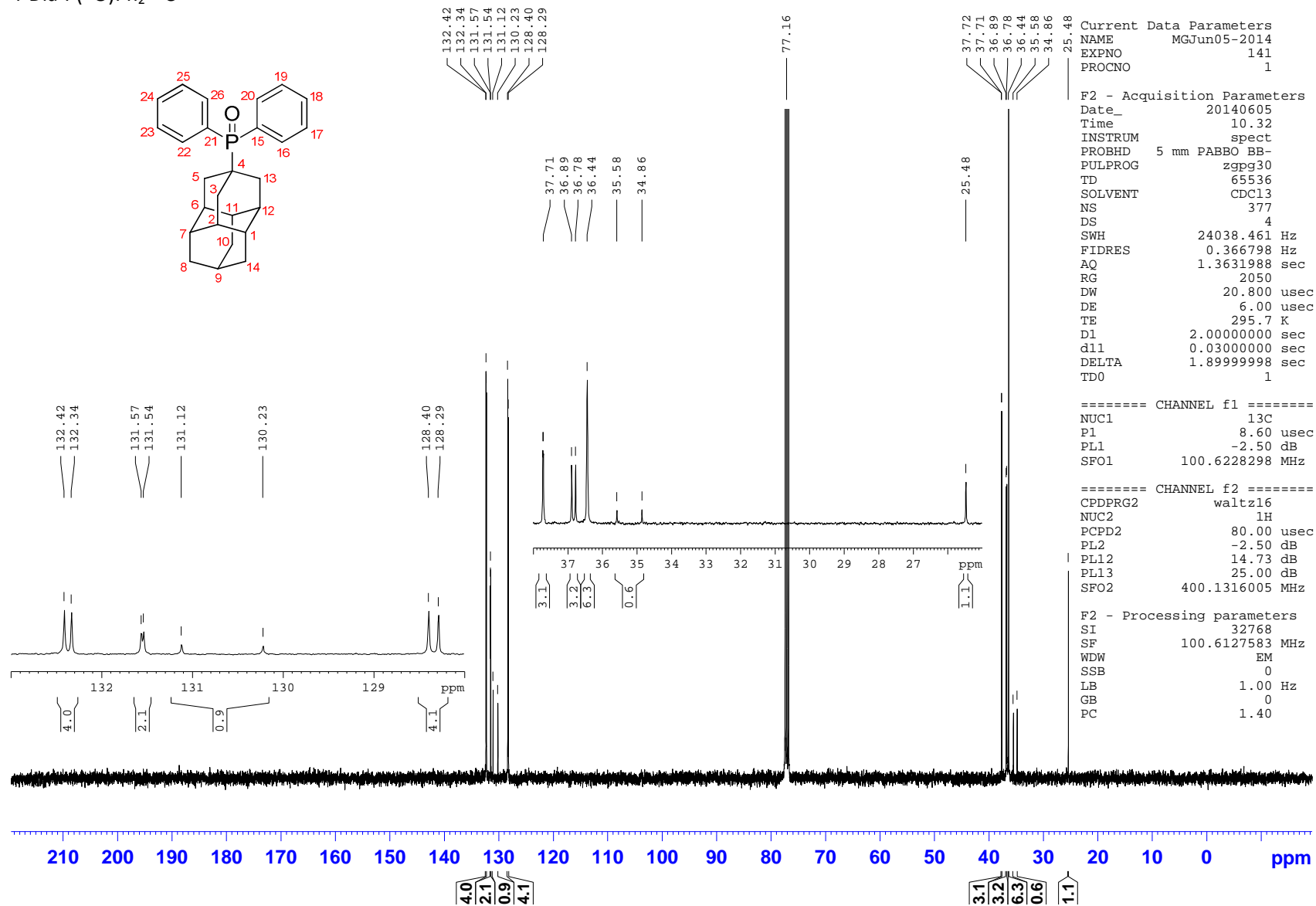


s) 4-Diamantylidiphenylphosphine oxide (**193**)

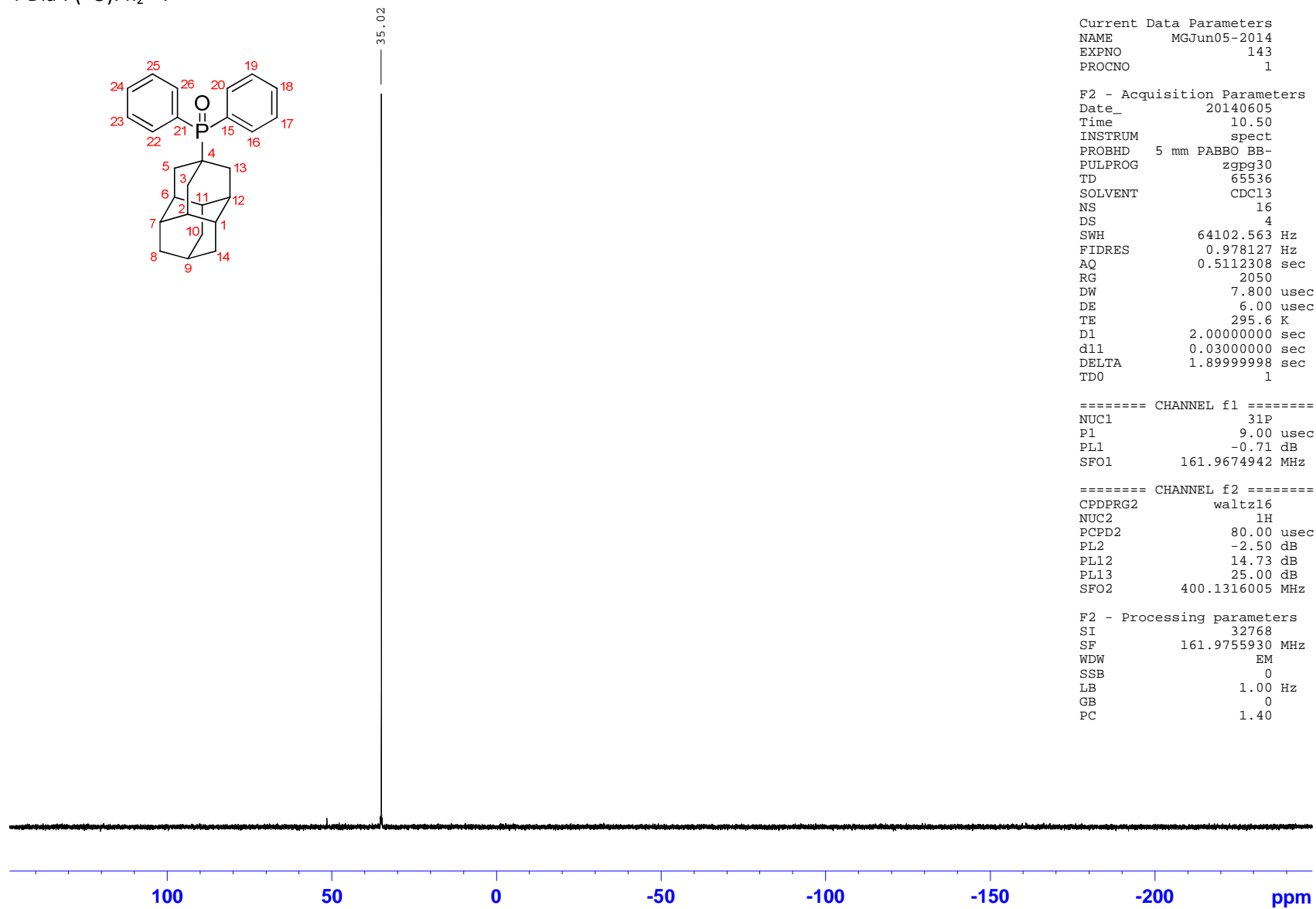
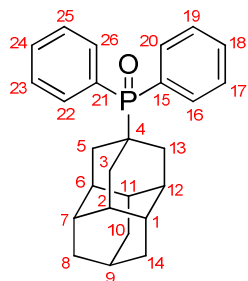
4-Dia-P(=O)Ph₂¹H



4-Dia-P(=O)Ph₂ ¹³C

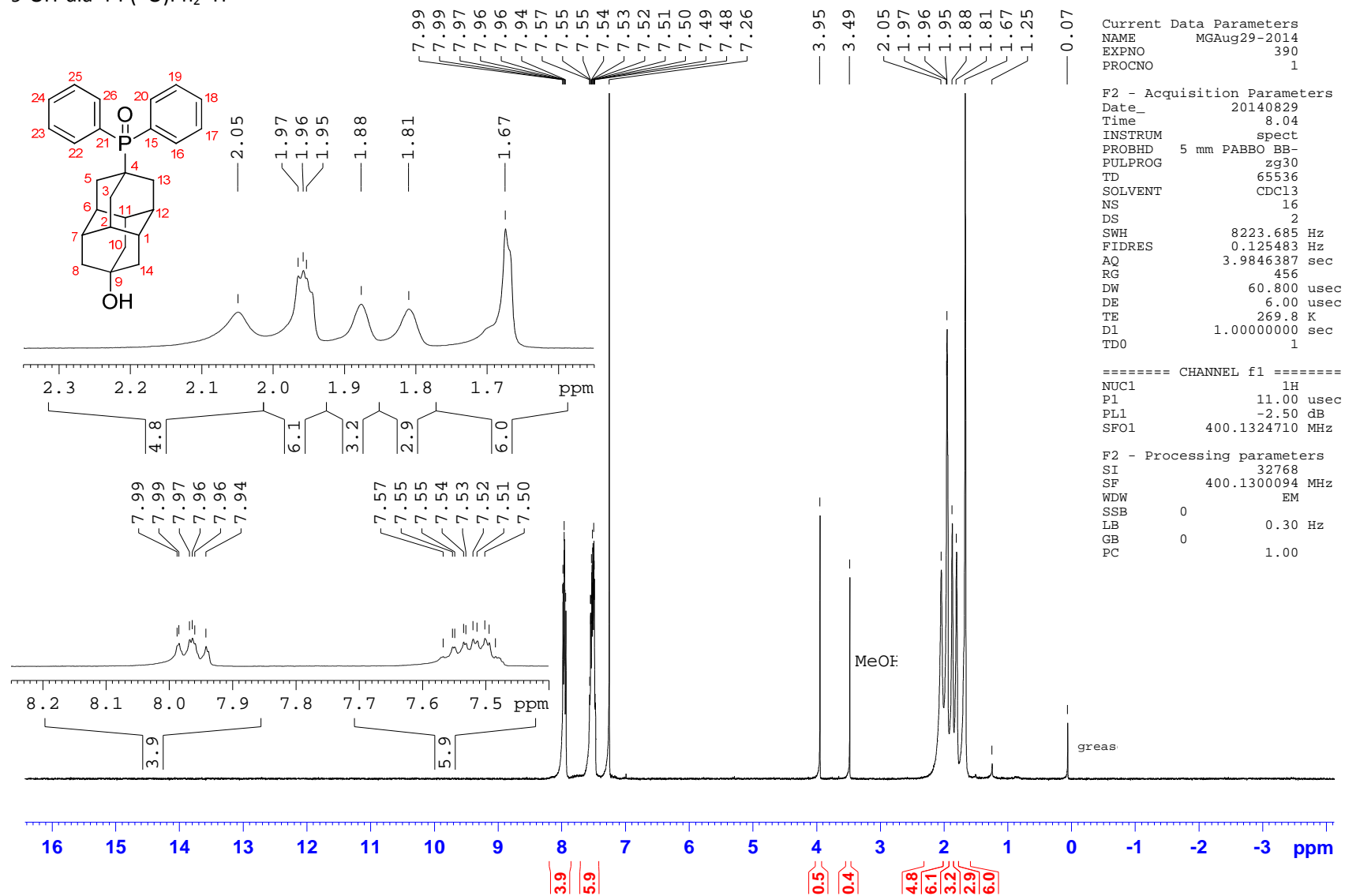


4-Dia-P(=O)Ph₂ ³¹P

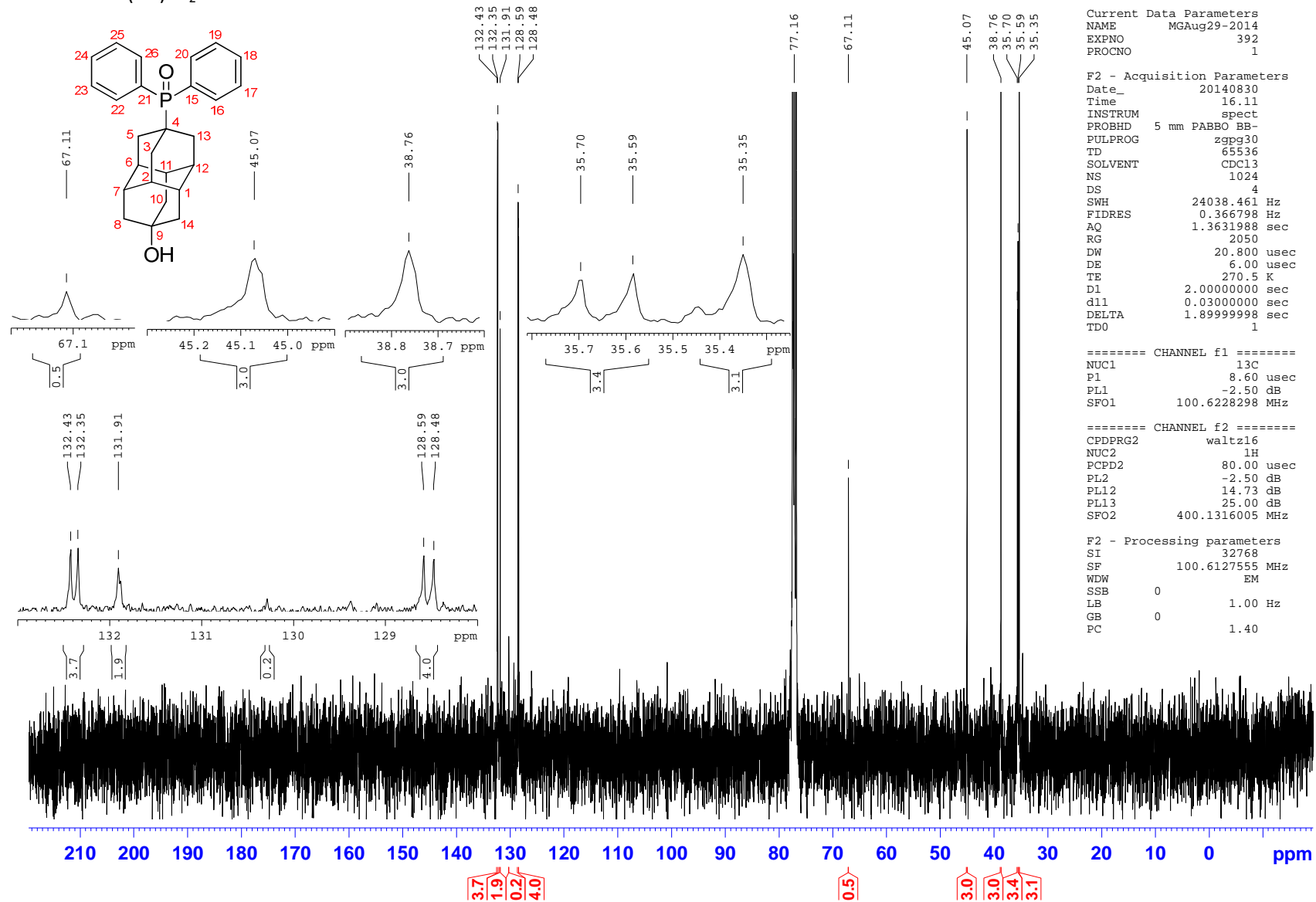


t) (9-Hydroxydiamant-4-yl)diphenylphosphine oxide (**194**)

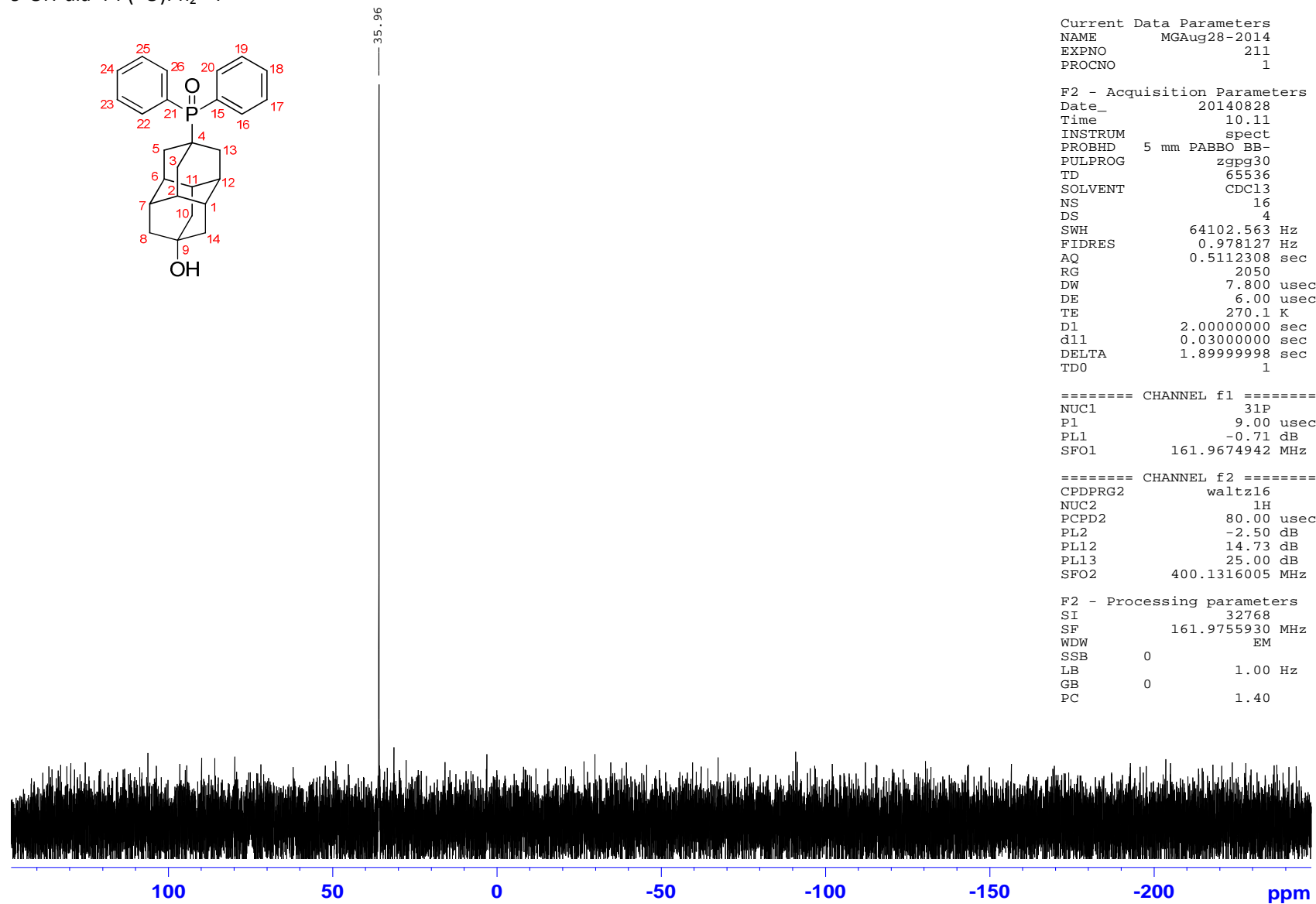
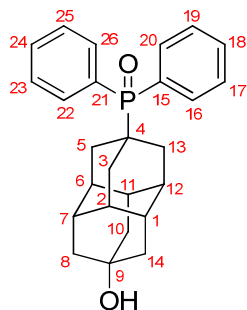
9-OH-dia-4-P(=O)Ph₂¹H



9-OH-dia-4-P(=O)Ph₂¹³C

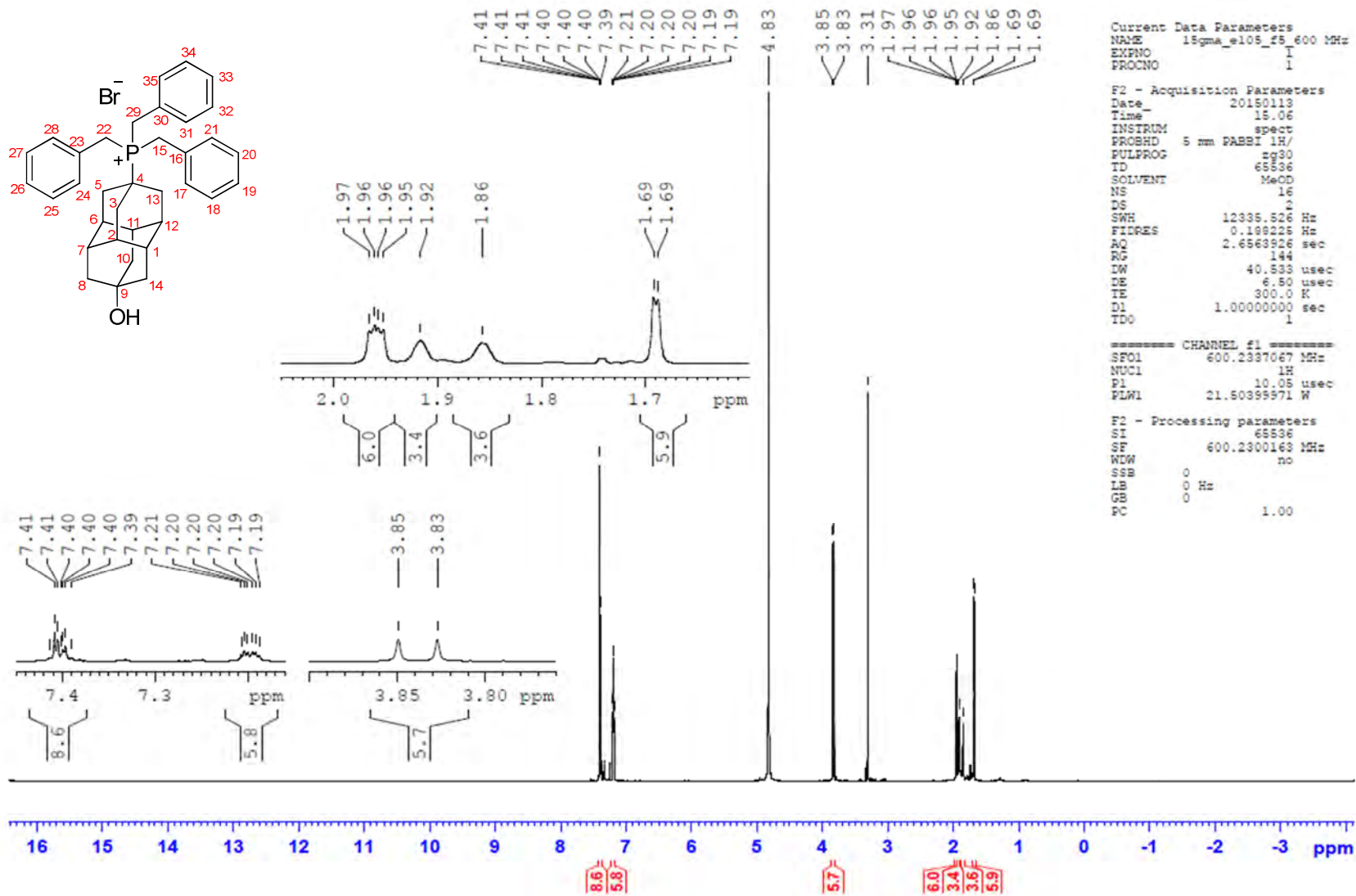


9-OH-dia-4-P(=O)Ph₂ ³¹P

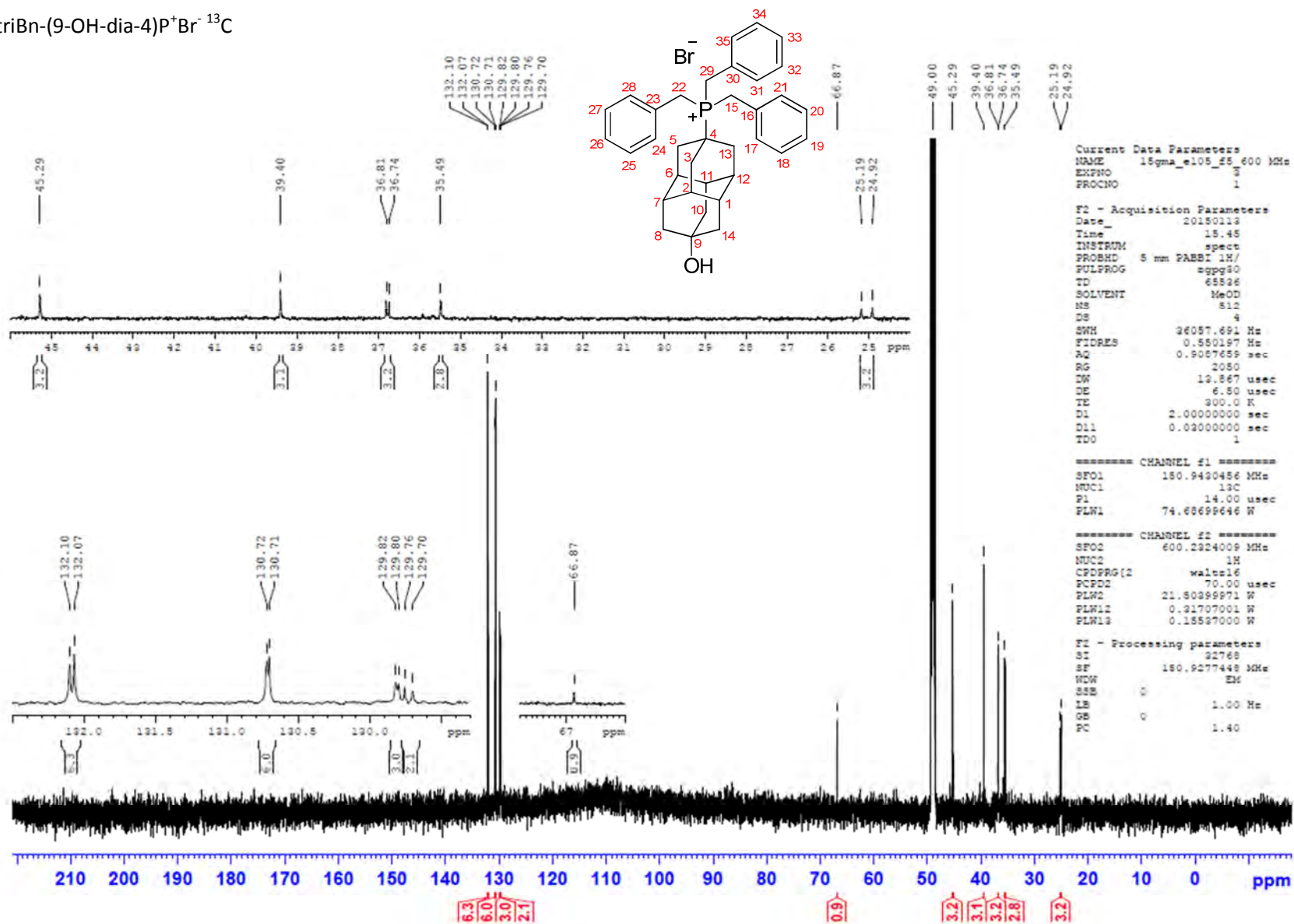


u) Tribenzyl(9-hydroxydiamantan-4-yl)phosphonium bromide (**195**)

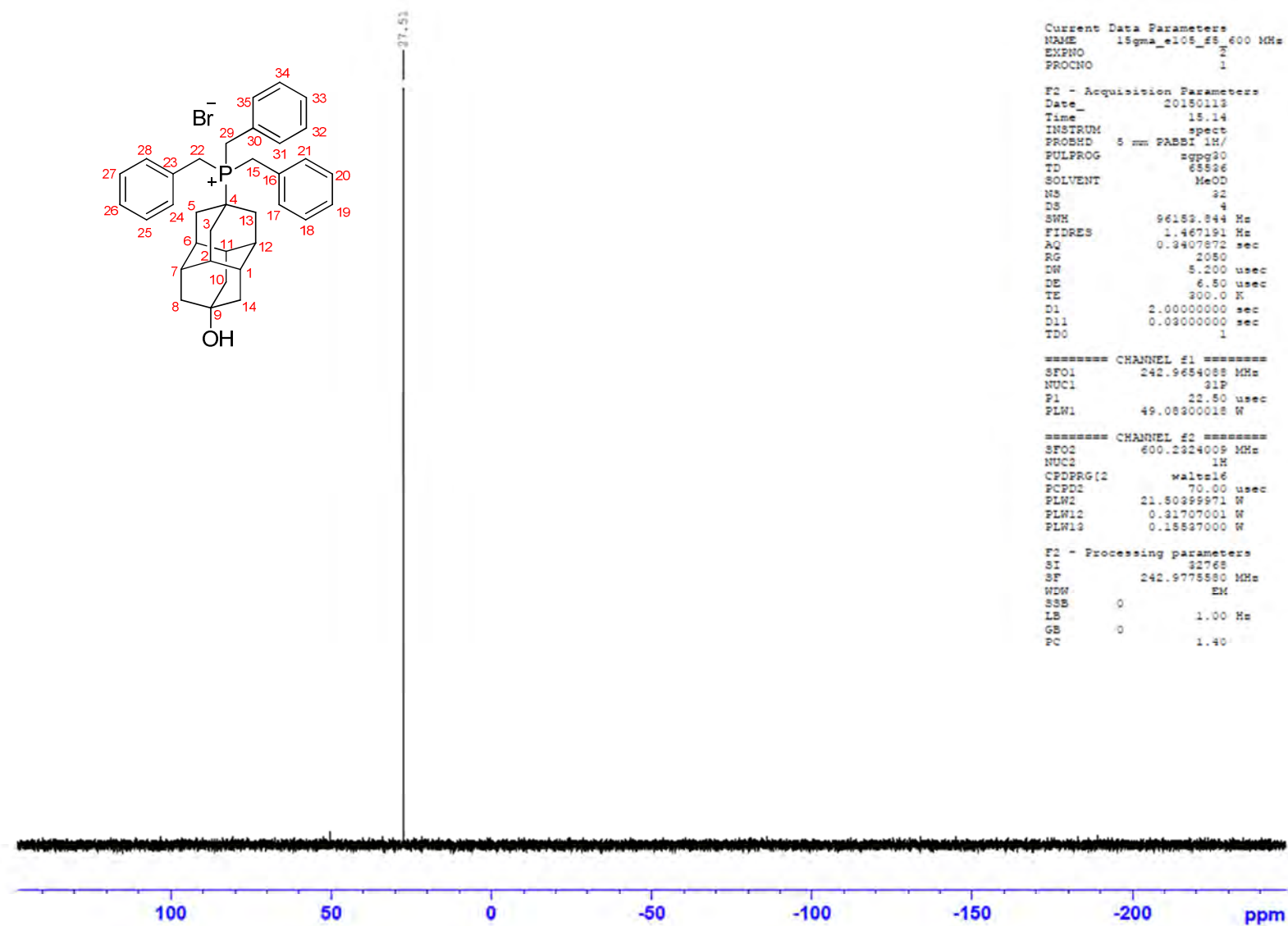
triBn-(9-OH-dia-4)P⁺Br⁻ H



triBn-(9-OH-dia-4)P⁺Br⁻ ¹³C

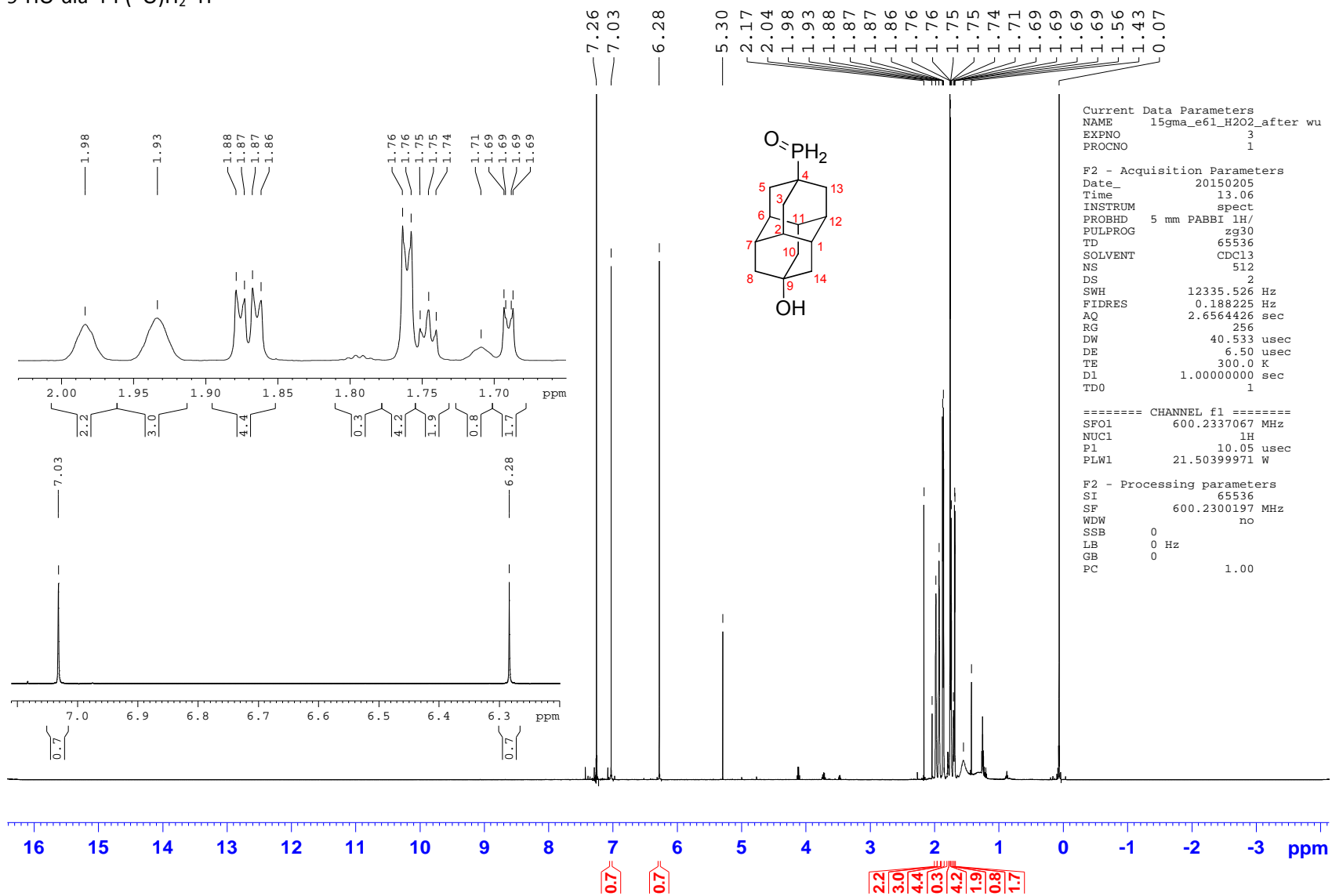


triBn-(9-OH-dia-4)P⁺Br⁻ ³¹P

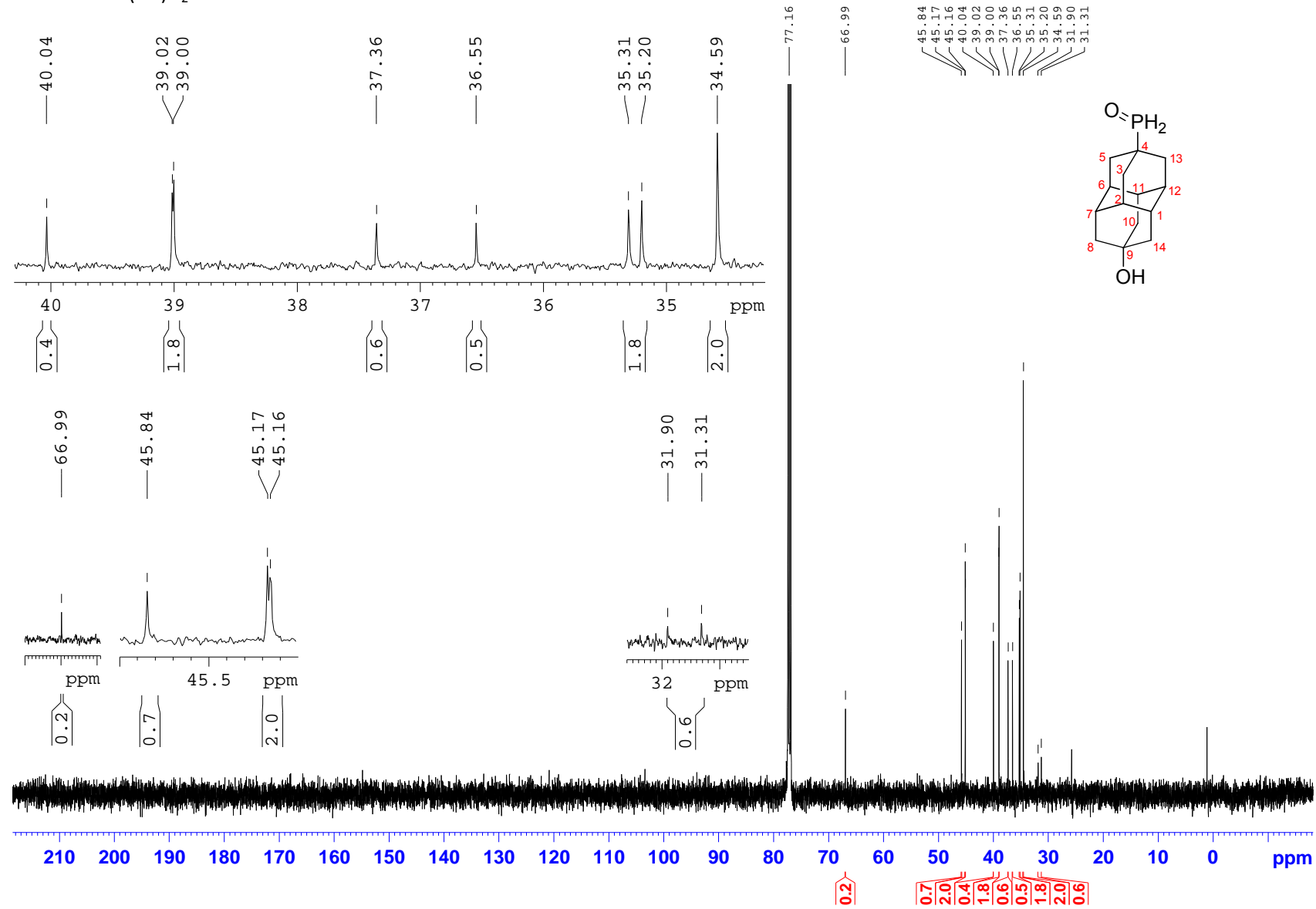


v) (9-Hydroxydiamant-4-yl)phosphine oxide (**196**)

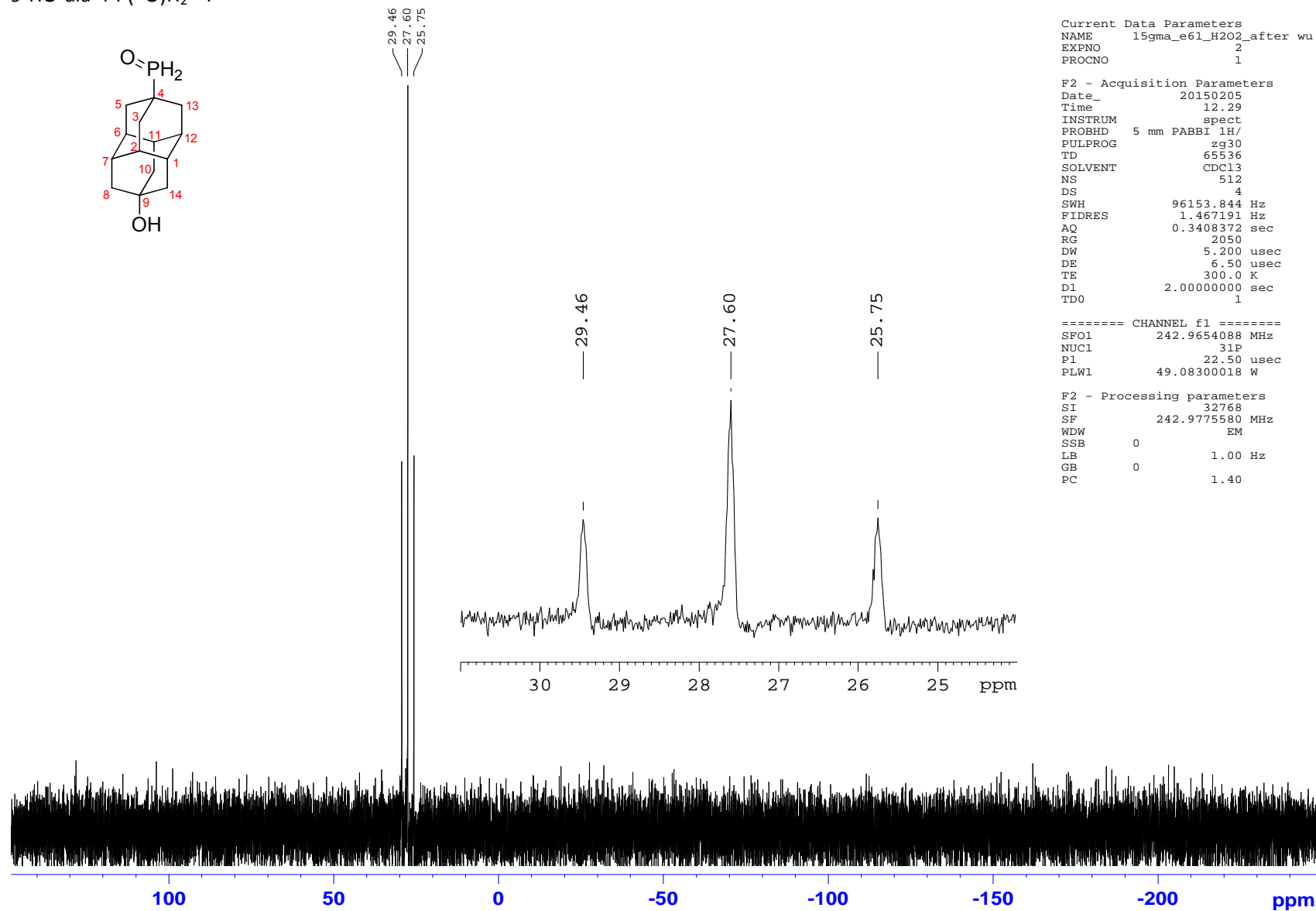
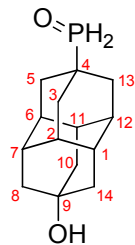
9-HO-dia-4-P(=O)H₂ ¹H



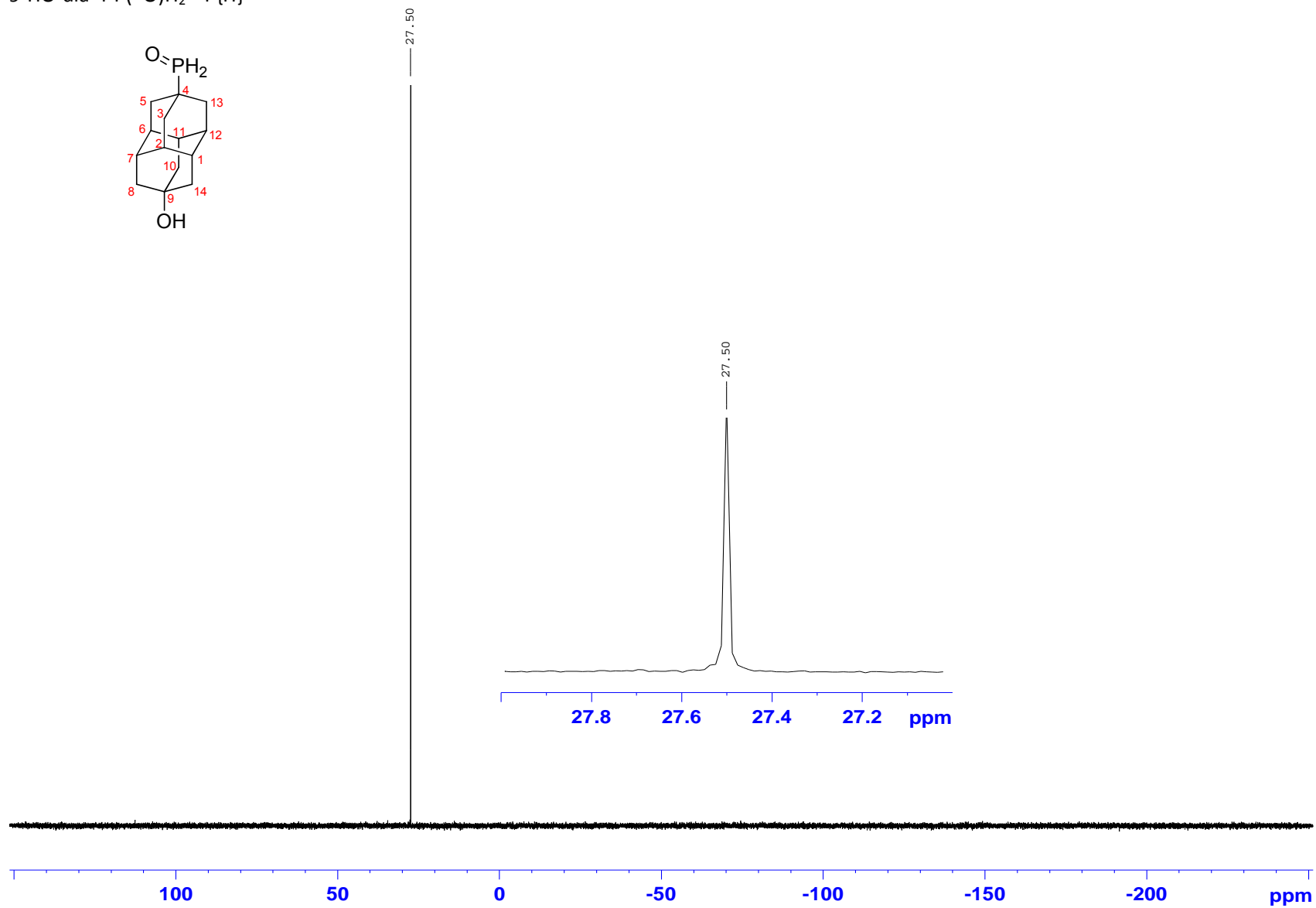
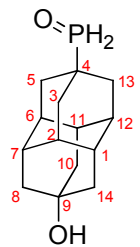
9-HO-dia-4-P(=O)H₂ ¹³C



9-HO-dia-4-P(=O)H₂ ³¹P

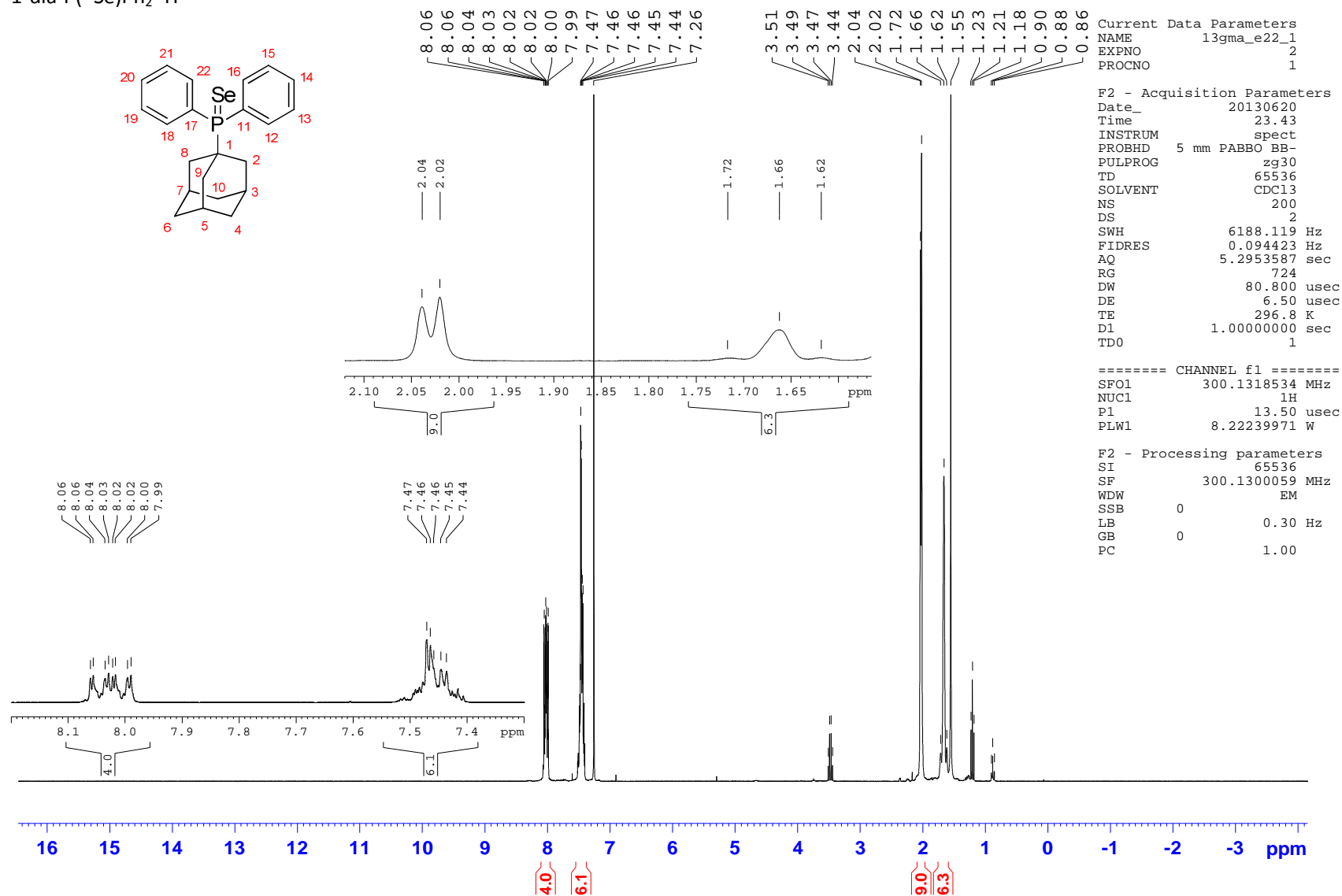


9-HO-dia-4-P(=O)H₂ ³¹P{H}

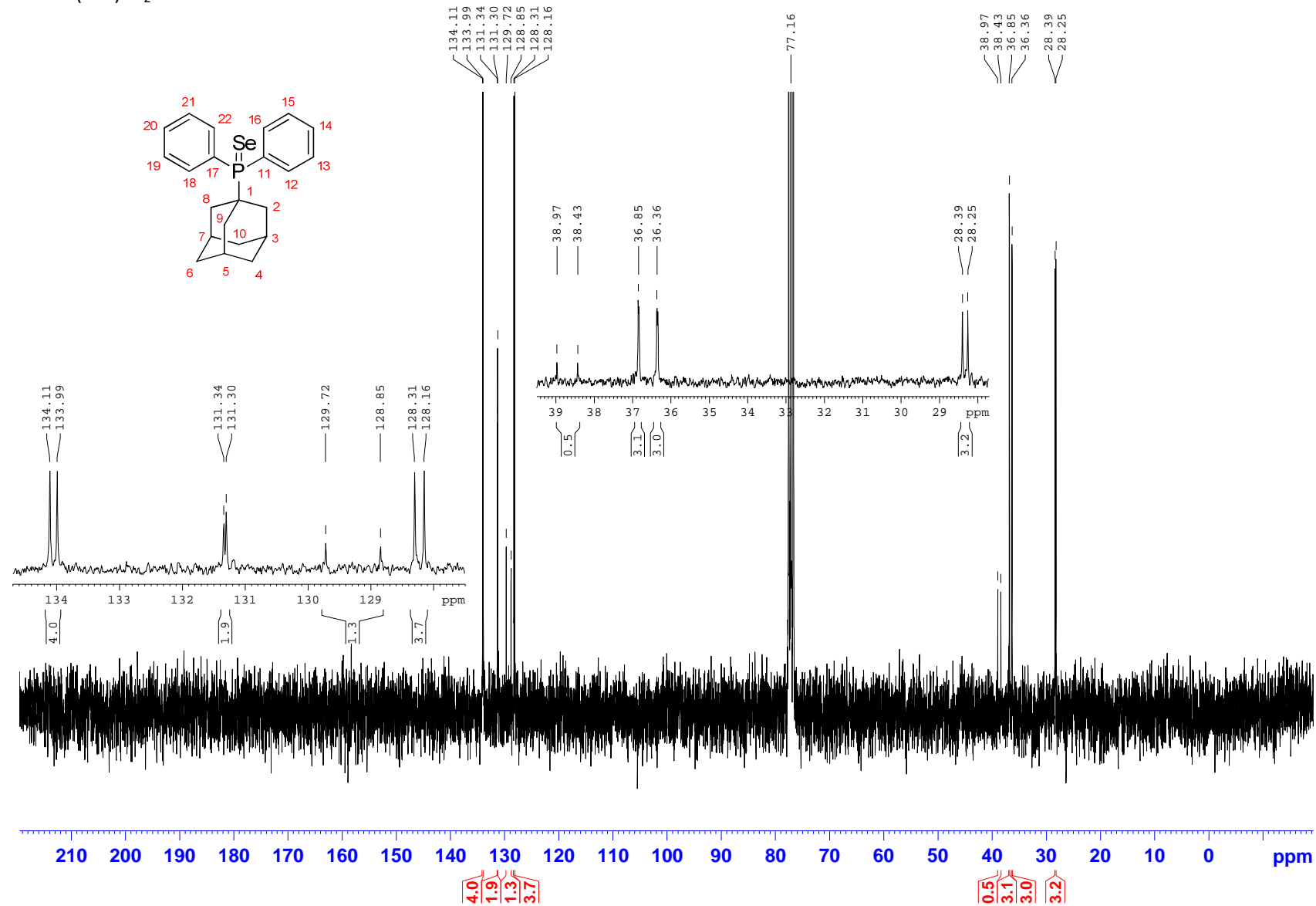


w) 1-Adamantylidiphenylphosphine selenide (**197**)

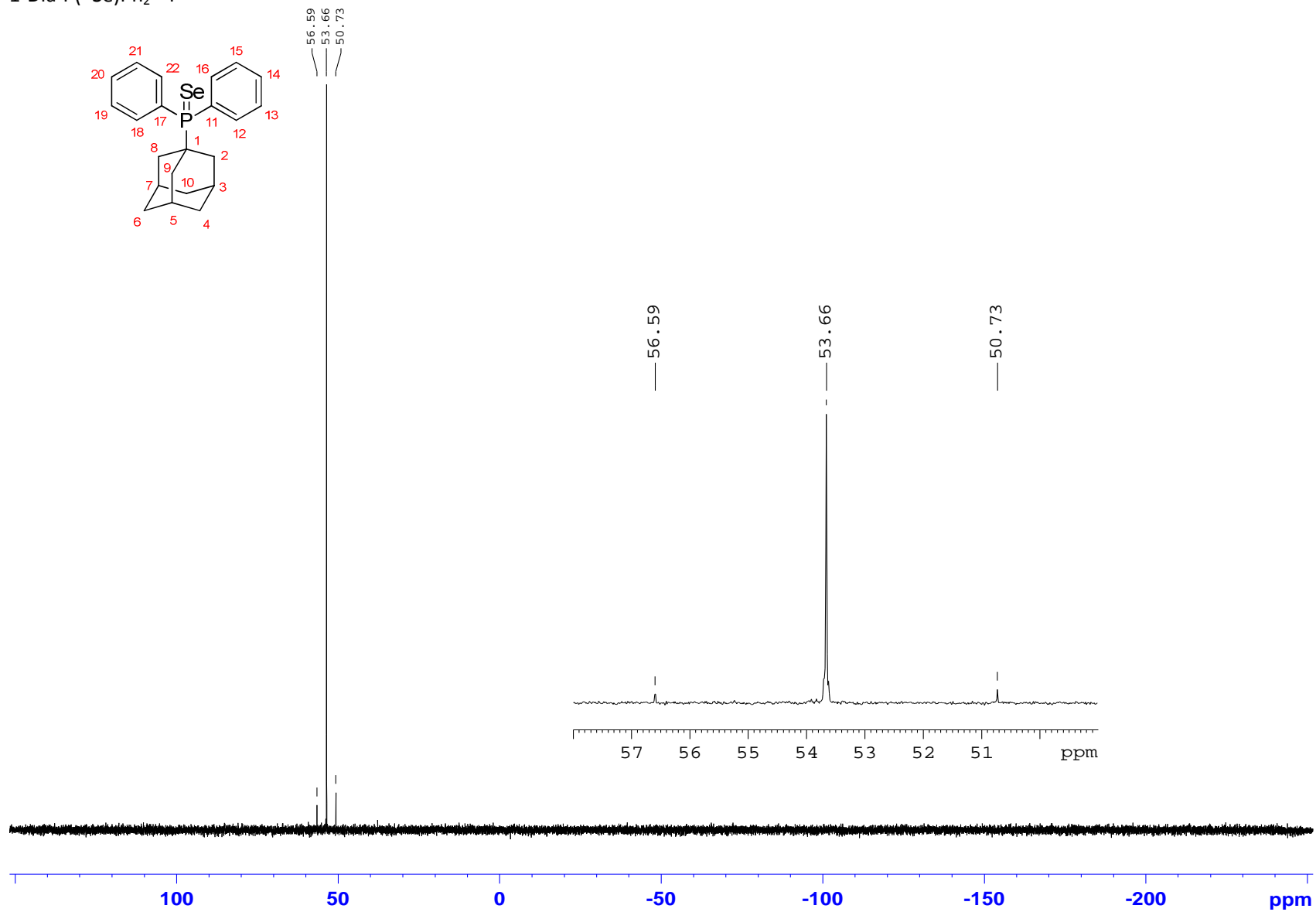
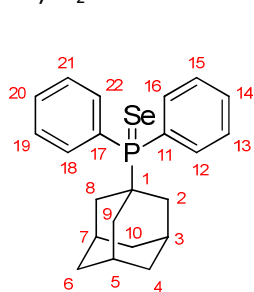
1-dia-P(=Se)Ph₂¹H



1-dia-P(=Se)Ph₂ ¹³C

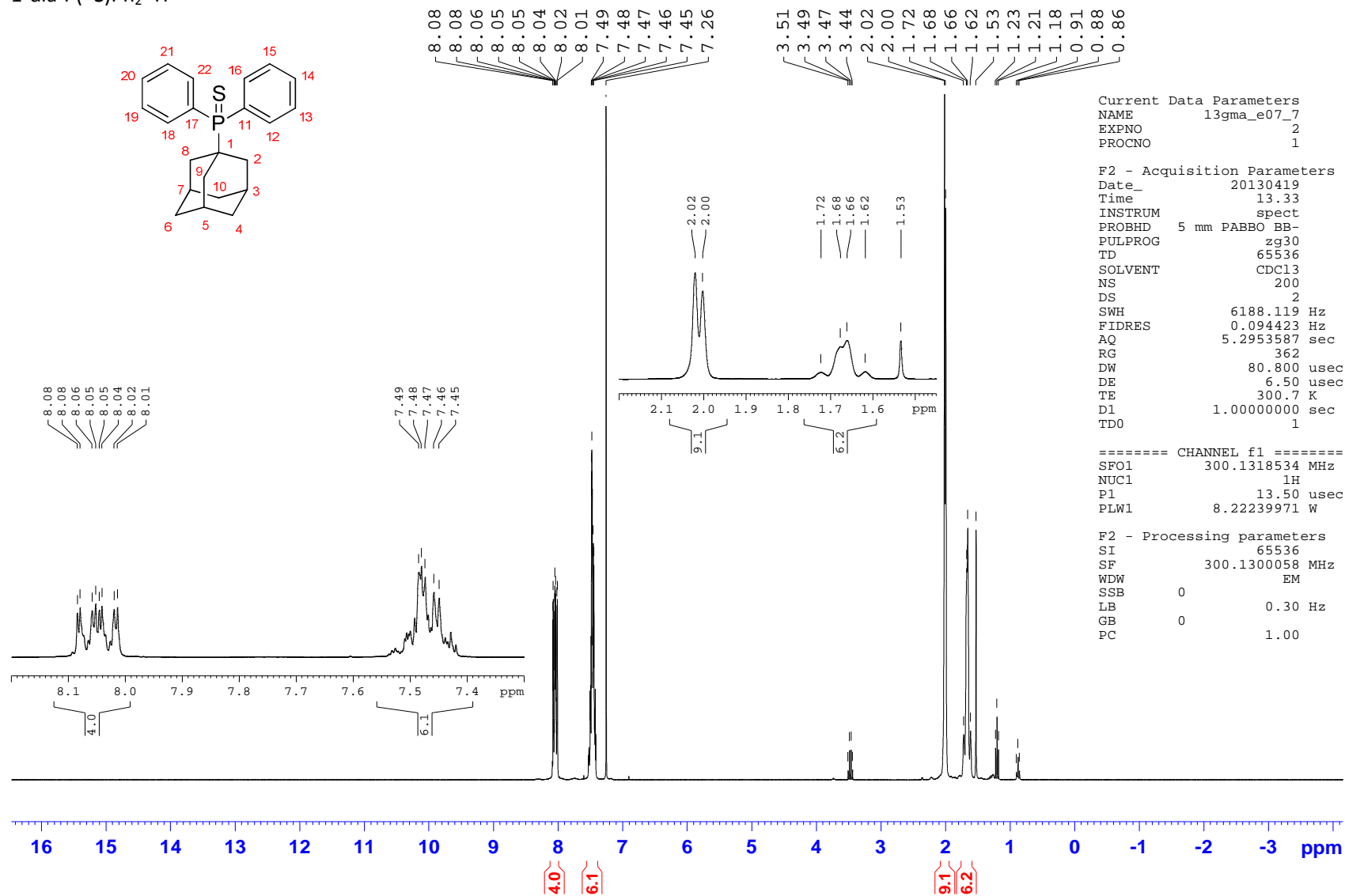


1-Dia-P(=Se)Ph₂ ³¹P

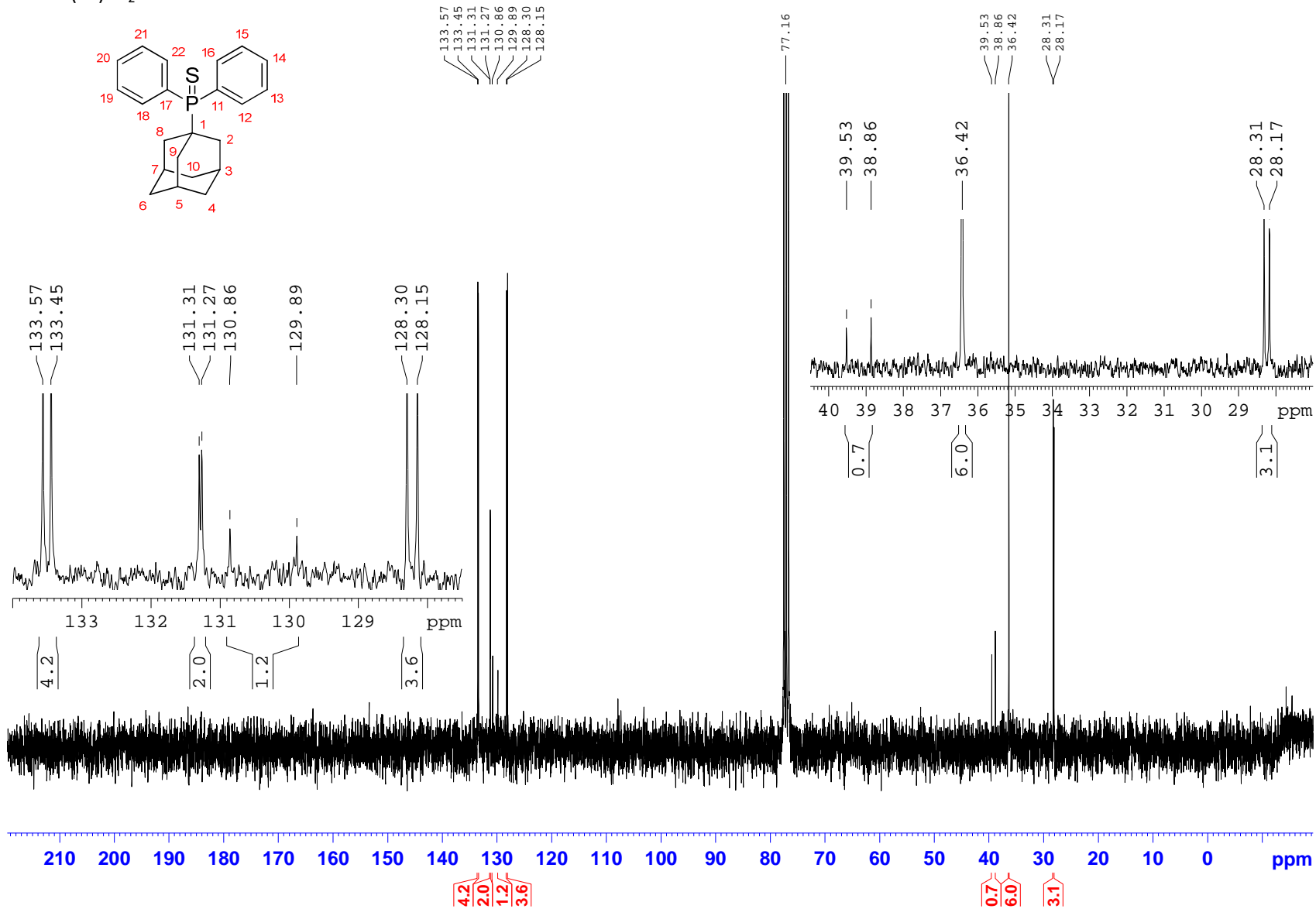


x) 1-Adamantylidiphenylphosphine sulphide (**198**)

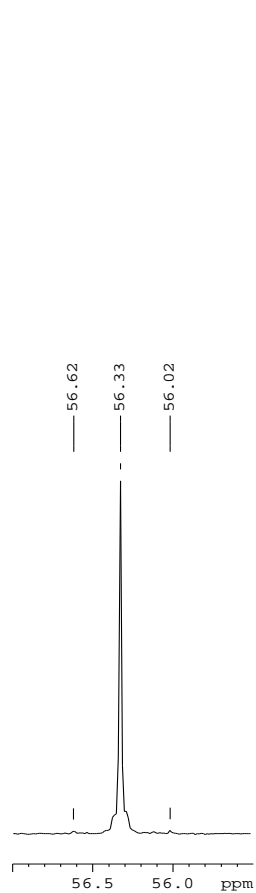
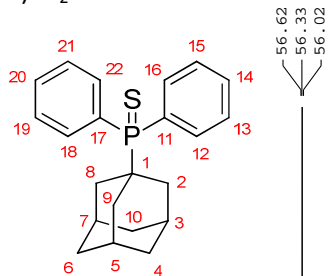
1-dia-P(=S)Ph₂¹H



1-dia-P(=S)Ph₂ ¹³C

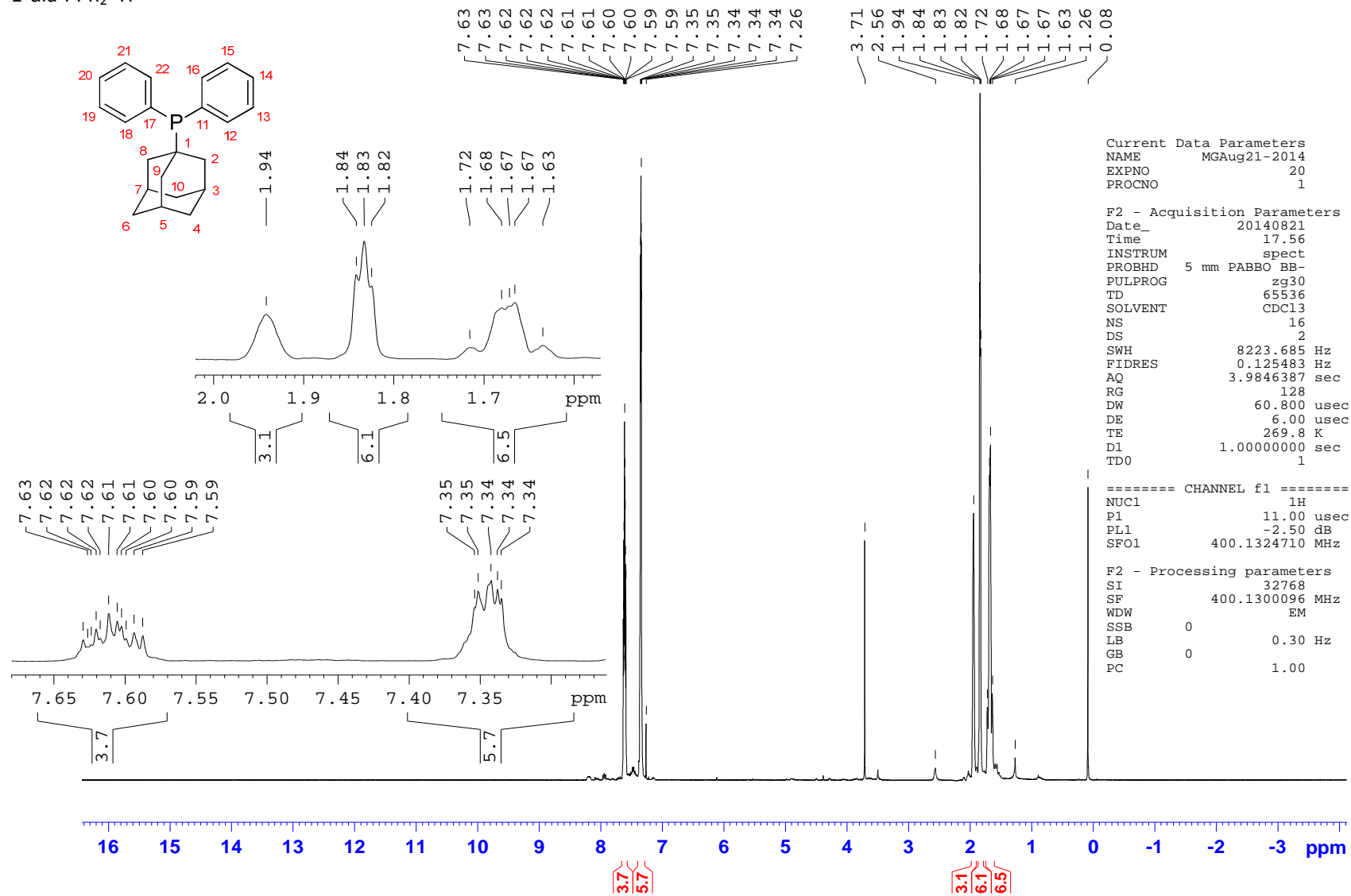


1-dia-P(=S)Ph₂ ³¹P

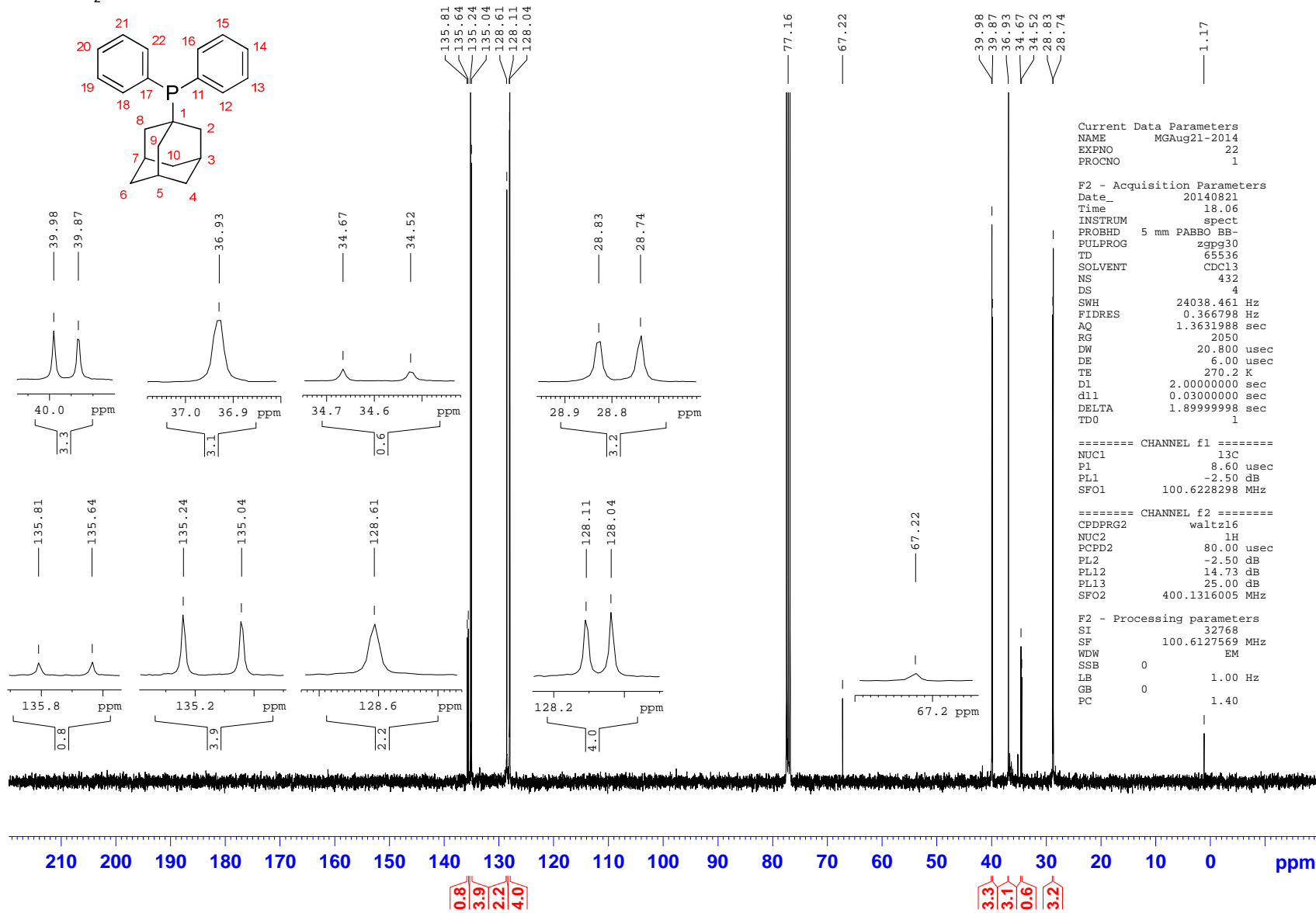


y) 1-Adamantylidiphenylphosphine (199)

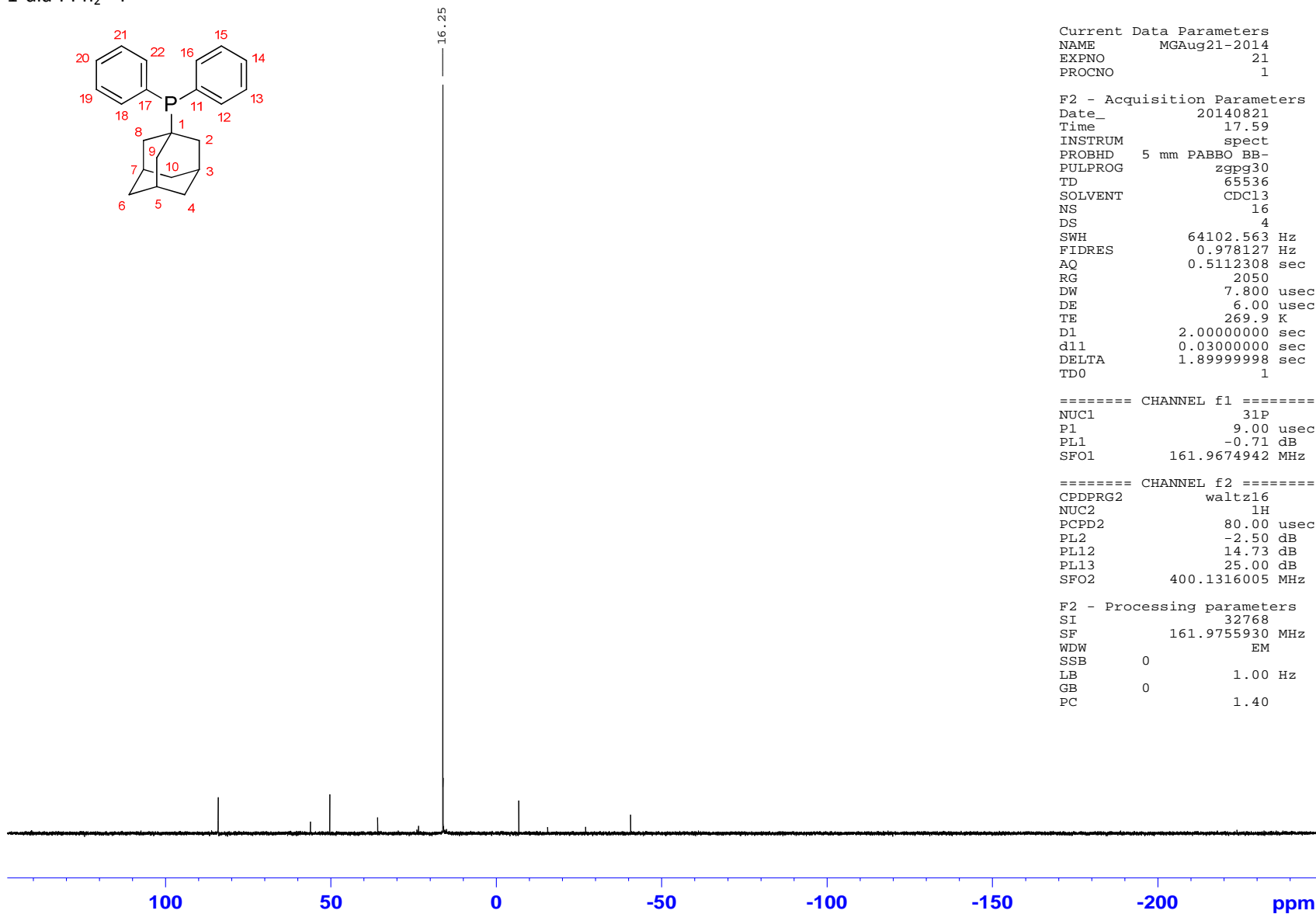
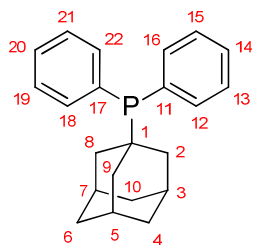
1-dia-PPh₂¹H



1-dia-PPh₂ ¹³C



1-dia-PPh₂ ³¹P



```

Current Data Parameters
NAME      MGAug21-2014
EXPNO    21
PROCNO    1

F2 - Acquisition Parameters
Date_    20140821
Time     17.59
INSTRUM  spect
PROBHD   5 mm PABBO BB-
PULPROG  zgpg30
TD       65536
SOLVENT  CDCl3
NS       16
DS       4
SWH      64102.563 Hz
FIDRES   0.978127 Hz
AQ       0.5112308 sec
RG       2050
DW       7.800 usec
DE       6.00 usec
TE       269.9 K
D1       2.00000000 sec
d11      0.03000000 sec
DELTA    1.89999998 sec
TD0      1

===== CHANNEL f1 =====
NUC1     31P
P1       9.00 usec
PL1     -0.71 dB
SFO1    161.9674942 MHz

===== CHANNEL f2 =====
CPDPRG2  waltz16
NUC2     1H
PCPD2    80.00 usec
PL2     -2.50 dB
PL12    14.73 dB
PL13    25.00 dB
SFO2    400.1316005 MHz

F2 - Processing parameters
SI       32768
SF      161.9755930 MHz
WDW      EM
SSB      0
LB       1.00 Hz
GB       0
PC       1.40
    
```

6.5. X-ray structure analyses of diamondoids

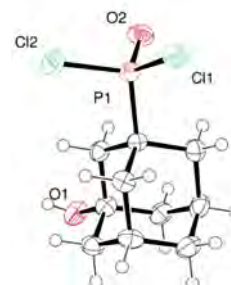
a) 4-Diamantylphosphonic dichloride (**22**)

CCDC No.	1054567
Empirical formula	C ₁₄ H ₁₉ OPCl ₂
Formula weight	305.16
Temperature/K	100
Crystal system	monoclinic
Space group	C2/c
a/Å	21.691(3)
b/Å	16.4132(18)
c/Å	15.261(2)
α/°	90
β/°	91.265(5)
γ/°	90
Volume/Å ³	5431.9(11)
Z	16
ρ _{calc} /cm ³	1.493
μ/mm ⁻¹	0.581
F(000)	2560.0
Crystal size/mm ³	0.45 × 0.35 × 0.17
Radiation	MoKα (λ = 0.71073)
2θ range for data collection/°	6.146 to 55.592
Index ranges	-28 ≤ h ≤ 28, -21 ≤ k ≤ 21, -19 ≤ l ≤ 19
Reflections collected	53928
Independent reflections	6298 [R _{int} = 0.0805, R _{sigma} = 0.0435]
Data/restraints/parameters	6298/0/326
Goodness-of-fit on F ²	1.063
Final R indexes [I ≥ 2σ (I)]	R ₁ = 0.0672, wR ₂ = 0.1989
Final R indexes [all data]	R ₁ = 0.0894, wR ₂ = 0.2193
Largest diff. peak/hole / e Å ⁻³	0.81/-0.58



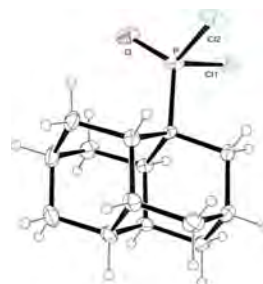
b) (3-Hydroxyadamant-1-yl)phosphonic dichloride (**178**)

CCDC No.	1053891	
Empirical formula	C ₂₀ H ₃₀ Cl ₂ O ₄ P ₂	
Formula weight	538.18	
Temperature	150(2) K	
Wavelength	0.71073 Å	
Crystal system	Orthorhombic	
Space group	Pbca	
Unit cell dimensions	a = 17.865(4) Å	α = 90°.
	b = 11.720(2) Å	β = 90°.
	c = 22.556(5) Å	γ = 90°.
Volume	4722.7(16) Å ³	
Z	8	
Density (calculated)	1.514 Mg/m ³	
Absorption coefficient	0.662 mm ⁻¹	
F(000)	2240	
Crystal size	0.450 x 0.120 x 0.050 mm ³	
Theta range for data collection	1.806 to 27.476°.	
Index ranges	-23 ≤ h ≤ 22, -15 ≤ k ≤ 15, -29 ≤ l ≤ 28	
Reflections collected	42127	
Independent reflections	5405 [R(int) = 0.0806]	
Completeness to theta = 25.242°	100.0 %	
Absorption correction	Empirical	
Max. and min. transmission	0.76884 and 0.72322	
Refinement method	Full-matrix least-squares on F ²	
Data / restraints / parameters	5405 / 0 / 275	
Goodness-of-fit on F ²	1.029	
Final R indices [I > 2σ(I)]	R1 = 0.0500, wR2 = 0.1220	
R indices (all data)	R1 = 0.0837, wR2 = 0.1339	
Extinction coefficient	n/a	
Largest diff. peak and hole	1.057 and -0.359 e.Å ⁻³	



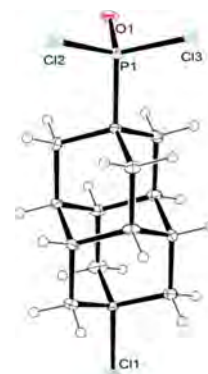
c) 1-Diamantylphosphonic dichloride (**181**)

Identification code	shelx	
Empirical formula	C ₁₄ H ₁₉ Cl ₂ OP	
Formula weight	305.16	
Temperature	100(2) K	
Wavelength	0.71073 Å	
Crystal system	Monoclinic	
Space group	P 21	
Unit cell dimensions	a = 6.547(3) Å	α = 90°.
	b = 14.435(7) Å	β = 108.659(18)°.
	c = 7.735(4) Å	γ = 90°.
Volume	692.5(6) Å ³	
Z	2	
Density (calculated)	1.463 Mg/m ³	
Absorption coefficient	0.569 mm ⁻¹	
F(000)	320	
Theta range for data collection	2.779 to 27.487°.	
Index ranges	-8<=h<=8, -18<=k<=18, -9<=l<=10	
Reflections collected	11813	
Independent reflections	3153 [R(int) = 0.0451]	
Completeness to theta = 26.000°	99.6 %	
Refinement method	Full-matrix least-squares on F ²	
Data / restraints / parameters	3153 / 1 / 164	
Goodness-of-fit on F ²	1.092	
Final R indices [I>2sigma(I)]	R1 = 0.0370, wR2 = 0.0831	
R indices (all data)	R1 = 0.0457, wR2 = 0.0889	
Absolute structure parameter	0.10(11)	
Extinction coefficient	n/a	
Largest diff. peak and hole	0.485 and -0.359 e.Å ⁻³	



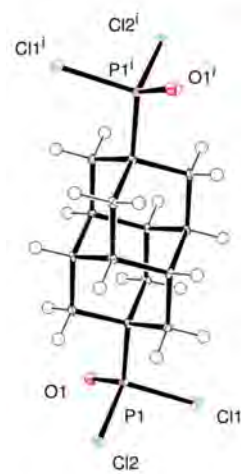
d) (9-Chlorodiamant-4-yl)phosphonic dichloride (**184**)

CCDC No.	1054565
Empirical formula	C ₁₄ H ₁₈ Cl ₃ OP
Formula weight	339.60
Temperature/K	115
Crystal system	monoclinic
Space group	P2 ₁
a/Å	7.2710(5)
b/Å	8.3207(4)
c/Å	12.3475(8)
α/°	90
β/°	102.708(4)
γ/°	90
Volume/Å ³	728.72(8)
Z	2
ρ _{calc} /g/cm ³	1.548
μ/mm ⁻¹	0.727
F(000)	352.0
Crystal size/mm ³	0.25 × 0.07 × 0.05
Radiation	MoKα (λ = 0.71073)
2θ range for data collection/°	5.99 to 58.414
Index ranges	-9 ≤ h ≤ 9, -11 ≤ k ≤ 11, -16 ≤ l ≤ 15
Reflections collected	8997
Independent reflections	3780 [R _{int} = 0.0421, R _{sigma} = 0.0755]
Data/restraints/parameters	3780/1/172
Goodness-of-fit on F ²	0.986
Final R indexes [I ≥ 2σ (I)]	R ₁ = 0.0412, wR ₂ = 0.0699
Final R indexes [all data]	R ₁ = 0.0680, wR ₂ = 0.0781
Largest diff. peak/hole / e Å ⁻³	0.37/-0.34
Flack parameter	0.04(6)



e) (4,9-Diamantyl)diphosphonic dichloride (**185**)

CCDC No.	1053886	
Empirical formula	$C_{14}H_{18}Cl_4O_2P_2$	
Formula weight	422.02	
Temperature	100(2) K	
Wavelength	0.71073 Å	
Crystal system	Triclinic	
Space group	P-1	
Unit cell dimensions	$a = 6.3875(5)$ Å	$\alpha = 95.801(2)^\circ$
	$b = 8.1583(7)$ Å	$\beta = 108.129(2)^\circ$
	$c = 9.1125(7)$ Å	$\gamma = 111.841(2)^\circ$
Volume	$406.04(6)$ Å ³	
Z	1	
Density (calculated)	1.726 Mg/m ³	
Absorption coefficient	0.928 mm ⁻¹	
F(000)	216	
Crystal size	$0.161 \times 0.065 \times 0.037$ mm ³	
Theta range for data collection	2.426 to 26.732°	
Index ranges	$-8 \leq h \leq 8$, $-10 \leq k \leq 10$, $-11 \leq l \leq 11$	
Reflections collected	17659	
Independent reflections	1716 [R(int) = 0.0369]	
Completeness to theta = 25.242°	99.7 %	
Absorption correction	Empirical	
Max. and min. transmission	0.7454 and 0.6708	
Refinement method	Full-matrix least-squares on F ²	
Data / restraints / parameters	1716 / 0 / 100	
Goodness-of-fit on F ²	1.532	
Final R indices [$I > 2\sigma(I)$]	R1 = 0.0338, wR2 = 0.1060	
R indices (all data)	R1 = 0.0354, wR2 = 0.1066	
Extinction coefficient	n/a	
Largest diff. peak and hole	0.453 and -0.480 e.Å ⁻³	



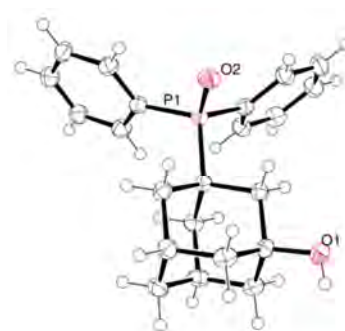
f) 1-Adamantyldiphenylphosphine oxide (**191**)

CCDC No.	1054566
Empirical formula	C ₂₂ H ₂₅ OP
Formula weight	336.39
Temperature/K	115
Crystal system	monoclinic
Space group	P2 ₁ /n
a/Å	8.9308(2)
b/Å	12.0815(5)
c/Å	16.2049(6)
α/°	90.00
β/°	90.127(2)
γ/°	90.00
Volume/Å ³	1748.46(10)
Z	4
ρ _{calc} /g/cm ³	1.278
μ/mm ⁻¹	0.163
F(000)	720.0
Crystal size/mm ³	0.38 × 0.2 × 0.1
Radiation	Mo Kα~1~ (λ = 0.71073)
2θ range for data collection/°	5.68 to 55.04
Index ranges	-10 ≤ h ≤ 11, -10 ≤ k ≤ 15, -21 ≤ l ≤ 19
Reflections collected	9232
Independent reflections	3931 [R _{int} = 0.0224, R _{sigma} = 0.0289]
Data/restraints/parameters	3931/0/217
Goodness-of-fit on F ²	1.100
Final R indexes [I >= 2σ (I)]	R ₁ = 0.0409, wR ₂ = 0.0947
Final R indexes [all data]	R ₁ = 0.0498, wR ₂ = 0.1010
Largest diff. peak/hole / e Å ⁻³	0.52/-0.33



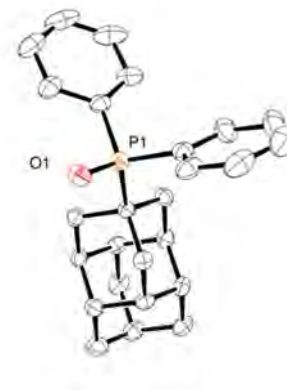
g) (3-Hydroxyadamant-1-yl)diphenylphosphine oxide (**192**)

CCDC No.	1053892	
Empirical formula	C ₂₂ H ₂₅ O ₂ P	
Formula weight	352.39	
Temperature	150(2) K	
Wavelength	0.71073 Å	
Crystal system	Monoclinic	
Space group	P2 ₁ /n	
Unit cell dimensions	a = 8.6126(17) Å	α = 90°.
	b = 12.987(3) Å	β = 99.46(3)°.
	c = 16.000(3) Å	γ = 90°.
Volume	1765.4(6) Å ³	
Z	4	
Density (calculated)	1.326 Mg/m ³	
Absorption coefficient	0.168 mm ⁻¹	
F(000)	752	
Crystal size	0.500 x 0.250 x 0.200 mm ³	
Theta range for data collection	2.031 to 30.070°.	
Index ranges	-12 ≤ h ≤ 12, -18 ≤ k ≤ 18, -21 ≤ l ≤ 22	
Reflections collected	47166	
Independent reflections	5146 [R(int) = 0.0654]	
Completeness to theta = 25.242°	99.9 %	
Absorption correction	Empirical	
Max. and min. transmission	0.7460 and 0.5991	
Refinement method	Full-matrix least-squares on F ²	
Data / restraints / parameters	5146 / 0 / 228	
Goodness-of-fit on F ²	1.094	
Final R indices [I > 2σ(I)]	R1 = 0.0397, wR2 = 0.1078	
R indices (all data)	R1 = 0.0547, wR2 = 0.1133	
Extinction coefficient	n/a	
Largest diff. peak and hole	0.338 and -0.321 e.Å ⁻³	



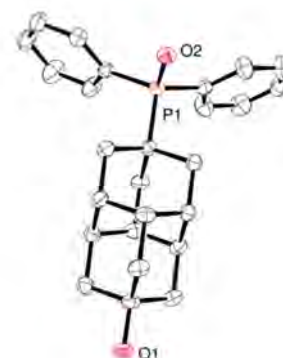
h) 4-Diamantylidiphenylphosphine oxide (**193**)

CCDC No.	1053890	
Empirical formula	C ₂₇ H ₃₃ O ₂ P	
Formula weight	420.50	
Temperature	150(2) K	
Wavelength	0.71073 Å	
Crystal system	Orthorhombic	
Space group	Pnma	
Unit cell dimensions	a = 11.550(2) Å	α = 90°.
	b = 12.931(3) Å	β = 90°.
	c = 14.982(3) Å	γ = 90°.
Volume	2237.6(8) Å ³	
Z	4	
Density (calculated)	1.248 Mg/m ³	
Absorption coefficient	0.144 mm ⁻¹	
F(000)	904	
Crystal size	0.700 x 0.300 x 0.250 mm ³	
Theta range for data collection	2.226 to 25.020°.	
Index ranges	-13 ≤ h ≤ 13, -15 ≤ k ≤ 15, -17 ≤ l ≤ 17	
Reflections collected	22179	
Independent reflections	2074 [R(int) = 0.0674]	
Completeness to theta = 25.020°	100.0 %	
Absorption correction	Empirical	
Max. and min. transmission	0.7456 and 0.5841	
Refinement method	Full-matrix least-squares on F ²	
Data / restraints / parameters	2074 / 0 / 155	
Goodness-of-fit on F ²	1.042	
Final R indices [I > 2σ(I)]	R1 = 0.0382, wR2 = 0.0985	
R indices (all data)	R1 = 0.0514, wR2 = 0.1072	
Extinction coefficient	n/a	
Largest diff. peak and hole	0.322 and -0.338 e.Å ⁻³	



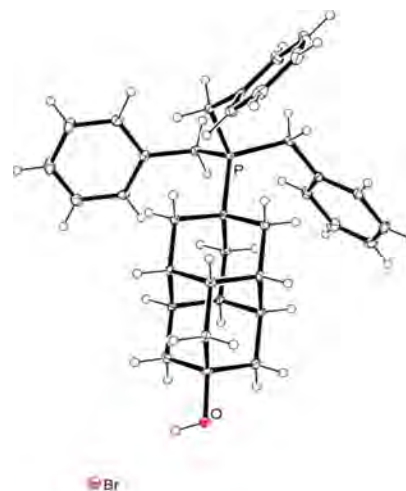
i) (9-hydroxydiamant-4-yl)diphenylphosphine oxide (**194**)

CCDC No.	1053889	
Empirical formula	C ₂₆ H ₂₉ O ₂ P	
Formula weight	404.46	
Temperature	150(2) K	
Wavelength	0.71073 Å	
Crystal system	Monoclinic	
Space group	P 21/n	
Unit cell dimensions	a = 9.2389(18) Å	α = 90°.
	b = 13.692(3) Å	β = 104.46(3)
	c = 16.878(3) Å	γ = 90°.
Volume	2067.3(8) Å ³	
Z	4	
Density (calculated)	1.299 Mg/m ³	
Absorption coefficient	0.153 mm ⁻¹	
F(000)	864	
Crystal size	0.300 x 0.200 x 0.050 mm ³	
Theta range for data collection	1.940 to 27.527°.	
Index ranges	-11 ≤ h ≤ 11, -17 ≤ k ≤ 17, -21 ≤ l ≤ 21	
Reflections collected	46347	
Independent reflections	4742 [R(int) = 0.1347]	
Completeness to theta = 25.242°	99.9 %	
Absorption correction	Empirical	
Refinement method	Full-matrix least-squares on F ²	
Data / restraints / parameters	4742 / 0 / 266	
Goodness-of-fit on F ²	1.028	
Final R indices [I > 2σ(I)]	R1 = 0.0461, wR2 = 0.1114	
R indices (all data)	R1 = 0.0828, wR2 = 0.1252	
Extinction coefficient	n/a	
Largest diff. peak and hole	0.236 and -0.325 e.Å ⁻³	



j) Tribenzyl(9-hydroxydiamant-4-yl)phosphonium salt (**195**)

CCDC No.	1054569
Empirical formula	C ₃₅ H ₄₀ BrOP
Formula weight	587.55
Temperature/K	100.0
Crystal system	monoclinic
Space group	P2 ₁ /c
a/Å	10.3888(5)
b/Å	14.2107(7)
c/Å	19.5603(10)
α/°	90
β/°	100.963(2)
γ/°	90
Volume/Å ³	2835.0(2)
Z	4
ρ _{calc} /g/cm ³	1.377
μ/mm ⁻¹	1.534
F(000)	1232.0
Crystal size/mm ³	0.25 × 0.15 × 0.1
Radiation	MoKα (λ = 0.71073)
2θ range for data collection/°	5.734 to 55.032
Index ranges	-13 ≤ h ≤ 13, -18 ≤ k ≤ 18, -25 ≤ l ≤ 25
Reflections collected	58402
Independent reflections	6492 [R _{int} = 0.0598, R _{sigma} = 0.0326]
Data/restraints/parameters	6492/0/344
Goodness-of-fit on F ²	1.016
Final R indexes [I ≥ 2σ (I)]	R ₁ = 0.0338, wR ₂ = 0.0755
Final R indexes [all data]	R ₁ = 0.0534, wR ₂ = 0.0840
Largest diff. peak/hole / e Å ⁻³	0.54/-0.46



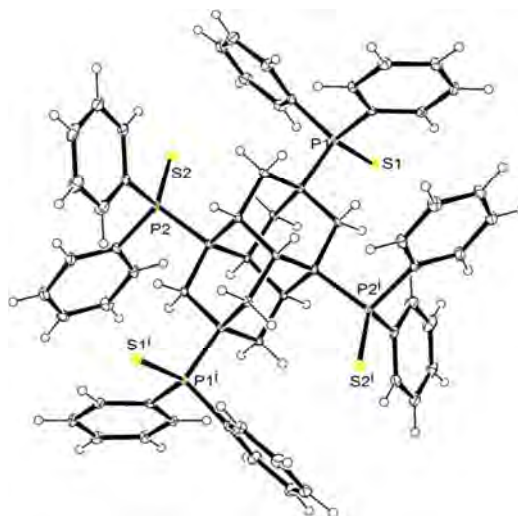
k) 1-Adamantylidiphenylphosphine sulphide (**198**)

N° CCDC	1054568	
Empirical formula	C ₂₂ H ₂₅ PS	
Formula weight	352.45	
Temperature	115(2) K	
Wavelength	0.71073 Å	
Crystal system	Orthorhombic	
Space group	P n m a	
Unit cell dimensions	a = 11.2136(3) Å	α = 90°.
	b = 12.6017(4) Å	β = 90°.
	c = 13.2583(5) Å	γ = 90°.
Volume	1873.54(11) Å ³	
Z	4	
Density (calculated)	1.250 Mg/m ³	
Absorption coefficient	0.258 mm ⁻¹	
F(000)	752	
Crystal size	0.25 x 0.20 x 0.15 mm ³	
Theta range for data collection	3.57 to 27.48°.	
Index ranges	-11 ≤ h ≤ 14, -16 ≤ k ≤ 16, -17 ≤ l ≤ 17	
Reflections collected	6866	
Independent reflections	2231 [R(int) = 0.0321]	
Completeness to theta = 27.48°	99.3 %	
Max. and min. transmission	0.9623 and 0.9382	
Refinement method	Full-matrix least-squares on F ²	
Data / restraints / parameters	2231 / 0 / 118	
Goodness-of-fit on F ²	1.075	
Final R indices [I > 2σ(I)]	R1 = 0.0357, wR2 = 0.0770	
R indices (all data)	R1 = 0.0484, wR2 = 0.0840	
Largest diff. peak and hole	0.399 and -0.257 e.Å ⁻³	



I) 1,4,6,9-Diamantyltetradiphenylphosphine sulphide (**200**)

Formula	C ₆₂ H ₅₆ P ₄ S ₄
$D_{calc.}/\text{g cm}^{-3}$	1.396
μ/mm^{-1}	0.361
Formula Weight	1053.18
Colour	colourless
Shape	prism
Max Size/mm	0.24
Mid Size/mm	0.19
Min Size/mm	0.09
T/K	100
Crystal System	triclinic
Space Group	P-1
$a/\text{\AA}$	12.4115(7)
$b/\text{\AA}$	13.9020(8)
$c/\text{\AA}$	17.1270(10)
$\alpha/^\circ$	82.967(2)
$\beta/^\circ$	69.001(2)
$\gamma/^\circ$	65.284(2)
$V/\text{\AA}^3$	2504.9(3)
Z	2
Z'	1
$\vartheta_{min}/^\circ$	2.937
$\vartheta_{max}/^\circ$	27.560
Measured Refl.	81671
Independent Refl.	11517
Reflections Used	8595
R_{int}	0.0754
Parameters	631
Restraints	0
Largest Peak	0.524
Deepest Hole	-0.376
Goof	1.031
wR_2 (all data)	0.0959
wR_2	0.0847
R_1 (all data)	0.0716
R_1	0.0418



Conclusions and perspectives

Synthetic modifications of adamantane and diamantane are well developed. Their applications have covered multidisciplinary studies, including fields such as biology, materials, electronics, and catalysis. Therefore the versatility of diamondoids has been already largely proven and further exciting development are achievable. The present bibliographical chapter constitutes a valuable foundation for the carbon-metal organohybrid construction we aim based on functionalized diamondoids.

Readily accessible processes for the mild vapor deposition of functionalized diamondoids provide previously unobserved self-assembly of organic micro- and nanocrystals. Key thermodynamic data including sublimation enthalpy of several diamondoid derivatives have been determined from a new measurement protocol at solid-vapor thermodynamic equilibrium state (**Chapter 2**). The conditions of pressure used for the depositions are crucial and if appropriately adjusted lead to deposits resistant to high vacuum and high energy beams. Vapor deposition under atmospheric pressure of air or argon lead to unprecedented assemblies that apparently capture gases, and turn to hollow edifices upon gas evacuation. Depending on the type of functional group and its position on the diamondoid, the general structure of the discrete deposits can vary dramatically and anisotropic structures such as rods, needles, triangles or truncated octahedra form. Self-assembled edifices of sizes ranging from 20 nm to several hundred micrometres can be obtained with conservation of a similar geometry for a given diamondoid.

Our first approach for building hybrid carbon-metal ordered structures was based on the two steps self-assembly of functionalized diamondoids on silicon by vapor phase, followed by palladium deposition using low-temperature OMCVD promoted at 65 °C in the presence of H₂ reactive gas. This approach (as described in **Chapter 3**) clearly failed. By lowering the temperature and extending the duration of deposition, we forced the deposition of palladium, but without specific selectivity or ordering over the substrates. As a consequence, thick uniform Pd layers were observed. Apparently the affinity of palladium with the Si surface (partially oxidized or with OH surface groups) is stronger than with the hydroxylated or fluorinated diamantanes. The reported studies of the influence of functional group on surface have shown that the presence of hydrogen/hydroxyl-terminated surface initiated the Pd decomposition.^{1,2,3,4} But in our case, the presence of H and OH at the surface of diamantane cages did not produced enough affinity to palladium.

¹ Q.-H. Wu, M. Gunia, T. Strunskus, G. Witte, M. Muhler, C. Wöll. *Chem. Vap. Deposition*, **2005**, 11, 355-361. Deposition of palladium from a cyclopentadienyl-allyl-palladium precursor on Si-based substrates with various pretreatments: the role of surface Si-OH and Si-H species studied by X-ray photoelectron spectroscopy.

To solve this issue, we changed our approach and decided to generate strong covalent bonding between the functionalized diamondoids and the transition metal. Concerning palladium, its affinity with phosphorus is well-known. Therefore we anticipated that forming hybrids might be facilitated by introducing phosphino groups onto the diamondoids. The idea would be then to strongly coordinate the first palladium units that may in turn initiate nucleation of nanoparticles and growth of new hybrid edifices. The synthesis of a variety of original diamondoids functionalized with P-containing groups is the subject of **Chapter 4**.

We synthesized a full set of unprecedented functionalized diamondoid phosphines based on adamantyl and diamantyl frameworks. Our approach was to first investigate synthetic pathways on unfunctionalized and easily accessible adamantyl backbone, then to transfer these conditions to diamantane derivatives. We delivered synthetic roads to functionalized diamondoid phosphines and primary phosphines (**186, 188, 190**) (**Scheme 4.13**) based on adamantane and diamantane frameworks. Brønsted acids have a great potential for phosphorylations of diamondoids allowing dissymmetrization of symmetric substrate like **49** (**Scheme 4.11**). Facile unequal difunctionalization of these diamondoids was possible avoiding tedious sequences of protection/deprotection for hydroxylated and chlorinated diamondoid phosphines (**186, 188, 190**). In the course of our investigations we also synthesized various tertiary phosphines (**199, Scheme 4.17**) with their pentavalent oxides (**191, 192, 193, 194**), sulfides (**198**), selenides (**197**) and phosphonium salt (**195**), as well as other difunctionalized derivatives for which synthetic protocols and characterization are reported (**Scheme 4.14, 4.15, 4.16, and 4.17**). Unexpected air-stability of some primary diamondoid phosphines (**188, 190, Scheme 4.13**) were observed. The air-stability of these compounds is remarkable regarding their donating alkyl substituents. This discovery allowed us to use those **188, 190** preferentially for preparing hybrid material by chemical vapor deposition of organometallic complexes as described in the **Chapter 5**.

Our first attempt to build hybrid Pd-diamondoid on **Chapter 3** using hydroxydiamantane showed that palladium growth by CVD had no specific selectivity towards diamondoids. Changing the hydroxy group with P(V) phosphonic dichloride **182** could not increase the affinity and did not conduct the preferential growth of palladium over the diamondoid. However, by switching the strategy and using P(III) phosphine

² C. Liang, W. Xia, H. Soltani-Ahmadi, O. Schlüter, R. A. Fischer, M. Muhler. *Chem. Commun.*, **2005**, 282-284. The two-step chemical vapor deposition of Pd(allyl)Cp as an atom-efficient route to synthesize highly dispersed palladium nanoparticles on carbon nanofibers.

³ C. P. Mehnert, D. W. Weaver, J. Y. Ying. *J. Am. Chem. Soc.*, **1998**, 120, 12289-12296. Heterogeneous heck catalysis with palladium-grafted molecular sieves.

⁴ X. Mu, U. Bartmann, M. Guraya, G. W. Busser, U. Weckenmann, R. Fischer, M. Muhler. *Applied Catal. A: General*, **2003**, 248, 85-95. The preparation of Pd/SiO₂ catalysts by chemical vapor deposition in fluidized-bed reactor.

as anchoring sites, hybrid material **Pd@PH₂-Diam-OH** was achieved. By varying the duration of palladium deposition by CVD, we could control the growth of palladium. At shorter time (1 h run), SEM analysis showed that the metallic Pd nodules grew preferentially on Si support. XPS and TEM confirmed that the hybrid was present since the first one hour. After 3 h run, the SEM analysis showed that a new smooth layer appeared, covering the columnar self-assembly **190**, and nodules formed with size 100-400 nm that are dispersed all over the sample. And after more than 5 h run, the smooth layer was clearly visible by SEM, covering the columnar self-assembly, and the size of nodules increased with most of them about 700 nm. XPS measurement indicated that an insulator material **Pd@PH₂-Diam-OH** formed during the CVD deposition with P–Pd interaction. These characterizations revealed that the formation of the hybrid occurs at the very first stage of the deposition, and then could be in competition with nucleation and growth of the nodules (or rearrangement of the surface deposition in nodules).

To deeply understand about the mechanism of the growth that happened during CVD process, several additional experiments are prerequisite.

First, to get the X-Ray structure of resulted molecule by mixing Pd precursor [Pd(allyl)Cp] with hydroxyphosphine **190** would give some information about the species that was formed during the metal deposition.⁵

Second, try to have self-assembly of **190** by PVD that have cleaner environment (reduced pressure 10⁻⁶ mbar) and far more thinner (nano-size particles, like on the case PVD of 1-hydroxydiamantane) by controlling the size using quartz balance. We can also reduce the size by vapor deposition at lower temperature and shorter duration of deposition. From this deposit, we can study about the morphology of the thin layer self-assembly.

Third, using XPS, we can study the growth of palladium on PVD self-assembly at various duration of metal deposition. It will give more information about the species that are formed during the deposition, and we could master the conditions for controlling the growth. Furthermore, by reducing the thickness of deposit into nanometer-size, we could reduce the charging effects that we observed previously during XPS measurements and get the real binding energies (BE) to get a good interpretation of the hybrid species.

Fourth, to understand the role of heteroatom on diamondoid phosphine, different phosphines can be used (i.e. PH₂-diamantane-Cl, PH₂-diamantane-SH). Such of different form of self-assemblies are

⁵ R. A. Fischer, U. Weckenmann, C. Winter, J. Käshammer, V. Scheumann, S. Mittler. *J. Phys. IV France*, **2001**, 11, Pr3/1183-Pr3/1190. Area selective OMCVD of gold and palladium on self-assembled organic monolayers: control of nucleation sites.

expected, and using PH₂-diamantane-SH could open the access to build self-assembly monolayers (SAMs).

Fifth, we can learn more about versatility and selectivity of phosphine as anchoring sites by altering the palladium that was used for metal deposition with various types of metals, such as Pt, Au, or Ni. Phosphorus doped carbon material could increase the catalytic performance of platinum catalyst.⁶ With the addition of phosphorus, it can inhibit the aggregation and reduce the size of Pt nanoparticles that really important in improving chemical activity of catalysts. The phosphorus (doping on carbon) also played decisive role in enhancing the stability of platinum particles because it has strong interactions with platinum.⁷ Depositing of gold on diamondoid phosphine may be also very interesting. Gold on phosphorus supported carbon has recently been reported alter the physico-chemical properties.^{8,9} Pd nanoparticles on carbon could be used for selective heterogeneous nucleation and growth of Ni.¹⁰ Addition of phosphorus on material could improve the mechanical properties of nickel but it should be optimized because too low or high P can cause the embrittlement.¹¹

Further characterizations to uncover the attractive novel physical properties (optic, electronic, magnetic, and conductive “band-gap”) of organohybrid **Pd@PH₂-Diam-OH** due to the inclusion (doping) with metal centers are needed.

Determination of such exact bonding type of P–Pd by Raman spectroscopy,^{12,13} FT-IR,¹⁴ and EXAFS are required. With EXAFS, we also could characterize the interface of diamondoid/metal and get a better understanding the mechanism of the growth. To see more precisely the topology of hybrid and nodules,

⁶ P. Song, L. Zhu, X. Bo, A. Wang, G. Wang, L. Guo. *Electrochim. Acta*, **2014**, 127, 307-314. Pt nanoparticles incorporated into phosphorus-doped ordered mesoporous carbons: enhanced catalytic activity for methanol electrooxidation.

⁷ Y. Tong, X. Zang, Q. Wang, X. Xu. *Comp. Theor. Chem.*, **2015**, 1059, 1-6. The adsorption mechanism of platinum on phosphorus-doped single walled carbon nanotube.

⁸ V. J. Mayani, S. V. Mayani, S. W. Kim. *Bull. Korean Chem. Soc.*, **2014**, 35, 401-406. Development of gold phosphorus supported carbon nanocomposites.

⁹ V. J. Mayani, S. V. Mayani, S. W. Kim. *Mater. Lett.*, **2012**, 87, 90-93. Development of nanocarbon gold composite for heterogeneous catalytic oxidation.

¹⁰ S.-M. Bak, K.-H. Kim, C.-W. Lee, K.-B. Kim. *J. Mater. Chem.*, **2011**, 21, 1984-1990. Mesoporous nickel/carbon nanotube hybrid material prepared by electroless deposition.

¹¹ W. Liu, C. Ren, H. Han, J. Tan, Y. Zou, X. Zhou, P. Huai, H. Xu. *J. Applied Phys.*, **2014**, 115, 043706/1-043706/7. First-principles study of the effect of phosphorus on nickel grain boundary.

¹² G. M. Fuge, P. W. May, K. N. Rosser, S. R. J. Pearce, M. N. R. Ashfold. *Diamond Relat. Mater.*, **2004**, 13, 1442-1448. Laser raman and X-ray photoelectron spectroscopy of phosphorus containing diamond-like carbon films grown by pulsed laser ablation methods.

¹³ L. Landt, M. Staiger, D. Wolter, K. Klünder, P. Zimmermann, T. M. Willey, T. van Buuren, D. Brehmer, P. R. Schreiner. *J. Chem. Phys.*, **2010**, 132, 024710/1-024710/7. The influence of a single thiol group on the electronic and optical properties of the smallest diamondoid adamantane.

¹⁴ A. Khalafi-Nezhad, F. Pahani. *Green Chem.*, **2011**, 13, 2408-2415. Immobilized palladium nanoparticles on silica-starch substrate (PNP-SSS): as an efficient heterogeneous catalyst for Heck and copper-free Sonogashira reactions in water.

it can be analyzed by Atomic Force Microscopy (AFM).¹⁵ Characterization with SIMS (dynamic mode) allows getting the relative thickness of sample, or with SIMS (static mode) permits to determine the relative composition of the external layers.

To learn more about its electronic properties of the hybrid, Scanning Tunneling Spectroscopy (STS) needs to be performed.¹⁶ With this technique, we can explore if the hybrid has metallic properties by measuring their conductivity.

Envisaging the applications, the use of palladium nanoparticles on silica-starch substrate (PNP-SSS) inspires us for uses in catalyst. Panahi group developed this excellent catalyst by immobilizing the palladium nanoparticles on silica-(potato) starch for Heck, copper-free Sonogashira, and Suzuki reactions.^{14,17} This catalyst can be reused more than six times by simply filtration without remarkable loss of catalytic activity in water. The use of the hybrid as recoverable catalytic materials in such C–C cross-couplings is expected to give higher efficiency since the presence of phosphine in our hybrid can increase the catalytic activity. Some preliminary results in Pd-catalyzed reaction were done in our group using hydroxyphosphine **190** as ligand in water and it gives encouraging results.¹⁸

For application in electronics, by using the hybrid that containing transition metal as seeds for growing diamond-like films, the reactivity of such seed nanostructures are expected to promote the formation of diamond-like films under mild conditions through C–H activation and C–C coupling. Diamond now is considered as wide bandgap (WBG) semiconductor¹⁹ that will replace the silicon because it allows power electronic components to be smaller, more reliable, and more energy efficient than silicon. WBG semiconductors permit devices to operate at much higher temperatures, voltages, and frequencies making these materials significantly more powerful than those made from conventional semiconductor materials. But the challenge here is to manufacturing these WBG materials to be effective in their applications. Using the hybrid for promoting the growth of diamond at lower temperature could tackle the problem of precise construction of the diamond devices with specific size and thickness.

¹⁵ A. V. Simak, E. N. Loubnin, G. A. Shafeev, P. Doppelt. *Appl. Surf. Sci.*, **2002**, 186, 227-231. Laser-assisted deposition of Pd-doped diamond-like films from liquid hydrocarbons and their use for glass metallization.

¹⁶ H. N. Aiyer, V. Vijayakrishnan, G. N. Subbanna, C. N. R. Rao. *Surf. Sci.*, **1994**, 313, 392-398. Investigations of Pd clusters by the combined use of HREM, STM, high-energy spectroscopies and tunneling conductance measurements.

¹⁷ A. Khalafi-Nezhad, F. Pahani. *J. Organomet. Chem.*, **2012**, 2012, 141-146. Immobilized palladium nanoparticles on silica-starch substrate (PNP-SSS): as a stable and efficient heterogeneous catalyst for synthesis of *p*-teraryls using Suzuki reaction.

¹⁸ L. Joucla, N. Batail, L. Djakovitch. *Adv. Synth. Catal.*, **2010**, 352, 2929-2936. "On water" direct and site-selective Pd-catalysed C-H arylation of (NH)-indoles.

¹⁹ United States Department of Energy, Advanced Manufacturing Office (April 2013), *Wide Bandgap Semiconductors: Pursuing the Promise*, Retrieved from manufacturing.energy.gov.

Such application in solar cells is also expected. Ma *et al.* has developed a material Pd doped amorphous carbon film on Si/SiO₂ supports by magnetron sputtering.²⁰ They found that this material has a high power conversion efficiency of 4.7%, which is much better than the Si doped amorphous carbon junctions reported. The palladium doping can greatly improve the photovoltaic characteristics but not for the case with Fe(Ni) doping. Recently, Partridge group found that addition of 1-10 nm of nanodiamond could improve the efficiency of solar cell up to 17.2%.²¹ These works lead us to think about the probability for application in this field. By combining these two materials as hybrid, we can expect a high improvement of solar cell efficiency.

Another application is fabrication of Pd membrane for gas separation. Inorganic membranes with high permeation selectivity for hydrogen have potential for application in industries because of their high thermal, chemical, and mechanical stability. For this reason, they have been studied using various materials such as silica and palladium. But these developments encounter several difficulties; it must be operated at a high temperature (>300 °C) to obtain a viable hydrogen permeation rate.²² In consequence, it required stability of the membrane at high temperature. Baker group prepared ultrathin Pd/Ag alloy films (50 nm) on polymeric supports.²³ Because this composite is limited by thermal stability of the support, Lin group tried to improve it using porous ceramic supports. They mentioned that surface roughness of the support was critical to obtain gas-tight and selective membrane.^{24,25} Depositing palladium metal on a phosphine-containing membrane at very low temperature by CVD permits to access various type of membranes since the recent type is usually suffers in thermal stability, difficulties in controlling the film thickness, and adhesion on support.

²⁰ M. Ma, Q. Xue, H. Chen, X. Zhou, D. Xia, C. Lv, J. Xie. *Appl. Phys. Lett.*, **2010**, 97, 061902/1-061902-3. Photovoltaic characteristics of Pd doped amorphous carbon film/SiO₂/Si.

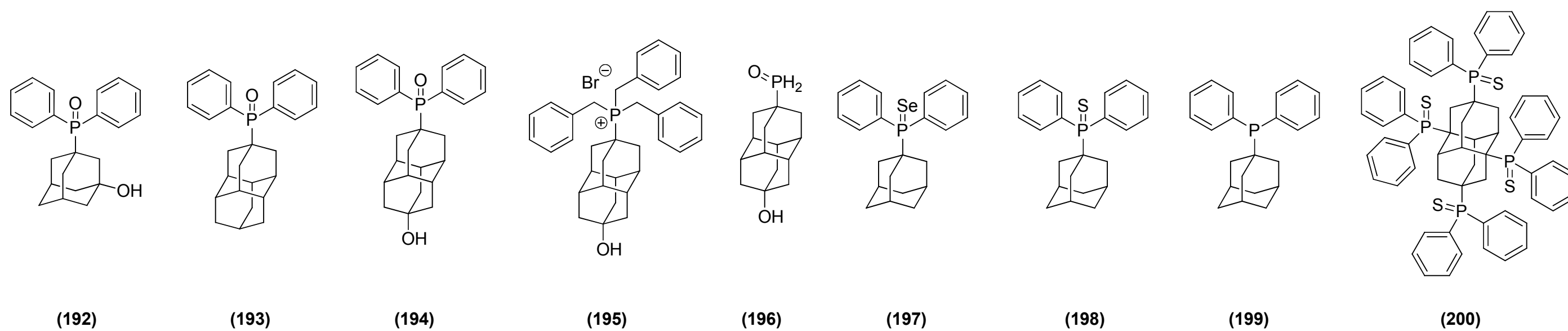
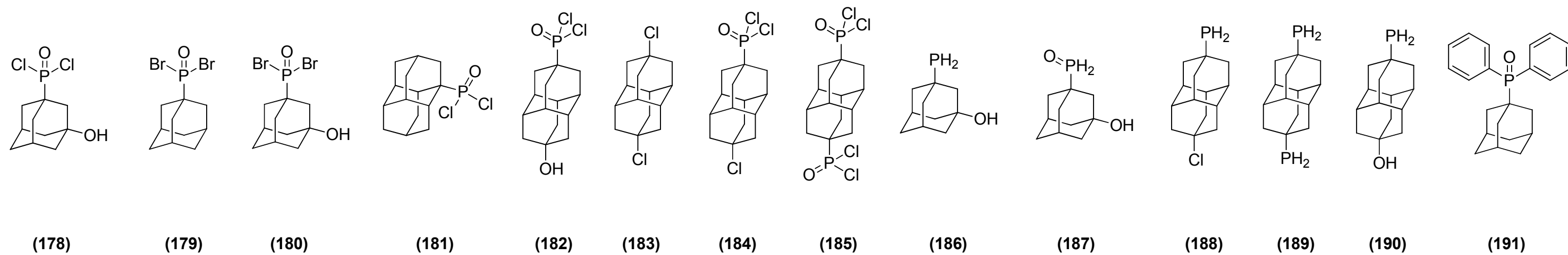
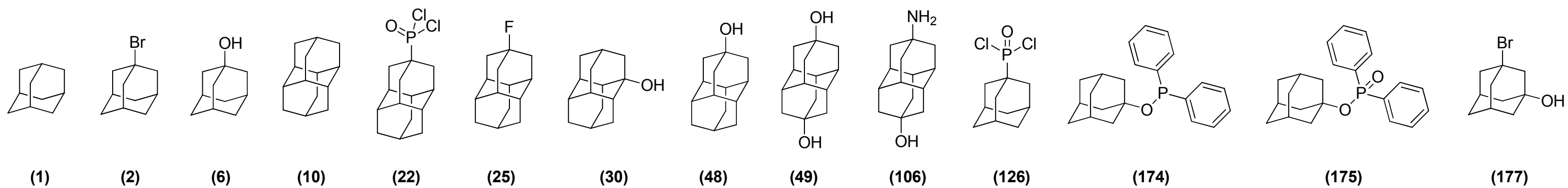
²¹ C. A. Bertelo, S. Gaboury, R. Partridge. *PCT Int. Appl.*, **2015**, WO 2015042555 A1 20150326. Nanodiamond coatings for solar cells.

²² G. Xomeritakis, Y. S. Lin. *J. Membrane Sci.*, **1996**, 120, 261-272. Fabrication of a thin palladium membrane supported in a porous ceramic substrate by chemical vapor deposition.

²³ A. L. Athayde, R. W. Baker, P. Nguyen. *J. Membrane Sci.*, **1994**, 94, 299-311. Metal composite membranes for hydrogen separation.

²⁴ V. Jayaraman, Y. S. Lin, M. Pakala, R. Y. Lin. *J. Membrane Sci.*, **1995**, 99, 89-100. Fabrication of ultrathin membranes on ceramic supports by sputter deposition.

²⁵ V. Jayaraman, Y. S. Lin. *J. Membrane Sci.*, **1995**, 104, 251-262. Synthesis and hydrogen permeation properties of ultrathin palladium-silver alloy membranes.



Structures numbering